Synthesis, Spectroscopic and Electrochemical Properties of Squaraine Polymers

Dissertation zur Erlangung
des naturwissenschaftlichen Doktorgrades der
Julius-Maximilians-Universität Würzburg

vorgelegt von
Sebastian Fabian Völker

aus Neckarelz

Würzburg 2014

Eingereicht bei der Fakultät für Chemie und Pharmazie am

01.07.2014

Gutachter der schriftlichen Arbeit

1. Gutachter: Prof. Dr. Christoph Lambert

2. Gutachter: Prof. Dr. Frank Würthner

Prüfer des öffentlichen Promotionskolloquiums

1. Prüfer: Prof. Dr. Christoph Lambert

2. Prüfer: Prof. Dr. Frank Würthner

3. Prüfer: Prof. Dr. Volker Engel

Datum des öffentlichen Promotionskolloquiums

01.08.2014

Doktorurkunde ausgehändigt am

Die vorliegende Arbeit wurde in der Zeit von Juni 2009 bis Juni 2014 am Institut für Organische Chemie der Universität Würzburg angefertigt.

Mein besonderer Dank gilt

Herrn Prof. Dr. Christoph Lambert

für die Vergabe des vielseitigen und interessanten Themas, den damit verbundenen Diskussionen sowie der Förderung, dem Vertrauen und den Freiheiten bei dessen Bearbeitung.

COPYRIGHT

7. *Singlet-Singlet Exciton Annihilation in an Exciton-Coupled Squaraine-Squaraine Copolymer: A Model towards Hetero-J-Aggregates,* S. F. Völker, A. Schmiedel, M. Holzapfel, K. Renziehausen, V. Engel, C. Lambert, *J. Chem. Phys. C.* **2014**, *accepted* –

CONTENTS

ABBREVIATIONS

BHJ	bulk heterojunction
COD	1,5-cyclooctadiene
CS	charge separation
CT	charge transfer
CV	cyclic voltammetry
dppf	1,1'-bis(diphenylphosphino)ferrocen
DPV	differential pulse voltammetry
EL	electroluminescence
GPC	gel permeation chromatography
MV	mixed valence
NDI	naphthalene diimide
OLED	organic light emitting diode
OSWV	*Osteryoung* square wave voltammetry
P3HT	poly(3-hexylthiophene)
PEDOT:PSS	poly(3,4-ethylenedioxythiophene):polystyrenesulfonate
PCBM	[6,6]-phenyl-C_{61}-butyric acid methyl ester
PL	photoluminescence
SEC	spectroelectrochemistry
TBAHFP	tetrabutylammonium hexafluorophospate
(TD)DFT	(time dependent) density functional theory

1 Introduction

1.1 Squaraines

Classification

Squaraines, which are quite often also referred to as squarylium dyes, belong to the family of polymethine dyes. Some members of this family are shown in Chart 1. Representative examples shown therein are defined by two heteroatoms which are connected by a polymethine chain consisting of an odd number of repeating methine units " = CH – " which results in conjugated systems. Depending on the heteroatoms, these systems can be cationic, anionic, zwitterionic or neutral.

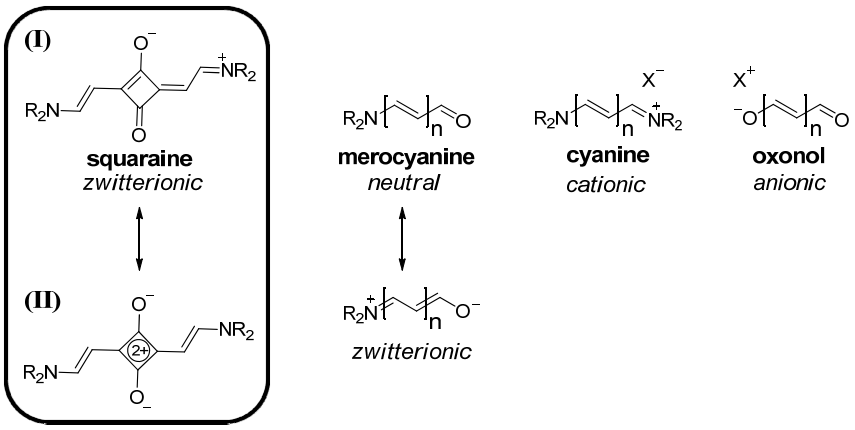

Chart 1 Schematic drawing of some members of the polymethine dye family.

Cyanine dyes are cationic species and one amine and one iminium group terminate the polymethine chain. In the "classical" cyanines, these nitrogen atoms are part of a heterocycle but there are also others like hemicyanines where there is only one nitrogen-containing heterocycle, for example. In oxonols, oxygen atoms are at the end of the polymethine chain, one in carboxylic form and the other one as alcohol. At neutral pH values they are commonly anionic. A neutral species of polymethine dyes are merocyanines. In these compounds, one nitrogen and one oxygen are located at the ends of the polymethine chain. They have a "push-pull" system and possess a distinct zwitterionic character which leads to a strong dipole moment of the chromophore.

Squaraines represent a real zwitterionic species. They are neutral overall, however, a neutral mesomeric structure can usually not be written with exception of special cases. The betaine structure can be expressed either as a dipolar cyanine structure (I) or a cyclobutenediyliumdiolate (II). The former might be responsible that squaraines are often referred to as cyanine dyes as well as the fact that their structure appears as if an oxocyclobutenolate core was inserted into the cyanine structure. In addition they show some similar properties such as strong and sharp absorption in the red to NIR region. However, squaraines should be seen as a separate class because they are zwitterionic and they consist of a donor–acceptor–donor (D–A–D) structure due to the strong electron withdrawing central moiety, in contrast to cyanines. For stabilisation of the D–A–D system, strong electron donating groups like heterocycles or electron rich aromatic units such as aniline derivatives are usually found in squaraine dyes.

History and Evolution

In 1959, *Cohen*, *Lacher*, and *Park* claimed the first synthesis of diketocyclobutenediol, nowadays better known as squaric acid (Chart 2), by aqueous hydrolysis of alkoxy and halogen persubstituted cyclobutenes.[1] This dibasic acid is highly acidic with $pK_{S1} \sim 1$ and $pK_{S2} \sim 2.2$ but surprisingly it is only poorly soluble in water (2%), which could be explained by strong hydrogen bonding which was observed in IR studies.[1-3]

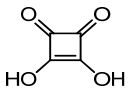

Chart 2 Squaric acid

It took another few years until 1965 when *Treibs* and *Jacob* (*T&J*) reported on dyes obtained upon reaction of highly reactive pyrroles or phloroglucinol (1,3,5-trihydroxybenzene) with squaric acid in ethanol.[4] They prepared both monomeric dyes (Chart 3, **S1** and **S2**, repectively) suffering from poor solubility and one pyrrole squaraine polymer (**PS1**) that was completely insoluble in common solvents.

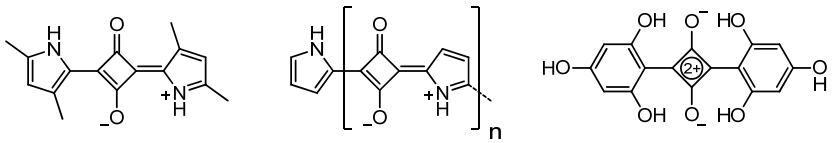

Chart 3 The first squaraines (**S1**, **S2**, and **PS1**) reported by *Treibs* and *Jacob* (*T&J*).[4]

This initiated an intense research on those dyes, giving rise to frequently new reports on squaraine dyes, containing diverse heterocyclic or aromatic compounds. Independently *Sprenger* and *Ziegenbein* (*S&Z*) as well as *T&J* synthesised the first indolenine squaraine (**S3**, Chart 4, p. 7), however, using different procedures. While *T&J* used acetic anhydride[5] as solvent, *S&Z* already used a mixture of 1-butanol and benzene under azeotropic removal of resulting water[6], a method that should become the standard in squaraine synthesis albeit nowadays quite often benzene is exchanged by toluene. *S&Z* also prepared squaraine dyes with benzothiazole (**S4**), benzoselenazole (**S5**), and 2-methylchinoline (**S7**).[6] *S&Z* and *T&J* also condensed indole[5], azulene[7], or tertiary aromatic amines[8] (**S8**) with squaric acid to obtain the corresponding dyes. In addition, instead of squaric acid they applied its diethyl ester, a squarate, in this condensation reaction and obtained differently coloured dyes but with the same molecular mass. Unlike the squaraine dyes, where the squaric acid core is substituted in the 2- and 4-position, those dyes were cyclobutenedione derivatives substituted in 3- and 4-position of the central ring absorbing light at higher energy and also showing different IR spectra (see below) compared to the 2,4-squaraine isomers with the same terminating groups.

T&J were interested in the mechanism of the new condensation reaction. Therefore they prepared a series of a proposed intermediate where only one nucleophile is attached at the squaric acid, a so-called semisquaraine. From this intermediate they were able to synthesise several asymmetrical squaraine dyes for the first time.[9] In this work, they also give an overview of the IR spectra concerning the vibrations of the central core unit, which were used to determine the structure. While both the semisquaraines and the 3,4-substitued derivatives show IR signals at ~ 1770 cm^{-1} and ~ 1720 cm^{-1} relating to the cyclobutenone groups, none of these signals is observed for the squaraine dyes. With 2,4-substitution at the central ring, these dyes show a signal at ~ 1615 cm^{-1} instead, reflecting the delocalised character of this chromophore.

It hast to be noted that the name “squaraine” was not used until it was proposed by *Schmidt* in a small side note of his review on reactions of squaric acid and squaric acid derivatives in 1980.[3] The name was derived from the combination of the *squar*ic acid and the bet*aine* character of the dyes.

T&J also proofed that it was possible to perform a pyrrole exchange reaction where one heterocycle of a squaraine dye was exchanged by a pyrrole upon heating the mixture of the squaraine and pyrrole in glacial acetic acid. They also prepared a bis-squaraine which is similar in the structure to **PS1** with n = 2 (Chart 3).[9]

Synthesis and Mechanism

As already mentioned above, from the method of *S&Z* to prepare squaraine dyes a standard procedure has been developed which is widely used. In this procedure, two equivalents of the nucleophilic aromatic molecule and one equivalent of squaric acid are condensed in a solvent mixture of toluene and 1-butanol (mostly in an 1:1 ratio) under the azeotropic distillation of resulting water using a *Dean-Stark* trap (example shown in Scheme 1). Commonly, the reaction time is between 1–18 h and the purification is either performed by column chromatography and/or crystallisation.

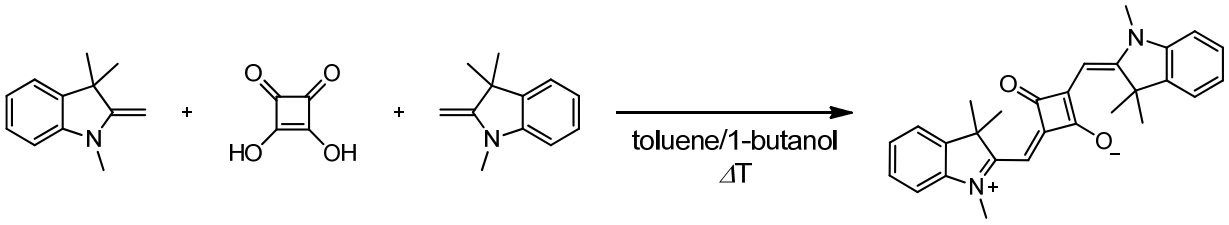

Scheme 1 Standard reaction for squaraine synthesis.

Shortly after the first reports on the synthesis of squaraine dyes the mechanism of the reaction was proposed[5] and was reported slightly modified later for the case when 1-butanol is part of the solvent mixture[10] instead of acetic acid as in the former publication. In the latter, the first step is proposed to be the formation of a “half ester” (in brackets, Scheme 2) of the squaric acid, whose formation was already described by *Cohen et al.*[11] The actual nucleophilic attack of the nucleophilic compound takes place

at this vinylogous ester in 4-position followed by the removal of 1-butanol (or water as for the former case when the attack takes place at the acid) like in a classic ester condensation reaction. This yields the intermediate semisquaraine acid (yellow). In the next step a formal ketone and a vinylogous carboxylic acid compete for the 2nd nucleophile which attacks at the former due to its higher reactivity. Elimination of water in favour of the formation of the conjugation yields the symmetric squaraine (blue).

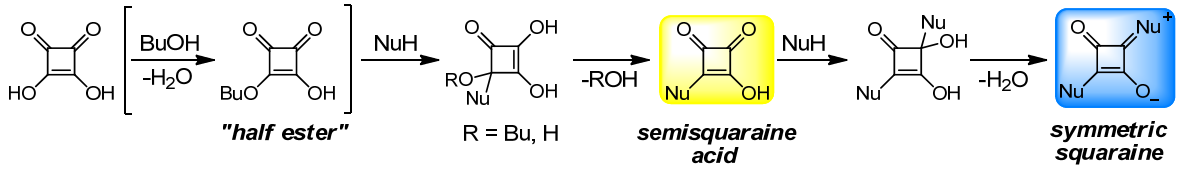

Scheme 2 Proposed reaction mechanism of the condensation reaction to symmetric squaraines.

For the synthesis of asymmetric squaraines more steps are necessary. Even though one could think that simple condensation reaction of the squaric acid with a mixture of the two different nucleophilic aromatic compounds would lead to the desired asymmetric dyes, it was reported that this usually leads to either one exclusively formed symmetric dye that contains the more nucleophilic aromatic moiety or to a mixture of all combinations that are generally difficult to separate.[12] For this reason a more target-oriented approach has been developed.

The first step is the synthesis of a semisquaraine derivative (Scheme 3). The straightforward approach of simply using equivalent amounts of squaric acid and the nucleophilic aromatic reactant, however, only resulted in symmetric squaraine dyes as shown in Scheme 2 and the reaction could not be stopped at the semisquaraine stage.[12] Therefore, not the squaric acid but its activated forms in terms of the ethyl or butyl ester (squarate) or its acid chloride are used. Those can be obtained by heating the squaric acid in the respective alcohol or by reaction with $SOCl_2$ in DMF, respectively.[3] For the semisquaraine synthesis varyous synthetic methods can be applied. Similarly to the synthesis of the symmetric squaraines, a condensation reaction of the nucleophile with one equivalent of the squarate in an alcohol or acetic acid results in the respective semisquaraine ester. The reaction of the nucleophile with squaric acid chloride in an inert solvent such as benzene or Et_2O yields the semisquaraine chloride. Using a stannyl

squarate derivative, it is also possible to apply a *Stille*-type coupling reaction to obtain a semisquaraine ester. Direct nucleophilic substitution at the semisquaraine ester or chloride however generate the 3,4-disubstituted cyclobutenedione derivatives and not the 2,4-disubstituted products, the squaraines. Therefore, either acidic or basic hydrolysis of the semisquaraine derivatives to the semisquaraine acid is mandatory for further synthesis of squaraines. The semisquaraine acid can be condensed with another nucleophilic aromatic compound applying the standard reaction conditions to obtain the asymmetric squaraine dye.

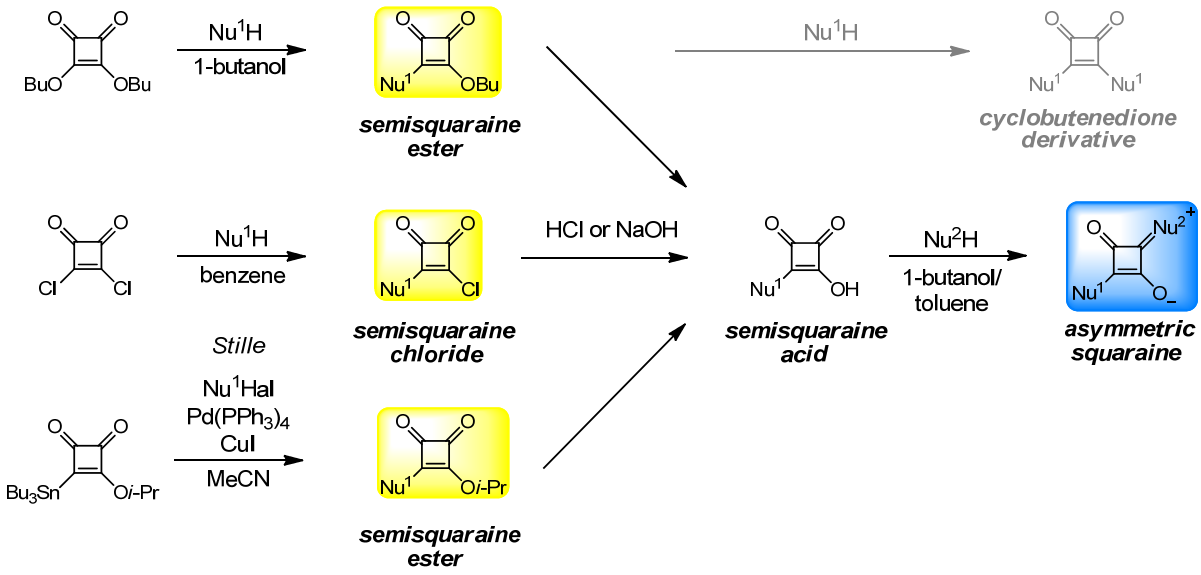

Scheme 3 Potential reaction pathways to asymmetric squaraines.

It has to be noted that there are several other procedures reported for both squaraine or semisquaraine synthesis,[3, 10, 13] nevertheless only the most commonly used ones are described herein.

Variety and Properties

As it might be obvious from the reaction mechanism, there are several nucleophilic compounds that can be applied for the synthesis of squaraine dyes. And indeed, a plethora of diverse types of squaraines was reported. The parent structures of some of the squaraines that have extensively been investigated are depicted in Chart 4 to give an idea about the variety of the dyes.

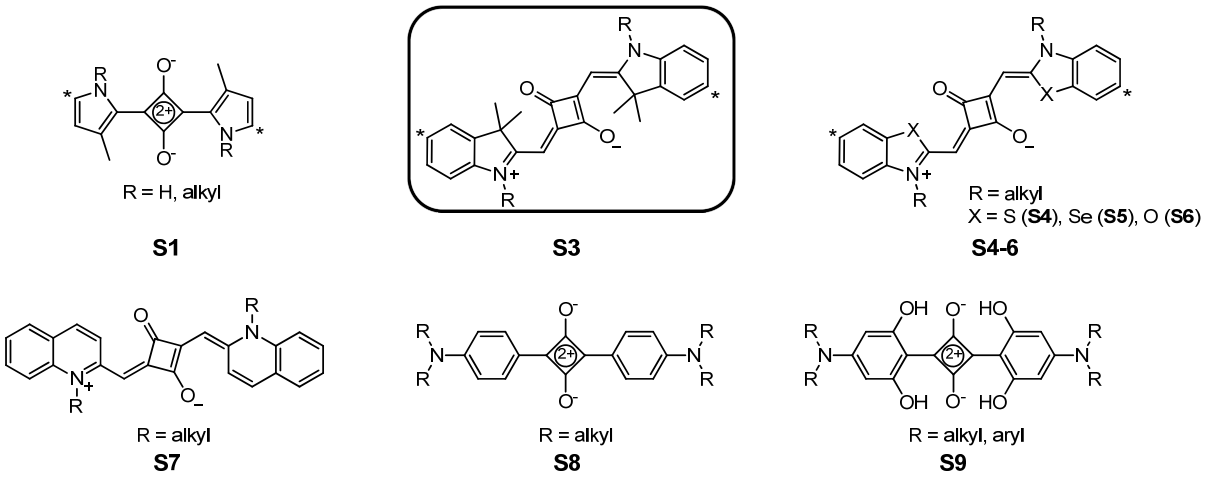

Chart 4 Selection of squaraine dyes **S1** and **S3**–**S9**. The stars designate the position where further functionalisation is often found. The frame accents the type of squaraine used in this work.

Squaraine dyes usually show a planar backbone and those carrying two identical donor moieties are usually centrosymmetric[14-15]. This corresponds to a *trans*-configuration for those squaraines that feature a methylene bridge between the outer donor groups and the central squaric acid core such as the indolenine squaraines[16-17] **S3**, for example. Centrosymmetric squaraines commonly have a vanishing dipole moment in the ground state.

The ability to form aggregates strongly depends on the outer donors of the squaraines. Indolenine squaraines barely show aggregation formation in solution most probably due to the two methyl groups at the indolenine ring which are pointing out of the elsewise planar system and therefore might hinder aggregate formation. Only in strongly aqueous media, where these dyes are barely soluble without solubilising groups, the formation of aggregates was reported.[18] More planar squaraines, such as those carrying chinoline[19-20], benzothiazole[21], pyrrole[22] units or aniline derivatives[23-24] more readily form aggregates, sometimes even in pure organic solvents. However, in the solid state even indolenine squaraines may form aggregates.[25]

The most prominent feature of squaraine dyes is their sharp and intense absorption and fluorescence in the visible red to NIR region, very similar to cyanine dyes (Figure 1). This is one of the reasons why they are sometimes referred to as members of the cyanine dye family as mentioned before. The *Stokes* shift is commonly rather small, which, in

addition to the narrow and intense low energy absorption, is indicative of delocalisation and small reorganisation energy of the excited state. The absorption band shows a steep rise at the low energy side with large extinction coefficients of $\varepsilon \sim 1–4 \times 10^5$ M^{-1} cm^{-1} at the maximum and a smaller vibronic shoulder at the high energy side, which is frequently (but not always) observed. This pronounced absorption band arises from a HOMO→LUMO transition from the S_0 to the S_1 state of the donor-acceptor-donor structure. At higher energies, one-photon excitation into the S_2 state is forbidden due to symmetry reasons and in the absorption spectra there is a decent gap of absorption.[26] Depending on the aromatic units used, additional absorptions are found at the high energy edge of the visible (Vis) and in the ultraviolet (UV) region.

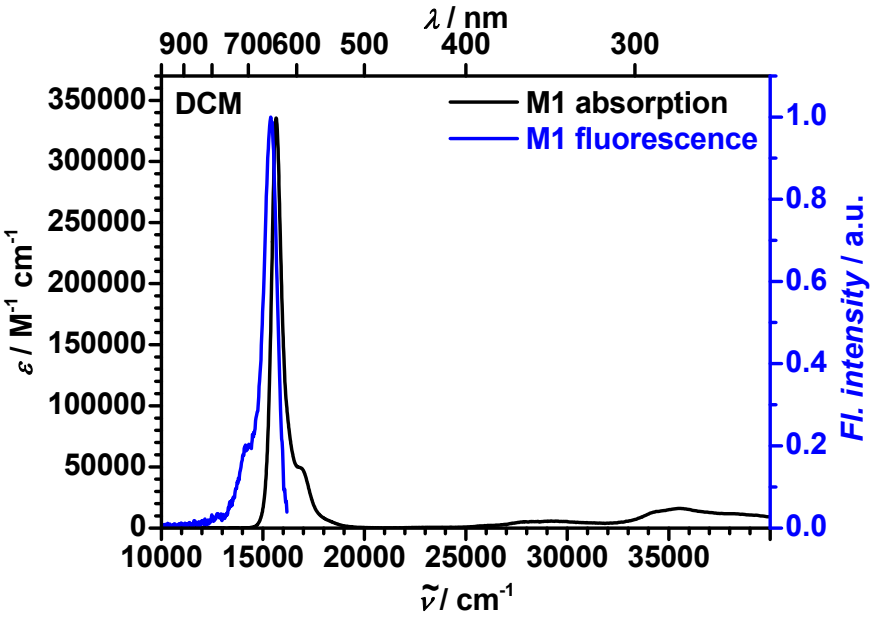

Figure 1 Typical absorption and fluorescence spectra of an indolenine squaraine dye of the type **S3**. The selected dye (**M1**) will be discussed in chapter 3.1 (p. 45).

There are various options to tune the absorption properties of squaraines. The HOMO and LUMO orbitals of an indolenine squaraine such as **S3** are depicted in Figure 2. As can be seen, the HOMO is spread over the complete π-system of the polymethine chain, the central ring including the oxygen atoms as well as the indolenine moiety at the periphery. In the LUMO orbital, there is still, but minor, contribution of the aromatic unit, whereas the largest orbital coefficients are found on the polymethine chain. Depending on the method applied for the calculation of the molecular orbitals, the

contribution of the aromatic unit to the LUMO may be even weaker or nearly vanishes, whereas it might be even more pronounced in the HOMO.[27-30]

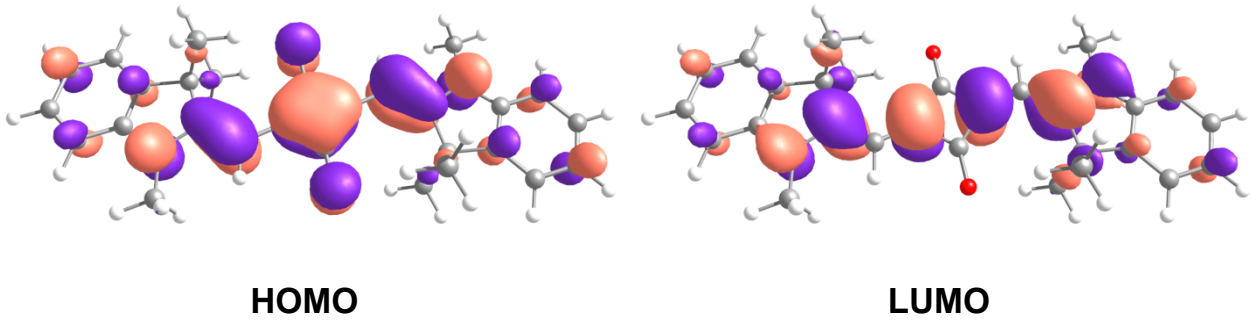

Figure 2 HOMO and LUMO orbitals of an indolenine squaraine calculated at B3LYP/6–31G* level of theory.

The stronger the electron donor, the higher is the HOMO level and the energy difference between HOMO and LUMO is decreased. This leads to a red shift of the main absorption band. Additionally, implementation of further electron donating moieties at the periphery of the dye can also result in a rise of the HOMO energy level and a shift of the absorption towards lower energy. Typical positions where those additional donors are commonly attached are marked with an asterisk in Chart 4.

In a similar manner, the LUMO level can be lowered by the substitution of one of the central oxygen atoms by a stronger electron acceptor. This also leads to a red shift of the main absorption band. The introduction of the core substituent is mainly performed at the semisquaraine stage where at the same time the synthesis of asymmetric dyes is enabled.[31-34] In limited cases, mainly for the exchange of oxygen in favour of sulphur, methoxy, or an amine (Chart 5, **S10**–**S14**), this can be done at the final squaraine stage.[31, 35-36] If symmetrical squaraines of the type **S11** or **S15** are desired this can also be achieved by a condensation reaction of the aromatic nucleophiles with the respective squaric acid derivative, such as the dithiosquarate in case of **S11**.

Depending on the steric demand of the electron accepting unit, the squaraine adopts a *cis*-[28, 34] instead of the common *trans*-configuration. Some of the substituents are shown for an indolenine squaraine (**S16**–**S21**) in Chart 5.[31-37] The highlighted squaraine **S15**

carries the dicyanomethylene group, which is the one that induces the largest red shift and will also be of major interest in this work.

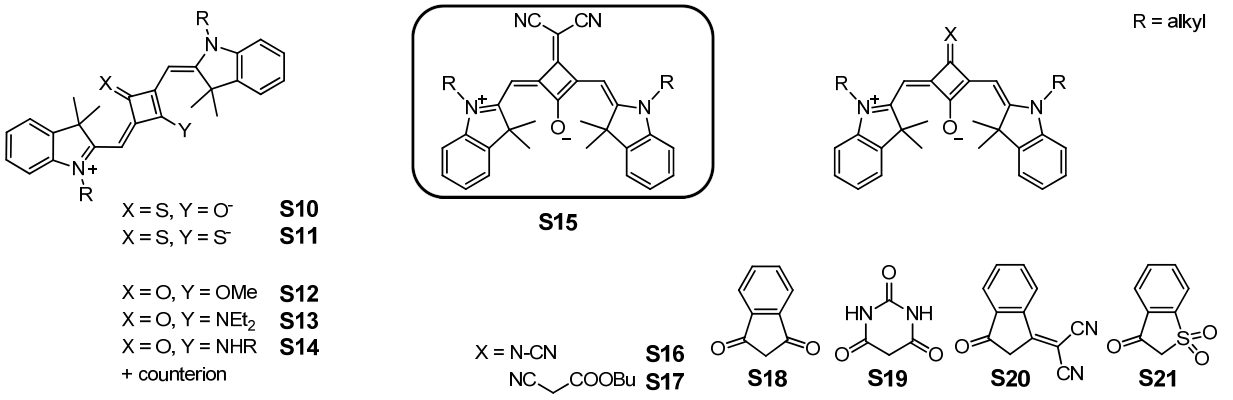

Chart 5 Core-substituted squaraine dyes **S10**–**S21**. The frame accents the type of squaraine used in this work.

Applications

General

Due to their absorption and fluorescence properties, squaraine dyes have been tested and used for a broad variety of applications. They have been reported as sensitive markers for several cations such as Cs^{+}[38], Ca^{2+}[39], and Hg^{2+}[40-41] as well as anions like CN^{-}[42]. This application is based on different mechanisms such as reducing the intensity of the main absorption (bleaching of the solution) due to inclusion of ions in crown-ether moieties being attached to the dye, changing the overall absorption properties (change of colour of the solution) by binding of ions to the central oxygen atoms or the formation of dimeric aggregates what also results in a change of absorption.

It was also shown that squaraines can detect thiol containing compounds.[43] In this case the thiol attacks the central ring at the 2-position. This perturbation of the delocalised π-system leads to a complete bleaching of the solution (Scheme 4). Based on this colourless squaraine–thiol conjugate, there have been additional studies in terms of Hg^{2+}[44-45] or CO_2[46] sensing when the thiol is removed from the squaraine and the colour is restored.

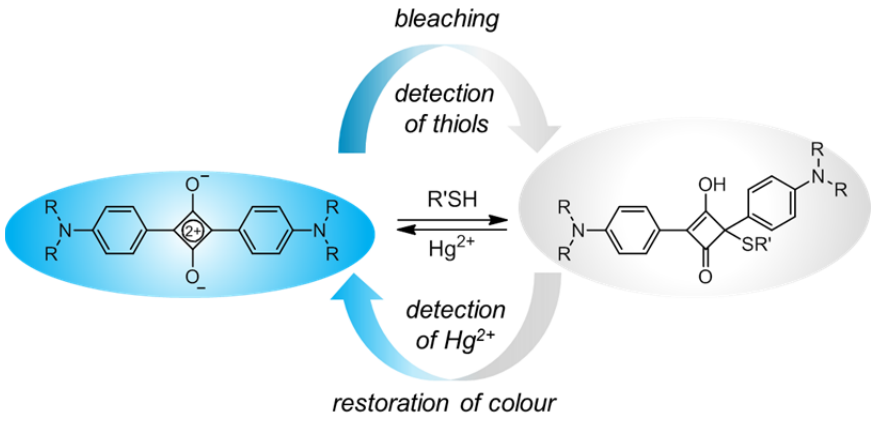

Scheme 4 Mechanism for the detection of both thiols and Hg^{2+}.

Besides, squaraines are tested in the field of bioimaging as protein markers and NIR fluorescence probes. Here, both free and rotaxane capped squaraines are applied.[31-32, 47-53] Especially absorption and fluorescence in the range of 600–1200 nm (~ 8300–16700 cm^{-1}) are of major importance due to increased penetration depth and reduced absorption and light scattering properties of the human tissue in this spectroscopic window.[54] Another medical aspect taking advantage of these features is the photodynamic therapy (PDT). Here both the labelling of biomolecules as well as a certain ability of triplet formation and singlet oxygen sensitisation is favoured.[55-58]

Moreover, the potential as materials for data imaging,[59] as photoconductors for xerographic devices,[60] and as materials with non-linear optical properties[27, 29, 61-68] was successfully proved. Besides, a recent investigation showed the use of dicyanomethylene substituted benzoselenazole squaraines in organic thin-film transistors (OTFTs). In this thorough study, remarkable hole mobilities of 0.45–1.3 $cm^2\ V^{-1}\ s^{-1}$ were reported for solution-sheared and vacuum deposited OTFTs.[69]

Squaraines in photovoltaic devices

The intense absorption in the red to NIR region gave rise to a series of investigations of squaraines in both dye-sensitised solar cells (DSSCs) or organic solar cells (mainly bulk heterojunction (BHJ)). The main structures of squaraines used for these devices interestingly slightly differ depending on the application.

For the DSSCs, attaching the dye to e.g. TiO_2 is necessary. Therefore, an anchor group is needed in the squaraine molecule. In most cases this group is a carboxylic acid which has been implemented in just one aromatic unit of the squaraine which results in asymmetric dyes. In the majority of the reports, at least one indolenine group is part of the squaraine dye, whereas a lot of different moieties have been used as the second aromatic unit on the other side of the central squaric ring. Here, the asymmetry is used to generate a drift flow direction for the electrons. Upon excitation the electrons can be injected *via* the anchor group into the conduction band of TiO_2 and from there to the electrodes. In the indolenine moiety, the anchor group can be attached to either the benzene ring or to the alkyl chain which is connected to the nitrogen. There have been many reports in recent years using both monomeric[70-79] and oligomeric[74, 80-81] squaraines with some of them absorbing light even beyond 900 nm (< 11100 cm^{-1})[81]. Efficiencies of DSSCs were in the order of 1–5% for most of the dyes used. An efficiency over 6% could be achieved in cosensitised solar cells with using a squaraine dye in combination with another dye.[82-83]

Semisquaraine acids were also applied as sensitisers for DSSCs. As they already carry a carboxylic acid which can be used as anchor group, there is no need to add a further anchor group to the molecule. Some semisquaraine acids absorb light up to 500 nm (20000 cm^{-1}) and those showing matching electronic levels were successfully applied in DSSCs.[84]

In organic BHJ solar cells, mostly symmetric squaraines were applied due to the ease of synthesis and no needs for anchor groups. Squaraines of the type **S3** were applied with efficiencies barely exceeding 2%.[85-89]. However, apart from pyrrole squaraine dyes,[90-92] the majority of reports deals with **S9** type squaraines. Efficiencies up to 4.6% were

obtained for dyes with *iso*-butyl groups (Chart 6, **S9a**) at the nitrogen atoms.[93-95] Since 2010 the preference for the moieties at the nitrogen atoms seems to lie in aromatic groups such as benzene or naphthalene (**S9b**). *Forrest et al.* frequently published recent results of optimised organic solar cells with by now efficiencies up to 5.9%.[14, 96-100]

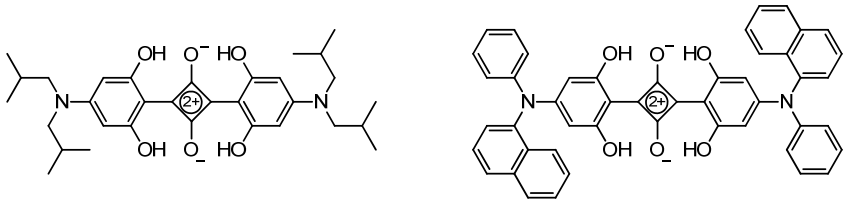

S9a **S9b**

Chart 6 Squaraine dyes **S9a** and **S9b** used in recent most efficient organic BHJ solar cells.[14, 93-100]

1.2 Oligo- and Polysquaraines

Oligosquaraines

There are few reports on oligomeric squaraine dyes which mainly describe *N*-*N*-dialkylaniline squaraine dimers (Chart 7, **OS1**) in which the monomers are linked by saturated bridges. A rigid linear dimer, a cyclic dimer, as well as several dimers connected by alkyl chains of various lengths were investigated and the formation of H-aggregates (for some explanation on H-aggregates in general, see next chapter) under certain circumstances was described.[101-102] Those H-aggregates showed blue shifted absorption bands in the visible region of the spectrum. While some dimers were used for ion sensing by a folding mechanism, others, including one tris-squaraine, showed self-assembly properties.[39, 103-104] In addition, the synthesis and spectroscopic properties of a series of conjugated bis- to tetrakis-squaraines, centrally connected *via* a vinylene-phenylene unit, was reported.[105]

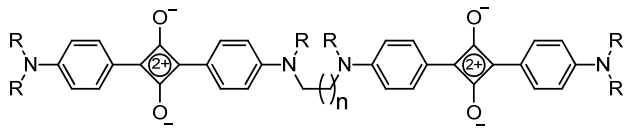

OS1

Chart 7 Dimer **OS1** of *N*,*N*-dialkylaniline squaraine.[101-102]

In terms of indolenine squaraines, *Yagi et al.* synthesised a series of bis-squaraines using a broad variety of arene and thiophene units as bridges (Chart 8, **OS2**). In a first step, these bridges and a stannyl derivative of the squarate were used in a *Stille*-type coupling to form bis-semisquaraine esters which were subsequently hydrolysed to the bis-semisquaraine acids. Double condensation with indolenine, oxazole or benzothiazole gave the corresponding bis-squaraines which showed strongly bridge-dependent absorption down to the NIR.[106] Using the same stannyl squarate, *Maeda* and *Yagi* were able to attach a semisquaraine derivative to an indolenine squaraine *via* the 5-position of the indolenine moiety (**OS3**). By the subsequent addition of up to four semisquaraine derivatives, an immense bathochromic shift was induced and the absorption maximum of the largest compound is at 940 nm (10600 cm^{-1}).[74, 81, 107]

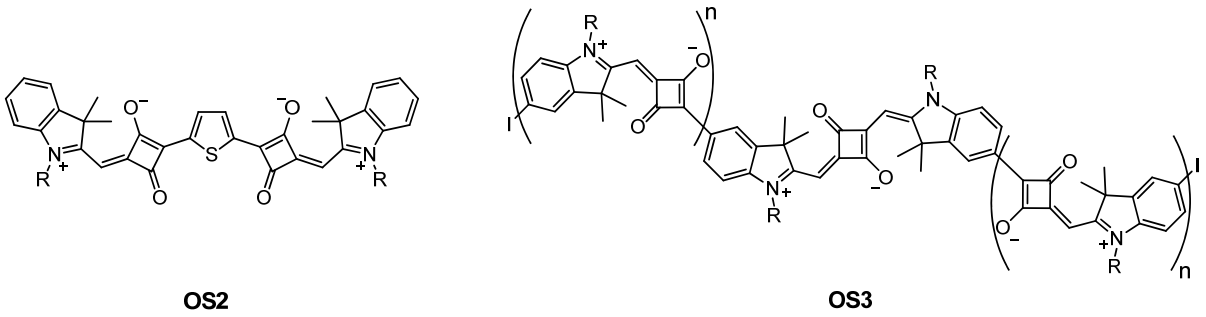

OS2 **OS3**

Chart 8 Oligosquaraines **OS2** and **OS3** by *Yagi et al.* and *Maeda et al*.[74, 81, 106-107]

In a more classical manner, both thiophene (**OS4**)[67] and fluorene (**OS5**)[108] units were used to bridge indolenine squaraines to form dimers, or in case of thiophene, a series of oligomers up to the pentamer (Chart 9). The fluorene was attached *via* alkyne linkers by *Sonogashira* coupling and the thiophene *via* direct C-C link by *Stille* coupling reaction. All oligomers showed two-photon absorption properties and the induced red shift were distinctly more pronounced for the thiophene bridges.

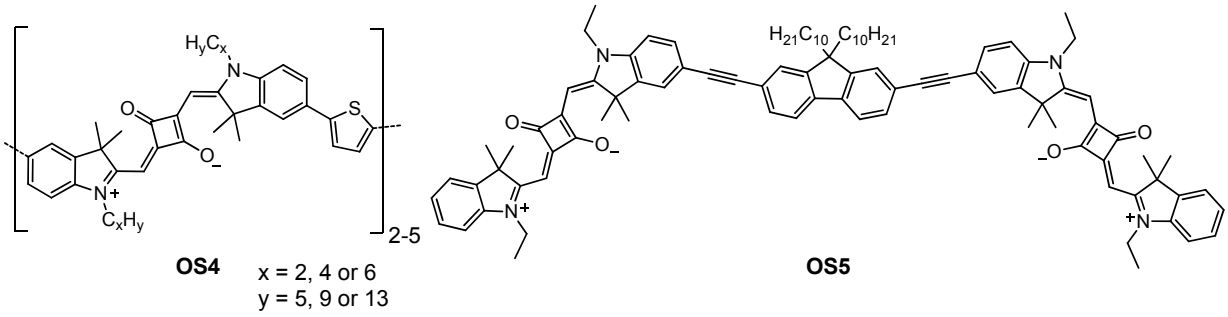

OS4 x = 2, 4 or 6
y = 5, 9 or 13

OS5

Chart 9 Thiophene and fluorene-bridged oligosquaraines **OS4** and **OS5**, respectively.[67, 108]

Polysquaraines

The synthesis of polymers is another way to tune both the spectroscopic as well as the electrochemical properties of substances. In case of polysquaraines, there have been various approaches since *T&J* described an insoluble solid after the condensation reaction of a pyrrole derivative with the squaric acid (Chart 10, **PS1**).[4] Low solubility and the formation of both 2,4- and 3,4-dicondensation products were the issues of a later attempt of the synthesis of a carbazole squaraine polymer using either polyphosphoric acid or dimethylsulfoxide (DMSO) as solvent.[109]

In 1993 *Havinga et al.* suggested that by alternation of donor and acceptor moieties in a conjugated polymer, small band gaps should be obtained.[110] An idea that was theoretically supported by *Brocks et al.* who proposed small band gaps for polysquaraines.[111] Indeed, *Havinga et al.* synthesised a series of polysquaraines using indolenine derivatives (Chart 10, **PS2**) or terthiophene to build polymers with band gaps of ~ 1.3 eV and an absorption beyond 900 nm (< 11100 cm^{-1}).[110, 112-113]

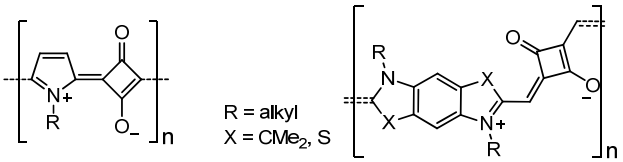

PS1 **PS2**

Chart 10 Simplified pyrrole squaraine polymer **PS1** as reported by *T&J*[4] and low band gap polysquaraines **PS2** by *Havinga et al*.[110, 112-113]

The majority of reports focusses on various substituted pyrrole derivatives with solubilising alkyl groups either at the nitrogen or at a carbon of the pyrrole.[68, 114-120] Nevertheless, in these cases no real low band gap polymers could be obtained. One explanation was that the structure of these polymers can be seen as squaraine chromophores that are bridged by a central squaric moiety, e.g. an electron acceptor ([D–A–D–][A–]) that might weaken the influence of the electron rich pyrrole moieties in the D–A–D structure. For this reason, the idea to insert additional electron donating units to bridge the monomeric squaraine chromophores arose. In this effort, dialkoxybenzene[121-122] (**PS3**, Chart 11), fluorene[123] (**PS4**) or thiophene[124] (**PS5**) units were inserted *via* vinylene linkers to synthesise copolymers with band gaps ~ 1 eV and broad absorption in the NIR up to 1000 nm (10000 cm^{-1}). Those copolymers were derived through the synthesis of bridged bis-pyrrole precursors and subsequent condensation reaction with squaric acid.

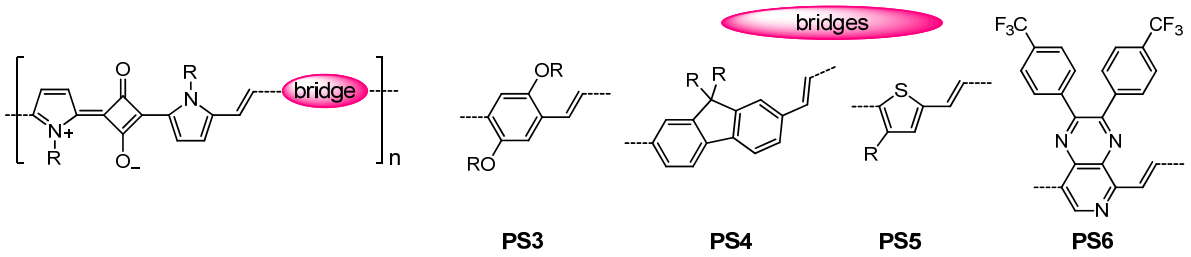

Chart 11 Various donor-bridged pyrroles squaraine polymers **PS3**–**PS6**.[121-125]

In the case of the donor-bridged pyrrole squaraine polymer **PS3**, the bridge was further extended by implementation of additional electron donating moieties. These polymers were synthesised by Pd- and Cu-catalysed *Sonogashira* coupling reaction from a symmetric dibrominated monomeric squaraine analogue of **PS3** with the respective acetylene-substituted precursors. As additional donors, dialkyl- and dialkoxythiophene[126], 2,7-carbazole[127], and yet another dialkoxybenzene[127] were applied, resulting in polymers with absorption up to ~ 800 nm (12500 cm^{-1}) in solution and up to nearly 1000 nm (10000 cm^{-1}) in thin films.

In a similar manner, an electron accepting unit was used as a bridge. For the copolymer consisting of pyrrole squaraine and pyridopyrazine (Chart 11, **PS6**) an even broader absorption from ~ 600–1100 nm (~ 9100–16700 cm^{-1}) in solution was obtained with a band gap ~ 1 eV.[125] This copolymer and its monomeric model compound showed two-photon absorption between 1460–1640 nm (~ 6100–6800 cm^{-1}).

The synthetic most convenient approach to polysquaraines was introduced by *Hecht et al.* by utilising a two step, one pot procedure starting with phloroglucinol (1,3,5-trihydroxybenzene) and secondary non-aromatic amines and, finally, addition of squaric acid.[128] These authors thus obtained polysquaraines with non-conjugating bridges (**PS7**–**PS9**, Chart 12) which they used for cation-sensing through folding and unfolding of the polymer chain. The cation complexation was monitored by the rise of an H-aggregate absorption band in the absorption spectra.

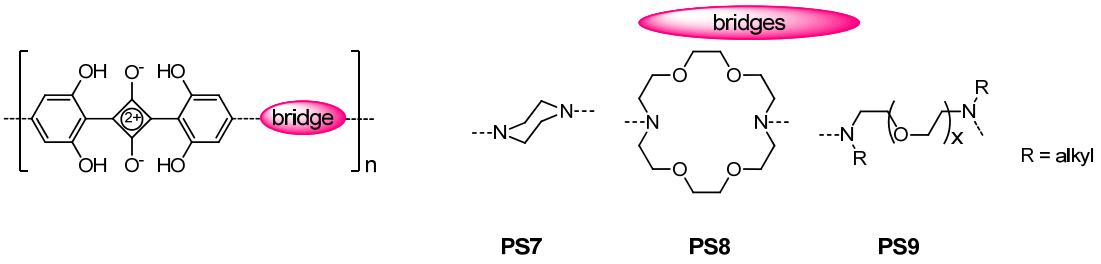

Chart 12 Polysquaraines **PS7**–**PS9** with non-conjugated bridges by *Hecht et al.*[128]

The majority of the polysquaraines so far mentioned was synthesised by either condensation of the nucleophilic moieties with squaric acid or *Sonogashira* coupling reaction in the final polycondensation step. Both reaction types exhibit slight drawbacks. For the former, the formation of unfavoured 3,4-dicondensation products can not completely be ruled out, even though it is unlikely in the commonly used solvent mixture of 1-butanol and toluene. For the latter, homocouplings between the terminal alkyne compounds can occur *via Glaser* coupling reaction.

In terms of indolenine or benzothiazole squaraine polymers, not much progress with regard to new compounds or further investigations was communicated for a while after the reports of *Havinga et al.* in the early 1990s.[110, 112-113] In these polymers, a "double" indolenine or benzothiazole sharing the same benzene core were used and polycondensated with squaric acid. This mergence of the chromophores and their strong conjugation resulted in absorption up to > 900 nm (< 11100 cm^{-1}).

During the time of the development of this work, *Maeda et al.* and *Kuster et al.* reported on their work on bridged indolenine squaraines.[30, 88] Searching for polymers with a broad absorption in the visible to NIR region, *Maeda et al.* used diverse substituted phenylene units as bridges, where the monomeric squaraine chromophores were linked in either *meta*- (Chart 13, **PS10**) or *para*-position (**PS11a**) of the phenylene.[88] Nevertheless, the bathochromic shift of the main absorption band as well as the intended broadening was only minor. Similar behaviour was found by *Kuster et al.* who synthesised a series of donor-bridged indolenine squaraine polymers.[30] In contrast to *Maeda et al.*, they used more electron rich bridging units. The achieved red shift depending on the bridging units was in the order fluorene (**PS13**) > phenylene (**PS11a**) > 2,5-dialkoxyphenylene (**PS11c**) > tetrafluorophenylene (**PS12**). All those bridges were

inserted *via* Pd-catalysed *Suzuki* coupling which resulted in direct C-C linkages between the aromatic units.

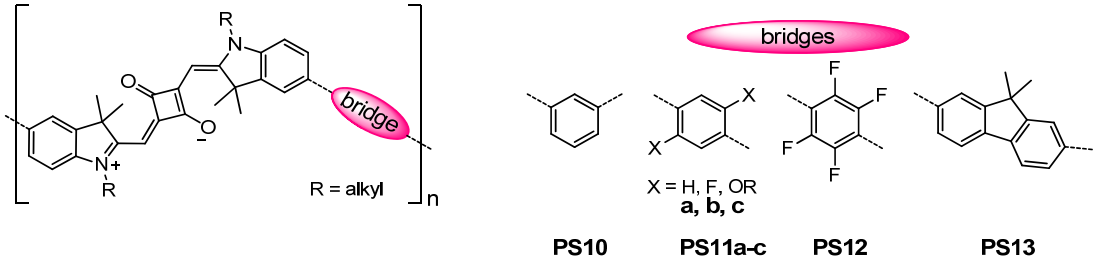

Chart 13 Various bridged indolenine squaraine polymers **PS10**–**PS13**.[30, 88]

In contrast to the indolenine polysquaraines mentioned, it was possible to induce a bathochromic shift and to achieve a broadening of the main absorption band. As previously mentioned in the oligomer section, this was demonstrated by *Scherer et al.* who produced a series of oligomers up to the pentamer using thiophene units as bridges, thereby achieving a bathochromic shift from 14900 cm^{-1} for a monomer to 13800 cm^{-1} for the pentamer in $CHCl_3$.[67] In this work, exciton coupling theory was successfully applied to explain the spectroscopic properties.

The exciton coupling theory will play a significant role in this work in order to explain spectroscopic properties of squaraine polymers. Therefore, a detailed description of it will be given in the next chapter.

1.3 Exciton Coupling

In this chapter, an overview about the exciton coupling theory is given, both in a more pictorial sense as well as in a quantum chemical approach, mainly following the work of *Kasha* in the 1960s.[129-131] In the first part however, the interpretation of *Kiprianov*[132] on the appearance of new absorption bands in dimeric chromophores will be summarised, also in a more pictorial way.

1.3.1 *Interaction of Conjugated Chromophores*

Early investigations[132-135] on the absorption properties of dye molecules showed that for a dye molecule that contains two conjugated chromophores, the absorption spectrum of the dye is not necessarily a superposition of the spectra of the two isolated chromophores. They lose their individuality and absorb light as a new single chromophore due to delocalisation caused by the conjugation. However, *Kiprianov*[132] described this behaviour in a simplified way and postulated that this is only valid if the single chromophores absorb light of similar energy and lie in a straight line. Only in this ideal case the two absorption bands of the isolated chromophores would merge to one absorption band at higher or lower energy. In case the chromophores do not lie in the same line, a splitting of the absorption band would be observed instead of one single merged band. For the case that the chromophores absorbed at distinctly different energies, no interaction would be observed even though they are conjugated.

This behaviour is demonstrated by the absorption properties of two dimeric cyanine dyes (**D1**, **D2**) and their isolated single chromophores (Chart 14, **C1**–**C3**). In case of **D1**, the chromophore **C1** (~ 422 nm (23700 cm^{-1})) is a trimethine cyanine dye and **C2** a pentamethine cyanine dye (~ 558 nm (12900 cm^{-1})) and the absorption maxima of the isolated chromophores clearly differ. In the dimer **D1**, those maxima were found at nearly identical energies as those of the single chromophores. On the contrary, for **D2** they were observed at distinctly different energies at 522 nm (19200 cm^{-1}) and 581 nm (17200 cm^{-1}) compared to those of the single chromophores **C3** (562 nm (17800 cm^{-1})) and **C2** (558 nm (17900 cm^{-1})), which are both pentamethine cyanine dyes.

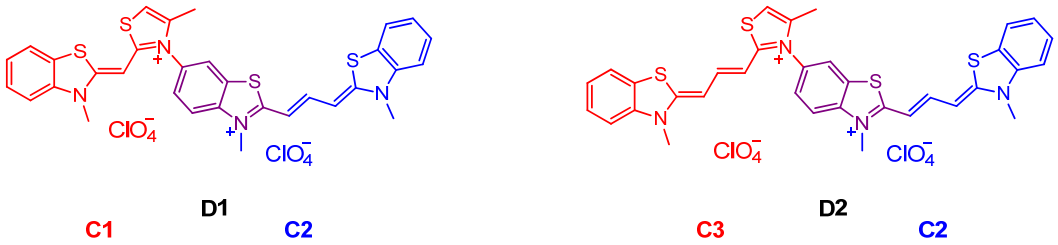

Chart 14 Two dimeric cyanine dyes **D1** and **D2**. The single chromophores **C1–C3** are depicted either in red or blue, the purple heterocycle is part of all single chromophores.

Kiprianov illustrated this behaviour in a pictorial way by comparing the two conjugated chromophores with two coupled oscillators, e.g. two pendulums. If they are of different length (correlated to the absorption of light of different energy), they will barely influence each other and both of them will keep their individual frequency. However, if they are of similar length they do influence each other and can move with two frequencies, depending on whether they oscillate in phase or out of phase.

H- and J-Aggregates

Concerning the energies of the absorption of dimeric chromophores, the oscillations of electrons in the chromophore that have been excited by light comply with vibrations of a dipole. Figure 3 shows the limiting cases of two dipoles that lie in the same plane. On the left hand side, the dipoles are stacked and have a face-to-face orientation. In this orientation they can either be arranged in a way that the dipoles repel (top) or attract (bottom) each other. Obviously, the latter orientation is more stabilised and excitation would require less energy. However, due the opposed alignment of the dipoles of the single chromophores, the total aggregate dipole vanishes, whereas it increases for the repulsive alignment. Consequently, only the in phase positioning can interact with an oscillating light wave and absorption is therefore shifted to higher energy in this case with twice the oscillator strength of the single chromophore. Due to the hypsochromic shift of the absorption band it is called H-band and the alignment an H-aggregate.

On the right hand side of Figure 3 the two dipoles are on a straight line next to each other in a head-to-tail fashion and the behaviour is reversed. In the repulsive alignment the

total aggregate dipole vanishes (top), whereas the dipoles point in the same direction for the attractive (bottom) arrangement. For this reason only the absorption band with less energy is seen in absorption spectroscopy. This bathochromic shifted absorption band is called J-band (apparently with respect to *E. E. Jelley*[136] who was one of the first, besides *G. Scheibe*[137], who reported about those bands in the 1930s) and the respective arrangement J-aggregate.

However, the cases described are cases of ideal arrangement. Once the chromophores are not perfectly in line, both absorption bands will be observed.

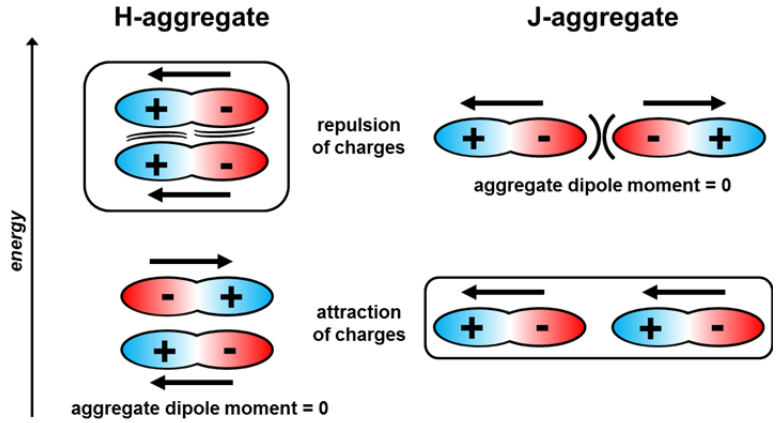

Figure 3 H-aggregate and J-aggregate alignments of dipoles. The frames accent the allowed alignment for electronic excitation by light.

1.3.2 *Kasha* and the Exciton Model

Excitons are regarded as bound electron-hole pairs that are generated upon excitation and are held together by electrostatic Coulomb forces. To distinguish between the different formulations of excitons that are present, the distribution of the electron in relation to its corresponding hole is one important factor. In 1931, *Frenkel* was among the first to describe excitons upon electromagnetic excitation in an argon crystal.[138] Due to a strong binding energy, the electron was considered to be "closely bound" to the respective hole and the exciton to be localised. In addition, there is the so called "atomic exciton" or also *Wannier-Mott* exciton, which is discussed as "loosely bound" and is used to describe atomic or ionic crystals where the excited electron is spread over several

neighbouring lattice sites compared to the corresponding hole, which is a result of a low binding energy.

Herein this work, the *Frenkel* exciton shall be of interest. This treatment of excitons was further developed by *Davydov* (*Davydov* splitting) in terms of a "molecular exciton" description, used to discuss excitations in molecular crystals or molecular aggregates. Here, the excitons are considered as tightly bound because the wave function of the excited electron is still bound to its corresponding molecule and there is only negligible electron exchange to neighbouring molecules. *Davydov*, as well as *Simpson* and *Peterson*[139] further divided the molecular excitons into two subtypes, whose theoretical origin is somewhat different but leads to an essentially similar classification. Herein, the classification of the latter is used which is based on the absorption properties of both unperturbed chromophores as well as on the exciton band width of the aggregate. In the case when twice the value of the exciton band width ($2 \times \Delta E$) is significantly larger than the band width of the single chromophore unit ($\Delta\varepsilon$) in the aggregate ($\frac{2 \times \Delta E}{\Delta\varepsilon} \gg 1$), it is considered a "strong coupling" case. For the inverse case of $\frac{2 \times \Delta E}{\Delta\varepsilon} \ll 1$ it is referred to as the "weak coupling" case. The former will be of major interest in this work. There, the *Born-Oppenheimer* approximation can be used to separate electronic and vibrational wave functions. Hence the focus is on the interacting electronic states.

In the exciton model, the interaction of electronic states is described. The model will be explained for the simplified case of a dimer that consists of two identical chromophores A and B. As a prerequisite for the model, the chromophores have only a negligible overlap of the wavefunctions in the ground state and both behave as individual compounds.

If the two chromophores in the dimer are in close enough vicinity, the former degenerate excited states split into two new states, due to excitonic interaction. These new excitonic states can be seen as a splitting of the absorption bands in the chromophore aggregate (Figure 4).

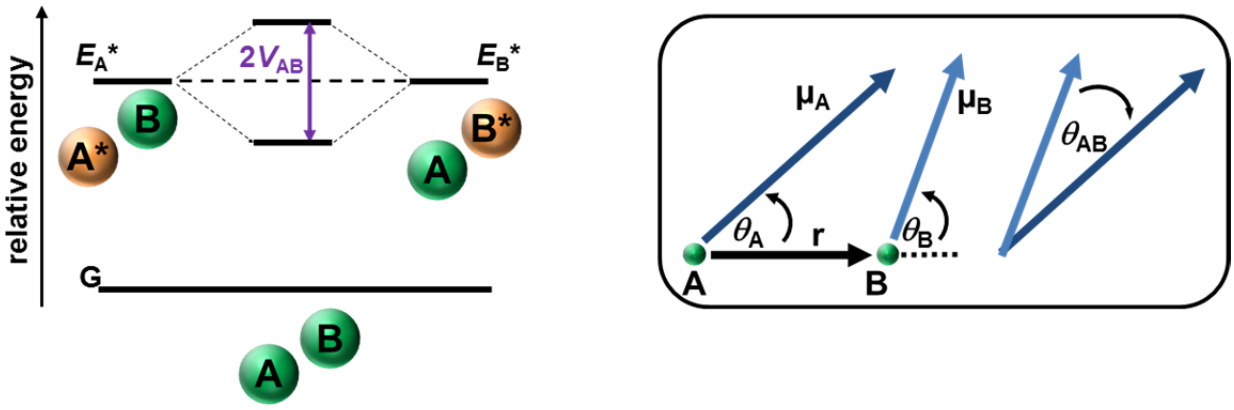

Figure 4 Schematic energy diagram for a dimer consisting of two equal chromophores A and B (left) and relative orientation of the respective individual transition moment vectors (right).

The size of the excitonic splitting ΔE in the dimer is $2V_{AB}$, with the exciton coupling energy V_{AB} which is dependent on the size, orientation, and distance of the individual transition moments of the respective chromophores.[129-130, 140]

$$V_{AB} = \frac{1}{hc4\pi\varepsilon_0}\frac{\mu_A\mu_B}{r^3}\kappa \qquad (1)$$

$$= \frac{1}{hc4\pi\varepsilon_0}\frac{\mu_A\mu_B}{r^3}(\cos\theta_{AB} - 3\cos\theta_A\cos\theta_B),$$

where κ is an orientation factor, in which θ_{AB} defines the angle between the transition moment vectors $\boldsymbol{\mu}_A$ and $\boldsymbol{\mu}_B$ of the chromophores A and B, respectively, and θ_A and θ_B are the angles of the respective transition moment vectors with the direction A→B. For now, the equation is stated as it is. The origin of this equation is derived in the following quantum chemical section.

In case of an infinite polymer (no end-effect of chromophores), the excitonic splitting is twice as large ($4V_{AB}$) due to the *nearest neighbour* approximation (interaction only with the direct neighbouring chromophores) because every chromophore has two neighbours to interact with instead of just one as in the dimer. In addition, the absorption band might become narrower compared to those of the single chromophores. This is attributed to the fact that the excitation is delocalised over many molecules because the excitation energy is transferred rapidly between the chromophores before vibrational relaxation can take

place. It is also referred to as exchange narrowing, which has been observed for J-aggregates,[141-142] resulting from the coherent excitation of several chromophore units. This leads to only minor deviations of the average excited state energy of the excited compound.

The selection rules to determine the allowed transitions for the respective arrangements of the chromophores in dimers and polymers are obtained from a simplified model. It is assumed that a transition dipole moment is directed along the long molecular axis of the single chromophore and that the single chromophores are in one plane along the dimer or polymer axis. Considering a parallel orientation of the single chromophores, different arrangements like H-type or J-type can be obtained by variation of the angle θ_A of the chromophores to the dimer or polymer axis from 90→0° (Figure 4, Figure 5). Figure 5 and Figure 6 show the energy diagrams of the exciton splitting and the corresponding structures of the dimers and polymers, respectively. The chromophores are designated by grey rectangles, the transition dipole moments by blue double arrows inside the rectangle and its phase relation is indicated by blue single arrows inside the diagrams. The red arrows indicate the direction of the total aggregate transition dipole moment and the dashed vertical lines indicate nodes between the phases of the transition dipole moments. These nodes are not to be mistaken by nodes arising in molecular orbitals but accent a change of phase of the adjacent transition dipole moments. The diagrams are simplified (*Van der Waals* interactions are neglected for example) because the main focus is on the allowed excitonic states and the corresponding exciton splitting energies V_{AB}, which is for the sake of clarity only indicated for the J-type alignment (Figure 5). The dashed lines in the diagram display forbidden excitonic states, whereas solid lines represent allowed excitonic states and the respective solid arrows demonstrate the allowed transitions.

To determine the allowed transitions to the respective excitonic states, the question whether the transition dipole moments of neighbouring chromophores are in phase or out of phase is of importance. The vector sum of the respective transition dipole moments has to be formed and generally, only in phase arrangements of the transition dipole moments result in allowed transitions, because this leads to an enhancement of the total

aggregate transition dipole moment in the same direction (red arrows). On the other hand, out of phase arrangements result in a vector sum of the aggregate transition dipole moment of zero. Those arrangements can therefore not contribute to the light absorption.

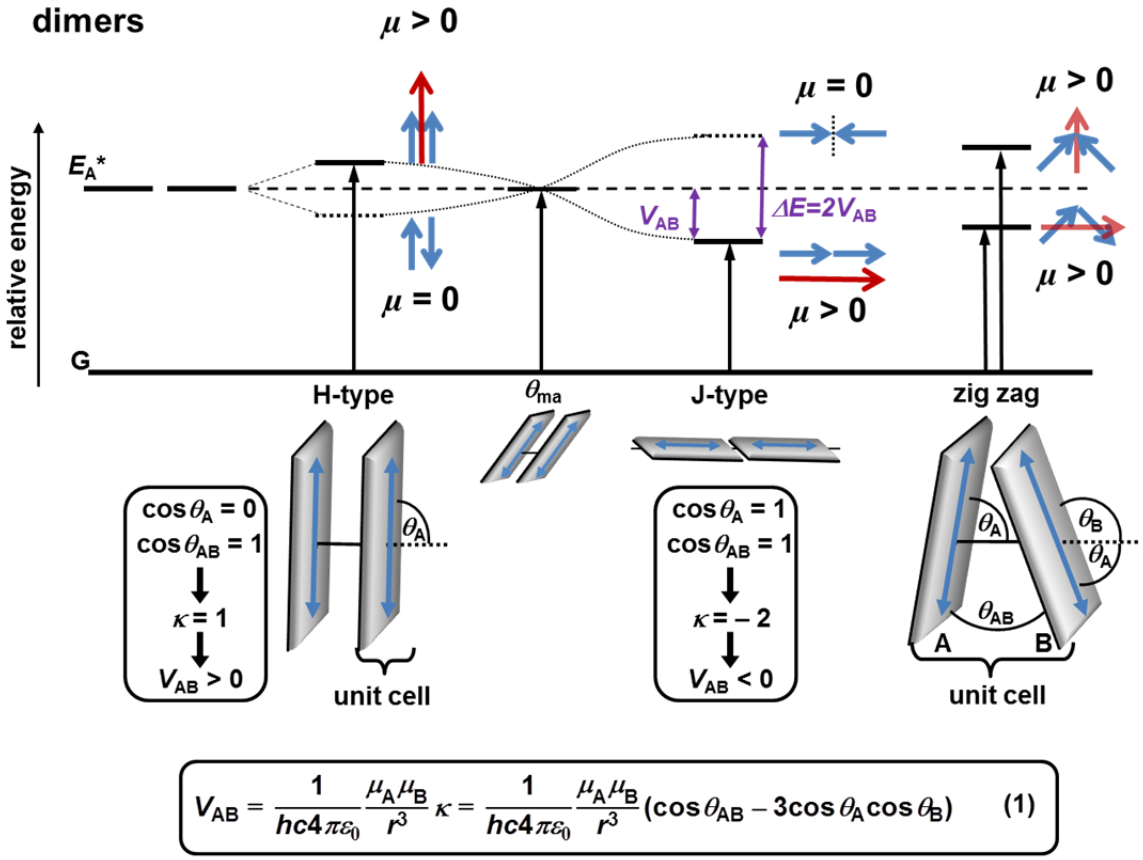

Figure 5 Energy diagram and structures of dimers. The chromophores are designated by grey rectangles, the dipoles by blue double arrows inside the rectangle, and the phase relation is indicated by single arrows inside the diagrams. The red arrows indicate the direction of the total dipole and the dashed vertical lines indicate nodes between the dipoles. V_{AB} is the excitonic interaction energy and θ_{ma} is the magic angle (54.7°). The depicted equation is used to estimate the electronic coupling and is derived below.

The relative energy of those states depends, as it was also described in the previous chapter (Figure 3, p. 22), on the repulsion or the attraction of the dipoles, where the former leads to an increase, the latter to a decrease in energy. In case of the dimers this is clearly seen for the H-type and J-type structures. Only the transition to the excitonic state higher in energy is allowed for the H-type structure, whereas it is forbidden for the lower. This leads to an increase of energy for the absorption and consequently a blue shift in the spectrum. For the J-type structure, transition into the lower excitonic state is

allowed and transition in the higher is forbidden, hence leading to a red shift of the absorption.

Not only the absorption properties, but also the fluorescence properties of H- and J-type aggregates clearly differ. Upon excitation, rapid internal conversion into the lowest excited state takes place. In a J-type aggregate, the lowest excited state is allowed and fluorescence can occur. In contrast, in an H-type aggregate there is usually no fluorescence because this can only take place from the lowest excited state (according to *Kasha*'s rule) which is forbidden in this case.

In a molecule with *N* identical chromophores (the polymer is represented by four to six units), an *N*-fold number of degenerated excited states may be formed which, due to excitonic interaction, split into *N* non-degenerate excitonic states (Figure 6). However not all of them are allowed by electronic transition from the ground state. The number of allowed states can readily be estimated by the geometry of the aggregate molecule and is dependent on the amount of single chromophores needed to build one repeating unit cell. In a complete parallel arrangement, one chromophore represents one unit cell and only absorption into one excitonic state is allowed, as it is the case for H- and J-type arrangements. For all other excitonic states there is at least one node found that indicates a change of phase between the dipoles and the overall dipole value vanishes, leading to forbidden transitions into those states. Again it has to be noted that this is the case for a perfect alignment of the structures. If this is not the case, additional absorption bands will be observed.

When the single chromophores are aligned in an alternating zig-zag manner and two of them build a repeating unit cell, two absorptions with mutually perpendicular orientation into two excitonic states are allowed.

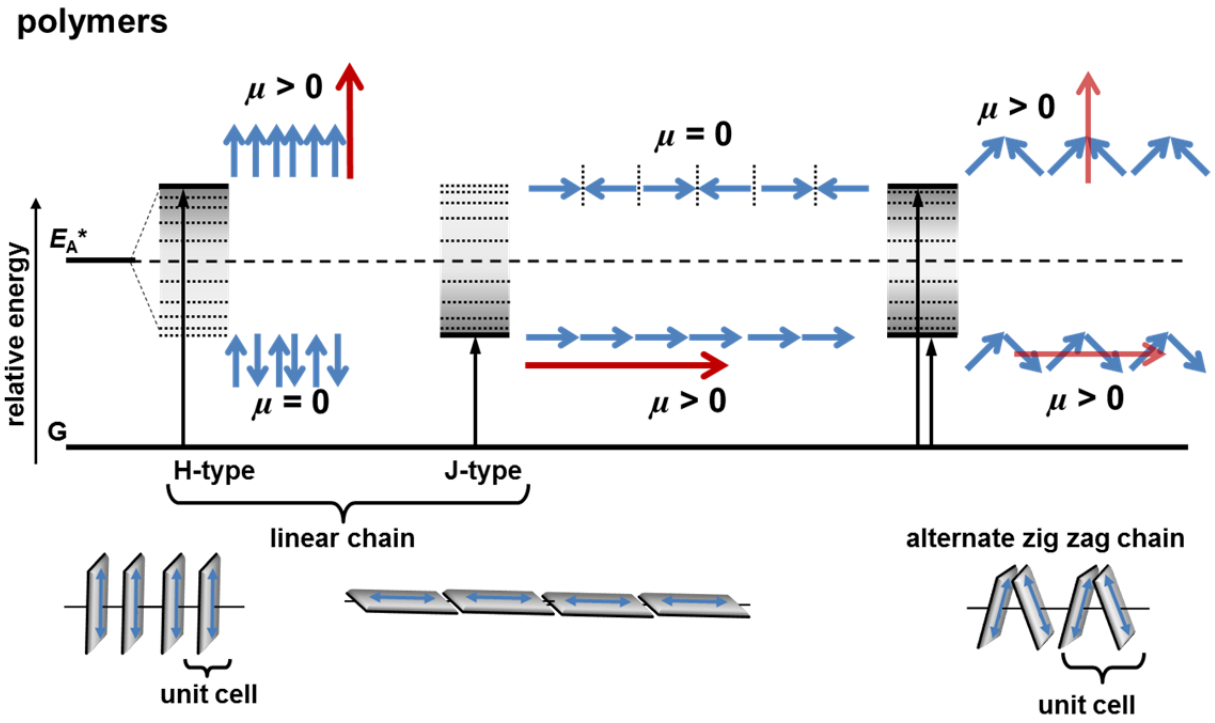

Figure 6 Energy diagram and structures of polymers. The chromophores are designated by grey rectangles, the dipoles by blue double arrows inside the rectangle and the phase relation is indicated by single arrows inside the diagrams. The red arrows indicate the direction of the total dipole and the dashed vertical lines indicate nodes between the dipoles. V_{AB} is the excitonic interaction energy. The example of the magic angle θ_{ma} (54.7°) as for the dimers is not shown but is essentially the same.

Quantum Chemical Approach

The interaction potential V_{AB} and the exciton band width ΔE[129-131]

First, the simple case of a dimer is considered. The quantum mechanical approach starts with the *Schrödinger* equation

$$\hat{H}\,\Psi = E\,\Psi \tag{2}$$

with the hamiltonian $\hat{H}$, the wave function Ψ and the energy eigenvalue E. The ground state wave function of a dimer that consists of two chromophores A and B is given by

$$\Psi_{\mathrm{G}} = \psi_{\mathrm{A}}\,\psi_{\mathrm{B}}, \tag{3}$$

where ψ_{A} and ψ_{B} are the ground state wave functions of the single chromophores. The hamiltonian of the dimer is

$$\hat{H} = \hat{H}_{\mathrm{A}} + \hat{H}_{\mathrm{B}} + \hat{V}_{\mathrm{AB}} \tag{4}$$

with $\hat{H}_{\mathrm{A}}$ and $\hat{H}_{\mathrm{B}}$ as operators for the isolated chromophores A and B, respectively, and $\hat{V}_{\mathrm{AB}}$ the intermolecular perturbation potential.

The excited state wave function is a linear combination of wave functions of the particular cases (including the respective coefficients c_1 and c_2) where either chromophore A or B is excited, marked with an asterisk. This localisation of an exciton on a chromophore is a prerequisite for the application of the excitonic model.

$$\Psi_{\mathrm{E}} = c_1\,\psi_{\mathrm{A}}^{*}\,\psi_{\mathrm{B}} + c_2\,\psi_{\mathrm{A}}\,\psi_{\mathrm{B}}^{*} \tag{5}$$

$$\hat{H}\,\Psi_{\mathrm{E}} = E_{\mathrm{E}}\,\Psi_{\mathrm{E}} \tag{6}$$

In order to find the eigenfunctions with the eigenenvalues of minimal energy, equation (6) is expanded with Ψ'_{E} and integrated over the total space.

$$\int \Psi'_{\mathrm{E}}\hat{H}\,\Psi_{\mathrm{E}}\,d\tau = E_{\mathrm{E}}\int \Psi'_{\mathrm{E}}\,\Psi_{\mathrm{E}}\,d\tau \tag{7}$$

$$E_{E_0} = \frac{\int \Psi'_E \hat{H} \Psi_E d\tau}{\int \Psi'_E \Psi_E d\tau} \tag{8}$$

and similar (integration over all coordinates of chromophores A and B)

$$\hat{H}(c_1 \psi^*_A \psi_B + c_2 \psi_A \psi^*_B) = E_E(c_1 \psi^*_A \psi_B + c_2 \psi_A \psi^*_B) \tag{9}$$

$$E_{E_0} = \frac{\iint (c_1 \psi^*_A \psi_B + c_2 \psi_A \psi^*_B)' \hat{H}(c_1 \psi^*_A \psi_B + c_2 \psi_A \psi^*_B) \, d\tau_A d\tau_B}{\iint (c_1 \psi^*_A \psi_B + c_2 \psi_A \psi^*_B)' (c_1 \psi^*_A \psi_B + c_2 \psi_A \psi^*_B) \, d\tau_A d\tau_B}. \tag{10}$$

At this point the implementation of matrix elements is necessary. Those are the

coulomb integral,
$$H_{AA} = H_{BB} = \iint \psi^*_A \psi_B \hat{H} \psi^*_A \psi_B \, d\tau_A d\tau_B \tag{11}$$

electronic coupling integral,
$$V_{AB} = V_{BA} = \iint \psi^*_A \psi_B \hat{H} \psi_A \psi^*_B \, d\tau_A d\tau_B \tag{12}$$

and overlap integrals
$$S_{AA} = S_{BB} = \iint (\psi^*_A \psi_B)(\psi^*_A \psi_B) \, d\tau_A d\tau_B$$
$$S_{AB} = S_{BA} = \iint (\psi^*_A \psi_B)(\psi_A \psi^*_B) \, d\tau_A d\tau_B. \tag{13}$$

This results in

$$E_E = \frac{c_1^2 H_{AA} + 2c_1 c_2 V_{AB} + c_2^2 H_{BB}}{c_1^2 S_{AA} + 2c_1 c_2 S_{AB} + c_2^2 S_{BB}}. \tag{14}$$

$$E_E(c_1^2 S_{AA} + 2c_1 c_2 S_{AB} + c_2^2 S_{BB}) = c_1^2 H_{AA} + 2c_1 c_2 V_{AB} + c_2^2 H_{BB}. \tag{15}$$

Because the lowest energy values are searched, equation (15) is differentiated over both c_1 and c_2 and in accordance to the variational principle $\frac{dE_E}{dc_1} = \frac{dE_E}{dc_2} = 0$. For simplification $(c_1^2 S_{AA} + 2c_1 c_2 S_{AB} + c_2^2 S_{BB}) = X$ and $(c_1^2 H_{AA} + 2c_1 c_2 V_{AB} + c_2^2 H_{BB}) = Y$ and by applying the product rule:

$\frac{d}{dc_1}$:
$$\frac{dE_E}{dc_1} \times X + E_E \times \frac{dX}{dc_1} = \frac{dY}{dc_1} \tag{16}$$

Because $\frac{dE_E}{dc_1} = 0$, the first term vanishes and equation (16) is reduced to

$$E_E \times \frac{dX}{dc_1} = \frac{dY}{dc_1} \tag{17}$$

$$2c_1 S_{AA} E_E + 2c_2 S_{AB} E_E = 2c_1 H_{AA} + 2c_2 V_{AB} \tag{18}$$

$$c_1(H_{AA} - S_{AA} E_E) + c_2(V_{AB} - S_{AB} E_E) = 0. \tag{19}$$

In a similar manner equation (20) is obtained:

$$\frac{d}{dc_2}: \qquad c_1(V_{AB} - S_{AB} E_E) + c_2(H_{BB} - S_{BB} E_E) = 0 \tag{20}$$

Out of equations (19) and (20), a determinant of the coefficients c_1 and c_2 can be built and set equal to zero for non-trivial solutions:

$$\begin{vmatrix} H_{AA} - S_{AA} E_E & V_{AB} - S_{AB} E_E \\ V_{AB} - S_{AB} E_E & H_{BB} - S_{BB} E_E \end{vmatrix} = 0 \tag{21}$$

Due to normalisation $S_{AA} = S_{BB} = 1$. Additionally, exciton coupling theory requires negligible electronic overlap between adjacent chromophores. Therefore $S_{AB} = 0$ which leads to (note: $H_{AA} = H_{BB}$):

$$\begin{vmatrix} H_{AA} - E_E & V_{AB} \\ V_{AB} & H_{AA} - E_E \end{vmatrix} = 0. \tag{22}$$

This determinant gives

$$(H_{AA} - E_E)^2 - V_{AB}^2 = 0 \tag{23}$$

and solving the quadratic formula yields two energies for the excited states

$$E_E' = H_{AA} - V_{AB} = E_A^* - V_{AB} \tag{24}$$

$$E_E'' = H_{AA} + V_{AB} = E_A^* + V_{AB}, \tag{25}$$

where H_{AA} is the lowest excited state energy of the isolated chromophore and will further be denoted as E_A^*. It follows that the exciton band width ΔE, which is the energy difference between the highest and lowest excited state, for a dimer of equal chromophores only depends on the electronic coupling integral V_{AB} and is

$$\Delta E = 2\, V_{AB}. \tag{26}$$

The respective zeroth order wave functions are

$$\Psi_{\mathrm{E}}' = \frac{1}{\sqrt{2}} (\psi_{\mathrm{A}}^{*} \psi_{\mathrm{B}} - \psi_{\mathrm{A}} \psi_{\mathrm{B}}^{*}) \tag{27}$$

$$\Psi_{\mathrm{E}}'' = \frac{1}{\sqrt{2}} (\psi_{\mathrm{A}}^{*} \psi_{\mathrm{B}} + \psi_{\mathrm{A}} \psi_{\mathrm{B}}^{*}). \tag{28}$$

The solution of the matrix element eq. (12) shows that this is only dependent on the perturbation or interaction potential $\hat{V}_{\mathrm{AB}}$ and yields the simplified exciton splitting term V_{AB}, which represents the interaction energy between chromophores A and B due to the exchange of excitation energy. Note that for ease of survey, the *Dirac* notation is occasionally used.

$$\begin{aligned} V_{\mathrm{AB}} &= \iint \psi_{\mathrm{A}}^{*} \, \psi_{\mathrm{B}} \, \hat{H} \, \psi_{\mathrm{A}} \psi_{\mathrm{B}}^{*} \, d\tau_{\mathrm{A}} d\tau_{\mathrm{B}} \\ &= \langle \psi_{\mathrm{A}}^{*} \psi_{\mathrm{B}} \, | \hat{H}_{\mathrm{A}} + \hat{H}_{\mathrm{B}} + \hat{V}_{\mathrm{AB}} | \, \psi_{\mathrm{A}} \psi_{\mathrm{B}}^{*} \rangle \\ &= \langle \psi_{\mathrm{B}} | \psi_{\mathrm{B}}^{*} \rangle \langle \psi_{\mathrm{A}}^{*} | \hat{H}_{\mathrm{A}} | \psi_{\mathrm{A}} \rangle + \langle \psi_{\mathrm{A}}^{*} | \psi_{\mathrm{A}} \rangle \langle \psi_{\mathrm{B}} | \hat{H}_{\mathrm{B}} | \psi_{\mathrm{B}}^{*} \rangle + \langle \psi_{\mathrm{A}}^{*} \psi_{\mathrm{B}} | \hat{V}_{\mathrm{AB}} | \psi_{\mathrm{A}} \psi_{\mathrm{B}}^{*} \rangle \end{aligned} \tag{29}$$

Due to orthogonality $\langle \psi_{\mathrm{A}}^{*} | \psi_{\mathrm{A}} \rangle = 0$, as is $\langle \psi_{\mathrm{B}} | \psi_{\mathrm{B}}^{*} \rangle = 0$ and it follows

$$V_{\mathrm{AB}} = \iint \psi_{\mathrm{A}}^{*} \, \psi_{\mathrm{B}} \, \hat{V}_{\mathrm{AB}} \psi_{\mathrm{A}} \psi_{\mathrm{B}}^{*} \, d\tau_{\mathrm{A}} d\tau_{\mathrm{B}}. \tag{30}$$

The perturbation potential is a coulombic intermolecular interaction term. Multipole expansion gives

$$V_{\mathrm{coul}} = V_{\mathrm{mono\text{-}mono}} + V_{\mathrm{mono\text{-}di}} + V_{\mathrm{di\text{-}di}} + V_{\mathrm{quad\text{-}quad}} + \ldots \tag{31}$$

For dipole allowed excitations, the dipole-dipole term dominates and the others are neglected and point-dipole point-dipole approximation gives in atomic units

$$\hat{V}_{AB} = \frac{e^2}{r_{AB}^3} \sum_{ij} (2z_A^i z_B^j - x_A^i x_B^j - y_A^i y_B^j), \tag{32}$$

where e is the elementary charge, r_{AB} the distance between the point-dipoles in chromophores A and B, z_A^i is the z-coordinate for the ith electron in chromophore A and so forth. The z-axis is parallel to the line connecting the centres of the chromophores (r) (Figure 7) and summation is carried out over all electrons in each chromophore.

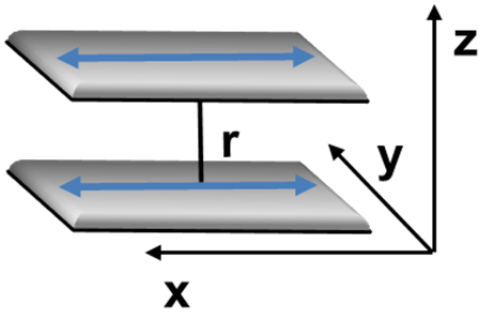

Figure 7 Parallel H-type dimer in an x,y,z-frame. The grey rectangles represent the plane of a chromophore and the blue double arrows indicate the orientation of the transition moments.

In order to switch from atomic units to SI units, equation (32) is devided by $4\pi\varepsilon_0$. To derive V_{AB} in cm^{-1}, it is further divided by hc and becomes

$$\hat{V}_{AB} = \frac{1}{hc4\pi\varepsilon_0} \frac{e^2}{r_{AB}^3} \sum_{ij} (2z_A^i z_B^j - x_A^i x_B^j - y_A^i y_B^j). \tag{33}$$

where h is *Planck*'s constant in [Js], c the speed of light in [cm s^{-1}], ε_0 the electric permittivity of vacuum in [C^2 J^{-1} m^{-1}], e in [C], r_{AB} in [m], and the coordinates (z_A^i for example) in [m].

Identification of the transition dipole moment μ in V_{AB}

Mostly, excitation by light induces displacement of electrons only in one direction and only one term remains. For example, an x-polarised transition in an H-type conformation

of two chromophores in a dimer is assumed, with the transition moments of both chromophores directed along the x-axis (Figure 7).

In this case, equation (33) is reduced to

$$\hat{V}_{AB} = \frac{1}{hc4\pi\varepsilon_0}\frac{e^2}{r_{AB}^3}\sum_{ij}(x_A^i\, x_B^j). \tag{34}$$

Insertion into equation (30) gives

$$V_{AB} = \frac{1}{hc4\pi\varepsilon_0}\ \frac{e^2}{r_{AB}^3}\iint \psi_A^*\,\psi_B\,(\sum_{ij} x_A^i\, x_B^j)\psi_A\,\psi_B^*\ d\tau_A d\tau_B. \tag{35}$$

and factorisation of equation (35) yields

$$V_{AB} = \frac{1}{hc4\pi\varepsilon_0}\ \frac{1}{r_{AB}^3}\int \psi_A^*\,(\sum_{ij} ex_A^i)\psi_A\ d\tau_A\ \int \psi_B\,(\sum_{ij} ex_B^j)\psi_B^*\ d\tau_B. \tag{36}$$

It can be seen that each integral implies the transition moment integral μ in x-direction of an individual monomeric chromophore with the respective electric dipole operator $\hat{\mu}_A$.

$$\mu_A = \int \psi_A^*\,(\sum_{ij} ex_A^i)\psi_A\ d\tau_A = \int \psi_A^*\,\hat{\mu}_A\,\psi_A\ d\tau_A \tag{37}$$

Therefore, it follows that for the parallel dimer with H-type arrangement the interaction energy is proportional to the transition moment squared (for $\mu_A = \mu_B$) and the inverse cube of the radius:

$$V_{AB} = \frac{1}{hc4\pi\varepsilon_0}\ \frac{\mu_A\mu_B}{r_{AB}^3}. \tag{38}$$

As mentioned before, this is the case for a perfect H-type arrangement of the chromophores and was meant as a simple example to accent the role of the transition moment μ in the exchange integral V_{AB}. The general dependence of the geometry will be discussed below.

Selection rules

Even though for a dimer there are two excited states formed by exciton coupling, they are not inevitably both observed in the absorption spectrum. The question to which excited state the transition from the ground state is allowed is a matter of geometry. For illustration, the transition moments μ' and μ'' for excitation from the ground state to the respective excited states E_E' and E_E'' are evaluated.

$$\mu' = \iint \Psi_G (\hat{\mu}_A + \hat{\mu}_B) \Psi_{E'} \, d\tau_A d\tau_B \tag{39}$$

$$\mu'' = \iint \Psi_G (\hat{\mu}_A + \hat{\mu}_B) \Psi_{E''} \, d\tau_A d\tau_B \tag{40}$$

Here, $\hat{\mu}_A$ and $\hat{\mu}_B$ are the electric dipole operators which correspond to the electronic coordinates of the respective chromophores.

$$\mu' = \frac{1}{\sqrt{2}} \iint (\psi_A \psi_B)(\hat{\mu}_A + \hat{\mu}_B)(\psi_A^* \psi_B - \psi_A \psi_B^*) \, d\tau_A d\tau_B \tag{41}$$

$$\mu'' = \frac{1}{\sqrt{2}} \iint (\psi_A \psi_B)(\hat{\mu}_A + \hat{\mu}_B)(\psi_A^* \psi_B + \psi_A \psi_B^*) \, d\tau_A d\tau_B \tag{42}$$

Because of normalisation $\langle \psi_B | \psi_B \rangle = 1$ and orthogonality $\langle \psi_B | \psi_B^* \rangle = 0$, (likewise for Ψ_A), this gives equation (43)

$$\begin{aligned} \mu' &= \frac{1}{\sqrt{2}} (\langle \psi_B | \psi_B \rangle \langle \psi_A | \hat{\mu}_A | \psi_A^* \rangle - \langle \psi_B | \psi_B^* \rangle \langle \psi_A | \hat{\mu}_A | \psi_A^* \rangle \\ &\quad + \langle \psi_A | \psi_A^* \rangle \langle \psi_B | \hat{\mu}_B | \psi_B^* \rangle - \langle \psi_A | \psi_A \rangle \langle \psi_B | \hat{\mu}_B | \psi_B^* \rangle) \\ &= \frac{1}{\sqrt{2}} (\int (\psi_A \hat{\mu}_A \psi_A^*) \, d\tau_A - \int (\psi_B \hat{\mu}_B \psi_B^*) \, d\tau_B) \\ \mu' &= \frac{1}{\sqrt{2}} (\mu_A - \mu_B) \end{aligned} \tag{43}$$

and in an analogous manner

$$\mu'' = \frac{1}{\sqrt{2}} (\mu_A + \mu_B). \tag{44}$$

Assuming that chromophore A and B are equal and therefore $\mu_A = \mu_B$, this results in

$$\mu' = 0 \tag{45}$$

$$\mu'' = \frac{2\mu_A}{\sqrt{2}}, \tag{46}$$

which shows that only one of the two transitions is allowed and will be observed. Since the oscillator strength *f* is proportional to the square of the transition moment, it follows that the observed oscillator strength is twice that of the isolated chromophore.

$$f = \frac{8\pi^2 m_e c \tilde{\nu}_{abs}}{3he^2}\mu^2 \tag{47}$$

$$\mu^2 = \frac{3hc\varepsilon_0 \ln 10}{2000\pi^2 N_{Av}} \frac{9n}{(n^2+2)^2} \int \frac{\varepsilon}{\tilde{\nu}} d\tilde{\nu} \tag{48}$$

Here, m_e is the mass of an electron, *e* the elementary charge, $\tilde{\nu}_{abs} = \frac{\int \varepsilon \, d\tilde{\nu}}{\int \frac{\varepsilon}{\tilde{\nu}} d\tilde{\nu}}$ the averaged reduced absorption energy, *c* the speed of light, ε_0 the electric permittivity of vacuum, *h* *Planck*'s constant, N_{Av} *Avogadro*'s number, and *n* the refractive index.

Geometry dependence of V_{AB}

For mutual orientation of the molecules with respect to the molecular axes in an x,y,z-frame as in Figure 7, the interaction energy is given by

$$V_{AB} = \frac{1}{hc4\pi\varepsilon_0} \frac{\mu_A \mu_B}{r_{AB}^3} (2\cos\theta_A^z \cos\theta_B^z - \cos\theta_A^x \cos\theta_B^x - \cos\theta_A^y \cos\theta_B^y), \tag{49}$$

where θ_A^z is the angle of the transition moment of chromophore A with the z-axis and so forth. The last term changes when all values are given with respect to each other without the need of an x,y,z-frame and eventually eq. (1) from the previous section is obtained,

$$V_{AB} = \frac{1}{hc4\pi\varepsilon_0}\frac{\mu_A\mu_B}{r^3}\kappa$$
$$= \frac{1}{hc4\pi\varepsilon_0}\frac{\mu_A\mu_B}{r^3}(\cos\theta_{AB} - 3\cos\theta_A\cos\theta_B), \quad (1)$$

where θ_{AB} defines the angle between the transition moment vectors $\boldsymbol{\mu}_A$ and $\boldsymbol{\mu}_B$ of the chromophores A and B, respectively, and θ_A and θ_B are the angles of the respective transition moment vectors with the direction A→B. Those units are in Figure 8 A for illustration. The last term of equation (1) defines an orientation factor κ, which can also be expressed as

$$\kappa = \boldsymbol{\mu}_A\boldsymbol{\mu}_B - 3(\boldsymbol{\mu}_A\mathbf{r}_{AB})(\boldsymbol{\mu}_B\mathbf{r}_{AB}), \quad (50)$$

where $\boldsymbol{\mu}_A$ and $\boldsymbol{\mu}_B$ are unit vectors of the transition moments μ_A and μ_B localised on the respective chromophores and $\mathbf{r}_{AB}$ is the unit vector connecting the two transition moments. For a random orientation $\kappa^2 = 2/3$.

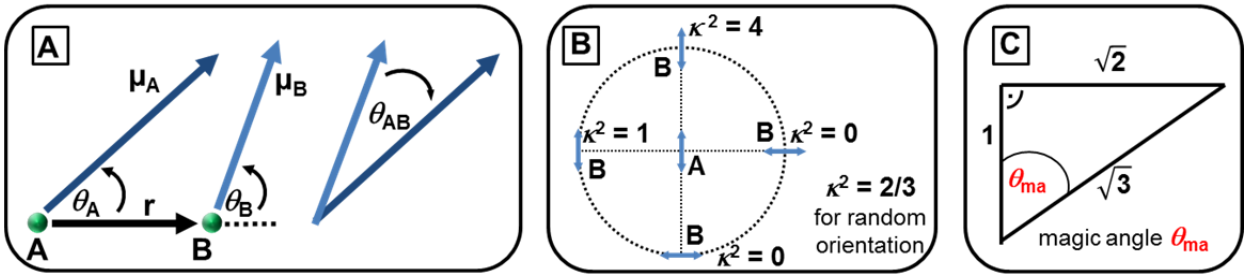

Figure 8 A: Units for the orientations of adjacent chromophores A and B: r is the distance between A and B, θ_{AB} defines the angle between the transition moment vectors $\boldsymbol{\mu}_A$ and $\boldsymbol{\mu}_B$ of the chromophores A and B, respectively, and θ_A and θ_B are the angles of the respective transition moment vector with the direction A→B. B: κ^2 values for extreme orientations. C: Origin of the magic angle.

Simplification of V_{AB}

In equation (1) the general dependence of V_{AB} on the geometric factors is given. For certain arrangements of the single chromophores, this equation can be simplified. To illustrate the concept, two general cases will be discussed that can be applied to both dimers and polymers equally well. In both cases it is assumed for simplicity that the

transition moments of the chromophores are in the plane of the chromophores along the long molecular axis. Additionally, the transition moments of the chromophores only build an angle to the dimer (polymer) axis going through the centres of the chromophores (see Figure 5 and Figure 6, p. 28).

In the 1st case, all chromophores are parallel to each other (linear chain polymer), meaning they are translatory equivalent. Therefore, $\theta_A = \theta_B$ and $\theta_{AB} = 0$ ($\cos(0) = 1$). Applying these angles to equation (1) reduces it to

$$V_{AB} = \frac{1}{hc4\pi\varepsilon_0}\frac{\mu_A\mu_B}{r^3}(1 - 3\cos^2\theta_A). \tag{51}$$

With all chromophores parallel to each other, both limiting cases such as the H-type ($\theta_A = 90° \rightarrow \cos(90) = 0$) and the J-type ($\theta_A = 0° \rightarrow \cos(0) = 1$) arrangement can be described by variation of θ_A. In this particular case, the interaction energy even vanishes if $\theta_A = \arccos(\frac{1}{\sqrt{3}}) = 54.7°$, which is the magic angle θ_{ma} (the geometric origin of the magic angle is shown in Figure 8 C). In this case the latter term vanishes ($(1 - 3\cos^2(54.7)) = 0$) and there is no interaction. It follows that:

H-type: $$V_{AB} = \frac{1}{hc4\pi\varepsilon_0}\frac{\mu_A\mu_B}{r^3} \tag{52}$$

J-type: $$V_{AB} = -\frac{1}{hc4\pi\varepsilon_0}\frac{2\mu_A\mu_B}{r^3} \tag{53}$$

θ_{ma}: $$V_{AB} = 0 \tag{54}$$

Eq. (52) and (53) show that the excitonic splitting is twice as large for a J-type arrangement as it is for an H-type arrangement if the transition moments and the distances are the same. It can also be seen that for an H-type arrangement $V_{AB} > 0$ and for a J-type arrangement $V_{AB} < 0$, therefore leading to a shift of the absorption to higher and lower energy, respectively.

Independent of the angle θ_A, the transition moments for the linear chain polymers into the excited states are $\mu = 0$ for the forbidden state and $\mu = \sqrt{N}\,\mu_A$ for the allowed excited state, where N accounts for the number of chromophores. Due to $f \propto \mu^2$ (eq. (47), the

oscillator strength in the polymer has the *N*-fold value compared to the monomer. This is in agreement with the example of the H-type dimer and eq. (45) and (46).

In the 2nd case, the transition moments are not parallel. Instead, there is an alternate zig-zag arrangement (and in a polymer two chromophores build one unit cell). The angles between the transition moments and the dimer (polymer) axis are given with respect to θ_A and are $\theta_B = 180° - \theta_A$ and $\theta_{AB} = 180 - 2\theta_A$ (Figure 5, p. 26). Following relations of cosine functions are needed

$$\cos(a + b) = \cos(a)\cos(b) - \sin(a)\sin(b) \tag{55}$$

$$\cos(a - b) = \cos(a)\cos(b) + \sin(a)\sin(b) \tag{56}$$

$$\sin^2 a + \cos^2 a = 1 \tag{57}$$

for a little mathematical excursion in order to reduce equation (1), where only the latter term shall be used for the calculation:

$$\begin{aligned}
&\cos\theta_{AB} - 3\cos\theta_A\cos\theta_B \\
&= \cos(180 - 2\theta_A) - 3\cos\theta_A\cos(180 - \theta_A) \\
&= \cos(180)\cos(2\theta_A) + \sin(180)\sin(2\theta_A) - \\
&3\cos\theta_A(\cos(180)\cos(\theta_A) + \sin(180)\sin(\theta_A)) \\
&= -\cos(2\theta_A) + 3\cos^2\theta_A \\
&= -\cos(\theta_A+\theta_A) + 3\cos^2\theta_A \\
&= -(\cos\theta_A\cos\theta_A - \sin\theta_A\sin\theta_A) + 3\cos^2\theta_A \\
&= \sin^2\theta_A - \cos^2\theta_A + 3\cos^2\theta_A \\
&= \sin^2\theta_A + 2\cos^2\theta_A \\
&= \sin^2\theta_A + \cos^2\theta_A + \cos^2\theta_A \\
&= 1 + \cos^2\theta_A.
\end{aligned} \tag{58}$$

Therefore, the interaction energy for the dimer (polymer) with alternate zig-zag arrangement is

$$V_{AB} = \frac{1}{hc4\pi\varepsilon_0}\frac{\mu_A\mu_B}{r^3}(1 + \cos^2\theta_A). \tag{59}$$

For both cases, the exciton band width $\Delta E = 2V_{AB}$ for a dimer. If the nearest-neighbour approximation is used, $\Delta E = 4V_{AB}$ in a polymer because each chromophore has two neighbours (no end-effect) instead of one as in the dimer.

The intensity of the absorption of the alternate zig-zag polymer is also dependening on the geometry. The total transition moments to the lowest and highest exciton states of a dimer or polymer are

$$\mu' = \sqrt{N}\,\mu_A \cos\,\theta_A \tag{60}$$

$$\mu'' = \sqrt{N}\,\mu_A \sin\,\theta_A, \tag{61}$$

where N is the number of chromophores.

Energies of the excited states

The pathway to determine the eigenstate energies of the excitonic states is described in a general way for polymers which works just as well for dimers.

The wave function of a ground state polymer with N identical chromophores is described by the sum of localised wave functions

$$\Psi_k = \prod_{n=1}^{N} \psi_n\,, \tag{62}$$

where ψ_n is the localised wave function of chromophore n in the ground state and k defines a quantum number ($k = 0, \pm1, \ldots N/2$). The wave function of the excited state with lowest energy is described by

$$\Phi_a = \psi_a^* \prod_{\substack{n=1 \\ n \neq a}}^{N} \psi_n\,, \tag{63}$$

where ψ_a^* is the localised wave function of chromophore A in the lowest energy excited state. There is a total of N localised wave functions of the type as in equation (63) where chromophore A is in the excited state and all others are in their ground state. The wave functions Φ_a are non-stationary. Stationary wave functions are obtained by symmetry adapted linear combinations

$$\Psi_0 = \frac{1}{\sqrt{N}} (\Phi_{a=1} + \Phi_{a=2} + \cdots \Phi_{a=N}). \tag{64}$$

Due to a periodical distribution of the chromophores, the *Bloch*[143] theorem can be applied and the wave functions can be described as *Wannier*[144] functions.

$$\Psi_k = \frac{1}{\sqrt{N}} \sum_{a=1}^{N} e^{2\pi ika/N} \Phi_a \tag{65}$$

The eigenstate energies of the excited states are given by

$$E_k = E_A^* + 2V_{AB} \left(\frac{N-1}{N}\right) \cos\left(\frac{2\pi k}{N}\right), \tag{66}$$

where E_A^* is the lowest excited state energy of the isolated chromophore A (as H_{AA} in equations (24) and (25), p. 31) and k is a quantum number that runs from $k = 0, \pm 1, \pm 2, \ldots, N/2$. The cosine term becomes maximum for $k = 0$ and $k = N/2$, leading to highest and lowest energies of the excitonic manifold. For an infinitely long polymer, the term $(N-1)/N$ approaches unity.

That this relation also works for dimers can easily be shown. For a dimer, $N = 2$ and it follows that $k = 0$ and $k = N/2$. For these k the cosine term becomes 1 and –1 and the energies $E_k = E_A^* + V_{AB}$ and $E_k = E_A^* - V_{AB}$ as seen in equations (24) and (25).

2 Scope of the work

This work partly follows the work of *Grahn et al.*[67], where a series of thiophene-bridged squaraine oligomers (**OS4**, Chart 9, p. 15) was prepared and the broadened absorption spectra were explained by exciton coupling theory, and the work of *Havinga et al.*[110, 112-113] who proposed low band gap polymers by the implementation of alternating electron donating and accepting units. There, a polysquaraine with fused indolenine units (**PS2**, Chart 10, p. 16) was already prepared showing a band gap of ~ 1.3 eV and absorption beyond 900 nm (< 11100 cm^{-1}). Therefore, the parent structure of the squaraine used in this work is an indolenine squaraine which shall be modified at different positions to tune the optical properties. The indolenine unit, which is substituted with two methyl groups at the 3-position, was chosen because in cyanine dyes it hinders the aggregation of the dyes in solution.[145] This feature should simplify the spectroscopic and electrochemical analysis of the compounds.

One basic idea for tuning the properties is the insertion of additional electron donating or withdrawing units. Standard unsubstituted squaraines already possess a low HOMO–LUMO gap and therefore absorption at low energy. The addition of electron donors at the periphery of the dye (commonly the 5-position of the indolenine unit) should lead to an increase of the HOMO energy level, the implementation of additional electron acceptors to a decrease of the LUMO energy level and both methods should therefore result in a decrease of the HOMO–LUMO gap and absorption at lower energy. In addition, one central oxygen atom can be replaced by the strong electron withdrawing dicyanomethylene group that also lowers the LUMO energy level and additionally induces a change of relative configuration of the indolenine units from *trans* to *cis*.

As mentioned above, the broad absorption spectra of the oligosquaraines were explained to be caused by exciton coupling. This is another potential approach to influence the spectroscopic properties of compounds. The exciton coupling energy V_{AB} is proportional to the transition dipole moments (eq. (1), p. 24) of the respective chromophores (the orientation of the transition dipole moments of the squaraines are depicted with green

double arrows in Figure 9). The high extinction coefficients at low energy of the squaraine dyes do in fact result in large transition dipole moments and should therefore lead to a strong exciton coupling energy.

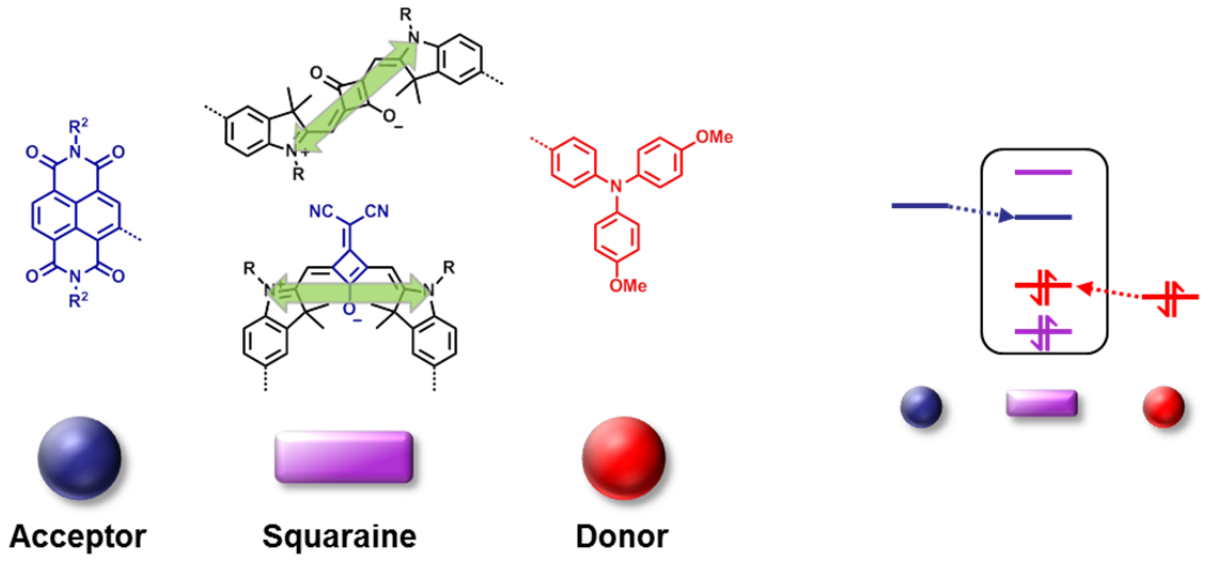

Figure 9 Structures of the parent squaraine dyes and examples for electron donating (red) and accepting (blue) units in addition to an energy level sketch. The green double arrows show the orientation of the transition dipole moments of the low energy absorption of the squaraines.

In this work, polymeric squaraine dyes shall be synthesised and explored regarding their spectroscopic and electrochemical properties. The goal is to create low band gap polymers with a broad and low energy absorption in the red to NIR region. If the squaraine shows suitable properties, their utilisation in optoelectronic devices such as organic solar cells for example can be explored in cooperations. Before doing so, monomeric model dyes shall be prepared and investigated in order to a) get an understanding of the impact of additional electron accepting and donating units on the squaraine system, b) evaluate the usefulness of the polymer synthesis and c) have a model system to compare the properties of the respective polymer with. In general, three different approaches shall be followed. The first two are the investigations of donor–squaraine and acceptor–squaraine copolymers and their respective model compounds, taking advantage of the increased HOMO or decreased LUMO energy levels. Here, also the electronic interactions between the different redox centres are of major interest. The third approach is the synthesis of homopolymers consisting exclusively of squaraine

chromophores. In those polymers the focus will be on the excitonic interaction that should be present due to the large transition moments and the close distance of the chromophores.

3 Results & Discussion

3.1 Reference Squaraines and Functionalised Squaraines[1]

3.1.1 Introduction

In order to be able to prepare a broad variety of squaraine dyes, functionalised squaraines are mandatory. Therefore, a series of symmetric and asymmetric squaraines with bromine or boronic ester moieties was synthesised. Both moieties enable the use of the Pd-catalysed *Suzuki* cross coupling reaction for further derivatisation. In addition, with the bromine-substituted squaraines in hand, the Ni-mediated *Yamamoto* homocoupling reaction can be performed, among others. Besides, non-functionalised squaraines were prepared as reference dyes in order to compare the spectroscopic and electrochemical properties.

All compounds that were prepared are indolenine squaraines and are based on two parent chromophore structures. The first is a typical squaraine with two oxygens at the central squaric core (**S3**), which will be called the "standard" squaraine. In the second, one oxygen is replaced by a stronger electron accepting dicyanomethylene group (**S15**), which forces those dyes in a *cis*-like conformation due to the steric demand of this group.

3.1.2 Synthesis

Reference Squaraines

The synthesis of basic indolenine squaraine dyes is straight forward. Simple dyes can be easily obtained in a few steps by alkylation of an indolenine derivative and subsequent

[1] Reproduced or adapted in part with permission from *Synthesis, Electrochemical, and Optical Properties of Low Band Gap Homo- and Copolymers Based on Squaraine Dyes*, S. F. Völker, T. Dellermann, H. Ceymann, M. Holzapfel, C. Lambert, *J. Polym. Sci., Part A: Polym. Chem.* **2014**, *52*, 890-911. Copyright (2014) WILEY-VCH Verlag GmbH & Co. KGaA, Weinheim.

dicondensation with squaric acid or a derivative. As reference compounds for this work, non-functionalised dyes were synthesised (Scheme 5). Therefore, the alkylating agent 3,7-dimethyloctyl tosylate **1** was prepared from the corresponding alcohol according to literature procedures.[146] Then, commercially available 2,3,3-trimethylindolenine was alkylated with **1** in $MeNO_2$ to yield the quaternary salt **2**. In situ deprotonation of **2** with pyridine to the highly nucleophilic methylene base and subsequent reaction with half an equivalent of squaric acid in a solvent mixture of toluene and 1-butanol (1:1) with azeotropic distillation of water using a *Dean-Stark* trap yielded the non-functionalised symmetric dye **M1**, which adopts a *trans*-configuration.[16] During the condensation, the reaction mixture turns into a strongly blue coloured solution, out of which the dye is isolated by flash column chromatography.

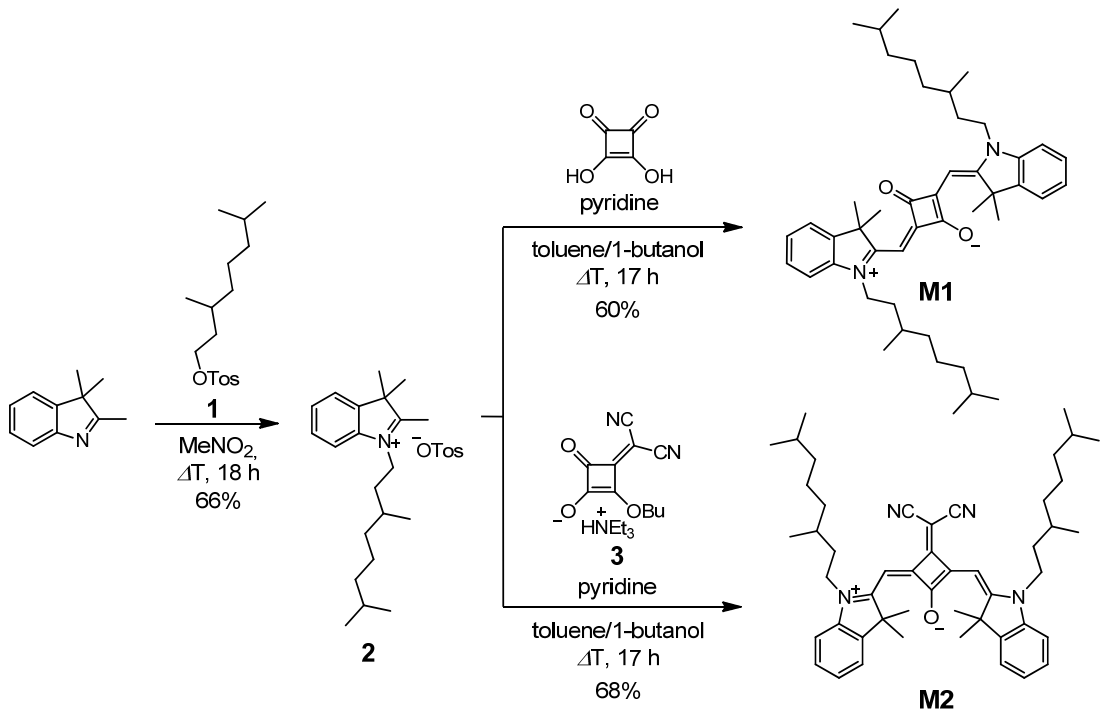

Scheme 5 Synthesis of reference squaraines **M1** and **M2**.

When the squaric acid is replaced by triethylammonium 2-butoxy-3-(dicyanomethylene)-4-oxocyclobut-1-enolate (**3**), which is obtained according to literature procedures from 3,4-dibutoxy-3-cyclobutene-1,2-dione and malononitrile,[147] the in other aspects same reaction conditions yield the dicyanomethylene-substituted symmetric dye **M2**. This dye is also purified by flash column chromatography of the, this time green, reaction mixture. On the contrary to **M1**, this dye adopts a *cis*-

configuration due to the steric demand of the dicyanomethylene group.[85] This description of the dicondensation reactions to **M1** and **M2** states the standard procedure to obtain squaraine dyes, which is used throughout this work if it is not stated elsewise.

Functionalised Squaraines

For further derivatisation of the squaraine dyes, functional groups are necessary. As functional analogue to the above shown indolenine derivative, 5-bromo-2,3,3-trimethylindolenine (**4**) was synthesised *via Fischer* indole synthesis from *p*-bromophenylhydrazine hydrochloride and isopropylmethyl ketone in glacial acetic acid similar to literature procedures (Scheme 6).[148] In prospect of potential solubility issues of squaraine polymers, both a long linear and a branched alkyl chain were chosen for the *N*-alkylation of the indolenine derivative. Alkylation with either 3,7-dimethyloctyl tosylate or 1-iodohexadecane in $MeNO_2$ gave the brominated quaternary salts **5** and **6**, respectively. In the following, **5** was suspended in a mixture of Et_2O and aqueous NaOH (1–2 M) solution. Under vigorous stirring, the suspended quaternary salt is deprotonated to the nucleophilic methylene base **7** which readily dissolves in the Et_2O layer and is obtained upon evaporation of the solvent. The further usage of **7** is shown in Scheme 23 (p. 158).

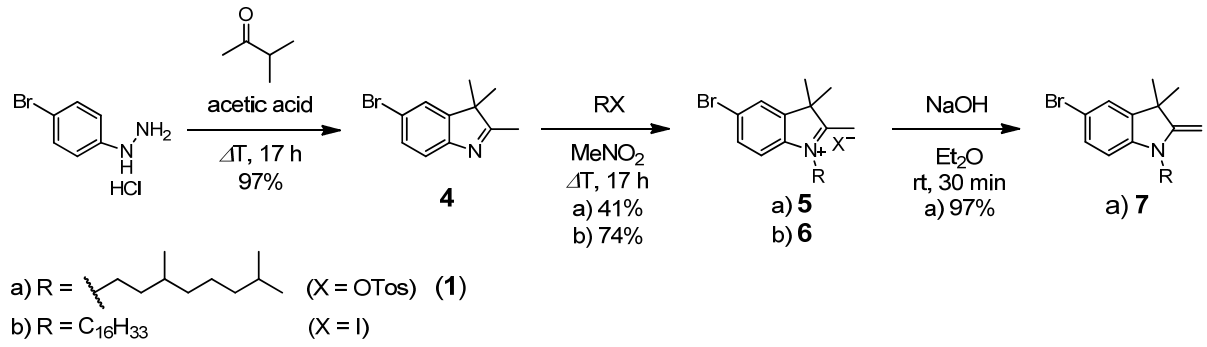

Scheme 6 Synthesis of functionalised indolenine precursors **4**–**7**.

For the synthesis of asymmetrical dyes, the synthetic route is slightly more laborious compared to the symmetric squaraines. Condensation of the quaternary salts **5** and **6** with one equivalent of either 3,4-diethoxy-3-cyclobutene-1,2-dione or 3,4-dibutoxy-3-

cyclobutene-1,2-dione, the ethyl- and butyl ester derivatives of the squaric acid, in the presence of triethylamine gave the semisquaraine ethyl- and butyl esters **8** and **9**, respectively (Scheme 7). Subsequent hydrolysis under acidic conditions yielded the semisquaraine acids **10** and **11**, respectively. The monobrominated asymmetric dye **M3** was obtained after condensation reaction of **10** and the non-functionalised quaternary salt **2** in the presence of pyridine.

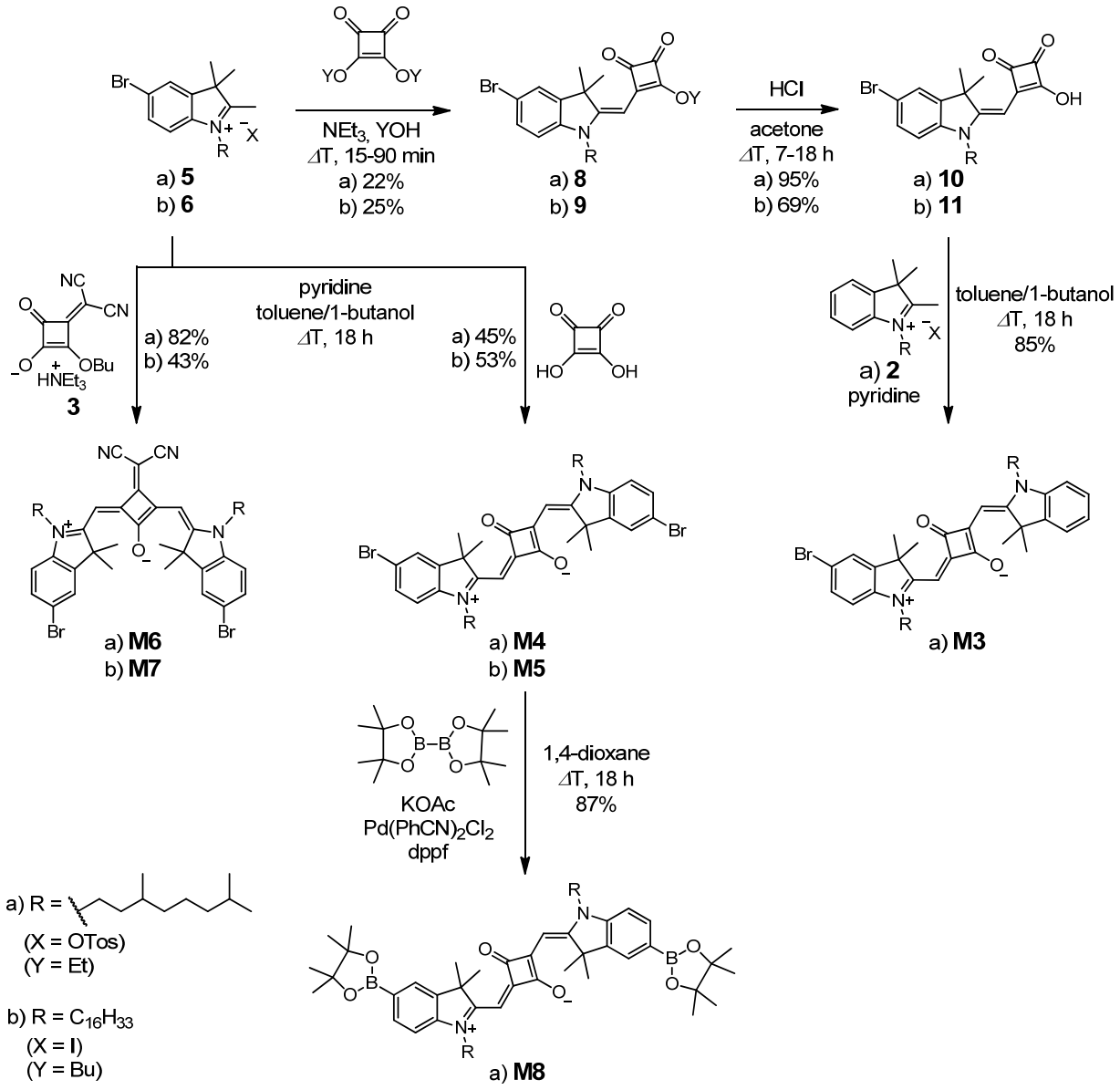

Scheme 7 Synthesis of precursors **8–11** and functionalised squaraines **M3**–**M8**.

The dibrominated dyes **M4** and **M5** were obtained by the standard procedure of the dicondensation reactions of squaric acid with **5** and **6**, respectively. Replacement of squaric acid by **3** resulted in the dicyanomethylene-substituted dyes **M6** and **M7**,

respectively. Furthermore, the bromine atoms in **M4** were substituted by boronic ester groups *via* the Pd-catalysed *Miyaura* borylation reaction using bis(pinacolato)diboron, $Pd(PhCN)_2Cl_2$, 1,1'-bis(diphenylphosphino)ferrocene (dppf), and KOAc as base, resulting in **M8** in high yields.

For a somewhat larger steric demand, the two methyl groups at the 3-position of the indolenine were replaced by a cyclohexyl moiety. Consequently, the corresponding indolenine **12** was synthesised *via Fischer* indole synthesis of *p*-bromophenylhydrazine hydrochloride and 1-cyclohexylethanone (Scheme 8). Alkylation with **1** to the quaternary salt **13** and subsequent dicondensation reaction with **3** gave the dicyanomethylene-substituted dye **M9**.

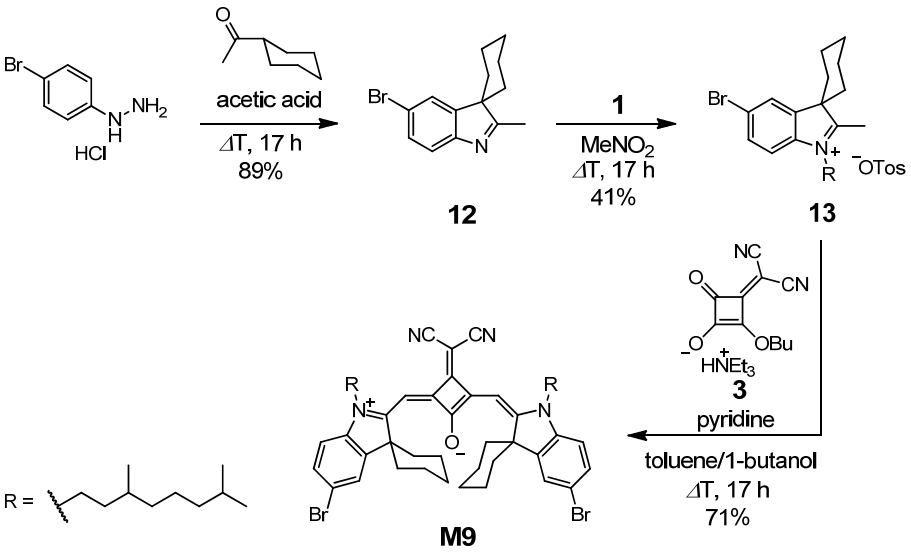

Scheme 8 Synthesis of precursors **12** and **13** and cyclohexyl-substituted dye **M9**.

3.1.3 Absorption Spectroscopy

The basic absorption and fluorescence properties of squaraine dyes are given by the corresponding spectra of the non-functionalised reference dyes **M1** and **M2** in DCM (Figure 10 and Figure 12). The described features are typical for standard and dicyanomethylene-substituted indolenine squaraine dyes. Furthermore, the transition moments μ were obtained by integration of the main low energy absorption band and calculated according to equation (48),[149]

$$\mu_{eg}^2 = \frac{3hc\varepsilon_0 \ln 10}{2000\pi^2 N_{Av}} \frac{9n}{(n^2+2)^2} \int \frac{\varepsilon}{\tilde{\nu}} d\tilde{\nu} \,. \tag{48}$$

All absorption and fluorescence data is listed in Table 1 (p. 55).

Due to the donor-acceptor-donor structure, **M1** shows a very intense and sharp absorption band in the orange to red region of the visible spectrum with the maximum at 15700 cm^{-1} and an extinction coefficient of $\varepsilon \sim 336000$ M^{-1} cm^{-1}. This band originates from a HOMO→LUMO transition and rises steep at the low energy side, while on the high energy side there is a small shoulder originating from vibronic progression. This transition is polarised along the long molecular axis[150-151] and the transition moment is μ_{eg} = 11.4 D. Additionally, minor transitions can be seen around 29000 cm^{-1} and 35000 cm^{-1}.

In **M2**, one oxygen atom of the central squaric ring has been substituted by a dicyanomethylene group. In consequence, the electron acceptor strength of the central squaric moiety is increased (see cyclic voltammetry section 3.1.5). Due to this increase, corresponding to a lowering of the LUMO energy level, and while the indolenine groups of the dye remain the same, the absorption maximum is shifted towards lower energy to the red region of the visible spectrum to 14600 cm^{-1} with a transition moment of μ_{eg} = 10.6 D and an extinction coefficient of 207000 M^{-1} cm^{-1}. In contrast to **M1**, there are additional prominent transitions between 21000–29000 cm^{-1} which are typical of the dicyanomethylene-substituted squaraines. A more detailed description of the absorption spectra, including the molecular orbitals that are involved, is shown in chapter 3.3.7 and Figure 49 (p. 142) for the dibrominated dyes **M5** and **M7** in combination with TDDFT (time dependent density functional theory) calculations.

Generally, when DCM is exchanged by toluene (not shown) there is no major influence on the absorption properties of the basic standard squaraine dyes such as **M1** and, if at all, the maximum is only slightly shifted towards lower energy. For dicyanomethylene-substituted dyes such as **M2**, this effect is slightly larger and the maximum is shifted around 200 cm^{-1} to lower energy.

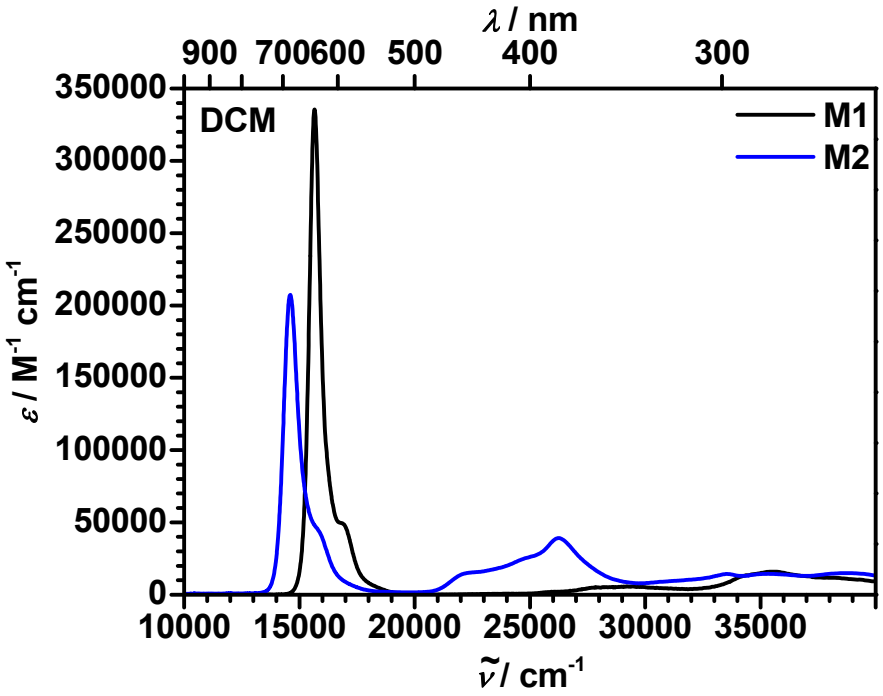

Figure 10 Absorption spectra of the non-functionalised reference dyes **M1** and **M2** in DCM.

The focus in this work lies on the alteration of the dominant main low energy absorption band. Therefore, most absorption spectra will be magnified in the red to NIR region to point out the absorption properties of the dyes.

The insertion of functional groups such as bromine or boronic esters does not alter the shape of the low energy absorption bands, which still retain the typical cyanine-like structure. However, in DCM each of these substituents shifts the maximum to lower energy. Bromine acts as a π-donor and σ-acceptor and compared to **M1** each bromine atom induces a red shift of 100 cm^{-1} (**M3**–**M5**), which is also true for the dicyanomethylene-substituted squaraines **M2**, **M6**, and **M7**. For the boronic ester-substituted dye **M8**, the boron atom acts as a π-acceptor[152-153], which can lead to significant delocalisation when implemented in an organic system, and also as a σ-donor due to its lower electronegativity compared to carbon for example. Therefore, a small red shift of the absorption maximum is induced.

In **M9**, the two methyl groups at the indolenine moiety are extended to a cyclohexyl group, which results in a slight red shift of ca. 100–200 cm^{-1} compared to the similar dyes **M6** and **M7**.

The extinction coefficients of all dyes are rather large. In general they are ~ 50% higher for the standard dyes **M1, M3**–**M5**, and **M8** (310000–336000 M^{-1} cm^{-1}) compared to the dicyanomethylene-substituted dyes **M2**, **M6**, and **M7** (207000–220000 M^{-1} cm^{-1}).

The alkyl chains do not have any significant impact on the absorption properties. This can be seen for **M4** and **M5** as well as for **M6** and **M7**, respectively. These pairs of dyes only differ in the alkyl chains attached at the indolenine nitrogen atom where **M4** and **M6** carry the branched 3,7-dimethyloctane chain whereas **M5** and **M7** (dashed lines in Figure 11 and Figure 13) carry the linear $C_{16}H_{33}$ chain. Both the energy of the absorption maxima as well as the extinction coefficients barely differ.

Consequently, in these systems presented here, the sometimes varying alkyl chains are not discussed in terms of the optical properties.

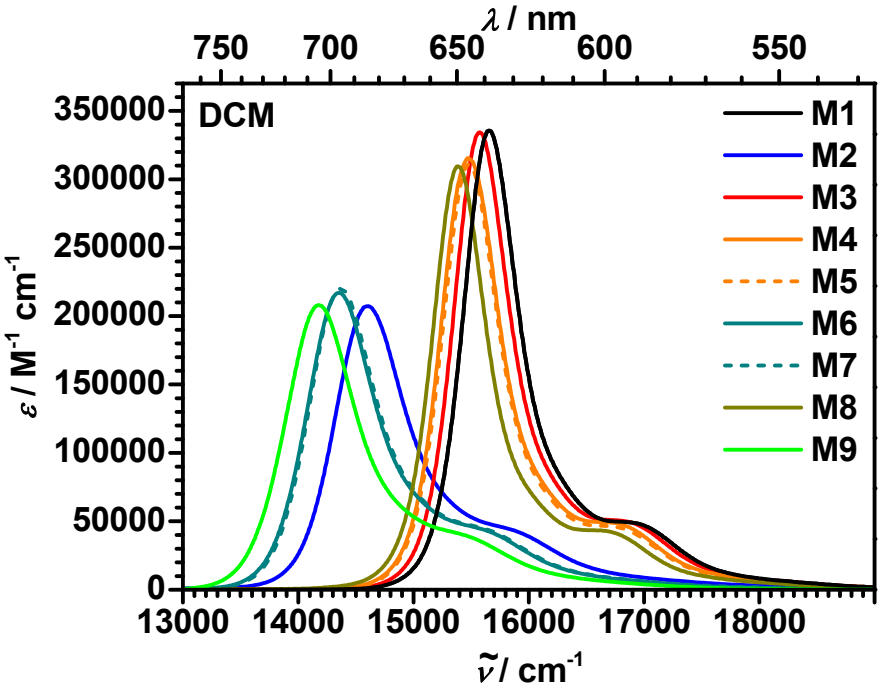

Figure 11 Absorption spectra in DCM of reference dyes **M1** and **M2** as well as the functionalised dyes **M3**–**M9**. The dashed lines indicate that the compound is similar to the one shown in the same colour (solid line) and only the alkyl chains at the nitrogen atoms differ.

3.1.4 Fluorescence Spectroscopy

The fluorescence spectra of **M1** and **M2** in DCM are depicted in Figure 12 together with the corresponding absorption spectra. They are mirror images to the main low energy absorption band with a steep rise of the band at the high energy side and a vibronic shoulder at the low energy side. Typically, there is only a minor *Stokes* shift, which is mostly somewhat larger for the dicyanomethylene-substituted dyes than for the basic squaraine dyes and is around 100–400 cm^{-1} for simple indolenine squaraines.

Similar to the absorption properties, the spectra are shifted very little, if at all, towards lower energy when DCM is exchanged by toluene (not shown). In general, the fluorescence quantum yields are higher in non-polar solvents such as toluene or cyclohexane than in DCM. The quantum yields Φ_{fl} for both dyes are around 0.20 in DCM and around 0.40 in toluene.[1]

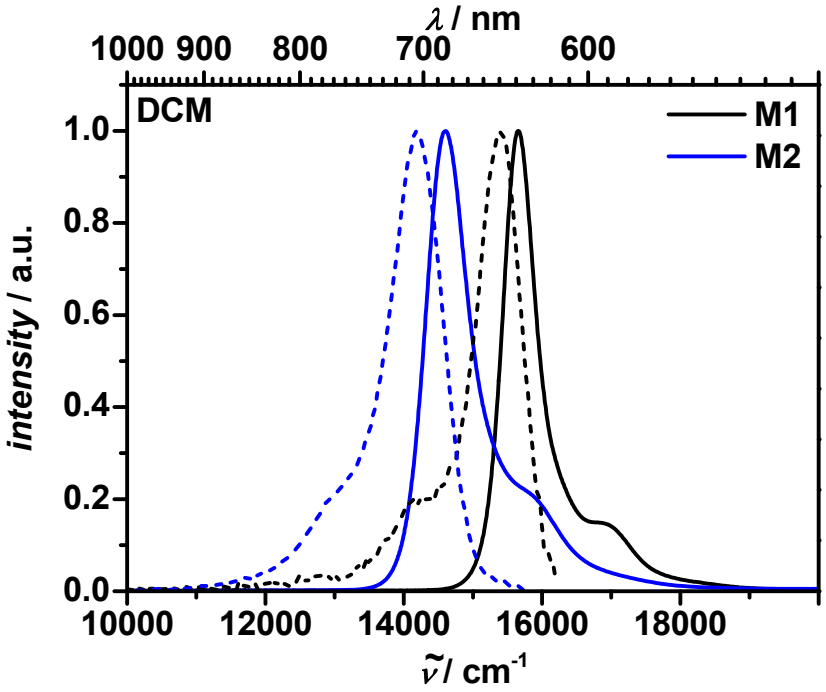

Figure 12 Normalised absorption (solid lines) and fluorescence (dashed lines) spectra of **M1** and **M2** in DCM.

[1] During the writing process, the quantum efficiency of oxazine 1 was determined to be 0.15 by an absolute measurement using an integration sphere. However, the values reported for the squaraine dyes herein are still referenced against the quantum efficiency of 0.11 as they were published to avoid confusion. Nevertheless, it has to be noted that the correct quantum efficiencies are larger by a factor of 0.15 / 0.11 ≈ 1.36.

The fluorescence lifetimes τ_{fl} of the monomeric squaraines show a monoexponential decay and are in the lower ns region. In toluene they are 1.9 ns for **M1** and 4.5 ns for **M2**. Generally the fluorescence lifetimes are nearly twice as large for the dicyanomethylene-substituted dyes compared to the basic squaraines.

The shapes of the fluorescence bands of the functionalised squaraines **M3**–**M8** (Figure 13) are nearly identical for all the dyes. They are mirror images to the absorption spectra (Figure 11) and all compounds show a small *Stokes* shift of ca. 200–400 cm^{-1}. In consequence, the energies of the fluorescence maxima are shifted to lower energy analogous to the absorption maxima.

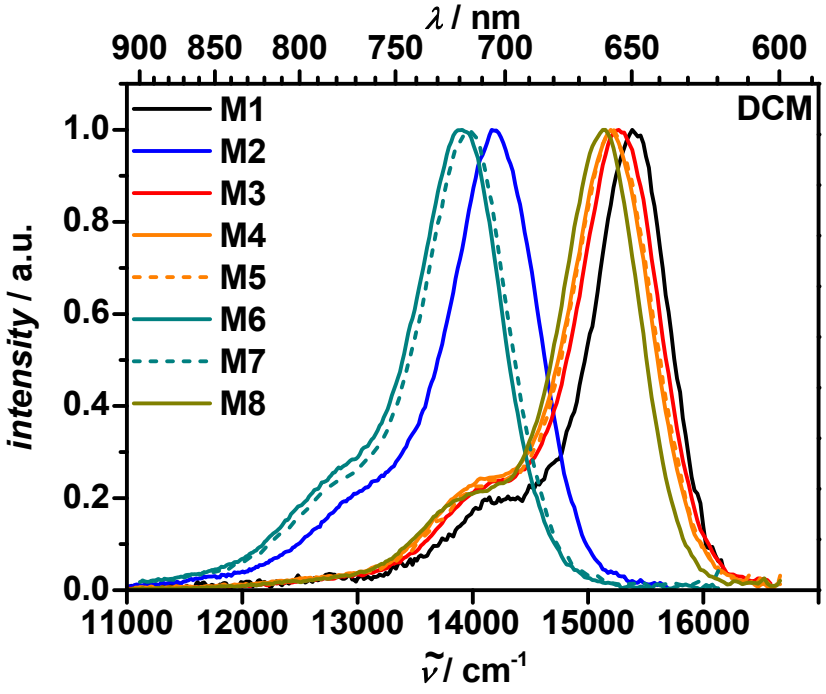

Figure 13 Normalised fluorescence spectra in DCM of reference dyes **M1** and **M2** as well as functionalised dyes **M3**–**M8**. The dashed lines indicate that the compound is similar to the one shown in the same colour (solid line) and only the alkyl chains at the nitrogen atoms differ.

The fluorescence quantum yields of the dyes are ca. 0.20–0.60 and the fluorescence lifetimes range between 1–5 ns. The bromine-substituted squaraines show a slightly higher fluorescence quantum yield compared to the reference dyes. This is in agreement with the systematic investigation by *Würthner et al.*[28], where the quantum yields of a series of halogenated and a non-halogenated squaraine dyes were investigated.

Table 1 Absorption maxima, extinction coefficients, transition moments, fluorescence maxima, fluorescence quantum yields, and fluorescence lifetimes of squaraine monomers **M1**–**M9**. cy = cyclohexane.

	solvent	λ / nm	$\tilde{\nu}_{max}$ / cm^{-1}	ε_{max} / $M^{-1}cm^{-1}$	μ_{eg} / D	λ_{fl} / nm	$\tilde{\nu}_{fl}$ / cm^{-1}	Φ_{fl}[a]	τ_{fl} / ns
M1	DCM	639	15700	336000	11.4	649	15400	0.19	1.0
	toluene	644	15500	340000	11.1	649	15400	0.35	1.9
M2	DCM	685	14600	207000	10.6	706	14200	0.25	-
	toluene	700	14300	236000	10.1	716	14000	0.41	4.5
M3	DCM	642	15600	334000	11.5	655	15300	0.18	1.4
	toluene	647	15500	327000	10.9	658	15200	0.46	1.8
M4	DCM	646	15500	316000	11.5	658	15200	0.33	1.3
	toluene	651	15400	354000	11.2	660	15200	0.45	-
	cy	646	15500	244000	9.3	657	15200	0.41	1.7
M5	DCM	646	15500	311000	12.4	656	15200	0.33	1.3
	cy	646	15500	348000	11.4	654	15300	0.51	1.7
	$CHCl_3$	646	15500	362000	11.6	654	15300	0.49	-
M6	DCM	697	14300	217000	10.7	719	13900	0.40	2.5
	toluene	711	14100	230000	10.4	726	13800	0.56	4.0
	cy	720	13900	217000	10.5	743	13500	0.50	3.9
M7	DCM	696	14400	220000	11.3	716	14000	0.46	2.7
	toluene	711	14100	194000	9.6	726	13800	0.57	4.1
	cy	720	13900	180000	9.4	739	13500	0.55	4.1
M8	DCM	650	15400	310000	11.0	660	15200	0.24	1.6
	toluene	656	15300	278000	10.4	665	15000	0.39	2.0
M9	DCM	706	14200	208000	10.5	-	-	-	-
	toluene	719	13900	220000	10.0	-	-	-	-

- was not measured. [a] During the writing process, the quantum efficiency of oxazine 1 was determined to be 0.15 by an absolute measurement using an integration sphere. However, the values reported for the squaraine dyes herein are still referenced against the quantum efficiency of 0.11 (see experimental section 5.1.2) as they were published to avoid confusion. Nevertheless, it has to be noted that the correct quantum efficiencies are larger by a factor of $0.15 / 0.11 \approx 1.36$.

3.1.5 Cyclic Voltammetry

Cyclic voltammetry measurements were carried out in DCM solution for most squaraine dyes using tetrabutylammonium hexafluorophosphate (TBAHFP, 0.2 M) as supporting electrolyte. In case of particular interest in the reduction processes, THF was used as

solvent. The values are referenced to the ferrocene/ferrocenium (Fc/Fc^+) redox couple. The data is listed in Table 2 (p. 58).

The typical result of cyclic voltammetry measurements of indolenine squaraine dyes is presented in case of the bromine-substituted dyes **M5** and **M7** and depicted in Figure 14 A. There is one reduction process of the central squaric ring unit and two oxidation processes. For **M5** in DCM the half-wave potential of the reduction is at a rather low potential of –1.61 V and those of the oxidations at 110 and 580 mV. Thin layer measurements revealed that the reduction is chemically irreversible, whereas both oxidations are reversible.

To visualise the impact of the dicyanomethylene group, the cyclic voltammogram of **M7** is depicted in the same figure as **M5** (Figure 14 A). Due to the dicyanomethylene moiety in the central squaric unit, the reduction occurs at more positive value (–1.41 V). In addition to this, also the 1st oxidation takes place at a higher potential (207 mV), whereas the second oxidation process is barely influenced (576 mV). This shows that the central core becomes a stronger acceptor upon exchange of one oxygen at the squaric core by a dicyanomethylene group as already indicated in the absorption spectroscopy.

When THF is used as solvent instead of DCM, the accessible potential window of the solvent is at more negative values. Therefore it was possible to record the 2nd reduction of the squaraine dyes. Both **M1** and **M6** (Figure 14 B and C, respectively) show a reduction process at –2.63 V and –2.31 V, respectively. These chemically irreversible reductions are accompanied by belated back oxidation processes starting at ca. –700 mV and –400 mV, respectively. That these belated back oxidation processes correspond to the 2nd reduction can clearly be seen because they only appear when the 2nd reduction process has been recorded before in the same cycle. The arrows indicate the initial recording direction. The irreversible 2nd reduction has also been shown for an azulene squaraine dye but in this case, no belated back oxidation was observed.[154] The 2nd oxidation of **M6** could not be recorded within the operation window of THF.

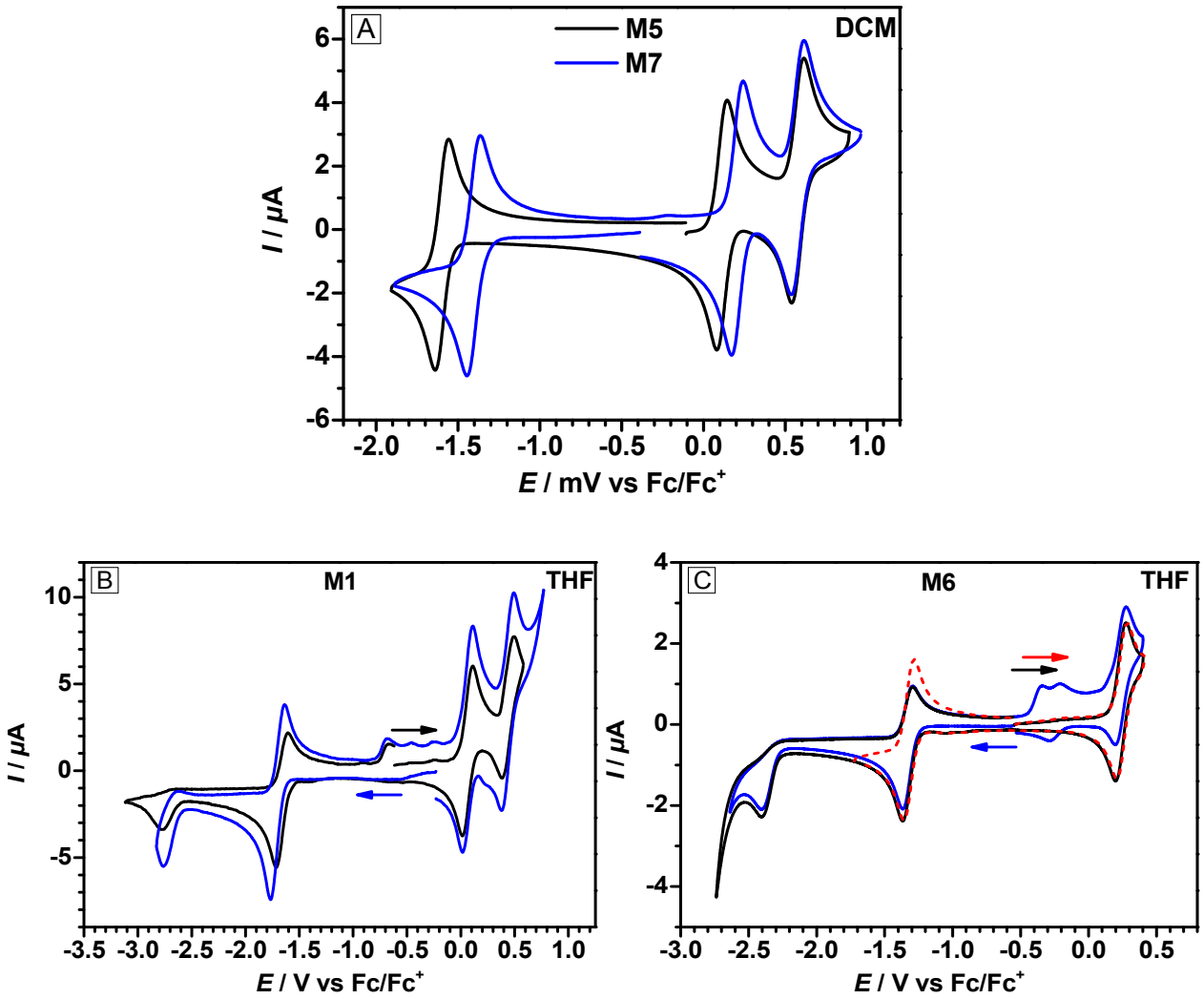

Figure 14 Cyclic voltammograms of **M5** and **M7** in DCM/TBAHFP (0.2 M) (A), and **M1** (B) and **M6** (C) in THF/TBAHFP (0.2 M) at a scan rate of 250 mV s^{-1}. In B and C the black and blue lines indicate voltammograms that were recorded in different initial directions. In C the voltammogram in the red dashed line only shows the 1st oxidation and 1st reduction.

HOMO and LUMO energy levels were calculated from the half-wave potentials. The potential of Fc/Fc^+ in TBAHFP/DCM is 0.46 eV and in TBAHFP/THF 0.56 eV vs. the saturated calomel electrode (SCE).[155] Furthermore, the potential of SCE is 0.244 vs. the normal hydrogen electrode (NHE), which has an absolute potential of 4.46 eV vs. vacuum.[156] Therefore, in DCM $E_{HOMO/LUMO} = -5.16\ eV - E_{1/2}^{Ox1/Red1}$ and the electrochemically derived band gap is $E_{gap}^{CV} = E_{LUMO} - E_{HOMO}$. In THF, –5.16 eV is replaced by –5.26 eV.

The HOMO and LUMO energy levels $E_{HOMO/LUMO}$ of the reference and the functionalised dyes are rather similar and the values range from –5.37 eV to –5.22 eV and –3.47 eV to –3.76 eV, respectively, leading to electrochemically obtained band gaps (the term "band gap" might not be correct for monomeric compounds, however, it will be used throughout this work for easier comparison to the band gaps of the polymers) of 1.61–1.80 eV. There is some deviation for **M6** but due to the similarity to **M7** this is attributed to the THF solvent that was used in the cyclic voltammetry measurements of **M6**.

The optical band gaps E_{gap}^{opt} were obtained from the onset of the lowest energy transition on the low energy side in the absorption spectra. Therefore, the 1st derivation of the absorption spectra was calculated to determine the inflexion point where a tangent was placed. The intersection point of the tangent with the x-axis in eV gave the optical band gap E_{gap}^{opt}. Comparison of the optical and the electrochemical band gaps shows, that the optically obtained values are 0.06–0.10 eV higher than the electrochemical values. **M1** and **M6** are left out for this comparison due to the different solvents used in the cyclic voltammetry and absorption spectroscopy.

Table 2 Redox potentials, HOMO and LUMO energy levels, and band gaps obtained by electrochemical (E_{gap}^{CV}) and optical (E_{gap}^{opt}) methods of squaraines **M1** and **M5**–**M8**.

	solvent	$E_{1/2}^{Red2}$ / mV	$E_{1/2}^{Red1}$ / mV	$E_{1/2}^{Ox1}$ / mV	$E_{1/2}^{Ox2}$ / mV	E_{HOMO} / eV[d]	E_{LUMO} / eV[d]	E_{gap}^{CV} / eV[d]	E_{gap}^{opt} / eV[e]
M1	THF[a]	–2631[c]	–1660	64	442	–5.32	–3.60	1.72	1.88
M5	DCM[a]		–1610	110	580	–5.27	–3.55	1.72	1.86
M6	THF[b]	–2312	–1320	245		–5.51	–3.94	1.57	1.71
M7	DCM[a]		–1405	207	576	–5.37	–3.76	1.61	1.71
M8	DCM[b]		–1678	71	524	–5.22	–3.47	1.75	1.85

[a] Ag/AgCl pseudo-reference electrode; [b] Ag/AgCl "leak free" electrode; [c] potentials extracted from DPV; [d] determined according to the procedure described in 5.1.4; [e] determined in DCM according to the procedure in 5.1.1.

3.1.6 Conclusion

To sum up, the syntheses of both reference and functionalised squaraines is straight forward. Symmetric and asymmetric dyes with bromine or boronic ester moieties can easily be obtained in decent yields and allow further derivatisation.

The absorption maxima of standard indolenine squaraines and dicyanomethylene-substituted squaraines are at ~ 15500 cm^{-1} and ~ 14300 cm^{-1}, respectively, and are slightly red-shifted by σ- or π-donating properties of the substituents. In general, the large extinction coefficients of the standard squaraines (~ 300000 M^{-1} cm^{-1}) are ~ 50% higher compared to the dicyanomethylene-substituted ones (200000 M^{-1} cm^{-1}).

All squaraines show decent fluorescence (Φ_{fl} = 0.20–0.60) with higher quantum yields in apolar solvents and a monoexponential decay in the low ns regime. The *Stokes* shift is commonly rather small (~ 300 cm^{-1}) and the fluorescence band a mirror image to the absorption band.

In DCM, the squaraines usually show one reduction and two oxidation processes. The stronger electron accepting feature of the dicyanomethylene moiety is clearly reflected in the higher reduction potentials and the resulting lower LUMO energy levels. A second (irreversible) reduction which is below –2 V can only be obtained in THF.

3.2 Homopolymers & Squaraine-Squaraine Copolymer

3.2.1 Introduction

In the previously mentioned work of *Grahn et al.*[67] thiophene-bridged indolenine squaraine oligomers up to the pentamer were synthesised (**OS4**, Chart 9, p. 15). Thereby, a distinct red shift and broadening of the main absorption band were induced. These features were explained by exciton coupling theory. In doing so, an absorption maximum of 15500 cm^{-1} (742 nm) was predicted for a potential polymer of this kind. In addition, the thiophene bridge does not act as a conjugative "π-bridge" but more as an insulating spacer. Inspired by this work, an indolenine squaraine homopolymer without the thiophene bridges was synthesised. Since the polymer synthesis does not require a stepwise approach as do the oligomers, a polymer with broad absorption in the red to NIR region should be obtained in a simple way. Besides, there is the indolenine squaraine polymer (**PS2**, Chart 10, p. 16) of *Havinga et al.*[112]. This polymer was obtained by the polycondensation of two fused indolenine units with squaric acid which resulted in the closest "distance" of the electron rich indolenine units. This polymer shows an absorption maximum at 11700 cm^{-1} (855 nm) in solution.

In a similar manner to the standard squaraine homopolymers, dicyanomethylene-substituted squaraines were polymerised to obtain homopolymers based on parent squaraine chromophores that already absorb light at lower energy than the standard squaraines and which exhibit a *cis*-like structure. The *cis*-configuration could lead to different superstructures of the polymer.

Eventually, the combination of both a standard indolenine squaraine and a dicyanomethylene-substituted squaraine was realised in a squaraine–squaraine copolymer in order to combine the different spectroscopic properties of the parent chromophores within one polymer.

3.2.2 Standard Squaraine Homopolymers[1]

Synthesis

For the polycondensation reaction of the dibrominated squaraines to the homopolymers, the Ni-mediated *Yamamoto* coupling reaction was chosen for the aromatic C–C linkage. The polymer **P2** was already described in the foregoing diploma thesis to this work[157] and its synthesis is also shown in Scheme 9 for the sake of completeness. In the presence of 1,5-cyclooctadiene (COD) and 2,2'-bipyridine, a slight excess of $Ni(COD)_2$ was used as Ni(0) source in a solvent mixture of DMF and toluene (1:1) to polycondensate **M5** to the homopolymer **P2**. The reaction was performed at room temperature over a period of 6 d. After several *Soxhlet* extractions **P2** was obtained in good yield with a number average molecular mass of $M_n \sim 28000$, which corresponds to a degree of polymerisation of $X_n \sim 33$. However, solubility was a problem and **P2** was only soluble in $CHCl_3$ and solvent mixtures consisting of both a chlorinated solvent and an alcohol. The size of the polymers was estimated by analytical gel permeation chromatography (GPC) in $CHCl_3$ with polystyrene standards and the data are found in Table 25 (p. 210).

In order to increase the solubility of the polymer, the linear alkyl chains at the nitrogen atoms were replaced by branched 3,7-dimethyloctane chains and the polycondensation of **M4** to **P1A** was carried out under the same reaction conditions. The resulting polymer **P1A**, with a number average molecular weight of $M_n \sim 31000$ and a degree of polymerisation of $X_n \sim 46$, is ~ 30% longer than the previous polymer **P2**, but solubility was again restricted to $CHCl_3$ and the above mentioned solvent mixtures. As **P1A** proved poorly soluble in pure solvents, pure DMF was used as the solvent for the *Yamamoto* coupling of **M4** under elsewise identical reaction conditions to provoke precipitation of the polymers at an earlier stage of the polycondensation reaction to get

[1] Reproduced or adapted in part with permission from a) *Polymeric Squaraine Dyes as Electron Donors in Bulk Heterojunction Solar Cells*, S. F. Völker, S. Uemura, M. Limpinsel, M. Mingebach, C. Deibel, V. Dyakonov, C. Lambert, *Macromol. Chem. Phys.* **2010**, *211*, 1098-1108. Copyright (2010) WILEY-VCH Verlag GmbH & Co. KGaA, Weinheim; b) *Synthesis, Electrochemical, and Optical Properties of Low Band Gap Homo- and Copolymers Based on Squaraine Dyes*, S. F. Völker, T. Dellermann, H. Ceymann, M. Holzapfel, C. Lambert, *J. Polym. Sci., Part A: Polym. Chem.* **2014**, *52*, 890-911. Copyright (2014) WILEY-VCH Verlag GmbH & Co. KGaA, Weinheim.

shorter and thus possibly better soluble polymers. Indeed, this reaction resulted in the shorter polymer **P1B** ($M_n \sim 8100$, $X_n \sim 12$) with increased solubility (soluble in pure DCM and pure PhCN for example), however in lower yields.

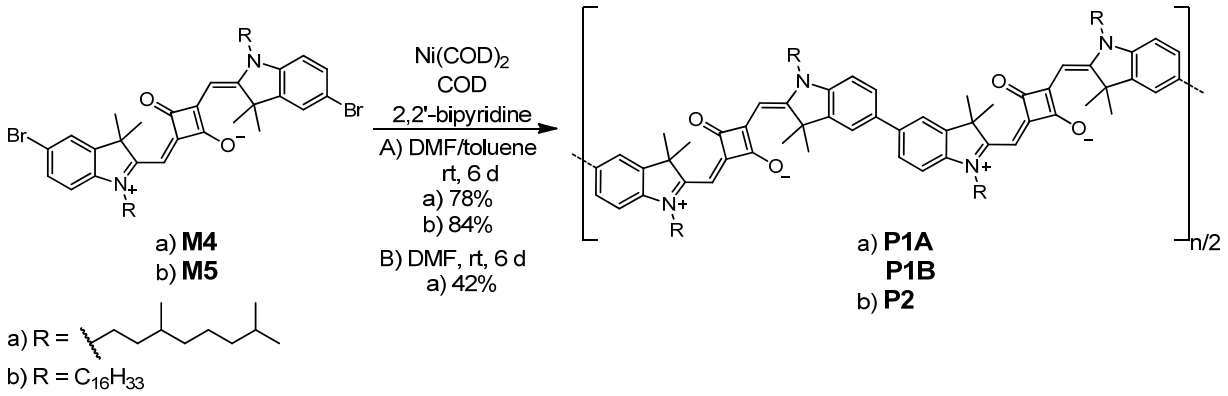

Scheme 9 Synthesis of homopolymers **P1A**, **P1B**, and **P2**.

Absorption Spectroscopy

Absorption and fluorescence spectra were recorded in $CHCl_3$ only (Table 3), due to the limited solubility of the polymers in other pure solvents. The homopolymers **P1A**, **P1B**, and **P2** show a broad main absorption band, covering a range of ~ 4000 cm^{-1} with a distinct intense absorption feature at the low energy side (Figure 15). The maximum of **P1A** is shifted by 2100 cm^{-1} to 13500 cm^{-1} compared to **M1** and the transition moment for the whole low energy band is $\mu_{eg} = 11.8$ D (monomer unit)$^{-1}$. The maximum of the absorption band of **P1B** is at 13600 cm^{-1}, at only slightly lower energy than **P1A** which shows that the effective conjugation length is reached at a degree of polymerisation $X_n = 12$ if not at already shorter lengths of the polymer. Besides, the maxima of **P1A** and **P2** are at the same energy despite the significant size difference of $X_n = 46$ and 33, respectively.

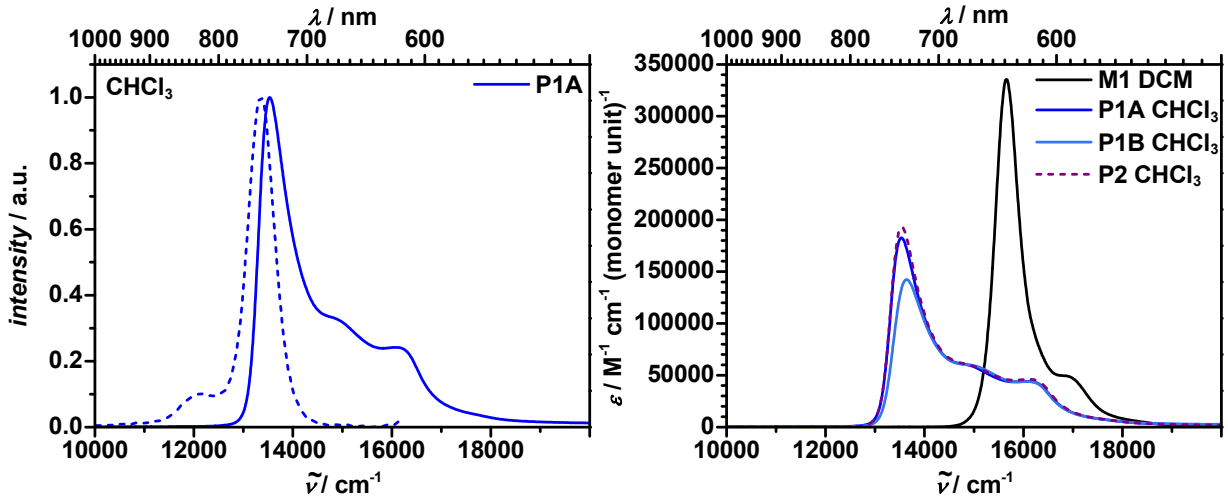

Figure 15 Left: Normalised absorption (solid line) and fluorescence (dashed line) spectra of **P1A** in $CHCl_3$. Right: Absorption spectra of **M1** in DCM and of the polymers **P1A**, **P1B**, and **P2** in $CHCl_3$.

Fluorescence Spectroscopy

In contrast to the monomeric compounds (Figure 12), the fluorescence spectra of the homopolymers are no mirror images to their absorption spectra but more like a mirror image to the monomer absorption spectra (Figure 15, left; due to the similarity of the spectra of the polymers and for the sake of a better survey, only the spectra of **P1A** are shown). The *Stokes* shift is as small as for the monomers (100–300 cm^{-1}) and fluorescence obviously only occurs from the lowest energy excitonic state with a quantum yield of around 0.25 (Table 3). The polymers exhibit biexponential fluorescence decays with both lifetimes in the low ns regime. The shorter lifetime of 1 ns is in the same range as those of the monomers and contributes with 97%. The slightly longer lifetime is around 8 ns.

Table 3 Absorption maxima, extinction coefficients, transition moments, fluorescence maxima, fluorescence quantum yields, and fluorescence lifetimes of homopolymers **P1A/B** and **P2**. Extinction coefficients ε and transition moments μ_{eg} of the polymers are given per monomer unit.

	solvent	λ_{abs} / nm	$\tilde{\nu}_{abs}$ / cm^{-1}	ε / $M^{-1}cm^{-1}$	μ_{eg} / D	λ_{fl} / nm	$\tilde{\nu}_{fl}$ / cm^{-1}	Φ_{fl}[a]	τ_{fl} / ns
M1	DCM	639	15700	336000	11.4	649	15400	0.19	1.0
	toluene	644	15500	340000	11.1	649	15400	0.35	1.9
P1A	$CHCl_3$	739	13500	183000	11.8	749	13400	0.28	1.0 (97.1) 8.1 (2.9)
	toluene	x	x	x	x	x	x	x	x
P1B	$CHCl_3$	733	13600	142000	11.1	744	13400	0.25	1.1 (97.0) 7.7 (3.0)
	toluene	x	x	x	x	x	x	x	x
P2	$CHCl_3$	738	13600	190000	12.2	751	13300	0.29	-
	toluene	x	x	x	x	x	x	x	x

- was not measured; x could not be determined. The values in brackets are the relative amplitudes of the corresponding fluorescence lifetimes. [a] During the writing process, the quantum efficiency of oxazine 1 was determined to be 0.15 by an absolute measurement using an integration sphere. However, the values reported for the squaraine dyes herein are still referenced against the quantum efficiency of 0.11 (see experimental section 5.1.2) as they were published to avoid confusion. Nevertheless, it has to be noted that the correct quantum efficiencies are larger by a factor of $0.15 / 0.11 \approx 1.36$.

Cyclic Voltammetry

The cyclic voltammograms of the bromine-substituted monomer **M5** and the polymers **P2** and **P1B** are all rather similar (Figure 16) despite the large size differences. The half-wave potentials $E_{1/2}$ of the reduction range between –1.66 and –1.69 V, those of the 1st oxidation between 60–110 mV, and those of the 2nd oxidation between 570–580 mV (Table 4). However, the redox waves of the polymers are broadened which can be interpreted by minor interaction of two adjacent monomeric units. Nevertheless, the remarkably small differences of the redox potentials show that in the ground state there is only a weak electronic interaction and the chromophores behave as almost independent redox moieties. According to the similar redox potentials, also the HOMO and LUMO energies $E_{HOMO/LUMO}$ of ca. –5.30 eV and –3.50 eV, respectively, barely differ.

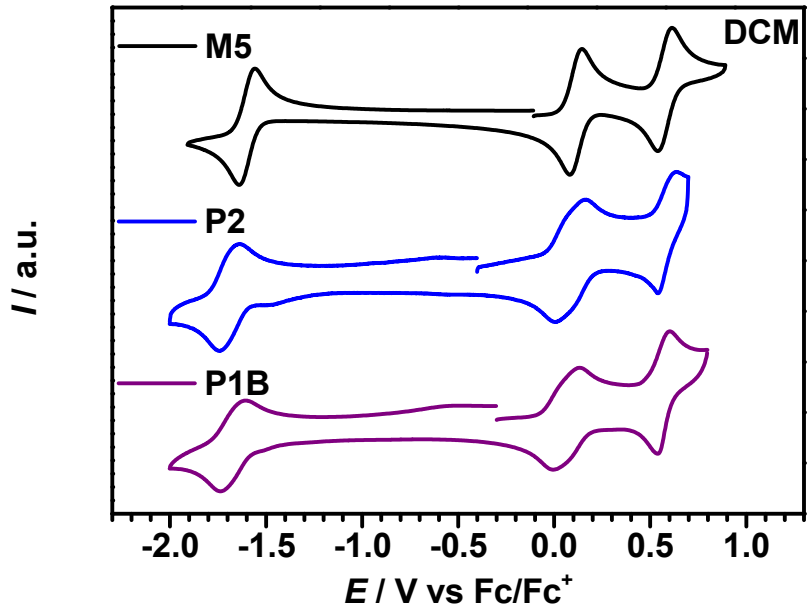

Figure 16 Cyclic voltammograms of **M5**, **P2**, and **P1B** in DCM/TBAHFP (0.1–0.2 M) at a scan rate of 250 mV s^{-1}.

Table 4 Redox potentials, HOMO and LUMO energy levels and band gaps obtained by electrochemical (E_{gap}^{CV}) and optical (E_{gap}^{opt}) methods of homopolymers **P1B** and **P2** together with monomeric dye **M5**.

	solvent	$E_{1/2}^{Red1}$ / mV	$E_{1/2}^{Ox1}$ / mV	$E_{1/2}^{Ox2}$ / mV	E_{HOMO} / eV[b]	E_{LUMO} / eV[b]	E_{gap}^{CV} / eV[b]	E_{gap}^{opt} / eV[c]
M5	DCM[a]	–1610	110	580	–5.27	–3.55	1.72	1.86
P2[e]	DCM[a]	–1690	90	590	–5.25	–3.47	1.77	1.63[d]
P1B	DCM[a]	–1671	62	570	–5.22	–3.49	1.73	1.63

[a] Ag/AgCl pseudo-reference electrode; [b] determined according to the procedure described in 5.1.4; [c] determined in DCM according to the procedure in 5.1.1; [d] determined in $CHCl_3$; [e] the polymer solution was filtered because the polymer did not completely dissolve in the solvent.

As has been seen for the spectroscopic properties, the effective conjugation length of the polymer is reached for **P1B** with $X_n = 12$. Considering the better solubility of the shorter polymer and the nearly size-independent electrochemical properties of squaraine

homopolymers, the increase in length of **P1B** may only affect morphological but not electronic properties.

Exciton Coupling

In analogy to the interpretation of the shifts and broadening of absorption bands in thiophene-bridged squaraine oligomers (**OS4**, Chart 9, p. 15),[67] the absorption features of the homopolymers **P1A**, **P1B**, and **P2** can be partly explained by exciton coupling theory.[130, 158] Exciton coupling of localised transition moments within the polymer chains shows mainly J-type behaviour (= red shift) with some H-type (= blue shift) contribution.

Two different possible idealised polymer structures are conceivable (Figure 17): a linear chain in which the monomers (and thus the polarisation of the allowed lowest energy transition) form a herring bone structure with an angle θ_A relative to the vector connecting the centres of the monomers (structure **Y**), and, alternatively, a zig-zag chain (**Z**) with angle θ_A. For the former, exciton coupling theory predicts a single allowed transition into the lowest energy exciton state (J aggregate). However, this is only the case for an ideal J-type structure with $\theta_A = 0°$. If $\theta_A \neq 0°$, transitions into exciton states of higher energy are also allowed but with lower intensity (see eq. (60) and (61) on p. 40 and eq. (48) on p. 36).

The exciton band width ΔE (difference of lowest and highest exciton energy) for the linear chain polymer is given by equation (67) in the point-dipole approximation where r is the centre-to-centre distance of the monomer units in the polymer.[159]

$$\Delta E = E_{\text{highest}} - E_{\text{lowest}} = 4V_{AB} = 4\frac{1}{hc4\pi\varepsilon_0}\frac{\mu_A\mu_B}{r^3}(1 - 3\cos^2\theta_A) \qquad (67)$$

For the alternative zig-zag arrangement, both excitations into the highest and the lowest exciton band are allowed, and the band width is given by equation (68).

$$\Delta E = E_{\text{highest}} - E_{\text{lowest}} = 4V_{\text{AB}} = 4\frac{1}{hc4\pi\varepsilon_0}\frac{\mu_{\text{A}}\mu_{\text{B}}}{r^3}(1+\cos^2\theta_{\text{A}}) \qquad (68)$$

From Figure 15 (p. 63) it is obvious that there is a transition at even higher energy (~ 16100 cm^{-1}) than the monomer HOMO→LUMO peak. This is caused either by the non-ideal J-type alignment (**Y**) of the polymer with $\theta_A \neq 0°$, or by the presence of zig-zag superstructure (**Z**). For both polymer types, the nearest-neighbour approximation leads to an exciton band width ΔE that corresponds to four times the electronic exciton coupling energy V_{AB}.[129] Assuming an angle θ_A of ca. 15° for **Y** and of 35° for **Z** (from AM1 optimisations[160]) gives roughly the same exciton band width. Thus, irrespective of the actual presence of either type **Y** or **Z** polymer section, the electronic coupling can be derived from the energy distance of the highest and lowest transition peak which is 2560 cm^{-1} and, thus, leads to $V_{AB} = \Delta E/4 = 640$ cm^{-1} as an average for the polymer **P2**. The point-dipole approximation (equation (68) with $r = 15$ Å and $\mu_{eg} = 11.9$ D) yields $V_{AB} = 370$ cm^{-1} for type **Z** conformer and $V_{AB} = 330$ cm^{-1} (with equation (67) and r = 16 Å) for type **Y**. Although these values are about half of that derived from the observed band width they essentially support the excitonic model. However, it does not explain all optical features of the squaraine polymers and it can not be excluded that direct conjugational effects also add to the observed absorption band within the polymer. Therefore, semiempirical CNDO/S2 calculations were performed (see below).

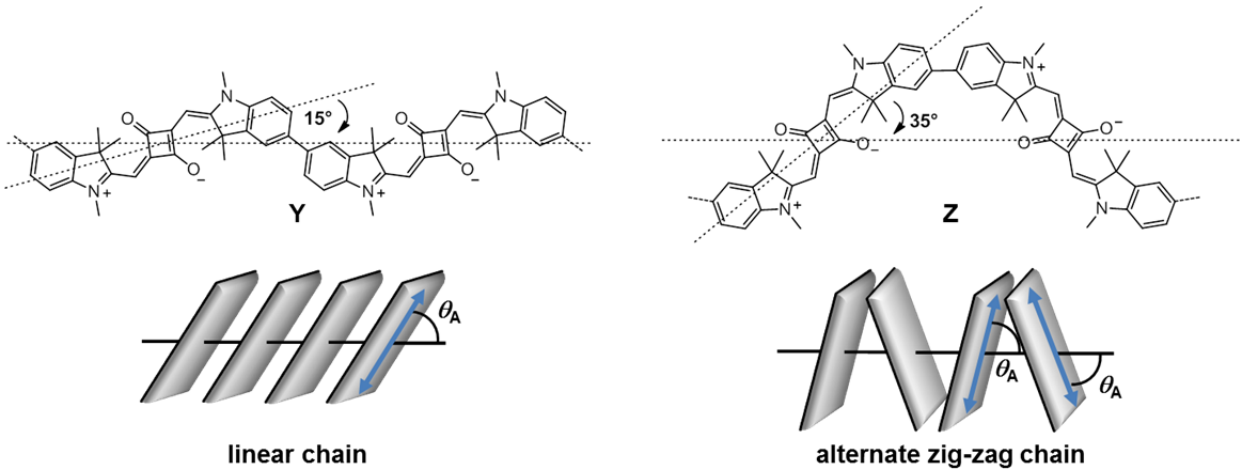

Figure 17 AM1 optimised polymer sections with elongated herring bone (**Y**) and zig-zag structure (**Z**).

Semiempirical Calculations[1]

In order to gain a deeper insight into the electronic structure of the polymers and the interaction of monomers, and to probe the effect of conjugation, semiempirical calculations were performed. Also the interaction with bridge molecules such as thiophene or carbazole was investigated for the corresponding copolymers, however, these results are described in section 3.4.8. First, the structure of a model hexamer was optimised using again the AM1 hamiltonian.[160] For simplicity and the ease of optimisation, the alkyl chains were replaced by methyl groups. The most elongated structure that could be modelled (**Y**-type) was used and other conformers that may have more strongly bent zig-zag structures (**Z**-type) were neglected. Therefore, the stretched conformers were investigated only. In these conformers the angle between the chromophores approaches 0° leading to a J-type exciton behaviour for which only transitions into the lowest excited state of the exciton manifold are optically allowed. Although the effective conjugation length may not be reached with a hexamer, it is close to.

In order to probe the effect of direct conjugation, the dihedral angle between the squaraine monomers was modified (Figure 18). Thus, a dihedral angle of 0° will enhance conjugation, an angle of 90° will inhibit conjugation and will leave exciton coupling (besides some hyperconjugative effects) to be the only mechanism at work for interaction. Using the thus obtained geometry, CNDO/S2 calculations[161] were performed to get the excited states. The electronic exciton coupling energy V_{AB} was again estimated by $V_{AB} = \Delta E/4$ where ΔE is the energy difference between the lowest and highest excited state of the excitonic manifold, respectively.

[1] The semiempirical calculations were performed by *Dr. Marco Holzapfel* or *Prof. Dr. Christoph Lambert*.

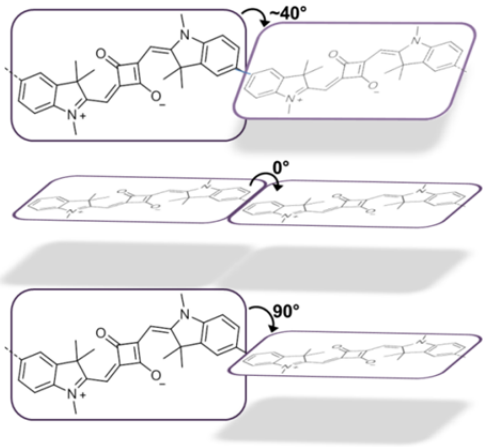

Figure 18 Models of polymer sections showing the different dihedral angles between two squaraine subunits.

For **P2** (likewise **P1A** or **P1B**, but due to the similarity **P2** will be used as in the previous chapter), AM1 optimisations gave, as expected, planar squaraines and dihedral angles between them of 39–41°. The CNDO/S2 calculated transition energies and oscillator strengths of this model hexamer together with those of the monomer **M1** are given in Table 5. Additionally, the exited states energies of an optimised dimer were calculated. Therefore, the optimised geometry of the hexamer model was used and the model reduced to a dimer.

Table 5 CNDO/S2 excited states energies ($\tilde{\nu}$), corresponding oscillator strengths (*f*), and electronic coupling energies (*V*) based on AM1 optimised geometries of hexameric structures of polymers of the type **P2**.

structure	$\tilde{\nu}$ / cm^{-1} *f*						V_{AB} / cm^{-1}
monomer (M1)	16678 1.79						
dimer[a]	16500 3.92	18065 0.19					783
polymer optimised	16437 9.79	17019 0.07	17682 0.74	18346 0.01	18886 0.32	19122 0.80	671
polymer dihedral angle = 0°	15997 10.39	16655 0.04	17429 0.81	18199 0.00	18823 0.35	19095 0.00	774
polymer dihedral angle = 90°	16817 6.67	17341 0.10	17922 0.78	18435 0.24	18831 0.91	18906 3.08	522

[a] the dimer structure was taken from the optimisation of the polymer.

The CNDO/S2 calculations of the monomeric model compound **M1** gave a lowest energy transition of ca. 16700 cm^{-1} which is around 1000 cm^{-1} too high in energy compared to experiment. For the dimeric compound, exciton coupling theory yields two excited states. The one at lower energy is allowed and carries roughly twice the oscillator strength of the monomer while the one at higher energy is forbidden and exhibits only minor oscillator strength. For dimers, the exciton coupling energy V_{AB} is half of the exciton splitting and therefore derived by $V_{AB} = \Delta E/2$ instead of $V_{AB} = \Delta E/4$ which is the case of infinitely long polymers.

The CNDO/S2 computation of the model hexamers of **P2** gave six lowest energy transitions in a close energy range which form the exciton manifold. The lowest energy transition carries almost all of the oscillator strength which is thus ca. 6-fold of the one of the respective monomer. This situation thus resembles a typical J-aggregate behaviour. However, only a slight decrease of the lowest energy compared to the monomer **M1** is predicted. This contrasts the experimental behaviour where a quite remarkable red shift of 2100 cm^{-1} was found. Nevertheless, the calculated exciton coupling energy $V_{AB} = 671$ cm^{-1} is in excellent agreement with one fourth of the experimentally observed band width (640 cm^{-1} from the peak to peak width of the highest and lowest energy peak in Figure 15).

Artificial planarisation of the polymer leads to an increase of apparent exciton coupling energy (774 cm^{-1}) and 90° orientation between the squaraine dyes to a decrease to 522 cm^{-1}. From these values it is apparent that ca. 78% of the electronic coupling of the optimised polymer stems from exciton coupling interactions and the remainder from conjugation.

Conclusion

In order to synthesise homopolymers with broad low energy absorption, the Ni-mediated *Yamamoto* homocoupling reaction proved rather useful. It even performed so well, that the polycondensation reaction proceeded until large amounts of the polymers precipitated in the reaction solution. However, this resulted in polymers **P1A** and **P2**

whose solubility is limited to $CHCl_3$ and solvent mixtures. The exchange of the linear alkyl chain (**P2**) by a branched one **(P1A**) did not lead to a polymer with increased solubility, but to a larger polymer with the same solubility issue. Nevertheless, by exchange of the solvent mixture from toluene/DMF to pure DMF it was possible to synthesise smaller polymers (**P1B**) with increased solubility.

The absorption spectra of all polymers are red-shifted compared to parent squaraine **M1** and strongly broadened. By analysis of the spectra, the use of the point-dipole approximation, and semiempirical calculations, these features were attributed to be mainly caused by exciton coupling of the chromophores and to some minor extend also to conjugational effects. At least two different superstructures of the polymer contribute to the spectra. The strong lowest energy absorption is induced by a linear J-type arrangement whereas a zig-zag type structure explains the additional transitions at higher energies (Figure 15, p. 63). However, while the strong red shift reflects a decreased optical band gap of the polymers compared to parent squaraine **M1**, the electrochemically determined band gap was barely influenced, indicating negligible interaction of the chromophores in the ground state in contrast to the exciton coupling of excited states.

To sum up, the synthesis of squaraine homopolymers and the resulting occurrence of exciton coupling is a good approach in order to generate compounds with broad and red-shifted absorption in the red to NIR region. The centre-to-centre distance of the chromophores plays a role in the exciton coupling strength (see eq. (1)) and the planarity of the polymer contributes to conjugational effects. For this reason, the initially synthesised homopolymer of *Havinga et al.* (**PS2**, Chart 10, p. 16), where two indolenine units are fused in one moiety, might constitute the upper limit for indolenine squaraine polymers in terms of broad low energy absorption.

3.2.3 Dicyanomethylene-Substituted *cis*-Squaraine Homopolymers[1]

Synthesis

The polycondensation reactions of the dicyanomethylene-substituted dyes **M6** and **M7** to the polymers **P3** and **P4**, respectively, were carried out likewise to the polycondensations of **M4** and **M5**. Only in case of **M6**, the reaction was performed at 65°C over a period of 6 d (Scheme 10). Various solvents were used for the *Soxhlet* extractions to purify the polymers. The number average molecular weights M_n of the total crude polycondensation products of **P3** and **P4** are ~ 6100 and ~ 8300, the degrees of polymerisation X_n are ~ 7 and ~ 11, respectively.

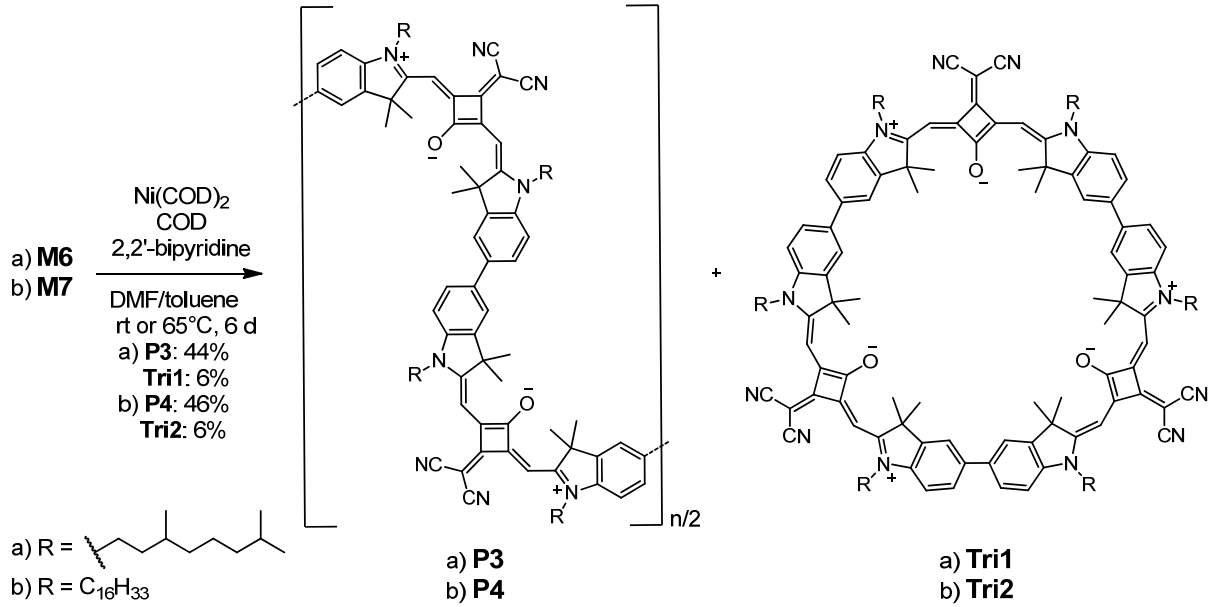

Scheme 10 Synthesis of homopolymers **P3** and **P4** and the cyclic trimers **Tri1** and **Tri2**.

In order to investigate the influence of molecular weight on the optical properties, the crude polymers were separated on a preparative recycling GPC ($CHCl_3$) to yield batches of polymers of different molecular weight distribution. Since the main part of the polymers was soluble in acetone, this fraction was used for the separation. In a first run on the preparative recycling GPC the fractions **P3-1** (**P4-1**) and **P3-2** (**P4-2**) were

[1] Reproduced or adapted in part with permission from *Exciton Coupling Effects in Polymeric cis-Indolenine Squaraine Dyes*, S. F. Völker, C. Lambert, *Chem. Mater.* **2012**, *24*, 2541-2553. Copyright 2012 American Chemical Society.

separated as indicated by the dotted lines in Figure 19. In this process, an eye-catching peak was observed in the chromatograms of both polycondensation reactions at a similar retention time which could be isolated in this process. This peak refers to a cyclic trimer (Scheme 10) as was confirmed by mass spectrometry and NMR spectra and whose formation is facilitated by the *cis*-structure of the squaraine monomer. These cyclic trimers (**Tri1**, **Tri2**) could be isolated in 6% yield and will be described in more detail in chapter 3.6 (p. 197). The polymeric fractions show relatively small polydispersities (M_w/M_n = 1.2–1.8) due to the preparative splitting. The number average molecular weights M_n are ~ 17500 (**P4-1**) and ~ 25600 (**P3-1**) for the heavier molecular weight fractions and ~ 6600 (**P4-2**) and ~ 8600 (**P3-2**) for the lighter ones (Table 25, p. 210). As the optical properties of the hexadecyl and 3,7-dimethyloctyl-substituted squaraines do not differ, the four polymers can thus be viewed as being a series with increasing number average degree of polymerisation X_n: 7.4 (**P4-2**), 11.8 (**P3-2**), 19.7 (**P4-1**), and 35.5 (**P3-1**). The polydispersity increases with increasing degree of polymerisation. All those polymers are well soluble in solvents like $CHCl_3$, DCM, toluene, 1,2-dichlorobenzene, and chlorobenzene.

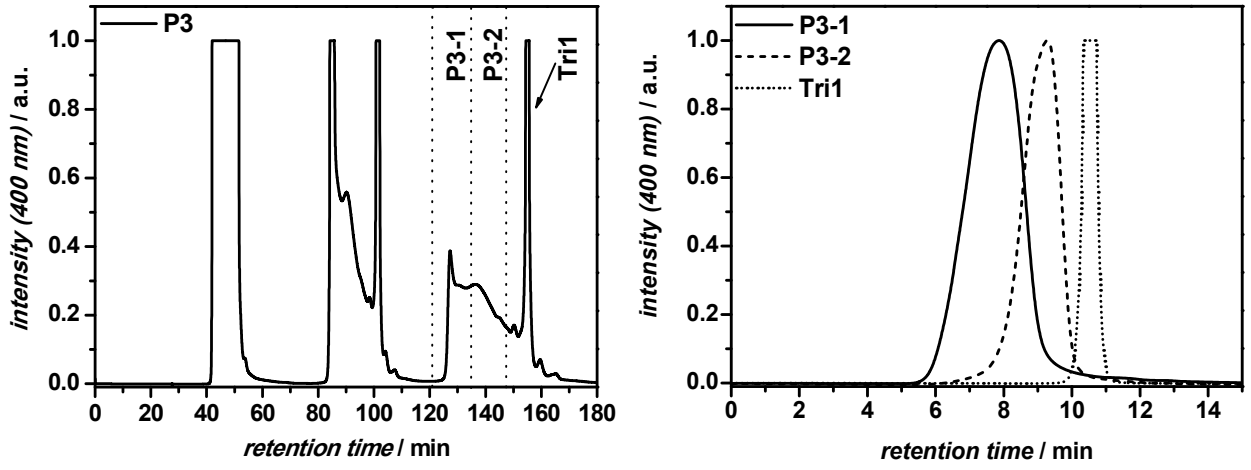

Figure 19 Chromatograms of preparative recycling GPC of **P3** (left) and of analytic GPC of the isolated fractions **P3-1**, **P3-2**, and the cyclic trimer **Tri1**.

Polymerisation of the dicyanomethylene-substituted dye **M9** was performed similarly to **M6** at 65°C for 6 d (Scheme 11). Likewise, a cyclic trimer (**Tri3**) was obtained in nearly the same yield as the previous timers **Tri1** and **Tri2**. In addition to this, even a cyclic

tetramer (**Tet1**) could be isolated, even though in only very low yield. The macrocyclic compounds are described in more detail in chapter 3.6 (p. 197).

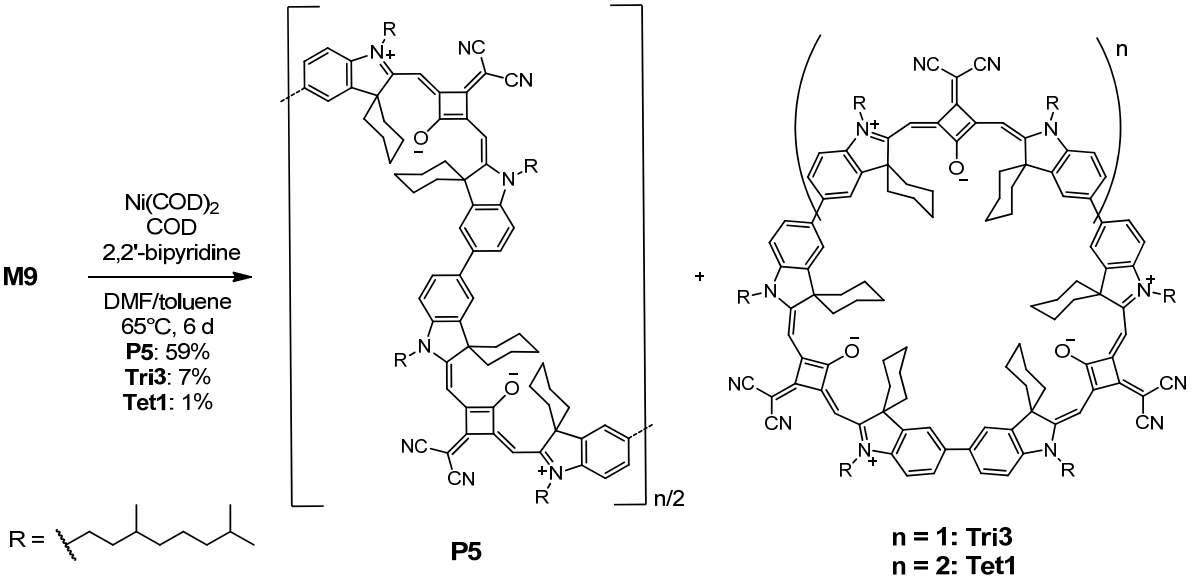

Scheme 11 Synthesis of the homopolymer **P5** and the macrocycles **Tri3** and **Tet1**.

Absorption Spectroscopy

The dicyanomethylene-substituted *cis*-indolenine squaraine homopolymers have a distinct better solubility in various solvents compared to the homopolymers **P1A**, **P1B**, and **P2**. Therefore it was possible to perform absorption spectroscopy in additional solvents to $CHCl_3$.

The polymers **P3-1**, **P3-2**, **P4-1**, and **P4-2** all display a broad absorption in the visible red to NIR region (Table 6, p. 80) which covers a range of ~ 3500 cm^{-1}. In DCM, the maximum is at the low energy side of this broad absorption band at 13000 cm^{-1} (Figure 20), which is 1600 cm^{-1} lower compared to the monomer **M2** (14600 cm^{-1}). The extinction coefficients are around 70000 M^{-1} cm^{-1} (monomer unit)$^{-1}$, but even though they are remarkably smaller compared to the monomer (236000 M^{-1} cm^{-1}), the transition moments are rather similar with values of 10.6 D for **M2** and 9.6 D (monomer unit)$^{-1}$ for **P3-1**.

In toluene the shape of the broad absorption band differs to the one in DCM and shows three almost equally intense (~ 55000 M^{-1} cm^{-1} (monomer unit)$^{-1}$) maxima around 12900 cm^{-1}, 13600 cm^{-1}, and 14500 cm^{-1}. The spectra of the polymers are nearly identical irrespective of molecular weight and the alkyl chain substituent. In particular, the transition moment of the main absorption band in toluene is around 9 D (monomer unit)$^{-1}$ for all polymers.

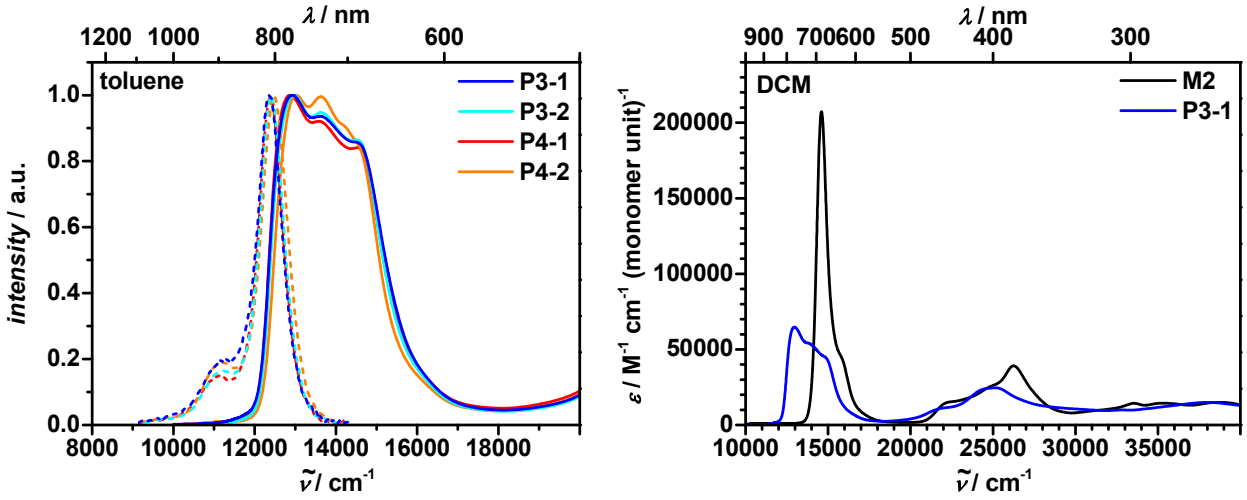

Figure 20 Left: Normalised absorption (solid lines) and fluorescence (dashed lines) spectra of **P3-1/2** and **P4-1/2** in toluene. Right: Absorption spectra of **M2** and **P3-1** in DCM.

The homopolymer **P5** has not been split into several fractions and therefore still shows a higher polydispersity of 2.66. Comparison with **P4-1**, which is closest in the number average degree of polymerisation (**P5**: X_n = 15.8; **P4-1**: X_n =19.7), shows that in $CHCl_3$ the lowest energy absorption band is slightly shifted to lower energy (Table 6, p. 80), as already seen for the monomer **M9** (Figure 11, p. 52) but elsewise the absorption spectrum barely differs (not shown).

For simplicity, the following discussion will focus on **P3-1** which is the largest of the polymers of this kind. Due to the distinct difference of the proportions of the local maxima in the absorption spectra of the polymers in toluene and DCM, absorption spectra of **P3-1** were also measured in a series of solvents that differ in polarity, aromatic character, and hydrogen bond donor property (Figure 21). Comparison of the spectra in $CHCl_3$, DCM, and toluene reveals that the local maxima are at the same energy but the bands at higher energies increase in relative intensity from $CHCl_3$ to toluene. In PhCN

the three local maxima have nearly the same intensity but a weak shoulder, due to a fourth band at even higher energy, is visible. In DMF this shoulder is more pronounced and shifts the maximum of the highest energy band to even higher energies while the maxima of the other bands at lower energy decrease in intensity. In acetone, where the polymer is not completely soluble, this trend further increases: now the former shoulder at highest energy is the maximum absorption and all other bands show decreasing relative intensities on going to lower energy. The absorption maximum at highest energy shifts hypsochromic from 14800 cm^{-1} (PhCN) to 15100 cm^{-1} (DMF) and to 15400 cm^{-1} (acetone). Again the measured transition moments of the main transitions range between 8.9 D (monomer unit)$^{-1}$ (PhCN, toluene) and 9.6 D (monomer unit)$^{-1}$ ($CHCl_3$, DCM).

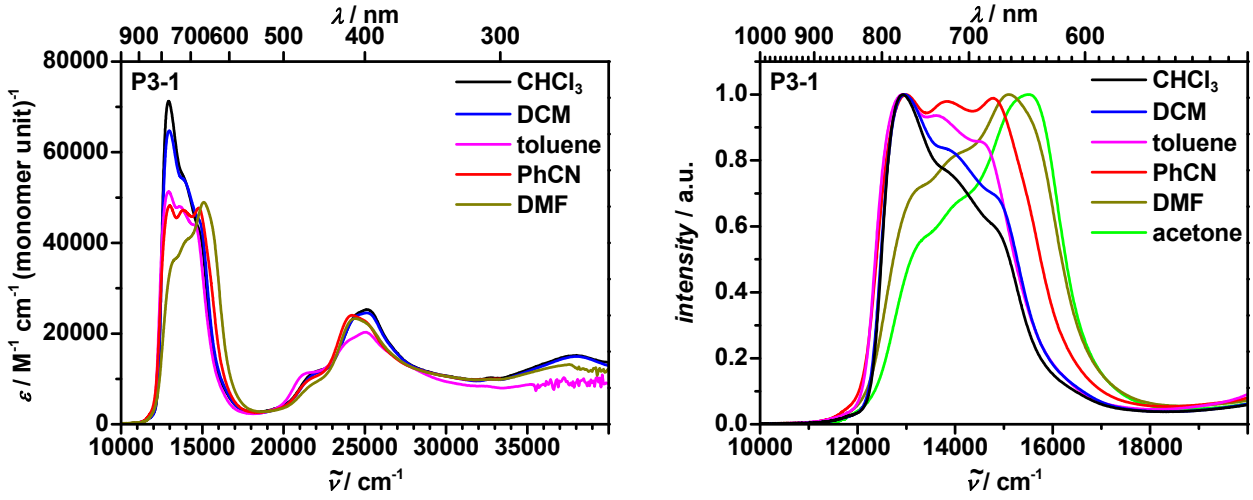

Figure 21 Left: Absorption spectra of **P3-1** in various solvents. Right: Normalised absorption spectra of **P3-1** in various solvents magnified at the low energy band.

In addition to the absorption spectra in solution, solid state absorption spectra of **P3-1** in a film were measured. Therefore, a solution of **P3-1** was spin-coated onto a glass substrate (2.5 mg ml^{-1}, 2000 r min^{-1}). Taking into account the differences of the absorption spectra in different solvents, the question is whether these properties are maintained in the film when prepared from solutions in different solvents. Thus, three solvents were chosen to prepare concentrated solutions for spin-coating: $CHCl_3$, DMF, and toluene. The spectra of the films were then measured with an integration sphere.

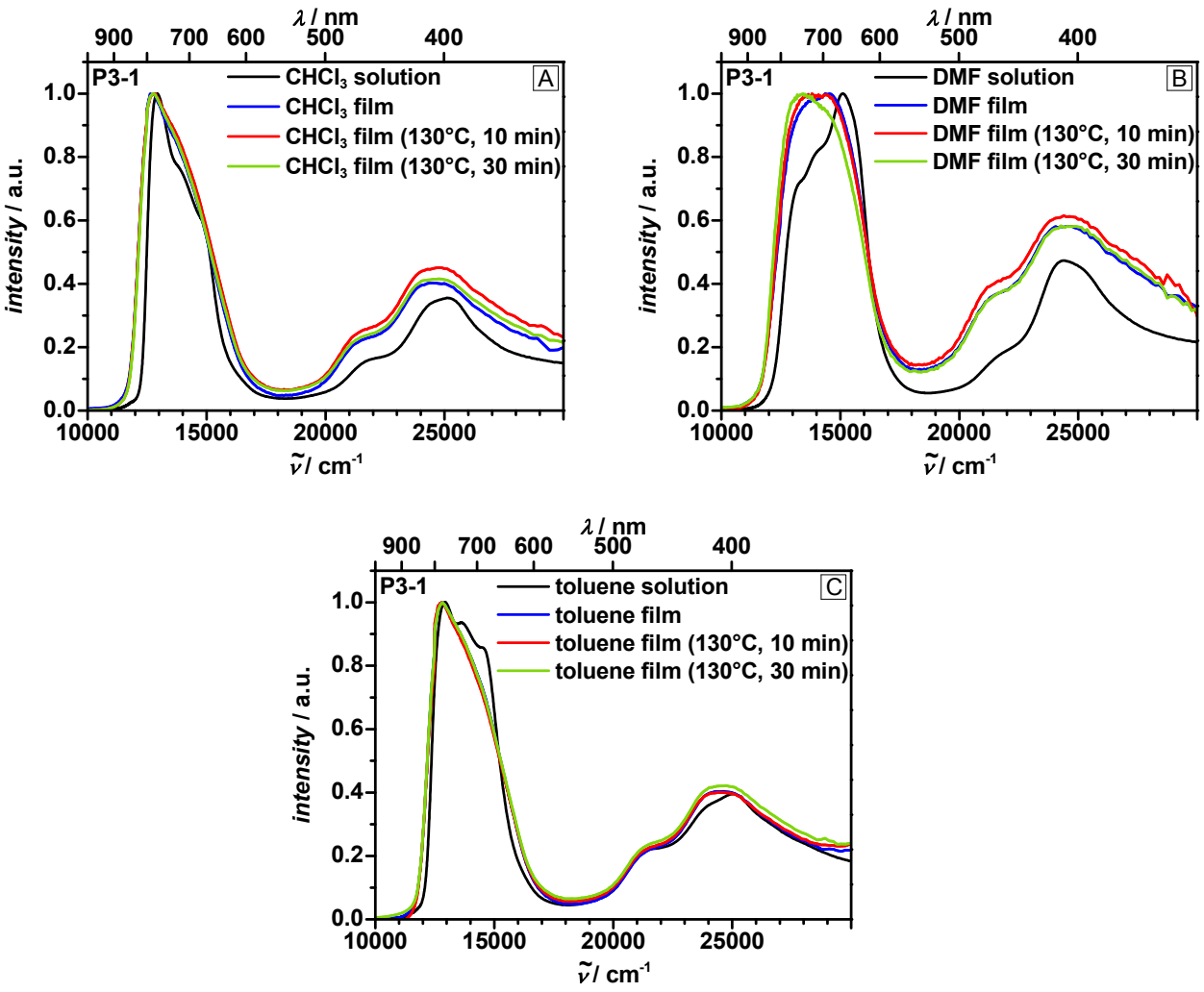

Figure 22 Normalised absorption spectra of **P3-1** in solution and in solid state as film spin-coated from $CHCl_3$ (A), DMF (B), and toluene (C).

For all films in common is the fact that the main absorption band loses its structure with the three local maxima and a slight broadening and bathochromic shift is observed. For films spin-coated from $CHCl_3$ solution (Figure 22 A) and toluene (C) the spectra are nearly identical and quite similar to the spectra measured in $CHCl_3$ solution with the maximum at 12800 cm^{-1}. However, in case of DMF (B) the situation is different. Similar to the spectrum in solution, the absorption maximum of the film is found at the high energy side of the main absorption band at 14500 cm^{-1} with a pronounced bathochromic shift. As annealing can lead to a structural reorganisation in the films, the absorption spectra were recorded again after annealing the substrates for 10 min and 30 min at 130°C. While no changes were observed in the films prepared from $CHCl_3$ and toluene, the one prepared from DMF shows significant differences upon annealing. As mentioned above, the maximum is at the high energy side of the main absorption band right after

film preparation. After 10 min at 130°C, a plateau is found from 13500–14500 cm^{-1} and after 30 min of annealing the maximum moves to the low energy side of the absorption band at 13400 cm^{-1}. Thus it appears that there is a thermodynamically favoured structure which is already present in solutions and in films of $CHCl_3$ and toluene but not in DMF solution and its pristine film, but which is gradually formed upon annealing of the films.

Fluorescence Spectroscopy

In contrast to the monomer model dye **M2**, the polymers **P3-1**, **P3-2**, **P4-1**, and **P4-2** (from here abbreviated as **P3/4**) all show fluorescence only in toluene. Similar to the homopolymers **P1A**, **P1B**, and **P2** (from here abbreviated as **P1/2**) the shape of the fluorescence band is no mirror image to the absorption band but looks like the fluorescence band of the monomer (Figure 20, p. 75), only shifted to lower energy (~ 12400 cm^{-1}). Despite the varying size of the polymers all spectra look nearly identical and the *Stokes* shift is around 500–600 cm^{-1} (Table 6, p. 80).

The fluorescence quantum yields Φ_{fl} of the polymers are lower compared to **M2** (0.41) and decrease with increasing degree of polymerisation from 0.19 ($X_n = 7.4$) to 0.06 ($X_n = 35.5$).

Fluorescence lifetimes τ_{fl} were measured in the ns time regime and the compounds were excited with a 650 nm laser diode. For all polymers, biexponential decays are observed with lifetimes around 5.6 ns and 1.6 ns (Figure 23). However, a closer inspection of the biexponential decays revealed an increase of the relative amplitude of the shorter component with increasing X_n.

While the excitation wavelength for both static and time-resolved fluorescence measurements was chosen for technical reasons (fixed laser diode wavelength, small *Stokes* shift) to be at the high energy side of the absorption bands, it is unlikely that the emission spectra or the kinetics are influenced by this choice as fast energy transfer dynamics beyond the time resolution of our set-up (ca. 200 ps by deconvolution with IRF) are assumed.

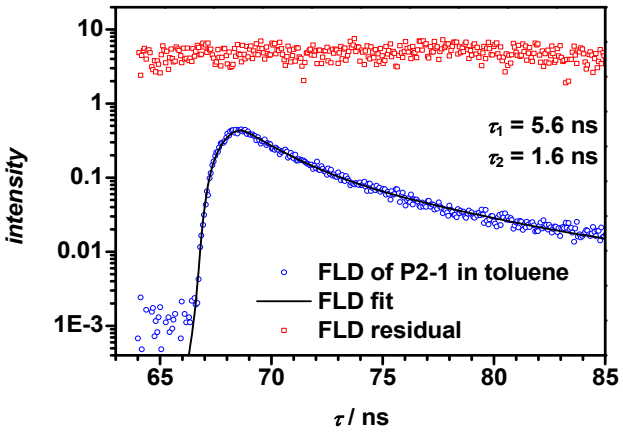

Figure 23 Fluorescence decay of **P3-1** in toluene. Excitation energy $\tilde{\nu}$ = 15400 cm^{-1} (λ = 650 nm).

The fluorescence quantum yield Φ_{fl} and the fluorescence τ_{fl} lifetime were used to calculate the average rate constant of the fluorescent decay $\bar{k}_{fl}$ and the non-radiative decay $\bar{k}_{nr}$ using equations (69) and (70). For the polymers the average fluorescence lifetime was used, which was obtained by equation (71) to calculate the rate constants, where α_x are the relative amplitudes of the corresponding lifetimes.

$$\bar{k}_{fl} = \frac{\Phi_{fl}}{\tau_{fl}} \tag{69}$$

$$\bar{k}_{nr} = \frac{1-\Phi_{fl}}{\tau_{fl}} \tag{70}$$

$$\bar{\tau} = \frac{\alpha_1 \tau_1^2 + \alpha_2 \tau_2^2}{\alpha_1 \tau_1 + \alpha_2 \tau_2} \tag{71}$$

Table 6 Degree of polymerisation, absorption maxima, extinction coefficients, transition moments, fluorescence maxima, fluorescence quantum yields, fluorescence lifetimes, and rate constants of the fluorescent and non-radiative decays of homopolymers **P3/4** in toluene. Extinction coefficients ε and transition moments μ_{eg} of the polymers are given per monomer unit.

	X_n	$\tilde{\nu}_{abs}$ / cm^{-1}	ε_{abs} / M^{-1}cm^{-1}	μ_{eg} / D	$\tilde{\nu}_{fl}$ / cm^{-1}	Φ_{fl}[a]	τ_{fl} / ns	$\bar{\tau}$ / ns	$\bar{k}_{fl}$ /10^8 s^{-1}	$\bar{k}_{nr}$ /10^8 s^{-1}
M2		14300	236000	10.1	14000	0.41	4.5		0.91	1.31
M9		13900	220000	10.0	-	-	-	-	-	-
		13000	61000	9.1	12500	0.19	5.4 [0.26]	3.7	0.52	2.20
P4-2	7.4						1.6 [0.74]			
		(13100)	(67000)	(10.0)	x	x	x	x	x	x
		13000	56000	9.0	12400	0.13	5.7 [0.18]	3.4	0.38	2.53
P3-2	11.8						1.8 [0.82]			
		(13000)	(74000)	(10.4)	x	x	x	x	x	x
		12900	59000	9.3	12400	0.10	5.7 [0.16]	3.2	0.31	2.78
P4-1	19.7						1.6 [0.84]			
		(12900)	(71000)	(9.9)	x	x	x	x	x	x
P3-1	35.5									
toluene		12900	51000	8.9	12300	0.06	5.6 [0.14]	3.1	0.19	3.03
							1.6 [0.86		x	x
DCM		(13000)	(65000)	(9.6)	x	x	x	x	x	x
$CHCl_3$		12900	71000	9.6	x	x	x	x	x	x
PhCN		13000	48000	8.9	x	x	x	x	x	x
DMF		15100	49000	9.0	x	x	x	x	x	x
P5	15.8									
$CHCl_3$		12800	77400	9.9	12400	0.02	-	-	-	-

The values in round brackets refer to measurements in DCM. The values in square brackets are the relative amplitudes of the corresponding fluorescence lifetimes; - was not measured; x could not be determined. [a] During the writing process, the quantum efficiency of oxazine 1 was determined to be 0.15 by an absolute measurement using an integration sphere. However, the values reported for the squaraine dyes herein are still referenced against the quantum efficiency of 0.11 (see experimental section 5.1.2) as they were published to avoid confusion. Nevertheless, it has to be noted that the correct quantum efficiencies are larger by a factor of $0.15 / 0.11 \approx 1.36$.

Cyclic Voltammetry

The electronic properties were investigated for one monomeric dye (**M7**) and two homopolymers of different size (**P3-1** and **P3-2**). In similarity to the *trans*-homopolymers shown above (**P1/2**), no major differences are observed in the cyclic voltammograms. All compounds show one reduction wave and two oxidation waves. While those of **M7** are rather sharp, those of the polymers are broadened. However, the half-wave redox potentials only differ by less than 60 mV in all processes and are found at ca. –1460 mV (reduction), 175 mV (1st oxidation), and 575 mV (2nd oxidation). Similar values are observed for **P5** (not shown) whose 2nd oxidation was not recorded due to a solvent batch of minor quality. As shown before for **P1/2**, also for the dicyanomethylene-substituted homopolymers there is only minor electronic interaction between the single chromophores in the ground state.

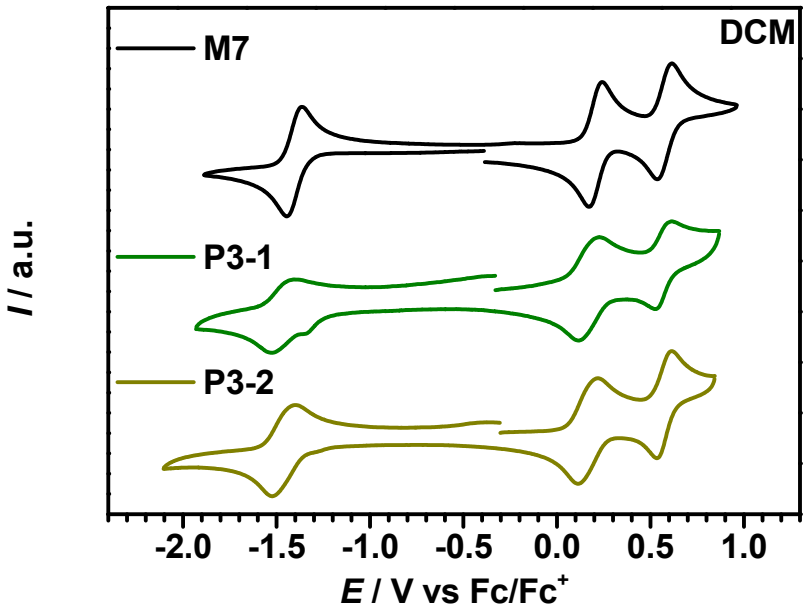

Figure 24 Cyclic voltammogram of monomer **M7** and homopolymers **P3-1** and **P3-2** in DCM/TBAHFP (0.1–0.2 M) at a scan rate of 250 mV s^{-1}.

Table 7 Redox potentials, HOMO and LUMO energy levels and band gaps obtained by electrochemical (E_{gap}^{CV}) and optical (E_{gap}^{opt}) methods of homopolymers **P3-1**, **P3-2**, and **P5** together with monomer **M7**.

	solvent	$E_{1/2}^{Red1}$ / mV	$E_{1/2}^{Ox1}$ / mV	$E_{1/2}^{Ox2}$ / mV	E_{HOMO} / eV[c]	E_{LUMO} / eV[c]	E_{gap}^{CV} / eV[c]	E_{gap}^{opt} / eV[d]
M7	DCM[a]	–1405	207	576	–5.37	–3.76	1.61	1.71
P3-1	DCM[a]	–1465	175	573	–5.34	–3.70	1.64	1.52
P3-2	DCM[a]	–1463	165	574	–5.33	–3.70	1.63	1.52
P5	DCM[b]	–1485	146		–5.30	–3.67	1.63	1.51[e]

[a] Ag/AgCl pseudo-reference electrode; [b] Ag/AgCl "leak free" electrode; [c] determined according to the procedure described in 5.1.4; [d] determined in DCM according to the procedure in 5.1.1; [e] determined in $CHCl_3$ likewise to the procedure in DCM.

Exciton Coupling[1]

When the *cis*-indolenine homopolymers **P3/4** are compared with the *trans*-indolenine homopolymers **P1/2**, it can be seen that even though the polymer weight is similar, the absorption spectra differ. While the lowest energy absorption band of **P3/4** in toluene comprises three almost equally intense features within 12000–17500 cm^{-1}, that of **P1/2** is highly asymmetric with a very intense band at the lowest energy side of the band manifold between 13000–17300 cm^{-1}. Those spectral features were discussed to stem from exciton coupling of localised transition states mainly with less contribution from conjugational effects (chapter 3.2.2). This seems also to be reasonable for **P3/4** as the electrochemical characterisation indicates weak electronic interactions of the squaraine chromophores in the ground state (see below).

Likewise to the *trans*-indolenine homopolymers, semiempirical AM1 calculations[160] were performed on hexameric models of the *cis*-indolenine homopolymers (Figure 25; again, for simplicity and the ease of optimisation, the alkyl chains were replaced by methyl groups so the modelled hexamers are suitable for **P3** and **P4**). Owing to the bent *cis*-structure of the parent chromophore, the stiff but conformationally flexible biaryl

[1] Semiempirical calculations were performed by *Prof. Dr. Christoph Lambert*.

axis and the fact that cyclic trimers could be isolated in the synthetic process, several different macromolecular superstructures are conceivable. Therefore, apart from an elongated zig-zag form, also a helical, an open loop, and a mixed structure with both helical and zig-zag contributions were optimised.

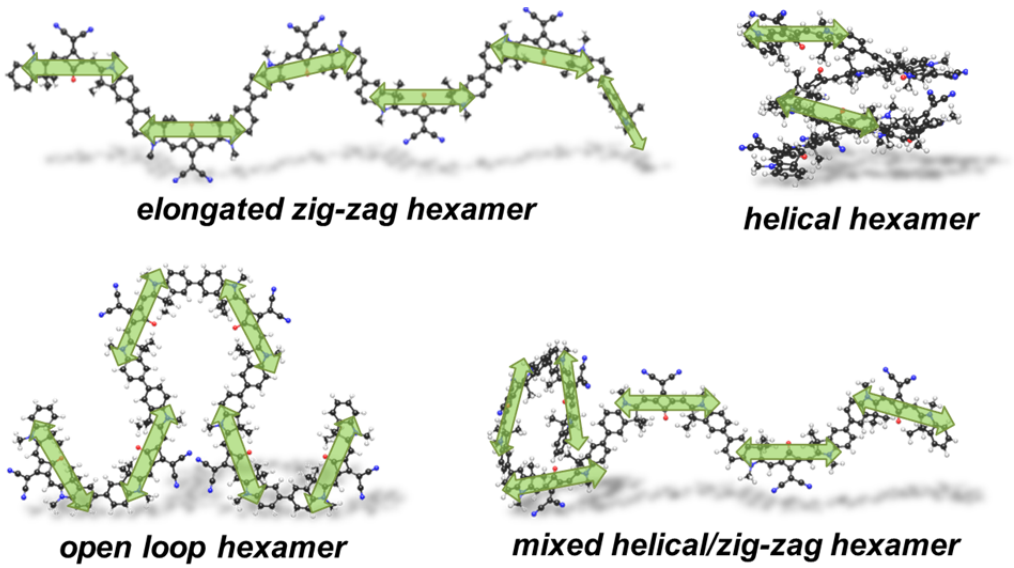

Figure 25 AM1 optimised superstructures (for simplicity the alkyl chains are replaced by methyl groups) of the elongated zig-zag, helical, open loop, and mixed helical/zig-zag hexamer. The orientation of localised transition moments of the lowest energy squaraine transition is indicated by the green arrows.

The elongated zig-zag structure shows an angle of ~ 114° between the centres of the squaric ring. The helical motif has ca. 2.7 monomer units per helix turn and the squaraine chromophores possess a tilt and shift π-stack arrangement where the alkyl chains extend radially from the tube formed by the helix (not shown because the alkyl chains have been replaced by methyl groups in the calculations). Alternatively to the helix, an open loop structure can be formed. In reality, mixtures of these structures may be present in a polymer strand as indicated for the mixed helical/zig-zag hexamer.

For the interpretation of the absorption spectra by exciton coupling theory, it has to be kept in mind that the transition moment of the lowest energy transition of a monomeric squaraine chromophore is polarised along the long molecular axis, i.e. along the *N*-*N*-vector or the indolenine nitrogen atoms. Owing to the C_{2v} symmetry of the monomeric unit there is also a short axis polarised transition, which is at significantly higher energy and does not play a role in the discussion here.

For the elongated zig-zag hexamer, exciton coupling theory predicts a single intense transition at low energy and five transitions at higher energy (J-type behaviour). This is in agreement with what is found by CNDO/S2 calculations: a strong transition at 14700 cm^{-1} and five almost negligible transitions between 15300–16900 cm^{-1} (Table 8). Much in contrast, in case of the helix-like arrangement, exciton coupling theory predicts two different excitonic interactions: one H-type behaviour (parallel orientation of transition moments) due to the stacked π-systems and another interaction that is the consequence of two consecutive chromophores which are arranged in a ca. 70° angle. Together both excitonic interactions lead to two allowed transitions into higher lying states, followed by four states that are forbidden. The CNDO/S2 calculations indeed give two strong transitions at 17800 and 17500 cm^{-1} and four very weak lower energy transitions between 17200–15300 cm^{-1}. The open loop hexamer also shows a very prominent single band but at intermediate energy (16500 cm^{-1}). Interestingly, the individual energies of the six transitions of these three hexamers are very similar and only their associated transition moments vary. Finally, in a mixed helical/zig-zag structure four transitions are observed, two at low and two at high energy.

Table 8 CNDO/S2 excited states energies ($\tilde{\nu}$) and corresponding oscillator strengths (*f*) based on AM1 optimised geometries of hexameric structures of polymers of the type **P3/4**.

structure	$\tilde{\nu}$ / cm^{-1} *f*					
elongated zig-zag hexamer	**14700** **7.1**	15300 0.4	15900 1.2	16400 0.1	16800 0.3	16900 0.4
helical hexamer	15300 0.2	16000 0.3	16500 0.1	17200 0.5	**17500** **3.6**	**18000** **3.9**
open loop hexamer	14700 1.2	15200 0.8	15700 1.9	**16500** **5.5**	16800 0.2	17200 0.8
mixed hexamer	**14700** **2.2**	**15100** **2.6**	15900 0.6	16700 0.3	**16900** **1.9**	**17000** **2.2**

It can be assumed that in solution the polymers **P3/4** display both helix-like sequences or loops as well as elongated structures. Thus, the experimentally observed absorption spectra will show a superposition of the spectral features that are associated with these superstructures, that is, two bands at the high energy side for the helix sections, one single band at the low energy side for the elongated sections, and one in the middle of the excitonic manifold as being present in the open-loop form. In fact, three bands are observed in toluene but four in the more polar solvents (Figure 21, p. 76). The fact that these spectral features are clearly visible suggests that indeed only a limited number of structures/conformers is present in solution.

From the band width of the excitonic manifold, the electronic coupling energy is estimated experimentally (from the energy difference between the absorption maxima in acetone (highest energy) and $CHCl_3$ (lowest energy)) as $V_{AB} = \Delta E/4 \approx 625\ cm^{-1}$. However, it might be more appropriate to estimate the coupling energy only in one solvent which yields, $V_{AB} = 480\ cm^{-1}$ in $CHCl_3$. However, since there is no real maximum at the high energy side in this solvent, this is a rough estimate. The theoretically obtained electronic coupling energy is $575\ cm^{-1}$ for the mixed hexamer structure. All in all, the values agree very well with that of the *trans*-indolenine homopolymers **P1/2** ($640\ cm^{-1}$).

Following *Kasha*`s rule, fluorescence is expected to be emitted from the lowest excited state of the excitonic manifold irrespective of the excitation energy into this manifold. This obviously occurs for the polymers, which can be seen from the shape of the fluorescence band, which is a mirror image of the monomer absorption but distinctly shifted to lower energy. The two different time constants of the fluorescence decay may be interpreted as being caused by two different superstructures, e.g. helical vs. elongated zig-zag. According to the *Strickler-Berg* equation (72)[162], H-type states with vanishing transition moment should have a small fluorescence rate constant k_{fl}. Therefore, the lowest energy state of the helical structure should be a dark state with a small fluorescence rate constant k_{fl}, while the one of the zig-zag structure (J-type band) should be allowed and thus should be associated with a significant k_{fl}.

$$k_{fl} = \frac{1}{\tau_{fl}} = \frac{16\times10^6\pi^3}{3h\varepsilon_0}\frac{n(n^2+2)^2}{9}\frac{g_g}{g_e}\frac{\int I_{fl}\, d\tilde{\nu}}{\int \tilde{\nu}^{-3} I_{fl}\, d\tilde{\nu}}\mu_{fl}^2 \qquad (72)$$

Here, n is the refractive index of the solvent, h is the *Planck* constant, ε_0 the permittivity of the free space, g_g and g_e the degeneracy of the ground and the excited state, respectively, μ_{fl} the transition moment of the fluorescence, and I_{fl} the fluorescence intensity plotted versus the wavenumber.

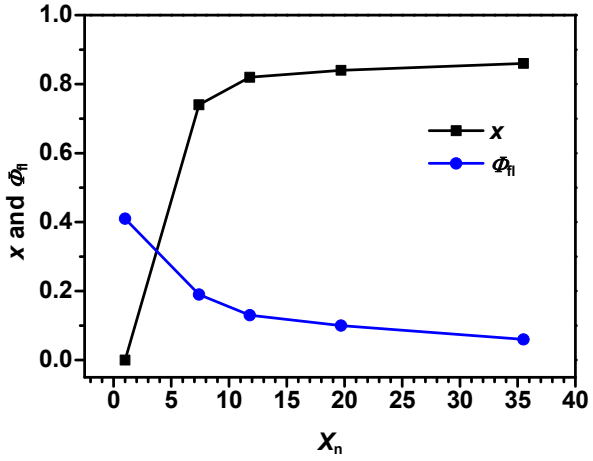

Figure 26 Dependency of the fluorescence quantum yield and the mole fraction of helix superstructure on the degree of polymerisation.

In the following, the relative amplitudes of the biexponential decay is interpreted as the mole fraction x and $1–x$, respectively, of two different superstructures present within one polymer strand. As will be argued below, the shorter lifetime (mole fraction $1–x$) is likely to be associated with the helix or open-loop structures while the long lifetime (mole fraction x) refers to the elongated zig-zag chain. A plot of the mole fraction x vs. the degree of polymerisation X_n (Figure 26) shows an increase and approaches a limiting value of ca. 0.86. This appears to be reasonable as longer chains possess a higher probability to form loops and helix structures than shorter chains. In a reversed trend, the fluorescence quantum yield decreases with the chain length and approaches ca. 0.06. Surprisingly, the absorption spectra in toluene do not reflect this change of mole fraction with increasing degree of polymerisation. From these observations and equation (69)–(71) the following characteristics can be derived for purely zig-zag ($\tau_{fl} = 5.6$ ns, $\Phi_{fl} = 0.41$, $k_{fl} = 1.1 \times 10^8$ s^{-1}, $k_{nr} = 7.3 \times 10^7$ s^{-1}) and helix structure ($\tau_{fl} = 1.6$ ns, $\Phi_{fl} = 0$,

$k_{fl} = 0\ s^{-1}$, $k_{nr} = 6.3 \times 10^8\ s^{-1}$) which are also given in Figure 9 (p. 52). The assignment of the helix-type structure to the short-lifetime component is made because in the limiting case of infinitely long chains this structure must have a vanishing fluorescence rate constant as required for an H-type superstructure. This model requires that energy transfer between the two different superstructures is slow relative to the decay rates.

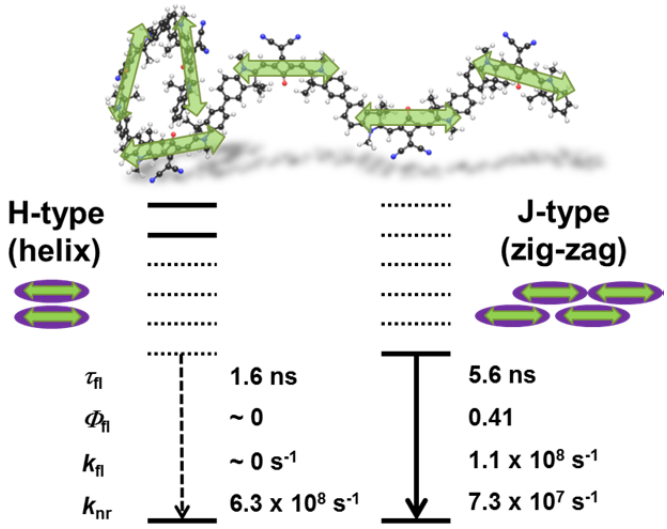

Figure 27 Relaxation pathways depending on the superstructure (helix or zig-zag).

Taking the above outlined structural model into account, the solvatochromic behaviour of the excitonic manifold can be explained by a fractional increase of helix or open loop structures relative to the zig-zag chain. While solvents that may form C–H hydrogen bonds to the squaric acid oxygen such as DCM and $CHCl_3$ favour a zig-zag chain, more polar solvents such as DMF or acetone that are unable to solvate the negative charge of the squaric acid core induce a folding to yield a more helix-like arrangement.

An interesting point concerns the optical properties of the films: While the films spin-coated from $CHCl_3$ or toluene clearly show a J-type behaviour and, consequently, a large mole fraction of zig-zag structures, the pristine film formed from DMF clearly displays a more pronounced H-type in the absorption spectra, which indicates large fractions of helix or open loop structures. Obviously, these structural motifs are maintained when spin-coating from solutions in DMF. Annealing then leads to a break-up of these structures to yield more zig-zag fractions. This aspect highlights the possibility to induce

supramolecular structures by choosing the appropriate solvent for film forming applications.

Conclusion

The first polymers on the basis of dicyanomethylene substituted squaraines were synthesised by *Yamamoto* homocoupling reaction. In comparison to the homopolymers described above (**P1** and **P2**), the polymers **P3** and **P4** show an increased solubility in various solvents what allowed a more detailed spectroscopic study.

The polymers show a rather broad absorption in the red to NIR region with distinct maxima but a narrow fluorescence, red-shifted relative to the monomer emission. With increasing degree of polymerisation the fluorescence quantum yield decreases. These features can best be described by formation of an excitonic manifold due to at least two different superstructures, a zig-zag chain and a helix-like arrangement. While the former shows typical J-type behavior, the latter may be conceived as an H-type aggregate. The fractions to which these structures are formed depend on the chain length and the solvent. Controlling the superstructure will allow to tune the optical properties which, in a first attempt, was successfully done in films.

3.2.4 Squaraine–Squaraine Copolymer[1]

Synthesis

Besides the homopolymers, a squaraine–squaraine copolymer, which comprises both a standard squaraine dye as well as a dicyanomethylene-substituted dye, was prepared. This was achieved *via* the Pd-catalysed *Suzuki* coupling reaction of the diboronic ester squaraine derivative **M8** and the dibrominated dicyanomethylene-substituted squaraine **M6** (Scheme 12). The reaction was performed under aqueous conditions (THF/H_2O) using $NaHCO_3$ as a base and $Pd(PPh_3)_4$ as Pd(0) source. The mixture was heated to reflux for 6 d to obtain the copolymer **P6** ($M_n \sim 32800$, $X_n \sim 23$).

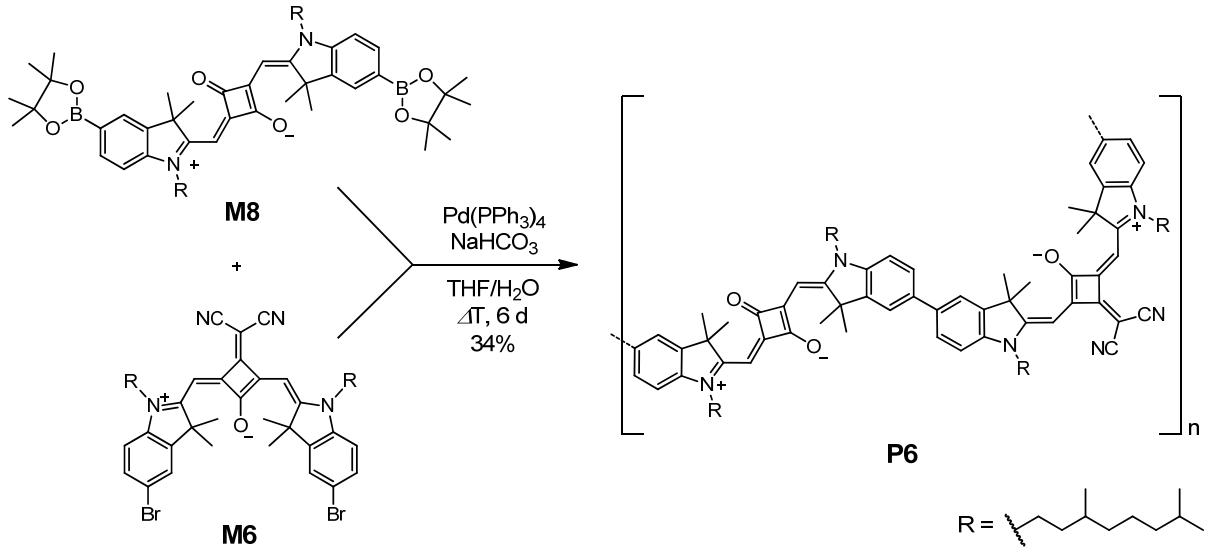

Scheme 12 Synthesis of the squaraine–squaraine copolymer **P6**.

Cyclic Voltammetry

The cyclic voltammetry measurement was carried out in DCM solution with TBAHFP (0.2 M) as supporting electrolyte. The cyclic voltammogram of **P6** is shown in Figure

[1] Reproduced or adapted in part with permission from *Singlet-Singlet Exciton Annihilation in an Exciton-Coupled Squaraine-Squaraine Copolymer: A Model towards Hetero-J-Aggregates,* S. F. Völker, A. Schmiedel, M. Holzapfel, K. Renziehausen, V. Engel, C. Lambert, *J. Chem. Phys. C.* **2014**, *accepted* – Copyright (2014) American Chemical Society.

28, where the cyclic voltammograms of model dyes **M5** and **M7** are also depicted for comparison.

The cyclic voltammogram of **P6** nearly looks like a superposition of those of the separate monomeric subunits. It can be seen that the subunits still have their independent chromophore character and the potentials of **P6** can clearly be allocated. The 1st oxidation at 57 mV and the 2nd reduction at –1.62 V can be assigned to the standard squaraine moiety (**M5**), whereas the 1st reduction at –1.38 V and the 2nd oxidation at 189 mV can be assigned to the dicyanomethylene-substituted squaraine moiety (**M7**). The 3rd oxidation at 583 mV is in the area of the 2nd oxidation processes of both subunits. The sharpened peak of the back-reduction process is an indication of adsorbed molecules on the electrode, which might precipitate at the three- or fourfold oxidised state. Integration of the signals in the differential pulse voltammetry (DPV) measurement reveals the contribution of two electrons to this signal and therefore the second oxidation of both subunits. The values of the redox potentials of **P6** were extracted from the DPV, because no half-wave potentials of the two reduction processes could be derived from the CV, once the 2nd reduction was recorded.

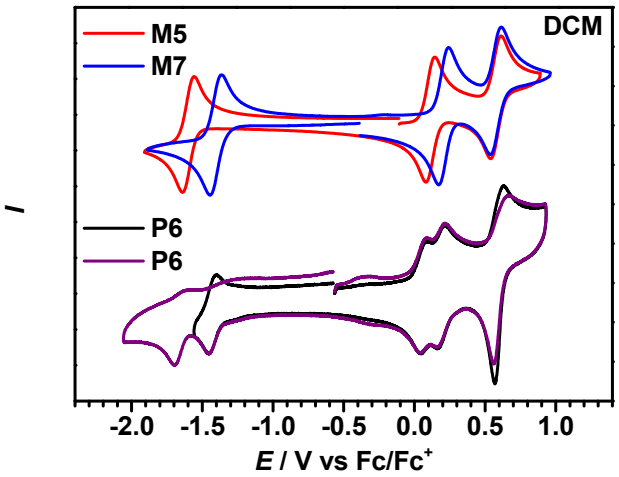

Figure 28 Cyclic voltammogram of squaraine–squaraine copolymer **P6** and model dyes **M5** and **M7** in DCM/TBAHFP (0.2 M) at a scan rate of 250 mV s^{-1}. The purple voltammogram of **P6** includes a second (irreversible) reduction.

Due to the contribution of both subunits to the redox potentials of the copolymer, its electrochemical derived band gap of 1.44 eV is lower than those of the monomers. The

similarity of the redox potentials compared with the monomeric compounds shows that there is barely an electronic interaction between the monomeric subunits in the ground state.

Table 9 Redox potentials, HOMO and LUMO energy levels, and band gaps obtained by electrochemical (E_{gap}^{CV}) and optical (E_{gap}^{opt}) methods of squaraine–squaraine copolymer **P6** and model dyes **M5** and **M7**.

	$E_{1/2}^{Red}$ / mV	$E_{1/2}^{Red}$ / mV	$E_{1/2}^{Ox}$ / mV	$E_{1/2}^{Ox}$ / mV	$E_{1/2}^{Ox}$ / mV	E_{HOMO} / eV[d]	E_{LUMO} / eV[d]	E_{gap}^{CV} / eV[d]	E_{gap}^{opt} / eV[e]
M5[a]	–1610		110		580	–5.27	–3.55	1.72	1.86
M7[a]		–1405		207	576	–5.37	–3.76	1.61	1.71
P6[b]	–1620[c]	–1380[c]	57[c]	189[c]	583[c]	–5.21	–3.77	1.44	

[a] Ag/AgCl pseudo-reference electrode; [b] Ag/AgCl "leak free" electrode; [c] potentials extracted from DPV; [d] determined according to the procedure described in 5.1.4; [e] determined in DCM for the monomers and $CHCl_3$ for the polymer according to the procedure in 5.1.1.

Extension of the Exciton Coupling Theory for Alternating Copolymers

To interpret the optical properties of the squaraine–squaraine copolymer, it is necessary to work out the exciton coupling theory for an alternating copolymer or for simplification for a heterodimer (note that even though the molecule consisting of two different chromophores is not a real dimer, it will be denoted as heterodimer for easier comparison). This was achieved in cooperation with *Prof. Dr. Volker Engel* and *Klaus Renziehausen* from the department of physical and theoretical chemistry at the Julius-Maximilians-University of Würzburg.

Because the dimer consists of two chromophores A and B, the energies of the isolated excited chromophores H_{AA} and H_{BB} are not equal ($H_{AA} \neq H_{BB}$) as it was assumed for the homodimer in chapter 1.3.2. Note that H_{AA} and H_{BB} are denoted as E_A^* and E_B^*, respectively. Therefore, the determinant eq. (22) (p. 31) and the resulting eq. (23) become

$$\begin{vmatrix} E_A^* - E_E & V_{AB} \\ V_{AB} & E_B^* - E_E \end{vmatrix} = 0 \tag{73}$$

and

$$(E_A^* - E_E)(E_B^* - E_E) - V_{AB}^2 = 0, \tag{74}$$

respectively, and it follows

$$E_E = \frac{(E_A^* + E_B^*) \pm \sqrt{(E_A^* + E_B^*)^2 - 4(E_A^* E_B^* - V_{AB}^2)}}{2}. \tag{75}$$

With the averaged energy of the two excited chromophores $\overline{E} = (E_A^* + E_B^*)/2$ and half of the energy difference of the isolated excited chromophores $E_{dev} = (E_A^* - E_B^*)/2$ where $E_A^* > E_B^*$, eq. (75) simplifies to eq. (76)

$$E_E = \overline{E} \pm \sqrt{E_{dev}^2 + V_{AB}^2}, \tag{76}$$

resulting in an exciton band width of $\Delta E = 2\sqrt{E_{dev}^2 + V_{AB}^2}$ for a heterodimer. Analogous to eq. (66), with neglect of the $(N-1)/N$ term, and with respect to the nearest-neighbour approximation the energies of the alternating copolymer can be obtained by

$$E_E = \overline{E} \pm \sqrt{E_{dev}^2 + (2V_{AB}\cos(\frac{2\pi k}{N}))^2}. \tag{77}$$

For the copolymer, the quantum number k is $k = 0, \pm 1, \pm 2, \ldots N/4$, where N is the number of chromophores (both A and B). The exciton band width for the copolymer is

$$\Delta E = 2\sqrt{E_{dev}^2 + 4V_{AB}^2}, \tag{78}$$

which simplifies to $\Delta E = 4V_{AB}$ for the homopolymer. It can be seen, that the exciton band width of the copolymer is even larger which in principle should also lead to an even broader absorption. However, for the copolymer eq. (78) predicts a gap of energy states in the excitonic manifold which is $2E_{dev}^2$. For pictorial presentation, the energy diagrams of a heterodimer, an alternate copolymer, and a homopolymer are depicted in Figure 29.

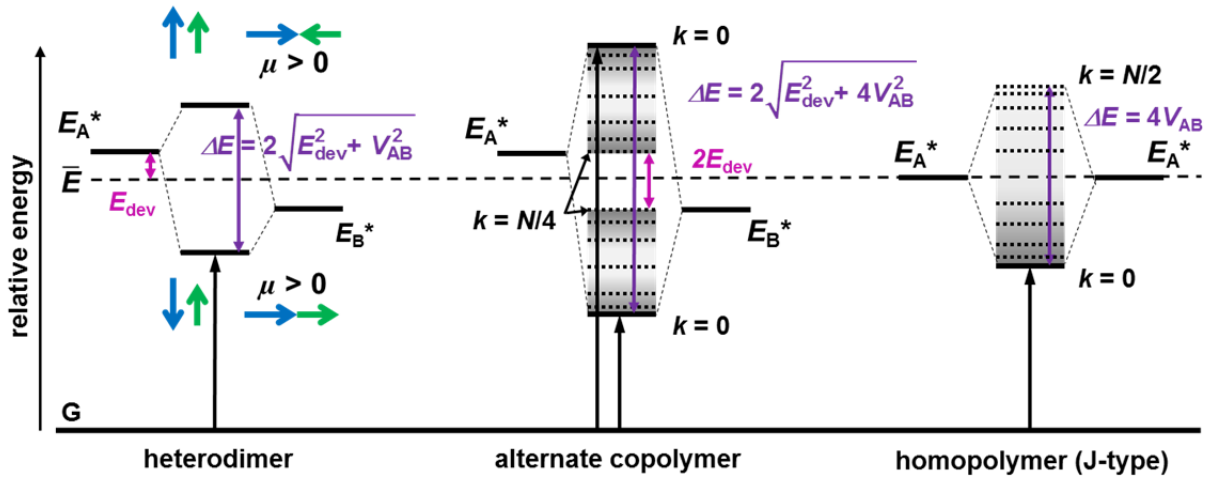

Figure 29 Schematic energy diagrams of a heterodimer, an alternate copolymer, and a homopolymer. For the heterodimer, the phase relation of the transition dipole moments of chromophore A and B are given in blue and green arrows. ΔE is the exciton band width, E_A* and E_B* the energies of the lowest excited state of the isolated chromophores A and B, respectively, $\bar{E} = (E_A* + E_B*)/2$ the averaged energy of the excited chromophores A and B, $E_{dev} = (E_A* + E_B*)/2$, and G the ground state energy.

Absorption Spectroscopy

The absorption spectrum of **P6** in $CHCl_3$ is depicted in Figure 30 (left) together with those of the homopolymers **P1A** and **P3-1**, and the monomers **M1** and **M2** (Table 10, p. 99). As described in the previous chapters, the spectra of the homopolymers **P1A** and **P3-1** in $CHCl_3$ are strongly broadened and red-shifted compared to their parent squaraines **M1** and **M2**, respectively, with the absorption maxima at the low energy side. This was explained by exciton coupling theory and the presence of different superstructures of the polymers. Here the low energy maxima arise from linear J-type structures (where only excitation into the lowest excited state is allowed) and the

transitions at higher energies from either a zig-zag structure of **P1A** or a helix-like structure of **P3-1**. As a reminder, in the zig-zag structure two chromophores built a unit cell and excitations into both the highest and lowest excitonic states are allowed, whereas the helix structure has H-type character and only a transition into the highest excitonic state is allowed.

For the copolymer **P6**, the absorption spectrum is also strongly broadened compared to both parent squaraines **M1** and **M2**. The main absorption band reaches from 12000 cm^{-1} to nearly 18000 cm^{-1} with the absorption maximum at the low energy side at 13000 cm^{-1} and another distinct absorption at the high energy side at 15200 cm^{-1}. The whole band almost covers the absorption bands of the homopolymers, but does not quite reach the low energy side of **P3-1** and the high energy side of **P1A**. The maximum of **P6** at the low energy side is indicative of an elongated structure with J-type character, where the bent **M2** moiety might induce a zig-zag motif. However, for a copolymer, both the transitions into the lowest and highest excitonic state are allowed, which is clearly reflected by the pronounced peak at the high energy side.

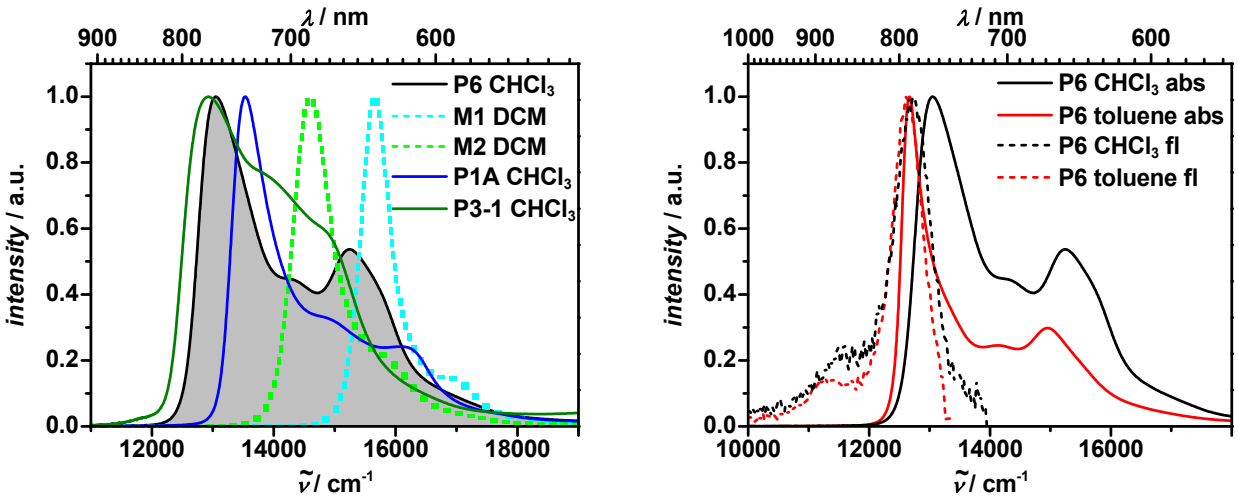

Figure 30 Left: Normalised absorption spectra the polymers **P6**, **P1A**, and **P3–1** in $CHCl_3$ and the parent monomers **M1** and **M2** in DCM. Right: Normalised absorption (solid lines) and fluorescence (dashed lines) spectra of **P6** in toluene and $CHCl_3$.

The absorption of **P6** is solvent dependent (Figure 31, left) in a similar way as it is for **P3-1** (Figure 21, p. 76). In DCM the spectrum is rather similar to $CHCl_3$ and therefore not shown. In more polar solvents such as DMF and PhCN, there is less intensity of the

low energy absorption band, which is roughly of equal value as the band at the high energy edge. The latter is significantly broader and in total there are contributions above 100000 M^{-1} cm^{-1} (**M1**–**M2** unit)$^{-1}$ from ~ 12800–16200 cm^{-1}. The most remarkable absorption properties are observed in toluene, which shows a really sharp and intense (478000 M^{-1} cm^{-1} (**M1**–**M2** unit)$^{-1}$) lowest energy absorption band at 12600 cm^{-1}. The transition dipole moments of the complete excitonic manifold in all solvents are rather similar with values ~ 14–16 D (**M1**–**M2** unit)$^{-1}$, which shows that they are nearly solvent independent.

The squared transition moments of the copolymer **P6** in toluene (μ_{eg}^2 = 243 D^2) are in excellent agreement with the sum of the squared transition moments of the parent monomers **M1** (11.1 D) and **M2** (10.1 D), which is 225 D^2. It has to be noted though, that due to solubility issues in toluene, the copolymer was first dissolved in $CHCl_3$ and then diluted with toluene to a ratio of toluene/$CHCl_3$ 99:1.

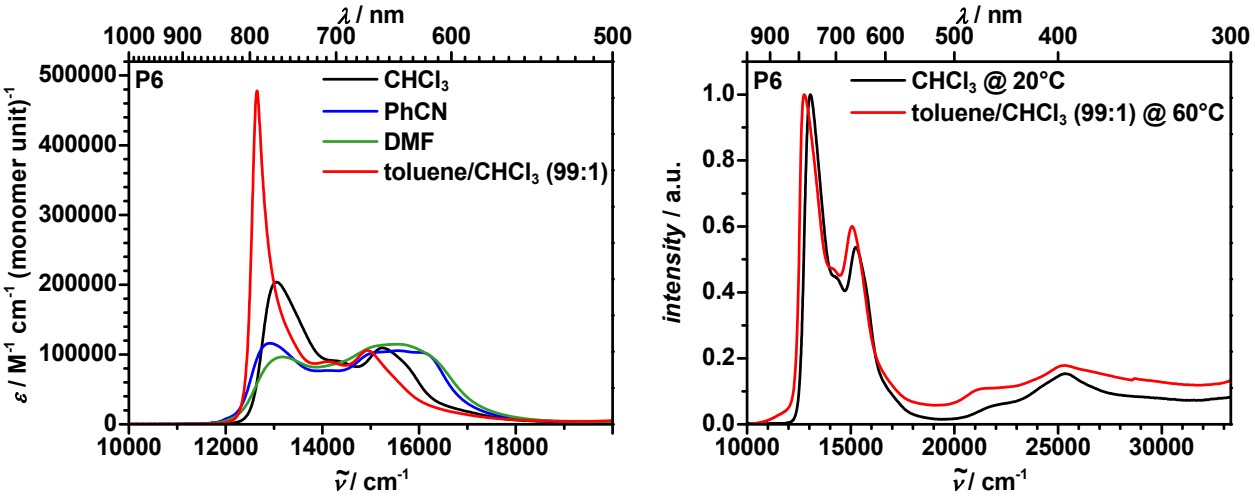

Figure 31 Left: Absorption spectra of **P6** in various solvents. Right: Normalised absorption spectra in $CHCl_3$ at 20°C and in toluene at 60°C.

For further discussions only the spectra in $CHCl_3$ and toluene will be considered. Comparison shows, as mentioned above, that in toluene the lowest energy absorption band is rather sharp. At 2/3 of the maximum band height the band width is $\Delta\tilde{\nu}_{2/3}$ = 820 cm^{-1} in $CHCl_3$ and only 250 cm^{-1} in toluene, while for **M2** in toluene it is 480 cm^{-1}. This small band width in toluene could be indicative of so-called "exchange narrowing" that has been described for diverse J-aggregates.[141-142] It can be explained

by the coherent excitation of several coupled chromophores. This leads to only minor deviations of the average excited state energy of those chromophores. The effective coherence length N_{eff}[163-164] can be calculated by eq. (79). *Knapp* introduced N_{eff} for the scaling of the line width for a purely electronic aggregate hamiltonian with strong electronic coupling and static disorder.[141] Later, it was shown that exchange narrowing also occurs if vibrational degrees of freedom are included and disorder is neglected. A thorough discussion on the subject of exchange narrowing has been published by *Walczak et al.*[142] and in a very recent work, *Scholes et al.* present a perspective on the measurement of exciton localisation.[165] Alltogheter, there is a demand for a more sophisticated theory and even though there are certainly limitations of equation (79), it is used herein for a rough estimate of the coherence length value. Here the band widths at 2/3 height are used because of the overlap of higher energy transitions at 1/2 height. Due to the lack of a **M1**–**M2** "monomer" model, the band width of **M2** in toluene (480 cm^{-1}) is used as $\Delta\tilde{\nu}_{2/3}(M)$ and for **P6** $\Delta\tilde{\nu}_{2/3}(P) = 250\ cm^{-1}$ in toluene.

$$\sqrt{N_{eff}} = \frac{\Delta\tilde{\nu}_{2/3}(M)}{\Delta\tilde{\nu}_{2/3}(P)} \qquad (79)$$

This results in an effective coherence length of $N_{eff} = 3.7$ which means, that an exciton is delocalised over $[\mathbf{M1–M2}]_{3.7}$. This delocalisation of excitation and exchange narrowing has been shown for J-aggregates as mentioned above, but to the best of knowledge not for a conjugated polymer.

The large deviation of the band width in toluene and $CHCl_3$ might be caused by a higher degree of order of the copolymer in toluene, whereas a certain amount of disorder might be responsible for the band width in $CHCl_3$, which is even larger than the one of a parent monomer. To see how temperature might influence the (dis)order of the copolymer, temperature dependent absorption spectra were recorded both in $CHCl_3$ (20–40°C) and in toluene (20–80°C). While there was no change to be observed in $CHCl_3$ (after density compensation), in toluene the lowest energy transition band decreases in intensity and eventually is even slightly blue-shifted at higher temperature. The normalised absorption spectrum in toluene at 60°C is similar (only minor red-shifted) to the spectrum in $CHCl_3$

(Figure 31, right). An explanation for this behaviour can only be proposed. Maybe the polymer chains of **P6** form some sort of helical double strands that unknot upon heating. Such potential double strands could also lead to a stiffening of the polymer chains and therefore induce a higher degree of order which results in the narrow absorption band. However, there is a broad distribution of chain lengths of the polymer and it seems unlikely that this favours aggregate formation. Since there is no proof for this proposal, the polymer will be treated as single stranded in the following.

Similar to the homopolymer **P3-1**, solid state absorption spectra of **P6** in a film were recorded in addition to the absorption spectra in solution (Figure 32). Therefore, a solution of **P6** was spin-coated on a glass substrate (2.0 mg ml^{-1}, 2000 r min^{-1}). Due to the different solution absorption spectra, the question is again if these properties are maintained in the film. Four different solvents were chosen to prepare solutions for spin-coating: $CHCl_3$, DMF, toluene, and PhCN. After the spectra of the pristine films were measured, the substrates were annealed at 130°C. Additional spectra were recorded after 10 min and further 30°min (40 min in total).

The film absorption spectra of **P6** in $CHCl_3$ (Figure 32, A) and toluene (C) are rather similar. The main absorption band is less structured and broadened to both the high and low energy side with the absorption maximum at the low energy side and red-shifted by 200–400 cm^{-1} compared to the solution spectra. The 2nd distinct peak at the high energy side which is observed in the solution spectra is not apparent in the film, however there is a prominent shoulder at ~ 15100 cm^{-1}. Upon annealing, the structure of the absorption bands barely change but there is a slight decrease of the intensity at the absorption maximum which is more pronounced in the case of toluene. For DMF (B) and PhCN (D) the absorption maxima of the pristine film spectra are at ~ 15600 cm^{-1}. These absorption bands at the high energy side are similar to those in solution, however, in solution there is a sharp absorption at the low energy side at ~ 13000 cm^{-1} where only a shoulder is found in the film spectra. Upon annealing, the high energy absorption bands decrease in intensity and are slightly red-shifted to ~ 15000 cm^{-1}. In addition the former shoulder at the low energy side slightly increases in intensity but to a smaller extent. In total, the properties of the solid state spectra of **P6** are similar to those of **P3-1** and it appears that

there is a thermodynamically favoured structure which is already present in solutions and films of $CHCl_3$ and toluene but not in DMF and PhCN solution and its pristine films.

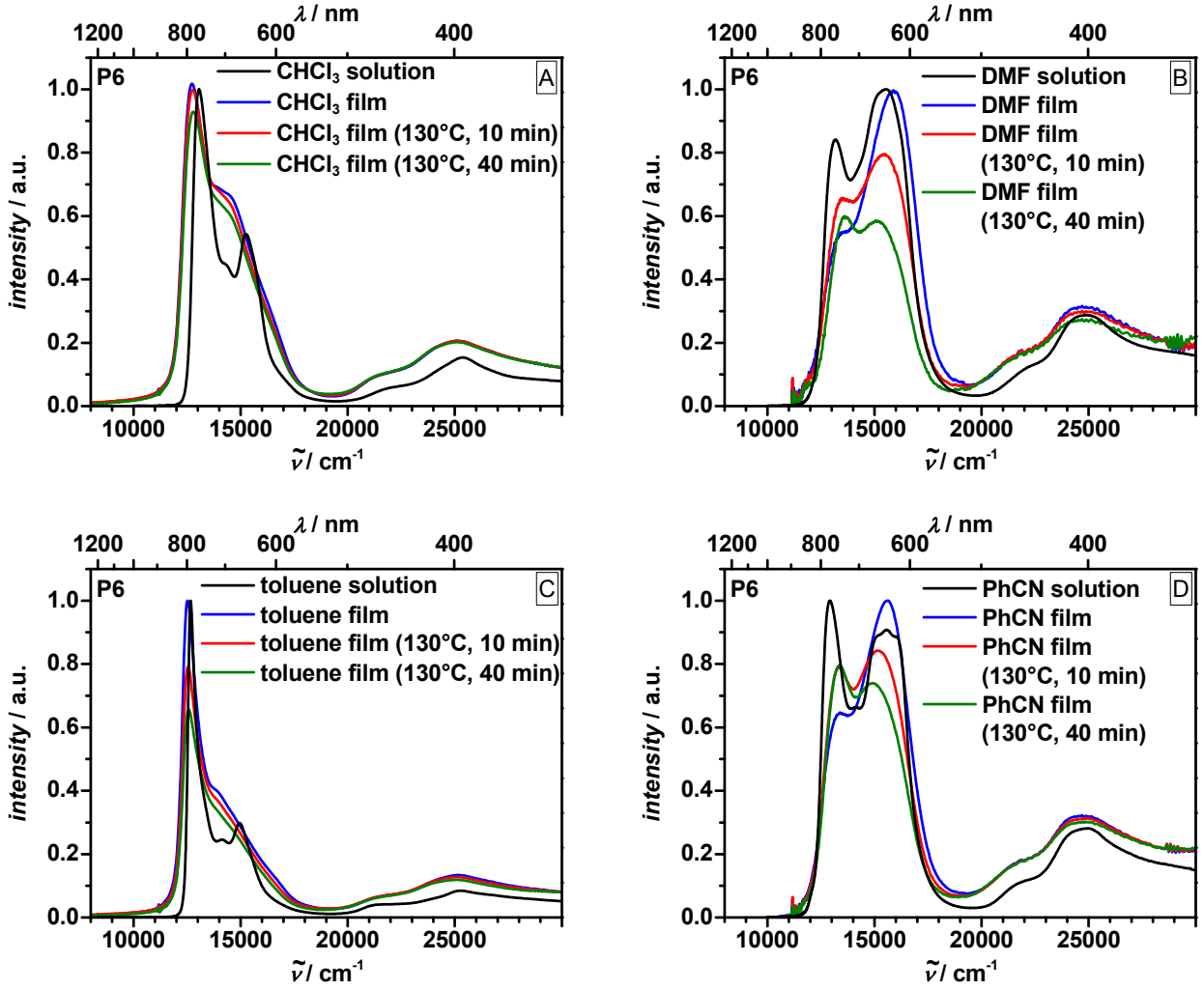

Figure 32 Absorption spectra of **P6** in solution and in solid state as thin film spin-coated from $CHCl_3$ (A), DMF (B), toluene (C), and PhCN (D). The solution spectra and the neat film spectra were normalised, the annealed film spectra were proportionately plotted.

Fluorescence Spectroscopy

The fluorescence spectra of **P6** (Figure 30, right) in $CHCl_3$ and toluene are rather similar and nearly mirror images to the absorption bands of the parent squaraine monomer. In similarity to the homopolymers **P1A** and **P3-1**, this shows that the fluorescence only occurs from the lowest excited state. Besides, the 2/3 fluorescence band widths of **P6** have nearly the same value (460 cm^{-1} in toluene and 550 cm^{-1} in $CHCl_3$) as the absorption bands of **M2** (480 cm^{-1} in toluene and 560 cm^{-1} in $CHCl_3$). Compared with

the narrow absorption band of **P6** in toluene, this indicates that while the absorption occurs into a delocalised excited state, the fluorescence occurs from a more disordered localised excited state. Copolymer **P6** shows low fluorescence quantum yields of $\Phi_{fl} = 0.01$ in $CHCl_3$ and 0.09 in toluene. The respective fluorescence decays are biexponential and the fluorescence lifetimes are longer in toluene (0.60 and 1.7 ns) than in $CHCl_3$ (0.13 and 0.28 ns) which also reflects the deviation of the quantum yields.

Table 10 Absorption maxima, extinction coefficients, transition moments, fluorescence maxima, fluorescence quantum yields, and fluorescence lifetimes of polymers **P1A**, **P3-1**, and **P6** and reference squaraines **M1** and **M2**. Extinction coefficients ε and transition moments μ_{eg} of the polymers are given per monomer unit (which in case of **P6** is a unit consisting of [**M1**–**M2**]).

	solvent	λ_{abs} / nm	$\tilde{\nu}_{abs}$ / cm^{-1}	ε / $M^{-1}cm^{-1}$	μ_{eg} / D	λ_{fl} / nm	$\tilde{\nu}_{fl}$ / cm^{-1}	Φ_{fl}[a]	τ_{fl} / ns
M1	DCM	639	15700	336000	11.4	649	15400	0.19	1.0
	toluene	644	15500	340000	11.1	649	15400	0.35	1.9
M2	DCM	685	14600	207000	10.6	706	14200	0.25	-
	toluene	700	14300	236000	10.1	716	14000	0.41	4.5
P1A	$CHCl_3$	739	13500	183000	11.8	749	13400	0.28	1.0 (97.1) 8.1 (2.9)
	toluene	x	x	x	x	x	x	x	x
P3-1	$CHCl_3$	773	12900	71000	9.6		x	x	x
	DCM	772	13000	65000	9.6		x	x	x
	toluene	775	12900	51000	8.9		12300	0.06	5.6 (0.14) 1.6 (0.86)
	PhCN	770	13000	48000	8.9		x	x	x
	DMF	663	15100	49000	9.0		x	x	x
P6	$CHCl_3$	766	13000	204000	14.9	785	12700	0.01	0.13 (0.73)[b] 0.28 (0.27)[b]
	DCM	767	13000	199000	15.6	x	x	x	x
	toluene	790	12600	478000	15.6	793	12600	0.09	0.60 (0.51)[b] 1.7 (0.49)[b]
	PhCN	774	12900	117000	14.2	x	x	x	x
	DMF	643	15600	115000	14.8	x	x	x	x

- was not measured; x could not be determined. The values in brackets are the relative amplitudes of the corresponding fluorescence lifetime. [a] During the writing process, the quantum efficiency of oxazine 1 was determined to be 0.15 by an absolute measurement using an integration sphere. However, the values reported for the squaraine dyes herein are still referenced against the quantum efficiency of 0.11 (see experimental section 5.1.2) as they were published to avoid confusion. Nevertheless, it has to be noted that the correct quantum efficiencies are larger by a factor of $0.15 / 0.11 \approx 1.36$. [b] values were obtained by time correlated single photon counting (TCSPC).

Exciton Coupling

The exciton coupling energy of the copolymer can be estimated either by evalutation of eq. (1) (p. 24), where the point-dipole approximation was applied, or by eq. (78) (p. 92) where the coupling energy V_{AB} is obtained from the experimental absorption spectrum and the difference of the excited state energies of the parent squaraines **M1** and **M2**. For the former, an angle of 0° between the transition dipole moments of the squaraine chromophores is assumed (to obtain maximum coupling energy, even though the angle is certainly larger) and a DFT computed distance between the chromophore centres of 17 Å. This yields exciton coupling energies of $V_{AB} = 230$ cm^{-1} in toluene and 250 cm^{-1} in $CHCl_3$. For the latter equation, the exciton band width is estimated from the absorption spectra to be 2190 and 2260 cm^{-1} in toluene and $CHCl_3$, respectively. The excited states energy differences of **M1** and **M2** are 1200 and 1100 cm^{-1}, leading to E_{dev} values of 600 and 550 cm^{-1} in toluene and $CHCl_3$, respectively. This results in exciton coupling energies of 480 cm^{-1} in toluene and 470 cm^{-1} in $CHCl_3$, roughly twice the one obtained by the former method. This is in similarity to the homopolymer **P2**, where the experimentally obtained electronic coupling energy is also roughly twice of the one obtained by the point-dipole approximation and eq. (1) (p. 24). However, the semiempirical calculations of the electronic coupling energy of **P2** gave values with reasonable agreement to those that have been obtained experimentally (see chapter 3.2.2). Therefore, the value of $V_{AB} = 480$ cm^{-1} seems to be more relieable. Obviously, the question arises whether the point-dipole approximation is appropriate in this case. A potential issue, which could lead to the collapse of the approximation, is a too close chromophore-chromophore distance in respect to the actual chromophore size.[166] For this case, *Beenken* and *Pullerits* showed that for the calculation of the electronic coupling energy, the point-dipole approximation is inferior to other methods such as the "line-dipole" approximation or the explicit calculation of transition densities at the chromophores and their interaction.[167]

The gap of energy states that is predicted by the exciton coupling theory for an alternating copolymer is not clearly visible but indicated by the lower intensity of absorption between the strong transition at lowest energy and the smaller but still

pronounced band at the high energy edge of the exciton manifold. The fact that there is no "real" gap could be explained by either molecular disorder from the perfect J-type structure and/or vibronic progression of the electronic states.

Transient Absorption Spectroscopy[1]

In order to probe the photoinduced dynamics of the copolymer, transient absorption spectroscopy was performed in the fs time regime. The samples were excited at the absorption maximum of 13100 cm^{-1} in $CHCl_3$ and both at the maximum (12700 cm^{-1}) and at higher energy of the excitonic manifold (15000 cm^{-1}) in toluene. Due to the high extinction coefficient of **P6**, the pump power was varied in order to check for the occurrence of multiple excitations of the polymer which could result in exciton-exciton annihilation processes. In addition, the number and the distribution of excitons that are generated during one laser pulse were estimated. Therefore, the probability of excitation P_m of one monomer subunit [**M1–M2**] is calculated by eq. (80)

$$P_m = 1 - \exp\left(-\frac{E}{(\frac{hc}{\lambda})\pi(\frac{D}{2})^2} \frac{1000 \ln(10)\varepsilon}{N_{Av}} \right) \tag{80}$$

with the energy per pulse E, *Planck*`s constant $h$, the speed of light $c$, the wavelength of the laser beam $\lambda$, the diameter of the laser beam $D$, the extinction coefficient of the compound $\varepsilon$ (taken as per monomer unit [**M1–M2**]), and *Avogadro*`s number N_{Av}. The first term of the exponential determines the number of photons per area and the last term is the absorption cross section.[168] In order to account for the fact, that the probe beam of the white light continuum has a distinct smaller diameter than the pump beam (D = 0.053 cm at $1/e^2$ maximum intensity), the pump energy has to be multiplied by a factor of $\lim_{x\to 0}\left(\frac{\mathrm{erf}(x)}{x} / \frac{\mathrm{erf}(\sqrt{2})}{\sqrt{2}}\right) \approx 1.672$, which is the ratio of the energy at the centre of a

[1] Femtosecond transient absorption spectroscopy measurements were performed by *Alexander Schmiedel* and the analysis was carried out by *Dr. Marco Holzapfel*.

Gaussian shaped laser pulse and the average energy at $1/e^2$ intensity. For the distribution of the multiple excitations in one polymer strand a hypergeometric function (eq. (81)) is used.

$$P_k = \frac{\binom{P_m}{k}\binom{1000-P_m}{n-k}}{\binom{1000}{n}} \tag{81}$$

Here, P_m is the excitation probability of one monomeric subunit [**M1–M2**] in thousandth (from eq. (80)), k is the number of excitations within the polymer and n is the number of monomer units in the average polymer strand, which is 23.4. ($X_n = 23.4$, see Table 25, p. 210).[169] In Table 11, for a pump energy of 50 nJ per pulse, the P_m and P_k values are listed for the respective excitation wavelength in the respective solvent. As can be seen, even for the low pump energy of 50 nJ per pulse, the excitation probability in toluene at 12700 cm^{-1} is already $P_m = 0.24$ and the highest probability of the multiple excitation is found for k = 5 with $P_k = 0.19$. Also for the excitation at higher energy in toluene or at the maximum in $CHCl_3$, where there are distinct lower extinction coefficients, multiple excitations should occur and have to be considered in the experiments.

Table 11 Excitation probabilities P_m and values of the distribution of multiple excitations P_k according to eq. (80) and (81) at a pump energy of $E = 50$ nJ per pulse at the given excitation wavelengths with the respective extinction coefficient per monomer unit [**M1–M2**].

solvent	$\varepsilon(\lambda)$	λ	P_m[a]	P_k[b]					
$\tilde{\nu}$ / **cm^{-1}**	/ **M^{-1}cm^{-1}**	/**10^{-9} m**		**k=1**	**k=2**	**k=3**	**k=4**	**k=5**	**k=6**
$CHCl_3$ 13100	204000	765	0.11	0.19	0.27	0.23	0.14	0.066	0.024
toluene 12700	478000	789	0.24	0.012	0.044	0.10	0.16	0.19	0.18
toluene 15000	105000	669	0.05	0.38	0.22	0.079	0.020	0.0037	0.00054

[a] for the calculation of eq. (80) h in Js, c in ms^{-1}, N_{Av} in mol^{-1}, and $D = 0.053$ cm are used. Due to the fact that the probe beam of the white light continuum has a distinct smaller diameter than the pump beam ($D = 0.053$ cm at $1/e^2$ maximum intensity), the pump energy of $E = 50$ nJ per pulse is multiplied by 1.672 which results in 83.6 nJ and is used in Joule. [b] for the calculation of eq. (81), P_m from eq. (80) is used in thousandth.

The transient absorption spectra of **P6** in $CHCl_3$ (excitation at 13100 cm^{-1}) with a pump energy of 50 nJ per pulse at different delay times (time zero is at 1.40 ps) are shown in Figure 33 (those in toluene are rather similar and only slightly shifted and therefore not shown). In the first 300 fs a strong ground state bleach (GSB) at the absorption maximum is observed, which is slightly shifted over time to 12900 cm^{-1}. In addition there is a small dip at 15300 cm^{-1}. This is accompanied by a small excited state absorption (ESA) shifting from 13200 to 13500 cm^{-1}, one ESA band at 14800 cm^{-1}, and a broad ESA from 16000–24000 cm^{-1}. The ESA at 13500 cm^{-1} rapidly decays and in the following, the spectra mainly consist of the strong GSB which is slightly more shifted to lower energy, potentially caused by vibrational relaxation,[170] and the broad ESA. Those two signals both decay multiexponentially in the following within 1 ns.

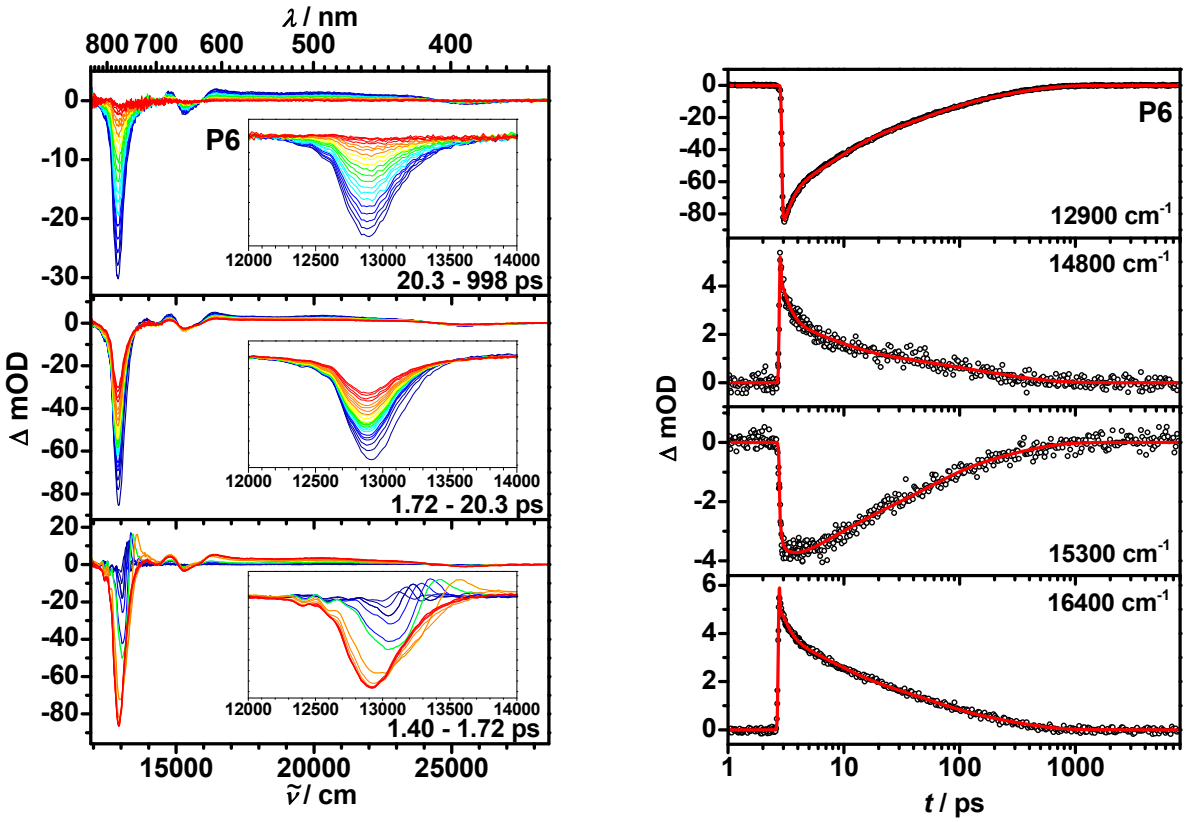

Figure 33 Left: Transient absorption spectra of **P6** in $CHCl_3$ excited at 13100 cm^{-1} with a pump energy of 50 nJ per pulse. The spectra are shown at different delay times. Time zero is at 1.40 ps. Early spectra are in blue, later ones in red. Right: Time decay traces at different energies and global target fit (red line) according to Scheme 13.

As mentioned above, the transient absorption spectra were recorded at varying pump energies (50, 100, 200, and 400 nJ per pulse) in order to check for multiple excitations and singlet-singlet annihilation (SSA). However, while the spectra barely differ with the

varying pump energies, distinct differences can be made out in the decay traces (normalised at $t = 0$), especially at early times (Figure 34), pointing to annihilation processes.

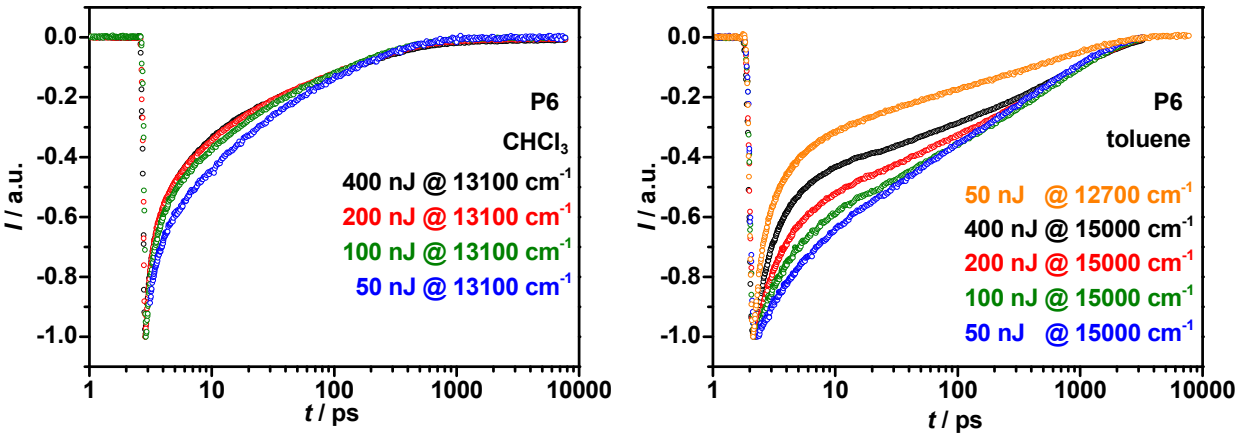

Figure 34 Left: Transient absorption decay traces of **P6** in $CHCl_3$ at (excitation at 13100 cm^{-1}) for the given pump energies per pulse. Right: Transient absorption decay traces of **P6** in toluene for the given pump energies per pulse at the given excitation wavenumber.

For SSA, there are various theories that are used to describe the process. One theory, which is commonly used for large aggregates or solid films of conjugated polymers where the process is diffusion controlled, uses the solvation of different rate equations (in the form of $\delta n/\delta t = -kn(t)-\gamma(t)n(t)^2$ for example, where k is the first order decay rate constant and $\gamma(t)$ the rate constant for the time dependent second order annihilation process).[171-174] However, in the present case the fits based on solutions of this kind of rate equation could not reproduce the experiment.

For small aggregates (a polymer in dilute solution can be considered accordingly), where the diffusion length of an exciton is large compared to the average distance of the excitons, it was shown that annihilation can be ascertained by the static rate of equilibrated excitons.[169, 174] On these roots, a kinetic scheme for the deactivation of the copolymer was developed (Scheme 13). In this scheme, the formation of both single excitons and "biexcitons" is assumed (**A**) right after excitation, where a biexciton is considered as two excitons in close vicinity, like in neighbouring monomer units M of the form [**M1**–**M2**]. Such a biexciton is treated as a discrete species, which can recombine into one ground state monomer unit and one higher excited monomer unit

which in turn rapidly decays to the lowest excited state to form a single exciton again. The subsequent decay of non-interacting excitons (**B**) to the ground state occurs stepwise over several species (**C**–**D** (and **E** in toluene)), which can be considered as being either slightly different in geometry or as a distribution of states due to the chain length distribution of the polymers.

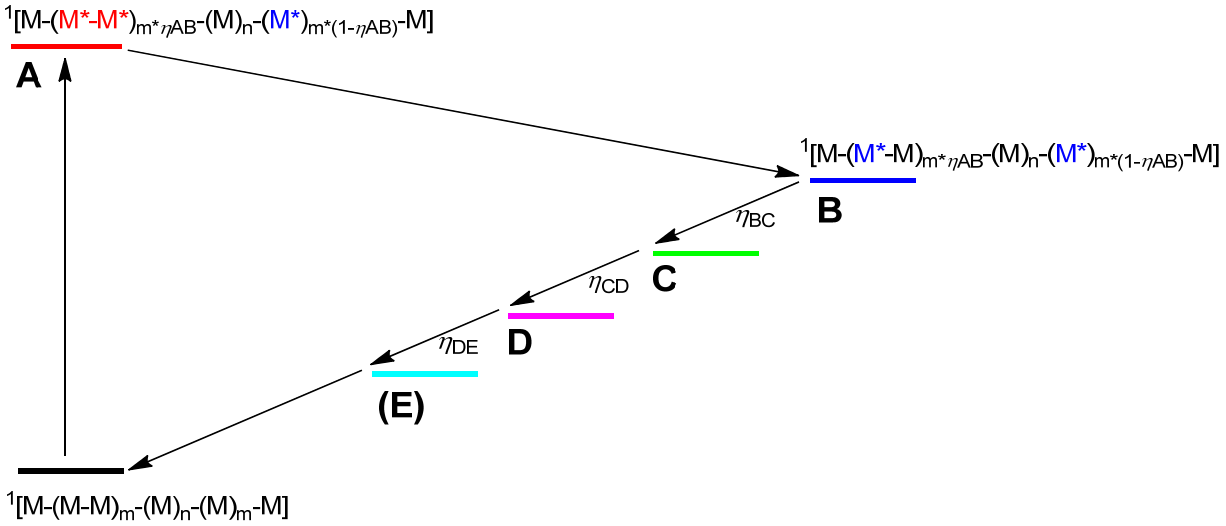

Scheme 13 Kinetic scheme for the deactivation of the copolymer. The asterisk denotes an excited monomeric unit M, which is a subunit of the form [**M1**–**M2**], monoexcitons are in blue and biexcitons in red. Upon photoexcitation there is a mixture of polymer strands with an overall population of biexcitons η_{AB} and monoexcitons $1-\eta_{AB}$. The subsequent efficiencies η_{BC} and so forth denote the respective decay step, while the remainder $1-\eta_{BC}$ denotes the direct decay to the ground state (not shown).

In addition, a further kinetic analysis was performed based on a *Kohlrausch* equation (eq. (82)) and the so-called stretched exponential:[175]

$$I(t) = \exp[-(t/\tau_0)^{\beta}] \tag{82}$$

For $\beta = 1$ the typical exponential function is obtained, whereas it is stretched for values of $0 < \beta < 1$. Using this equation, the decay trace at 15000 cm^{-1} was fitted between 10–8000 ps and a lifetime of $\tau_0 = 63$ ps with a stretching exponent of $\beta = 0.47$ was obtained. Nevertheless, in order to accurately fit the decay at very early times right after the excitation, two additional exponential functions were necessary resulting in $\tau_1 = 0.32$ ps,

$\tau_2 = 2.65$ ps, and $\tau_0 = 23$ ps with $\beta = 0.36$. In this way, two discrete lifetimes were obtained in addition to one broad distribution of lifetimes.

By performing a global target fit to the transient maps according to the proposed scheme (it was assumed that the extinction coefficient of a biexciton is twice as large as of a single exciton and that those of the GSB of the species **B–E** are the same), species associated difference spectra (SADS) (Figure 35), lifetimes, and efficiencies η_x for the different processes were obtained (Table 12, p. 108). In both solvents, the species **A** is characterised by the pronounced GSB with a lifetime of < 1 ps. For the species **B–D**, which barely differ among each other in shape and intensity, this bleach is slightly shifted to lower energy. Despite the different solvents and excitation wavenumbers, the shape of the SADS and the decay times hardly differ. The most prominent difference is the long living (> 1 ns) species **E** that is only present in toluene. For the excitation in toluene at 15000 cm^{-1}, the SADS of **E** shows a different GSB (at higher energy) compared to all SADS described above. Note that at 12500 cm^{-1} there is a positive peak in the SADS of **E** which originates from stray light.

In both solvents the 2/3 band widths of the SADS of **B–D** are considerably smaller compared to the respective absorption bands. They vary between 300–340 cm^{-1} in $CHCl_3$ and ~ 170 cm^{-1} in toluene. In Figure 35 D, it can be seen that the SADS of **B** in toluene (excitation at 15000 cm^{-1}) and the respective inverted absorption spectrum perfectly match at the low energy flank but not at the high energy one. A difference spectrum of those two is calculated in order to estimate an ESA spectrum. This shows a pronounced absorption at > 13000 cm^{-1}, maybe arising from two-photon states. A superposition of this two-photon absorption and the GSB seems to be responsible for the narrow band width in the SADS. However, a stimulated emission that could be expected at the low energy side (see the inverted fluorescence spectrum divided by $\tilde{\nu}^2$) is not observed.

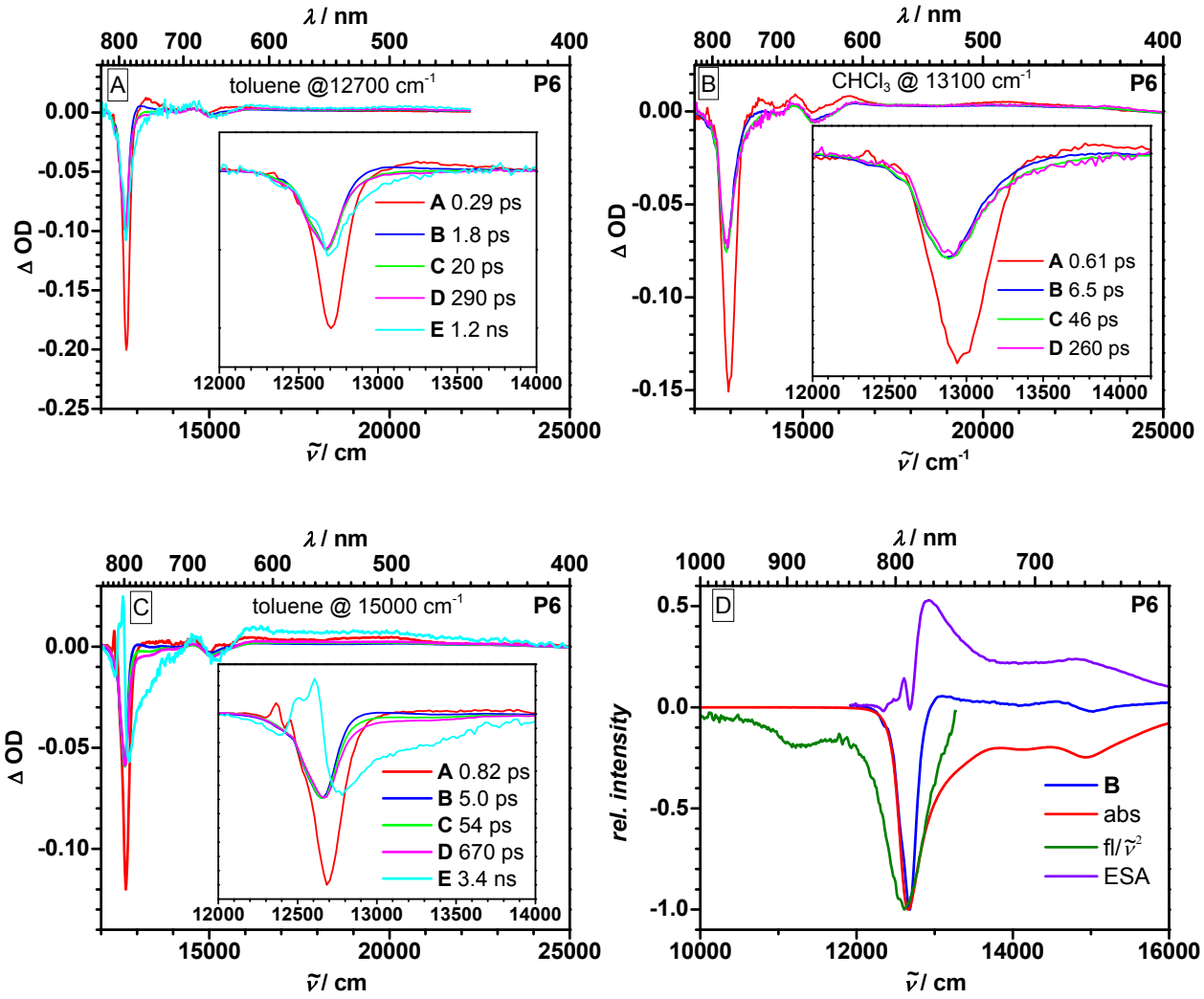

Figure 35 SADS of **P6** from the global fits A) in toluene (excitation at 12700 cm^{-1}), B) in $CHCl_3$ (excitation at 13100 cm^{-1}), C) in toluene (excitation at 15000 cm^{-1}); D) Normalised SADS of **B** in toluene (excitation at 15000 cm^{-1}), inverted absorption spectrum, inverted fluorescence spectrum (divided by $\tilde{\nu}^2$), and simulated ESA (calculated from the difference of SADS and absorption spectrum).

Considering the various pump energies, in $CHCl_3$ (excited at 13100 cm^{-1}) the efficiency η of the formation of biexciton **A** is strongly energy dependent and steadily increases with increasing pump energy (50→400 nJ per pulse) from 0.25 to 0.43. In toluene the efficiencies rise from 0.11 to 0.35 (excited at 15000 cm^{-1}) and even to 0.45 when excited at 12700 cm^{-1} with 50 nJ per pulse. In the latter series, the lifetime τ_A decreases with increasing pump energy. Also the other efficiencies and lifetimes in toluene follow essentially the same trend. Therefore, the pump energy influences both early and late processes. It could be assumed that at later times due to geometry relaxations, the excitons become localised. These localised excitons have a slower diffusion and

therefore the formation of "biexcitons" and consequently their annihilation is delayed because it is now a diffusion-dominated process. Nevertheless, the first rapid lifetime τ_A can be assigned to exciton annihilation. One should keep in mind that at this short timescale (hundreds of fs) alternative processes occur such as localisation of excitation for example.[176] However, since the annihilation rates are not independent of the pump energy, the assumptions made for the model might not be completely ideal.

In toluene (excitation at 12700 cm^{-1}) the efficiency η is already 0.45 at 50 nJ $pulse^{-1}$ and no dependency on the pump energy can be concluded. In addition, the decay here is even more rapid as at 400 nJ per $pulse^{-1}$ in toluene (excited at 15000 cm^{-1}) as can be seen in Figure 34. This might indicate a saturation effect that is already present at low pump energies, potentially due to the high extinction coefficient at 12700 cm^{-1} in toluene.

Table 12 Results of the global target fit to the transient maps of **P6** at the given pump energies per pulse: lifetimes and efficiencies for the processes that are depicted in Scheme 13.

	E / nJ $pulse^{-1}$	η	τ_A/ps	τ_B/ps	η_{BC}	τ_C/ps	η_{CD}	τ_D/ps	η_{DE}	τ_E/ns
$CHCl_3$ 13100 cm^{-1}	50	0.25	0.61	6.4	0.50	46	0.38	260		
	100	0.31	0.54	4.9	0.52	38	0.40	270		
	200	0.39	0.40	4.2	0.47	44	0.38	360		
	400	0.43	0.57	5.9	0.45	96	0.21	1000		
toluene 12700 cm^{-1}	50	0.45	0.29	1.8	0.51	20	0.58	290	0.37	1.2
	100	0.47	0.26	1.5	0.51	18	0.57	290	0.42	1.6
	200	0.38	0.31	1.2	0.52	17	0.55	260	0.48	1.5
	400	0.41	0.29	1.5	0.53	16	0.59	200	0.53	1.5
toluene 15000 cm^{-1}	50	0.11	0.82	5.0	0.65	54	0.55	670	0.12	3.4
	100	0.16	0.66	3.9	0.65	54	0.60	720	0.14	2.6
	200	0.24	0.62	3.4	0.64	50	0.62	700	0.18	2.3
	400	0.35	0.56	2.9	0.62	42	0.67	600	0.27	2.0

Generally, with the exception of an additional long lifetime of a few ns in toluene, the lifetimes obtained for $CHCl_3$ and toluene (0.4–0.6 ps), which are in the range of recenctly investigated helical π-stacks of perylene diimide aggregates,[177] do not much differ. This finding is somewhat unexpected. Due to the rather narrow absorption band in toluene that was postulated to be caused by a more ordered J-type structure and exchange narrowing, one would expect a faster relaxation of the excited state due to delocalisation. This could indicate that the rate limiting process for exciton annihilation on the short timescale is not exciton diffusion but static annihilation of two excitons in close vicinity.

Exciton Diffusion

The exciton diffusion process can be understood as a *Förster* type energy transfer between adjacent chromophores. It can be viewed as the process of dipole allowed relaxation (fluorescence) and attendant dipole allowed excitation (absorption) at chromophores at nearby sites m and n in the form $S_1^{m} \rightarrow S_0^{m}$ / $S_0^{n} \rightarrow S_1^{n}$. As a prerequisite for a fast energy transfer, this process requires the spectral overlap of the respective absorption and fluorescence spectra, which is the case due to the small *Stokes* shift. The SSA can be seen as the simultaneous occurrence of dipole allowed relaxation (fluorescence) and dipole allowed excitation (ESA) in the form $S_1^{m} \rightarrow S_0^{m}$ / $S_1^{n} \rightarrow S_x^{n}$. This process also requires spectral overlap. Due to the slightly blue-shifted ESA, this overlap should be smaller than the one mentioned above and therefore result in a lower rate. Consequently, the SSA process is slower than the exciton diffusion which makes the SSA the rate limiting process. In order to support this, the energy transfer rate k_{FT} was estimated according to *Förster* theory and the *Golden rule* expression (eq. (83)),[166, 178] where eq. (84) is used for convenience in order to use the electronic coupling values V_{AB} (obtained from the respective absorption spectra, see p. 100) in cm^{-1}.

$$k_{FT} = \frac{2\pi}{\hbar} V_{AB}^2 \, \rho(\tilde{\nu}) \tag{83}$$

$$k_{FT} = 4\pi^2 c V_{AB}^2 \rho(\tilde{\nu}) \tag{84}$$

The value $\rho(\tilde{\nu})$ is given by $\rho(\tilde{\nu}) = \int I_f(\tilde{\nu})\varepsilon(\tilde{\nu})\tilde{\nu}^{-4} d(\tilde{\nu})$ as the spectral overlap of the reduced and area normalised emission and absorption spectra, respectively, on the wavenumber scale.

In $CHCl_3$, the electron coupling energy V_{AB} is 470 cm^{-1}, $\rho(\tilde{\nu}) = 2.6 \times 10^{-4}$ cm^{-1}, and thus $k_{FT} = 68$ ps^{-1}. In toluene, the energy transfer rate is even higher with $k_{FT} = 110$ ps^{-1} ($V_{AB} = 480$ cm^{-1}, $\rho(\tilde{\nu}) = 4.1 \times 10^{-4}$ cm^{-1}). Those transfer rates are about one order of magnitude larger than those reported for an intrachain exciton transfer in the conjugated and rather rigid polymer polyindenofluorene.[179] However, those equations are used to describe an incoherent process, but as also at least some order of coherent energy migration (exciton coupling) is assumed, the question on the accuracy of the obtained rate constants arises. The coherent processes are described by eq. (85), which again is transformed for more convenience to eq. (86), to use the values of the electronic coupling in cm^{-1}.[131]

$$k_{coh} = \frac{2V_{AB}}{h} \tag{85}$$

$$k_{coh} = 2cV_{AB} \tag{86}$$

Applying those equations, energy transfer rates of 28 ps^{-1} ($CHCl_3$) and 29 ps^{-1} (toluene) are obtained. Even though the values of the two estimations differ, the obtained energy transfer rates are distinctly larger than those of the exciton-exciton annihilation which are ~ 1–3 ps^{-1}. This reflects that the annihilation process is the rate limiting process in this system at high pump energies.

With the estimated energy transfer rates k_{FT}, it is now possible to calculate the exciton diffusion constant D (eq. (87)) and with that the averaged exciton diffusion length L_D (eq. (88)), which indicates how far an exciton travels before it decays to the ground state.

$$D = k_{\mathrm{FT}} \frac{a^2}{2} \tag{87}$$

$$L_{\mathrm{D}} = \sqrt{2D\overline{\tau}} \tag{88}$$

$$R_0 = a \sqrt[6]{k_{\mathrm{FT}}\,\overline{\tau}} \tag{89}$$

For a, the end-to-end distance of the monomeric subunit [**M1–M2**] (a = 3.5 nm) is used as the minimum size of an exciton. The value $\overline{\tau}$ is the average fluorescence lifetime of the polymer, obtained from the fluorescence lifetime measurements and eq. (71) (p. 79) ($\overline{\tau} = \sum_i \alpha_i \tau_i^2 / \sum_i \alpha_i \tau_i$, Table 10, p. 99). For $CHCl_3$ an exciton diffusion constant of $D = 420\ \mathrm{nm^2\ ps^{-1}}$ is obtained and an average exciton diffusion length of $L_{\mathrm{D}} = 410$ nm ($\overline{\tau} \approx 0.20$ ns). For toluene the values are slightly larger with $D = 670\ \mathrm{nm^2\ ps^{-1}}$ and $L_{\mathrm{D}} = 1370$ nm ($\overline{\tau} \approx 1.4$ ns). If the previously calculated effective coherence length is regarded as the actual exciton size, the diffusion lengths become even greater. In both cases, the obtained exciton diffusion lengths are about one order of magnitude larger than the average polymer size (23.4 × 3.5 nm ≈ 82 nm). That means that an exciton can travel forth and back several times before it decays to the ground state. Nevertheless, in those estimations, the effects of exciton traps for example, that would certainly shorten the diffusion length, are not considered. The estimated *Förster* radii (eq. (89)) are R_0 = 17 nm ($CHCl_3$) and 26 nm (toluene).

Conclusion

After the synthesis of two different kinds of squaraine homopolymers (**P1–P4**), an alternating copolymer consisting of those two different parent squaraines (**M1** and **M2**) was synthesised by *Suzuki* cross coupling reaction. Likewise to the homopolymers, there is barely any interaction of the single chromophores in the ground state which is reflected by cyclic voltammetry measurements which reveal nearly identical redox potentials of the polymers compared to the respective parent squaraines. The copolymer

P6 also shows a strong red-shifted and broadened low energy absorption band. In addition, there is a significant transition at the high energy edge of the excitonic manifold, which can be explained by exciton coupling theory which was extended for alternating copolymers. Similar to the dicyanomethylene-substituted homopolymers **P3** and **P4**, the broad absorption band of the copolymer **P6** also shows a strong solvent dependency, which might be attributed to the presence of different superstructures. Especially in toluene, an extreme intense and narrow lowest energy absorption band is observed and assigned to what is called "exchange narrowing". Additionally, a large exciton diffusion length and large exciton diffusion constant were determined. As also a strong pump energy dependence was observed for the decay (in particular at early times), the latter accounts for the fact that singlet-singlet annihilation is the rate limiting step in the deactivation process of the excited polymer in solution. This is extraordinary compared to other conjugated polymers, where in the solid state the exciton diffusion is the rate limiting process.

Also in terms of the spectral narrowing and exciton diffusion length, **P6** behaves unlike other conjugated polymers. The exciton diffusion length exceeds those of other conjugated polymers by 1–2 orders of magnitude,[180] however, potential exciton trap sites have not been considered in the present case. Even cyanine polymers[181] or the vastly investigated polymer poly-3-hexylthiophene (P3HT), which usually show highly ordered domains, do not show similar properties as **P6**.[182-183] The exhibited properties of **P6** are more J-aggregate like and may be compared to some cyanine and perylene diimide J-aggregates.[184-186] This and the benefit of the chemical robustness of a polymer make **P6** a new and peculiar model system for excitonic features of hetero J-aggregates.

3.3 Donor-Substituted Squaraine Monomers[1]

3.3.1 Introduction

Several electron donating moieties have been attached at the periphery of a squaraine dye in order to lower the HOMO energy level and therefore induce a bathochromic shift of the absorption band. The chosen units were *p*-methoxy-substituted triarylamines (**M13**) and *p*-methoxy-substituted diarylamines (**M10** and **M11**), in which the donor is closer to the squaraine to shorten the *N*-*N*-distance of the additional redox centres and to avoid twisting effects that might be present in the "biaryl" bridge in **M13**. The diarylamine was also attached at a dicyanomethylene-substituted squaraine to realise a squaraine with both a strong donor at the periphery and a strong acceptor in the centre (**M12**). In addition to di- and triarylamines, more rigid carbazoles that were linked *via* their 2- or 3-position or the nitrogen, and *N*-methylpiperazines were attached at the periphery (**M14–M19**).

3.3.2 Synthesis

Diarylamine-Substituted Squaraine Monomers

In prospect to synthesise various symmetric and asymmetric squaraine dyes, an additional amine donor was attached at an early stage of the reaction sequence towards the squaraine dyes. Thus, **4** was treated with bis(4-methoxyphenyl)amine in a Pd-catalysed *Buchwald-Hartwig* coupling reaction to give aminoindolenine **14** (Scheme 14). This indolenine was alkylated with 1-iodohexadecane to the quaternary salt **15**, the precursor for three different squaraines **M10**, **M11**, and **M12**. Condensation of **15** with

[1] Reproduced or adapted in part with permission from a) *Squaraine Dyes as Efficient Coupling Bridges between Triarylamine Redox Centres*, S. F. Völker, M. Renz, M. Kaupp, C. Lambert, *Chem. Eur. J.* **2011**, *17*, 14147-14163. Copyright (2011) WILEY-VCH Verlag GmbH & Co. KGaA, Weinheim; b) *Synthesis, Electrochemical, and Optical Properties of Low Band Gap Homo- and Copolymers Based on Squaraine Dyes*, S. F. Völker, T. Dellermann, H. Ceymann, M. Holzapfel, C. Lambert, *J. Polym. Sci., Part A: Polym. Chem.* **2014**, *52*, 890-911. Copyright (2014) WILEY-VCH Verlag GmbH & Co. KGaA, Weinheim.
Parts of this chapter have been investigated in a bachelor thesis under the supvervision of S. F. Völker: T. Dellermann, Bachelor thesis, Julius-Maximilians Universität (Würzburg), **2011**.

one equivalent of **11** resulted in the asymmetric squaraine **M10**, whereas dicondensation reactions with half an equivalent of squaric acid or **3** resulted in the symmetric squaraine dyes **M11** and **M12**, respectively.

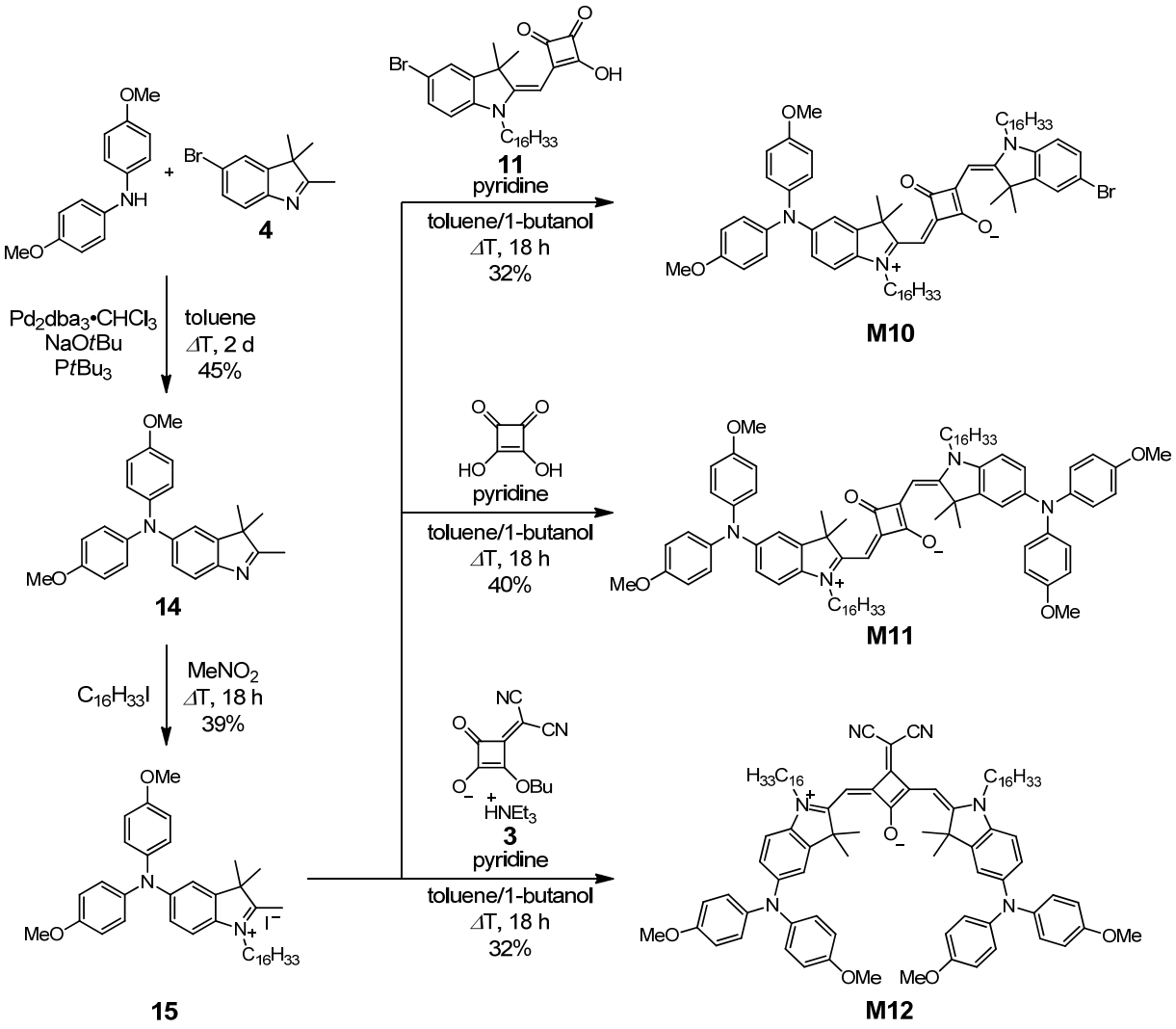

Scheme 14 Synthesis of precursors **14** and **15** and diarylamine-substituted squaraines **M10**–**M12**.

Triarylamine-Substituted Squaraine Monomer

In addition to the diarylamine-substituted dyes, the squaraine **M13**, which comprises triarylamine moieties at the periphery, was synthesised (Scheme 15). Compared to **M11** this dye comprises an additional phenyl linker between the diarylamine moieties and the squaraine core. First, the bromine atom of the triarylamine **16**, which was synthesised according to literature procedures,[187] was replaced by a boronic ester moiety. Thus,

after lithiation of **16** and subsequent addition of triisopropylborate, the isopropyl group at the resulting boronic ester moiety was hydrolysed with aqueous HCl to the free boronic acid. The boronic pinacole ester-substituted triarylamine **17** was obtained after refluxing the crude product overnight in the presence of pinacole. Eventually, *Suzuki* coupling reaction of **M5** and **17** with $Pd(PPh_3)_4$ and Na_2CO_3 as base under aqueous conditions (toluene/H_2O) was performed. After flash column chromatography, little amounts of monosubstituted side product were removed by crystallisation of pure **M13** from acetone solution.

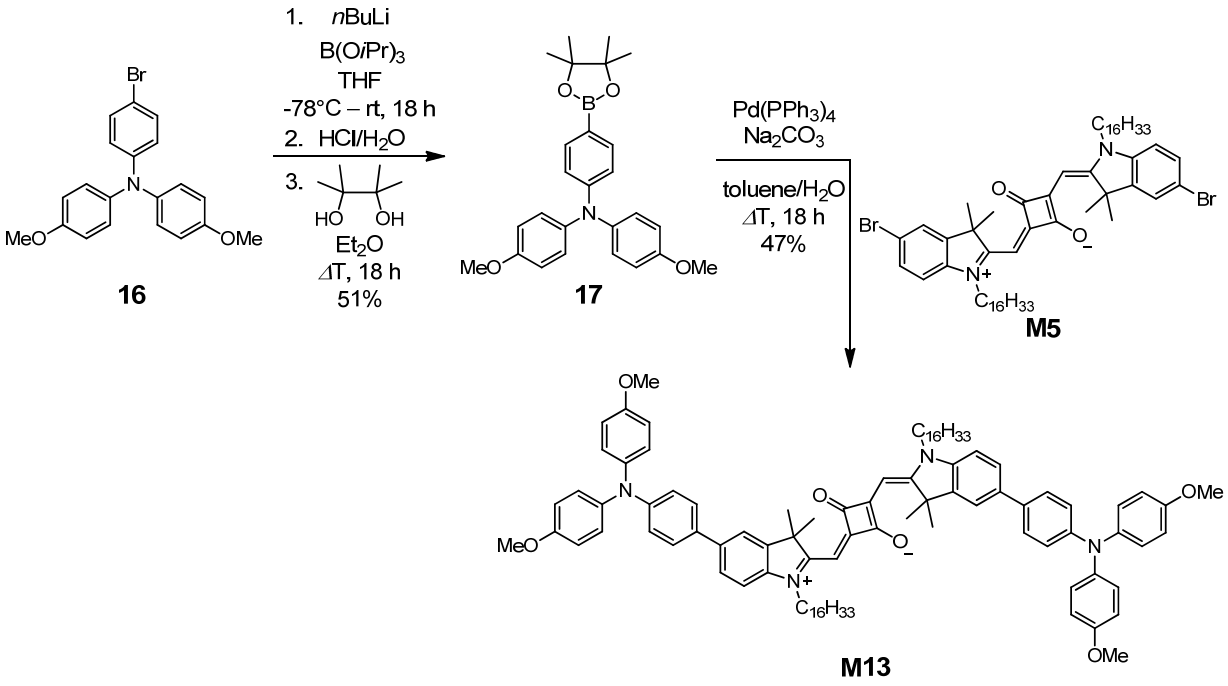

Scheme 15 Synthesis of precursors **16** and **17** and triarylamine-substituted squaraine **M13**.

Carbazole-Substituted Squaraine Monomers

Triarylamines possess a propeller-like structure which shows some flexibility.[188] In order to increase conjugation, the triarylamine was replaced by the more rigid carbazole unit which was connected either *via* its 2- or 3-position to the squaraines.

The synthesis of the carbazole precursors is straight forward and rather similar for all carbazoles used in this work (Scheme 16). All non-alkylated brominated carbazoles were synthesised according to literature procedures.

Deprotonation of the monobrominated carbazoles **18**[189] and **21**[190] with NaH and subsequent alkylation with 3,7-dimethyloctyl bromide gave the alkylated carbazoles **19** and **22**, respectively, in very good to moderate yields. The boronic ester was attached *via* halogen-lithium exchange in THF using *n*BuLi and subsequent addition of the borolane to give the boronic esters **20** and **23**, respectively.

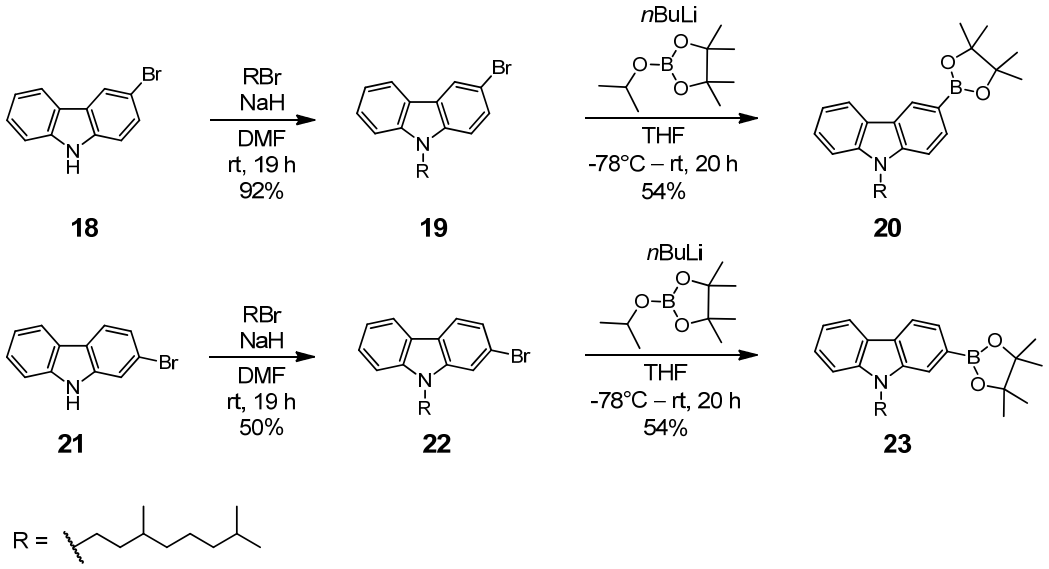

Scheme 16 Synthesis of carbazole precursors **19**, **20**, **22**, and **23**.

Suzuki coupling of squaraine **M6** with carbazole **20** in toluene/water (Scheme 17) gave both di- and monosubstituted squaraines **M14** and **M15**, respectively, after separation by preparative recycling GPC. In the monosubstituted dye **M15** the bromine was replaced by hydrogen during the reaction. Squaraine **M4** was coupled with both **20** and **23** to yield the substituted squaraines **M16** and **M17**, respectively, to investigate the impact of the different linking positions of the carbazoles.

In addition, a carbazole unit was connected *via* its *N*-position to a squaraine dye which yields an asymmetric dye conjugate. *Buchwald-Hartwig* coupling reaction of monobrominated squaraine **M3** with 3,6-dichloro-9*H*-carbazole gave substituted squaraine **M18**. In this reaction, the temperature plays a particularly crucial role. Under refluxing conditions the product could not be isolated. There were always mixtures with substances where additional carbazole units were coupled to the one that was already attached at the squaraine core. This could be avoided by reducing the temperature to 80°C for a reaction time of 18 h.

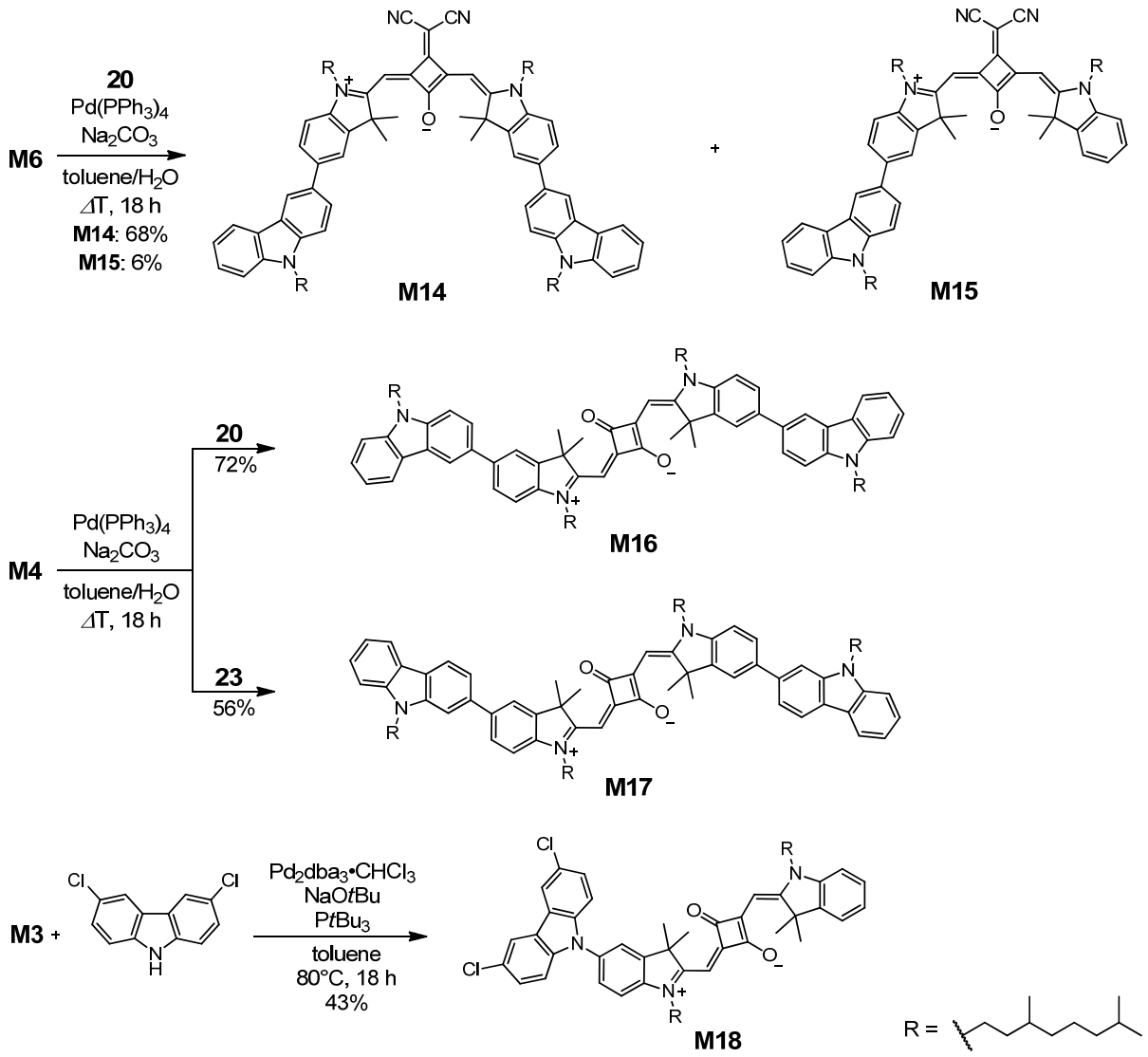

Scheme 17 Synthesis of carbazole-substituted squaraines **M14**–**M18**.

Piperazine-Substituted Squaraine Monomer

Piperazine was chosen as a non-conjugating electron donor that may be used as a bridge to connect squaraine dyes in a copolymer. Therefore, for the monomeric model compound *N*-methylpiperazine was attached at the periphery of a squaraine. As the *Buchwald-Hartwig* coupling reaction did not prove successful for the polymerisation step for a similar system at an earlier stage, a different synthetic route was followed also for the monomer where the piperazine was attached to the methylene base before the dye condensation synthesis (Scheme 18).

Buchwald-Hartwig reaction of the methylene base **7** with *N*-methylpiperazine gave **24** which was treated with squaric acid in a dicondensation reaction to yield the model compound **M19** in moderate yield.

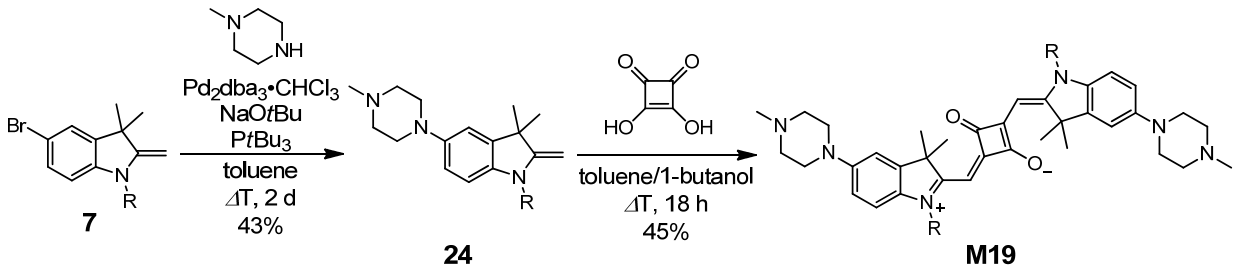

Scheme 18 Synthesis of piperazine precursor **24** and squaraine **M19**.

3.3.3 Absorption Spectroscopy

The influence of *p*-methoxy-substituted arylamine moieties on the absorption properties of a squaraine dye is depicted in the spectra measured in DCM solution in Figure 36 (Table 13, p. 123). As can be seen, all additional electron donors at the periphery induce a shift of the lowest energy absorption band towards lower energy compared to the reference dye **M1**.

The absorption maximum of **M10**, which incorporates one bromine atom and one diarylamine moiety at the periphery, is shifted by 900 cm^{-1}. The substitution of the bromine by another diarylamine results in a total shift of 1500 cm^{-1} in **M11** with the absorption maximum at 14200 cm^{-1}.

The impact of the triarylamine groups is not as pronounced as it is for the diarylamines and the shift is only 900 cm^{-1} in total for **M13**. This indicates a weaker electronic interaction of the triarylamines with the indolenine squaraine core which might be due to the twisted biaryl moiety connecting the two. The absorption maximum of **M13** is found at the same energy as for **M10** at 14800 cm^{-1}.

In the higher energy region, the substituted dyes **M10**, **M11**, and **M13** show additional bands at ca. 33000 cm^{-1} and in case of triarylamine-substituted squaraine **M13** another

one at ca. 30000 cm^{-1} which are not found for the reference dye. Hence, they can be assigned to the arylamine moieties.

The extinction coefficients of the diarylamine-substituted dyes **M10** and **M11** (~ 150000 M^{-1} cm^{-1}) are roughly half of that of the triarylamine-substituted dye **M13** and reference dye **M1** (~ 310000 M^{-1} cm^{-1}). The transition moments are between 9.9–13.6 D with the lowest value for **M10** in cyclohexane (9.9 D). In this series, **M13** shows the highest values of 12.5–13.9 D.

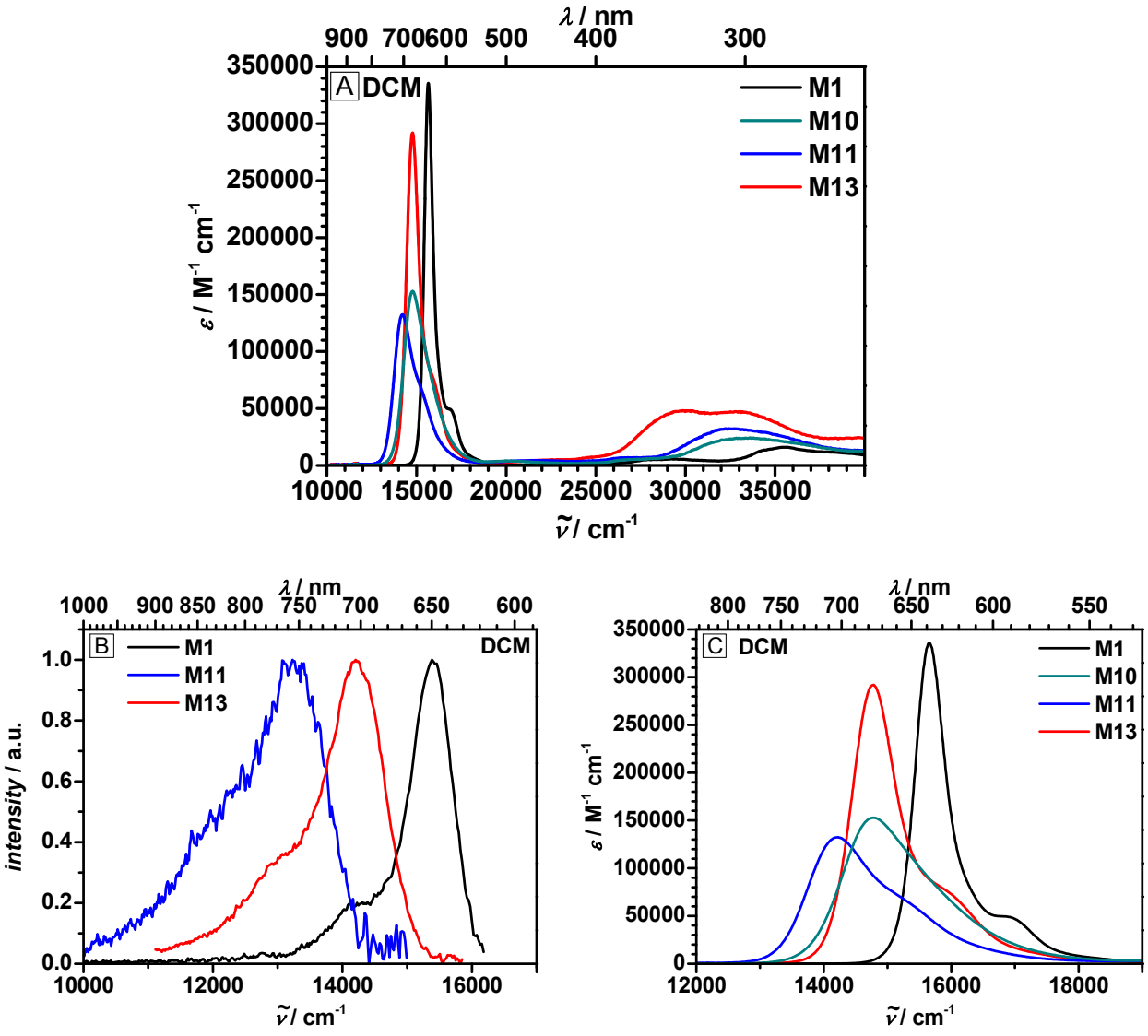

Figure 36 Complete (A) and magnified (C) absorption spectra and normalised fluorescence (excitation between 600–640 nm) spectra (B) of di- and triarylamine-substituted squaraines **M10**, **M11**, and **M13**.

In Figure 37 the absorption and fluorescence spectra of the carbazole- and piperazine-substituted squaraines in DCM are shown. The asymmetric dye **M18** shows a minor shift

of the absorption maximum of 200 cm^{-1} compared to **M1**. For the symmetric carbazole dyes **M16** and **M17** it appears as if the position of connection of the carbazole moieties has no influence on the absorption maxima which are both shifted by 800 cm^{-1} to 14900 cm^{-1}. However, the higher energy bands between 25000–40000 cm^{-1} differ in shape and energy.

Furhtermore, the piperazine moieties shift the absorption maximum by 1000 cm^{-1} to 14700 cm^{-1} but the extinction coefficient is only around 200000 M^{-1} cm^{-1}. In addition, it shows barely any additional transitions in the higher energy region.

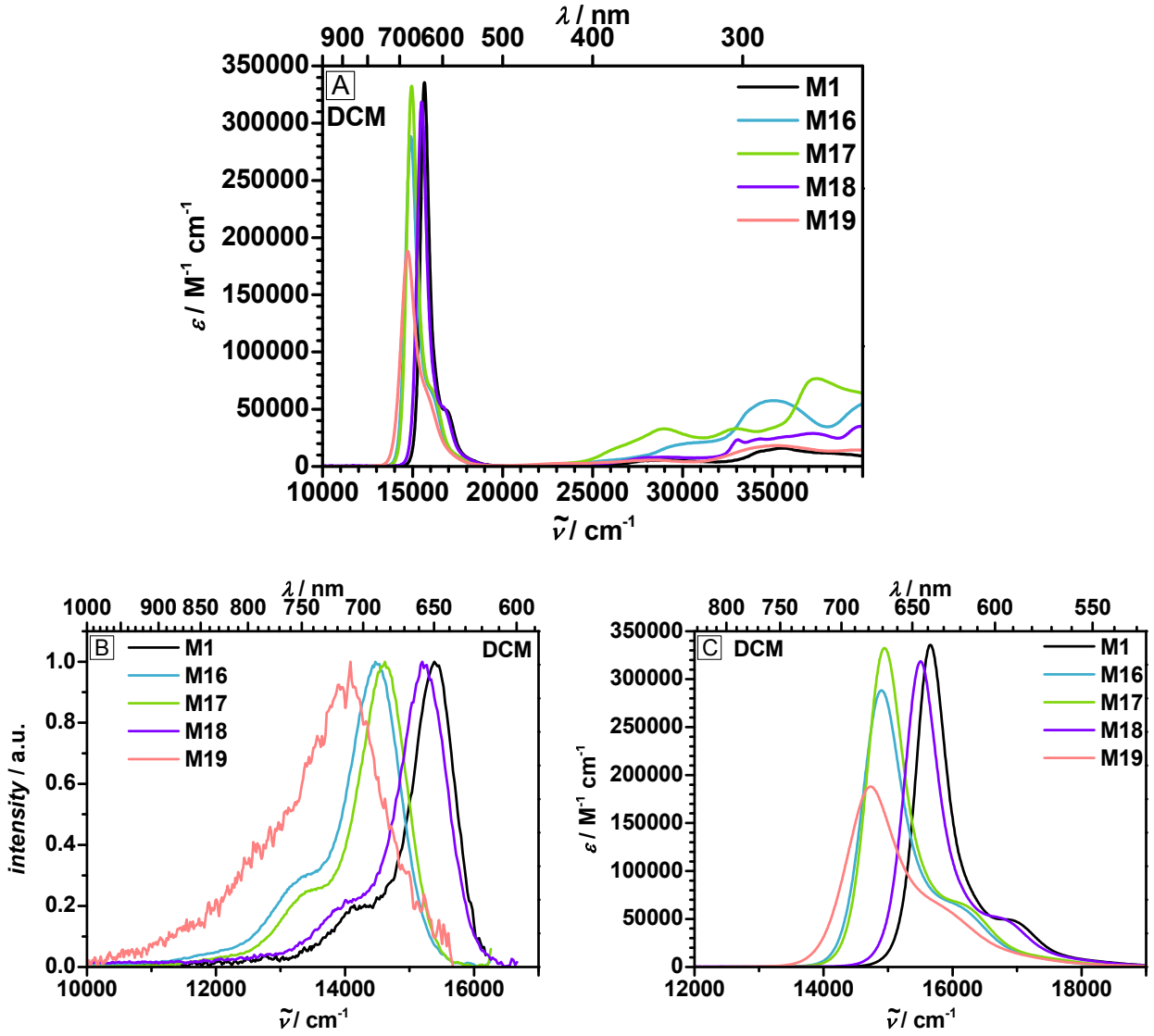

Figure 37 Complete (A) and magnified (C) absorption spectra and normalised fluorescence (excitation between 600–640 nm) spectra (B) of carbazole- and piperazine-substituted squaraines **M16–M19**.

The absorption and fluorescence spectra of the squaraine dyes that are both substituted by the dicyanomethylene group at the centre of the dye and by additional electron donors at the periphery are shown in Figure 38. The carbazole moieties of **M14** induce a red shift of the absorption maximum of 700 cm^{-1}, compared to **M2**, likewise to the standard squaraines where the carbazoles induce a shift of 800 cm^{-1} compared to **M1**. While it was shown for **M16** and **M17** that the position of the linkage of the carbazole unit to the squaraine core does barely influence the absorption maximum, the amount of units does. The absorption maximum of asymmetric dye **M15** (14200 cm^{-1}), which incorporates only one carbazole unit, is only shifted by 400 cm^{-1} to lower energy compared to reference dye **M2**.

In the squaraine **M12**, both the strong electron accepting dicyanomethylene moiety in the centre as well as the so far strongest red shifting electron donor (*p*-methoxy-substituted diarylamine) are united in one dye. For the standard dyes it was already shown that the dicyanomethylene and two diarylamine groups induce a red shift of 1000–1100 cm^{-1} and 1500 cm^{-1}, respectively. Consequently, compared to **M1** the absorption maximum of **M12** is red-shifted by 2500 cm^{-1} to 13200 cm^{-1} which reflects that the influence of the substituents sums up if combined, as already shown above.

In general, comparison of the absorption maxima of the monomeric squaraines indicates that the induced red shifts of the absorption maxima caused by the substituents, follow an additive character in DCM.

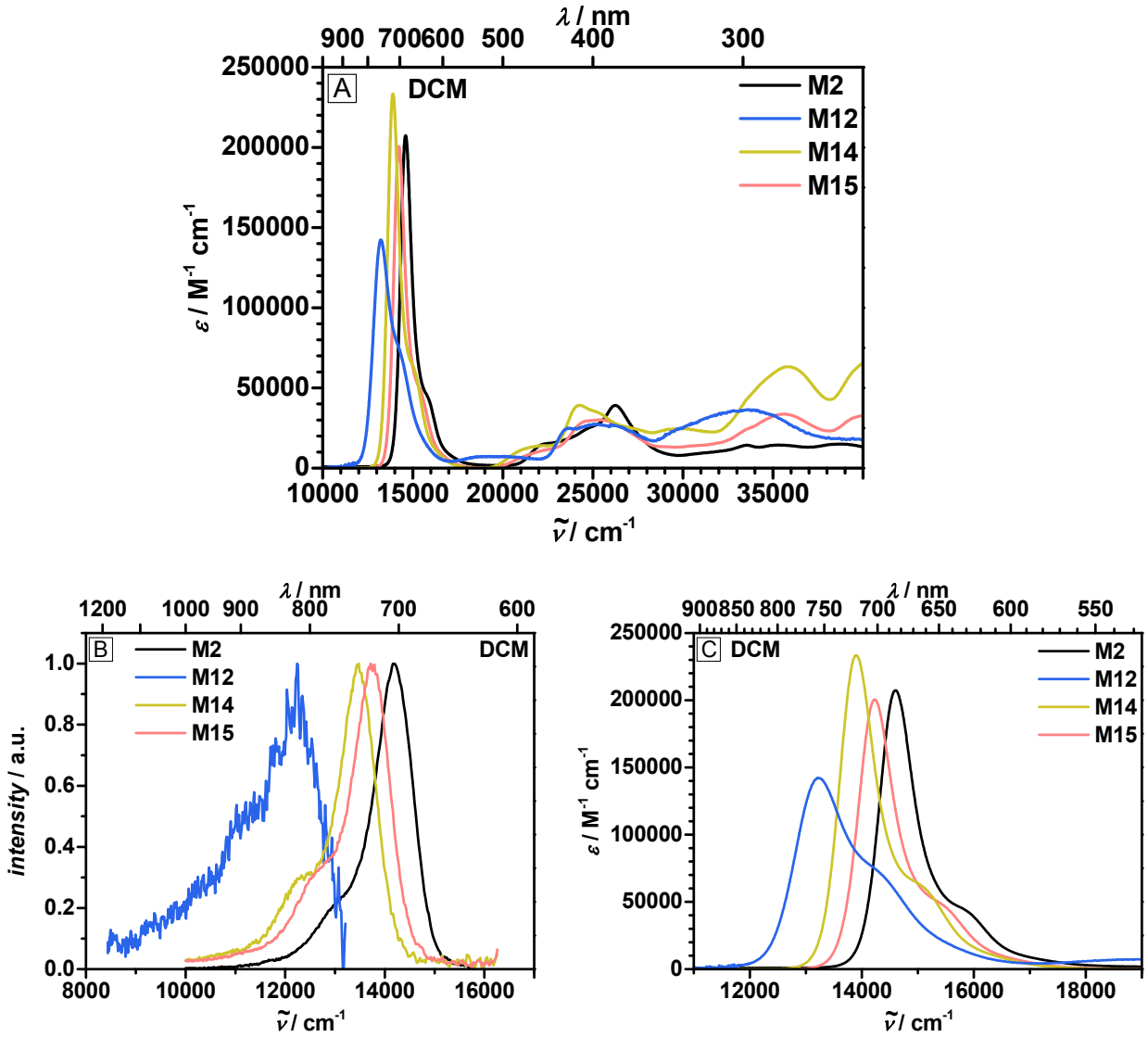

Figure 38 Complete (A) and magnified (C) absorption spectra and normalised fluorescence (excitation between 600–640 nm) spectra (B) of dicyanomethylene-substituted squaraines **M12**, **M14**, and **M15**.

Table 13 Absorption maxima, extinction coefficients, transition moments, fluorescence maxima, fluorescence quantum yields, and fluorescence lifetimes of donor-substituted squaraines **M10–M19** and reference dyes **M1** and **M2**. cy = cyclohexane.

	solvent	λ_{abs} / nm	$\tilde{\nu}_{abs}$ / cm^{-1}	ε / $M^{-1}cm^{-1}$	μ_{eg} / D	λ_{fl} / nm	$\tilde{\nu}_{fl}$ / cm^{-1}	Φ_{fl}[a]	τ_{fl} / ns
M1	DCM	639	15700	336000	11.4	649	15400	0.19	1.0
	toluene	644	15500	340000	11.1	649	15400	0.35	1.9
M2	DCM	685	14600	207000	10.6	706	14200	0.25	-
	toluene	700	14300	236000	10.1	716	14000	0.41	4.5
M10	DCM	677	14800	153000	12.6	x	x	x	x
	cy	677	14800	152000	9.9	694	14400	0.34	1.9
M11	DCM	703	14200	132000	12.3	756	13200	0.04[b]	0.29
	toluene	706	14200	193000	11.4	730	13700	0.30	2.2
	cy	697	14300	189000	11.9	716	14000	0.52	2.4
M12	DCM	756	13200	142000	12.3	817	12200	0.01[c]	< 0.1
	cy	766	13100	206000	11.5	802	12500	0.13	1.6
M13	DCM	677	14800	292000	13.6	704	14200	0.24	0.83
	toluene	681	14700	314000	12.5	695	14400	0.48	2.5
	cy	672	14900	351000	12.9	684	14600	0.72	2.3
M14	DCM	719	13900	233000	11.7	742	13500	0.14	3.7
	toluene	731	13700	236000	10.9	747	13400	0.47	3.7
	cy	733	13600	245000	11.3	758	13200	0.54	-
M15	DCM	703	14200	200000	10.6	729	13700	0.16	3.7
	toluene	715	14000	179000	9.3	732	13700	0.51	3.7
	cy	720	13900	197000	10.1	742	13500	0.47	-
M16	DCM	671	14900	288000	12.3	691	14500	0.44	2.6
	toluene	674	14800	298000	11.5	687	14600	0.49	2.7
	cy	667	15000	328000	12.0	681	14700	0.60	-
M17	DCM	669	14900	332000	12.7	684	14600	0.51	2.5
	toluene	673	14800	355000	12.2	684	14600	0.55	2.5
	cy	666	15000	294000	11.2	681	14700	0.58	-
M18	DCM	645	15500	318000	11.7	658	15200	0.30	1.3
	toluene	649	15400	312000	11.0	660	15200	0.40	2.0
	cy	644	15500	248000	9.8	655	15300	0.47	-
M19	DCM	679	14700	188000	11.3	710	14100	0.03	0.19 (91.6) 1.1 (8.1) 6.2 (0.3)
	toluene	682	14700	202000	10.8	706	14200	0.24	1.7

- was not measured; x could not be determined. The values in brackets are the relative amplitudes of the corresponding fluorescence lifetime. [a] During the writing process, the quantum efficiency of oxazine 1 was determined to be 0.15 by an absolute measurement using an integration sphere. However, the values reported for the squaraine dyes herein are still referenced against the quantum efficiency of 0.11 (see experimental section 5.1.2) as they were published to avoid confusion. Nevertheless, it has to be noted that the correct quantum efficiencies are larger by a factor of $0.15/0.11 \approx 1.36$. [b] The quantum yield was published too large by one order of magnitude ($\Phi_{fl} = 0.42$) due to a mistake in the calculations.[191-192] [c] The quantum yield was published too large by one order of magnitude ($\Phi_{fl} = 0.12$) due to a mistake in the calculations.[191]

3.3.4 Fluorescence Spectroscopy

The donor-substituted squaraine monomers show some remarkable trends concerning their fluorescence properties. In general, the fluorescence spectra are mirror images to the lowest energy absorption bands. The *Stokes* shifts are rather small in cyclohexane (200–400 cm^{-1}) and toluene (200–500 cm^{-1}) for all compounds with the exception of **M12** (600 cm^{-1}). In DCM the *Stokes* shifts are of a similar value for the carbazole-substituted squaraines **M14**–**M18** but somewhat larger (600 cm^{-1}) for the piperazine- and triarylamine-substituted squaraines **M19** and **M13**, respectively. The by far largest shifts are observed for the diarylamine-substituted dyes **M11** and **M12** whose fluorescence maxima are shifted by 1000 cm^{-1}. The fluorescence maxima of **M11** are at 13200 cm^{-1} in moderate polar DCM and at 14000 cm^{-1} in apolar cyclohexane and have the largest energy difference between each other of all monomers. This indicates that there is some charge transfer (CT) contribution in the excited state.

For most of the dyes, the fluorescence bands are at higher energy in the apolar solvents cyclohexane and toluene, and at lower energy in DCM ($\tilde{\nu}_{fl(cy)} > \tilde{\nu}_{fl(toluene)} > \tilde{\nu}_{fl(DCM)}$). Only for the dyes **M14** and **M15**, that incorporate both the central dicyanomethylene group and either one or two carbazole moieties at the periphery, this trend is reversed.

Generally, the fluorescence quantum yields Φ_{fl} are higher in the apolar solvents cyclohexane and toluene than in DCM. While the values are relatively high at ca. 0.50 in all solvents for carbazole-substituted dyes **M16** and **M17**, the fluorescence quantum yields are below 0.05 in DCM for the piperazine squaraine **M19** and diarylamine-substituted dyes **M11** and **M12**. Asymmetric diarylamine-substituted squaraine **M10** does not fluoresce at all in DCM but has a fluorescence quantum yield of 0.34 in cyclohexane. The highest Φ_{fl} observed is 0.72 in cyclohexane for **M13**.

Independently of the solvent, all donor-substituted squaraine monomers show a monoexponential fluorescence decay. The excited state lifetimes vary between a few hundred ps (**M11**–**M13** in DCM) and ca. 4 ns (**M14** and **M15** in toluene) and are similar to values reported for other squaraine systems in literature.[26, 32, 64, 101, 193-194] Only **M19**

shows three fluorescence lifetimes in DCM. However, due to the poor signal to noise ratio the accuracy of this is limited.

3.3.5 Cyclic Voltammetry

In the cyclic voltammetry experiments of the donor-substituted squaraine dyes, the focus is obviously on the oxidation processes. The second reduction that was shown above for the reference dyes will not be discussed in this chapter. Therefore, all measurements were carried out in DCM solution (TBAHFP, 0.2 M) due to the larger operation window for positive potentials compared to THF. High care had to be taken in the drying of DCM, because it was only possible to record the up to six oxidation processes in very dry solvent. Therefore, DCM, which has already been predried over CaH_2, was freshly distilled and poured on activated neutral alumina oxide under nitrogen atmosphere for further drying. In MeCN, this potential window is even larger for positive potentials, however, the squaraines investigated in this work are not soluble in this solvent. The data of the cyclic voltammetry measurements can be found in Table 14 (p. 130).

In Figure 39 the cyclic voltammograms of **M5** and **M10** are depicted and the effect of an additional diarylamine moiety on the redox properties of a squaraine is clearly visible. While there are two oxidation and one reduction processes in dibrominated **M5**, four oxidation processes are recorded for **M10**. All of them are one-electron processes and consequently, two can be assigned to the squaraine core and two have their origin in the additional diarylamine group. The 1st oxidation of **M10** is at 170 mV lower potential ($E_{1/2}^{Ox1} = -59$ mV) compared to **M5** and also the reduction is at 80 mV lower potential ($E_{1/2}^{Red1} = -1.69$ V). The 4th oxidation is found at 1.05 V.

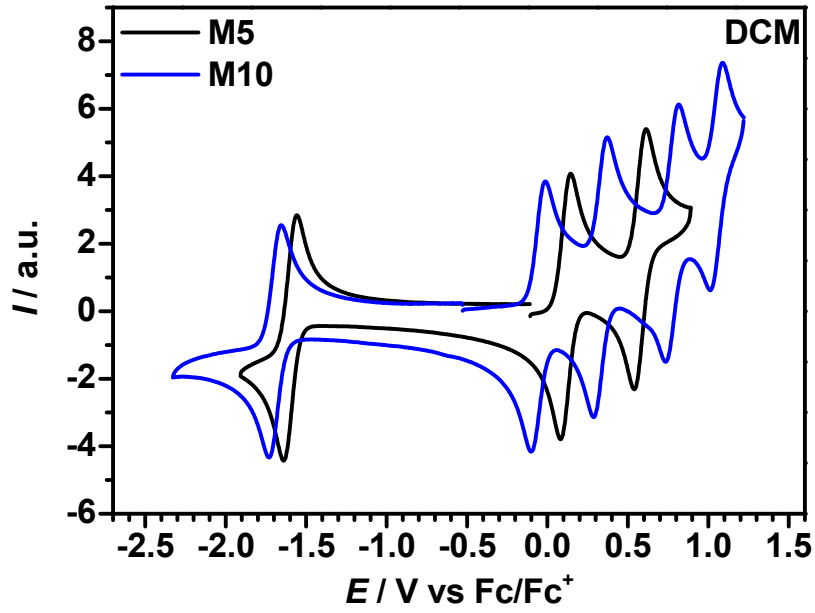

Figure 39 Cyclic voltammograms of **M5** and **M10** in DCM/TBAHFP (0.2 M) at a scan rate of 250 mV s^{-1}.

The voltammograms of both dyes that are substituted with two diarylamine groups (**M11** and **M12**) are shown in Figure 40 (left). For both of them, five oxidation waves are resolved. The first four waves are one-electron processes whereas the 5th wave covers the transfer of two electrons. Digital fitting with DigiSim[195] reveals two oxidation potentials within the last oxidation wave with energy splitting of the single oxidations of 47 mV and 32 mV for **M11** and **M12**, respectively. This leads to a total of six oxidations, two for the parent squaraine system and two for each diarylamine substituent in agreement with **M10**. The strong electron donor properties of the additional diarylamine substituents are reflected at the remarkably low 1st oxidation potentials that are –190 and –111 mV for **M11** and **M12**, respectively. Similar to the dibrominated squaraines **M5** and **M7** (Figure 14, top), it can be observed that the dicyanomethylene group in the central ring leads to more positive potentials of the reduction and the 1st oxidation. All other oxidations are barely influenced. The 5th/6th oxidations occur at almost the same potential as the 4th of **M10** at ca. 1.04 V.

For **M13** the pattern of the oxidation potentials (Figure 40, right) is different compared to those of **M10** and **M11**. Here, alternating one- and apparent two-electron processes

are observed. The total number of oxidations sums up to six as in **M11**. However, the "two-electron" processes differ from each other. Digital fitting of the second oxidation wave yields two equal oxidation potentials for the 2nd and 3rd oxidation. Even for two non-interacting redox centres there should be a redox splitting of 35.6 mV for statistical reasons.[196] The 4th oxidation wave is separate and for the 5th and 6th oxidation again a redox splitting of 50 mV is obtained by the digital fit. The interpretation of these redox properties will be discussed in more detail in section 3.3.7.

It can clearly be seen that the addition of an electron donor dramatically reduces the first oxidation potential. This is a result of a delocalised character since both the 1st oxidation potential of an isolated indolenine squaraine such as **M1** or **M5** and the 1st oxidation of isolated triarylamines[197] are at distinctly higher potential.

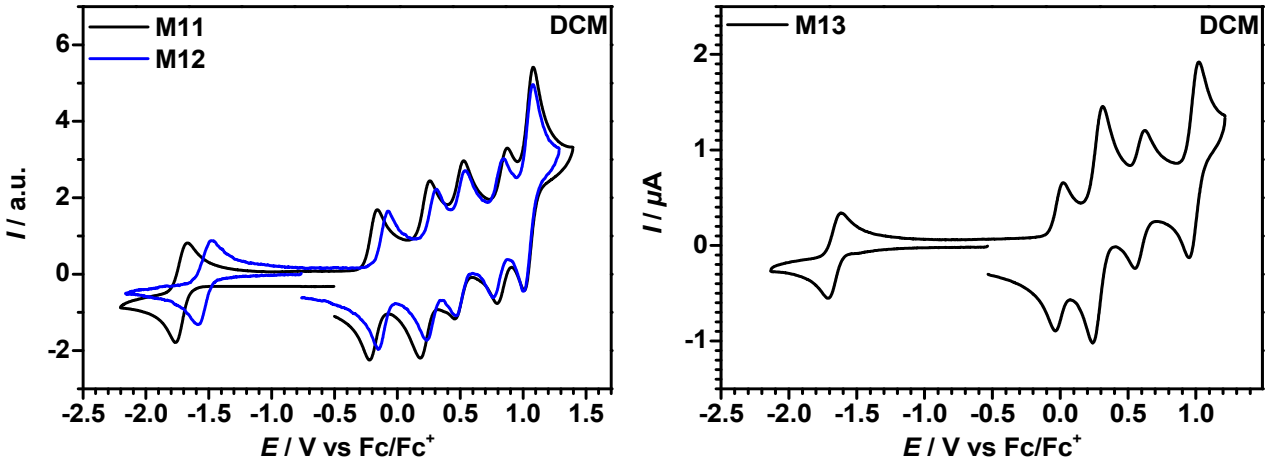

Figure 40 Cyclic voltammograms of monomer **M11** and **M12** (left) and **M13** (right) in DCM/TBAHFP (0.2 M) at a scan rate of 250 mV s^{-1}.

The voltammograms of the carbazole-substituted dyes are shown in Figure 41. Concerning the first two oxidation steps and the reduction, only slight differences are found for the squaraines **M17** and **M16** that are linked to carbazole either in the carbazole 2- or 3-position, respectively. The *N*-linked carbazole conjugate **M18** shows a somewhat lower reduction and higher oxidation potentials.

Comparison of the mono- and dicarbazole-substituted squaraines **M14** and **M15** shows that the additional carbazole moiety leads to 40–50 mV lower oxidation potentials. Scanning over a third, chemically irreversible, oxidation process for **M14**–**M17** leads to

a different back-reduction (dashed lines, not shown for **M17**). The irreversibility of the third process is likely to be due to the unprotected 6-position of the carbazole moieties where dimerisation could occur after oxidation of the carbazole moiety.[198-199] This interpretation is supported by the third clean reversible oxidation of **M18** where the 3- and 6-positions are protected by chlorine atoms and no further dimerisation of the carbazole moiety is possible.

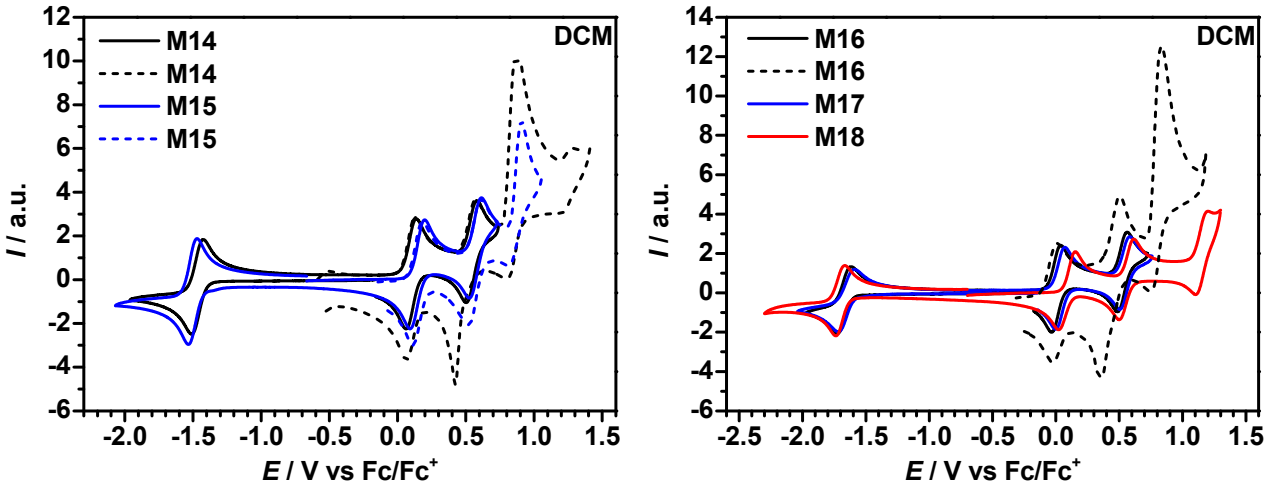

Figure 41 Cyclic voltammograms of monomer **M14** and **M15** (left) and **M16**–**M18** (right) in DCM/TBAHFP (0.2 M) at a scan rate of 250 mV s^{-1}. The voltammograms depicted in dashed lines cover a third oxidation process that is not included in the respective voltammograms depicted in solid lines.

Piperazine-substituted dye **M19** exhibits two clean oxidation waves and one reduction wave (Figure 42, black line). However, if the scan includes the third, chemically irreversible, oxidation process, no clean back-reduction is observed for this process. The half-wave potential of the 1st oxidation is the lowest found for all dyes investigated in this work and is found at –214 mV. Generally, the reduction and the 1st and 2nd oxidation potentials ($E_{1/2}$ = –1.71 V, –214 mV, and 231 mV, respectively) are rather similar compared to diarylamine-substituted squaraine **M11** ($E_{1/2}$ = –1.72 V, –190 mV, and 221 mV, respectively). This comparison indicates that the 1st oxidation is localised on the parent squaraine and not at either of the substituents.

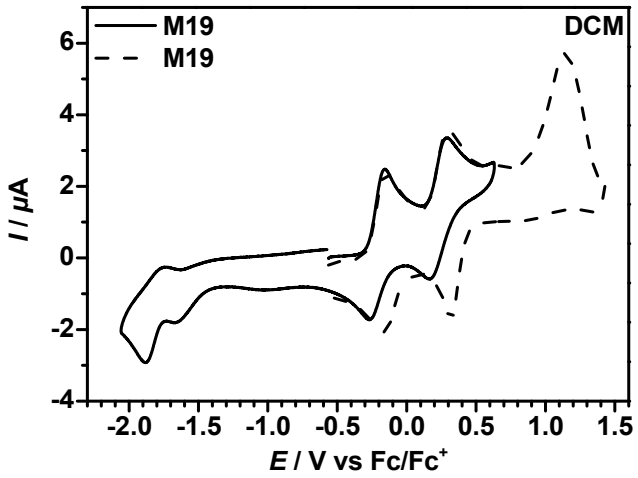

Figure 42 Cyclic voltammograms of monomer **M19** in DCM/TBAHFP (0.2 M) at a scan rate of 250 mV s^{-1}. The voltammogram depicted in dashed line covers a third oxidation process that is not included in the respective voltammogram depicted in solid line.

This low oxidation potential is not completely reflected in the absorption spectroscopy even though the absorption maximum is slightly shifted to lower energy compared to the reference dye **M1**. This can also be seen in the large deviation of the electrochemical and optical obtained band gaps E_{gap}^{CV} and E_{gap}^{opt}, respectively, shown below. Nevertheless, these results demonstrate the strong electron donating character of the piperazine moieties.

3.3.6 Band Gaps

The HOMO energy levels (E_{HOMO}) of all the donor-substituted squaraine dyes are between –4.95 eV for the squaraines with strong electron donating substituents (**M11**, **M12**, and **M19**) and –5.31 eV. The LUMO energy levels (E_{LUMO}) are between –3.44 eV and –3.69 eV, where the lowest values are found for squaraines incorporating the central dicyanomethylene group (**M12**, **M14**, and **M15**).

The band gaps range from 1.42 eV to 1.79 eV. The lowest is obtained for **M12**, the squaraine that comprises both the strong electron accepting dicyanomethylene group as well as the strong electron donating diarylamine moieties. The highest value is found for the asymmetric dye **M18** which even exceeds that of the reference or functionalised squaraines without an additional donor.

Table 14 Redox potentials, HOMO and LUMO energy levels and band gaps obtained by electrochemical (E_{gap}^{CV}) and optical (E_{gap}^{opt}) methods of donor-substituted squaraines **M10**–**M19** together with dibrominated squaraines **M5** and **M7**. All measurements were performed in DCM.

	$E_{1/2}^{Red1}$ / mV	$E_{1/2}^{Ox1}$ / mV	$E_{1/2}^{Ox2}$ / mV	$E_{1/2}^{Ox3}$ / mV	$E_{1/2}^{Ox4}$ / mV	$E_{1/2}^{Ox5}$ / mV	$E_{1/2}^{Ox6}$ / mV	E_{HOMO} / eV[d]	E_{LUMO} / eV[d]	E_{gap}^{CV} / eV[d]	E_{gap}^{opt} / eV[e]
M5[a]	–1610	110	580 *571*					–5.27	–3.55	1.72	1.86
M7[a]	–1405	207	576 *574*					-5.37	-3.76	1.61	1.71
M10[a]	–1692	59	329 *319*	775 *756*	1049 *1028*			–5.10	–3.47	1.63	1.71
M11[a]	–1717	–190	221 *244*	491 *458*	833 *803*	1045 *992*	1045 *1039*	–4.97	–3.44	1.53	1.65
M12[a]	–1535	–111	271 *305*	502 *493*	801 *792*	1038 *1013*	1038 *1045*	–5.05	–3.63	1.42	1.54
M13[a]	–1664	–6	277 *268*	277 *<286*	587 *586*	987 *958*	987 *1008*	–5.15	–3.50	1.65	1.75
M14[a]	–1468	96	542					–5.26	–3.69	1.57	1.65
M15[a]	–1502	146	570	802[c]				–5.31	–3.66	1.65	1.69
M16[a]	–1670	1	523					–5.16	–3.49	1.67	1.77
M17[a]	–1653	35	544					–5.20	–3.51	1.69	1.79
M18[a]	–1701	88	557	1151				–5.25	–3.46	1.79	1.86
M19[b]	–1711	–214	231	994[c]				–4.95	–3.45	1.50	1.73

[a] Ag/AgCl pseudo-reference electrode; [b] Ag/AgCl "leak free" electrode; [c] potentials extracted from DPV; [d] determined according to the procedure described in 5.1.4; [e] determined in DCM according to the procedure in 5.1.1; the values written in italics are obtained by digital fitting of the redox waves with DigiSim.[195]

3.3.7 Squaraines as Bridge Between two Redox Centres

Introduction

The absorption and redox properties of the di-/triarylamine-substituted dyes, and especially the strikingly different characteristics of **M11** and **M13**, urged the need for a more detailed investigation on their origin. Therefore, the matter of the interaction

between the di/-triarylamine moieties and the central squaraine core, as well as the interaction between the di/-triarylamine groups themselves was explored.

The electronic structure of the neutral compounds as well as the radical cations, diradical dications (and in one case triradical trication) was characterised using the interplay of spectroelectrochemistry experiments and TDDFT calculations, in addition to steady state absorption spectroscopy, fluorescence spectroscopy, and cyclic voltammetry. Even though squaraines are a popular class of dyes, the nature of the electronic structure of its radical cations is largely unexplored. The compounds chosen for this study are di-/triarylamine-substituted dyes **M10**–**M13** as well as **M5** and **M7** for comparison.

Albeit intensive research has been performed on the nature of bis(triarylamine) radical cation mixed valence (MV) systems with varying bridges in order to probe the interaction of the two triarylamine systems and to consequently determine their *Robin-Day*[200] classification (class I: charge localised on one redox centre → no interaction between redox centres; class II: charge mainly localised on one redox centre, however, it can be transferred to the other by thermal or optical activation; class III: charge delocalised over both redox centres and the bridge).[201-204] Considering the central squaraine chromophore as a bridge unit, its impact on the coupling between redox centres was investigated.

The following bis(triarylamine) radical cations illustrate some basic features of organic MV systems in solution: compounds **A-C** (Chart 4) all possess phenylene-vinylene bridging units with increasing length. Compound **A** has eleven bonds between the nitrogen atoms, and the charge in this bis(triarylamine) radical cation is completely delocalised.[204-205] On the other hand, compound **C** incorporates 29 bonds between the nitrogen atoms and shows essentially no interaction between the *N*-*N*-centres. In-between is compound **B** in which the positive charge is mainly localised at one of the two triarylamine moieties but significant interaction with the other triarylamine is visible through an inter-valence charge transfer band (IV-CT) in the NIR region of the absorption spectrum. Thus, compounds **A–C** cover the range from *Robin-Day* class III (**A**) over class II (**B**) to borderline class I/II (**C**) with (almost) no interaction.

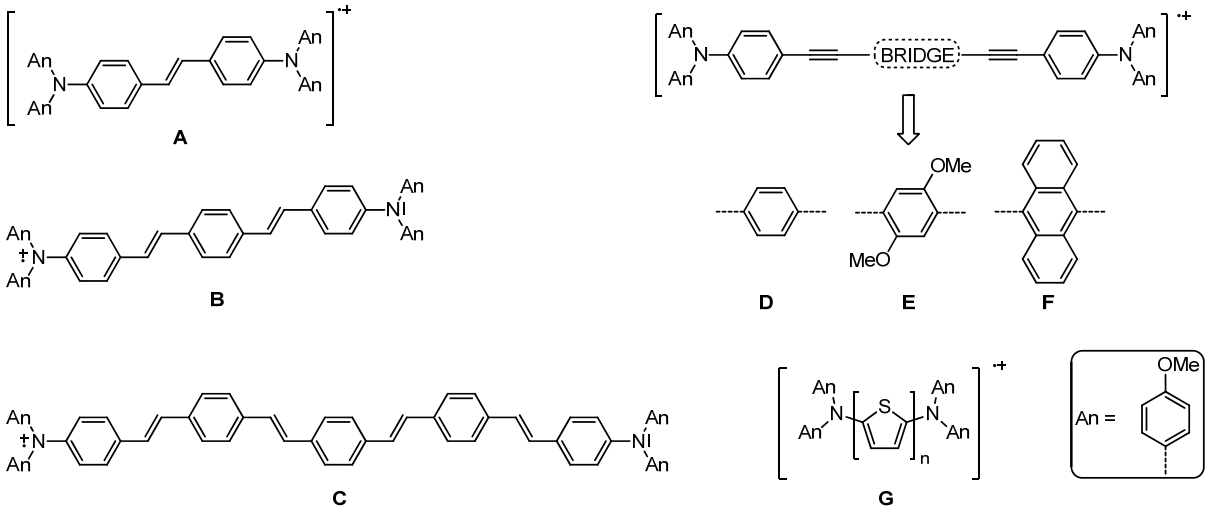

Chart 15 Bis(triarylamine) radical cations **A**–**G**.

Furthermore, it could be demonstrated that it is possible to completely alter the electron transfer (ET) behaviour of bis(triarylamine) radical cations only by bridge state modification, even though the *N*-*N*-distance remains constant.[201] In compound **D** in DCM the charge is mainly localised on one of the redox centres, whereas in **E** the charge is increasingly delocalised between the bridge and one of the redox centres. MV system **F** is right at the class II/III borderline: in MeCN it appears to be a class II compound, whereas in DCM there is experimental evidence that the charge is symmetrically delocalised over the anthracene bridge and the adjacent phenylethynyl groups, and it is therefore a class III compound. This behaviour is due to the increasing donor character of the bridge where the charge gets more and more stabilised and leads to a valence delocalised system with a bridge localised ground state in **F**. This is not because the bridge unit might be easier oxidised than the triarylamine redox centres (which is not the case for **F** since isolated anthracene possesses a higher oxidation potential than the isolated triarylamine) but a direct consequence of the delocalisation and class III character. Recent DFT calculations (similar to those performed in this work) predict **F** to be a completely delocalised class III compound in each of those solvents.[206] Similar results were obtained for bis(triarylamine) radical cations with other electron-rich bridges.[207-209]

In a related computational work, *Lacroix et al.* studied the influence of the bridge length on the electronic structure of electron-rich MV compounds by analysing thiophene-

bridged bis(dianisylamine) radical cations **G** with various numbers (*n*) of bridge units.[210] Here it was shown that for *n* = 1, 2 the charge is symmetrically delocalised and those compounds can therefore be placed into class III. However for n > 4 (e.g. *N*-*N*-distance of 21 bonds for n = 5) the substances are class II since the charge is localised on one of the redox centres.

Thus, with increasing length of the bridge, delocalised systems might cross over to real MV systems with a localised charge. On the other hand, systems with a localised charge can turn into valence delocalised systems with a bridge ground state when a more electron-rich bridge is used.

Using a squaraine as an electron rich bridge unit with low 1st oxidation potential, these studies are extended. The relative sharp and intense lowest energy absorption band of a squaraine indicates a strong delocalisation of the excited state and consequently a small reorganisation energy which should support delocalisation of charge between adjacent triarylamine redox centres in a squaraine based, potentially MV, system. Furthermore, the oxidation potential of isolated squaraines is in the same range as those of isolated triarylamines. Compared to e.g. the anthracene bridge of compound **F**, this should further increase the coupling between the adjacent triarylamines and allow creating extended valence delocalised systems.

Oxidation Sequence

Comparison of the cyclic voltammograms of **M11** and **M13** (Figure 40, p. 127) and their different oxidation patterns gives rise to the question why the second and the third oxidation process in **M13** cannot be seen separately, in contrast to all other compounds. The difference between **M11** and **M13** is an additional phenylene unit in **M13** between each diarylamine moiety and the central indolenine squaraine chromophore.

It is assumed that the first oxidation process in **M11**–**M13** occurs formally at the central indolenine squaraine unit whereas the second oxidation takes place at one of the di-

/triarylamine groups (1st and 2nd step Figure 44). This is confirmed also by the computed spin density distributions shown in Figure 43.

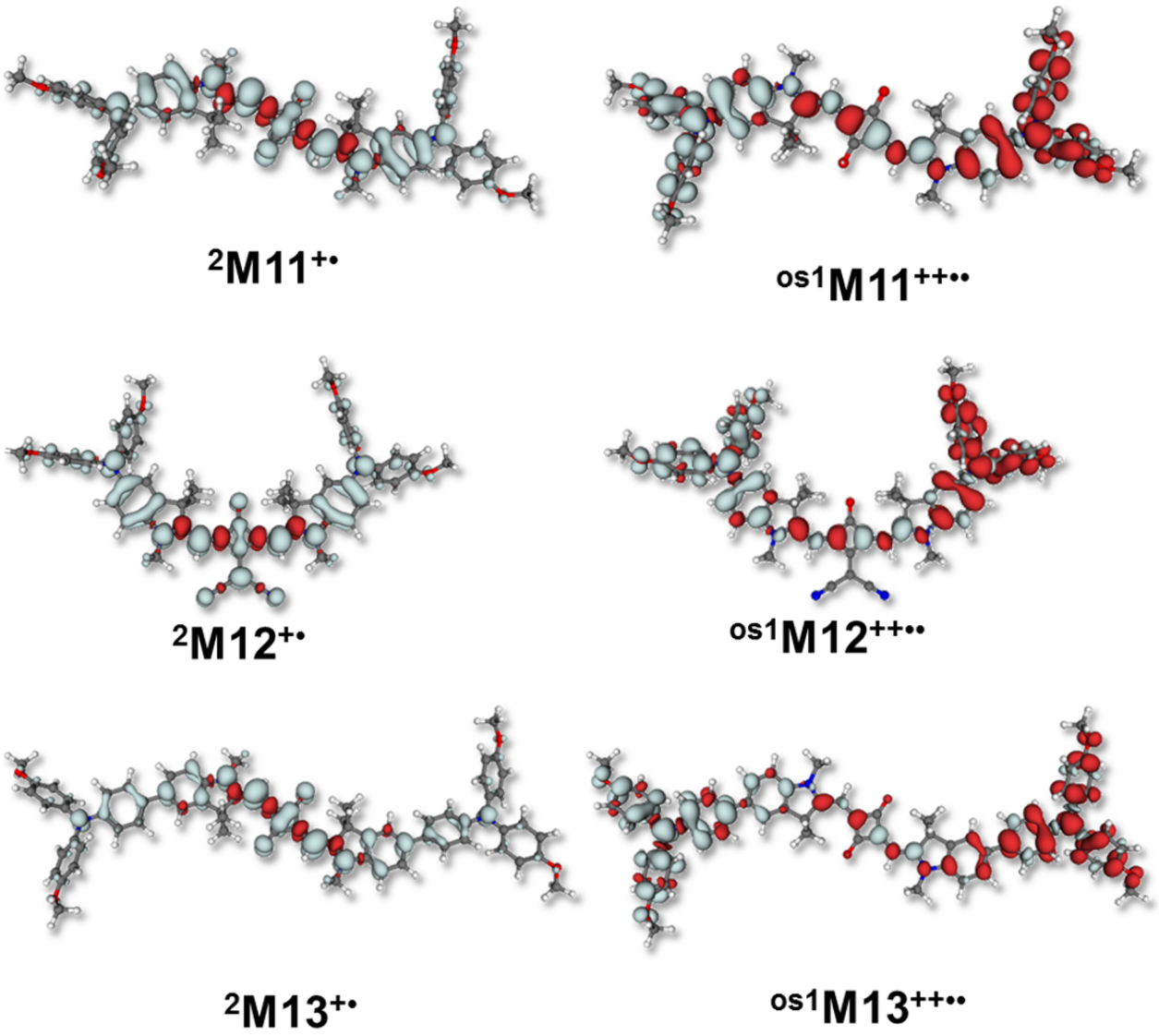

Figure 43 Spin density isosurface plots (values ± 0.001 a.u.) of the monoradical cations (left) and open shell (os) singlet diradical dications (right) of **M11** (top), **M12** (middle), and **M13** (bottom) (B3LYP/SVP).

Due to electrostatic repulsion of the two positive charges, a kinetically fast migration of the central positive charge to the second di-/triarylamine group (3rd step in Figure 44) is postulated. As it was already shown by the shifts of the main absorption band upon addition of further electron-donating moieties, the influence of the triarylamine units in **M13** is weaker than that of the diarylamine groups in **M11**. However, in the case of **M13**$^{++\bullet\bullet}$ the electrostatic interaction is still strong enough to repel the positive charges,

leading to a dication with the two positive charges being located at the triarylamine groups. The migration of charges results in the central indolenine squaraine being "neutral" again for $\mathbf{M11}^{++\bullet\bullet}$ and $\mathbf{M13}^{++\bullet\bullet}$.

In a 4th step (Figure 44) the central squaraine can once again be oxidised, yielding the trications $\mathbf{M11}^{+++\bullet\bullet\bullet}$ and $\mathbf{M13}^{+++\bullet\bullet\bullet}$. The main difference between **M11** and **M13** is the potential at which this third oxidation occurs: in $\mathbf{M13}^{++\bullet\bullet}$ the squaraine moiety can be oxidised at a distinctly lower potential, presumably just slightly higher than the first oxidation (which refers to the squaraine oxidation of neutral **M13**) because the electrostatic interaction is weak in this large chromophore system. This is supported by a digital fit which yields the same potential for the 2nd and 3rd oxidation. An upper bound for the latter is somewhat ambiguous because equal or slightly higher potentials for the third than second step yield both equally good fits. Thus, the third oxidation happens right after the charges have separated in $\mathbf{M13}^{++\bullet\bullet}$, which leads to the apparent two-electron process at the same potential. From this reasoning it is concluded that $E_{1/2}^{\mathrm{Ox1}} < E_{1/2}^{\mathrm{Ox3}} < E_{1/2}^{\mathrm{Ox2}}$ for **M13**.

For $\mathbf{M11}^{++\bullet\bullet}$ electrostatic repulsion of charges is stronger because of the smaller size extension of the chromophore compared to $\mathbf{M13}^{++\bullet\bullet}$. Therefore, the two positive charges have a strong influence on the third oxidation which thus appears at higher potential, indicating $E_{1/2}^{\mathrm{Ox1}} < E_{1/2}^{\mathrm{Ox2}} < E_{1/2}^{\mathrm{Ox3}}$ for **M11** with well separated oxidation processes. A further hint supporting this interpretation of only weakly coupled triarylamines in **M13** is the 4th oxidation $E_{1/2}^{\mathrm{Ox4}}$ of **M13** (*586* mV), which differs only slightly from $E_{1/2}^{\mathrm{Ox2}}$ of **M5** (*571* mV) and **M7** (*574* mV). It is therefore assumed that this oxidation occurs nearly "undisturbed" at the indolenine squaraine chromophore.

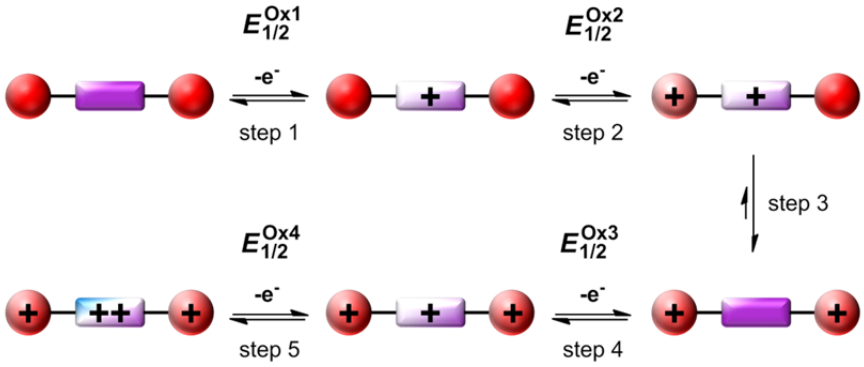

Figure 44 Proposed oxidation sequence of di- and triarylamine disubstituted squaraines.

In case of **M10** the first oxidation is also assumed to occur at the indolenine squaraine. This is supported by computed spin densities (Figure 45), which resemble that of the disubstituted chromophores. The 2nd oxidation occurs at the diarylamine group. For the 4th oxidation of **M10** and the 5th and 6th of **M11**–**M13**, similar values are observed. Consequently it can be assumed that these refer to the 2nd oxidation of the diarylamine/triarylamine moieties.

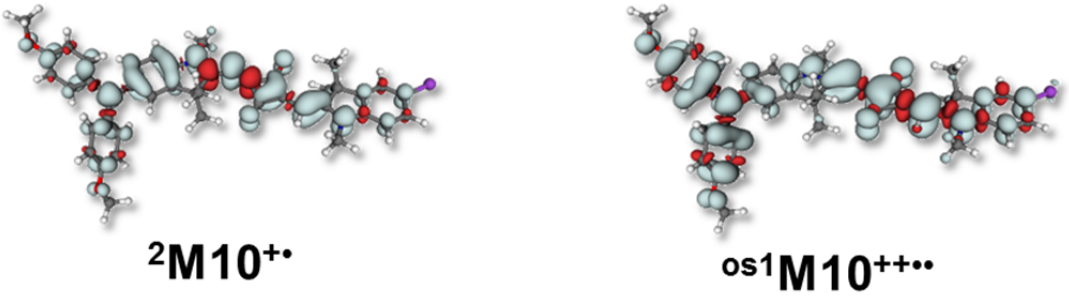

Figure 45 Spin density isosurface plots (values ± 0.001 a.u.) of the monoradical cation (left) and open shell (os) singlet diradical dication (right) of **M10** (B3LYP/SVP).

Spectroelectrochemistry

To gain further insight into the electronic structure of the compounds upon oxidation, spectroelectrochemical experiments in the UV/Vis/NIR region were performed to characterise the mono- and dications (and the trication of **M13**). Spectroelectrochemical investigations for different squaraines were reported earlier, but the information about indolenine squaraines is rare.[211-212] For a complete investigation the dibrominated

squaraines **M5** and **M7** were analysed in addition to the donor-substituted dyes **M10**–**M13**.

UV/Vis/NIR spectra of the successive electrochemical oxidation of the squaraine compounds were recorded in DCM with TBAHFP (0.2 M) as supporting electrolyte. The oxidation processes were recorded up to the second oxidation (in the case of **M13**, third oxidation) for which chemical reversibility of the processes could be proved.

The spectroelectrochemical data of all compounds was analysed with SPECFIT[213] and the UV/Vis/NIR spectra of the pure neutral squaraines (black lines), its radical cations (blue lines), diradical dications (green lines), and in the case of **M13** the triradical trication (red line) were extracted and are shown in Figure 46. The spectroscopic data are summarised in Table 15 (p. 150).

The most intense absorption bands of the squaraine monocations are located between 11500 cm^{-1} and 12100 cm^{-1} for the diarylamine-substituted squaraines **M10**–**M12** and between 14800 cm^{-1} and 15300 cm^{-1} for **M5**, **M7**, and **M13**. They all show similar large extinction coefficients on the order of 100000 $M^{-1}\,cm^{-1}$. The sharp and intense band shape (with the exception of $\mathbf{M13}^{+\bullet}$) indicates that the monoradical cations still have a cyanine-like, delocalised character. Another hint for delocalised monoradical cations are the computed relatively small dipole moments (Table 15, p. 150). Furthermore, all amine donor-substituted compounds show an additional absorption around 6000 cm^{-1} with an extinction coefficient of around 40000 $M^{-1}\,cm^{-1}$. A striking difference is a 2nd weaker absorption band of $\mathbf{M12}^{+\bullet}$ in that spectral region the origin of which is discussed below. By superimposition of the absorption spectra recorded during the oxidation process, isosbestic points can be observed for all compounds. Those reveal that only two species, whose concentrations are related linearly, exist. Therefore a formation of aggregates of the monoradical cations can be ruled out since this would disturb the linear relation of the neutral species and the monoradical cation and no isosbestic points could be observed.

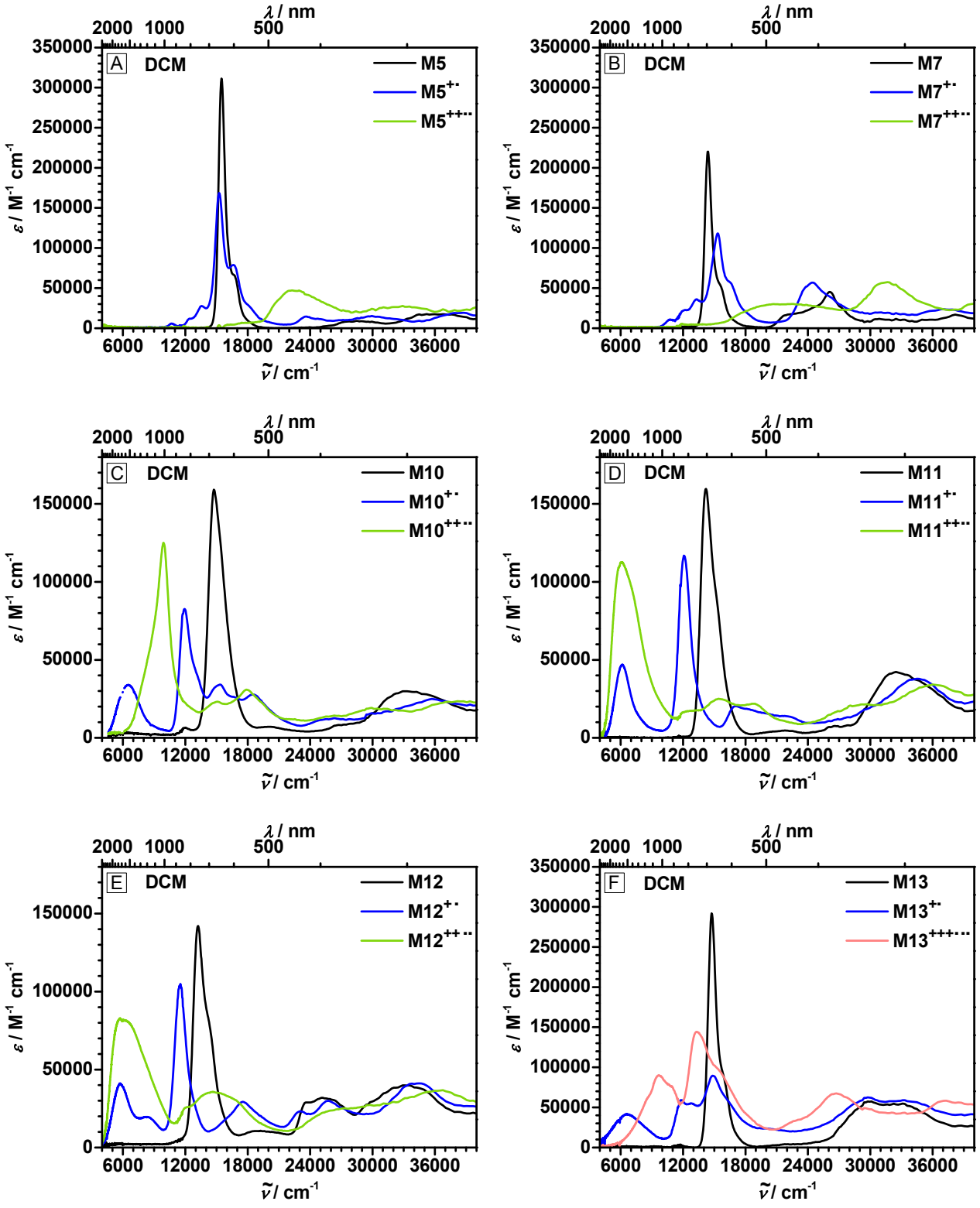

Figure 46 UV/Vis/NIR spectra of the neutral squaraines (black), monoradical cations (blue), diradical dications (green), and triradical trication (red) in DCM/TBAHFP (0.2 M).

An example of the overlaid absorption spectra is given for **M12** in Figure 47 (left, **M12**→**M12**$^{+\bullet}$; right, **M12**$^{+\bullet}$→**M12**$^{++\bullet\bullet}$) and isosbestic points are found at 12500 cm^{-1} and 15800 cm^{-1} (left) for example.

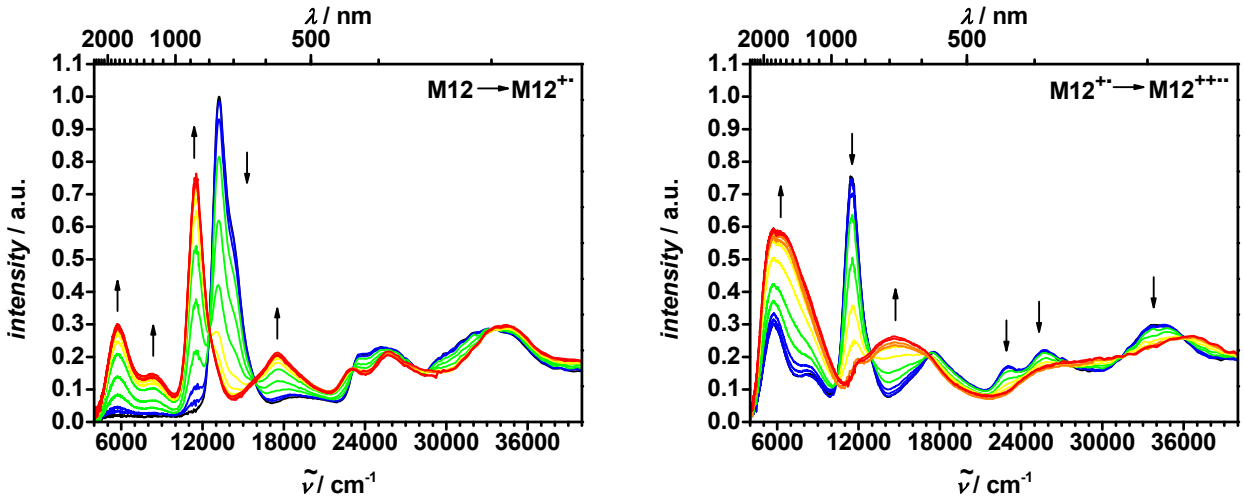

Figure 47 Normalised absorption spectra of the successive 1st (left) and 2nd oxidation (right) of **M12**, derived from the spectroelectrochemical experiment in DCM/TBAHFP (0.2 M).

Both **M11**$^{++\bullet\bullet}$ and **M12**$^{++\bullet\bullet}$ exhibit an intense absorption around 6000 cm^{-1} with a similar extinction coefficient of around 90000 M^{-1} cm^{-1}. Unlike the absorption spectra of the monoradical cation, the spectrum of **M10**$^{++\bullet\bullet}$ is different to those of **M11**$^{++\bullet\bullet}$ and **M12**$^{++\bullet\bullet}$. The main absorption band of **M10**$^{++\bullet\bullet}$ is located at 9900 cm^{-1} with an extinction coefficient of 125000 M^{-1} cm^{-1}. This difference could be due to the charge separation that occurs in **M11**$^{++\bullet\bullet}$ and **M12**$^{++\bullet\bullet}$ leading to the two amine centres being oxidised while this cannot take place in **M10**$^{++\bullet\bullet}$ where the single amine and the squaraine are oxidised.

In the case of **M13** only the monoradical cation can be compared with the other compounds because for reasons discussed above, dication formation is rapidly followed by triradical trication formation. The triradical trication is then the only species present at the given electrode potential. In fact, careful inspection of the spectroelectrochemistry data did not give any evidence for the presence of a sizeable **M13**$^{++\bullet\bullet}$ concentration during stepwise oxidation of **M13**$^{+\bullet}$ to **M13**$^{+++\bullet\bullet\bullet}$. For the triradical trication **M13**$^{+++\bullet\bullet\bullet}$, two strong absorption bands are found at 9700 cm^{-1} and 13300 cm^{-1}, with extinction coefficients of just below 100000 M^{-1} cm^{-1} and 144000 M^{-1} cm^{-1}, respectively.

Even though characteristic absorption spectra of the oxidised species were obtained, the interpretation of the observed bands remained difficult. Therefore, DFT and TDDFT calculations (cf. Computational Details in 5.1.11) were performed to support the experimental findings.

DFT & TDDFT-Calculations

The DFT and TDDFT calculations were performed in the group of *Martin Kaupp* at the Institut für Chemie at the Technische Universität Berlin for the neutral systems, the monoradical cations, and the diradical dications (and the triradical trication of **M13**) in order to compare the calculated with experimental excitation energies and to conclude about the electronic structure in case of favourable agreement. Several questions such as the localisation/delocalisation of positive charges or the spin multiplicity of the doubly charged species shall be addressed. In the latter case both the closed and open-shell singlet (treated as broken-symmetry solution), as well as the triplet species were evaluated to assess which one is in fact generated in the spectroelectrochemistry experiment. In case of **M13**, the doublet and quartet species of the triradical trication were calculated (the doublet again as broken-symmetry state). These calculations provide dipole moments, excitation energies, the corresponding transition moments, and oscillator strengths, as well as the contributions of various orbitals to the excitations.

An overview of some of the relevant molecular orbitals (MOs) is given in Figure 48. For easier comparison, the assignment of the HOMOs and LUMOs of the *neutral* molecules is retained even for the charged species even though it is incorrect.

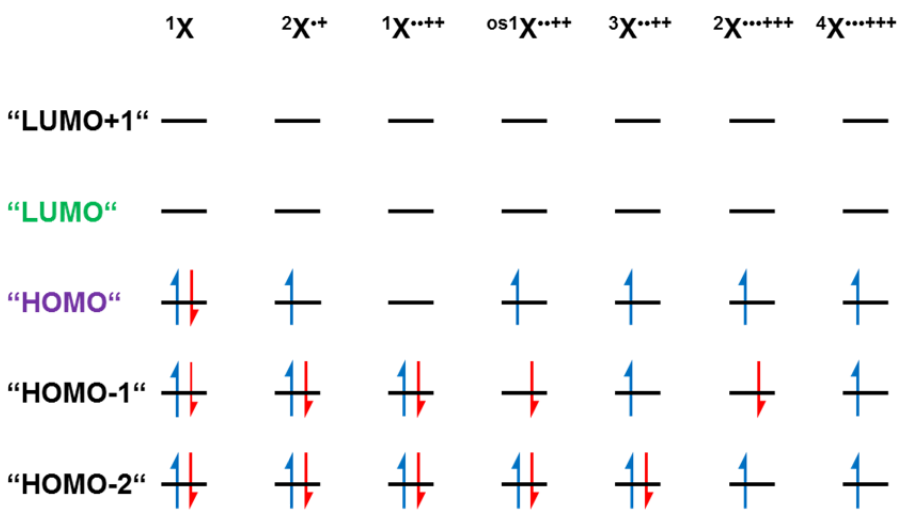

Figure 48 Molecular orbitals of the neutral and charged species of **M10**–**M13**. The "HOMO" and "LUMO", etc. descriptions are only valid for the neutral species but are retained for the charged species as well. ^{x}**X** stands for the compound; the superscript defines the spin multiplicity. os = open shell.

The TDDFT-B3LYP/SVP computed data are presented as stick spectra together with the experimental spectra. In these diagrams the strongest measured absorption band was normalised to the oscillator strength of the corresponding computed transition. The spectra of **M5** and **M7** are shown in Figure 49 (left and right, respectively), those of **M10**–**M13** are shown in Figure 50, Figure 52, Figure 54, and Figure 55, respectively.

For **M5** and **M7** theory and experiment agree very nicely for the neutral compounds and the radical cations, but not at all for the diradical dications. However, for both diradical dications the calculations reveal that the singlet is 80–90 kJ mol^{-1} lower in energy than the triplet. This is due to the highly delocalised charge in these two molecules compared to the other molecules. Therefore, the 2nd oxidation takes place in the same orbital without charge separation and thus favours the singlet state.

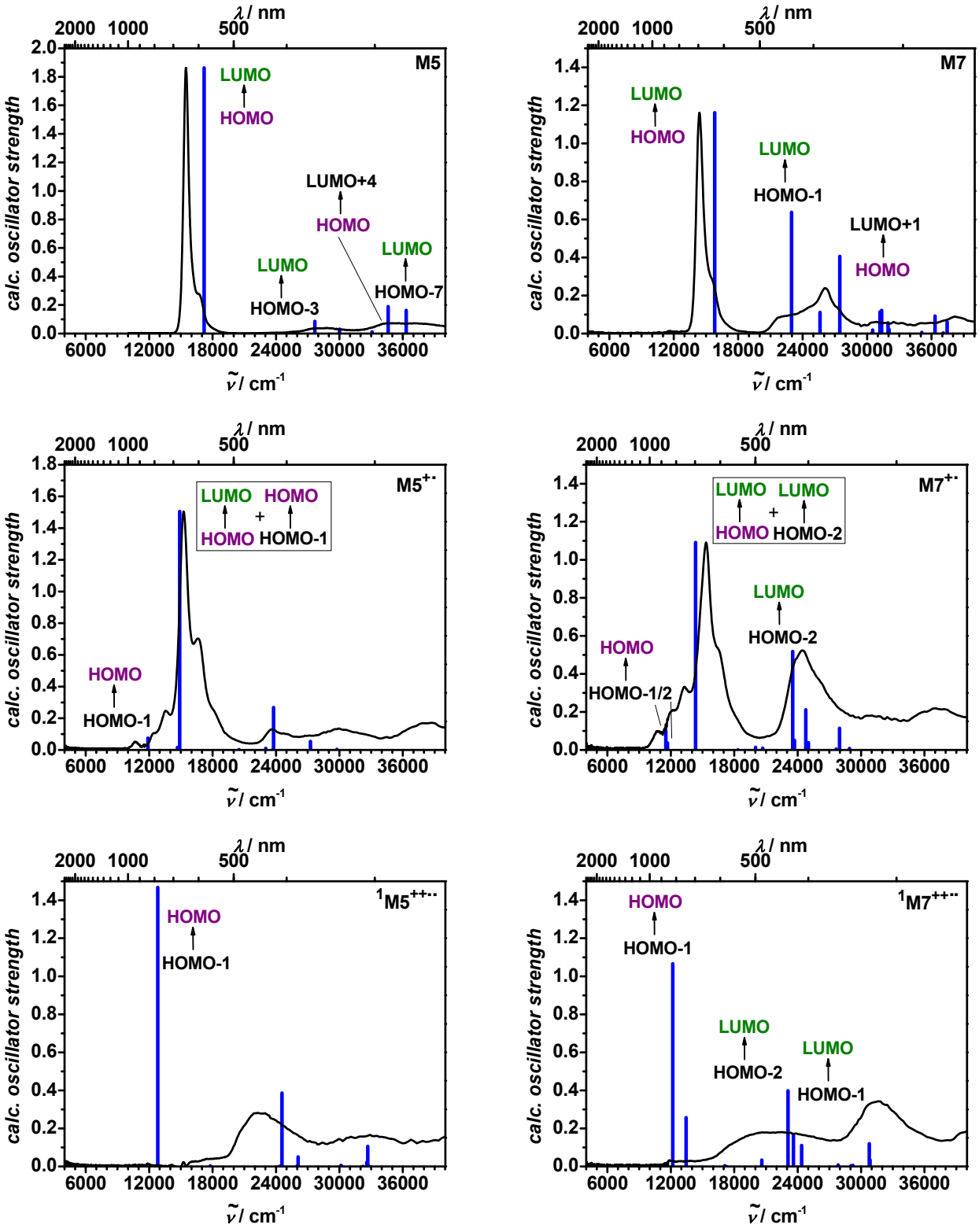

Figure 49 Combined UV/Vis/NIR spectra of the different species of **M5** (left) and **M7** (right). The "HOMO", "LUMO" etc. labels relate to the *neutral* molecule.

For all neutral compounds, the computed excitation energies are in excellent agreement with experiment for the lowest energy absorption. This transition is in all cases due to a

HOMO→LUMO excitation. The transition at higher energy is also at the appropriate energy but its oscillator strength comes out too large relative to the first excitation.

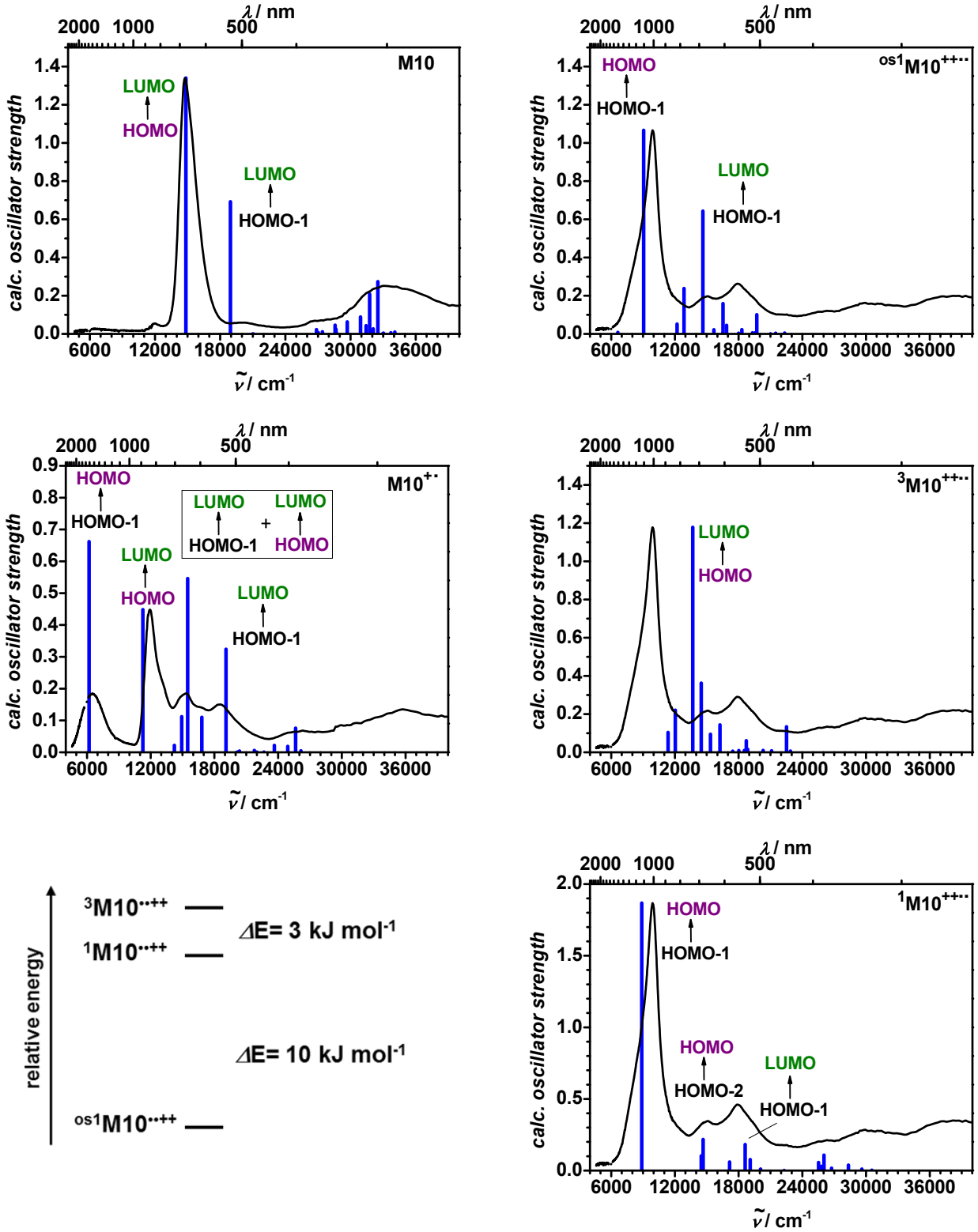

Figure 50 Combined UV/Vis/NIR spectra of the different species of **M10** and relative energies of the diradical dications. The "HOMO", "LUMO" etc. labels relate to the *neutral* molecule. os = open shell.

For the monoradical cations, the agreement with experiment is also very good, but excitation energies for the lowest energy transitions are somewhat too low. These (measured around 6000 cm^{-1}) are due to HOMO–1→HOMO excitations while the one at next higher energy is mainly due to a HOMO→LUMO excitation, slightly red-shifted compared to the equivalent transition in the neutral chromophores (for **M12**$^{+\bullet}$ there is a transition in-between which will be discussed below). The computed oscillator strength of the lowest energy transition comes out too large on a relative level, especially for **M11**$^{+\bullet}$ and **M12**$^{+\bullet}$. Inspection of the orbitals that are involved in these transitions shows that the monoradical cations are delocalised, and the lowest energy transition is due to a degenerate charge transfer from the triarylamine to the squaraine bridge in the case of **M11**$^{+\bullet}$ and **M12**$^{+\bullet}$. In this respect, "degenerate" refers to diabatic excited states that may be defined as having one positive charge on either of the two amine moieties. These two states mix and yield two non-degenerate adiabatic states, which can both be observed separately in **M12**$^{+\bullet}$: comparing the lowest energy absorption bands of **M11**$^{+\bullet}$ and **M12**$^{+\bullet}$, it can be seen that there is only one for **M11**$^{+\bullet}$ (6200 cm^{-1}) but two for **M12**$^{++\bullet\bullet}$ (5800 cm^{-1} and 8300 cm^{-1}). The latter corresponds to the HOMO–2→HOMO transition (Figure 54, blue). The analogous transition has no oscillator strength in **M11**$^{+\bullet}$ due to symmetry reasons: squaraine **M11**$^{+\bullet}$ has C_i symmetry. The appropriate orbitals possess a_u (HOMO–2), a_g (HOMO–1), and a_u (HOMO) symmetry (Figure 51).

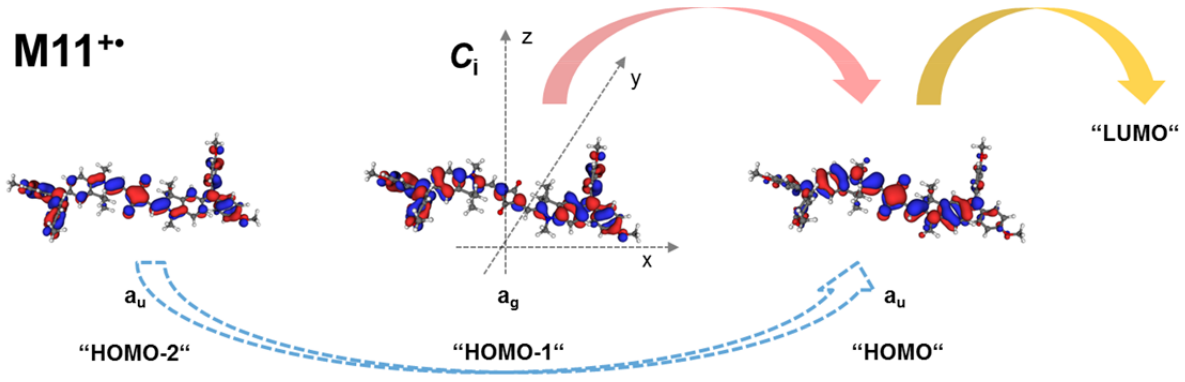

Figure 51 Molecular orbitals of **M11**$^{+\bullet}$ and its symmetry descriptions. The arrows indicate symmetry allowed (filled) and forbidden (blank, dashed line) transitions. The colours match those of the corresponding absorption bands in the spectra in Figure 52.

For a transition to be allowed, the direct product of the involved MOs and of the transition dipole moment vector has to include the totally symmetric descriptor a_g. This holds for the HOMO–1→HOMO (Figure 52, red) excitation but not for the HOMO–

2→HOMO excitation, which is thus forbidden. The most pronounced absorption in the monoradical cations still stems from a HOMO→LUMO transition (yellow) similar to the neutral compounds and is slightly red-shifted.

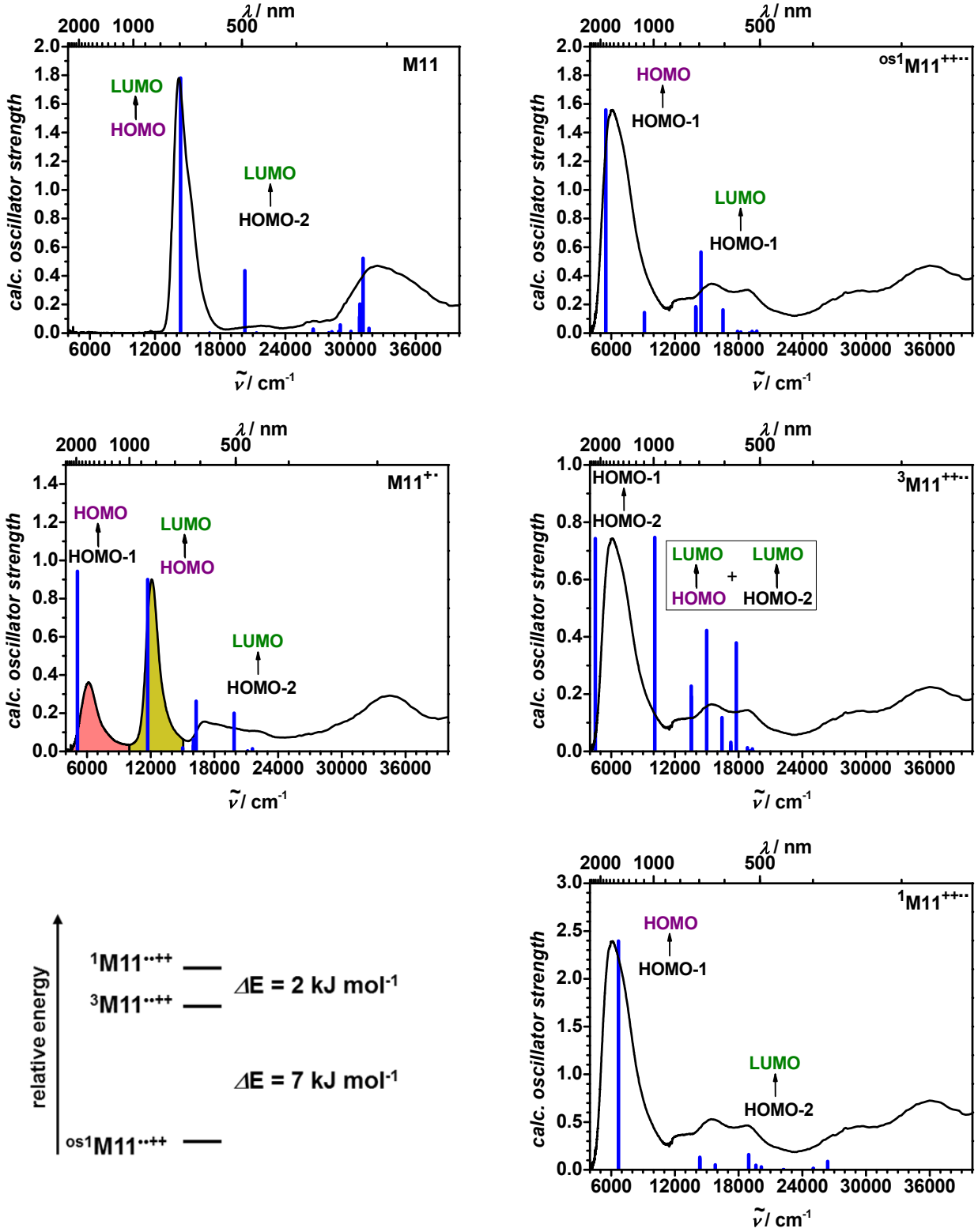

Figure 52 Combined UV/Vis/NIR spectra of the different species of **M11** and relative energies of the diradical dications. The "HOMO", "LUMO" etc. labels relate to the *neutral* molecule. The colours of the absorption bands match the transitions indicated in Figure 51. os = open shell.

For **M12**$^{+\bullet}$, the central dicyanomethylene group enforces the molecule to adopt C_2 symmetry due to sterical reasons. In this case the analogous orbitals have b (HOMO–2), a (HOMO–1), and b (HOMO) symmetry as seen in Figure 53. Therefore, the HOMO–1→HOMO (Figure 54, red) excitation is allowed with its transition moment polarised in x-direction, whereas the HOMO–2→HOMO excitation is also allowed but with its transition moment polarised in z-direction (blue). While this analysis explains the observation of the electronic transitions reasonably well, inspection of the HOMO orbitals and the spin density distribution (Figure 43, p. 134) demonstrates at the same time the essentially delocalised character of positive charge in the monocations. The very effective electronic coupling properties of the squaraine gives **M10**$^{+\bullet}$–**M13**$^{+\bullet}$ clearly *Robin-Day* class III character.

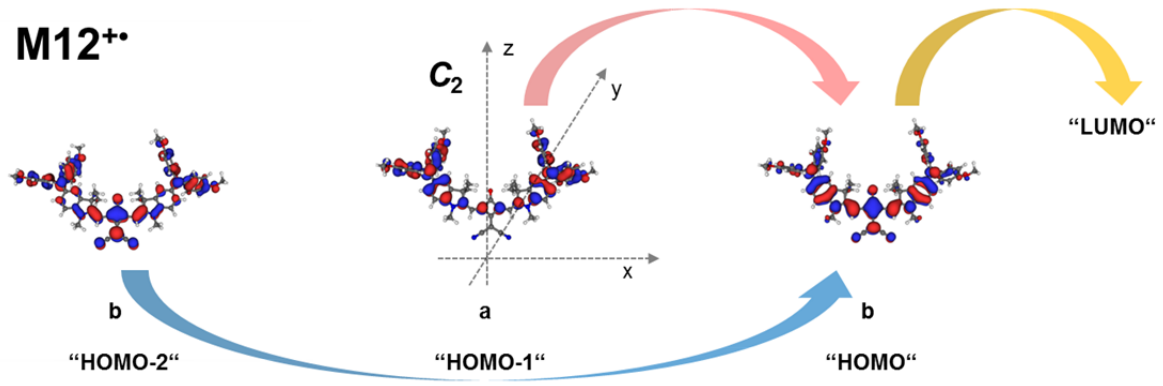

Figure 53 Molecular orbitals of **M12**$^{+\bullet}$ and its symmetry descriptions. The arrows indicate symmetry allowed transitions. The colours match those of the corresponding absorption bands in the spectra in Figure 54.

For the diradical dications the question of a triplet vs. singlet ground state arises. While for the triplet state it is obvious to use an unrestricted open-shell (os) wave function, for the singlet states both a restricted closed-shell and an unrestricted broken-symmetry open-shell state have been evaluated. For **M10**$^{++\bullet\bullet}$, a large disagreement (~ 4000 cm^{-1} in the lowest excitation energy) between calculated and experimental spectra for the triplet state is observed. The latter is thus excluded from further consideration. Computed spectra for the restricted closed-shell and the unrestricted broken-symmetry open-shell state agree both well with experiment. However, as the broken-symmetry state is below the closed-shell state by about 10 kJ mol^{-1} at the computational level employed, an antiferromagnetically coupled open-shell singlet is the most likely ground state for this

diradical dication. For the broken-symmetry state, the intense lowest energy transition corresponds to a HOMO–1→HOMO transition much as in the monoradical cation.

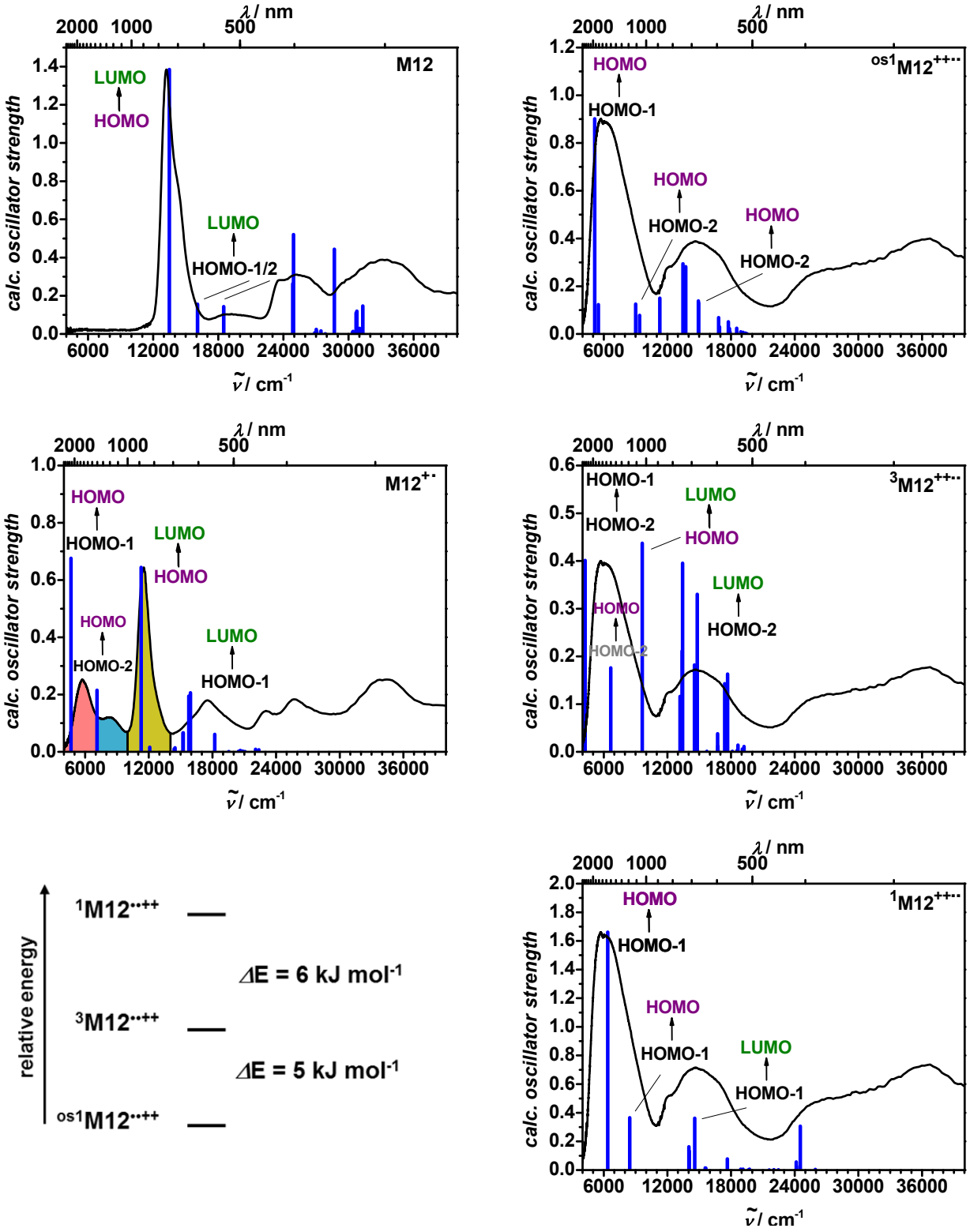

Figure 54 Combined UV/Vis/NIR spectra of the different species of **M12** and relative energies of the diradical dications. The "HOMO", "LUMO" etc. labels relate to the *neutral* molecule. The colours of the absorption bands match the transitions indicated in Figure 53. os = open shell.

The analogy of diradical dication and monoradical cation is even more evident for **M11**$^{++\bullet\bullet}$. Here again the triplet state can be ruled out, and the open-shell singlet state is favoured based on the lower energy of the broken-symmetry state, and on the excellent agreement of computed and experimental spectra. The lowest energy transition is again due to a HOMO–1→HOMO excitation much at the same energy as in the monoradical cation but with distinctly higher intensity (Figure 52). The diradical dication **M12**$^{++\bullet\bullet}$ behaves essentially analogously.

The $\langle S^2 \rangle$ spin expectation values of the broken-symmetry states of the diarylamine-substituted squaraine dications **M10**$^{++\bullet\bullet}$ (0.783), **M11**$^{++\bullet\bullet}$ (0.837), and **M12**$^{++\bullet\bullet}$ (0.886) indicate an almost equally weighted mixture of open-shell singlet and triplet character, consistent with the overall description of antiferromagnetic coupling between the amine radical cation units.

For **M13**$^{+\bullet}$ the calculation predicts a transition at 3300 cm^{-1}. It is assumed that this corresponds to the experimental absorption at 6600 cm^{-1} which is strongly underestimated compared to the other compounds. To confirm the absence of a transition at such low energy, the spectroelectrochemical experiment was additionally performed in deuterated chloroform from 3125 cm^{-1} to 40000 cm^{-1} since in this solvent the IR region is much less disturbed by solvent bands. The spectra were identical to those measured in DCM which attests the non-existence of absorption at lower energy.

For reasons discussed above the spectra of a **M13** diradical dication could not be measured but only that of the triradical trication. For **M13**$^{+++\bullet\bullet\bullet}$, the system may adopt a doublet or a quartet state. While the doublet seems to be the favoured state based on its lower energy, a quartet state or mixtures of both cannot definitely be ruled out as the quartet is only 3 kJ mol^{-1} higher in energy. The spin expectation value $\langle S^2 \rangle$ of the doublet (1.75) also indicates a broken-symmetry state, whereas the quartet (3.79) is close to a pure state. In both cases, the agreement of calculated spectra with experiment is satisfactory.

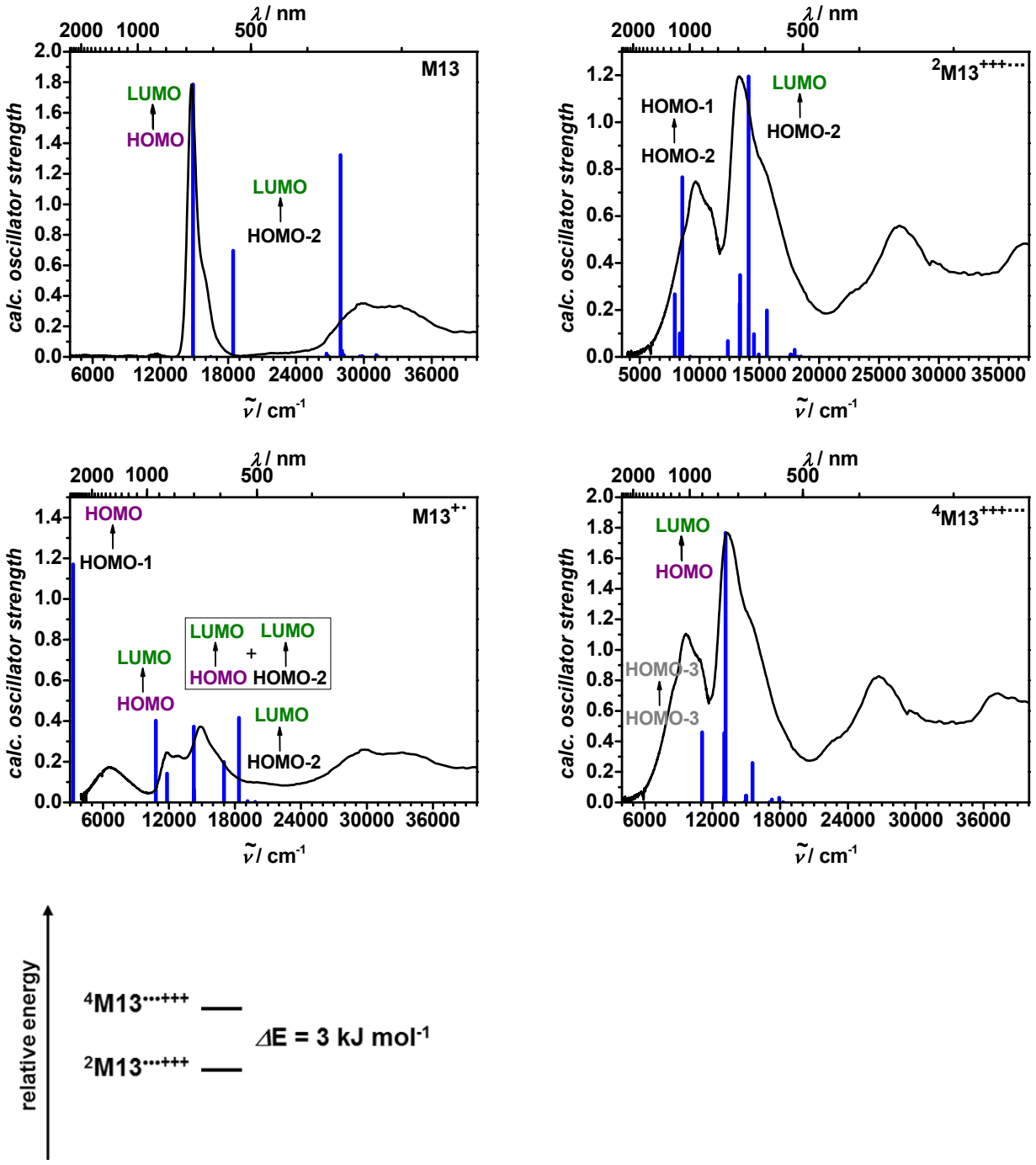

Figure 55 Combined UV/Vis/NIR spectra of the different species of **M13** and relative energies of the diradical dications. The "HOMO", "LUMO" etc. labels relate to the *neutral* molecule.

Table 15 Experimental and DFT calculated (in brackets) spectroscopic data of the neutral species, mono-, di-, and trications of the squaraines **M5**, **M7**, and **M10–M13**. Ground state dipole moments, absorption energies, extinction coefficients, and transition dipole moments.

	X	M5	M7	M10	M11	M12	M13
neutral **X**	μ_g / D	[0.1]	[5.3]	[4.5]	[5.3]	[12.4]	[0.4]
	$\tilde{\nu}_{abs}$ / cm^{-1}	15500 [17200]	14400 [15800]	14800 [14800]	14200 [14400]	13200 [13500]	14800 [14900]
	ε / M^{-1}cm^{-1}	311000	220000	153000	132000	142000	292000
	μ_{eg} / D	12.4 [15.2]	11.3 [12.5]	12.6 [13.9]	12.3 [16.2]	13.6 [14.8]	12.3 [16.0]
monocation $X^{+\cdot}$	μ_g / D	[0.1]	[2.2]	[9.7]	[5.0]	[9.26]	[0.4]
	$\tilde{\nu}_{abs}$ / cm^{-1}			6500 [6200]	6200 [5100]	5700 [4700] 8300 [7100]	6600 [3300]
	ε / M^{-1}cm^{-1}			34000	39000	41000 20000	42000
	μ_{eg} / D			10.4 [15.1]	9.9 [19.8]	9.4 [17.6] 7.5 [8.0]	13.4 [27.5]
	$\tilde{\nu}_{abs}$ / cm^{-1}	15200 [14900]	15300 [14300]	11900 [11300]	12100 [11700]	11500 [11300]	11800 [10800] 14800 [14300]
	ε / M^{-1}cm^{-1}	169000	118000	83000	97000	105000	59000 90000
	μ_{eg} / D	[14.7]	[12.7]	[9.2]	10.0 [12.8]	10.0 [11.0]	[7.5] [8.9]
dication $^{os1}X^{++\cdots}$	μ_g / D			[20.0]	[4.2]	[15.0]	
	$\tilde{\nu}_{abs}$ / cm^{-1}			9900 [9100]	6100 [5500]	5800 [5100]	
	ε / M^{-1}cm^{-1}			125000	93000	83000	
	μ_{eg} / D			[15.8]	[24.6]	[19.3]	
trication $^{2}X^{+++\cdots}$	μ_g / D						[0.62]
	$\tilde{\nu}_{abs}$ / cm^{-1}						[8600] 13300 [14100]
	ε / M^{-1}cm^{-1}						90000 144000
	μ_{eg} / D						[13.8] [13.4]

For the di- and trications only the data of the most beneficial state is shown. The spectra of the charged species were extracted with SPECFIT after analysis of the spectroelectrochemical experiments in DCM. Some transition moments could not be determined experimentally when there was a superposition of too many absorption bands. os = open shell.

Conclusion

While squaraine chromophores are a promising class of dyes for various applications, their radical cations have been largely unexplored. Thus, the electronic structure of the mono-, di-, and (in one case) trications of various squaraines with additional electron donating amine redox centres were thoroughly characterised by using a combination of cyclic voltammetry, spectroelectrochemistry, and DFT calculations.

Only by calculating the electronic spectra of all possible spin states and by comparison with the experimental spectra of the respective charged species, it was possible to draw definite conclusions about the electronic nature of the various cationic states. All squaraine monoradical cations turned out to be delocalised *Robin-Day* class III species due to the relatively low redox potential of the squaraine bridge. Substitution of a squaric ring oxygen by a dicyanomethylene group alters the symmetry of the indolenine squaraine dyes which has direct impact on the optical properties of the radical monocations. With an *N*-*N*-distance of 26 bonds between the triarylamine redox centres, **M13**$^{+\bullet}$ is to the best of knowledge the longest bis(triarylamine) radical cation that is completely delocalised. Compared to the phenylene-vinylene-bridged compounds **B** and **C**, and the anthracene-bridged compound **F** the strong impact of the squaraine bridge is obvious: e.g. compound **C** has an *N*-*N*-distance of 29 bonds, only three bonds longer than in **M13**, but shows practically no interaction between the redox centres and is therefore classified as class I/II borderline, while **M13**$^{+\bullet}$ is fully delocalised.

In contrast, the electronic situation is much more complex for the dications of the squaraine dyes: here it was shown that the energetically most stable computed state of dianisylamine-substituted squaraines is a broken-symmetry state and can better be described as a mixture of almost equal contributions of open shell singlet and triplet state. Thus, the true ground state is likely an antiferromagnetically coupled open-shell singlet.

Furthermore the redox properties of the triarylamine squaraine conjugates were explored and up to six oxidation processes assigned to the corresponding molecular moieties. It was shown that by weakening the coupling between the amine redox centres and the

central squaraine chromophore due to twisting of the π-system (biaryl moiety) and increasing length of the *N*-*N*-distance of the adjacent redox amine centres by two additional phenylene groups in **M13**, the redox potentials of the oxidations are altered strongly compared to **M11**. This leads to the unusual case of a reversed redox potential sequence for **M13**, where the third oxidation appears at lower (or almost equal) potential than the second.[214] In this case, formation of a diradical dication is impossible as is indeed observed by direct oxidation of $\mathbf{M13}^{+\bullet}$ to $\mathbf{M13}^{+++\bullet\bullet\bullet}$ in the spectroelectrochemistry experiments.

In conclusion, the electrochemical and spectroscopic data of the radical cations and diradical dications of amine-substituted indolenine squaraine chromophores demonstrate that the cyanine-like delocalised character present in the neutral chromophores is largely retained in the monoradical cations. They still show the typical intense squaraine HOMO→LUMO absorption besides additional HOMO–1→HOMO transitions while the latter dominate the spectral characteristics of the diradical dications.

3.4 Donor–Squaraine Copolymers[1]

3.4.1 Introduction

After the characterisation and study of the donor-substituted monomeric squaraine model compounds, respective copolymers were synthesised where the additional electron donating units bridge two squaraine chromophores. The goal was to create copolymers with broad absorption shifted even further into the NIR region compared to the model compounds. This concept of donor–squaraine copolymers was successfully realised for pyrrole squaraines where polymers with absorption up to 1000 nm (10000 cm^{-1}) and low band gaps around 1 eV were obtained.[121-124] However, during the preparation of this work, some donor-indolenine squaraine copolymers were reported, showing only minor red shift and broadening of the absorption spectra.[30, 88] On the contrary, as mentioned before, a series of thiophene-bridged indolenine squaraine oligomers (**OS4**, Chart 9, p. 15) shows absorption spectra with red-shifted and broadened low energy absorption bands.[67]

A series of copolymers from indolenine squaraine and various electron rich bridges was synthesised and the effect of exciton coupling and conjugation on the electronic and spectroscopic properties was investigated. In this series, saturated piperazine, unsaturated propeller like triarylamines, and more rigid unsaturated 2,7- and 3,6-carbazoles were used as bridging units. For the squaraine chromophores, both the standard oxygen squaraine as well as the dicyanomethylene-substituted squaraine were used.

The size of the polymers was determined by analytical GPC in $CHCl_3$ with polystyrene standards and the data is listed in chapter 3.7 (Table 25, p. 210).

---

[1] Reproduced or adapted in part with permission from *Synthesis, Electrochemical, and Optical Properties of Low Band Gap Homo- and Copolymers Based on Squaraine Dyes*, S. F. Völker, T. Dellermann, H. Ceymann, M. Holzapfel, C. Lambert, *J. Polym. Sci., Part A: Polym. Chem.* **2014**, *52*, 890-911. Copyright (2014) WILEY-VCH Verlag GmbH & Co. KGaA, Weinheim.
Parts of this chapter have been investigated in a bachelor thesis under the supvervision of S. F. Völker: T. Dellermann, Bachelor thesis, Julius-Maximilians Universität (Würzburg), **2011**.

3.4.2 Synthesis

Triarylamine–Squaraine Copolymers

For the synthesis of the copolymers, bifunctional precursors were necessary. The diboronic ester triarylamine derivative **26** was synthesised in two steps, applying the Cu-catalysed *Ullmann* coupling of bis(4-bromophenyl)amine and 1-iodo-4-methoxybenzene to **25** in the first step (Scheme 19). Halogen-metal exchange with *n*BuLi and subsequent addition of an appropriate borolane eventually gave the diboronic ester **26** in low yield.

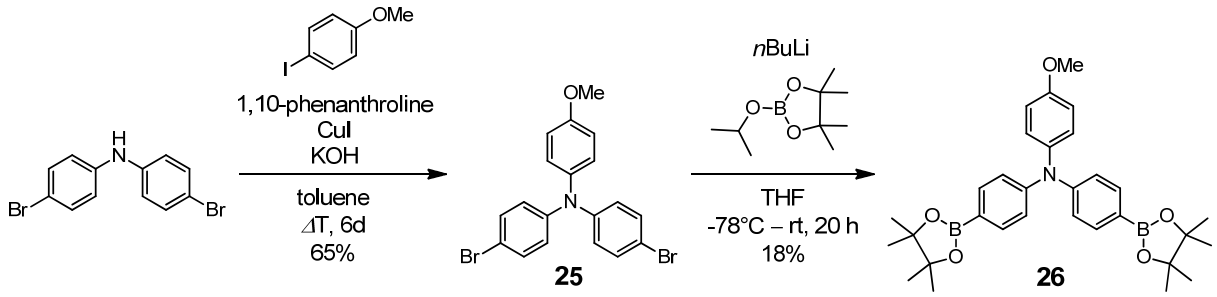

Scheme 19 Synthesis of the precursors **25** and **26**.

Copolymerisations of **26** with either **M6** or **M4** were carried out by *Suzuki* coupling reaction with $Pd(PPh_3)_4$ and $NaHCO_3$ and continuous heating in THF/water for 5 d to give the copolymers **P7** and **P8**, respectively (Scheme 20). In the former reaction, a cyclic dimer **Dim1** could be isolated in traces by preparative GPC from the hexane fractions that were obtained during the work-up of the reaction (see experimental section 5.2). **Dim1** will be described in more detail in chapter 3.6 (p. 197). The polymers are of similar size with a degree of polymerisation $X_n \sim 15$. However, in case of **P8** solubility turned out to be poor. A major part of the polymer was insoluble in common organic solvents. Therefore, the fraction that was used for all the physical characterisations throughout this work was the part that remained insoluble during treatment in a *Soxhlet* apparatus with DCM but dissolved when replacing DCM by $CHCl_3$.

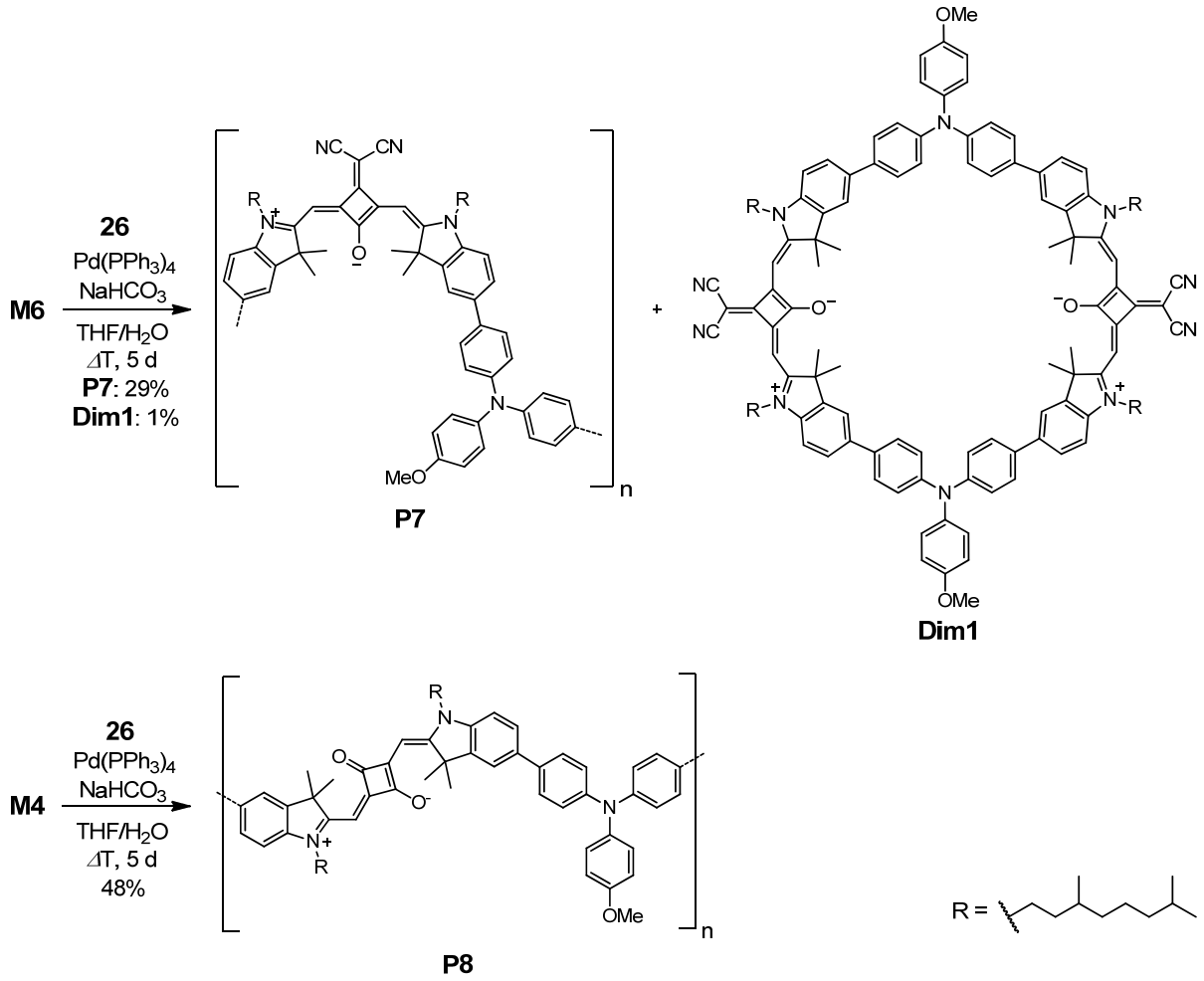

Scheme 20 Synthesis of triarylamine–squaraine copolymers **P7** and **P8** and the cyclic dimer **Dim1**.

Carbazole–Squaraine Copolymers

The difunctionalised carbazole precursors (Scheme 21) were obtained in a similar manner as the monofunctionalised analogues (Scheme 16, p. 116). Deprotonation of the dibrominated carbazoles **27**[215] and **30**[216], which were synthesised according to literature procedures, with either NaH or K_2CO_3 and subsequent alkylation with 3,7-dimethyloctyl bromide or tosylate in DMF gave the alkylated carbazoles **28** and **31**, respectively, in very good to moderate yields. The boronic esters were attached *via* halogen-lithium exchange in THF using *t*BuLi and subsequent addition of the borolane to give **29** and **32**.

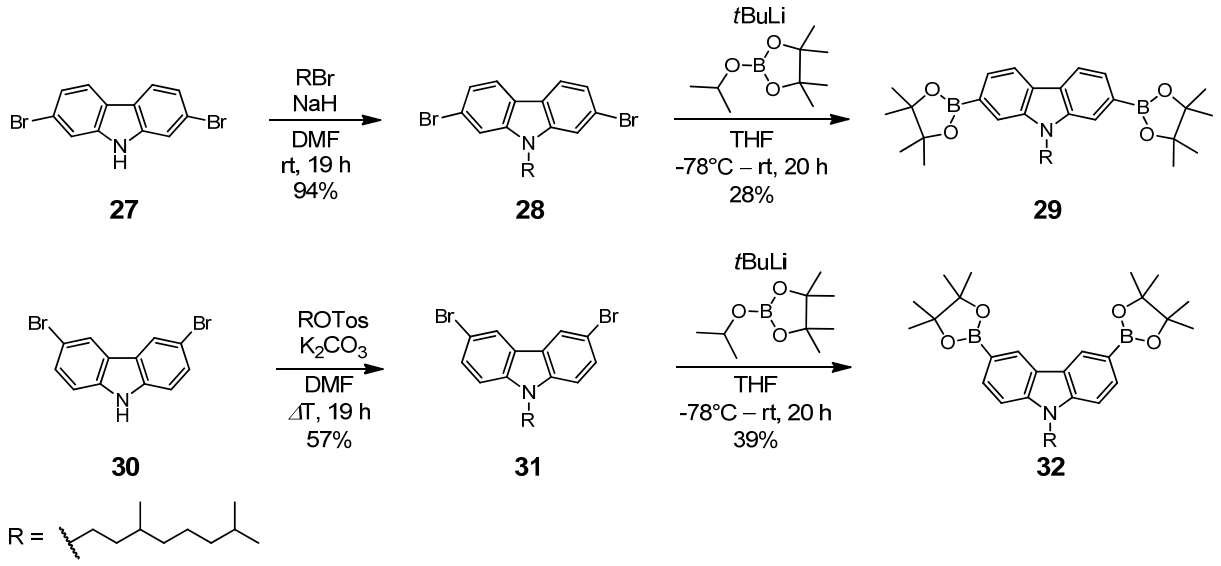

Scheme 21 Synthesis of carbazole precursors **28**, **29**, **31**, and **32**.

Suzuki coupling reaction of squaraine **M6** and carbazole **29** with $Pd(PPh_3)_4$ and Na_2CO_3 in toluene/water resulted in polymer **P9** in reasonable yield and mass distribution (M_n = 13700, X_n = 13), whereas the same reaction conditions for dibromosquaraine **M4** and carbazole diboronic ester **29** only gave low yield and much shorter polymers **P10** (M_n = 7090, X_n = 7.2) (Scheme 22). This is most likely due to the precipitation of shorter polymer strands during reaction in this particular solvent mixture after a couple of hours. However, the reaction of squaraine diboronic ester **M8** and dibromocarbazole **28** in THF/water proceeded very well to give longer polymers **P10** (M_n = 20900, X_n = 21) in higher yield. This fraction of the longer polymers **P10** was used for the characterisation throughout this work.

The copolymerisation reaction for **M4** and 3,6-disubstituted carbazole **32** in toluene/water gave good yields but short polymers **P11** (M_n = 6200, X_n = 6.4). The synthetic approach with reversed functionalities in THF/water, analogous to the synthesis of **P10**, was not pursued in this case, because no major differences neither of the optical properties between the 2,7-carbazole- or 3,6-carbazole-squaraine copolymers (**P10** and **P11**) nor of the optical and electrochemical properties of the monomeric model compounds (**M16** and **M17**) were observed.

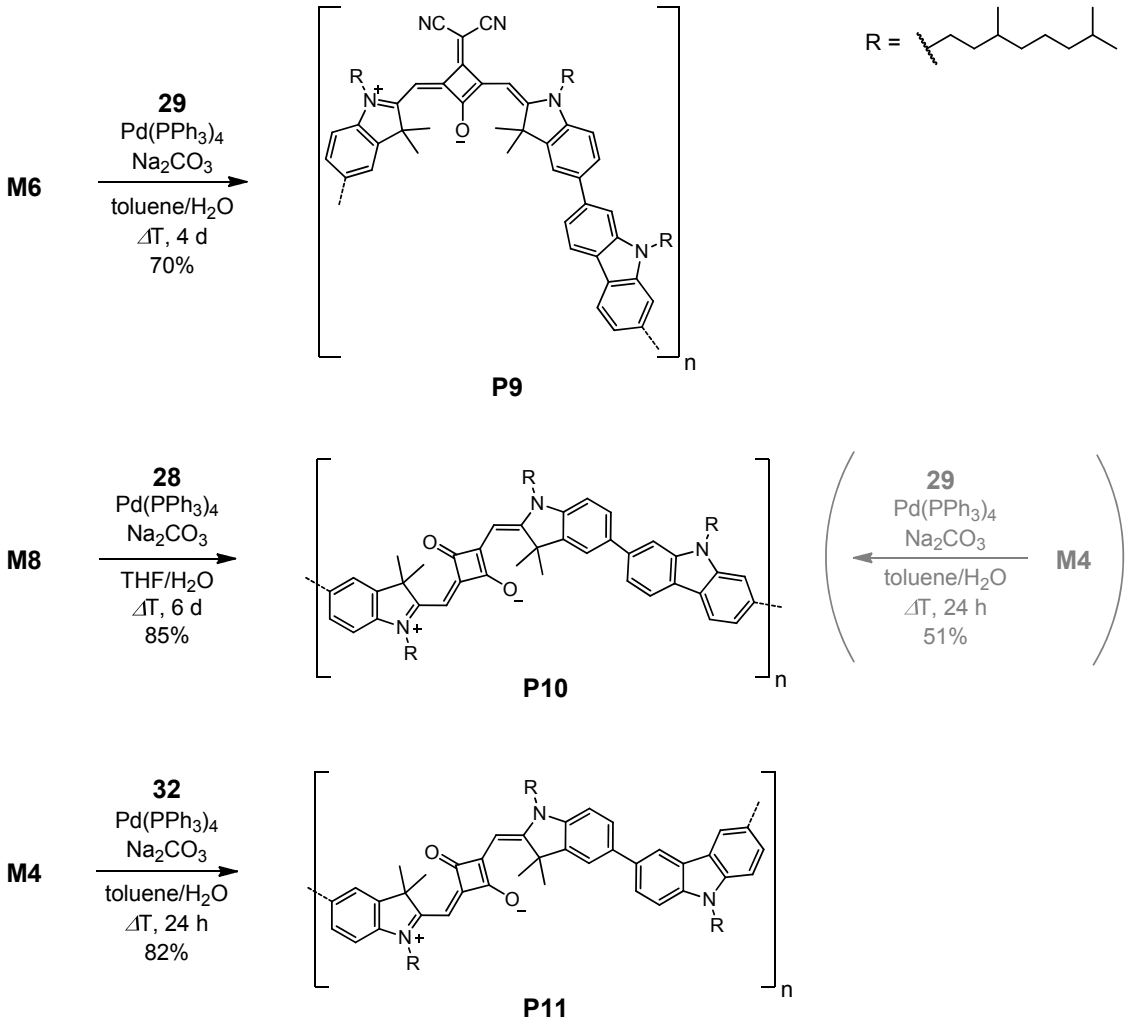

Scheme 22 Synthesis of carbazole–squaraine copolymers **P9**–**P11**.

Piperazine–Squaraine Copolymer

Analogous to the reaction sequences used for the **M19** monomer synthesis (Scheme 18, p. 118), a twofold *Buchwald-Hartwig* reaction of the methylene base **7** with piperazine was applied to give **33** (Scheme 23). Here, immediate recrystallisation of the crude product from ethanol proved essential to prevent the product from further side reactions. Polymerisation was then carried out analogously to the monomer squaraine condensation synthesis in toluene/1-butanol (1:1) using a *Dean-Stark* trap. However, the polycondensation reaction was performed under nitrogen atmosphere and the reaction time was extended to 6 d to obtain polymer **P12** (M_n = 9400, X_n = 12).

It is well known that in the condensation reaction of a squaric acid derivative with nucleophilic compounds the central ring can be disubstituted both in the 2,4-positions to the squaraine dye and in 3,4-positions to a cyclobutenedione compound. Therefore IR spectroscopy was used to check for unfavoured 3,4-substitution. The result is shown in section 3.7.2 (p. 211).

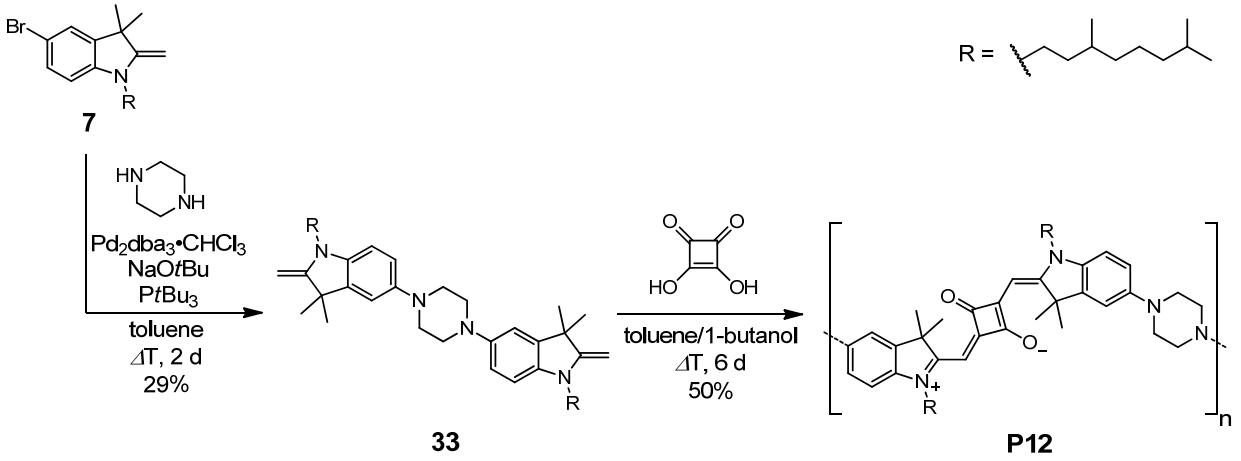

Scheme 23 Synthesis of piperazine precursor **33** and piperazine–squaraine copolymer **P12**.

3.4.3 Absorption Spectroscopy

For the absorption spectroscopy, the polymers were dissolved in $CHCl_3$ due to better solubility and the monomers in DCM due to better stability. The spectra of the monomers behave very similar in those two solvents which allows proper comparison.

Copolymerisation of a squaraine dye with either a 3,6- or 2,7-carbazole to polymers **P11** or **P10** has hardly any impact on the absorption (Figure 56, right) or fluorescence spectra (left) compared to the monomeric compounds **M16** and **M17**. The red shift of the absorption maxima of the polymers is only 100–300 cm^{-1} (Table 16) and the maxima are at 14800 cm^{-1} (**P11**) and 14600 cm^{-1} (**P10**) and there is only little broadening of the absorption band. This indicates only little electronic coupling between the squaraine chromophores and the carbazole bridges.

The absorption band of the carbazole–dicyanomethylene squaraine copolymer **P9** is also rather narrow but at lower energy (13800 cm^{-1}) as expected for a dicyanomethylene-substituted squaraine dye.

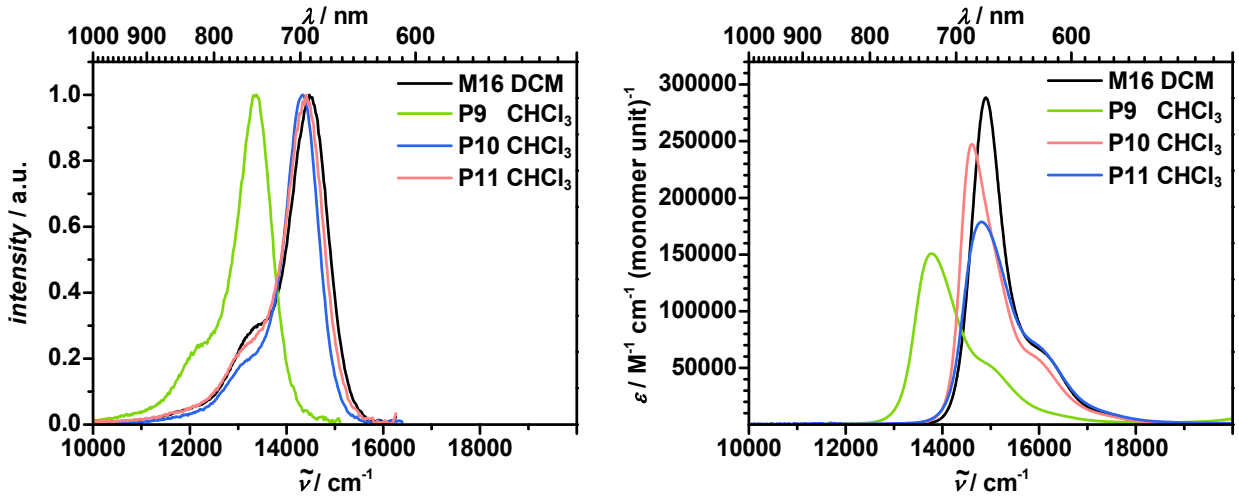

Figure 56 Absorption spectra (right) and normalised fluorescence spectra (left) of carbazole squaraine monomer **M16** and copolymers **P9**–**P11**.

For the triarylamine–squaraine copolymers (**P7**, **P8**) the absorption spectra are essentially similar to the one of the monomeric dye conjugate (**M13** vs. **P8**) concerning the peak with highest intensity (Figure 57). However, for **P8** in $CHCl_3$ there is a small but significant band at lower energy (13800 cm^{-1}) which is absent in toluene. Polymer **P7** also shows a similar but even weaker absorption peak at lower energy (12700 cm^{-1}) than the most intense signal. In addition, the signal at ca. 15000 cm^{-1} which usually appears as a shoulder in all squaraine dyes is now more pronounced and shows a distinct peak maximum.

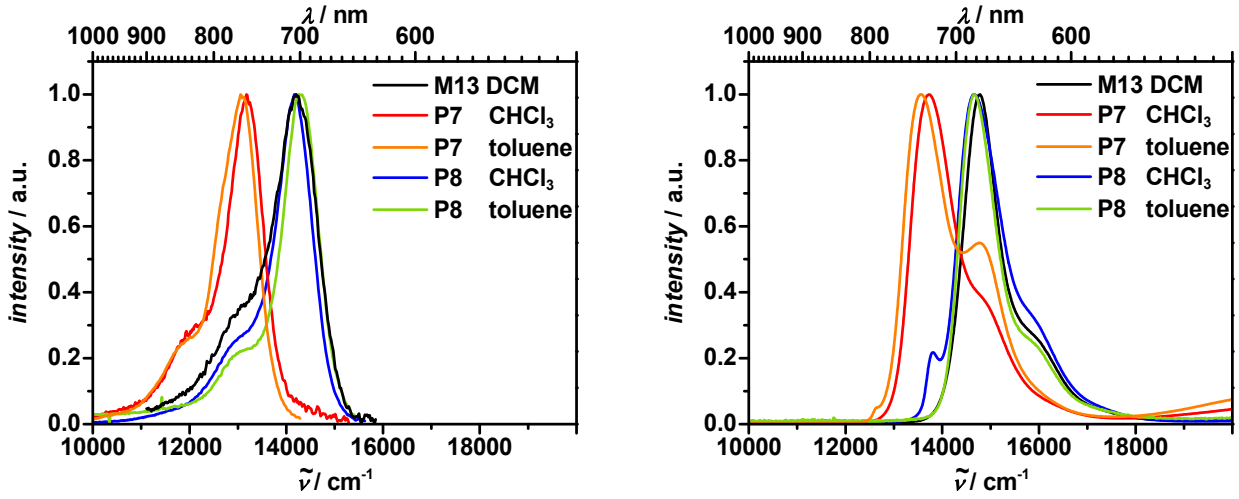

Figure 57 Absorption spectra (right) and normalised fluorescence spectra (left) of triarylamine squaraine monomer **M13** and copolymers **P7** and **P8**.

The copolymer of squaraine and piperazine **P12** also displays an absorption spectrum that is similar to **M19** (Figure 58, left). But again, a low energy band of low intensity is found at 13100 cm^{-1} both in $CHCl_3$ and in toluene (not shown). These low energy bands of **P7**, **P8**, and **P12** are plotted together in Figure 58 (right) for better comparison. The origin of these features is not fully understood but as they only appear for copolymers of squaraines with amine donors it is supposed that they are caused by charge transfer interactions which only occur in some conformers, possibly in those in which the donor is coplanar to the squaraine dye. Semiempirical computations indeed suggest a lowering of excitation energy in such fully coplanar conformers, see below (section 3.4.8).

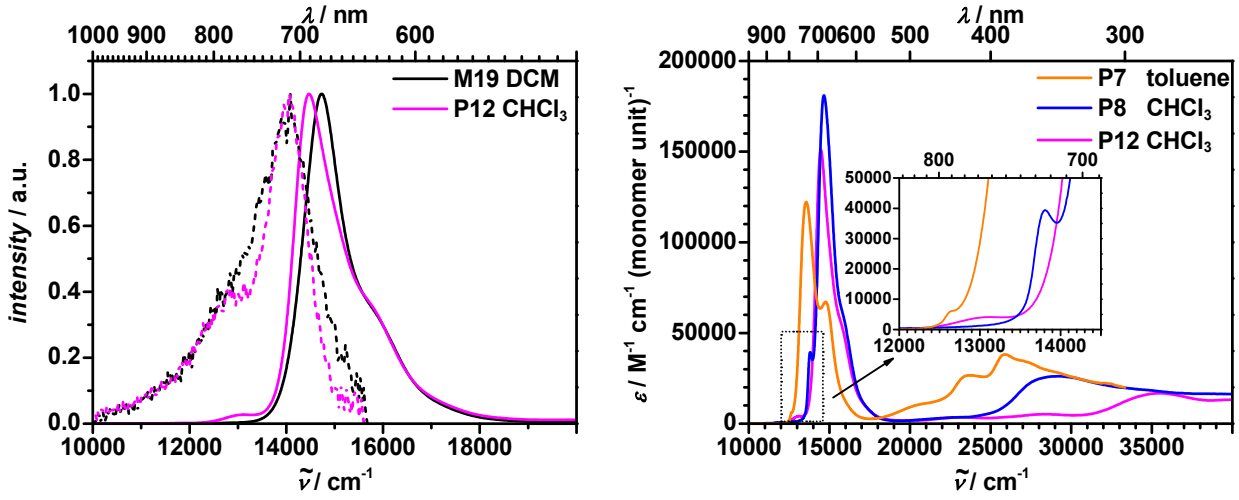

Figure 58 Absorption spectra (solid line) and fluorescence spectra (dashed line) of piperazine squaraine monomer **M19** and copolymers **P12** and **P8** (left) and complete absorption spectra of donor–squaraine copolymers **P7**, **P8**, and **P12** (right).

3.4.4 Fluorescence Spectroscopy

The fluorescence spectra of all copolymers show essentially mirror image behaviour to the absorption spectra with exception of the weak low energy band of **P7**, **P8**, and **P12** that do not show any equivalent signal in the fluorescence spectra.

The fluorescence quantum yield Φ_{fl} for **P12** (0.02 in $CHCl_3$ and 0.16 in toluene) is only slightly smaller than for the analogous monomer **M19** (0.03 in DCM and 0.24 in toluene) which is due to the saturated piperazine bridge. All other polymers however show a much smaller fluorescence quantum yield than their monomers, e.g. for carbazole copolymer **P10** the quantum yield is 0.21 in $CHCl_3$ while it is 0.51 in DCM for **M17**.

For all copolymers biexponential fluorescence decays are observed. The shorter fluorescence lifetimes τ_{fl} are between 0.8–2.1 ns and dominate the decay with amplitudes exceeding 90%. The longer lifetimes are between 3.5–10 ns. However, for **P9** in toluene the longer lifetime makes two thirds of the amplitude whereas the shorter lifetime contributes with one third. All in common is the fact that the fluorescence lifetimes of the related monomers are right between the two lifetimes of the polymers. The lifetime found for **P12** in $CHCl_3$ is unreliable because of the low signal to noise ratio caused by the low quantum yield.

Table 16 Absorption maxima, extinction coefficients, transition moments, fluorescence maxima, fluorescence quantum yields, and fluorescence lifetimes of donor–squaraine copolymers **P7–P12** and corresponding model and reference dyes. Extinction coefficients ε and transition moments μ_{eg} of the polymers are given per monomer unit. cy = cyclohexane.

	solvent	λ_{abs} / nm	$\tilde{\nu}_{abs}$ / cm^{-1}	ε / $M^{-1}cm^{-1}$	μ_{eg} / D	λ_{fl} / nm	$\tilde{\nu}_{fl}$ / cm^{-1}	Φ_{fl} [a]	τ_{fl} / ns
M1	DCM	639	15700	336000	11.4	649	15400	0.19	1.0
	toluene	644	15500	340000	11.1	649	15400	0.35	1.9
M2	DCM	685	14600	207000	10.6	706	14200	0.25	-
	toluene	700	14300	236000	10.1	716	14000	0.41	4.5
M13	DCM	677	14800	292000	13.1	704	14200	0.24	0.83
	toluene	681	14700	314000	12.5	695	14400	0.48	2.5
	cy	672	14900	351000	12.9	684	14600	0.72	2.3
M16	DCM	671	14900	288000	12.3	691	14500	0.44	2.6
	toluene	674	14800	298000	11.5	687	14600	0.49	2.7
	cy	667	15000	328000	12.0	681	14700	0.60	-
M17	DCM	669	14900	332000	12.7	684	14600	0.51	2.5
	toluene	673	14800	355000	12.2	684	14600	0.55	2.5
	cy	666	15000	294000	11.2	681	14700	0.58	-
M19	DCM	679	14700	188000	11.3	710	14100	0.03	0.19 (91.6) 1.1 (8.1) 6.2 (0.3)
	toluene	682	14700	202000	10.8	706	14200	0.24	1.7
P7	$CHCl_3$	729	13700	160000	10.9	759	13200	0.07	0.88 (98.7) 10 (1.3)
	toluene	738	13500	122000	10.0	766	13100	0.10	2.0 (87.3) 6.2 (12.7)
P8	$CHCl_3$	682	14700	181000	11.4	705	14200	0.14	1.3 (97.4) 5.0 (2.6)
	toluene	682	14700	x	x	701	14300	0.22	2.1 (98.6) 8.7 (1.4)
P9	$CHCl_3$	726	13800	151000	10.5	748	13400	0.09	1.7 (93.1) 6.4 (6.9)
	toluene	735	13600	90000	8.1	755	13200	0.20	0.84 (31.1) 3.5 (68.9)
P10	$CHCl_3$	685	14600	247000	11.8	698	14300	0.28	1.3 (97.7) 5.0 (2.3)
	toluene	x	x	x	x	x	x	x	x
P11	$CHCl_3$	676	14800	179000	11.4	694	14400	0.22	1.6 (94.3) 5.5 (5.7)
	toluene	677	14800	152000	10.1	692	14500	0.39	2.1 (91.6) 6.0 (8.4)
P12	$CHCl_3$	691	14500	151000	10.5	711	14100	0.02	0.58
	toluene	693	14400	x	x	709	14100	0.16	1.2 (93.4) 4.1 (6.6)

- was not measured; x could not be determined. The values in brackets are the relative amplitudes of the corresponding fluorescence lifetime. [a] During the writing process, the quantum efficiency of oxazine 1 was determined to be 0.15 by an absolute measurement using an integration sphere. However, the values reported for the squaraine dyes herein are still referenced against the quantum efficiency of 0.11 (see experimental section 5.1.2) as they were published to avoid confusion. Nevertheless, it has to be noted that the correct quantum efficiencies are larger by a factor of $0.15 / 0.11 \approx 1.36$.

3.4.5 Spectroscopy Summary

To sum up, the optical behaviour of all the copolymers is rather similar, no matter if the bridge is saturated (piperazine) or unsaturated, rigid (carbazole) or propeller like (triarylamine) and does not differ very much from those of the analogous monomers. These kinds of bridges obviously do not provide any significant coupling of individual squaraine chromophores by π-conjugation and the distance of chromophores is widened in such a way that exciton coupling decreases to an extent which is not noticeable.

A similar behaviour was reported by *Kuster* and *Geiger* for indolenine squaraines.[30] These authors synthesised a series of linear squaraine dimers and oligomers and investigated the impact of various bridges. They also found only little broadening and small bathochromic shifts of the absorption bands. The induced red shift of the bridges was in the order tetrafluorophenylene < 2,5-dialkyloxyphenylene < phenylene < fluorene. *Maeda et al*. bridged indolenine squaraines *via* phenylene units.[88] These dyes were linked in *para*- or *meta*-positions also leading to little broadening and red shift which was more pronounced for the *para*-linked system.

As mentioned before, also thiophenes were used as bridges in squaraine oligomers (**OS4**, Chart 9, p. 15).[67] Much in contrast to the observations stated above, both a broadening as well as a significant red shift was observed. The absorption maximum of a pentamer was found at 13800 cm^{-1} in $CHCl_3$ compared to 14900 cm^{-1} for a dithienyl-substituted indolenine squaraine monomer. In contrast to the phenylene bridges in the work of *Kuster* and *Geiger* (and the carbazole and triarylamine bridges used in this study), which show a computed torsional angle of 36–41°, thiophene bridges may adopt a more coplanar conformation with the squaraine π-system thus enhancing π-conjugation. Semiempirical AM1 computations for model hexamers indeed gave dihedral angles of 22–32°, see below (section 3.4.8).

However, for *N*-alkylpyrrole squaraine dyes, significant broadening and red shift of the absorption was reported upon copolymerisation with an electron rich bridge. *Ajayaghosh* and *Eldo* used 2,5-dialkoxydivinylbenzene to bridge *N*-alkylpyrrole squaraines to form conjugated polymers with intense and broad absorption in the NIR region and low band

gaps.[121-122] Into that system, *Zhang* et al. inserted additional donors such as thiophene derivatives, 2,7-carbazole or another 2,5-dialkoxyphenylene *via* the *Sonogashira* coupling and also obtained low band gap polymers with broad absorption in the NIR region.[126-127] In all these cases the conjugation pathway is provided by vinylene groups (and ethynyl groups in the latter cases) which allow a better coplanar orientation of aromatic and heterocyclic ring moieties.

So far, as described above, the broadening and red shift is stronger in the homopolymers **P1**–**P5**, where no bridges are used and the squaraine chromophores are directly linked *via* single C–C bonds between the indolenine rings. Thus, taken together the information given above, the exciton coupling model to explain the optical properties should be modified to include conjugational effects at least to some extend. Therefore, semiempirical calculations have been performed to reveal insights of the electronic structure of the dyes, which is found in section 3.4.8.

3.4.6 Cyclic Voltammetry

All donor–squaraine copolymers show one reduction wave and up to four oxidation waves when measured in DCM/TBAHFP (0.2 M) (Table 17). The voltammograms of the carbazole–squaraine copolymers **P9** (Figure 59, left) and **P10** (right) display a very symmetric reduction wave with a small peak separation of only 20–30 mV. The same is true for the first two oxidation processes of **P10** (8 mV and 32 mV). It is assumed that these polymers adsorb to the electrode which then might lead to the observed behaviour typical of thin layers where diffusion processes do not lead to the usually observed hysteresis behaviour of cyclic voltammograms under semi-infinite boundary conditions in solution. The polymerisation does not have a strong impact on the potentials of **P10** as both reduction and oxidation values are in the same range as those of the model monomer **M17** (Figure 41, right, p. 129; Table 17, p. 167). Also the potentials of **P12** (Figure 60, right) do not differ very much from those of the parent monomer **M19** (Figure 42, p.129).

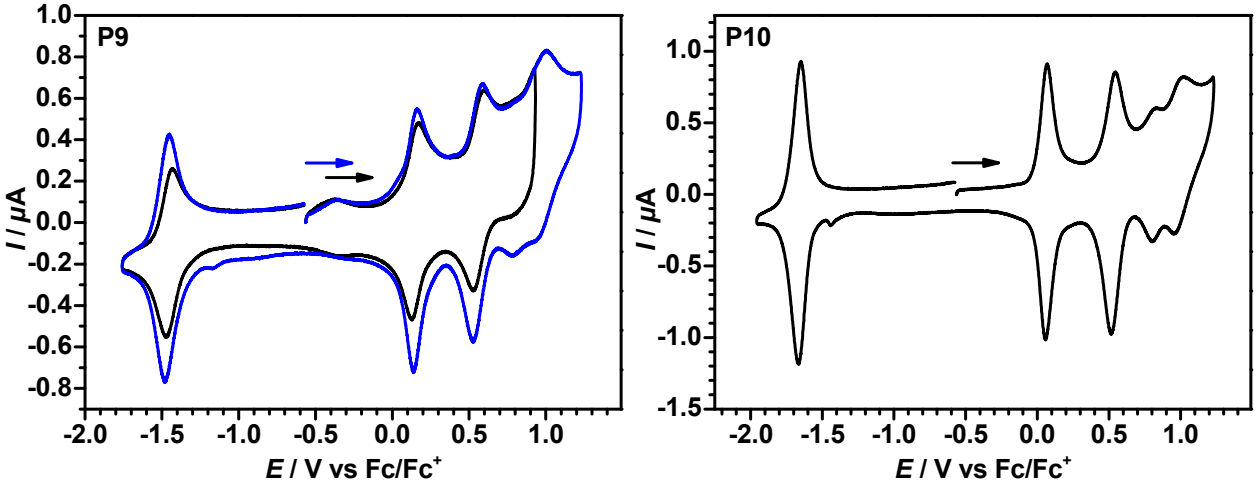

Figure 59 Cyclic voltammograms of polymers **P9** (left) and **P10** (right) in DCM/TBAHFP (0.2 M) at a scan rate of 250 mV s^{-1}. The blue voltammogram of **P9** covers a third oxidation process.

In case of the triarylamine–squaraine copolymers **P7** (Figure 60, left) and **P8** (Figure 61, left), the back-reduction peak becomes distinctly sharper when a potential high enough to cover the fourth oxidation was applied. This sharp wave is a sign for adsorbed polymers on the electrode that might have precipitated at the four-fold oxidised state. In contrast, when only the third oxidation process is covered (black voltammogram of **P7** in Figure 60, left), the back-reduction shows the normal reversible signal.

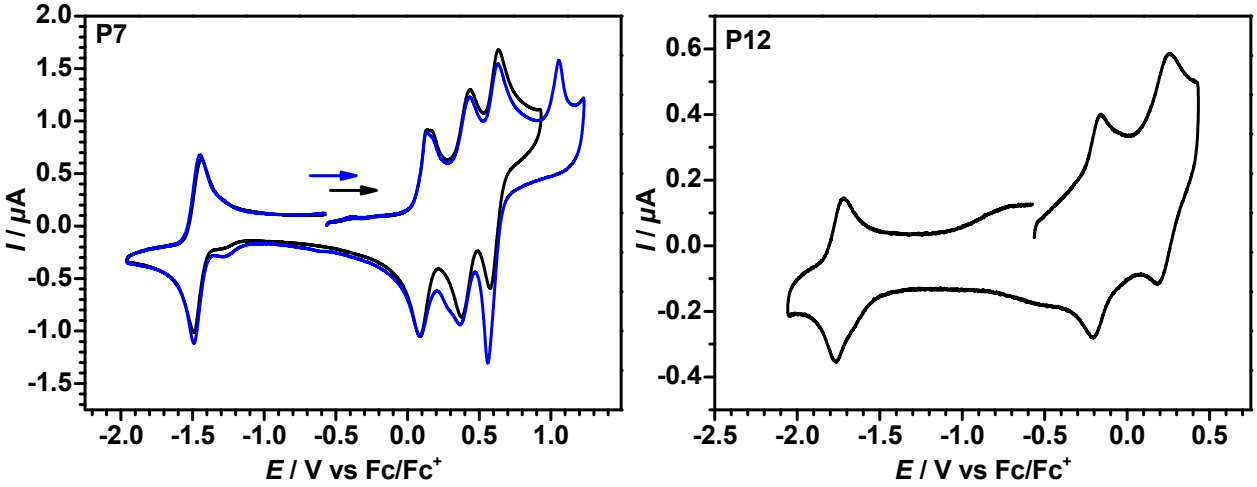

Figure 60 Cyclic voltammograms of polymers **P7** (left) and **P12** (right) in DCM/TBAHFP (0.2 M) at a scan rate of 250 mV s^{-1}. The blue voltammogram of **P7** covers a fourth oxidation process.

Triarylamine–squaraine copolymer **P8**, which was measured in $CDCl_3$, does not show a clean reduction wave within the operating window of the solvent. In this particular case, also the voltammogram of the differential pulse voltammetry (DPV) measurements is shown in Figure 61 (right). However, the values of the potentials have to be taken with care because polymer **P8** was measured against the redox couple of decamethylferrocene/decamethylferrocenium in $CDCl_3$ and just a correlation against the redox couple of ferrocene/ferrocenium in $CHCl_3$ was found in literature.[217] The deviations of the values of the redox potentials might be small but have to be taken into account.

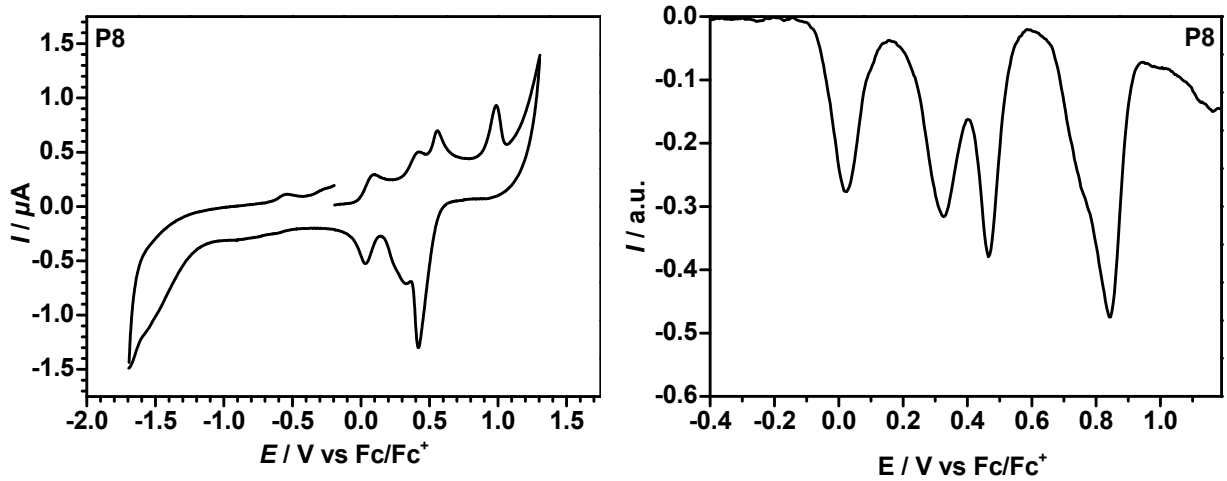

Figure 61 Cyclic voltammogram (left) and differential pulse voltammogram (right) of polymer **P8** in $CDCl_3$/TBAHFP (0.2 M) at a scan rate of 250 mV s^{-1} and 20 mV s^{-1}, respectively.

Table 17 Redox potentials, HOMO and LUMO energy levels and band gaps obtained by electrochemical (E_{gap}^{CV}) and optical (E_{gap}^{opt}) methods of donor–squaraine copolymers **P7**–**P10** and **P12** together with corresponding monomeric model dyes.

	$E_{1/2}^{Red1}$ / mV	$E_{1/2}^{Ox1}$ / mV	$E_{1/2}^{Ox2}$ / mV	$E_{1/2}^{Ox3}$ / mV	$E_{1/2}^{Ox4}$ / mV	E_{HOMO} / eV[d]	E_{LUMO} / eV[d]	E_{gap}^{CV} / eV[d]	E_{gap}^{opt} / eV[e]
M5[a]	–1610	110	580 *571*			–5.27	–3.55	1.72	1.86
M7[a]	–1405	207	576 *574*			–5.37	–3.76	1.61	1.71
M13[a]	–1664	–6	277 *268*	277 *<286*	587 *586*	–5.15	–3.50	1.65	1.75
M17[a]	–1653	35	544			–5.20	–3.51	1.69	1.79
M19[b]	–1711	–214	231	994[a]		–4.95	–3.45	1.50	1.73
P7[b]	–1466	112	407	607		–5.27	–3.69	1.58	1.62
P8 $CDCl_3$		(25[c])	(325[c])	(465[c])	(843[c])				1.68/1.74
P9[b]	–1454	147	563			–5.31	–3.71	1.60	1.63
P10[b]	–1656	60	530			–5.22	–3.50	1.72	1.76
P12[b]	–1744	–183	219			–4.98	–3.42	1.56	1.54/1.72

[a] Ag/AgCl pseudo-reference electrode; [b] Ag/AgCl "leak free" electrode; [c] potentials extracted from DPV; [d] determined according to the procedure described in 5.1.4; [e] determined in DCM for the monomers and $CHCl_3$ for the polymers according to the procedure in 5.1.1; the values written in brackets have to be taken with care because there might be a deviation because of the correlation of the decamethylferrocene/decamethylferrocenium redox couple to the redox couple of ferrocene/ferrocenium in $CHCl_3$[217] and not in $CDCl_3$; the values written in italics are obtained by digital fitting of the redox waves with DigiSim.[195]

3.4.7 Band Gaps

HOMO and LUMO energies as well as electrochemical and optical band gaps were obtained in the same manner as stated above (3.3.6). Only for **P8** no values have been determined for various reasons. First, there might be some deviation in the values due to the solvent used in the cyclic voltammetric measurements (see above) and second, since no reduction was recorded, the HOMO energy level cannot be calculated in any event.

The HOMO energy levels of the donor–squaraine copolymers are between –4.98 eV for the piperazine–squaraine copolymer **P12** and –5.31 eV. The LUMO energy levels are

between –3.42 eV and –3.71 eV. The band gaps range between 1.54–1.76 eV and comparison of the band gaps determined by optical and electrochemical methods shows that the latter values are generally slightly lower than the optical derived values. However, it has to be kept in mind that for the polymers $CHCl_3$ was used for the optical experiments while DCM was used for the cyclic voltammetry. Nevertheless, the absorption properties of those systems are rather similar in DCM and $CHCl_3$ and therefore the band gaps are in good agreement.

The band gaps and the HOMO and LUMO energies of the copolymers do not differ very much to the corresponding monomeric squaraine dyes. For example, comparison of monomer **M19** with polymer **P12** shows that the difference of all the values is less than 60 meV. The same holds true for **M17** and **P10** where the differences are even below 30 meV.

As already seen in the absorption section above, there is no major impact on the optical or electrochemical properties upon polymerisation indicating only limited interaction of the single squaraine units over the bridges.

3.4.8 Semiempirical Calculations & Exciton Coupling

Likewise to the homopolymer **P2** (chapter 3.2.2), semiempirical calculations were performed to gain insight into the electronic structure of the polymers and in this case in particular into the interaction with bridge molecules in the copolymers. As representative examples, carbazole-squaraine copolymer **P10** was chosen as well as a thiophene-squaraine copolymer of the type **OS4** , that has been investigated by *Grahn et al*. in form of monodisperse oligomers up to the pentamer (Chart 9, p. 15).[67] Similarly, structures of model monomers, dimers, and hexamers were optimised using the AM1 hamiltonian and the most elongated structure that could be modelled was employed. Moreover, the dihedral angle between the squaraine chromophore and the bridge moieties was modified to both 0° and 90° to probe the effect of direct and no conjugation, respectively. For the dimers, the optimised model of the hexameric structure was used and reduced to a dimer model. As expected, AM1 optimisation gave planar squaraine chromophores and

dihedral angles between squaraine and bridge of 22–32° for **OS4** (Chart 9, p. 15) and 40–46° for **P10**. The lowest energy transitions of the monomeric compounds, calculated by CNDO/S2, were around 17000 cm^{-1}, which is around 1000–2000 cm^{-1} too high in energy, what might be a systematic problem of the CNDO/S2 parameterisation.

Again, the electronic coupling energy was obtained by $V_{AB} = \Delta E/2$ for the dimers, and nearest-neighbour approximation lead to $V_{AB} = \Delta E/4$ for the polymers. Those, as well as the transition energies and corresponding oscillator strengths obtained by CNDO/S2 calculations are shown in Table 18 (p. 171) for the monomers (bridge–squaraine–bridge), dimers (bridge–[squaraine–bridge]$_2$), and hexamers (bridge–[squaraine–bridge]$_6$).

Likewise to the homopolymer **P2**, the coupling energies obtained for the dimeric structures are somewhat higher than those of the optimised hexamers, indicating that the model hexamers do not fully reach polymeric character, concerning the full exciton band width of $4 \times V_{AB}$. The oscillator strengths for both model dimers and hexamers are mainly on the lowest energy transition with the ca. 2- and 5-fold values compared to the monomer, illustrating the J-type behaviour.

For the optimised geometry, the coupling energies V_{AB} for **OS4** and **P10** are 442 and 170 cm^{-1}, respectively (V_{AB} = 671 cm^{-1} for **P2**). However, for the completely planar structure the energies are 507 and 214 cm^{-1}, respectively. In other words, the coupling energies drop in the order V_{AB}(**P2**) > V_{AB}(**OS4**) > V_{AB}(**P10**) as do the excitonic contributions to this energy, which are 78% for **P2**, 66% for **OS4**, and ca. 50% for **P10**. This decreasing contribution can be explained by the dependence of V_{AB} on the inverse cube of the distance r_{AB} in the point-dipole approximation according to equation (1)[218]

$$V_{AB} = \frac{1}{hc4\pi\varepsilon_0} \frac{\mu_A \mu_B}{r_{AB}^3} \kappa, \qquad (1)$$

where κ is an orientation factor (see chapter 1.3, eq. (1) (p. 24) and $\mu_A = \mu_B$ is the transition moment of a squaraine monomer.

Thus, the CNDO/S2 calculations can explain the small changes in the carbazole–squaraine copolymer compared to the monomer model compound and the distinctly stronger coupling in **OS4** and **P2**. However, the fact that both **P2** and **OS4** (but not **P10**) show distinctly lower energies of their lowest transitions than the respective monomer is still unexplained. Nevertheless, for all polymers, the lowest transition energy is somewhat lower for the 0° conformer than for the optimised geometry which supports the assumption that conformational issues are responsible for the small low energy peaks seen in the spectra of Figure 58 (right, p. 160).

It is tempting to argue that the experimentally observed missing shift of lowest energy absorption of e.g. **P10** vs. **M18** is caused by a small effective conjugation length which might even be confined to only the monomer. However, even in the case of the 90°-twisted polymer where conjugation is blocked, the CNDO/S2 calculations indicate a significant exciton coupling interaction. Particularly in this case, the semiempirical computations predict a hypsochromic shift of the allowed lowest energy transition upon polymer formation. Thus, from a missing bathochromic shift, one cannot conclude about the absence of exciton coupling interactions because the whole excitonic manifold can be shifted to higher energies, for what reasons so ever. Thus, it remains to be elucidated how the lowest energy transition within the exciton manifold depends on the degree of excitonic interaction and the degree of polymerisation.

Table 18 CNDO/S2 excited states energies ($\tilde{\nu}$), corresponding oscillator strengths (*f*), and electronic coupling energies (*V*) based on AM1 optimised geometries.

	structure	$\tilde{\nu}$ / cm^{-1} *f*						V_{AB} / cm^{-1}
P2	**monomer (M1)**	16678 1.79						
	dimer[b]	16500 3.92	18065 0.19					783
	polymer[c] **optimised**	16437 9.79	17019 0.07	17682 0.74	18346 0.01	18886 0.32	19122 0.80	671
	polymer[c] **dihedral angle = 0°**	15997 10.39	16655 0.04	17429 0.81	18199 0.00	18823 0.35	19095 0.00	774
	polymer[c] **dihedral angle = 90°**	16817 6.67	17341 0.10	17922 0.78	18435 0.24	18831 0.91	18906 3.08	522
OS4	**monomer**[a]	16659 2.28						
	dimer[b]	16365 4.24	17412 0.29					524
	polymer[c] **optimised**	16774 10.23	17093 0.23	17594 0.44	18002 0.03	18358 0.16	18541 1.88	442
	polymer[c] **dihedral angle = 0°**	16449 11.22	16873 0.04	17380 0.61	17876 0.04	18274 0.23	18475 0.82	507
	polymer[c] **dihedral angle = 90°**	17554 5.04	17785 0.25	18050 1.55	18316 0.20	18568 0.42	18723 4.82	295
P10	**monomer (M18)**[a]	17105 2.35						
	dimer[b]	17211 4.44	17663 0.13					226
	polymer[c] **optimised**	17828 11.30	17978 0.36	18156 0.49	18306 0.01	18452 0.22	18507 0.36	170
	polymer[c] **dihedral angle = 0°**	17532 11.74	17730 0.11	17939 0.58	18145 0.02	18316 0.20	18387 0.55	214
	polymer[c] **dihedral angle = 90°**	18331 10.45	18407 0.46	18490 0.62	18568 0.00	18630 0.12	18670 0.21	85

[a] The monomer consists of the sequence bridge–squaraine–bridge; [b] the dimer consist of the sequence (bridge–[squaraine–bridge]$_2$) whose structure was taken from the optimisation of the polymer; [c] the polymers consists of the sequence (bridge–[squaraine–bridge]$_6$).

3.4.9 Conclusion

The idea of the insertion of electron donors as bridges between indolenine squaraines in order to generate a broad absorption in the NIR region was pursued. Therefore, a series of donor–squaraine copolymers and respective monomeric model compounds were synthesised using diverse synthetic strategies. No matter if transition metal-catalysed/mediated reactions or polycondensation reactions were applied, polymers could always be obtained in sufficient yield and molecular weight.

The impact of various bridges on the spectroscopic and electrochemical properties was investigated. For this purpose, saturated (piperazine), unsaturated rigid (3,6- and 2,7-carbazole), and propeller like (triarylamine) groups were chosen. While the absorption maxima of the model compounds generally shift bathochromically upon extension of the π-system at the periphery or the addition of donors (both σ and π), copolymerisation of a squaraine dye and a donor did not have a major impact on the absorption spectra. These were only marginally broadened and red-shifted compared to the model compounds. Furthermore, the electrochemical properties remained rather similar to their monomeric model conjugates. This behaviour was observed for all bridges and is explained to be caused by a decrease of exciton coupling energy with a power-3-dependence on the chromophore distance provoked by insertion of the bridging groups. However, conjugative effects also play a role for the interchromophore interactions and may reach ca. 50% for longer squaraine separations as in **P10**.

3.5 Acceptor-Substituted Squaraine Monomers and Copolymer[1]

After the synthesis and characterisation of homo- and copolymers and in order to complement the series of polysquaraines, both weak and strong electron accepting units were attached at the periphery of a standard squaraine dye. As weak electron acceptor, a triarylborane was chosen and as strong electron acceptor, a naphthalene diimide (NDI) was used. If one looks at a squaraine as an electron donor in total (and neglects the internal D–A–D structure), implementation of an electron accepting unit as a bridge leads to a D–A copolymer. Since it is know that the alternate arrangement of conjugated electron donating and accepting units can lead to low band gap polymers this concept was pursued.

Due to their potential application in organic optoelectronic devices such as organic solar cells[219-220] or organic field effect transistors (OFETs)[220-221], there is a major focus on low band gap polymers in current research. Charge and energy transfer processes are fundamental processes in optoelectronic devices and consequently, the dynamics of charges and excitons are of great importance for a better insight.[176, 222-223] Upon excitation of a low band gap polymer from the ground state to an excited state, the time dependency of the localisation vs. the delocalisation of the generated exciton and the potential transfer of excitons along the polymer chain or between polymer chains are of interest.[180, 224] In addition, attention is drawn to the formation of charge transfer states as well as charge separated states.[225-229] All these processes need to be understood at a molecular level and eventually in the bulk material to be able to optimise optoelectronic devices. In this order, both homopolymers[230-232] as well as copolymers[233-234] have been investigated in regard of their photoinduced dynamics in solution and the solid state.

---

[1] Reproduced or adapted in part with permission from a) *Synthesis, Electrochemical, and Optical Properties of Low Band Gap Homo- and Copolymers Based on Squaraine Dyes*, S. F. Völker, T. Dellermann, H. Ceymann, M. Holzapfel, C. Lambert, *J. Polym. Sci., Part A: Polym. Chem.* **2014**, *52*, 890-911. Copyright (2014) WILEY-VCH Verlag GmbH & Co. KGaA, Weinheim; b) *Charge TransferDynamics in Squaraine-Naphthalene Diimide Copolymers*, S. F. Völker, A. Schmiedel, M. Holzapfel, C. Böhm, C. Lambert, *Phys. Chem. Chem. Phys.* **2013**, *15*, 19831-19844. – Reproduced or adapted in part by permission of the PCCP Owner Societies.
Parts of this chapter have been investigated in a bachelor thesis under the supvervision of S. F. Völker: C. Böhm, Bachelor thesis, Julius-Maximilians Universität (Würzburg), **2012**.

Due to reasons that become apparent below, the photoinduced dynamics of the NDI–squaraine copolymer were investigated whereas the synthesis of a triarylborane–squaraine copolymer was neglected.

3.5.1 Triarylborane–Squaraine Monomer

Synthesis

To investigate the impact of additional acceptor units at the periphery of the dye molecule, triarylboranes, where the boron centre is protected by six methyl groups in *ortho*-position to the boron atom, were attached (Scheme 24). This acceptor–squaraine–acceptor dye is topologically similar to the donor–squaraine–donor dyes described in chapter 3.3. Overnight heating of **M8** and triarylborane **34**, which was synthesised from 1,4-dibromo-2,3,5,6-tetramethylbenzene and dimesitylfluoroborane according to literature procedures,[235] with $Pd(PPh_3)_4$ and Na_2CO_3 in a solvent mixture of toluene and water resulted in **M20** in high yield.

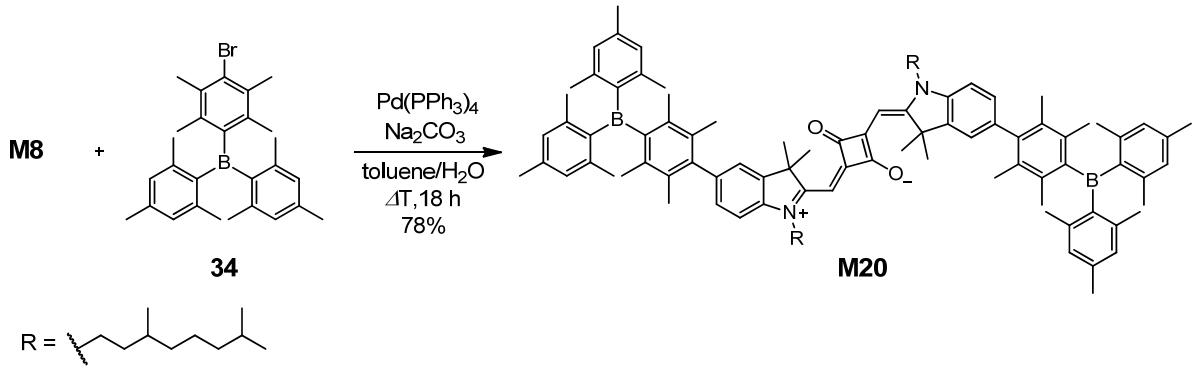

Scheme 24 Synthesis of triarylborane-substituted squaraine **M20**.

Absorption Spectroscopy

The triarylborane-substituted dye **M20** has a remarkably large extinction coefficient of $\varepsilon = 432000\ M^{-1}\ cm^{-1}$ in DCM (Figure 62, left) while it is $308000\ M^{-1}\ cm^{-1}$ in toluene (not shown). The shape of the lowest energy absorption band is typical cyanine-like with

the steep rise at the low energy side and the shoulder at the high energy side. There are additional transitions at ca. 30000 cm^{-1} that may be attributed to the triarylborane moieties. The absorption maximum is at 15300 cm^{-1} in both toluene and DCM and is red-shifted by 200 and 400 cm^{-1}, respectively, compared to reference squaraine **M1**. Even though the triarylboranes are formal π-electron acceptors due to the free p_z orbital, they can also act as σ-donors due to the lower electronegativity of the boron compared to carbon[152-153] and shift the absorption maximum to lower energy. Also conformational issues certainly play a role which may inhibit efficient π-overlap due to the steric demanding duryl bridge between the indolenine and the boron centre.

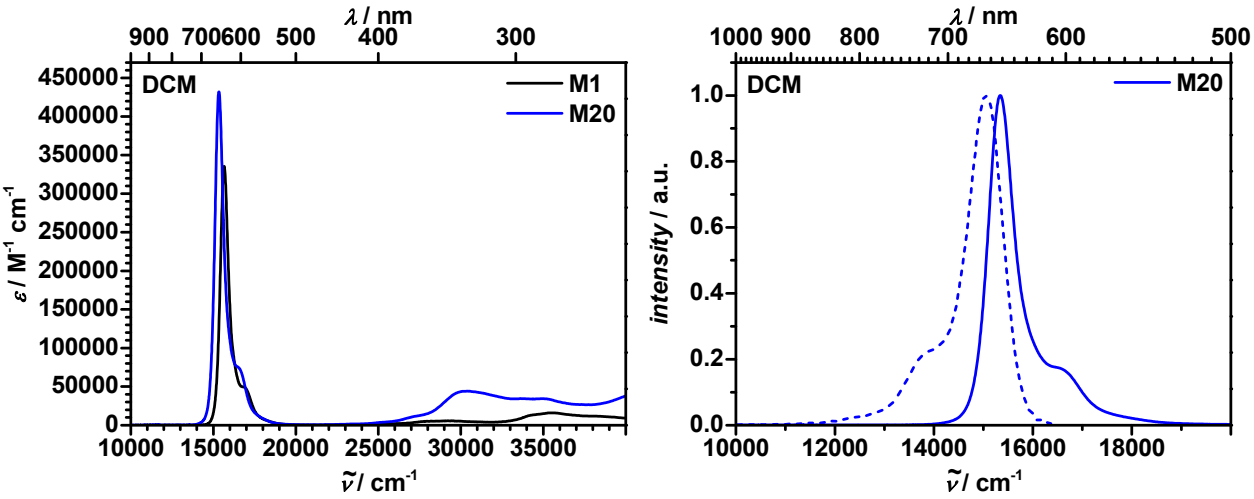

Figure 62 Left: Complete absorption spectra of **M1** and **M20**. Right: Normalised absorption (solid line) and fluorescence spectra (dashed line) of **M20**.

Fluorescence Spectroscopy

The fluorescence band is a mirror image to the lowest energy absorption band and the *Stokes* shift is 300 cm^{-1} (Figure 62, left). The fluorescence quantum yield Φ_{fl} is 0.30 in DCM and 0.42 in toluene, similar to the other monomeric dyes. Also the fluorescence lifetime of ca. 2 ns is analogue to the other squaraines.

Table 19 Absorption maxima, extinction coefficients, transition moments, fluorescence maxima, fluorescence quantum yields, and fluorescence lifetimes of triarylborane-substituted squaraine **M20** and reference dye **M1**.

	solvent	λ_{abs} / nm	$\tilde{\nu}_{abs}$ / cm^{-1}	ε / $M^{-1}cm^{-1}$	μ_{eg} / D	λ_{fl} / nm	$\tilde{\nu}_{fl}$ / cm^{-1}	Φ_{fl}[a]	τ_{fl} / ns
M1	DCM	639	15700	336000	11.4	649	15400	0.19	1.0
	toluene	644	15500	340000	11.1	649	15400	0.35	1.9
M20	DCM	652	15300	432000	13.7	665	15000	0.30	1.7
	toluene	655	15300	308000	10.8	666	15000	0.42	2.1

[a] During the writing process, the quantum efficiency of oxazine 1 was determined to be 0.15 by an absolute measurement using an integration sphere. However, the values reported for the squaraine dyes herein are still referenced against the quantum efficiency of 0.11 (see experimental section 5.1.2) as they were published to avoid confusion. Nevertheless, it has to be noted that the correct quantum efficiencies are larger by a factor of $0.15 / 0.11 \approx 1.36$.

Cyclic Voltammetry

Due to the electron deficient boron centre, the triarylborane moieties can act as electron acceptors. Therefore, the reduction processes of the squaraine **M20** were of particular interest and the experiments were carried out in THF/TBAHFP (0.2 M) (Figure 63). The half-wave potentials of the two oxidations ($E_{1/2}^{Ox1}$ = 64 mV, $E_{1/2}^{Ox2}$ = 454 mV) and the first reduction ($E_{1/2}^{Red1}$ = –1.65 V) are nearly identical to reference dye **M1** ($E_{1/2}^{Ox1}$ = 64 mV, $E_{1/2}^{Ox2}$ = 442 mV, and $E_{1/2}^{Red1}$ = –1.66 V) which was also measured in THF/TBAHFP (0.2 M) (Figure 14). Obviously, there is no effect of the triarylborane moieties on those redox potentials.

In addition to the above mentioned oxidation and reduction processes, two reduction processes below –2 V are observed. Similar to **M1**, one of this additional reduction processes is chemically irreversible and leads to a belated back oxidation process starting at ca. –700 mV. Differential pulse voltammetry (Figure 63, right) shows that the second of these additional reduction processes covers two electrons. Thus, the reduction processes at –2.65 V are assigned to the two triarylborane moieties, whose values are similar to those found for other triarylboranes[236], and the two reductions at –2.49 V and –1.65 V are ascribed to the squaraine moiety. Hence, only the 2nd reduction of the squaraine is influenced and shifted by ~ 140 mV to higher potential.

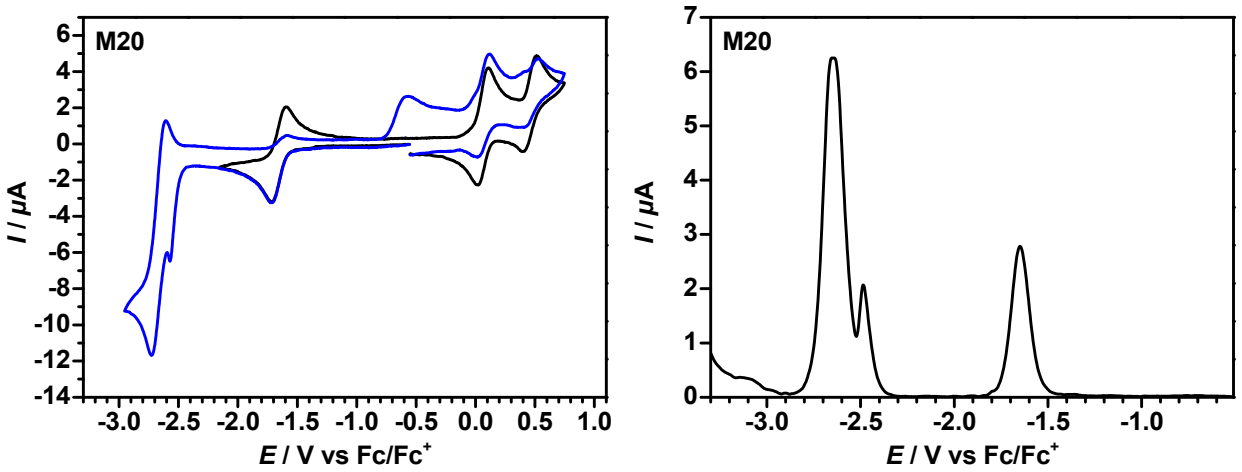

Figure 63 Cyclic voltammograms (left) and differential pulse voltammogram (right) of **M20** in THF/TBAHFP (0.2 M) at a scan rate of 250 mV s^{-1} and 20 mV s^{-1}, respectively. The blue voltammogram covers the additional reduction processes.

Table 20 Redox potentials, HOMO and LUMO energy levels and band gaps obtained by electrochemical (E_{gap}^{CV}) and optical (E_{gap}^{opt}) methods of **M20** and reference dye **M1**. The electrochemical experiments were performed in THF for both compounds.

	$E_{1/2}^{Red3}$ / mV	$E_{1/2}^{Red2}$ / mV	$E_{1/2}^{Red1}$ / mV	$E_{1/2}^{Ox1}$ / mV	$E_{1/2}^{Ox2}$ / mV	E_{HOMO} / eV[d]	E_{LUMO} / eV[d]	E_{gap}^{CV} / eV[d]	E_{gap}^{opt} / eV[e]
M1[a]		–2631[c]	–1660	64	442	–5.32	–3.60	1.72	1.88
M20[b]	–2647[c]	–2487[c]	–1655 –1647[c]	64	454	–5.32	–3.61	1.71	1.84

[a] Ag/AgCl pseudo-reference electrode; [b] Ag/AgCl "leak free" electrode; [c] potentials extracted from DPV; [d] determined according to the procedure described in 5.1.4; [e] determined in DCM according to the procedure in 5.1.1.

Conclusion

The dye **M20** does not show any remarkable differences of neither the absorption nor the electrochemical properties compared to reference squaraine **M1**. The reduction potential of the triarylborane moiety is at even lower potential than the second irreversible reduction of the squaraine core. Due to the only minor differences of these properties of

the monomeric dye **M20** compared to reference squaraine **M1**, the synthesis of a corresponding polymer was not attempted.

3.5.2 NDI–Squaraine Monomers and Copolymer

In the previous chapter it was shown that the addition of a weak electron accepting moiety, such as the triarylborane, barely influences the spectroscopic and electrochemical properties of the squaraine dye. NDIs on the other hand are strong electron acceptors[237-238] which were successfully applied in OFETs[239] or as side chain acceptors in double cable oligomers.[240] In principle, NDI can be connected to squaraines by the nitrogen or *via* the naphthalene core. The latter was chosen as this allows a better conjugation and, thus, stronger electronic communication between the squaraine and NDI chromophores. In contrast, communication of chromophores *via* the NDI nitrogen is expected to be quite week as the NDI's π-LUMO and HOMO possess nodes through the nitrogen centres.[241]

Synthesis

NDI-Substituted Squaraine Monomers

The synthesis of the NDI precursors **35** and **36** (Scheme 25) was performed analogously to literature procedures.[242-244] Naphthalene-1,4,5,8-tetracarboxyanhydride was brominated with dibromoisocyanuric acid in sulphuric acid. The crude product, which contained a mixture of varying brominated species, was subsequently used without further purification, because separation of the various products is easier at the diimide stage. After imidation with 2-ethylhexylamine in glacial acetic acid, **35** and **36** were isolated by column chromatography and/or precipitation in 6 and 37% yield over two steps.

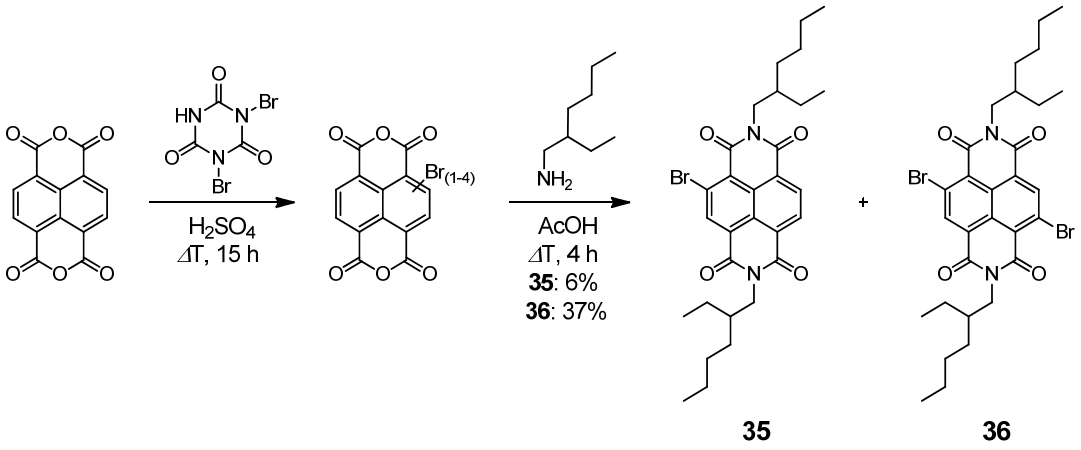

Scheme 25 Synthesis of mono- and difunctionalised NDI precursors **35** and **36**.

The synthesis of monomer **M21** was accomplished by *Suzuki* coupling of the appropriate squaraine diboronic ester **M8** and bromonaphthalene **35** with $Pd(PPh_3)_4$ and Na_2CO_3 in a mixture of 1,4-dioxane and water, similar to a literature procedure (Scheme 26).[245] This reaction also yields a squaraine dye that is substituted with one NDI but still has one boronic ester left unreacted (**M22**). The dyes were purified by column chromatography and subsequent recycling GPC.

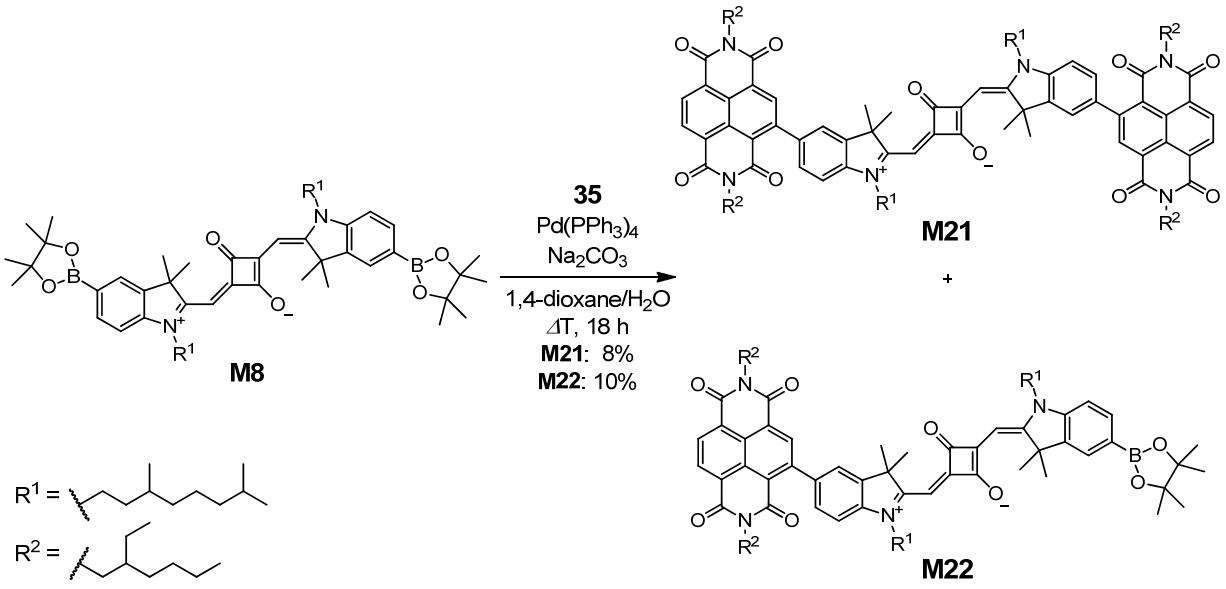

Scheme 26 Synthesis of mono- and disubstituted NDI–squaraines **M21** and **M22**, respectively.

NDI–Squaraine Copolymer

Similar to the reaction of the NDI-substituted squaraine monomers **M21** and **M22**, the reaction of **M8** and dibromonaphthalene diimide **36** in a solvent mixture of 1,4-dioxane and water with $Pd(PPh_3)_4$ and Na_2CO_3 was carried out but gave only low yields and small oligomers (M_n = 6200, M_w = 8900, X_n = 5.3, PDI = 1.45). However, the use of $NaHCO_3$ in THF (Scheme 27) and water gave much better yields and longer polymers **P13** which were purified by *Soxhlet* extractions in several solvents (M_n = 28000, X_n = 24).

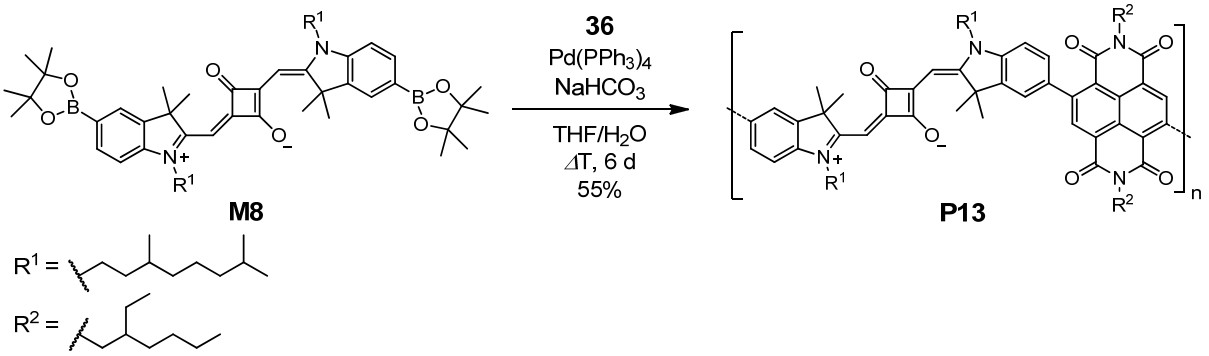

Scheme 27 Synthesis of NDI–squaraine copolymer **P13**.

Absorption Spectroscopy

The reference indolenine squaraine dye **M1** shows a strong and sharp absorption at 15700 cm^{-1} in DCM as shown before. Parent naphthalene diimide **NDI1** (Chart 16) has the characteristic lowest energy absorption at 26300 cm^{-1} with vibrational progression in DCM (Figure 64, left).[244, 246-247] Even though **NDI1** comprises aromatic instead of alkyl groups at the nitrogen atoms, it was chosen for comparison because it has been investigated in the group of *Lambert* and the difference of the absorption properties is negligible.[246] For the monomeric conjugates **M21** and **M22** as well as the polymer **P13** one expects to find these features in addition to those emerging from interaction between the squaraine and the NDI.

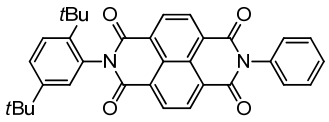

NDI1

Chart 16 Reference naphthalene diimide **NDI1**.

E.g. it is well known, that NDIs substituted with donor substituents at the naphthalene core show an additional CT band at lower energy, depending on the substituent.[237, 241, 248] However, for most NDIs (even for NDI with four amino substituents) the CT absorption does not exceed 15600 cm^{-1}.[240] It needs a combination of strong donors plus an extension of the π-system to push that CT absorption further into the red spectral region.[249] For example, two *N*,*N*-dihexylanilines being attached to the NDI core *via* acetylene bridges push the CT band down to 14500 cm^{-1}. Upon protonation of these aniline moieties, this band disappears which proves the CT character of this transition.[237] For a NDI core-substituted with two *ortho*-phenylenediamine moieties *via* their nitrogen atoms, the CT band was even shifted down to 12900 cm^{-1} in DCM.[250]

The absorption spectra of disubstituted NDI squaraine dye **M21** and the corresponding copolymer **P13** are shown together with the reference squaraine **M1**, parent **NDI1** (Figure 64, left), and with monosubstituted NDI squaraine **M22** (Figure 64, right). The monomers **M21** and **M22** show a broad low energy absorption band between ca. 10000–20000 cm^{-1}, which extends to both the higher and lower energy side compared to parent squaraine **M1**. They are the only squaraine monomers in this work, where the shape of this band clearly differs from all other squaraines and the typical structure such as the steep rise at the low energy side together with a vibronic shoulder at the high energy side is not apparent. At ca. 26000–30000 cm^{-1} the local π-π^* absorption of NDI with its typical vibronic progression is clearly visible. It is also apparent that for **M21** the ratio of parent squaraine chromophore to NDI moiety (1:2) is different to **M22** and **P13** (1:1) where the extinction coefficient of the local NDI absorption bands is roughly twice the value for the former.

Squaraine **M21** was used as monomeric model compound for **P13** and therefore **M22** was not further investigated in detail.

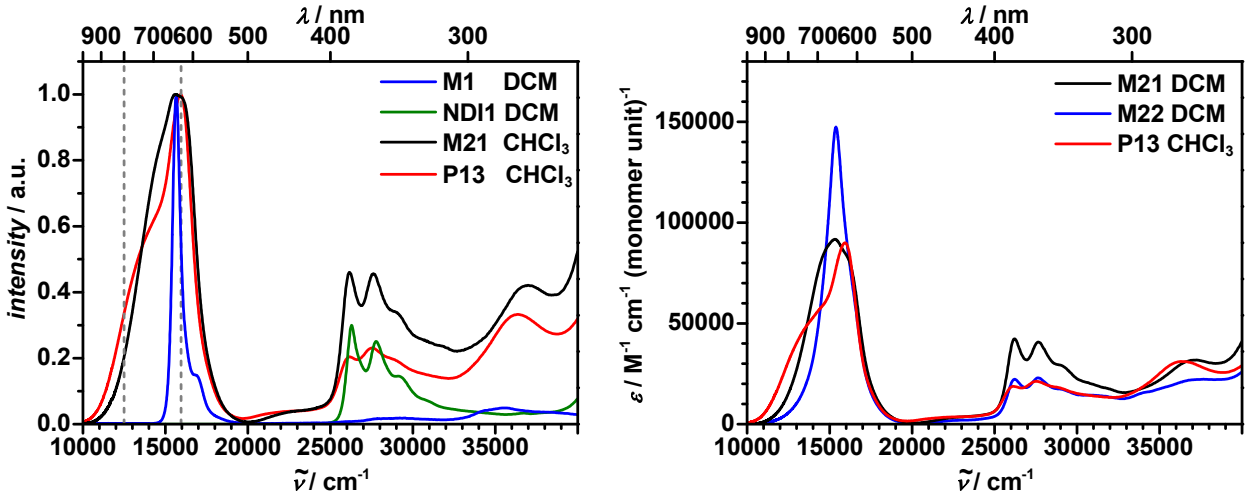

Figure 64 Left: Normalised absorption spectra of **M21** and **P13** together with reference squaraine **M1** and NDI derivative **NDI1** (normalised to an arbitrary value of 0.3). The vertical dashed lines indicate the excitation energy of the pump-probe experiment. Right: Absorption spectra of monomers **M21** and **M22** and copolymer **P13**.

The broad low energy absorption band of **M21** strongly depends on the solvent and a bathochromic shift of the maximum of this band is observed (Figure 65). It is assumed that this band consists of an overlapping local squaraine transition and CT band which is caused by partial CT from the squaraine to the NDI moiety. At higher energy the local π-π* transitions only differ slightly in cyclohexane, where they are hypsochromically shifted to 26500 cm^{-1}.

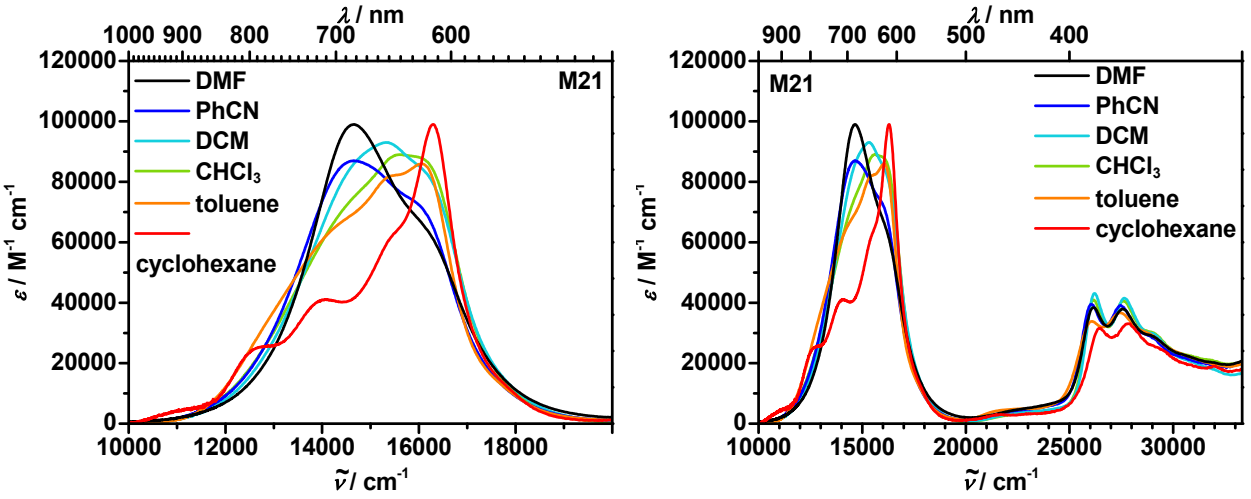

Figure 65 Magnified (left) and complete (right) absorption spectra of **M21** in various solvents.

While both squaraine and NDI dyes are susceptible to aggregation, concentration dependence on the spectral shape was checked and indeed, strong deviations were found

for cyclohexane but not for the other solvents. In cyclohexane at high concentration the peak at 16300 cm^{-1} is highest (Figure 66, left). This behaviour points towards an H-aggregate formation. Whether the NDI or the squaraine moiety is responsible for this effect is unknown.

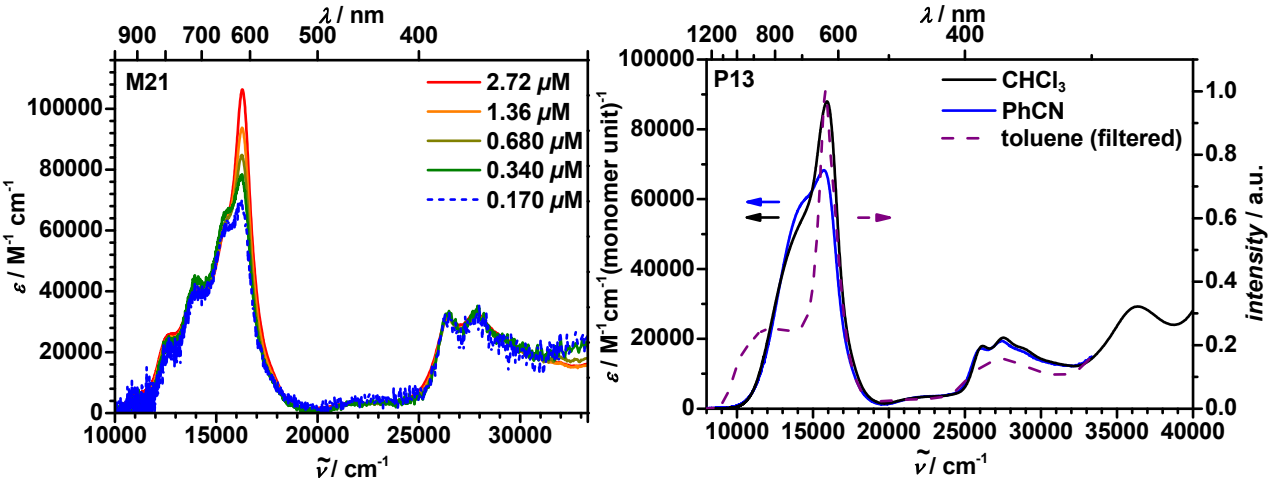

Figure 66 Left: Absorption spectra of **M21** in cyclohexane at different concentrations. The spectra were normalised to the extinction coefficient at 26500 cm^{-1} (378 nm) of the 2.72 μM solution. Right: Absorption spectra of **P13** in several solvents. The polymer was not completely soluble in toluene, therefore an extinction coefficient could not be determined.

From the strong shift of lowest energy absorption of **M21** vs. parent **M1** and **NDI1** (Figure 64, left), it can be concluded that there are strong electronic interactions between these moieties which are possibly of CT nature. In order to gain a more detailed insight, quantum chemical calculations were performed both at density functional level and at semiempirical level. First **M21** was optimised at CAM-B3LYP/6-31G* in approximate C_i symmetry.[251] TDDFT computations including a COSMO solvent model for $CHCl_3$ give three lowest energy excited singlet states: 17200 cm^{-1} (oscillator strength $f = 2.2$), 20800 cm^{-1} ($f = 0.0$), and 21300 cm^{-1} ($f = 0.1$). Looking at the orbitals involved, these transitions may be interpreted as CT transitions between the squaraine localised HOMO and the NDI localised LUMOs as well as the squaraine LUMO. Taking this DFT optimised geometry, the excited state was also computed by the semiempirical CNDO/S2 method[161] which proved to be useful in describing optical properties of squaraine dyes. These CIS computations also gave three lowest energy singlet excited states: 17500 cm^{-1} ($f = 2.1$), 20100 cm^{-1} ($f = 0.0$), and 20500 cm^{-1} ($f = 0.1$) which are in

excellent agreement with the DFT results. However, in both types of calculations the computed transition energies are too high compared to the experimental values. It is also unlikely that the broad absorption in **M21** is caused by only one electronic transition. It is assumed that all three transitions contribute to the broad band and that, unlike the computed predictions, owing to symmetry breaking all three transitions are electronically allowed.

The experimental absorption spectra of the polymer **P13** are even more unusual (Figure 66, right). In $CHCl_3$ there is a prominent absorption at 15900 cm^{-1} with a pronounced shoulder at ca. 14000 cm^{-1}. This shoulder is even more intense in benzonitrile (PhCN). In toluene the shoulder is less intense but strongly shifted towards lower energy so that the lowest energy absorption extends down to ca. 9000 cm^{-1}. Again, concentration dependent spectra show no evidence for aggregation in these three solvents. It has to be mentioned that **P13** was not completely soluble in toluene and the suspension was filtered prior to the absorption measurement. Later, when the polymer was applied in a ternary solar cell, an absorption spectrum of a spin-coated thin film (from chlorobenzene solution) was recorded (chapter 3.8.3, Figure 83, left, p. 226). This spectrum matches the one recorded in toluene solution, indicating either undissolved particles in the toluene solution smaller than the pore size of the filter (~ 0.1 μm) or dissolved aggregates that already arrange in the same way as in thin film.

In order to gain insight into the electronic nature of the polymer, a model hexamer of **P13** was optimised with the AM1 hamiltonian[252] and the transition energies as well as the oscillator strength were again computed by CNDO/S2. This calculation gave a series of 15 lowest energy transitions between 22800 and 17900 cm^{-1}. The most intense ones are that at 17900 cm^{-1} (f = 5.1), 18400 cm^{-1} (f = 0.7) and 19600 cm^{-1} (f = 0.8). In that way, these results are similar to the ones of **M21**. In all these calculations, the lowest energy transition allowed is a squaraine localised transition and the higher energy ones possess some CT character. In comparison with the experiment, it can be assumed that the energy of these CT states are estimated to be too high and that they are actually lower in energy than the squaraine localised state.

Table 21 Absorption maxima, extinction coefficients, transition moments, fluorescence quantum yields, and band gaps obtained by electrochemical (E_{gap}^{CV}) and optical (E_{gap}^{opt}) methods of **M1**, **M21**, **M22**, and **P13**. Extinction coefficient ε and transition moment μ_{eg} of the polymer are given per monomer unit. cy = cyclohexane.

	solvent	λ_{abs} / nm	$\tilde{\nu}_{abs}$ / cm^{-1}	ε / $M^{-1}cm^{-1}$	μ_{eg} / D	Φ_{fl}[a]	E_{gap}^{opt} / cm^{-1} (eV)[b]	E_{gap}^{CV} / eV[c]
M1	DCM	639	15700	336000	11.4	0.19	15200 (1.88)	1.72
	toluene	644	15500	340000	11.1	0.35	-	-
M21	PhCN	683	14600	87000	12.0	x	12500 (1.55)	x
	DMF	682	14700	99000	12.5	x	12900 (1.60)	x
	DCM	653	15300	93000	12.6	x	12400 (1.54)	1.05
	$CHCl_3$	639	15600	89000	12.5	x	12100 (1.50)	x
	toluene	623	16100	86000	12.0	x	11700 (1.46)	x
	cy	614	16300	106000[c]	11.4[a]	x	10100 (1.26)	x
M22	DCM	650	15400	147000	12.0	x	x	x
	toluene	652	15300	143000	11.6	x	x	x
P13	PhCN	636	15700	70000	11.3	x	11300 (1.40)	x
	$CHCl_3$	627	15900	88000	12.4	x	11100 (1.38)	1.20[d]
	toluene	632	15800	x	x	x	9200 (1.14)	x

- was not measured; x could not be determined. [a] During the writing process, the quantum efficiency of oxazine 1 was determined to be 0.15 by an absolute measurement using an integration sphere. However, the values reported for the squaraine dyes herein are still referenced against the quantum efficiency of 0.11 (see experimental section 5.1.2) as they were published to avoid confusion. Nevertheless, it has to be noted that the correct quantum efficiencies are larger by a factor of $0.15/0.11 \approx 1.36$. [b] determined according to the procedure in 5.1.1. [c] determined according to the procedure described in 0; [d] determined in $CDCl_3$; [d] extinction coefficient determined at the concentration of 2.72 μM.

Cyclic Voltammetry

Electrochemical investigation of the redox potentials as well as spectroelectrochemical measurements of the associated changes of UV/Vis/NIR-absorption spectra shall give information about possible CT states that may also be formed upon optical excitation. The cyclic voltammogram of the model dye **M21** in DCM shows two oxidation waves and three reduction waves (Figure 67, left). The first two reduction waves have roughly twice the intensity than the third one and refer to the two naphthalene diimide units[246] whereas the third belongs to the squaraine core as do the two oxidation waves ($E_{1/2}$ = 23 mV and 516 mV). Digital fitting[195] confirmed that each of the first two reduction waves comprises two reduction processes with half-wave potentials of $E_{1/2}$ = –1.03 V, –1.09 V, –1.48 V, and –1.54 V determined by digital fitting. For comparison, the

half-wave potentials of non-substituted NDI are $E_{1/2} = -1.11$ V and –1.54 V.[246] The last reduction at $E_{1/2} = -1.88$ V is that of the squaraine core, which possesses the most negative potential for the 1st reduction of the squaraine core of all dyes investigated in this work. For comparison **M5** shows half-wave potentials of $E_{1/2} = -1.66$ V, 110 mV, and 580 mV in DCM.

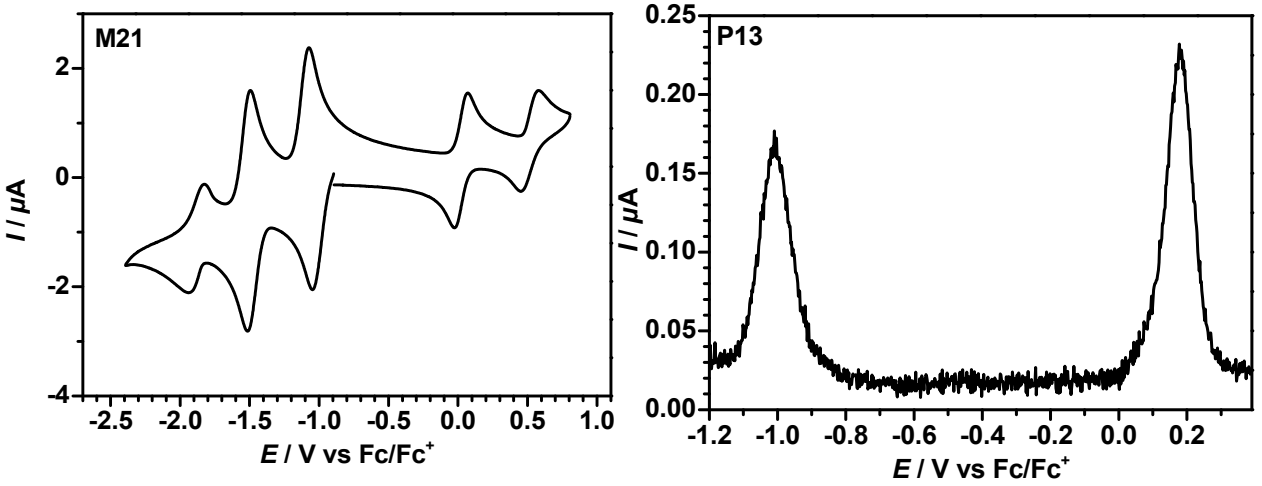

Figure 67 Left: Cyclic voltammogram of **M21** in DCM/TBAHFP (0.2 M) at a scan rate of 250 mV s^{-1}. Right: *Osteryoung* square wave voltammogram of **P13** in $CDCl_3$/TBAHFP (0.2 M) at 50 mV s^{-1}.

Polymer **P13** is sufficiently soluble in $CHCl_3$ (or $CDCl_3$) only but in this solvent the reduction is chemically irreversible in contrast to the oxidation. Thus, the redox potentials ($E_{1/2} = -1.03$ V and 180 mV) were determined by *Osteryoung* square wave voltammetry (OSWV) which is given in Figure 67 (right). It has to be kept in mind that due to the chemical irreversibility, OSWV does not provide exact thermodynamic redox potentials but close approximations. From *Weller* approach[253] (equation (90)) the formation of a charge separated state (squaraine oxidised and NDI reduced) is estimated to have an energy of $\Delta G^0_{1CS} = 0.93$ eV in $CDCl_3$.

$$\Delta G^0_{1CS} = \frac{N_A}{1000} ze\left(E^{ox1}_D - E^{red1}_A\right) - \frac{N_{Av}e^2}{1000}\frac{1}{4\pi\varepsilon_0}\left(\left(\frac{1}{2r_D}+\frac{1}{2r_A}\right)\left(\frac{1}{\varepsilon_r}-\frac{1}{\varepsilon_s}\right)+\frac{1}{\varepsilon_s r_{DA}}\right) \quad (90)$$

Here, E_D^{ox1} and E_A^{red1} are the redox potentials of the first oxidation of the donor and the first reduction of the acceptor, respectively, r_D (= 5.5 Å) is the radius of the donor (squaraine), r_A (= 4.0 Å) the radius of the acceptor (NDI) and r_{DA} (= 11 Å) the donor-acceptor centre-to-centre distance as determined from the Connolly molecular surfaces of the subunits calculated with ChemBio3D Ultra[254]. N_{Av} is *Avogadro*'s constant, e the elementary charge, ε_0 the permittivity of vacuum, and ε_r and ε_s the permitivities of the solvents used for the cyclic voltammetry and the spectroscopy, respectively.

Table 22 Redox potentials, HOMO and LUMO energy levels, and band gaps obtained by electrochemical (E_{gap}^{CV}) and optical (E_{gap}^{opt}) methods of monomer **M5**, NDI-substituted dye **M21**, and NDI–squaraine copolymer **P13**.

	$E_{1/2}^{Red5}$ / mV	$E_{1/2}^{Red4}$ / mV	$E_{1/2}^{Red3}$ / mV	$E_{1/2}^{Red2}$ / mV	$E_{1/2}^{Red1}$ / mV	$E_{1/2}^{Ox1}$ / mV	$E_{1/2}^{Ox2}$ / mV	E_{HOMO} / eV[d]	E_{LUMO} / eV[d]	E_{gap}^{CV} / eV[d]
M5[a] DCM					–1610	110	580	–5.27	–3.55	1.72
M21[a] DCM	–1883	–1504 *–1540*	–1504 *–1480*	–1060 *–1090*	–1060 *–1030*	23	516	–5.17	–4.09	1.08
P13[b] $CDCl_3$					–1025[c]	177				1.20

[a] Ag/Ag/Cl pseudo-reference electrode; [b] Ag/AgCl "leak free" electrode; [c] potentials extracted from OSWV; [d] determined according to the procedure described in 5.1.4; the values written in italics are obtained by digital fitting of the redox waves with DigiSim.[195]

Spectroelectrochemistry

For estimating the changes that may occur upon photoexcitation, UV/Vis/NIR-spectroelectrochemical measurements of **M21** were performed in DCM/TBAHFP (0.2 M). Oxidation of **M21** leads to a sharpening of the lowest energy absorption peak (Figure 68 A) much in the same way as oxidation of the dibromo indolenine squaraine **M5** (Figure 68 C) and the maximum is found at 14900 cm^{-1}. This excellent match of the spectra of the monocations up to 24000 cm^{-1} (Figure 68 D) indicates that the CT character of the squaraine HOMO to NDI LUMO transition is lost upon oxidation of the

squaraine moiety and only localised squaraine transitions are found in that region. The local π-π* NDI transitions above 26000 cm^{-1} remain unchanged.

Reduction of the NDI moieties leads to a decrease of the typical NDI-bands[237] at 26200 and 27700 cm^{-1} (Figure 68 B) and to an increase of signals at 20700 and 15200 cm^{-1}. The latter is caused by a superposition of the intense squaraine band and of transitions arising from reduced NDI[237-238] which can be found between 10000–20000 cm^{-1} depending on the specific substitution pattern at the NDI.

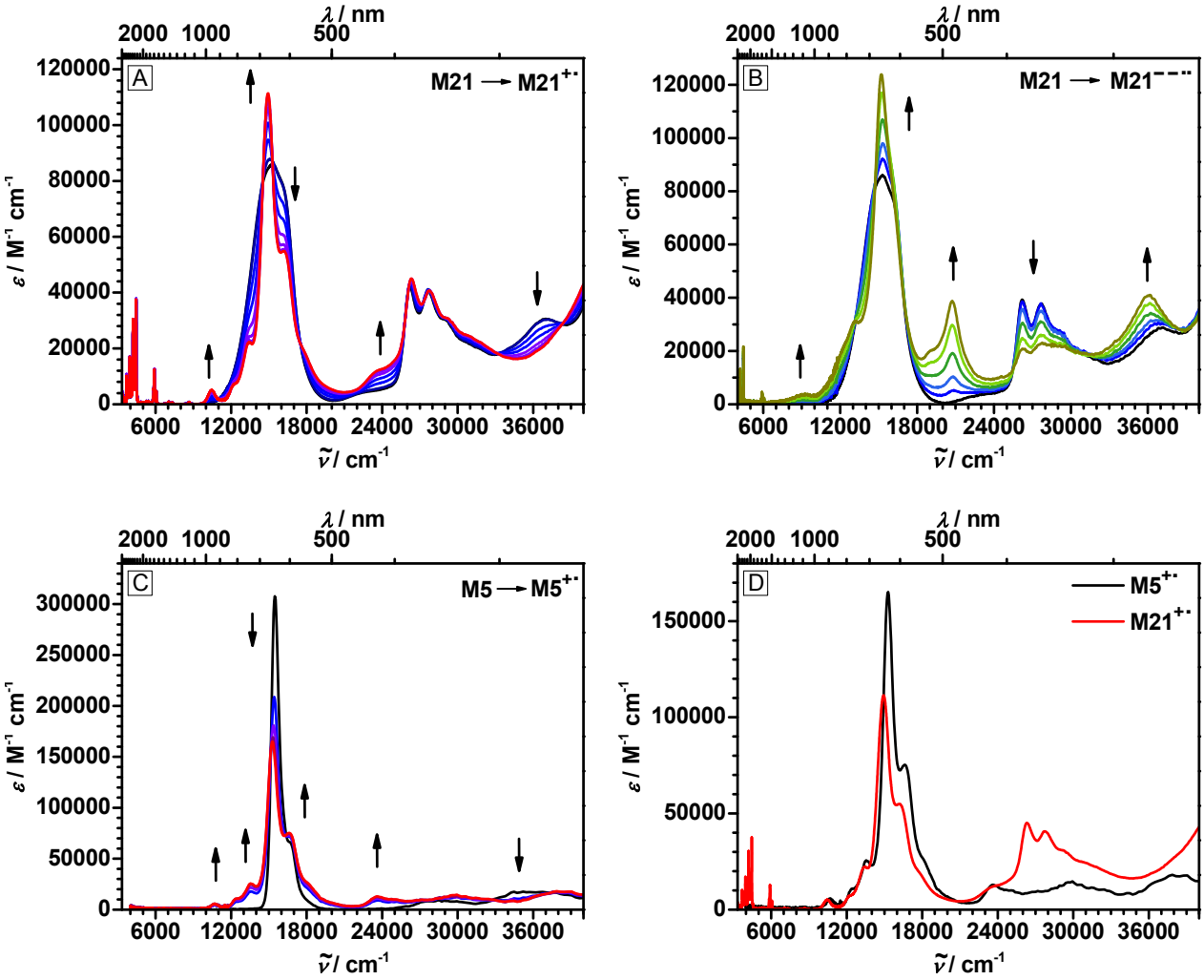

Figure 68 UV/Vis/NIR-Spectroelectrochemistry of **M21** and **M5** in DCM/TBAHFP (0.2 M). The black spectra are the initial spectra. A: 1st oxidation of **M21**; B: 1st and 2nd reduction of **M21**; C: 1st oxidation of **M5**; D: comparison of the spectra of the monocations **M5**$^{+\cdot}$ and **M21**$^{+\cdot}$.

Transient Absorption Spectroscopy

Neither the monomer **M21** nor the polymer **P13** shows any appreciable fluorescence in the above-mentioned solvents. This behaviour is quite unusual for squaraine dyes which are commonly known as efficient fluorescence dyes and points towards a rapid quenching mechanism, possibly caused by CT processes. Thus, the excited state lifetime was probed by transient absorption spectroscopy in $CHCl_3$. For **M21**, a solution in $CHCl_3$ was excited at 16000 cm^{-1} with 140 fs pulses and the transient spectra were probed with 100 fs white light continuum. From the transient spectra given in Figure 69 (left) a prominent ground state bleach (GSB) between 14000–17000 cm^{-1} and excited state absorption (ESA) both at lower and at higher energy can be seen. The latter one is particularly broad and extends up to 26000 cm^{-1}.

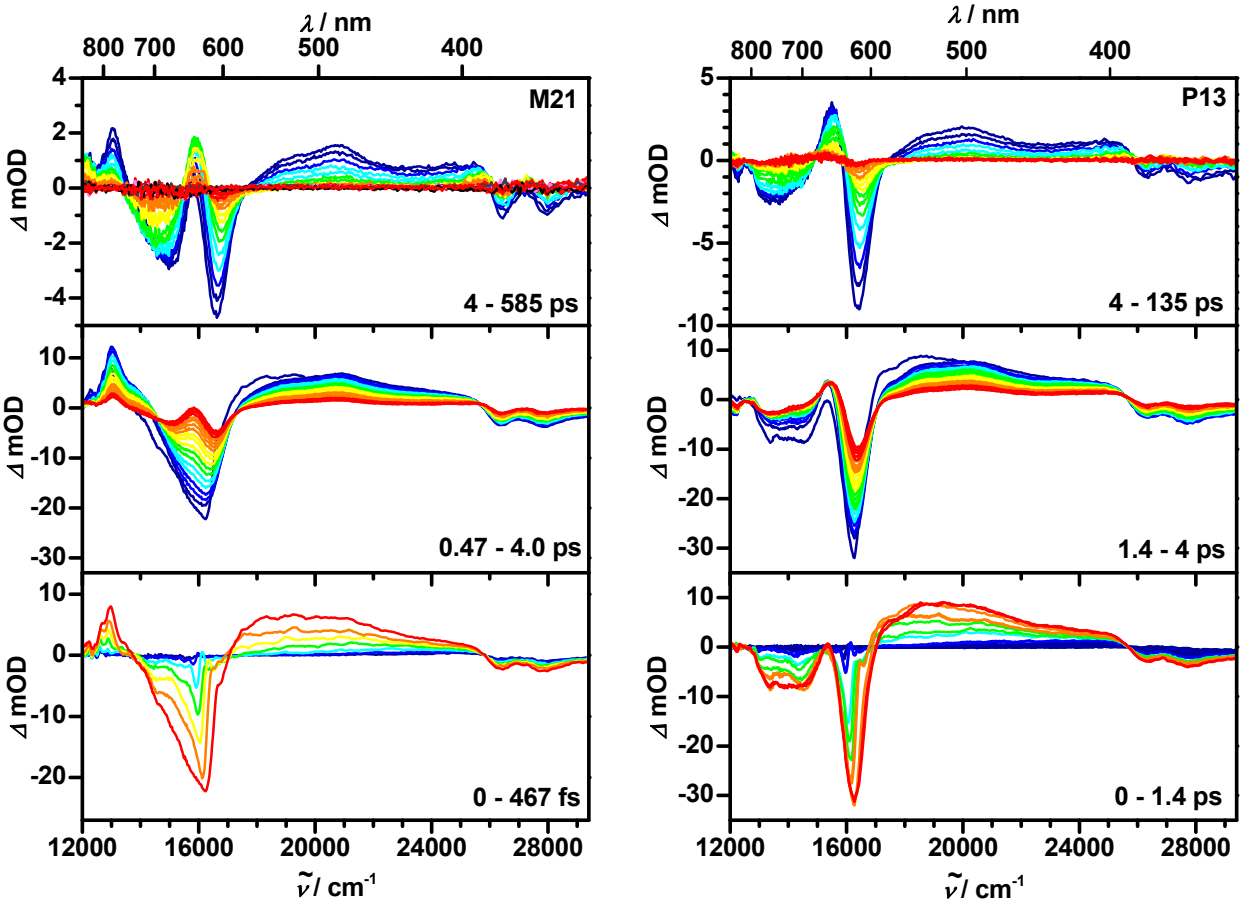

Figure 69 Transient absorption spectra of **M21** and **P13** in $CHCl_3$ at 16000 cm^{-1} pump energy. Spectra at early times are given in dark blue, spectra at later times in red.

Comparison with the absorption spectrum (Figure 65) shows that the GSB is strongly overlaid by ESA because the lowest energy absorption of **M21** covers a much broader region between 11000 and 19000 cm^{-1}. In addition there is a GSB signal between ca. 26000 and 30000 cm^{-1} which is typical of the vibronic structure of NDI.[237] All these signals rise with the instrument response and decrease rapidly (on the order of ca. 1 ps), giving rise to an ESA at ca. 16000 cm^{-1} which increases relatively to all other features.

A better interpretation of the transient data can be done on the basis of a singular value decomposition of the transient (wavenumber × time) map, which yields the number of independent spectral components, and a subsequent global fit to the transient map. These deconvolutions were done using the GLOTARAN software[255], which allows a target fit to a kinetic model which is given in Figure 71 (p. 193). In this figure, the various states discussed below are shown together with the corresponding lifetimes. Additionally the efficiencies/percentages of the different processes are shown as well as the energies of some of the states. The values concerning **M21** are given in brackets. All lifetimes given in the text/figure are extracted from the global fit and belong to the corresponding species.

The species associated difference spectra (SADS) of this target fit are given in Figure 70 (A). The first SADS component (black line, $\tau = 48$ fs) shows a sharp GSB at 16400 cm^{-1} (the small peak at 16000 cm^{-1} is caused by the coherent artefact of the pump wavelength) and broad and much weaker ESA above 17000 cm^{-1}. As the squaraine moiety is predominantly excited at 16000 cm^{-1} pump energy, these features can safely be assigned to the localised excitation of the squaraine. Two SADS follow which are both characterised by a much broader GSB around 16000 cm^{-1} and ESA above 17000 cm^{-1}. Furthermore, both show the typical vibronic GSB features of NDI above 26000 cm^{-1}. These two states can be interpreted as hot (orange line, $\tau = 1.0$ ps) and relaxed CT state (red line, $\tau = 1.2$ ps) because there is a significant sharpening of the GSB of the second transient spectrum at 16400 cm^{-1} which is interpreted to be caused by vibrational cooling.[256-258] This process may also include conformational relaxation,[259-262] e.g. changes of the dihedral angle between squaraine and NDI. This CT state transforms into a species that has a lifetime of 5.6 ps (blue line). The SADS of this species again shows

the NDI GSB features above 26000 cm^{-1} but a strong ESA at 15900 cm^{-1} which overlays the GSB in this region to produce an alternating spectral pattern between 12000 and 18000 cm^{-1}.

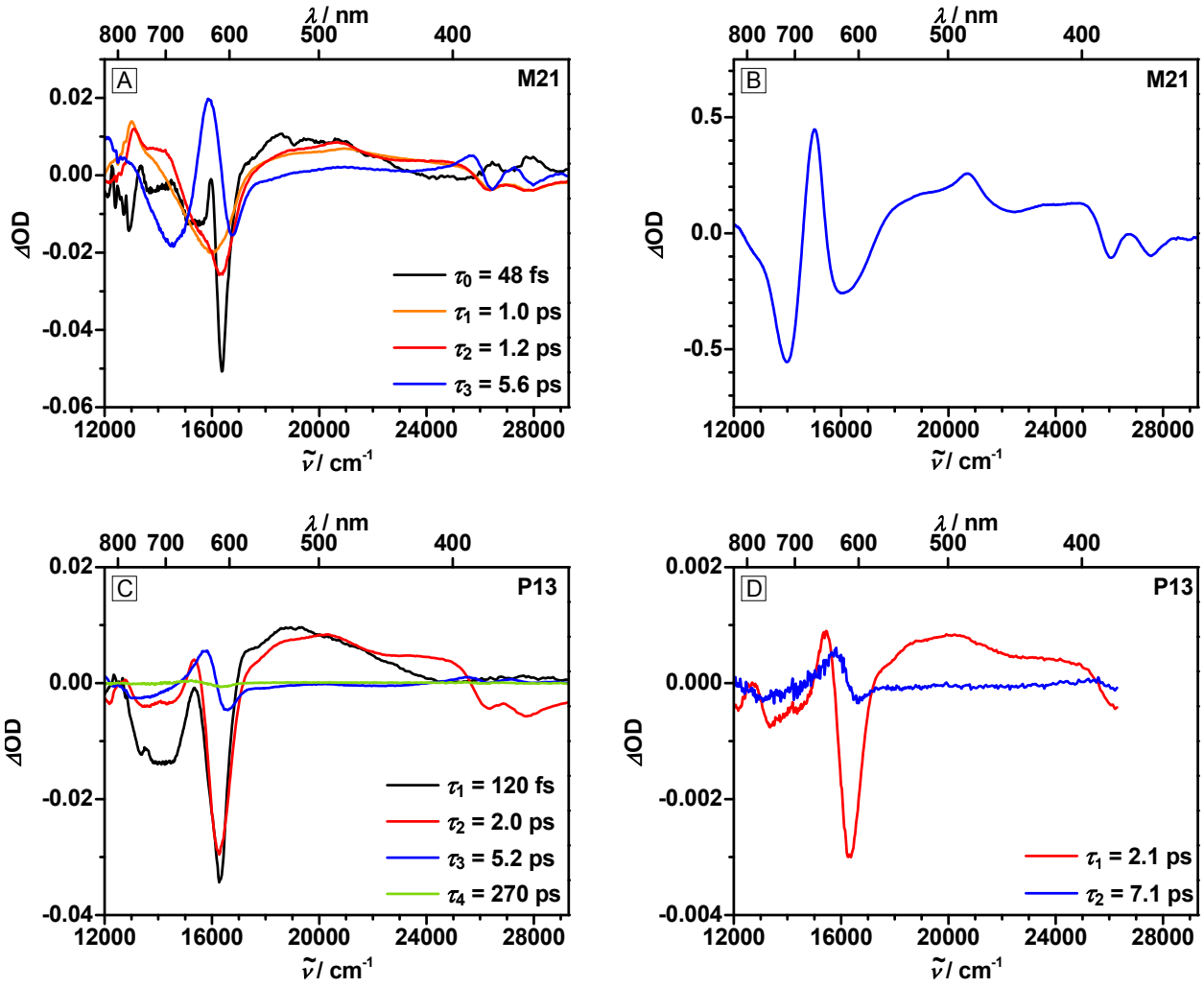

Figure 70 A: SADS of **M21** in $CHCl_3$ at 16000 cm^{-1} pump energy; B: Sum of difference spectra of radical cation and half of the diradical dianion of **M21** generated by spectroelectrochemistry in DCM; C: EADS of **P13** in $CHCl_3$ at 16000 cm^{-1} pump energy; D: EADS of **P13** at a pump energy of 12500 cm^{-1}.

From the spectroelectrochemical experiments of radical cation and diradical dianion of **M21** the spectra of a possible charge separated state (CS) can be constructed by adding the difference spectrum of the radical cation and half of the difference spectrum of the dianion (because two reduced NDI moieties contribute to this spectrum). This constructed spectrum is given in Figure 70 (B) and proves that the SADS (τ = 5.6 ps) in Figure 70 (A) is indeed that of a charge separated state in which the squaraine is oxidised and one NDI is reduced. The target fit to the transient map of **M21** was done under the

assumption that the NDI GSB above 26000 cm^{-1} possesses the same intensity in all components. In order to achieve this, the efficiencies of processes had to be adjusted which are given in Figure 71. From these efficiencies it is clear that the CS state of **M21** is only formed in ca. 22% quantum yield. Most excitation is lost by direct recombination of the CT state down to the ground state. In conclusion, for **M21** the formation of a CS state, possibly *via* CT states as intermediates, could unequivocally be proved.

For the polymer **P13** analogous transient absorption measurements were performed which are shown in Figure 69 (right) for a pump energy at 16000 cm^{-1}. While most features appear to be similar to the monomer, there is a significant GSB around 13000–15000 cm^{-1} already at very early times ($t < 4$ ps) while there is ESA in **M21**. Global analysis yields four independent spectral contributions. Here, evolution associated difference spectra (EADS) for a sequential kinetic model are used for interpretation (Figure 70 C), because there are no spectral signatures which would allow estimating efficiencies for a target model. Besides this, using EADS for **P13** and the SADS for **M21** is equivalent. The first EADS of **P13** has a lifetime of 120 fs (black line) and shows a strong GSB between 13000 and 17000 cm^{-1} with a pronounced dip at 15300 cm^{-1}. This dip comes from an overlaid ESA which becomes more pronounced at later times and was already seen in the SADS spectra of **M21** at 5.6 ps. In the EADS with $\tau = 120$ fs there is no GSB above 26000 cm^{-1} which indicates that only the squaraine moiety is excited. The subsequent EADS with $\tau = 2.0$ ps now shows an ESA at 15300 cm^{-1} and the GSB above 26000 cm^{-1} which indicates excitation of both, NDI and squaraine components and, in analogy to **M21**, the formation of a CT state. This state relaxes into a state with $\tau = 5.2$ ps (blue line) which has transient spectral features very similar to the CS state of **M21**. Because of this similarity it is assumed that a CS state (hereafter called CS_1 state) is also formed in **P13**. For the intensity of the associated EADS has much smaller amplitude than the other signals and the analogous spectrum in **M21**, the formation must occur with an efficiency less than 100%. Unfortunately, spectroelectrochemistry cannot be measured appropriately to proof the CS character of this state because of the irreversibility of the reduction of **P13** but the analogy to **M21** is considered to be convincing. A fourth component with $\tau = 270$ ps (green line) also shows spectral characteristics similar to the CS_1 state but has very low amplitude. It can

be speculated that this CS_2 state is one in which the positive and negative charge are farther apart which explains the longer lifetime of this state compared to the CS_1 state with adjacent charges but the quantum yield of this state is certainly very low.

Analogous pump-probe experiments at 12500 cm^{-1} pump energy only excited the lower energy flank of the CT band. Accordingly, the transient spectra of localised squaraine excitation or hot CT states are not observed but the EADS of the relaxed CT state and subsequently that of the CS state (Figure 70 D).

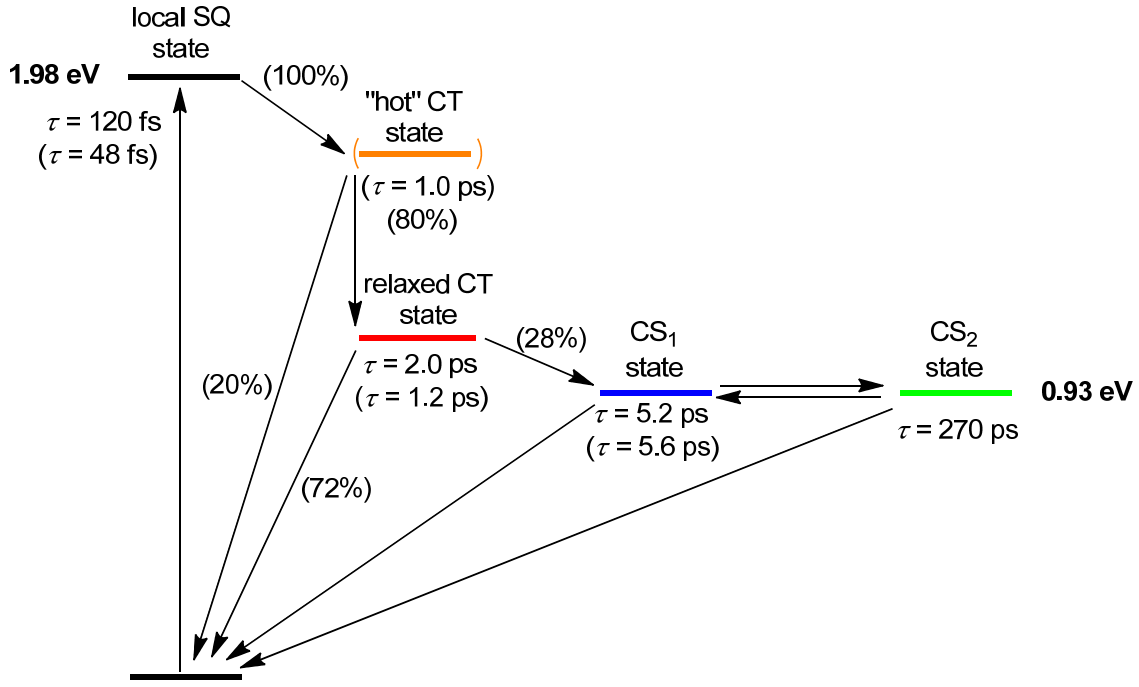

Figure 71 State energy diagram for **M21** (values in brackets) and **P13** in $CHCl_3$. All lifetimes are extracted from the global exponential fit and belong to the corresponding species. The "hot" CS state was observed for **M21** only.

Possible energy transfer processes can be traced by looking at the time dependent transient absorption anisotropy.[232, 263-264] Therefore, the transient anisotropy values $r(t)$ were measured at selected probe energies with parallel and perpendicular pump polarisation (Figure 72). As excitation energy, 12500 cm^{-1} was chosen to excite in the red absorption flank as only possible energy transfer processes between CT states localised on different sections within one polymer strand were of interest. Additionally, local relaxation processes should be avoided. Generally, the anisotropy in transient absorption experiments is the weighted average of the individual ESA, GSB, and

stimulated emission (SE) components. As these individual contributions are not known, the absolute values of anisotropy cannot be interpreted but for cases in which both positive (ESA) and negative (GSB or SE) amplitudes contribute, the anisotropy can reach any values $-\infty < r < +\infty$.[265] However, provided that these relative contributions do not vary with time, they may give evidence for time dependent changes of transition moments and, thus, possible energy or electron transfer processes in the polymer.

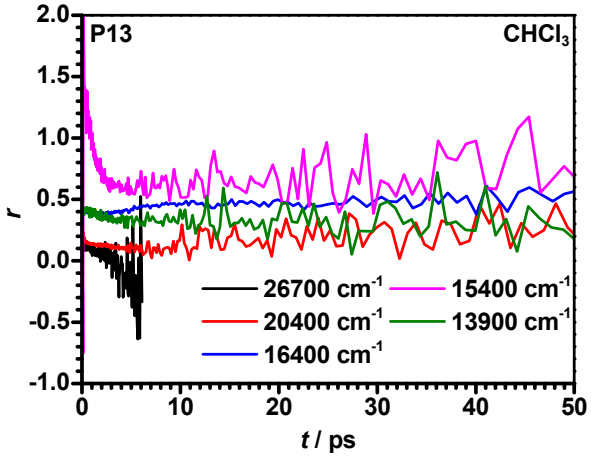

Figure 72 Anisotropy r(t) of **P13** in $CHCl_3$ for selected probe energies at 12500 cm^{-1} pump energy. There is no depolarisation until the signal/noise ration becomes too small.

In fact there was no appreciable variation of the anisotropy with time after ca. 1 ps and, in particular no depolarisation within the longest decay time (270 ps). It is concluded that there is neither significant energy transfer between different CT states nor is there any electron transfer of positive or negative charges to centres lying farther away that would lead to any depolarisation. Depolarisation caused by molecular motion is expected to be quite slow (>> ns) because of the size of the polymer. The strong variation of anisotropy at 15400 cm^{-1} within the first 3 ps is caused by a change of relative contribution of GSB and ESA with time (Figure 69, right, p. 189). To sum up, due to the strong variation of GSB and ESA within the first 3 ps, no clear conclusion can be drawn regarding energy transfer in this time span. However, it can be excluded for the following time owing to the constant anisotropy.

The formation of CT and subsequent CS states was recently postulated by *Riedle et al.*[266] for a monomeric phenylamino-substituted NDI derivative. These authors also

found an ultrafast charge separation within 3 ps in $CHCl_3$ but a significantly slower charge recombination. The very fast charge recombination in **M21** and **P13** is possibly caused by the fact that these systems are close to the *Marcus* optimal region where the ET barrier vanishes. To support this hypothesis the solvent reorganisation energy in $CHCl_3$ was estimated by the *Born* model[267] with equation (91) to be 0.49 eV[1],

$$\lambda_0 = \frac{e^2}{4\pi\varepsilon_0}\left(\frac{1}{2r_D}+\frac{1}{2r_A}-\frac{1}{r_{DA}}\right)\left(\frac{1}{n^2}-\frac{1}{\varepsilon_s}\right) \qquad (91)$$

where n is the refractive index of the solvent and all other values and constants are the same as for equation (90) (p. 186). The inner reorganisation energy for self-exchange of NDI is known to be 0.39 eV.[268] The inner reorganisation energy for the self-exchange reaction of unsubstituted squaraine was calculated by the "neutral-in-cation-geometry" method[269] using the Gaussian09 program[251] and the B3LYP/6-31+G* density functional-basis set combination. This yields 0.21 eV. Thus, an averaged inner reorganisation energy of 0.30 eV is obtained and, thus, a total reorganisation energy of 0.79 eV which is pretty close to the energy of the CS state of **P13** for which 0.93 eV are estimated by *Weller* approach. Therefore, the charge recombination of **P13** might indeed be at or close to the optimal region where the ET barrier is small or has vanished. Changing the solvent to a more apolar or more polar one would possibly give support for this interpretation but **P13** is unfortunately not soluble enough in other solvents besides $CHCl_3$ and benzonitrile.

Conclusion

In conclusion, both a squaraine dye with a weak (triarylborane) as well as a squaraine with a strong electron accepting unit (NDI) attached at the periphery were synthesised. While for the former (**M20**) only a minor influence of the acceptor on the spectroscopic

[1] As input for the *Marcus* equation 5.5 Å were used as the radius of the donor, 4.0 Å for the acceptor, and 11 Å for the donor-acceptor distance as determined from the Connolly molecular surfaces of the subunits calculated with ChemBio3D Ultra [CambridgeSoft, *ChemBio3D Ultra 3.0*, Revision 12.0.2.1076; Cambridge, U.K., 2010].

and electrochemical properties was observed, the properties of the latter (**M21**) were unique compared to all other dyes presented in this work. A broad and intense lowest energy absorption band was observed, which most probably consists of a superposition of the common local squaraine HOMO→LUMO transition and a partial CT squaraine to NDI transition, due to the strong electron accepting properties of the latter. Due to this and other peculiar features, also the corresponding alternant donor-acceptor polymer **P13** was prepared.

The polymer shows an optical band gap as low as 1.14–1.40 eV depending on the solvent. For both polymer **P13** and monomer **M21** the ultrafast formation of a CS state within a few ps could be proven. Intermediate states, which are believed to be CT states, are populated right after local photoexcitation of the squaraine chromophore and subsequently relax into the CS state. Charge recombination to the ground state also occurs within a few ps because the system is presumably close to the *Marcus* optimal region for barrierless ET. There is obviously neither appreciable charge nor energy transfer within the lifetime of the excited state, thus, the CS state is essentially confined within one donor-acceptor pair in the polymer strand. This means, that most of the CS or CT states collapse before the charges can further travel along the polymer chain, be it either as separated charges or as correlated electron-hole pairs. Only a small fraction may form CS states where the charges are farther apart. This confinement of excited states is due to the small or even vanishing oscillator strengths and weak spectral overlap of the CT and CS state absorption and emission spectra and therefore, a very slow hopping (= *Förster*) resonance energy transfer can be expected.[270] Charge migration appears also to be slow compared to the excited state lifetime, possibly because of high reorganisation energy.

This investigation shows that the excitons formed in **P13** would readily decay to form weakly bound electron-hole pairs (*Wannier-Mott* exciton) and finally fully separated charges which are unable to move independently within their lifetime.

3.6 Cyclic Squaraines

Even though the focus of this work is on squaraine polymers, also several conjugated macrocycles could be isolated as side products of diverse polymer syntheses. To the best of knowledge, they are the first of their kind and show remarkable spectroscopic properties and will be described in this chapter.

There is the cyclic dimer **Dim1** (Chart 17) that incorporates two squaraine chromophores bridged by two triarylamines. It was obtained as a by-product of the synthesis of the copolymer **P7**. In addition, there are three rather similar cyclic trimers **Tri1–Tri3** as well as one cyclic tetramer **Tet1**, which were obtained during the syntheses of the respective homopolymers. The trimers **Tri1** and **Tri2** (Chart 18) only differ in the alkyl chain on the nitrogen, whereas **Tri3** (Chart 18) and **Tet1** (Chart 19) incorporate a cyclohexyl moiety directly at the indolenine body instead of the CMe_2 moiety.

The spectroscopic data of all squaraine macrocycles is listed in Table 24 (p. 208). Due to limited availability of cyclic squaraine material, cyclic voltammetry experiments were only performed for **Tri1**.

3.6.1 Triarylamine–Squaraine Dimer

Synthesis

The cyclic triarylamine–squaraine dimer **Dim1** was obtained as a side product of the polymerisation reaction to the polymer **P7** (Scheme 20, p. 155). The dimer was isolated in 1% yield by preparative recycling GPC from the hexane fractions that accumulated during the work up (see experimental section 5.2). The formation of the cyclic compound is enabled by the *cis*-structure of the parent squaraine **M2**.

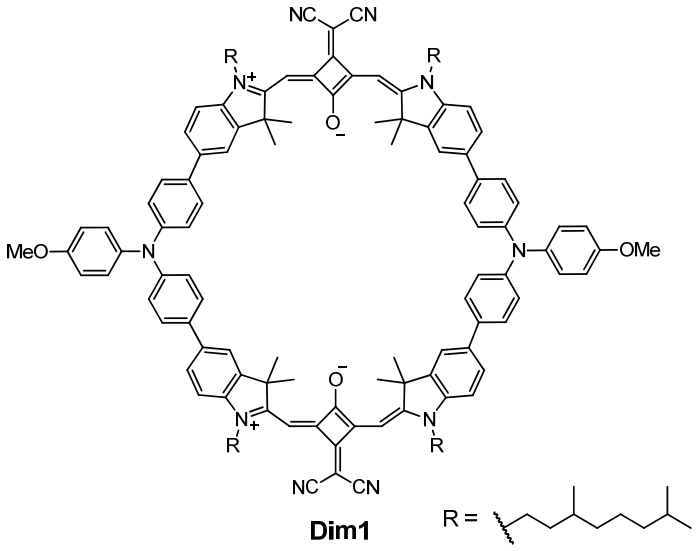

Dim1

Chart 17 Cyclic triarylamine–squaraine dimer **Dim1**.

Absorption Spectroscopy

The absorption spectrum of **Dim1** is similar to the one of the corresponding polymer **P7** (Figure 73, left) with the absorption maximum at the low energy side. Especially at higher energy the spectra are nearly identical, most probably due to the fact that both compounds incorporate the same ratio of squaraine chromophore and triarylamine moiety (1:1). The most striking difference is the intense low energy absorption band. Compared to the reference dye **M2**, the maximum of the dimer **Dim1** is less red-shifted (500 cm^{-1}) to 14100 cm^{-1} (Table 24, p. 208) whereas it is at 13700 cm^{-1} for the polymer **P7**. In addition, the shoulder at 14800 cm^{-1} is more pronounced for **Dim1** than for **P7**.

The shift of the absorption maximum of **Dim1** compared to **M2** can be explained by the triarylamine moieties and their electron donating character. However, the shift is not as pronounced as it was for triarylamine–squaraine model dye **M13** (Table 13, p. 123), where two triarylamines induced a bathochromic shift of 900 cm^{-1} compared to reference dye **M1**. Nevertheless, the impact of exciton coupling between the squaraine chromophores needs to be discussed. First, in chapter 3.4 it was shown that the interaction between squaraine chromophores that are connected by the electron rich bridges used in this work is small due to a twisting of the bridge units and an increased

distance between the squaraine centres. Second, the squaraine chromophores in the dimer clearly adopt an H-like conformation which would result in a hypsochromic shift of the absorption band. Taking all this into account, the conclusion can be derived that exciton coupling can be neglected in this case. One might argue that the shoulder at the high energy side of the main absorption band, which is even more pronounced in toluene, might be a result of excitonic interaction of the squaraines in the H-like conformation in the dimer. However, if this interaction existed it would result in a blue shifted absorption maximum and not only a shoulder. The structure of the dimer was optimised by simple semiempirical AM1 calculations. These computations indicate two planar squaraine chromophores which are in one plane and are connected by the propeller-like triarylamines as one can expect. However, the centre-to-centre distance between the squaraine chromophores might be too large to show pronounced exciton coupling effects.

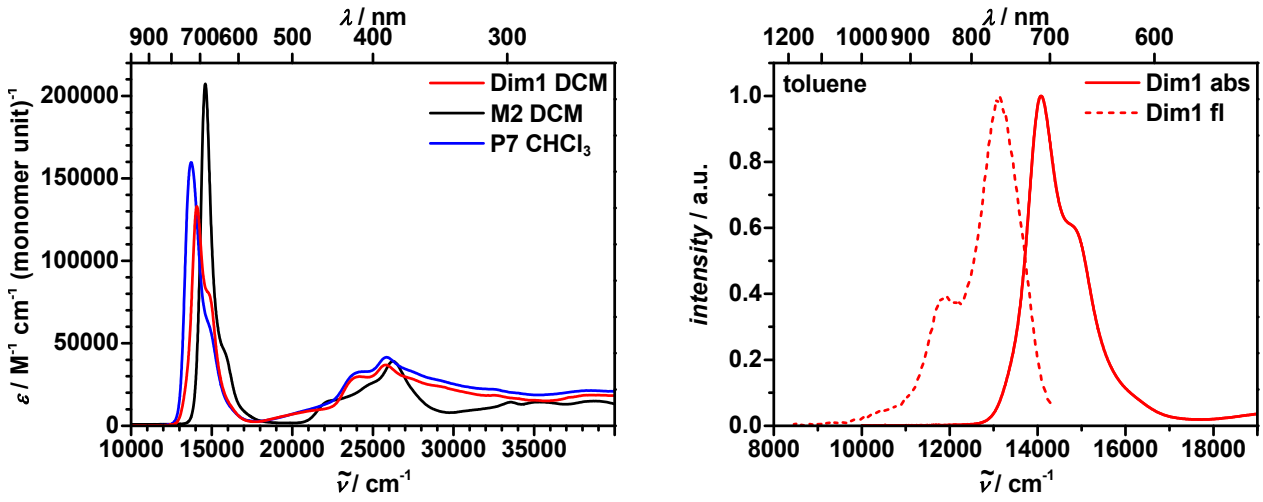

Figure 73 Left: Absorption spectra of **Dim1** (DCM), **M2** (DCM), and **P7** ($CHCl_3$). Right: Normalised absorption (solid line) and fluorescence spectra (dashed line) of **Dim1** in toluene.

Fluorescence Spectroscopy

The dimer **Dim1** is only fluorescent in toluene but not in DCM. The spectrum is not exactly a mirror image of the absorption because the shoulder is lower in intensity in the fluorescence spectrum (Figure 73, right). The *Stokes* shift of 700 cm^{-1} is among the

larger ones of the squaraine dyes. The fluorescence quantum yield of 0.26 is higher than that of the polymer **P7** (0.10 in toluene). The corresponding lifetime of 5.9 ns is greater than those of the monomers and similar to the larger one of **P7** (6.2 ns).

The existence of fluorescence, at least in toluene, is another indication for a negligible excitonic interaction. In an H-type conformation, the lowest excited state is a fluorescence forbidden dark state, which would lead to a quenching of the fluorescence. However, this is theoretically just the case for a perfect H-aggregate and deviation from the perfect symmetry can still result in the occurrence of fluorescence.[271]

3.6.2 Cyclic Trimers[1]

Synthesis

The cyclic trimers **Tri1**–**Tri3** (Chart 18) were a side product of the syntheses to the polymers **P3**–**P5**, respectively (Scheme 10, p. 72 and Scheme 11, p. 74). They were isolated in 6–7% yield each by preparative recycling GPC from the batches that were already purified by *Soxhlet* extractions. Remarkably, the yield of all trimers is nearly identical showing the reproducibility of this side reaction. As can be seen in the chromatogram (Figure 19, p. 73), the trimers were indicated by a prominent peak that occurred in each of the batches at rather similar retention times.

[1] Reproduced or adapted in part with permission from *Exciton Coupling Effects in Polymeric cis-Indolenine Squaraine Dyes*, S. F. Völker, C. Lambert, *Chem. Mater.* **2012**, *24*, 2541-2553. Copyright 2012 American Chemical Society.

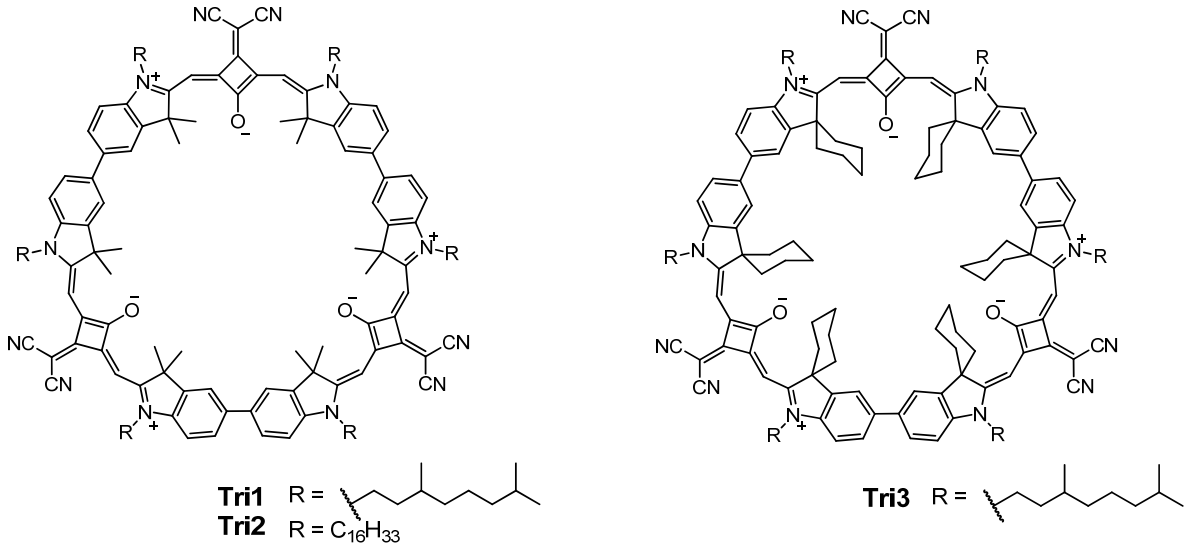

Chart 18 Cyclic squaraine trimers **Tri1**–**Tri3**.

Absorption Spectroscopy

As it was already shown for some functionalised dyes (**M6** and **M7** for example, Figure 11, p. 52), there is barely any difference in the spectroscopic or electrochemical properties depending on the alkyl chain on the nitrogen. Therefore, absorption spectra of **Tri2** will not be shown since they are more or less identical to those of **Tri1**. The absorption spectra of **Tri1** and **Tri3** are depicted in Figure 74. In comparison with reference dye **M2**, the absorption maximum of **Tri1** is at the same energy (14300 cm^{-1}, Table 24, p. 208). Besides, the extinction coefficients of $\varepsilon \sim 220000\ M^{-1}\ cm^{-1}$ (monomer unit)$^{-1}$ and transition moments of $\mu_{eg} \sim 10.5$ D (monomer unit)$^{-1}$ are rather similar. The maximum of **Tri3** is at slightly lower energy (14100 cm^{-1}), which is in accordance with the spectra of the model dyes **M6** and **M9** (Figure 11, p. 52), where it was already shown that the cyclohexyl moiety at the indolenine induces a slight red shift. Apart from that, the spectra of these two trimers are essentially the same. What catches the eye is a prominent shoulder at the low energy side of the main absorption band at around 13600 cm^{-1} with an extinction coefficient of $\varepsilon \sim 45000\ M^{-1}\ cm^{-1}$ (monomer unit)$^{-1}$. In addition, there is a rather small transition band ($\varepsilon \sim 4000\ M^{-1}\ cm^{-1}$ (monomer unit)$^{-1}$) at even lower energy at 12400 cm^{-1}.

In contrast to nearly all squaraine monomers in this work (with the exception of the NDI-substituted squaraines **M21** and **M22**), the absorption spectra of the cyclic trimers are the only squaraine absorption spectra that do not show a steep rise at the low energy side that goes from zero intensity straight to the maximum. Nevertheless, there is a steep rise, but as mentioned there are further transitions at lower energy, whose origin needs to be discussed. Therefore, the structure of the trimer was optimised by both semiempirical AM1 calculations[160] and at DFT level, using the B3LYP/6-31G* functional/basis set combination.[272-275] Both methods were in excellent agreement and the AM1-optimised structure is shown in Figure 75. The structure of the trimer proved to be asymmetric caused by some strain in the ring. While one squaraine moiety is planar, the other two adopt a bent structure, which deviates from planarity in order to close the cycle.

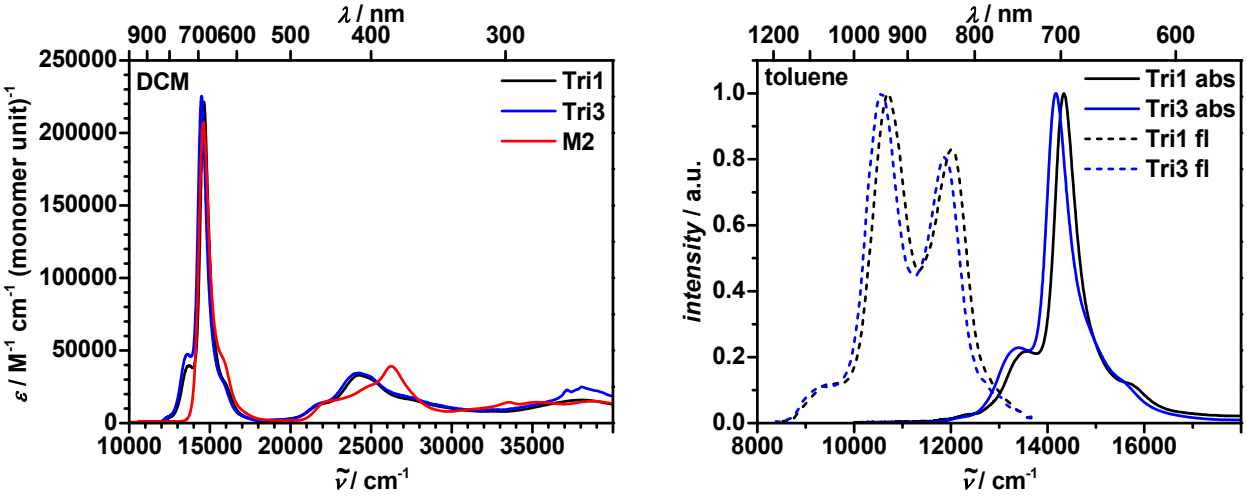

Figure 74 Left: Absorption spectra of cyclic trimers **Tri1** and **Tri3** as well as reference dye **M2** in DCM. Right: Normalised absorption (solid lines) and fluorescence spectra (dashed lines) of **Tri1** and **Tri3** in toluene.

If ideal C_3 symmetry of the trimer **Tri1** is assumed, simple exciton theory predicts an A-symmetric state into which electronic transition is forbidden and which is below two degenerate E states which are optically allowed.[130] Because of the asymmetry of the trimer the degeneracy will be lifted and the selection rules will not strictly apply. Semiempirical CNDO/S2 computations[161] indeed support this interpretation. Although the absolute transition energies are estimated to be too high by ca. 3000 cm^{-1} these calculations yield two allowed bands at 17000 and 16500 cm^{-1} and a very weak one at 14800 cm^{-1}. In fact we observe two bands at different energy (14300 and 13600 cm^{-1})

which are likely the "E-type" bands and a very weak one at lower energy (12400 cm^{-1}) which is supposedly the forbidden A-type band.

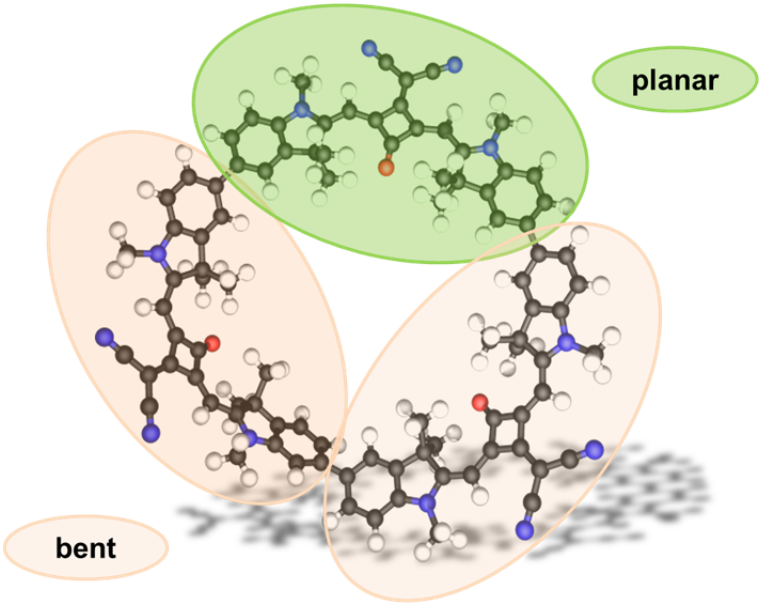

Figure 75 AM1 optimised preliminary structure of the cyclic trimer **Tri1**. The alky chains have been replaced by methyl groups for a better survey.

Fluorescence Spectroscopy

The cyclic trimers **Tri1**–**Tri3** do not fluoresce in DCM (similar to the respective homopolymers **P3** and **P4**) but show little fluorescence in toluene ($\Phi_{fl} \sim 0.10$). In contrast to both monomeric and polymeric squaraines in this work, the fluorescence spectra are neither a mirror image of the absorption spectra of the cyclic trimers nor of those of the squaraine monomers (Figure 74, right). The fluorescence spectra completely differ as do the absorption spectra (note that due to the similarity of the spectra among the cyclic trimers, only the spectrum of **Tri1** will be discussed). There are two rather intense fluorescence bands at 12000 cm^{-1} and 10700 cm^{-1} (maximum) with a small shoulder at lower energy at 9400 cm^{-1}. The smallest *Stokes* shift, which can be obtained by the difference of the highest energy fluorescence and the lowest energy absorption band, is ~ 400 cm^{-1}. However, if the maxima of both spectra are compared, the *Stokes* shift is huge with 3600 cm^{-1}. No other squaraine in this work shows either multiple

fluorescence bands (except of the cyclic tetramer **Tet1**, Figure 77, right, p. 207) or fluorescence that reaches so far into the NIR-region.

The very structured fluorescence spectrum with the large *Stokes* shift which extends into the NIR (< 12000 cm^{-1}) is somewhat unexpected. This behaviour may be interpreted in two different ways: one possibility is based on structure optimisations by semiempirical AM1 and DFT calculations which indicate a pronounced asymmetry of the trimer caused by some strain in the ring (Figure 75). While one squaraine chromophore retains its planarity, the other two appear to be bent in order to be able to close the cyclic structure. The strong distortion of two of the three squaraine chromophores might lead to a strong vibronic progression in the lowest energy emitting state. The observation of an almost unperturbed and unshifted narrow absorption band at 14300 cm^{-1} for the unperturbed squaraine chromophore but a much broader and weaker band at lower energy (13600 cm^{-1}) support this interpretation. The other interpretation is that two of the three chromophores behave different and almost independently which would lead to two different fluorescence emission bands. A similar observation has recently been made for strained small oligothiophene macrocycles[276] while *Law* et al. observed dual or triple fluorescence in squaraine dyes which these authors interpreted to be caused by conformationally different structures being present in solution or by solute-solvent complexes.[277-280] Dual (or triple) fluorescence from a squaraine trimer would however require negligible energy transfer within the trimer as otherwise only a single emission from the lowest of the three excitonic states would be observed. For this seems unlikely in such a small chromophore arrangement, the first interpretation is preferred.

In addition, even though semiempirical calculations and DFT calculations have already been performed, the cyclic trimers and the cyclic tetramer (see below) are subject of further theoretical investigations which unfortunately have not been completed during the completion of this thesis. In this effort, the structures of the macrocycles as well as their absorption and fluorescence spectra should be modelled. First results support the first interpretation described above. By simply modelling each monomer as a point-dipole in the centre of mass of the chromophore and placing them in one plane in an equilateral triangle or a square, the absorption spectra of the trimer or tetramer,

respectively, could be reproduced. Furthermore, by twisting one of the dipoles by an angle of 15° also the shape of the fluorescence spectrum of the cyclic trimer could be simulated, not yet the correct energy though, which is attributed to the simple model applied.

Cyclic Voltammetry

The cyclic voltammetry measurement of **Tri1** shows one reduction and two oxidation processes. Comparison of the redox potentials with monomer **M7** and homopolymer **P3-1** indicates that there is negligible electronic interaction within the chromophores in the ground state. Both reduction potential ($E_{1/2}^{\mathrm{Red1}} = -1.46$ V) and oxidation potentials ($E_{1/2}^{\mathrm{Ox}} = 167$ mV and 600 mV) differ by less than 50 mV (Table 23).

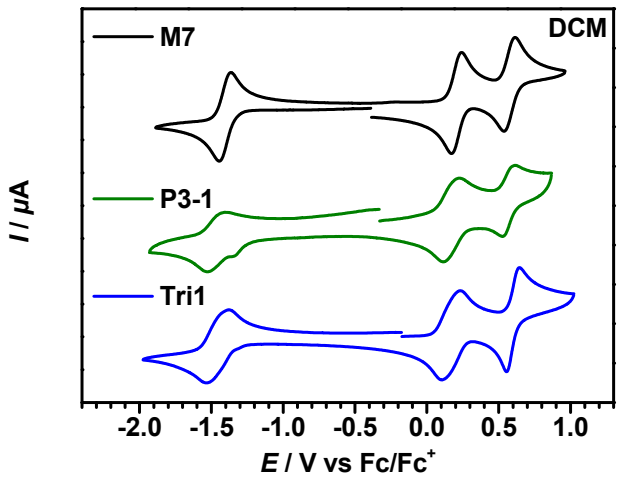

Figure 76 Cyclic voltammogram of monomer **M7**, homopolymer **P3-1**, and cyclic trimer **Tri1** in DCM/TBAHFP (0.1–0.2 M) at a scan rate of 250 mV s^{-1}.

Table 23 Redox potentials, HOMO and LUMO energy levels and band gaps obtained by electrochemical (E_{gap}^{CV}) and optical (E_{gap}^{opt}) methods of homopolymer **P3-1**, cyclic trimer **Tri1**, and monomer **M7**.

	solvent	$E_{1/2}^{Red1}$ / mV	$E_{1/2}^{Ox1}$ / mV	$E_{1/2}^{Ox2}$ / mV	E_{HOMO} / eV[c]	E_{LUMO} / eV[b]	E_{gap}^{CV} / eV[b]	E_{gap}^{opt} / eV[c]
M7	DCM[a]	–1405	207	576	–5.37	–3.76	1.61	1.71
P3–1	DCM[a]	–1465	175	573	–5.34	–3.70	1.64	1.52
Tri1	DCM[a]	–1456	167	600	–5.33	–3.70	1.62	1.60[d]

[a] Ag/AgCl pseudo-reference electrode; [b] determined according to the procedure described in 5.1.4; [c] determined in DCM according to the procedure in 5.1.1; [d] determined from a tangent at the pronounced shoulder at the low energy side of the main absorption band.

3.6.3 Cyclic Tetramer

Synthesis

In a similar manner to the cyclic trimer **Tri3**, the cyclic tetramer **Tet1** was obtained as side product of the respective polymer synthesis (**P5**) in 1% yield, (Scheme 11, p. 74).

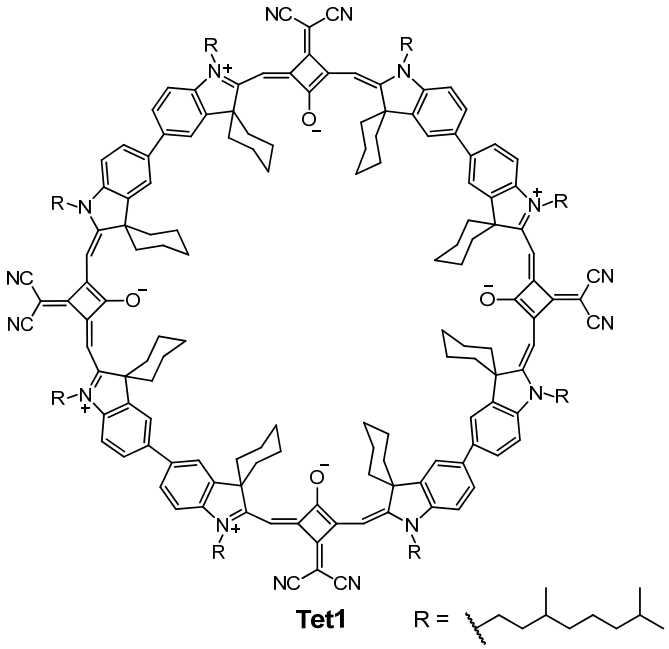

Tet1 R =

Chart 19 Cyclic squaraine tetramer **Tet1**.

Absorption Spectroscopy

For the cyclic tetramer **Tet1** the absorption spectra also differ to those of the squaraine monomers, polymers, or the other macrocycles. In DCM, the absorption maximum is red-shifted by 500 cm^{-1} compared to **M2** (14100 cm^{-1}) and the frequently observed band at the high energy side is only indicated by a small bump. In addition, there are bumps at the low energy side at ~ 12900 cm^{-1} and 13600 cm^{-1}. The latter two are most pronounced in toluene but shifted by 100 cm^{-1} to lower energy as is the absorption maximum. Especially the absorption at 13500 cm^{-1} is way more prominent having nearly the same intensity as the absorption maximum. The extinction coefficients per monomeric subunit and also the transition moments are the smallest for all cyclic squaraines with $\varepsilon \sim 90000\ M^{-1}\ cm^{-1}$ (monomer unit)$^{-1}$ and $\mu_{eg} \sim 9$ D (monomer unit)$^{-1}$, respectively.

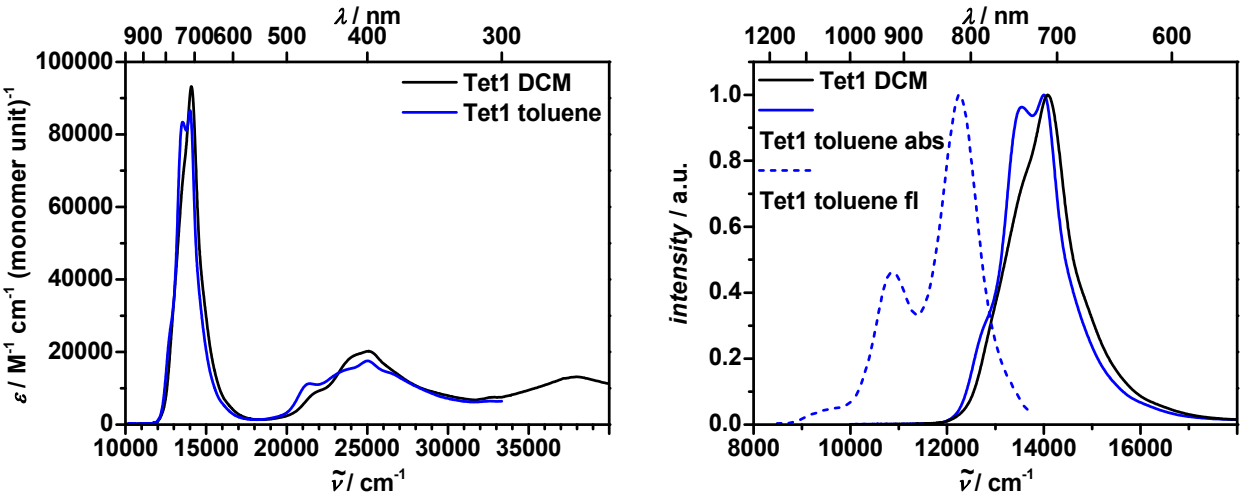

Figure 77 Left: Absorption spectra of the cyclic tetramer **Tet1** in DCM and toluene. Right: Normalised absorption spectra in DCM and toluene (solid lines) and fluorescence spectrum in toluene (dashed line) of **Tet1**.

Fluorescence Spectroscopy

In similarity to the other squaraine macrocycles, the cyclic tetramer **Tet1** shows no fluorescence in DCM but in toluene ($\Phi_{fl} = 0.10$). The fluorescence maximum is at 12400 cm^{-1} and there is another transition at 10900 cm^{-1} with roughly half the intensity. Additionally, a rather small fluorescence band is found at ~ 9500 cm^{-1}. The smallest

Stokes shift is ~ 400 cm^{-1} but again, the *Stokes* shift between the maxima is rather large (1600 cm^{-1}).

Likewise to the cyclic trimer, semiempirical AM1 optimisations of the tetramer also indicate the combination of both planar and bent squaraine chromophores in the macrocycle. However, more accurate calculations are in progress in order to determine the correct structure.

Table 24 Absorption maxima, extinction coefficients, transition moments, fluorescence maxima, fluorescence quantum yields, and fluorescence lifetimes of donor–squaraine copolymers **Dim1**, **Tri1–Tri3**, **Tet1**, reference dye **M2**, and model dye **M9**. Extinction coefficients ε and transition moments μ_{eg} of the cyclic oligomers are given per monomer unit.

	solvent	λ_{abs} / **nm**	$\tilde{\nu}_{abs}$ / **cm^{-1}**	ε / **M^{-1}cm^{-1}**	μ_{eg} / **D**	λ_{fl} / **nm**	$\tilde{\nu}_{fl}$ / **cm^{-1}**	Φ_{fl}[a]	τ_{fl} / **ns**
M2	DCM	685	14600	207000	10.6	706	14200	0.25	-
	toluene	700	14300	236000	10.1	716	14000	0.41	4.5
M9	DCM	706	14200	208000	10.5	-	-	-	-
	toluene	719	13900	220000	10.0	-	-	-	-
Dim1	DCM	710	14100	133000	9.8	x	x	x	x
	toluene	723	13800	136000	9.1	761	13100	0.26	5.9
Tri1	DCM	684	14600	221000	10.9	x	x	x	x
	toluene	697	14300	222000	10.7	926	10800	0.08	7.2
Tri2	DCM	684	14600	245000	11.2	x	x	x	x
	toluene	697	14300	198000	9.9	927	10800	0.11	6.8
Tri3	DCM	691	14500	225000	11.1	x	x	x	x
	toluene	706	14100	195000	10.1	938	10700	0.05	6.9
Tet1	DCM	710	14100	93200	9.1	x	x	x	x
	toluene	714	14000	87000	8.6	807	12400	0.10	1.4 (56.8) 6.5 (43.2)

- was not measured; x could not be determined. The values in brackets are the relative amplitudes of the corresponding fluorescence lifetime. [a] During the writing process, the quantum efficiency of oxazine 1 was determined to be 0.15 by an absolute measurement using an integration sphere. However, the values reported for the squaraine dyes herein are still referenced against the quantum efficiency of 0.11 (see experimental section 5.1.2) as they were published to avoid confusion. Nevertheless, it has to be noted that the correct quantum efficiencies are larger by a factor of 0.15 / 0.11 ≈ 1.36.

3.6.4 Conclusion

A series of unprecedented conjugated cyclic squaraines was synthesised. These macrocycles were isolated in low yields by preparative recycling GPC as side products of the respective polymer syntheses. The trimers and the tetramer show remarkable spectroscopic features which are most probably a result of the interplay of both planar and bent chromophores in the macrocycles. Especially the question of the origin of the unusual absorption and the structured fluorescence of the cyclic trimer in the NIR ($< 12000\ cm^{-1}$) is of major interest.

In order to fully understand the optical properties of the macrocycles, more accurate calculations of the structures are in progress. The obtained structures shall than be used to improve the so far simple model in purpose to accurately simulate the spectra.

Optimisations of the reaction conditions, such as high dilution reactions for example, in order to achieve higher yields of the macrocycles have not been pursued as well as investigations of the potential arrangement to 2- or 3-dimensional superstructures. However, this is not to be expected due to the non-planar structures of the macrocycles of this kind, neither for the triarylamine–squaraine dimer **Dim1**, nor for the homotrimers **Tri1**–**Tri3** or the homotetramer **Tet1**.

3.7 Polymer Characterisation[1]

3.7.1 Gel Permeation Chromatography (GPC)

Molecular weight distributions of all isolated polymers were determined by analytical GPC in $CHCl_3$ using polystyrene standards (Table 25).

Table 25 Polymer characterisation: number-average molecular weight (M_n), number average degree of polymerisation (X_n), weight-average molecular weight (M_w), and polydispersity (M_w/M_n). Analysis was performed in $CHCl_3$ with polystyrene as a standard.

	M_n	X_n	M_w	M_w/M_n
P1A	31000	45.9	80200	2.59
P1B	8100	12.0	22700	2.81
P2	28000	33.1	48100	1.72
P3-total	8300	11.4	27300	3.29
P3-1	25600	35.5	46700	1.82
P3-2	8600	11.8	11900	1.39
P4-total	6100	6.8	13600	2.23
P4-1	17500	19.7	27800	1.59
P4-2	6600	7.4	8300	1.25
P5	12700	15.8	41600	2.66
P6	32800	23.4	63400	1.93
P7	14700	14.7	31900	2.17
P8	15800	16.7	32800	2.07
P9	13700	13.3	73200	5.35
P10	20900	21.4	61500	2.94
P11	6200	6.4	20600	3.30
P12	9400	12.4	28800	3.07
P13	27200	23.4	76900	2.82

[1] Reproduced or adapted in part with permission from *Synthesis, Electrochemical, and Optical Properties of Low Band Gap Homo- and Copolymers Based on Squaraine Dyes*, S. F. Völker, T. Dellermann, H. Ceymann, M. Holzapfel, C. Lambert, *J. Polym. Sci., Part A: Polym. Chem.* **2014**, *52*, 890-911. Copyright (2014) WILEY-VCH Verlag GmbH & Co. KGaA, Weinheim.

In general the degree of polymerisation X_n depends on the solubility of the polymer under the given reaction conditions and varies from ca. 6 up to ca. 46. The polydispersity $PDI = M_w/M_n$ varies mainly between ca. 2–5 typical of polycondensation reactions which should ideally show a *Flory* distribution with $PDI = 2$. The deviation from this values can be understood by the work up extraction procedures which remove both very short (= very soluble) and very long (= insoluble) polymer fractions from the crude polymer product. The *PDI*s of **P3-1**, **P3-2**, **P4-1**, and **P4-2** are among the smallest which is due to the preparative splitting on the recycling GPC.

3.7.2 IR-Spectroscopy

It is well known that in the condensation reaction of a squaric acid derivative with nucleophilic compounds the central ring can be disubstituted both in the 2,4-positions to the squaraine dye and in 3,4-positions to a cyclobutenedione compound.[3, 109, 120] The solvent that is used in this condensation reaction step plays a crucial role, e.g. the use of a toluene/1-butanol solvent mixture usually gives 2,4-substituted products only. In the case of monomeric squaraine dyes, even traces of 3,4-substituted products can be removed *via* flash chromatography to give pure 2,4-isomeric squaraine products. A subsequent transition metal-catalysed or -mediated polycondensation reaction therefore will give polymers with only isomerically pure squaraine subunits where the central ring is disubstituted at the 2,4-positions. However, this may be different in cases where the squaraine forming reaction is the polycondensation step itself as for the bifunctional piperazine-bridged methylene base **33** and squaric acid that form **P12**. Therefore, even though it is unlikely, the formation of 3,4-substituted subunits cannot be completely ruled out. To prove their absence, IR spectroscopy was used. In case of 3,4-substitution, a diketone structure of the cyclobutene ring shows a C=O vibration at around 1680–1800 cm^{-1}.[9] Due to the delocalised character of 2,4-substituted units, this vibration is not observed in this case, but a vibration at around 1600 cm^{-1} should be seen as a result of the delocalisation of the chromophore. Thus, IR spectra of polymer **P12** and, for comparison, of monomers **M19** and **M1** were recorded. Figure 78 shows the complete IR spectra and a magnified part of **M19** and **P12** (inset). As can be seen for the monomers,

there is absolutely no signal at around 1680–1800 cm^{-1}. For the polymer very weak bands in this region indicate indeed negligible formation of 3,4-substituted squaraine moieties.

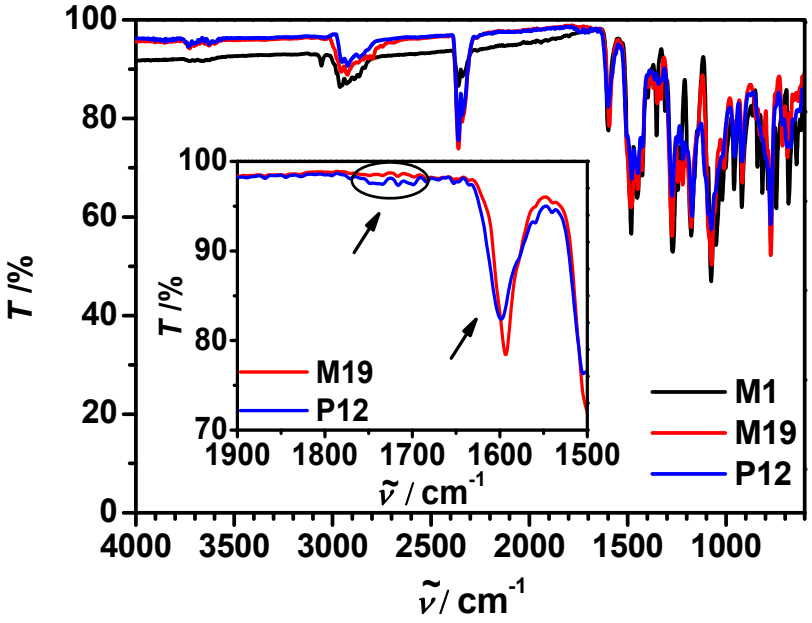

Figure 78 IR spectra of **M1**, **M19**, and **P12**.

3.8 Applications

3.8.1 Introduction to Organic Solar Cells

Theory[219, 281-285]

Organic solar cells mainly consist of two organic compounds, electron donor and electron acceptor, that are simply spoken sandwiched between two electrodes. As electron acceptor, fullerene derivatives such as [6,6]-phenyl-C_{61}-butyric acid methyl ester (PCBM) for example is widely used and shows ultrafast and highly efficient charge transfer from donor polymers.[286-287] In case of the electron donors a competition between small molecules[282, 288] and polymers[289-290] is in progress, achieving efficiencies ~ 8%.[291-293] Up to now, the poly(3-hexylthiophene)(P3HT)/PCBM couple is still the by far most widely studied donor/acceptor combination with more than 1000 relating publications between 2002–2010.[294]

The working principle of an organic solar cell contains several steps. At first, incident light is harvested by the photoactive layer, where the corresponding molecule, mainly the donor compound, is excited and forms a tightly bound electron-hole pair, an exciton. To be able to generate a current, the formed excitons need to dissociate into free charge carriers. Therefore, the excitons have to diffuse to the interface of the two organic compounds. The exciton diffusion length of some conjugated polymers is on the order of ~ 10 nm.[295-296] In classical bilayer devices the two compounds are deposited consecutively and form one more or less plain interface. In bulk heterojunction (BHJ) solar cells, due to the simultaneous deposition of donor- and acceptor material, an interpenetrating network of the two with a larger interface can be obtained. Once the excitons have migrated to the interface, charge separation can take place and an electron can jump from the LUMO of the donor to the LUMO of the acceptor while the hole remains in the HOMO of the donor. For this step, due to the exciton binding energy, which was estimated to be in the order of ~ 0.35 V, an offset of this value between the two LUMO levels is necessary.[297-298] The separated charges can now drift within the domain of one of the organic compounds to the electrodes where the charges have to be

efficiently collected for current generation. In this step, the morphology of the single domains is of major importance because it significantly influences the charge transport.

The most important physical properties of a solar cell can be obtained from current-voltage (*J-V*) characteristics and are depicted in Figure 81 (p. 218). They are briefly discussed in the following, however, for more detail or physical background, the corresponding literature needs to be addressed.

The open circuit voltage V_{OC} defines the highest voltage that can be obtained by the device and is a boundary value at the point where the value of the current density in the device is zero. The V_{OC} is mainly dependent on the HOMO energy of the electron donor and the LUMO energy of the acceptor. For an estimation of the V_{OC}, equation (92) can be used, where e is the elementary charge and the 0.3 V is an empirically derived value.[284]

$$V_{OC} = \frac{1}{e}\left(\left|E_{HOMO}^{Donor}\right| - \left|E_{LUMO}^{Acceptor}\right|\right) - 0.3\text{V} \tag{92}$$

The short circuit current J_{SC} is the maximum photocurrent that can be derived in a BHJ solar cell and is the boundary value at the point where the voltage in a device is zero. It depends on the number of absorbed photons that managed to form excitons, the dissociation of excitons to holes and electrons, charge transfer, and the charge transport to, as well as charge collection at the electrodes. For the charge transport properties the morphology of the applied compounds plays a crucial role.[299-301]

The fill factor *FF* describes the quality of the solar cell. It is the maximum rectangular area within a *J-V* curve and is expressed as the ratio of the products of the maximum voltage and current, V_{max} and J_{max} (maximum power output), respectively, to the product of the V_{OC} and J_{SC} (equation (93)).

$$FF = \frac{V_{max}J_{max}}{V_{OC}J_{SC}} \tag{93}$$

The external quantum efficiency *EQE* is a wavelength-dependent value and is described by the ratio of incident photons to the number of charge carriers that could generate a current. Obviously, a high extinction coefficient of the applied material is beneficial for the *EQE* as well as the properties important for the J_{SC}.

The power conversion efficiency *PCE* (sometimes also denoted as η) is described by the ratio of the power that is produced by the solar cell to the power of the incident light and several forms of its equation (94) can be used.

$$PCE = \frac{P_{max}}{P_{in}} \times 100\% = \frac{V_{max} J_{max}}{P_{in}} = FF \frac{V_{OC} J_{SC}}{P_{in}} \times 100\% \qquad (94)$$

Two representative examples of architecture of the organic solar cells that were used within the collaborations of this work are shown in Figure 79. However, a broad variety of different materials can be applied as well as additional exciton blocking layers and other additives. The “standard” architecture consists of a transparent indium tin oxide (ITO) bottom electrode which is covered with the conductive polymer poly(3,4-ethylenedioxythiophene):polystyrenesulfonate (PEDOT:PSS) and works as a cathode. The PEDOT:PSS functions as hole transporting layer. On top of this, the photoactive layer gets deposited and Ca/Al is used as top electrode (anode). In the inverted architecture[302] the ITO works as anode instead of cathode and is in this case covered with aluminium doped zinc oxide (AZO) on top of which the photoactive layer is deposited. This layer is covered by PEDOT:PSS and Ag is used as top electrode which in this case works as cathode and not as an anode as the metal in the standard architecture. The standard architecture was used in the binary BHJ solar cells, whereas the inverted architecture was used in the ternary solar cells. These will be described in the next sections.

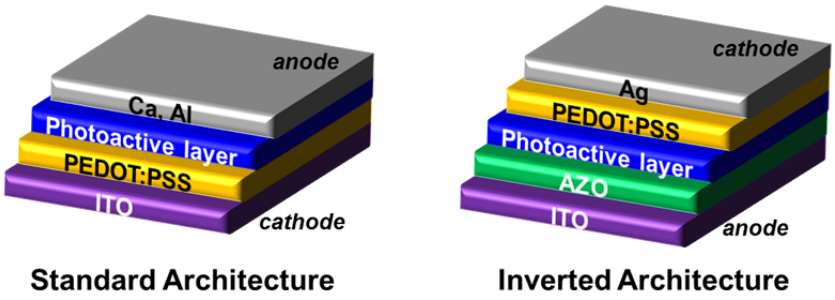

Figure 79 Standard and inverted architectures of bulk heterojunction solar cells. The former was used for the binary, the latter for the ternary devices.

3.8.2 Binary Bulk-Heterojunction Solar Cells[1]

Due to the broad absorption in the red to NIR region, the squaraine homopolymers were applied in organic bulk heterojunction (BHJ) solar cells in cooperation with *Dr. Markus Mingebach*, *Moritz Limpinsel*, *Stefan Walter*, *Prof. Dr. Carsten Deibel* and *Prof. Dr. Vladimir Dyakonov* from the department of experimental physics VI at the Julius-Maximilians-University of Würzburg. The squaraines were used as electron donors in the photoactive layer in combination with PCBM as an electron acceptor.

The devices were built with the "standard" architecture (Figure 79) consisting of ITO/PEDOT:PSS/photoactive layer (squaraine+PCBM)/Ca;Al. The complete procedure of the fabrication is described in the experimental section (5.1.12).

The first compound to be studied was **P2**, which was used in a series of solar cells with varying PCBM content and the devices were analysed at simulated AM 1.5 conditions. For comparison, devices of P3HT/PCBM were built and tested under identical conditions. However, due to the poor solubility of **P2**, $CHCl_3$ was used as solvent for the spin-coating of the **P2**/PCBM photoactive layer while chlorobenzene was used for P3HT/PCBM.

---

[1] Reproduced or adapted in part with permission from *Polymeric Squaraine Dyes as Electron Donors in Bulk Heterojunction Solar Cells*, S. F. Völker, S. Uemura, M. Limpinsel, M. Mingebach, C. Deibel, V. Dyakonov, C. Lambert, *Macromol. Chem. Phys.* **2010**, *211*, 1098-1108. Copyright (2010) WILEY-VCH Verlag GmbH & Co. KGaA, Weinheim.

To obtain absorption spectra of **P2** that are more related to the final device, spectra of **P2** in a film were recorded (Figure 80). Upon spin-coating a thin film of **P2** on a quartz or ITO (not shown) substrate, the maximum of the absorption is shifted to 757 nm. Interestingly, the shape of the absorption band changed considerably. The small peak at 621 nm which can be seen in the absorption spectrum of **P2** in solution is no longer observable in the absorption spectrum of the film. Furthermore, the absorption of a film of **P2** on an ITO substrate after annealing at 130°C for 10 min was investigated. These tempering conditions were the same as for the preparation of the solar cell devices which is described below. After annealing the absorption maximum is shifted even further to 778 nm. These effects might be due to a different alignment of the monomeric subunits in a film. According to the structural model explained above, this could result from a more uniform J-type structure with less zig-zag arrangements in the polymer strand. Furthermore, interchain excitonic effects might also contribute to the overall absorption spectrum.

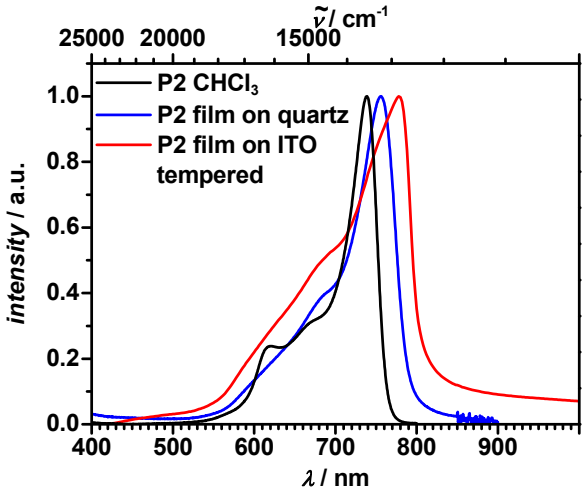

Figure 80 Absorption spectra of **P2** in $CHCl_3$ solution, as film on a quartz substrate and as film on an ITO substrate after annealing at 130°C for 10 min.

For analysis of the solar cell devices, their current-voltage (*J*-*V*) characteristics were investigated. The weight ratio of **P2**/PCBM was varied between 1:1 and 1:5 but only the results for the ratios 1:1–1:3 are listed in Table 26. At higher contents of PCBM, the devices were shunted and did not show any diode characteristics and are not further discussed. For the other devices, independently of the weight ratio, the open circuit voltage V_{OC} remains rather constant around 500 mV and only slight variations are

observed for the fill factor *FF* (28–34%). Those values are ~ 17% and ~ 33% lower, respectively, compared to the reference cell with P3HT. On the contrary, there is a major deviation of the values of the short circuit current J_{SC} which drops with increasing content of **P2** to < 1 mA cm^{-2}, which is not even 10% compared to the reference device (10.31 mA cm^{-2}). The overall efficiency *PCE* is strongly correlated to the J_{SC} and is highest for the device with a 1:1 ratio of **P2**/PCBM with *PCE* = 0.45% and a J_{SC} of 2.82 mA cm^{-2}. Nevertheless, the performance is inferior to the reference cell which shows an efficiency of 2.83%.

As an example, the *J-V* characteristics of both the best **P2**/PCBM as well as the reference P3HT/PCBM device are depicted in Figure 81, which clearly shows the supremacy of the reference device.

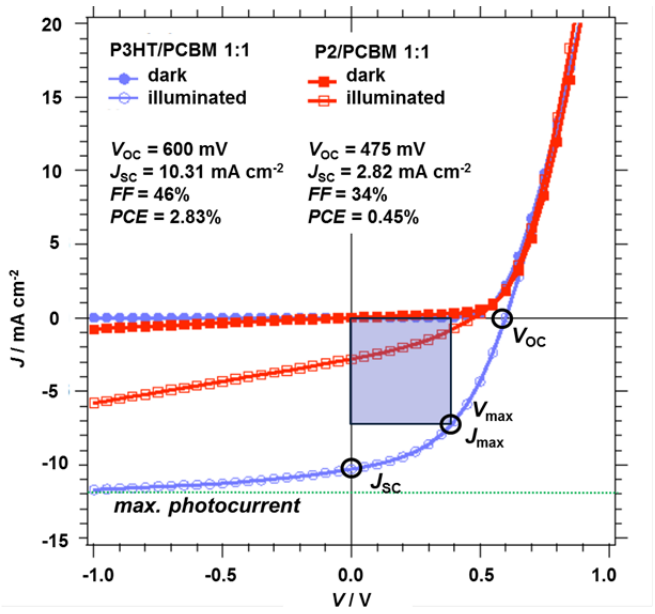

Figure 81 Current-voltage (*J-V*) characteristics of the **P2**/PCBM 1:1 (red) and the P3HT/PCBM 1:1 solar cells. The physical values such as $V_{OC/max}$ and $J_{SC/max}$ are also depicted for the reference device.

The *EQE* spectrum (Figure 82) shows that **P2** contributes to the photocurrent generation in the red to NIR region from 600–850 nm while PCBM is responsible for the photocurrent generation in the high energy region. The contribution is in agreement with the absorption spectra measured in a film where already the broadening of the absorption band beyond 800 nm was observed (Figure 80). In contrast, there is hardly any photocurrent generation of the reference cell at energies lower than 660 nm. However,

the *EQE* values are at ~ 60% at the maximum at ~ 520 nm, whereas they are lower than 20% over the whole spectrum for the device containing **P2**. This also reflects the higher efficiency of the reference cell.

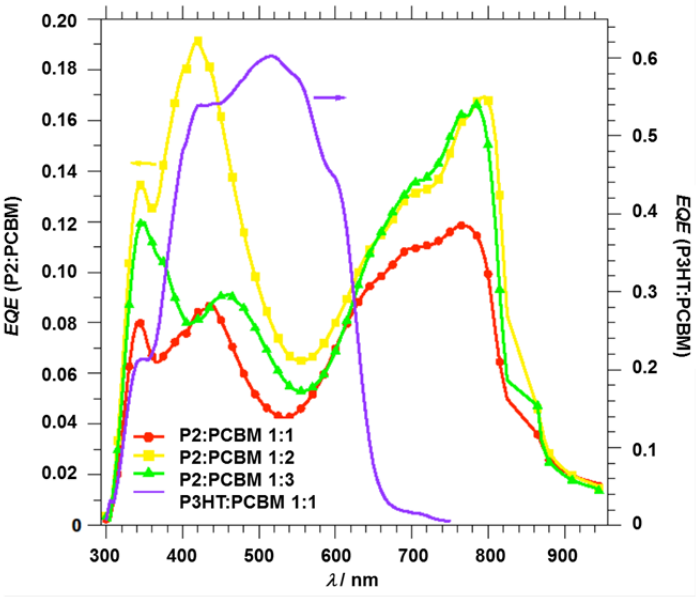

Figure 82 *EQE* of **P2**/PCBM solar cells with varying ratio (left axis) and of the P3HT/PCBM 1:1 reference cell (right axis).

To sum up, even though a larger area of the solar spectrum is covered for the light harvesting, the device suffers from the poor ability to efficiently generate a photocurrent upon absorption of light. From all this data it is obvious, that the major drawback of the **P2**/PCBM solar cells is the low *EQE* and consequently the low short circuit current. This again is correlated to the exciton and charge transport within a device and a sign of unfavoured morphology of the organic compounds in the device.

In the following, the impact of different side chains, different molecular weight, as well as different polymers in general on the device performance was investigated. The polymers **P1A** and **P1B** have the same basic structure than **P2** but carry a branched side chain instead of a linear one. **P1A** is slightly larger ($X_n = 45.9$) and **P1B** smaller ($X_n = 12.0$) than **P2** ($X_n = 33.1$). As mentioned in the synthetic section, the different sized polymers were obtained by different reaction conditions. Additionally, the dicyanomethylene group containing homopolymers **P3-1**, **P3-2**, **P4-1**, and **P4-2** were tested (the ending 1 corresponds to the fraction with higher molecular weight, the ending

2 to the fraction with lower molecular weight). All of them are of distinctively different molecular weight (Table 25, p. 210) which was achieved by splitting of the respective batch by preparative GPC. **P3-1** and **P3-2** carry the branched alky chain while **P4-1** and **P4-2** carry the linear one. Those polymers were applied in the BHJ solar cells with different weight ratios of PCBM. This time, only the devices with weight ratios of squaraine/PCBM 1:3 were tempered during the processing (60°C for 10 min).

Comparison of the standard homopolymers shows that all values of the larger polymer **P1A** are similar to those of **P2**, while those of **P1B** are distinctly smaller. Both efficiencies and short circuit currents remain low and the alkyl chain does not seem to have a major influence on the properties of the devices.

The devices containing the dicyanomethylene-substituted homopolymers **P3-1**, **P3-2**, **P4-1**, and **P4-2** all show higher V_{OC} between 500–600 mV, which reflects the lower HOMO levels of those polymers, which are ~ –100 meV lower than those of the standard homopolymers. Surprisingly, the V_{OC} of the smaller fractions are somewhat higher than those of the larger ones even though cyclic voltammetry revealed nearly identical HOMO levels for **P3-1** and **P3-2**. The J_{SC} values are again rather low and are all between ~ 1–2.5 mA cm^{-2} and also the *FF*s barely differ with values between 28–34%, similar to the other polymers. As a consequence, also the *PCE*s of the solar cells were not or only marginal improved and ranged between 0.13–0.50%.

To sum up, no clear trend on the properties of the devices can be observed for the tested polymers. Neither the different alkyl chains nor the different molecular weights seem to strongly influence the devices. No clear conclusion can be drawn on the effect of the tempering because comparable devices with ratios of squaraine/PCBM 1:3 that have not been tempered are missing.

Table 26 Characteristics of the solar cells. The superscripted letters define the concentration and the solvent used for the solar cell preparation.

Compound/PCBM	ratio	V_{OC} / mV	J_{SC} / mA cm^{-2}	*FF* / %	*PCE* / %
P3HT	1:1[a]	600	10.31	45.8	2.83
P2	1:1[b]	515	1.36	33.5	0.23
	1:1[c]	475	2.82	33.9	0.45
	1:2[c]	500	2.45	31.6	0.39
	1:3[c]	500	0.87	28.4	0.12
P1A	1:2[d]	450	0.85	30.0	0.11
	1:3[d]*	475	2.00	33.9	0.33
	1:4[d]	480	2.15	34.5	0.36
P1B	1:2[d]	415	0.50	25.0	0.05
	1:3[d]*	420	0.60	25.6	0.07
	1:4[d]	435	1.30	29.0	0.16
P3-1	1:1[e]	544	1.50	29.6	0.24
	1:2[e]	546	2.09	33.0	0.37
	1:3[e]*	333±141	2.50	28.1	0.25
	1:4[e]	565	2.23	33.0	0.41
P3-2	1:2[e]	570	1.80	29.7	0.31
	1:3[e]*	590	2.35	34.0	0.48
	1:4[e]	600	2.47	33.3	0.50
P4-1	1:1[e]	555	0.83	28.1	0.13
	1:2[e]	456	1.47	28.3	0.19
	1:3[e]*	559	1.88	32.2	0.34
	1:4[e]	531	1.67	31.3	0.28
P4-2	1:2[e]	555	1.25	28.0	0.20
	1:3[e]*	570	1.75	30.6	0.30
	1:4[e]	585	2.10	31.7	0.38

[a] c = 20 mg ml^{-1}, chlorobenzene, device annealed at 130°C for 10 min

[b] c = 15 mg ml^{-1}, $CHCl_3$, device annealed at 130°C for 10 min

[c] c = 10 mg ml^{-1}, $CHCl_3$, device annealed at 130°C for 10 min

[d] c = 30 mg ml^{-1}, $CHCl_3$

[e] c = 30 mg ml^{-1}, chlorobenzene

* annealing of the device at 60°C for 10 min.

All devices suffer from rather low J_{SC} values < 3 mA cm^{-2} which is the major reason for the poor performances. For BHJ solar cells with indolenine squaraine dyes and PCBM, these low values are not unusual and have been observed for both polysquaraine/PCBM[88] as well as monomeric squaraine/PCBM[85, 87] solar cells. In this respect, a comparative study on monomeric dyes such as both an indolenine squaraine (similar to **M1**) and the dicyanomethylene-substituted derivative (similar to **M2**) as well as the two respective benzothiazole squaraines was performed by *Würthner et al*.[85]

In general, the results were similar to those of the presented polymers here. However, upon annealing, the solar cell with dye **S22** (Chart 20) showed a formidable J_{SC} of 12.6 mA cm^{-2}, a value higher by one order of magnitude. **S22** crystallises in a densely packed arrangement and upon annealing structures of both J- and H-type aggregate are formed, depending on the annealing conditions. It was shown that only in the area of the J-type aggregates the J_{SC} is enhanced which attests that here exciton and charge carrier transport properties are improved.[85-86] However, the formation of J-type aggregates and the increased J_{SC} was on the expense of the V_{OC} which decreased to 300 mV and the *PCE* did not exceed 1.79%. In case of the indolenine squaraines, the two methyl groups at the indolenine ring might sterically be too demanding to allow for a favoured alignment of the molecules. Even in merocyanine dyes, which usually have a large tendency to form dimers in solution, implementation of this indolenine suppresses dimer formation.[303]

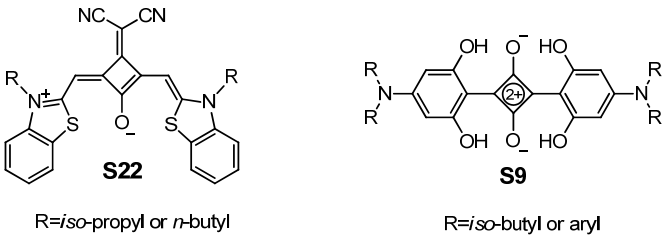

Chart 20 Squaraine dyes **S22** and **S9** with high efficiencies in organic solar cells.

Pyrrole squaraine dyes were also used in organic BHJ solar cells but suffered similar problems such as low J_{SC} and low *FF*s and did so far not exceed efficiencies of 2%.[90-92] A lot of effort was undertaken to improve organic solar cells, mainly bilayer cells with C_{60} fullerene as electron acceptor, that incorporate various *N*-*N*-substituted 3,5-

dihydroxyaniline squaraines (**S9**, Chart 20).[14, 98-100, 304] Those devices show large open circuit voltages of nearly 1 V and *PCE*s beyond 5%[98-99] with short circuit currents and fill factors around 7 mA cm^{-2} and 70%, respectively, and are so far the most efficient organic solar cells containing squaraine dyes. For only few other dyes such as a merocyanine[305], a porphyrin[306] or a copper phthalocyanine[307] for example (for the latter two a different device design was used), efficiencies beyond 5% could be shown.

However, it appears that the incorporation of sulphur containing heterocycles is mandatory for highly efficient small molecule organic solar cells. For those showing efficiencies between 6–7%, the donor materials incorporate at least one thiophene unit[308] or even further sulphur containing electron acceptors and donors[309-310]. The same is the case for the just recently reported molecule **SMPV1** (Chart 21), which boosts the *PCE* of a BHJ solar cell to beyond 8%, and a tandem cell to even above 10%.[291] Short circuit currents of all the latter mentioned devices are exceeding 12 mA cm^{-2} and open circuit voltages approach 1 V, while the fill factors are between 60–70%. In general, there are, among others, three detailed reviews on small molecule semiconductors from 2012 and 2013 that thoroughly show the different types of molecules that have been used in organic solar cells over the years.[282, 288, 311]

In terms of polymer solar cells, sulphur containing heterocycles also seem to be mandatory. The D–A copolymer **PCPDTBT** (Chart 21) was first reported in 2006[312] and consists of cyclopentadithiophene as electron donor and benzothiadiazole as electron acceptor and showed promising properties regarding organic solar cells. A broad variety of sulphur containing donor and acceptor units were applied in copolymers in the recent years, leading to solar cell efficiencies of 6–7%.[313-317] These compounds commonly exhibit a relative planar backbone, which allows good delocalisation, and they reveal J_{SC} and V_{OC} values above 12 mA cm^{-2} and 600–900 mV, respectively, with fill factors and *EQE*s around 60%. The copolymer **PBDTTPD** (Chart 21) even reaches 70% for the latter values and a V_{OC} close to 1 V leading to an overall efficiency of 8.5%.[293] This copolymer was also subject to very recent studies on different highly efficient charge separation pathways occurring in **PBDTTPD**/PCBM solar cells which are linked to the

bulk structure of the compounds.[301] In two reviews from 2011 and 2012 an overview of an extract of the large diversity of polymers can be obtained.[289-290]

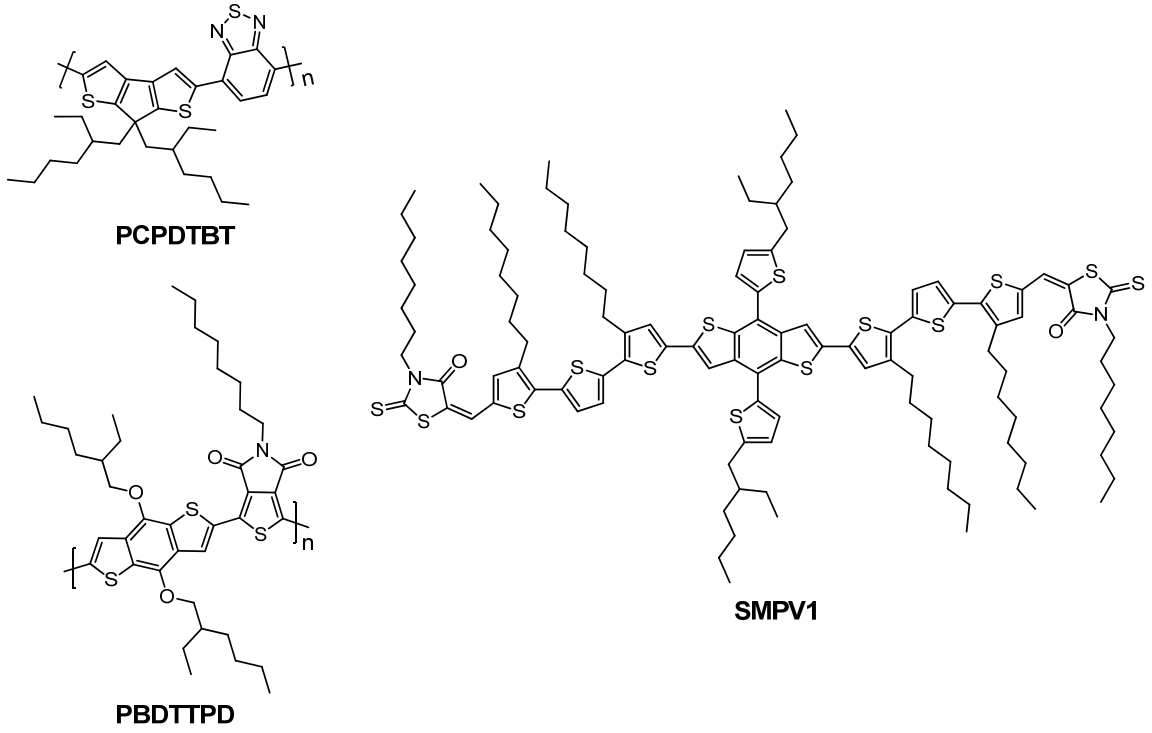

Chart 21 Highly efficient polymers (left) and small molecule (right) for organic solar cells.

3.8.3 Ternary Solar Cells

Theory

In addition to the "classical" organic BHJ solar cells, some of the squaraine dyes were applied in ternary solar cells in cooperation with *Parisa Khoram*, *Dr. Tayebeh Ameri* and *Prof. Dr. Christoph J. Brabec* from the institute Materials for Electronics and Energy Technology (*i*-MEET) at the Friedrich-Alexander University Erlangen-Nürnberg. The tested squaraines were model dye **M14** and the squaraine polymers **P1A**, **P4-1**, and **P13**. The obtained results are discussed briefly, more detail can be found in the master thesis of *Parisa Khoram*.[318]

In ternary solar cells a third compound, mostly called sensitiser, is used in the photoactive layer in addition to an already working donor/acceptor couple. The sensitiser usually is another electron donor and the idea is to use components that absorb light at

different energies so that the main part of the solar spectrum is covered and more photons can be harvested. There have been several approaches in the last few years and the amount of the sensitiser used (in comparison to the other donor) ranged from < 1 wt. %[319] up to equal amounts of the donors.[320] In the latter case, two polymers (**DTffBT** and **DTPyT**, Chart 22) which gave very similar and good results in binary devices with PCBM (J_{SC} ~ 12.5 mA cm^{-2}; V_{OC} ~ 880 mV; *FF* ~ 67%; *PCE* ~ 6.3%) were mixed. Due to the different absorption properties of the polymers but equally good J_{SC} values, the ternary devices showed higher *EQE*s from 350–800 nm what resulted in distinctly increased J_{SC} (13.7 mA cm^{-2}) and *PCE* (7.0%) while roughly maintaining the high V_{OC} and *FF*.

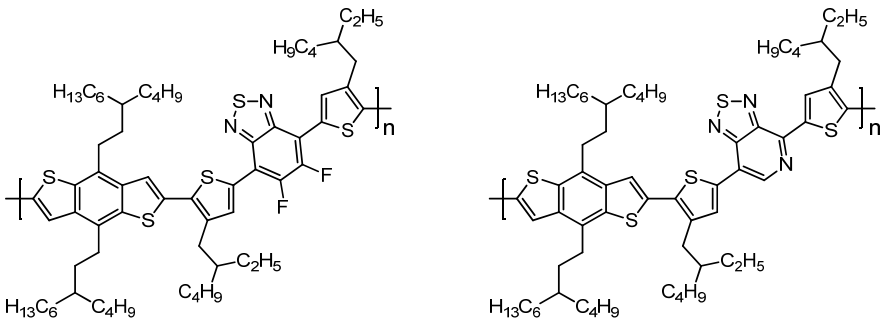

Chart 22 Polymers of an efficient ternary solar cell with the constitution **DTffBT**/**DTPyT**/PCBM of 0.5:0.5:1.

Choosing the right combination of materials may lead to additional charge transfer and transport pathways like cascade charge transfer, energy transfer or parallel-like charge transfer for example, depending on energy levels, band gaps, and the final morphology of the device. Those mechanisms and more information on ternary solar cells can be found in a sound recent review.[321]

In this cooperation, the idea was to take advantage of the good charge transport and light harvesting properties of the well-studied P3HT/PCBM host system and extend the spectral absorption by the addition of squaraine dyes that absorb in the red to NIR region. Even though there are more efficient solar cell systems, the above mentioned was chosen because it is the most studied one and results can easily be compared.

Due to the low J_{SC} values obtained in the binary devices (Table 26) the amount of squaraine was held low in order not to perturb the ordered P3HT domains and therefore hinder efficient charge transfer to the electrodes. The squaraines were supposed to harvest light in the red to NIR region and to open new pathways for charge or energy transfer between the P3HT/PCBM couple to increase the efficiency of the solar cell. This concept was already successfully proved for the P3HT/PCBM couple when it was blended with *N*,*N*-di-*iso*-butly-3,5-dihydroxyaniline squaraine dye (**S9**, Chart 20, p. 222).[322] Here small amounts of < 5% of squaraine resulted in more ordered packing of P3HT chains and enhanced phase separation. Additionally, efficient *Förster* resonant energy transfer (FRET) from excited P3HT to the squaraine was observed serving as an additionally pathway for the energy transfer. Overall this led to enhanced *EQE*, J_{SC}, and *PCE*.

In Figure 83 the absorption spectra of the films of P3HT and all the squaraines used in this study are shown as well as the fluorescence spectrum of P3HT. In addition, the HOMO and LUMO energy levels of those compounds are depicted. It can be seen that for all squaraines both the respective HOMO and LUMO energy levels lie in between those of P3HT and PCBM allowing cascade charge transfer. Also there is a distinct overlap of the P3HT fluorescence and the squaraine absorption, potentially allowing *Förster* resonant energy transfer (FRET) from the P3HT to the respective squaraine.

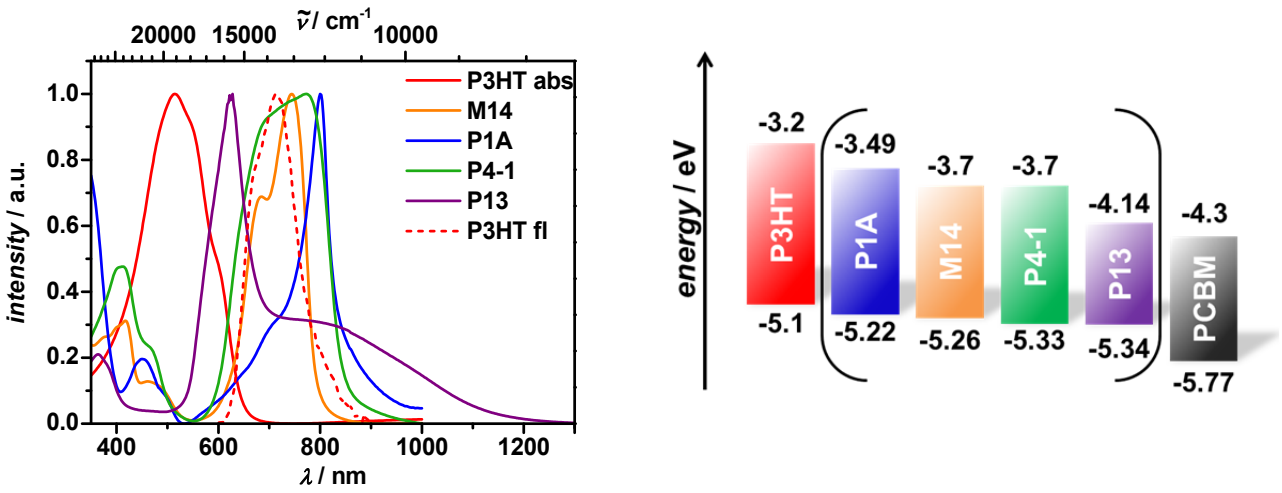

Figure 83 Left: Absorption spectra of films of P3HT and the squaraines **M14**, **P1A**, **P4-1**, and **P13** (solid lines) and fluorescence spectrum of P3HT (dashed line). Right: Energy levels of all applied substances.

P1A

Photoluminescence (PL) experiments were carried out to study the electronic interaction between the squaraine polymer and the host system (Figure 84, left). Therefore, films of pristine P3HT, pristine **P1A**, and binary films of P3HT/**P1A** (0.9:0.1) and of PCBM/**P1A** (1:1) were illuminated at 488 nm, where absorption of P3HT is dominant and there is barely any squaraine absorption (Figure 83). Comparison of these spectra reveals that PCBM quenches the PL of **P1A** by ~ 90%, indicating charge transfer from the latter to PCBM, which is in agreement with the photovoltaic activity observed for the binary BHJ solar cells described in the previous chapter. However, the PL of P3HT diminishes only slightly in the presence of **P1A**, indicating that no efficient charge or energy transfer occurs from P3HT to **P1A**. This might explain the in all aspects inferior performances of the ternary compared to the binary solar cells, because no extra pathway for charge or energy transfer was detected that might lead to an enhanced solar cell performance. It has to be noted that due to the solubility issues of **P1A** only chloroform could be used as solvent for the fabrication of the device and not chlorobenzene, which was used in all other cases.

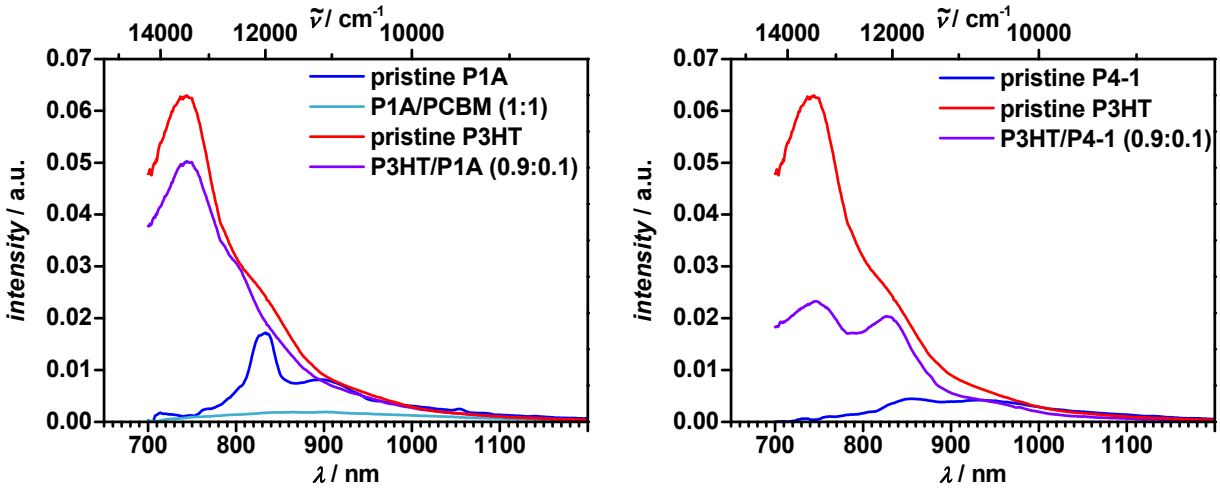

Figure 84 Photoluminescence spectra of films of pristine **P1A**, pristine P3HT and blends of **P1A**/PCBM (1:1) and P3HT/**P1A** (0.9:0.1) (left) and of pristine **P4-1**, pristine P3HT and the blend of P3HT/**P4-1**(0.9:0.1) (right) obtained upon excitation at 488 nm.

P4-1

Likewise to **P1A**, PL spectra of pristine and binary films were recorded. Excitation of the binary P3HT/**P4-1** (0.9:0.1) film at 488 nm showed a quenching of the PL of P3HT and a simultaneous increase of the PL originating form **P4-1** around 840 nm (Figure 84, right). Due to the fact that there is an overlap of the fluorescence spectrum of P3HT and the absorption spectrum of **P4-1**, *Förster* resonance energy transfer (FRET) might take place and potentially open an additional pathway for energy transfer, which could result in improved solar cell performances.

Ternary solar cells with a donor/acceptor ratio of 1:1 were built, where the sum of both P3HT and **P4-1** accounts for the total donor content, and the squaraine content was varied between 2–20% of the donor amount, resulting in solar cells with the constitution of P3HT/**P4-1**/PCBM of 0.9:0.1:1, for example. Comparison with the binary P3HT/PCBM solar cell showed that the implementation of **P4-1** does not have a big influence on V_{OC} but leads to a distinct decrease of J_{SC}, a minor decrease of *FF* and finally a decrease of *PCE*. With increasing **P4-1** content, the absorption spectra of the solar cells showed a slight blue shift of the absorption bands correlated to P3HT. This gave rise to the idea that the usually ordered P3HT domains are perturbed by the polysquaraine what could explain the drop of J_{SC} due to less efficient charge transport. In addition, AFM (atomic force microscopy) images showed agglomerates of **P4-1** already at a content of 5%. This for electron or energy transfer unfavoured microstructure might also contribute to the overall limited performances of the ternary solar cells.

In conclusion, the broad absorption of **P4-1** complements nicely with the absorption of P3HT and a broad spectral region for the light harvesting is covered. In addition the overlap of the P3HT fluorescence and **P4-1** absorption allows FRET. However, solar cell performance was low and it can be concluded that the morphology is the limiting factor and it seems like morphology control is mandatory to achieve higher *PCE*s for those ternary solar cells.

P13

The implementation of **P13** into the P3HT/PCBM host system did not lead to any improvement of the solar cells, but in contrast to an inferior performance. While the V_{OC} remained constant, there was a decrease of J_{SC}, *FF*, and *PCE* compared to the binary solar cell. PL experiments showed a reasonable PL quenching of P3HT by **P13**. However, the absorption spectra of both polymers do not really complement each other because the maximum of **P13** is found at ~ 630 nm where also P3HT absorbs. Therefore, due to the low contents of **P13** in the solar cells no major contribution of **P13** on the *EQE* was observed. Additionally, there is only a small offset between the LUMO levels of **P13** (–4.14 eV) and PCBM (–4.3 eV) that could prevent efficient charge transport and be responsible for the lower efficiencies of the solar cells.

M14

In addition to the polymers, **M14** was the only monomeric compound that was tested in the ternary solar cells. The absorption spectra of **M14** and P3HT match rather well (Figure 83) and a broad spectral region is covered. In addition, the PL experiments revealed a strong quenching of the PL of P3HT by **M14** as well as of the PL of **M14** by PCBM, illustrating an efficient charge or energy transfer between the respective compounds.

Implementation of up to 5% of **M14** into the P3HT/PCBM host system resulted in only a minor decrease of J_{SC} that was equalled out by slight increase of *FF* resulting in more or less similar *PCE*. The V_{OC} remained rather constant, likewise to the formerly described ternary solar cells with the polysquaraines. A higher content of **M14** induced a drop of both J_{SC} and *PCE*. Similar to **P4-1**, implementation of 20% of **M14** lead to a blue shift of the P3HT absorption, indicating a perturbation of its ordered morphology and resulting in lower J_{SC}. However, as the only example in this study, at low squaraine loads the performance of the ternary solar cell did not decrease compared to the binary one.

Several optimisation procedures have been carried out in order to boost the performance of a ternary solar cell and to outstrip the binary reference cell. An excerpt of the results is listed in Table 27. The content of **M14** was optimised while a ratio of P3HT/PCBM of 1:1 was held constant. Subsequently, the PCBM content was varied to find the optimal constitution of the ternary solar cell. Eventually the effect of solvent vapour annealing (SVA) was investigated and it was shown that it leads to enhanced performances in nearly all cases of the ternary and binary devices due to the formation of more favoured crystallinity of P3HT.[323-324] The squaraine and PCBM domains remained rather unaffected. After all, even the best ternary solar cell with a composition of P3HT/**M14**/PCBM 1:0.02:0.8 could not outperform the binary one, but showed similar values of V_{OC} = 570 mV, J_{SC} = 8.48 mA cm^{-2}, *FF* = 67.7%, and an overall efficiency of *PCE* = 3.30%.

Table 27 Characteristics of the ternary solar cells and the binary reference devices.

P3HT/M14/PCBM / wt. %	V_{OC} **/ mV**	J_{SC} **/ mA cm^{-2}**	***FF* / %**	***PCE* / %**
1:0:1	540	8.02	61.0	2.71
1:0:1*	560	8.82	66.0	3.29
0.98:0.02:1	560	7.05	55.8	2.16
0.98:0.02:1*	540	6.71	62.5	2.32
1:0.02:1	560	7.96	61.1	2.72
1:0.02:1*	570	8.14	67.9	3.18
1:0.05:1	550	6.15	60.2	2.02
1:0.05:1*	560	7.83	64.1	2.81
1:0.02:0.8	560	8.15	64.9	2.99
1:0.02:0.8*	570	8.48	67.7	3.30

* solvent vapour annealed.

Conclusion

For nearly all ternary solar cells, a drop of *PCE* was observed that mainly originated from decreasing J_{SC}. This again was a result of a lowering of the photocurrent generation that originated from P3HT. This reduction could not be compensated by the contribution of photocurrent generation in the red to NIR region of the squaraine dyes which was rather low. Therefore, it is obvious that replacing contents of P3HT with a squaraine that is not capable of charge transport to the same extend does necessarily result in lower J_{SC} and *PCE*. Keeping a high content of P3HT and slightly decreasing the content of PCBM in favour of a squaraine prevents the drop of J_{SC} but still the best ternary solar cell did not outperform the binary one due to low contributions of photocurrent generation of the squaraine sensitisers. In this case its amount is limited to below 5% in order to not perturb the ordered domains of P3HT. As it was already indicated for the binary squaraine/PCBM BHJ solar cells in the previous chapter, it was even more clearly emphasised in the studies of the ternary solar cells that the morphology of the squaraines is a crucial factor.

The indolenine moiety used in this work might not be the right heterocycle in a squaraine because it can be imagined that the two methyl groups that point out of the plane of the squaraine might hinder a favourable structure in thin film, which would allow efficient charge transport. Therefore, more detailed structure-property relations of squaraines need to be addressed in the future to find more suitable compounds since electronic properties can easily be adjusted.

3.8.4 Dye Doped OLEDs[1]

In cooperation with *Benedikt Stender* and *Prof. Jens Pflaum* from the department of experimental physics VI at the Julius-Maximilians-University of Würzburg, **M6** was applied as a NIR emitter in an OLED (organic light emitting diode). In this OLED, the fluorescent polymer "Super Yellow" PPV (**SY-PPV**), a derivative of the poly(phenylenevinylene) (PPV) polymer (Chart 23), was used as host molecule and the dye **M6** was implemented as guest into the polymer matrix. In this device, highly efficient energy transfer from the visible spectral region to the NIR was obtained and the mechanism of the energy transfer from the polymer to **M6** was investigated, using both electroluminescence (EL) and photoluminescence (PL) experiments.

SY-PPV exhibits a broad absorption in the visible region from ~ 18000–33000 cm^{-1} and a fluorescence ranging from ~ 13000–19300 cm^{-1} (Figure 85, left) with a fluorescence quantum yield in a film of 0.22.[325]

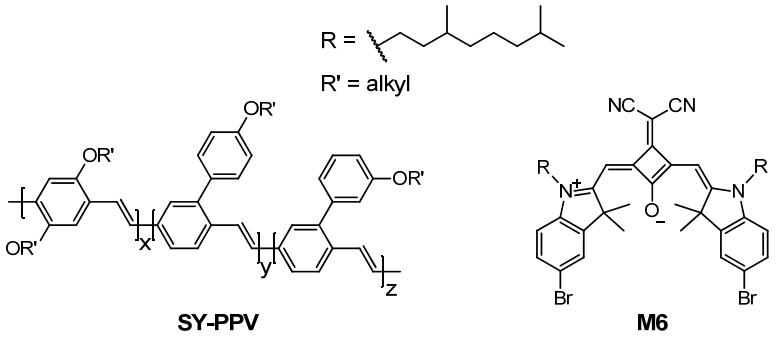

Chart 23 Molecular structures of the host matrix **SY-PPV** and the dopant **M6**.

In toluene the intense lowest energy absorption band of **M6** is found from 13000–17000 cm^{-1} with the maximum at 14100 cm^{-1}. The fluorescence is in the NIR with the maximum at 13800 cm^{-1} and a fluorescence quantum yield of 0.56. As can be seen in Figure 85 (left), there is a small overlap of the fluorescence spectrum of **SY-PPV** and the lowest energy absorption band of **M6**. All this makes **M6** a suitable candidate to work as

[1] Reproduced or adapted in part with permission from *Optoelectronic Processes in Squaraine Dye-Doped OLEDs for Emission in the Near-Infrared*, B. Stender, S. F. Völker, C. Lambert, J. Pflaum, *Adv. Mater.* **2013**, *25*, 2943-2947. Copyright (2013) WILEY-VCH Verlag GmbH & Co. KGaA, Weinheim.

dopant and NIR emitter in this OLED. In addition, the HOMO and LUMO energy levels of **M6** are between those of **SY-PPV** (Figure 85, right).

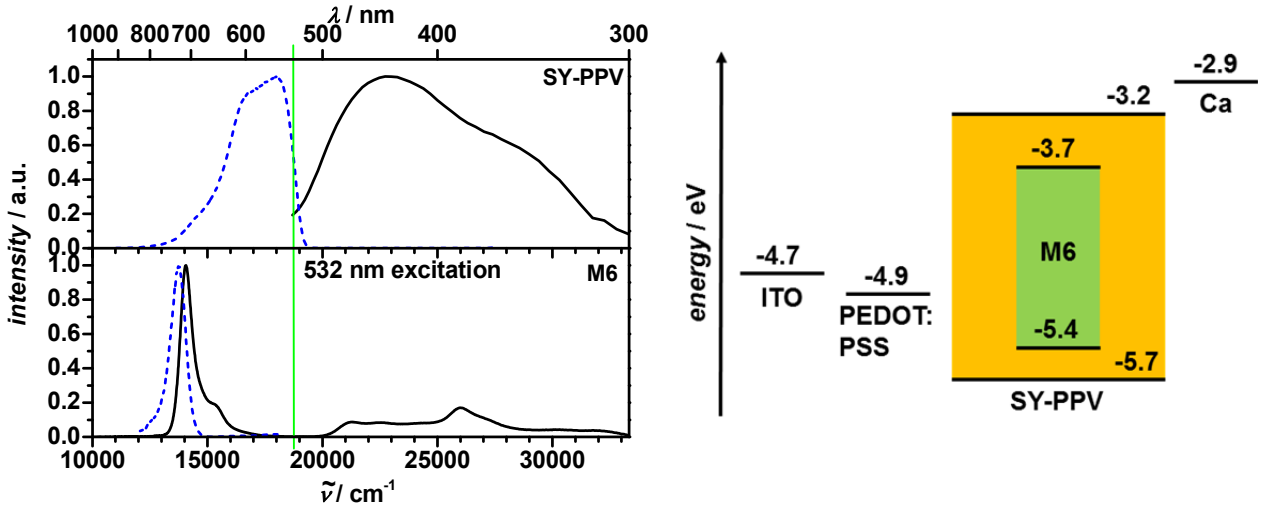

Figure 85 Left: Normalised absorption (solid black lines) and photoluminescence (dashed blue lines) spectra of the matrix polymer **SY-PPV** (top) and the dye dopant **M6** (bottom). The green line indicates the excitation wavelength used for the energy transfer experiments. Right: Energy levels of the substances incorporated in the OLED.

Spectral overlap is a prerequisite for *Förster* resonant energy transfer (FRET). Here, energy transfer takes place non-radiative from an excited donor molecule (here the polymer **SY-PPV**) to an acceptor molecule (here squaraine **M6**), which subsequently undergoes radiative relaxation. The *Förster* radius R_0 defines the mean distance between donor and acceptor molecules where 50% of energy transfer is obtained and is an indicator for the efficiency of the energy transfer. Equation (95)[326] (it has been corrected with respect to the original equation published by *Förster*)[140] is used to calculate the *Förster* radius,

$$R_0^6 = \frac{9\ln 10}{128\pi^5 n^4 N_{Av}} \kappa^2 \Phi_{PL} \int_0^\infty F_D(\lambda)\varepsilon_A(\lambda)\lambda^4 d\lambda \qquad (95)$$

with the orientation factor κ^2 (2/3 for random orientation), the fluorescence quantum yield of the donor Φ_{PL}, the refractive index of the surrounding media n, *Avogadro*'s number N_{Av}, and the spectral overlap integral between donor fluorescence and acceptor absorption are taken into account. Even though the spectral overlap is rather small, the

value of the overlap integral is decent due to the high extinction coefficient of the squaraine dye. The calculated *Förster* radius R_0 is 4.0 nm which assigns an efficient energy transfer.

In addition, the *Förster* radius was also determined experimentally by PL measurements and equation (96),

$$E = \frac{1}{1 + (\frac{R_0}{r})^6} = 1 - \frac{I_{DA}}{I_D} \qquad (96)$$

where E is the transfer efficiency, r the host-guest distance, I_{DA} denotes the intensity of the fluorescence peak maximum of the donor in the presence of the acceptor, and I_D that of the pure donor. From Figure 86 (left) it is apparent that 50% of energy transfer is reached at a concentration of **M6** of 0.17 wt.% and the resulting *Förster* radius is 3.0 nm and in very good agreement with the calculated radius of 4.0 nm.

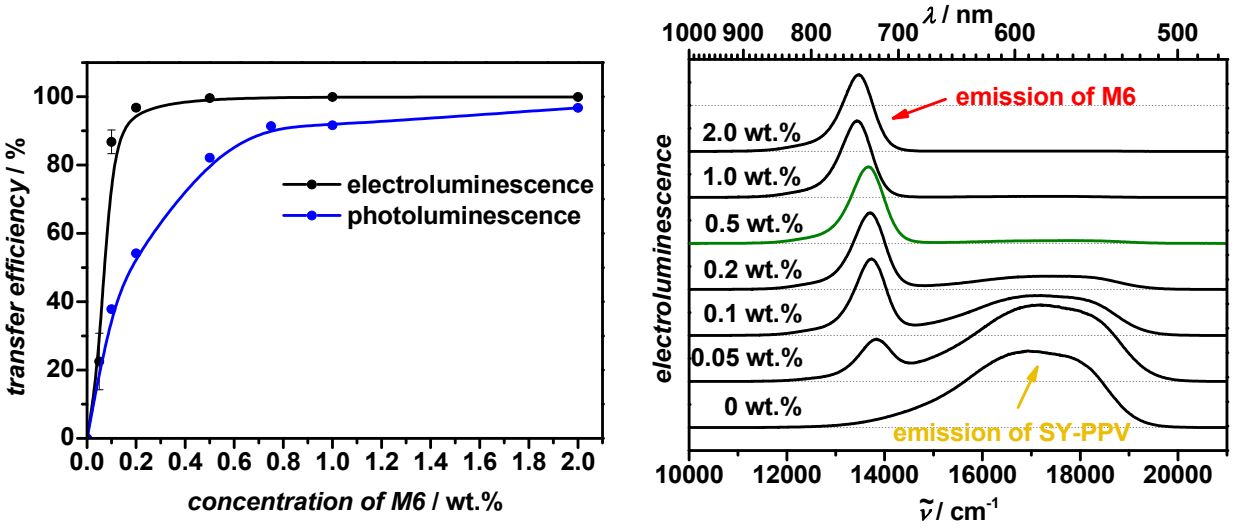

Figure 86 Left: Concentration dependent transfer efficiencies from polymer **SY-PPV** to squaraine **M6** determined by photoluminescence (excitation at 18800 cm^{-1}; 532 nm) and electroluminescence. Right: Normalised electroluminescence spectra at various concentrations of **M6** at an applied voltage of 6 V.

Besides, Figure 86 shows that in the electroluminescence measurements, the fluorescence of **SY-PPV** is almost completely quenched at a dye load of 0.5 wt.%, (green) which indicates that additional quenching mechanisms in addition to FRET play

a role. Further experiments could show that in the electrically driven devices, charge carrier dynamics dominate the NIR emission rather than FRET.

To sum up, it could be demonstrated that **M6** can be applied as NIR emitter in a solution processed squaraine doped thin film OLED which operates at room temperature. Additionally, the transfer mechanisms for both electroluminescence and photoluminescence of the device were elucidated. For a dye load as little as 0.05 wt.%, a turn-on voltage of 2 V, a maximum NIR quantum efficiency of 0.65%, and a power efficiency of 1.6 lm W^{-1} at 2.26 mA cm^{-2} were found (see literature[327]).

4 Summary

In this work the synthesis, the spectroscopic and electrochemical investigation as well as some applications of a broad diversity of indolenine squaraine dyes were presented. This diversity was based on two parent squaraine dyes, one standard *trans*-configured compound (**M1**) and one in which one central oxygen atom was replaced by a dicyanomethylene moiety (**M2**), which increased the acceptor strength and induced a *cis*-configuration. The variety of synthesised dyes included functionalised squaraine monomers, donor- and acceptor-substituted monomeric model squaraines, donor- and acceptor-squaraine copolymers, pure squaraine homopolymers, a squaraine-squaraine copolymer, as well as some conjugated cyclic oligomers.

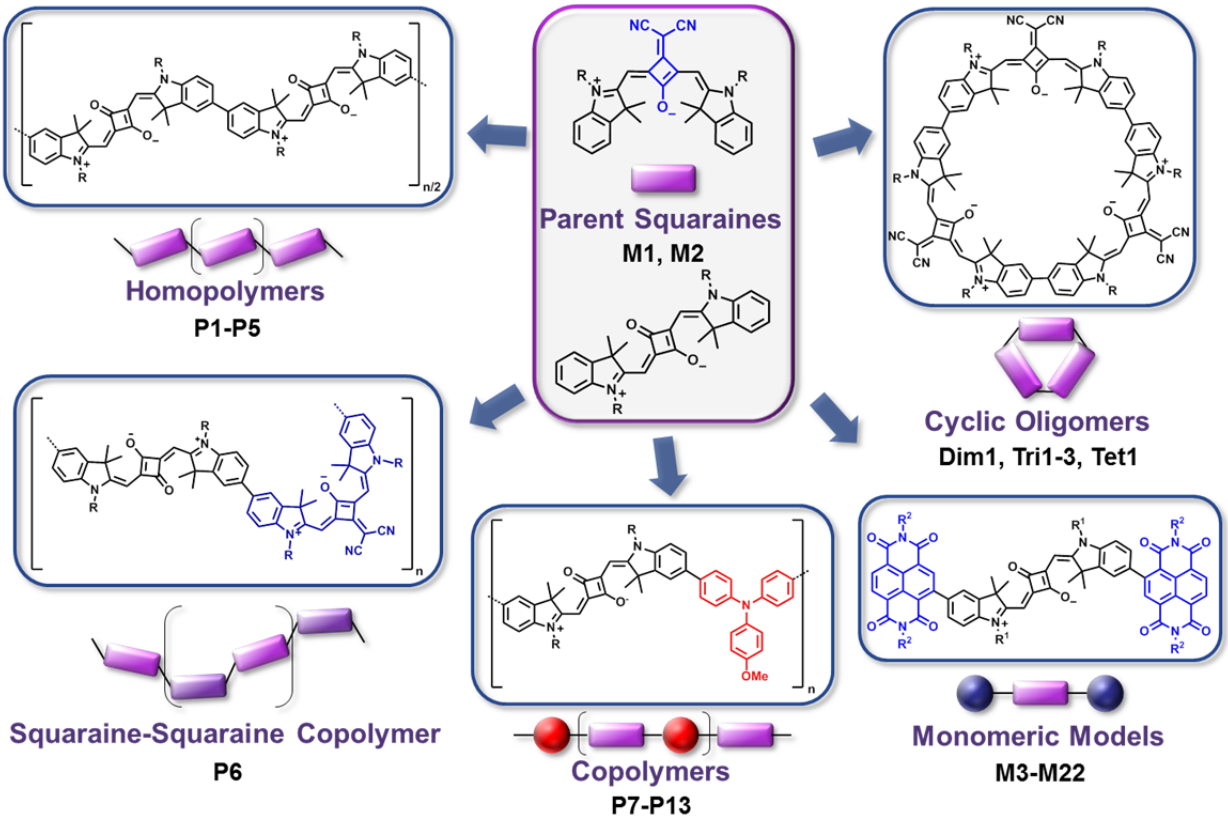

In order to be able to synthesise all these different kinds of dyes, several bromine and boronic ester derivatives were synthesised, which enabled the use of the *Suzuki* cross coupling reaction, to generate model dyes and copolymers. In addition, the bromine

derivatives were used to carry out the *Yamamoto* homocoupling reaction to the respective homopolymers and macrocycles.

The absorption maximum of unsubstituted reference dye **M1** was found at ~ 15500 cm^{-1}, while that of **M2** was red-shifted to ~ 14300 cm^{-1} due to the increased acceptor strength of the central unit. The extinction coefficients were in the order of ~ 300000 M^{-1} cm^{-1} and ~ 200000 M^{-1} cm^{-1}, respectively. It was found that the implementation of functional groups (**M3–M9**), additional electron donors (**M10–M19**) or acceptors (**M20–M22**) at the periphery lead to bathochromic shifts of the absorption depending on the strength of either σ- and/or π-donating properties of the substituents.

For the bis- and triarylamine substituted dyes **M10–M13** and the dibrominated dyes **M5** and **M7** the electronic structure of the mono- and diradical (di)cations was explored using the interplay of cyclic voltammetry, spectroelectrochemistry, and DFT calculations. It was demonstrated that the monoradical cations still show a cyanine-like character and are delocalised *Robin-Day* class III species due to the low redox potential of the squaraine bridge between the additional amine redox centres. To the best of my knowledge, this made $\mathbf{M13}^{+\bullet}$, with an *N*-*N*-distance of 26 bonds between the additional redox centres to the longest bis(triarylamine) radical cation that is completely delocalised. For the diradical dications, the situation was of larger complexity. The computed most stable energetic state of the dianisylamine-substituted dyes turned out to be a broken-symmetry state with almost equal contributions of an open-shell singlet and triplet state. In addition, it was shown that the HOMO–1→HOMO transition dominated the absorption spectra of the diradical dications where the *trans-/cis*-configuration of the squaraines had a direct impact due to symmetry reasons.

Based on the donor–squaraine model compounds **M10–M19**, a series of donor–squaraine copolymers was synthesised (**P7–P12**) in order to further red shift and broaden the low energy absorption band. However, these effects were only of marginal extent. Both the optical and the electrochemical derived band gaps were barely lowered compared to the respective monomeric model dyes. This was assigned to an increased squaraine-squaraine distance and resulting lower exciton coupling between the squaraine chromophores due to the bridging units. In addition, according to semiempirical

calculations the bridges were twisted out of the squaraine plane what reduced conjugational effects between the chromophores. To sum up, the idea to insert additional electron rich bridging units in order to create copolymers with broad and red-shifted absorption did not fully work out for the presented systems.

The addition of strong electron accepting NDI units at the periphery resulted in **M21**, the most unique monomeric model squaraine in this work. The common picture of a sharp low energy squaraine absorption completely altered due to the addition of the NDIs and a rather broad and solvent dependent low energy absorption was found. Spectroelectrochemical experiments and semiempirical calculations showed that this band is a superposition of the common squaraine HOMO→LUMO transition and a partial squaraine→NDI charge transfer transition. The latter was lost upon oxidation of the squaraine and the absorption spectrum of the monocation of **M21** was found to be nearly a 1:1 image of a pure squaraine monocation. Both the monomeric model **M21** and the respective copolymer **P13** showed low electrochemically obtained band gaps of 1.05–1.20 eV, which were the lowest of all squaraines in this work. For both dyes, transient absorption measurements in the fs-time regime revealed the ultrafast formation of a CS state *via* an intermediate CT state within a few ps. Besides, charge recombination to the ground state also occured within a few ps. In the polymer, there was barely any further energy or charge transfer within the excited state lifetime and therefore the CS state was confined on adjacent squaraine-NDI pairs and did not further travel along the polymer strand.

The Ni-mediated *Yamamoto* homocoupling reaction was applied for the synthesis of the homopolymers (**P1–P5**). In contrast to the donor–squaraine copolymers, those polymers revealed strongly red-shifted and broad absorption in the red to NIR region in addition to a sharp fluorescence. These features could be explained to originate mainly from the exciton coupling of localised excited states and the presence of different superstructures in solution. For the polymers **P1** and **P2**, an elongated J-type polymer chain caused the strong lowest energy absorption band whereas a zig-zag type arrangement of the single chromophores lead to transitions into both low and high energy excited states of the excitonic manifold. For the polymers **P3** and **P4**, several polymer fractions of different

size were investigated. Here, also an elongated chain with J-type character induced the lowest energy absorption band whereas a helical H-type arrangement caused transitions to higher energies of the excitonic manifold. The fractions to which these structures were formed depended on the chain length and the solvent. In thin film measurements, it was shown that the initially in solution formed superstructures were partly retained in the thin film but could be altered by annealing procedures. A control of the superstructures should enable the controlled tuning of the optical properties. Despite the strong interaction of the chromophores in the excited state, the redox potentials of the homopolymers barely differed to those of the respective reference dyes, indicating negligible electronic interaction in the ground state.

In addition squaraine-squaraine copolymer **P6**, consisting of alternating parent dyes **M1** and **M2**, was synthesised. Likewise to the homopolymers, a broad and red-shifted absorption was observed. This was explained by exciton coupling theory, which was extended to also suit alternating copolymers. In toluene, an extraordinary narrow and intense lowest energy absorption band was observed. This exchange narrowing might be a result of a highly ordered J-type structure of the polymer especially in this solvent because it was not found in others. The features of the polymer may be compared to typical J-aggregates formed from monomeric cyanine molecules for example and the polymer used as model for excitonic interactions in an alternating copolymer. Transient absorption measurements revealed a strong energy dependence of the decay traces of the copolymer, most strikingly at early decay times. This was assigned to the occurrence of multiple excitations of one polymer strand (due to the large extinction coefficients of the polymer) and resulting exciton-exciton annihilation. Due to the large exciton diffusion constants that were estimated, the static exciton-exciton annihilation was the rate limiting process of the decay, in contrast to other conjugated polymers, where in thin film measurements the decay was diffusion controlled.

To sum up, for the polymers consisting of exclusively squaraine chromophores, it was shown that the exciton coupling of single chromophores with strong transition dipole moments was a fruitful way to tune the absorption spectra.

As a side product of some of the polycondensation reactions, unprecedented cyclic conjugated oligomers such as the triarylamine-bridged dimer **Dim1**, the cyclic homotrimers **Tri1–Tri3**, and the tetramer **Tet1** were obtained by recycling GPC in low yields. Especially the cyclic trimers showed unusual absorption and even more extraordinary fluorescence properties. They showed multiple fluorescence bands in the NIR that covered a range from ~ 8000–12500 cm^{-1} (800–1250 nm). First hints from theoretical calculations indicated that the trimer was not fully planar but comprised a mixture of both planar and bent single squaraine chromophores. However, final results of the calculations were still missing at the time of writing.

In the last part of this work, the application of some monomeric and polymeric squaraines in binary and ternary bulk heterojunction solar cells was demonstrated. Also the utilisation as a dopant in a polymer matrix in an OLED device was shown. The homopolymers **P1–P4** were tested in the binary BHJ solar cells revealing poor performances and especially very low short circuit currents. The utilisation of the polymers **P3** and **P4** that carried the dicyanomethylene group resulted in higher open circuit voltages due to the lower LUMO energy levels but still an overall poor performance. Neither for the different alkyl chains nor for the size of the polymers was a trend observed. In the ternary BHJ solar cells, small amounts of either monomer **M14** or polymers **P1A**, **P4–1** or **P13** were added to a P3HT/PCBM system in order to generate an additional pathway for charge or energy transfer that should result in a better device performance. However, for none of the tested squaraines, improved solar cells could be built. In similarity to the binary solar cells, the short circuit currents were lower compared to a P3HT/PCBM reference device. These low short circuit currents indicated that the morphology of the squaraine dyes was the major limitation in those devices. It is possible that the dimethyl groups at the indolenine hindered a favoured alignment of the compounds that would allow decent charge transport. In the squaraine doped OLED the squaraine **M6** worked rather well as an NIR emitter. Already at low dye loads the fluorescence of the host polymer **SY-PPV** was completely quenchend and emission from the squaraine was observed. For electroluminescence measurements, a lower dye load (0.5 wt.%) compared to the photoluminescence measurements was sufficient, indicating

that apart from FRET additional quenching mechanisms were at work in the electrically driven devices such as charge carrier dynamics.

5 Experimental Section[1]

5.1 Materials & Methods

5.1.1 Absorption Spectroscopy

- JASCO V570 or V670 UV/Vis/NIR-Spectrophotometer
- Cary Model 5000 UV/Vis/NIR-Spectrometer

Experiments were carried out in 1 cm quartz cuvettes in Uvasol® solvents from Merck. The neat solvent was used as reference and the compounds were measured at various concentrations $\sim 10^{-7}$–10^{-5} mol l^{-1} to affirm linear behaviour (to exclude aggregate formation). The extinction coefficients are given per monomer unit for the polymers and cyclic oligomers. In case of the copolymers one monomer unit consists of one squaraine and one bridge unit.

The measurements of films of the polymer **P3-1** were performed on samples that were spin-coated (2000 rpm) from the respective solvent (2.5 mg ml^{-1}) onto a flat glass substrate. Those spectra were measured with an integrating sphere ($\phi = 15$ cm) on the Cary spectrometer.

---

[1] Reproduced or adapted in part with permission from a) *Polymeric Squaraine Dyes as Electron Donors in Bulk Heterojunction Solar Cells*, S. F. Völker, S. Uemura, M. Limpinsel, M. Mingebach, C. Deibel, V. Dyakonov, C. Lambert, *Macromol. Chem. Phys.* **2010**, *211*, 1098-1108. Copyright (2010) WILEY-VCH Verlag GmbH & Co. KGaA, Weinheim; b) *Squaraine Dyes as Efficient Coupling Bridges between Triarylamine Redox Centres*, S. F. Völker, M. Renz, M. Kaupp, C. Lambert, *Chem. Eur. J.* **2011**, *17*, 14147-14163. Copyright (2011) WILEY-VCH Verlag GmbH & Co. KGaA, Weinheim; c) *Exciton Coupling Effects in Polymeric cis-Indolenine Squaraine Dyes*, S. F. Völker, C. Lambert, *Chem. Mater.* **2012**, *24*, 2541-2553. Copyright 2012 American Chemical Society; d) *Charge TransferDynamics in Squaraine-Naphthalene Diimide Copolymers*, S. F. Völker, A. Schmiedel, M. Holzapfel, C. Böhm, C. Lambert, *Phys. Chem. Chem. Phys.* **2013**, *15*, 19831-19844. – Reproduced or adapted in part by permission of the PCCP Owner Societies; e) *Optoelectronic Processes in Squaraine Dye-Doped OLEDs for Emission in the Near-Infrared*, B. Stender, S. F. Völker, C. Lambert, J. Pflaum, *Adv. Mater.* **2013**, *25*, 2943-2947. Copyright (2013) WILEY-VCH Verlag GmbH & Co. KGaA, Weinheim; f) *Synthesis, Electrochemical, and Optical Properties of Low Band Gap Homo- and Copolymers Based on Squaraine Dyes*, S. F. Völker, T. Dellermann, H. Ceymann, M. Holzapfel, C. Lambert, *J. Polym. Sci., Part A: Polym. Chem.* **2014**, *52*, 890-911. Copyright (2014) WILEY-VCH Verlag GmbH & Co. KGaA, Weinheim; g) *Singlet-Singlet Exciton Annihilation in an Exciton-Coupled Squaraine-Squaraine Copolymer: A Model towards Hetero-J-Aggregates,* S. F. Völker, A. Schmiedel, M. Holzapfel, K. Renziehausen, V. Engel, C. Lambert, *J. Chem. Phys. C.* **2014**, *accepted* – Copyright (2014) American Chemical Society.

The optical band gaps E_{gap}^{opt} were determined by the intersection point of a tangent on the inflexion point of the low energy side of the low energy absorption band and the x-axis. Therefore the first deviation of the absorption spectrum was calculated to identify the inflexion point, which is found at the maximum/minimum of the first deviation.

5.1.2 Fluorescence Spectroscopy

- Photon Technology International (PTI) SQ-2000-4 Fluorescence Spectrometer with a xenon lamp (75 W)
- Photomultiplier (R928P) or InGaAs detector
- Edinburgh Instruments FLS980 fluorescence spectrometer[1]

Experiments were carried out in 1 cm quartz cuvettes in Uvasol® solvents from Merck. The dissolved samples were purged with argon for 10 min and oxazine 1 was used as fluorescence standard ($\Phi_{fl} = 0.11$ in ethanol[328])1. Quantum yields were determined using equation (97)

$$\Phi_{fl} = \Phi_{fl,\,Ref} \times \frac{I(\tilde{\nu}) \times OD_{Ref} \times (n_D^{20})^2}{I(\tilde{\nu})_{Ref} \times OD \times (n_{D,\,Ref}^{20})^2} \tag{97}$$

with the fluorescence quantum yield Φ_{fl}, the integrated emission band $I(\tilde{\nu})$, the optical density at the excitation wavelength OD, and the refractive index of the respective solvent n_D^{20}. The index "Ref" donates that the value corresponds to the fluorescence standard reference. The compounds were excited between 600–640 nm (15600–16700 cm^{-1}).

[1] During the writing process, the quantum efficiency of oxazine 1 was determined to be 0.15 by an absolute measurement using an integration sphere. However, the values reported for the squaraine dyes herein are still referenced against the quantum efficiency of 0.11 as they were published to avoid confusion. Nevertheless, it has to be noted that the correct quantum efficiencies are larger by a factor of $0.15 / 0.11 \approx 1.36$.

5.1.3 Fluorescence Lifetimes

- PTI TM-2/2003 Fluorescence Lifetimes Spectrofluorometer
  - 650 nm laser diode
- Edinburg Instruments TCSPC fluorescence lifetimes spectrometer FLS980 (**P6**)[1]
  - 656 nm laser diode

The samples were prepared similar to the steady state fluorescence experiments. The instrumental response was determined by using a scatter solution consisting of colloidal silicon in deionised water. Fitting of the decay curves with exponential decay functions yielded the fluorescence lifetimes.

The fluorescence quantum yield Φ_{fl} and the fluorescence τ_{fl} lifetime were used to calculate the average rate constant of the fluorescent decay $\bar{k}_{fl}$ and the non-radiative decay $\bar{k}_{nr}$ using equations (69) and (70). For the polymers the average fluorescence lifetime was used, which was obtained by equation (71) to calculate the rate constants, where α_x are the relative amplitudes of the corresponding lifetimes.

$$\bar{k}_{fl} = \frac{\Phi_{fl}}{\tau_{fl}} \tag{69}$$

$$\bar{k}_{nr} = \frac{1-\Phi_{fl}}{\tau_{fl}} \tag{70}$$

$$\bar{\tau} = \frac{\alpha_1 \tau_1^2 + \alpha_2 \tau_2^2}{\alpha_1 \tau_1 + \alpha_2 \tau_2} \tag{71}$$

[1] TCSPC fluorescence lifetime measurements of **P6** were performed by *Alexander Schmiedel*.

5.1.4 Cyclic Voltammetry (CV), Differential Pulse Voltammetry (DPV), and *Osteryoung* Square Wave Voltammetry (OSWV)

- BAS CV-50 W electrochemical workstation or Gamry Instruments Reference 600 Potentiostat/Galvanostat/ZRA

Three electrode setup with a platinum disc working electrode with a diameter of 1 mm, a platinum helical counter electrode and either a Ag/AgCl pseudo-reference electrode or a Ag/AgCl "leak free" electrode[329].

Solvent: DCM, $CDCl_3$ or THF with tetrabutylammonium hexafluorophosphate (TBAHFP) as supporting electrolyte (c = 0.1–0.2 M).

Experiments were carried out under argon atmosphere in a completely sealed glass vessel with solvents that were dried according to literature procedures. Prior to the experiments, the solvents were freshly distilled and poured onto activated neutral alumina oxide under nitrogen atmosphere for further drying. For thin layer measurements, the electrode was put on the polished flat surface of a glass hemisphere with a diameter of 8 mm. Several cycles were measured with a scan rate of 10 mV s^{-1}. The standard scan rate was 250 mV s^{-1} for the CV, 50 mV s^{-1} for the OSWV, and 20 mV s^{-1} for the DPV.

When the pseudo-reference electrode was used, the redox couple of decamethylferrocene/decamethylferrocenium was used as reference and the potentials were calculated against the ferrocene/ferrocenium redox couple.[217]

HOMO and LUMO ($E_{HOMO/LUMO}$) energy levels were obtained from the half-wave potentials of cyclic voltammetry measurements. The potential of Fc/Fc^+ in TBAHFP/DCM is 0.46 eV and in TBAHFP/THF 0.56 eV vs. the saturated calomel electrode (SCE).[155] Furthermore, the potential of SCE is 0.244 V vs. the normal hydrogen electrode (NHE)[330] which has an absolute potential of 4.46 eV vs. vacuum.[156] Therefore, the energy levels in DCM are $E_{HOMO/LUMO} = -5.16\ eV - E_{1/2}^{Ox1/Red1}$ and the electrochemically derived band gap $E_{gap}^{CV} = E_{LUMO} - E_{HOMO}$. In THF, –5.16 eV is replaced by –5.26 eV.

5.1.5 Spectroelectrochemistry

- JASCO V570 or V670 UV/Vis/NIR-Spectrophotometer
- Princeton Applied Research Potentiostat/Galvanostat Model 283

Three electrode setup with a platinum disc working electrode with 6 mm diameter, a gold-coated metal plate as counter electrode and a Ag/AgCl pseudo-reference electrode.

Solvent: DCM or $CDCl_3$ with tetrabutylammonium hexafluorophosphate (TBAHFP) as supporting electrolyte (c = 0.2 M).

Experiments were carried out in a cylindrical quartz cell and spectra were recorded in reflection mode at the polished working electrode through the transparent cell bottom. The electrode was adjusted at 100 μm height above the bottom by a μm screw. Using this method, the thin layer is entirely electrolysed during the measurement. The voltages were raised in steps of 25 or 100 mV and extinction coefficients were calculated against the neutral starting material.

5.1.6 NMR Spectroscopy

- Bruker Avance 400 FT-Spectrometer (^{1}H: 400.1 MHz; ^{13}C: 100.6 MHz)
- Bruker Avance DMX 600 FT-Spectrometer (^{1}H: 600.13 MHz; ^{13}C: 150.92 MHz)

The chemical shift is given in ppm relative to tetramethylsilane (TMS) as internal standard. The coupling constants J are quoted in Hertz (Hz).

The abbreviations used for declaration of the spin multiplicities and C-atom depictions are: s = singlet, d = doublet, t = triplet, q = quartet, m = multiplet, dd = doublet of doublet; prim = primary, sec = secondary, tert = tertiary, quart = quaternary.

Order of declaration: chemical shift (spin multiplicity, coupling constant, number of protons, assignment).

5.1.7 Mass Spectrometry

- Bruker Daltonik microTOF focus (high resolution ESI)
- Bruker Daltonik autoflex II (MALDI-TOF)

5.1.8 Gel Permeation Chromatography (GPC)

- Shimadzu: SPD-M20A (diode array detector), CBM-20A (system controller), LC-20AD (solvent delivery unit), DGU-20A9 (online degasser). Solvent: $CHCl_3$. Temperature: 20°C
  - Preparative: Recycling mode with two SDV columns (50 Å, 500 Å; particle size 10 μm, 20 × 600 mm) from PSS/Mainz, Germany.
  - Analytical: SDV column (mixed bed, "Linear S", 5 μm particle size, 8 × 300 mm) from PSS/Mainz, Germany. Polystyrene was used as calibration standard. Solutions of 1 mg/ml were used.

5.1.9 High Pressure Liquid Chromatography (HPLC)

- JASCO: LC-NetII ADC (interface box), PU-2080 plus (HPLC pump), DG-2080-53 (inline degasser), LV-2080-03 (solvent selection valve unit), UV-2077 (UV/vis detector), CHF122SC (fraction collector)

Experiments were carried out with a flow of 10 ml min^{-1} in the given solvents.

5.1.10 Femtosecond Transient Absorption Pump-Probe Spectroscopy[1]

- Ultrafast Systems: Helios transient spectrometer

[1] Femtosecond transient absorption spectroscopy measurements were performed by *Alexander Schmiedel* and the analysis was carried out by *Dr. Marco Holzapfel*.

- Newport Spectra Physics: Solstice femtosecond laser, pulse duration 100 fs

The pump wavenumbers of 12700 cm^{-1}, 13100 cm^{-1}, 15000 cm^{-1} (chapter 3.2.4) and of 12500 cm^{-1} and 16000 cm^{-1} (chapter 3.5.2) were generated by a OPA (TOPAS-C) with a pulse duration of ~ 140 fs. The fundamental of 12500 cm^{-1} was used to generate a white light continuum from 12500–25000 cm^{-1} to probe the excited samples. For the detailed setup see ref.[331] Experiments were carried out in quartz cuvettes (d = 2 mm) from Spectrocell (Oreland, PA) in Uvasol® solvents ($CHCl_3$, toluene) from Merck. The samples ($c = 1–5 \cdot 10^{-6}$ mol l^{-1} (monomer unit)$^{-1}$) were filtered and purged with argon for at least 30 min prior to the experiment. In chapter 3.5.2 the energy per pulse was 100–245 nJ at both excitation wavelengths. Linearity was checked from 50–400 nJ. Due to the strong GSB at the pump wavenumbers, the transient maps were corrected for stray light contributions before the analysis. In this, the amount of independent species n was estimated by singular value decomposition. Then a global fit on the transient map with GLOTARAN[332] was performed. There, a target model (i.e. branched model) was employed to modell the IRF (~ 150 fs), the white light dispersion (chirp), and the coherent artefact at time zero. The time characteristics of the employed model were those of the IRF plus an additional exponential function. Thus, the species associated or the evolution associated difference spectra (SADS and EADS, respectively) were obtained.

5.1.11 Computational Details[1]

The complete computational details of the (TD)DFT computations of chapter 3.3.7 (p. 130) are given in reference [191].

[1] Semiempirical AM1 and CNDO/S2 calculations as well as (TD)DFT calculations were performed by *Dr. Marco Holzapfel* and *Prof. Dr. Christoph Lambert.* The (TD)DFT calculations of chapter 3.3.7 were performed by *Dr. Manuel Renz* and *Prof. Dr. Martin Kaupp*.

5.1.12 Binary Solar Cell Preparation[1]

For the solar cell fabrication, conductive ITO/glass substrates were cleaned and coated with a thin layer of PEDOT:PSS under ambient conditions. All subsequent fabrication and measurement procedures were performed in a glove box under nitrogen atmosphere. The samples were annealed at 130°C for 10 min and subsequently the active layer was spin-coated. Respective concentration, solvent, and annealing condition of the coating of the active layer are given in Table 26 (p. 221). Subsequently, the metal contacts (Ca/Al: ~ 3 nm/120 nm) were thermally evaporated. The characterisation procedure is given in reference [157].

5.1.13 Ternary Solar Cell Preparation[2]

The procedure for the fabrication of the ternary BHJ solar cells is given in reference [318].

[1] Binary solar cell preparation and characterisation was performed by *Dr. Markus Mingebach*, *Moritz Limpinsel*, and *Stefan Walter* in the group of *Prof. Dr. Carsten Deibel* and *Prof. Dr. Vladmir Dyakonov* from the department of experimental physics VI at the Julius-Maximilians-University Würzburg.

[2] Ternary solar cell preparation and characterisation was performed by *Parisa Khoram* and *Dr. Tayebeh Ameri* in the group of *Prof. Dr. Christoph Brabec* from the institute Materials for Electronics and Energy Technology (*i*-MEET) at the Friedrich-Alexander University Erlangen-Nürnberg.

5.2 Synthesis

The reactions were performed in standard glass ware and chemicals that were obtained from commercial suppliers were used without further purification if not stated elsewise. For reactions under nitrogen atmosphere, the nitrogen was dried over Sicapent® from Merck and the oxygen was removed by copper catalyst R3-11 from BASF. The reaction vessels were heat dried in vacuum and the solvents dried according to common literature procedures and stored under nitrogen atmosphere. For flash column chromatography, silica gel (32–63 μm) from Merck was used.

As representative examples, the numbers for the assignment of the protons are shown for compound **2**.

5.2.1 Synthesis of Precursors 1–36

The precursors 3,7-dimethyloctyl bromide[333], 3,7-dimethyloctyl tosylate[146] (**1**), triethylammonium 2-butoxy-3-(dicyanomethylene)-4-oxocyclobut-1-enolate[147] (**3**), 5-bromo-1-hexadecyl-2,3,3-trimethyl-3*H*-indolium iodide (**6**)[157], triarylamine **16**[187], 3-bromo-9*H*-carbazole[189] (**18**), 2-bromo-9*H*-carbazole[190] (**21**) 2,7-dibromo-9*H*-carbazole[215] (**27**), 3,6-dibromo-9*H*-carbazole[216] (**30**), and triarylborane **34**[235] were synthesised according to literature procedures.

*Synthesis of 1-(3,7-dimethyloctyl)-3,3-dimethyl-3H-indol-1-ium tosylate (**2**)*

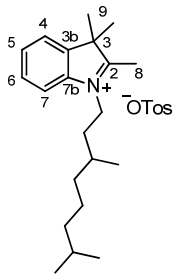

2,3,3-Trimethyl-3*H*-indole (2.00 g, 12.6 mmol) and 3,7-dimethyloctyl tosylate (**1**) (2.75 g, 8.79 mmol) were refluxed in $MeNO_2$ (10 ml) for 18 h. The solvent and remaining indole were removed under reduced pressure and the residue was digested with Et_2O several times.

Yield: 2.76 g (5.80 mmol, 66%) of a wine red solid

$C_{28}H_{41}NO_3S$ [471.70]

^{1}H-NMR (600.1 MHz, $CDCl_3$):

δ[ppm] = 7.64–7.60 (AA', 2 H), 7.56–7.49 (4 H), 7.05–7.01 (BB', 2 H), 4.73–4.62 (m, 2 H, NCH_2), 2.99 (s, 3 H, H-8), 2.29 (s, 3 H, $O_3SC_6H_4CH_3$), 1.85–1.77 (m, 1 H, C*H*), 1.66–1.58 (8 H, H-9, CH_2), 1.54–1.46 (m, 1 H, C*H*), 1.38–1.28 (m, 2 H, CH_2), 1.25–1.17 (m, 2 H, CH_2), 1.17–1.09 (m, 2 H, CH_2), 1.04 (d, ^3J = 6.0 Hz, 3 H, CH_3), 0.86 (d, ^3J = 6.5 Hz, 3 H, CH_3), 0.85 (d, ^3J = 6.6 Hz, 3 H, CH_3).

^{13}C-NMR (150.9 MHz, $CDCl_3$):

δ[ppm] = 195.7 (quart), 143.7 (quart), 141.8 (quart), 141.2 (quart), 138.8 (quart), 129.7 (tert), 129.2 (tert), 128.4 (tert), 125.9 (tert), 123.1 (tert), 115.0 (tert), 54.4 (quart), 47.4 (sec), 39.0 (sec), 36.9 (sec), 35.0 (sec), 31.0 (tert), 27.9 (tert),

24.6 (sec), 23.0 (prim)[1], 22.9 (prim)[1], 22.6 (prim)[1], 22.5 (prim)[1], 21.2 (prim), 19.5 (prim), 14.9 (prim).

ESI-MS pos (high resolution): $[M–OTos^-]^{\cdot+}$

calc.: 300.26858 m/z

found: 300.26840 m/z Δ = 0.58 ppm.

*Synthesis of 5-bromo-2,3,3-trimethyl-3H-indolenine (**4**)*[148]

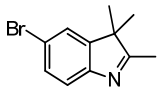

CA [54136–24–2]

p-Bromophenylhydrazine hydrochloride (15.1 g, 67.7 mmol), isopropylmethyl ketone (11.7 g, 135 mmol) and acetic acid (120 ml) were refluxed under nitrogen atmosphere for 6 h and stirred at room temperature (rt) for 18 h. The solvent was removed under reduced pressure and the residue was dissolved in Et_2O (150 ml) and H_2O (100 ml). After phase separation the aqueous phase was extracted with petroleum ether (PE) (2 × 100 ml) and Et_2O (100 ml). The combined organic phases were washed with aqueous KOH solution (10%, 3 × 100 ml) and H_2O (3 × 100 ml), dried over $MgSO_4$, the solvent was evaporated, and the remaining product was dried in vacuo. The product was used without further purification.
(If the crude product is distilled under reduced pressure, the obtained colourless oil turns into long colourless needles after a few days in the fridge.)

Yield: 15.6 g (65.7 mmol, 97%) of a dark brownish oil

$C_{11}H_{12}BrN$ [238.12]

[1] The signal of the primary C-atoms splits into two signals of equal intensity even though they are supposed just to give one single signal. Possibly this is due to the alkyl side chain, which has a stereocenter but is of racemic character.

^{1}H-NMR (400.1 MHz, $CDCl_3$):

δ [ppm] = 7.44–7.36 (3 H, H-4,-6,-7), 2.26 (s, 3 H, H-8), 1.30 (s, 6 H, H-9).

Synthesis of 5-bromo-1-(3,7-dimethyloctyl)-3,3-dimethyl-3H-indol-1-ium tosylate ***(5)***

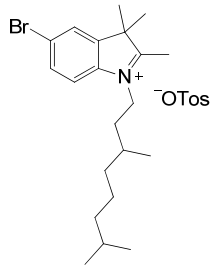

5-Bromo-2,3,3-trimethyl-3*H*-indole (**4**) (1.01 g, 4.23 mmol) and 3,7-dimethyloctyl tosylate (**1**) (1.78 g, 5.69 mmol) were dissolved in $MeNO_2$ under nitrogen atmosphere and refluxed for 17 h. After cooling to rt, Et_2O (40 ml) was added and the product crystallised within 1 h. The precipitate was filtered and washed with Et_2O.

Yield: 955 mg (1.73 mmol, 41%) of a light brown solid

$C_{28}H_{40}BrNO_3S$ [550.59]

^{1}H-NMR (600.1 MHz, $CDCl_3$):

δ [ppm] = 7.64 (dd, ^3J = 8.5 Hz, ^4J = 1.6 Hz, 1 H, H-6), 7.62 (d, ^4J = 1.6 Hz, 1 H, H-4), 7.59–7.54 (AA', 2 H), 7.42 (d, ^3J = 8.6 Hz, 1 H, H-7), 7.04–7.00 (BB', 2 H), 4.70–4.55 (m, 2 H, NCH_2), 2.94 (s, 3 H, H-8), 2.29 (s, 3 H, $O_3SC_6H_4CH_3$), 1.81–1.74 (m, 1 H, C*H*), 1.65–1.54 (8 H, H-9, CH_2), 1.54–1.45 (m, 1 H, C*H*), 1.36–1.25 (m, 2 H, CH_2), 1.24–1.16 (m, 2 H, CH_2), 1.15–1.07 (m, 2 H, CH_2), 1.01 (d, ^3J = 6.2 Hz, 3 H, CH_3), 0.85 (d, ^3J = 6.6 Hz, 6 H, CH_3).

^{13}C-NMR (150.9 MHz, $CDCl_3$):

δ [ppm] = 195.7 (quart), 143.6 (quart), 143.5 (quart), 140.3 (quart), 138.9 (quart), 132.5 (tert), 128.4 (tert), 126.6 (tert), 125.8 (tert), 124.1 (quart), 116.6 (tert), 54.5 (quart), 47.7 (sec), 39.0 (sec), 36.8 (sec), 34.9 (sec), 31.0 (tert), 27.9 (tert),

24.6 (sec), 22.90 (prim)[1], 22.85 (prim)[1], 22.6 (prim)[1], 22.5 (prim)[1], 21.3 (prim), 19.5 (prim), 15.0 (prim).

ESI-MS pos (high resolution): $[M–OTos^–]^{\cdot+}$

calc.: 378.17909 m/z

found: 378.17910 m/z Δ = 0.03 ppm.

Synthesis of 5-bromo-1-(3,7-dimethyloctyl)-3,3-dimethyl-2-methyleneindoline (7)

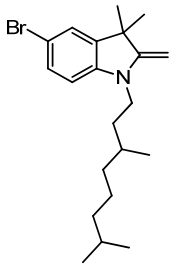

5-Bromo-1-(3,7-dimethyloctyl)-3,3-dimethyl-3*H*-indol-1-ium tosylate (**5**) (786 mg, 1.43 mmol) was suspended in Et_2O (20 ml) and aqueous NaOH (1 M, 20 ml, 20.0 mmol) was added. The mixture was stirred for 30 min and extracted with Et_2O (3 × 10 ml). The combined organic phases were washed with H_2O (2 × 10 ml), dried over $MgSO_4$, and the solvent was removed under reduced pressure. The compound was further used straight after ^{1}H-NMR proof.

Yield: 533 mg (1.41 mmol, 99%) of a yellowish liquid that turned red after a while

$C_{21}H_{32}BrN$ [378.39]

^{1}H-NMR (400.1 MHz, $CDCl_3$):

δ [ppm] = 7.20 (dd, ^3J = 8.3 Hz, ^4J = 2.0 Hz, 1 H, H-7), 7.14 (d, ^4J = 2.0 Hz, 1 H, H-4), 6.36 (d, ^3J = 8.3 Hz, 1 H, H-6), 3.88 (d, ^2J = 2.1 Hz, 1 H, C*H*), 3.85 (d,

[1] The signal of the primary C-atoms splits into two signals of equal intensity even though they are supposed just to give one single signal. Possibly this is due to the alkyl side chain, which has a stereocenter but is of racemic character.

^{2}J = 2.1 Hz, 1 H, C*H*), 3.53–3.38 (m, 2 H, NCH_2), 1.66–1.09 (16 H), 0.97 (d, ^{3}J = 6.5 Hz, 3 H, CH_3), 0.87 (d, ^{3}J = 6.6 Hz, 6 H, CH_3).

Synthesis of the semisquaraine ester ***8***

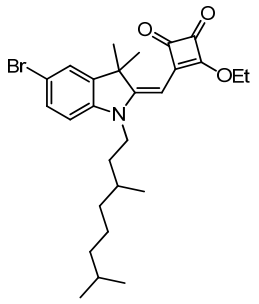

5-Bromo-1-(3,7-dimethyloctyl)-3,3-dimethyl-3*H*-indol-1-ium tosylate (**5**) (1.32 g, 2.40 mmol) was dissolved in EtOH (4 ml) and NEt_3 (1 ml) and heated to boiling point. 3,4-Diethoxycyclobut-3-en-1,2-dione (340 mg, 2.00 mmol) was added dropwise and the solution was refluxed for 2.5 h. The solvent was removed under reduced pressure and the residue purified by flash chromatography (eluent: PE/ethyl acetate (EA) 9:1). The crude product was recrystallised from EtOH.

Yield: 184 mg (366 μmol, 18%) of a yellow solid

$C_{27}H_{36}BrNO_3$ [502.48]

^{1}H-NMR (600.1 MHz, $CDCl_3$):

δ [ppm] = 7.37 (dd, ^{4}J = 2.0 Hz, ^{3}J = 8.3 Hz, 1 H, H-6), 7.35 (d, ^{3}J = 8.2 Hz, 1 H, H-4), 6.70 (d, ^{3}J = 8.3 Hz, 1 H, H-7), 5.37 (s, 1 H, C*H*), 4.88 (q, ^{3}J = 7.1 Hz, 2 H, OCH_2), 3.82–3.71 (m, 2 H, NCH_2), 1.73–1.63 (m, 1 H, C*H*), 1.63–1.59 (6 H, H-9), 1.56–1.49 (6 H, C*H*, CH_2, CH_3), 1.40–1.11 (6 H, CH_2), 1.03 (d, ^{3}J = 6.5 Hz, 3 H, CH_3), 0.87 (d, ^{3}J = 6.7 Hz, 6 H, CH_3).

^{13}C-NMR (150.9 MHz, $CDCl_3$):

δ [ppm] = 192.1 (quart), 188.1 (quart), 187.8 (quart), 173.7 (quart), 167.1 (quart), 143.0 (quart), 141.7 (quart), 130.6 (tert), 125.4 (tert), 115.1 (quart), 109.4 (tert), 81.8 (tert), 70.0 (sec), 47.9 (quart), 41.3 (sec), 39.1 (sec), 37.0 (sec), 32.8

(sec), 31.0 (tert), 27.9 (tert), 26.96 (prim)[1], 26.93 (prim)[1], 24.7 (sec), 22.65 (prim)[1], 27.57 (prim)[1], 19.7 (prim), 15.9 (prim).

*Synthesis of the semisquaraine ester **9***

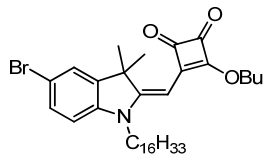

3,4-Dibutoxycyclobut-3-ene-1,2-dione (210 mg, 928 μmol) and 1-butanol (1 ml) were placed in a flask and **6** (548 mg, 928 μmol) was added in portions under vigorous stirring. Afterwards NEt_3 (330 μl, 2.32 mmol) was added and the solution refluxed for 18 h. The mixture was concentrated and Et_2O (10 ml) was added. The precipitate was filtered off and the solvent of the filtrate was evaporated under reduced pressure. The residue was purified by flash chromatography (eluent: pentane/Et_2O 7:1 → 6:1 → 3:1 → 1:4 → Et_2O/DCM 4:1) to obtain the yellow semisquaraine and blue squaraine in nearly equal yields. The semisquaraine was recrystallised from EtOH to give yellow needles.

Yield semisquaraine **9**: 142 mg (231 μmol, 25%) of yellow needles

(Yield squaraine (**M5**): 112 mg (112 μmol, 24%) of a green solid)

$C_{35}H_{52}BrNO_3$ [614.70]

^{1}H-NMR (600.1 MHz, $CDCl_3$):

δ [ppm] = 7.37 (dd, ^3J = 8.2 Hz, ^4J = 1.9 Hz, 1 H, H-6), 7.35 (d, ^4J = 1.6 Hz, 1 H, H-4), 6.72 (d, ^3J = 8.3 Hz, 1 H, H-7), 5.39 (s, 1 H, H-8), 4.85 (t, ^3J = 6.7 Hz, 2 H, OCH_2), 3.76 (t, ^3J = 7.5 Hz, 2 H, NCH_2), 1.89–1.83 (m, 2 H, CH_2), 1.74–1.68 (m, 2 H, CH_2), 1.60 (s, 6 H, H-9), 1.54–1.47 (m, 2 H, CH_2), 1.41–1.32

[1] The signal of the primary C-atoms splits into two signals of equal intensity even though they are supposed just to give one single signal. Possibly this is due to the alkyl side chain, which has a stereocenter but is of racemic character.

(4 H, CH_2), 1.31–1.21 (22 H, CH_2), 1.00 (t, ^3J = 7.4 Hz, 3 H, CH_3), 0.88 (t, ^3J = 7.0 Hz, 3 H, CH_3).

^{13}C-NMR (150.9 MHz, $CDCl_3$):

δ[ppm] = 192.5 (quart), 188.0 (quart), 187.9 (quart), 173.4 (quart), 167.2 (quart), 142.9 (quart), 141.9 (quart), 130.6 (tert), 125.4 (tert), 115.0 (quart), 109.6 (tert), 81.7 (tert), 73.9 (sec), 47.9 (quart), 43.1 (sec), 32.1 (sec), 31.9 (sec), 29.69 (sec), 29.68 (sec), 29.67 (sec), 29.65 (sec), 29.64 (sec), 29.59 (sec), 29.52 (sec), 29.45 (sec), 29.35 (sec), 29.27 (sec), 26.98 (sec), 26.95 (prim), 26.2 (sec), 22.7 (sec), 18.7 (sec), 14.1 (prim), 13.7 (prim).

ESI-MS pos (high resolution): [M^{+}]

calc.: 613.31251 m/z

found: 613.31250 m/z Δ = 0.02 ppm.

*Synthesis of the semisquaraine acid **10***

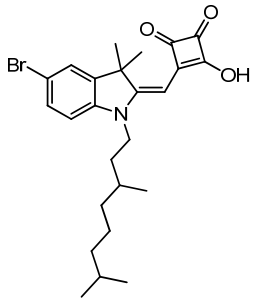

The semisquaraine ester **8** (211 mg, 420 μmol) was dissolved in acetone (15 ml) and heated to boiling point. HCl (2N in H_2O, 14 ml) was added and the mixture refluxed until TLC indicated a complete reaction. The solvent was removed under reduced pressure and the residue was dried in vacuo.

Yield: 189 mg (398 μmol, 95%) of a yellow-brown solid

$C_{25}H_{32}BrNO_3$ [474.43]

^{1}H-NMR (400.1 MHz, d^6-aceton):

δ [ppm] = 7.56 (d, ^{4}J = 2.0 Hz, 1 H, H-4), 7.45 (dd, ^{3}J = 8.4 Hz, ^{4}J = 2.0 Hz, 1 H, H-6), 7.03 (d, ^{3}J = 8.4 Hz, 1 H, H-7), 5.37 (s, 1 H, C*H*), 3.71–3.82 (m, 2 H, NCH_2), 1.82–1.71 (m, 1 H, C*H*), 1.70–1.48 (9 H, C*H*, CH_2, CH_3), 1.48–1.12 (6 H, CH_2), 1.05 (d, ^{3}J = 6.4 Hz, 3 H, CH_3), 0.86 (d, ^{3}J = 6.4 Hz, 6 H, CH_3).

^{13}C-NMR (150.9 MHz, $CDCl_3$):

δ [ppm] = 189.0 (quart), 186.0 (quart), 177.0 (quart), 170.3 (quart), 143.4 (quart), 141.2 (quart), 130.9 (tert), 125.7 (tert), 124.8 (quart), 116.7 (quart), 110.4 (tert), 83.2 (tert), 48.9 (quart), 42.1 (sec), 39.1 (sec), 37.0 (sec), 33.2 (sec), 31.0 (tert), 28.0 (tert), 26.8 (prim), 24.6 (sec), 22.7 (prim), 19.6 (prim).

*Synthesis of the semisquaraine acid **11***

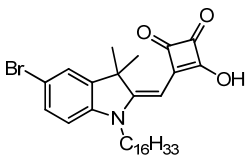

The semisquaraine ester **9** (240 mg, 390 μmol) was dissolved in acetone (30 ml) and heated to boiling point. HCl (2N in H_2O, 1.5 ml) was added and the solution refluxed for further 3 h. After 3 h, HCl (2N in H_2O, 7 ml) was added and the solution further refluxed for 18 h. The solvent was evaporated and the residue was dissolved in Et_2O (30 ml) and washed with H_2O (3 × 40 ml). The organic layer was dried over $MgSO_4$ and the solvent was removed in vacuo. The product was obtained by dropping a concentrated DCM solution into hexane and used without further purification.

Yield: 150 mg (269 μmol, 69%) of a brown solid

$C_{31}H_{44}BrNO_3$ [558.59]

^{1}H-NMR (400.1 MHz, d^6-acetone):

δ [ppm] = 7.55 (1 H, H-4), 7.42 (dd, ^{3}J = 8.3 Hz, ^{4}J = 1.9 Hz, 1 H, H-6), 7.05 (d, ^{3}J = 8.1 Hz, 1 H, H-7), 5.62 (s, 1 H, H-8), 4.05–3.85 (m, 2 H, NCH_2), 1.83–

2.73 (m, 2 H, CH_2), 1.66 (s, 6 H, H-9), 1.50–1.34 (4 H, CH_2), 1.34–1.21 (22 H, CH_2), 0.87 (t, ^3J = 7.0 Hz, 3 H, CH_3).

Synthesis of ***12***[334]

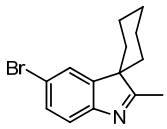

CA [468774–85–8]

p-Bromophenylhydrazin hydrochloride (8.07 g, 36.1 mmol), 1-cyclohexylethanone (5.47 g, 43.3 mmol) and acetic acid (80 ml) were refluxed for 6 h and stirred at rt for 18 h. The solvent was removed under reduced pressure and the residue was dissolved in Et_2O (80 ml) and H_2O (80 ml). The aqueous phase was extracted with PE (2 × 80 ml) and Et_2O (80 ml) and the combined organic phases were washed with aqueous KOH (10%, 5 × 80 ml), H_2O (6 × 80 ml) and brine (50 ml) and dried over $MgSO_4$. The solvent was evaporated under reduced pressure.

Yield: 8.94 g (32.1 mmol, 89%) of a brownish oil

$C_{14}H_{16}BrN$ [278.19]

^{1}H-NMR (400.1 MHz, $CDCl_3$):

δ [ppm] = 7.83 (d, ^3J = 1.8 Hz, 1 H), 7.49–7.41 (2 H), 2.30 (s, 3 H, CH_3), 2.10–1.20 (10 H, CH_2).

*Synthesis of **13***

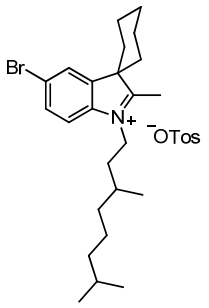

Indolenine derivative **12** (3.00 g, 10.8 mmol) and **1** (3.71 g, 11.9 mmol) were refluxed in $MeNO_2$ (12 ml) for 18 h. Et_2O (80 ml) was added and the solution was left at –30°C for 2 h. The precipitate was filtered and washed with Et_2O.

Yield: 2.59 g (4.38 mmol, 41%) of a light brown solid

$C_{31}H_{44}BrNO_3S$ [419.46]

^{1}H-NMR (400.1 MHz, $CDCl_3$):

δ [ppm] = 7.98 (d, ^4J = 1.6 Hz, 1 H), 7.69 (dd, ^3J = 8.6 Hz, ^4J = 1.7 Hz, 1 H), 7.58–7.54 (AA', 2 H), 7.47 (d, ^3J = 8.6 Hz, 1 H), 7.04–7.00 (BB', 2 H), 4.70–4.53 (m, 2 H, NCH_2), 2.95 (s, 3 H, CH_3), 2.28 (s, 3 H, CH_3), 2.15–1.45 (14 H), 1.36–1.10 (6 H), 1.00 (d, ^3J = 6.2 Hz, 3 H), 0.84 (d, ^3J = 6.6 Hz, 6 H).

^{13}C-NMR (100.6 MHz, $CDCl_3$):

δ [ppm] = 195.2 (quart), 144.0 (quart), 142.7 (quart), 140.8 (quart), 138.8 (quart), 132.3 (tert), 129.2 (tert), 128.5 (tert), 126.0 (tert), 123.2 (quart), 11.7 (tert), 58.7 (quart), 47.8 (sec), 39.1 (sec), 37.0 (sec), 35.1 (sec), 31.1 (tert), 30.5 (sec), 30.4 (sec), 28.0 (tert), 24.7 (sec), 24.3 (sec), 22.8 (prim)[1], 22.7 (prim)[1], 21.4 (prim), 20.7 (2 × sec), 19.6 (prim), 15.8 (prim).

[1] The signal of the primary C-atoms splits into two signals of equal intensity even though they are supposed just to give one single signal. Possibly this is due to the alkyl side chain, which has a stereocenter but is of racemic character.

*Synthesis of **14***

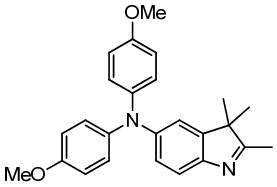

5-Bromo-2,3,3-trimethylindolenine (**4**) (314 mg, 1.32 mmol), P*t*Bu$_3$ (1 M in toluene, 80.0 μl, 79.1 μmol), 4,4'-dimethoxydiphenylamine (317 mg, 1.39 mmol) and NaO*t*Bu (190 mg, 1.98 mmol) were dissolved in dry toluene (8 ml) under a nitrogen atmosphere and the solution was degased with nitrogen for 15 min. Upon addition of $Pd_2dba_3 \cdot CHCl_3$ (54.6 mg, 52.7 μmol), the mixture was refluxed for 48 h. The solvent was removed under reduced pressure and the residue was purified by flash chromatography (eluent: DCM/EA 5:1). The crude product was used without further purification.

Yield: 230 mg (595 μmol, 45%)

$C_{25}H_{26}N_2O_2$ [386.49]

^{1}H-NMR (400.1 MHz, d^6-aceton):

δ [ppm] = 7.25 (d, ^3J = 8.2 Hz, 1 H, H-7), 7.15–6.95 (5 H), 6.87 (m, 4 H), 6.79 (dd, ^3J = 8.3 Hz, ^4J = 2.3 Hz, 1 H, H-6), 3.77 (s, 6 H, OCH_3), 2.17 (s, 3 H, H-8), 1.20 (s, 6 H, H-9).

ESI-MS pos (high resolution): $[M–HI]^+$

calc.: 386.19888 m/z

found: 386.19853 m/z Δ = 0.90 ppm.

*Synthesis of **15***

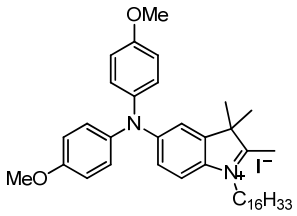

Compound **14** (314 mg, 812 μmol) and 1-iodohexadecane (429 mg, 1.22 mmol) were dissolved in MeCN (5 ml) and refluxed for 17 h. The mixture was concentrated and Et_2O (20 ml) was added. The resulting precipitate was filtered and washed with Et_2O.

Yield: 235 mg (318 μmol, 39%) of a brown solid

$C_{41}H_{59}IN_2O_2$ [738.83]

^{1}H-NMR (600.1 MHz, CD_2Cl_2):

δ[ppm] = 7.34 (d, ^3J = 8.9 Hz, 1 H, H-4), 7.12 (AA', 4 H), 6.92 (d, ^4J = 1.6 Hz, 1 H, H-7), 6.92–6.87 (5 H), 4.48 (t, ^3J = 7.6 Hz, 2 H, NCH_2), 3.80 (s, 6 H, OCH_3), 2.88 (s, 3 H, H-8), 1.90 (m, 2 H, NCH_2CH_2), 1.48 (s, 6 H, H-9), 1.44 (m, 2 H, CH_2), 1.35 (m, 2 H, CH_2), 1.32–1.12 (22 H), 0.87 (t, ^3J = 6.9 Hz, 3 H, CH_3).

^{13}C-NMR (150.9 MHz, CD_2Cl_2):

δ[ppm] = 189.7 (quart), 157.6 (quart), 151.6 (quart), 143.6 (quart), 139.4 (quart), 132.7 (quart), 128.0 (2 × tert), 118.1 (tert), 115.8 (tert), 115.4 (2 × tert), 112.1 (tert), 55.8 (prim), 54.2 (quart), 49.8, 32.2, 29.98, 29.97, 29.96, 29.94, 29.93, 29.88, 29.78, 29.65, 29.61, 29.41, 28.4, 27.0, 23.0 (each sec), 23.3 (2 × prim), 15.9 (prim), 14.2 (prim).

ESI-MS pos (high resolution): $[M–HI]^{\cdot+}$

calc.: 610.44928 m/z

found: 610.44929 m/z Δ = 0.02 ppm.

Synthesis of ***17***[335]

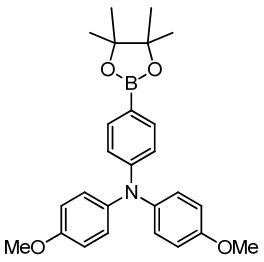

CA [875667–84–8]

4-Bromo-*N*,*N*-bis(4-methoxyphenyl)aniline (**16**) (2.59 g, 6.74 mmol) was dissolved in dry THF (30 ml) under nitrogen atmosphere and cooled to –78°C. *n*-BuLi (1.6 M in hexane, 4.75 ml, 7.41 mmol) was added slowly and the solution stirred at –78°C for 30 min. Triisopropyl borate (2.54 g, 13.5 mmol) was added and the reaction mixture was warmed slowly to rt within 2 h. The solution was treated with aqueous HCl (5%, 120 ml) and extracted with Et_2O (3 × 120 ml). The combined organic layers were dried over Na_2SO_4 and the mixture was concentrated to a volume of 200 ml. Pinacol (2.58 g, 21.8 mmol) was added and the reaction mixture was refluxed for 18 h. After cooling to rt the solvent was removed under reduced pressure and the residue was purified by flash chromatography (eluent: PE/DCM 1:2).

Yield: 1.47 g (3.41 mmol, 51%) of a colourless powder

$C_{26}H_{30}BNO_4$ [431.33]

^{1}H-NMR (400.1 MHz, d^6-aceton):

δ[ppm] = 7.53 (AA', 2 H), 7.08 (AA', 4 H), 6.92 (BB', 4 H), 6.77 (BB', 2 H), 3.80 (s, 6 H, OCH_3), 1.30 (s, 12 H, CH_3).

*Synthesis of 3-bromo-9-(3,7-dimethyloctyl)-carbazole **19***

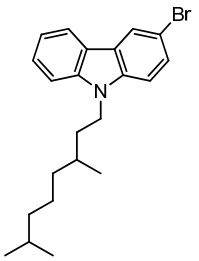

NaH (dispersion in mineral oil, 60%, 1.80 g, 45.0 mmol) was dissolved in dry THF (20 ml) under nitrogen atmosphere. Consecutively, 3-bromo-9*H*-carbazole (**18**) (8.85 g, 36.0 mmol) and 3,7-dimethyloctyl bromide (9.94 g, 45.0 mmol) were added and the solution refluxed for 36 h. The solvent was removed under reduced pressure and the residue dissolved in DCM (60 ml) and H_2O (30 ml). The phases were separated and the aqueous phase was extracted with DCM (2 × 60 ml). The combined organic phases were dried over $MgSO_4$ and the solvent was removed under reduced pressure. The residue was purified by flash chromatography (eluent: PE).

Yield: 12.8 g (33.1 mmol, 92%) of a colourless solid

$C_{22}H_{28}BrN$ [386.37]

^{1}H-NMR (400.1 MHz, $CDCl_3$):

δ [ppm] = 8.20 (dd, ^4J = 2.0 Hz, ^5J = 0.5 Hz, 1 H, H-4), 8.06–8.02 (m, 1 H, C*H*), 7.53 (dd, ^3J = 8.6 Hz, ^4J = 2.0 Hz, 1 H, H-2), 7.51–7.46 (m, 1 H, C*H*), 7.41–7.37 (m, 1 H, C*H*), 7.27 (dd, ^3J = 8.7 Hz, ^5J = 0.4 Hz, 1 H, H-1), 7.26–7.21 (m, 1 H, C*H*), 4.36–4.22 (m, 2 H, NCH_2), 1.90–1.80 (m, 1 H, C*H*), 1.69–1.58 (m, 1 H, C*H*), 1.58–1.45 (m, 2 H, CH_2), 1.39–1.28 (m, 2 H, CH_2), 1.28–1.18 (m, 2 H, CH_2), 1.18–1.08 (m, 2 H, CH_2), 1.02 (d, ^3J = 6.6 Hz, 3 H, CH_3), 0.85 (d, ^3J = 6.6 Hz, 6 H, CH_3).

^{13}C-NMR (100.6 MHz, $CDCl_3$):

δ [ppm] = 140.5 (quart), 138.9 (quart), 128.2 (tert), 126.3 (tert), 124.6 (quart), 123.1 (tert), 121.8 (quart), 120.6 (tert), 119.2 (tert), 111.5 (quart), 110.0 (tert),

108.8 (tert), 41.3 (sec), 39.2 (sec), 37.1 (sec), 35.5 (sec), 30.9 (tert), 27.9 (tert), 24.6 (sec), 22.64 (prim)[1], 22.56 (prim)[1], 19.7 (prim).

*Synthesis of **20***

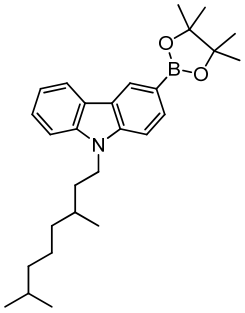

3-Bromo-9-(3,7-dimethyloctyl)-carbazole (**19**) (570 mg, 1.48 mmol) was dissolved in dry THF (10 ml) under nitrogen atmosphere and the solution cooled to –78°C. *n*BuLi (2.6 M in toluene, 624 μl, 1.62 mmol) was added dropwise and the mixture was stirred at –78°C for 2 h. After 2-isopropoxy-4,4,5,5-tetramethyl-1,3,2-dioxaborolane (549 mg, 2.95 mmol) was added, the solution was stirred at –78°C for further 2 h and at rt for 18 h. The reaction was quenched with H_2O (20 ml) and extracted with Et_2O (3 × 20 ml). The combined organic phases were dried over Na_2SO_4 and the solvent was removed under reduced pressure. The residue was purified by flash chromatography (eluent: PE/DCM 3:1 → DCM).

Yield: 345 mg (796 μmol, 54%) of a colourless oil

$C_{28}H_{40}BNO_2$ [433.44]

^{1}H-NMR (400.1 MHz, $CDCl_3$):

δ[ppm] = 8.61–8.58 (m, 1 H, C*H*), 8.15–8.11 (m, 1 H, C*H*), 7.92 (dd, ^3J = 8.0 Hz, ^4J = 1.2 Hz, 1 H, H-2), 7.49–7.43 (m, 1 H, C*H*), 7.42–7.38 (m, 2 H, C*H*), 7.38 (dd, ^3J = 8.0 Hz, ^5J = 0.4 Hz, 1 H, H-1), 4.38–4.25 (m, 2 H, NCH_2),

[1] The signal of the primary C-atoms splits into two signals of equal intensity even though they are supposed just to give one single signal. Possibly this is due to the alkyl side chain, which has a stereocenter but is of racemic character.

1.92–1.81 (m, 1 H, C*H*), 1.72–1.60 (m, 1 H, C*H*), 1.59–1.42 (m, 2 H, CH_2), 1.40 (s, 12 H, CH_3), 1.38–1.08 (6 H, CH_2), 1.03 (d, ^3J = 6.5 Hz, 3 H, CH_3), 0.85 (d, ^3J = 6.8 Hz, 6 H, CH_3).

^{13}C-NMR (150.9 MHz, $CDCl_3$):

δ [ppm] = 142.4 (quart), 140.3 (quart), 132.1 (tert), 127.8 (tert), 125.6 (tert), 123.1 (quart), 122.6 (quart), 120.6 (tert), 119.2 (tert), 108.6 (tert), 107.9 (tert), 83.552 (quart), 83.549 (2 × quart), 41.3 (sec), 39.2 (sec), 37.1 (sec), 35.5 (sec), 30.9 (tert), 27.9 (tert), 24.9 (prim), 24.6 (sec), 22.7 (prim)[1], 22.6 (prim)[1], 19.7 (prim).

Synthesis of 2-bromo-9-(3,7-dimethyloctyl)-carbazole ***22***

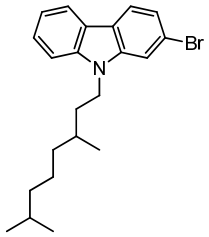

2-Bromo-9*H*-carbazole (**21**) (1.65 g, 6.70 mmol) was suspended in DMF (25 ml) and NaH (dispersion in mineral oil, 60%, 375 mg, 8.05 mmol) was added. After the mixture was stirred at rt for 1 h, 3,7-dimethyloctyl bromide (1.78 g, 8.05 mmol) was added and the mixture was stirred for another 18 h. H_2O (50 ml) was added and the solution was extracted with Et_2O (3 × 20 ml). The combined organic phases were dried over Na_2SO_4 and the solvent removed under reduced pressure. The residue was purified by flash chromatography (eluent: hexane).

Yield: 1.29 g (3.34 mmol, 50%) of a colourless solid

$C_{22}H_{28}BrN$ [386.37]

[1] The signal of the primary C-atoms splits into two signals of equal intensity even though they are supposed just to give one single signal. Possibly this is due to the alkyl side chain, which has a stereocenter but is of racemic character.

^{1}H-NMR (400.1 MHz, $CDCl_3$):

δ[ppm] = 8.08–8.04 (m, 1 H, C*H*), 7.93 (dd, ^3J = 8.0 Hz, ^5J = 0.4 Hz, 1H, H-4), 7.54–7.52 (m, 1 H, C*H*), 7.51–7.46 (m, 1 H, C*H*), 7.41–7.38 (m, 1 H, C*H*), 7.33 (dd, ^3J = 8.4 Hz, ^4J = 1.6 Hz, 1 H, H-3), 7.24–7.22 (m, 1 H, C*H*), 4.34–4.19 (m, 2 H, NCH_2), 1.93–1.79 (m, 1 H, C*H*), 1.73–1.60 (m, 1 H, CH_2), 1.59–1.48 (m, 2 H, CH_2), 1.43–1.30 (m, 2 H, CH_2), 1.30–1.18 (m, 2 H, CH_2), 1.18–1.10 (m, 2 H, CH_2), 1.04 (d, ^3J = 6.8 Hz, 3 H, CH_3), 0.87 (d, ^3J = 6.6 Hz, 6 H, CH_3).

^{13}C-NMR (100.6 MHz, $CDCl_3$):

δ [ppm] = 141.1 (quart), 140.4 (quart), 126.0 (tert), 122.4 (quart), 121.9 (tert), 121.8 (quart), 121.5 (tert), 120.4 (tert), 119.3 (tert), 119.2 (quart), 111.6 (tert), 108.8 (tert), 41.4 (sec), 39.2 (sec), 37.1 (sec), 35.5 (sec), 30.9 (tert), 28.0 (tert), 24.6 (sec), 22.7 (prim)[1], 22.6 (prim)[1], 19.8 (prim).

*Synthesis of **23***

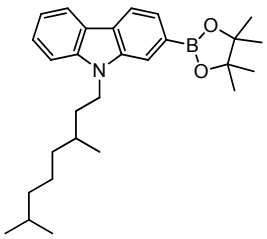

2-Bromo-9-(3,7-dimethyloctyl)-carbazole (**22**) (1.28 g, 3.32 mmol) was dissolved in dry THF (20 ml) under nitrogen atmosphere and the solution cooled to –78°C. *n*BuLi (2.6 M in toluene, 1.40 ml, 3.64 mmol) was added dropwise and the mixture was stirred at –78°C for 2 h. After 2-isopropoxy-4,4,5,5-tetramethyl-1,3,2-dioxaborolane (1.23 g, 6.63 mmol) was added, the solution was stirred at –78°C for further 2 h and at rt for 18 h. The reaction was quenched with H_2O (100 ml) and extracted with Et_2O

[1] The signal of the primary C-atoms splits into two signals of equal intensity even though they are supposed just to give one single signal. Possibly this is due to the alkyl side chain, which has a stereocenter but is of racemic character.

(3 × 60 ml). The combined organic phases were dried over Na_2SO_4 and the solvent was removed under reduced pressure. The residue was purified by flash chromatography (eluent: PE/DCM 5:1 → DCM).

Yield: 779 mg (1.80 mmol, 54%) of a brown oil

$C_{28}H_{40}BNO_2$ [433.44]

^{1}H-NMR (400.1 MHz, $CDCl_3$):

δ [ppm] = 8.14–8.09 (2 H, C*H*), 7.89–7.87 (m, 1 H, C*H*), 7.69 (dd, ^3J = 8.0 Hz, ^5J = 0.8 Hz, 1 H, H-4), 7.56–7.45 (m, 1 H, C*H*), 7.42–7.38 (m, 1 H, C*H*), 7.25–7.19 (m, 1 H, C*H*), 4.43–4.30 (m, 2 H, NCH_2), 1.93–1.82 (m, 1 H, C*H*), 1.75–1.62 (m, 1 H, C*H*), 1.61–1.47 (m, 2 H, CH_2), 1.41 (s, 12 H, CH_3), 1.45–1.10 (6 H, CH_2), 1.04 (d, ^3J = 6.4 Hz, 3 H, CH_3), 0.86 (d, ^3J = 6.4 Hz, 6 H, CH_3).

^{13}C-NMR (150.9 MHz, $CDCl_3$):

δ [ppm] = 140.8 (quart), 139.8 (quart), 126.1 (tert), 125.4 (quart), 124.9 (tert), 122.6 (quart), 120.8 (tert), 119.6 (tert), 118.6 (tert), 114.9 (tert), 108.7 (tert), 83.7 (3 × quart), 41.2 (sec), 39.2 (sec), 37.1 (sec), 35.7 (sec), 30.9 (tert), 27.9 (tert), 24.9 (prim), 24.6 (sec), 22.7 (prim)[1], 22.6 (prim)[1], 19.8 (prim).

[1] The signal of the primary C-atoms splits into two signals of equal intensity even though they are supposed just to give one single signal. Possibly this is due to the alkyl side chain, which has a stereocenter but is of racemic character.

*Synthesis of 1-(3,7-dimethyloctyl)-3,3-dimethyl-2-methylene-5-(4-methyl-piperazin-1-yl)indoline (**24**)*

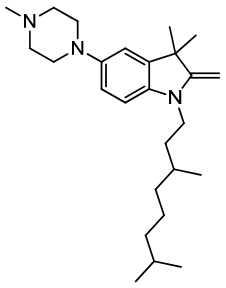

5-Bromo-1-(3,7-dimethyloctyl)-3,3-dimethyl-2-methyleneindoline (**7**) (447 mg, 1.18 mmol), 1-methylpiperazine (118 mg, 1.18 mmol), P*t*Bu$_3$ (1 M in toluene, 70.9 μl, 70.9 μmol) and NaO*t*Bu (170 mg, 1.77 mmol) were dissolved in dry toluene (7 ml) under nitrogen atmosphere and degassed in a stream of nitrogen for 10 min. $Pd_2dba_3{\cdot}CHCl_3$ (48.9 mg, 47.0 μmol) was added and the mixture was refluxed for 2 d. The solvent was removed under reduced pressure and the residue was purified by flash chromatography (eluent: EA/MeOH 6:1). The compound was further used straight after ^{1}H-NMR proof.

Yield: 200 mg (503 μmol, 43%) of a brown-blue solid

$C_{26}H_{43}N_3$ [397.64]

^{1}H-NMR (400.1 MHz, $CDCl_3$):

δ[ppm] = 6.83 (d, ^4J = 2.4 Hz, 1 H, H-4), 6.72 (dd, ^3J = 8.4 Hz, ^4J = 2.4 Hz, 1 H, H-6), 6.40 (d, ^3J = 8.3 Hz, 1 H, H-7), 3.78 (1 H, C*H*), 3.76 (1 H, C*H*), 3.52–3.38 (m, 2 H, NCH_2), 3.12–3.07 (m, 4 H, CH_2), 2.66–2.59 (m, 4 H, CH_2), 2.38 (s, 3 H, CH_3), 1.68–1.58 (m, 1 H, C*H*), 1.56–1.46 (m, 2 H, CH_2), 1.45–1.38 (m, 1 H, C*H*), 1.31 (s, 6 H, CH_3), 1.28–1.22 (m, 2 H, CH_2), 1.20–1.10 (4 H, CH_2), 0.96 (d, ^3J = 6.5 Hz, 3 H, CH_3), 0.86 (d, ^3J = 6.6 Hz, 6 H, CH_3).

ESI-MS pos (high resolution): [MH^+]

calc.: 398.35298 m/z

found: 398.35286 m/z Δ = 0.30 ppm.

*Synthesis of N,N-bis(4-bromophenyl)-4-methoxyaniline (**25**)*[336]

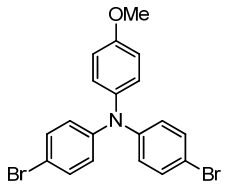

CA [100308–69–8]

Bis(4-bromophenyl)amine (1.00 g, 3.06 mmol), 4-iodoanisole (1.07 g, 4.59 mmol), 1,10-phenanthroline (10.5 mg, 58.1 μmol), CuI (11.1 mg, 58.1 μmol), and KOH (515 mg, 9.17 mmol) were suspended in dry toluene (20 ml) under nitrogen atmosphere and degassed with a stream of nitrogen for 10 min. After the mixture was refluxed for 6 d, the solvent was evaporated under reduced pressure and the residue was dissolved in DCM (40 ml) and H_2O (40 ml). Upon separation of the layers, the aqueous layer was extracted with DCM (3 × 40 ml). The combined organic layers were washed with a concentrated $Na_2S_2O_3$ solution (2 × 40 ml) and H_2O (40 ml) and dried over $MgSO_4$. The solvent was evaporated under reduced pressure and the residue purified by flash chromatography (eluent: PE/DCM 10:1).

Yield: 864 mg (2.00 mmol, 65%) of a colourless powder

$C_{19}H_{15}Br_2NO$ [433.14]

^{1}H-NMR (400.1 MHz, d^6-acetone):

δ [ppm] = 7.39 (AA‘, 4 H), 7.08 (AA‘, 2 H), 6.98–6.86 (6 H), 3.81 (s, 3 H, OCH_3).

*Synthesis of **26***

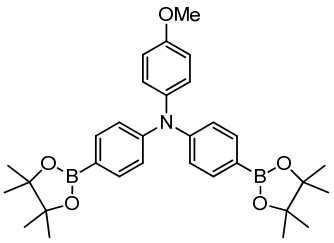

N,*N*-bis(4-bromophenyl)-4-methoxyaniline (**25**) (775 mg, 1.79 mmol) was dissolved in dry THF (20 ml) under nitrogen atmosphere and cooled to –78°C. *n*BuLi (1.6 M in hexane, 2.46 ml, 3.94 mmol) was added slowly and the mixture stirred at –78°C for 30 min. 2-Isopropoxy-4,4,5,5-tetramethyl-1,3,2-dioxoborolan (733 mg, 3.94 mmol) was added and the reaction mixture was warmed to rt slowly within 2 h. The solution was treated with aqueous HCl (5%, 36 ml) and extracted with Et_2O (3 × 25 ml). The combined organic layers were dried over Na_2SO_4 and the solvent evaporated under reduced pressure. The residue was purified by flash chromatography (eluent: PE/DCM 1:1) and the product was obtained as a colourless powder after recrystallisation from EtOH.

Yield: 172 mg (330 μmol, 18%) of a colourless powder

$C_{31}H_{39}B_2NO_5$ [527.27]

^{1}H-NMR (400.1 MHz, d^6-acetone):

δ[ppm] = 7.64 (AA', 4 H), 7.10 (AA', 2 H), 7.01 (BB', 4 H), 6.98 (BB', 2 H), 3.82 (3 H, OCH_3), 1.32 (s, 24 H, CH_3).

^{13}C-NMR (100.6 MHz, d^6-acetone):

δ[ppm] = 158.2 (quart), 151.3 (quart), 140.5 (quart), 136.7 (tert), 129.1 (tert), 122.4 (tert), 115.9 (tert), 84.3 (2 × quart), 55.8 (prim), 25.1 (prim).

*Synthesis of 2,7-dibromo-9-(3,7-dimethyloctyl)-carbazole (**28**)*

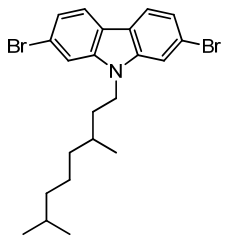

CA [1293358–80–1]

2,7-Dibromo-9*H*-carbazole (**27**) (3.00 g, 9.23 mmol) was suspended in DMF (50 ml) and NaH (dispersion in mineral oil, 60%, 520 mg, 13.0 mmol) was added. After the mixture was stirred at rt for 1 h, 3,7-dimethyloctyl bromide (2.45 g, 11.1 mmol) was added and the mixture was stirred for another 18 h. H_2O (50 ml) was added and the solution was extracted with Et_2O (3 × 20 ml). The combined organic phases were dried over Na_2SO_4 and the solvent removed under reduced pressure. The residue was purified by flash chromatography (eluent: hexane).

Yield: 3.96 g (8.49 mmol, 92%) of a colourless solid

$C_{22}H_{27}Br_2N$ [465.26]

^{1}H-NMR (400.1 MHz, $CDCl_3$):

δ [ppm] = 7.88 (dd, ^3J = 8.2 Hz, ^5J = 0.4 Hz, 2 H, H-4/5), 7.51 (d, ^4J = 1.4 Hz, 2 H, H-1/8), 7.34 (dd, ^3J = 8.3 Hz, ^4J = 1.6 Hz, 2 H, H-3/6), 4.28–4.13 (m, 2 H, NCH_2), 1.87–1.76 (m, 1 H, CH), 1.70–1.60 (m, 1 H, CH), 1.58–1.48 (m, 2 H, CH2), 1.42–1.30 (m, 2 H, CH_2), 1.30–1.20 (m, 2 H, CH_2), 1.20–1.10 (m, 2 H, CH_2), 1.03 (d, ^3J = 6.5 Hz, 3 H, CH_3), 0.87 (d, ^3J = 6.6 Hz, 6 H, CH_3).

*Synthesis of **29***

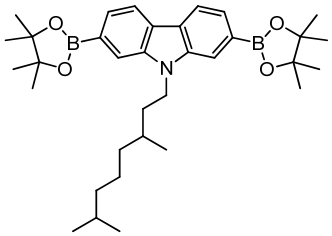

2,7-Dibromo-9-(3,7-dimethyloctyl)-carbazole (**28**) (1.50 g, 3.22 mmol) was dissolved in dry THF (40 ml) under nitrogen atmosphere and the solution cooled to –78°C. *t*BuLi (1.9 M in pentane, 7.47 ml, 14.2 mmol) was added dropwise and the mixture was stirred at –78°C for 4 h. After 2-isopropoxy-4,4,5,5-tetramethyl-1,3,2-dioxaborolane (2.40 g, 12.9 mmol) was added, the solution was stirred at –78°C for further 2 h and at rt for 48 h. The reaction was quenched with H_2O (50 ml) and extracted with Et_2O (3 × 40 ml). The combined organic phases were dried over Na_2SO_4 and the solvent was removed under reduced pressure. The residue was purified by flash chromatography (eluent: PE/DCM 1:1).

Yield: 499 mg (892 μmol, 28%) of a light brown solid

$C_{34}H_{51}B_2NO_4$ [559.40]

^{1}H-NMR (400.1 MHz, $CDCl_3$):

δ [ppm] = 8.12 (dd, ^3J = 7.6 Hz, ^5J = 0.8 Hz, 2 H, C*H*), 7.87–7.88 (m, 2 H, C*H*), 7.68 (dd, ^3J = 7.6 Hz, ^5J = 0.8, 2 H, C*H*), 4.48–4.37 (m, 2 H, NCH_2), 1.93–1.83 (m, 1 H, C*H*), 1.75–1.65 (m, 1 H, C*H*), 1.64–1.48 (4 H, CH_2), 1.40 (s, 24 H, CH_3), 1.33–1.11 (4 H, CH_2), 1.03 (d, ^3J = 6.8 Hz, 3 H, CH_3), 0.87 (d, ^3J = 6.4 Hz, 6 H, CH_3).

^{13}C-NMR (100.6 MHz, $CDCl_3$):

δ [ppm] = 140.5 (quart), 125.3 (quart), 125.0 (tert), 120.2 (tert), 115.3 (tert), 83.9 (2 × quart), 41.3 (sec), 39.4 (sec), 37.2 (sec), 36.0 (sec), 31.1 (tert), 28.1 (tert), 25.8 (prim), 24.7 (sec), 22.9 (prim)[1], 22.8 (prim)[1], 20.0 (prim).

*Synthesis of 3,6-dibromo-9-(3,7-dimethyloctyl)-carbazole (**31**)*[337]

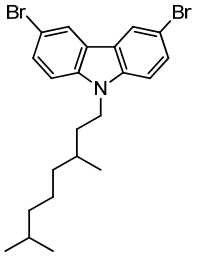

CA [409104–51–4]

3,6-Dibromo-9*H*-carbazole (**30**) (1.30 g, 4.00 mmol), 3,7-dimethyloctyl tosylate (**1**) (1.98 g, 6.32 mmol) and K_2CO_3 (1.66 g, 12.0 mmol) were stirred at 50°C in DMF (24 ml) under nitrogen atmosphere for 44 h. H_2O was added (70 ml) and the mixture was extracted with DCM (3 × 30 ml). The combined organic phases were washed with H_2O (2 × 30 ml), dried over Na_2SO_4 and the solvent removed under reduced pressure. The residue was purified by flash chromatography (eluent: hexane → hexane/DCM 2:1).

Yield: 1.06 g (2.27 mmol, 57%) of a colourless liquid that turned into a solid over night

$C_{22}H_{27}Br_2N$ [465.26]

^{1}H-NMR (400.1 MHz, $CDCl_3$):

δ [ppm] = 8.14 (d, ^4J = 1.8 Hz, 2 H, H-4/5), 7.55 (dd, ^3J = 8.7 Hz, ^4J = 1.9 Hz, 2 H, H-2/7), 7.26 (d, ^3J = 8.7 Hz, 2 H, H-1/8), 4.34–4.18 (m, 2 H, NCH_2), 1.87–1.76 (m, 1 H, C*H*), 1.66–1.55 (m, 1 H, C*H*), 1.55–1.44 (m, 2 H, CH_2), 1.38–1.24

[1] The signal of the primary C-atoms splits into two signals of equal intensity even though they are supposed just to give one single signal. Possibly this is due to the alkyl side chain, which has a stereocenter but is of racemic character.

(m, 2 H, CH_2), 1.24–1.14 (m, 2 H, CH_2), 1.14–1.06 (m, 2 H, CH_2), 1.01 (d, ^3J = 6.6 Hz, 3 H, CH_3), 0.85 (d, ^3J = 6.6 Hz, 6 H, CH_3).

*Synthesis of **32***

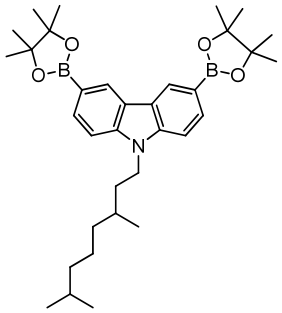

3,6-Dibromo-9-(3,7-dimethyloctyl)-carbazole (**31**) (1.00 g, 2.15 mmol) was dissolved in dry THF (20 ml) under nitrogen atmosphere and the solution cooled to –78°C. *t*BuLi (1.7 M in pentane, 7.56 ml, 12.9 mmol) was added dropwise and the mixture was stirred at –78°C for 4 h. After 2-isopropoxy-4,4,5,5-tetramethyl-1,3,2-dioxaborolane (1.60 g, 8.60 mmol) was added, the solution was stirred at –78°C for further 2 h and at rt for 48 h. The reaction was quenched with H_2O (50 ml) and extracted with Et_2O (3 × 40 ml). The combined organic phases were dried over Na_2SO_4 and the solvent was removed under reduced pressure. The residue was purified by flash chromatography (eluent: PE/DCM 1:1).

Yield: 526 mg (940 μmol, 44%) of a light brown solid

$C_{34}H_{51}B_2NO_4$ [559.40]

^{1}H-NMR (400.1 MHz, $CDCl_3$):

δ [ppm] = 8.67–8.65 (m, 2 H, H-4/5), 7.89 (dd, ^3J = 8.0 Hz, ^4J = 1.2 Hz, 2 H, H-2/7), 7.37 (dd, ^3J = 8.0 Hz, ^4J = 0.4, 2 H, H-1/8), 4.28–4.37 (m, 2 H, NCH_2), 1.83–1.73 (m, 1 H, C*H*), 1.62–1.52 (m, 1 H, C*H*), 1.50–1.45 (m, 2 H, CH_2), 1.45–1.37 (m, 2 H, CH_2), 1.32 (s, 24 H, CH_3), 1.28–1.08 (m, 2 H, CH_2), 1.08–1.00 (m, 2 H, CH_2), 0.94 (d, ^3J = 6.8 Hz, 3 H, CH_3), 0.77 (d, ^3J = 6.8 Hz, 6 H, CH_3).

^{13}C-NMR (100.6 MHz, $CDCl_3$):

δ[ppm] = 142.7 (quart), 132.1 (tert), 128.3 (tert), 123.1 (quart), 108.1 (tert), 83.7 (2 × quart), 41.4 (sec), 39.4 (sec), 37.3 (sec), 35.7 (sec), 31.3 (tert), 28.1 (tert), 25.1 (prim), 24.7 (sec), 22.8 (prim)[1], 22.7 (prim)[1], 19.9 (prim).

*Synthesis of 1,4-bis(1-(3,7-dimethyloctyl)-3,3-dimethyl-2-methyleneindolin-5-yl)piperazine (**33**)*

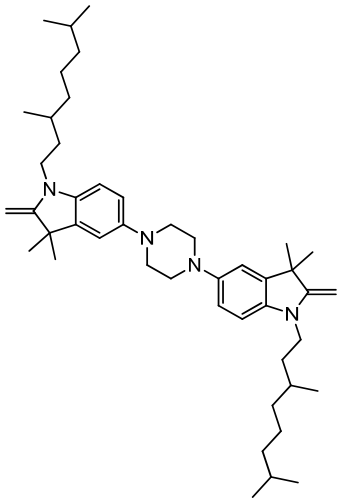

5-Bromo-1-(3,7-dimethyloctyl)-3,3-dimethyl-2-methyleneindoline (**7**) (710 mg, 1.88 mmol), piperazine (81.0 mg, 938 μmol), NaO*t*Bu (270 mg, 2.81 mmol), and P*t*Bu_3 (1 M in toluene, 113 μl, 113 μmol) were dissolved in dry toluene (8 ml) under inert nitrogen atmosphere (8 ml) and degassed in a stream of nitrogen for 10 min. $Pd_2dba_3 \cdot CHCl_3$ (78.0 mg, 75.0 μmol) was added and the solution was refluxed for 2 d. The solvent was removed under reduced pressure and the residue purified by flash chromatography (eluent: PE/EA/NEt_3 5:1:0.1). The raw product was immediately recrystallised from EtOH.

Yield: 187 mg (275 μmol, 29%) of a grey solid

[1] The signal of the primary C-atoms splits into two signals of equal intensity even though they are supposed just to give one single signal. Possibly this is due to the alkyl side chain, which has a stereocenter but is of racemic character.

$C_{46}H_{72}N_4$ [681.09]

^{1}H-NMR (600.1 MHz, d^6-acetone):

δ [ppm] = 6.99 (d, ^4J = 2.4 Hz, 2 H, H-4), 6.76 (dd, ^3J = 8.3 Hz, ^4J = 1.6 Hz, 2 H, H-6), 6.52 (d, ^3J = 8.3 Hz, 2 H, H-7), 3.83–3.77 (4 H, C*H*), 3.58–3.48 (m, 4 H, NCH_2), 3.16 (s, 8 H, NCH_2), 1.68–1.64 (m, 2 H, C*H*), 1.58–1.48 (m, 4 H, CH_2), 1.44–1.12 (26 H), 0.99 (d, ^3J = 6.7, 6 H, CH_3), 0.86 (d, ^3J = 6.7 Hz, 12 H, CH_3).

^{13}C-NMR (150.9 MHz, d^6-acetone):

δ [ppm] = 162.4 (quart), 146.19 (quart), 141.04 (quart), 139.1 (quart), 116.6 (tert), 114.3 (tert), 105.74 (tert), 72.6 (sec), 52.4 (sec), 45.1 (quart), 40.9 (sec), 39.9 (sec), 37.9 (sec), 33.1 (sec), 31.6 (tert), 30.4 (prim)[1], 30.3 (prim)[1], 28.7 (tert), 25.5 (sec), 23.0 (prim)[1], 22.9 (prim)[1], 20.2 (prim).

*Synthesis of N,N'-di(2-ethylhexyl)-2-bromonaphthalene diimide (**35**) and N,N'-di(2-ethylhexyl)-2,6-dibromonaphthalene diimide (**36**)*[243]

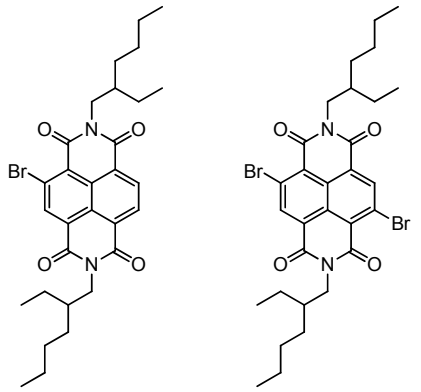

35 **36**

36: CA [861402–48–4]

[1] The signal of the primary C-atoms splits into two signals of equal intensity even though they are supposed just to give one single signal. Possibly this is due to the alkyl side chain, which has a stereocenter but is of racemic character.

A suspension of naphthalene-1,4,5,8-tetracarboxydianhydride (3.00 g, 11.2 mmol) in conc. H_2SO_4 (15 ml) was dripped into a solution of dibromoisocyanuric acid (6.42 mg, 22.4 mmol) in conc. H_2SO_4 (15 ml). The mixture was then stirred at 135°C for 15 h. After cooling to rt, the mixture was poured onto ice. The resulting precipitate was filtered, washed with H_2O (3 × 20 ml) and MeOH (3 × 20 ml), and dried in vacuo to yield a yellow powder (5.21 g).

This crude product and 2-ethylhexylamine (6.32 g, 48.9 mmol) were dissolved in glacial acetic acid (150 ml) under nitrogen atmosphere and the resulting mixture was stirred at 120°C for 4 h. Under reduced pressure, the mixture was concentrated to 20% of its volume and subsequently poured onto MeOH (300 ml). The precipitate was filtered, washed with MeOH, and dried in vacuo. The crude product was dissolved in PE/DCM (1:1) and the remaining insoluble yellow solid was filtered off. The solvent of the filtrate was removed under reduced pressure and the procedure was repeated with PE/DCM (2:1). The filtered solid turned out to be pure **36**. The solvent of the filtrate was removed under reduced pressure and the residue was purified by column chromatography (eluent: PE/DCM 1:1 → 2:3) to yield first additional **36** (total: 2.71 g, 4.18 mmol, 37%) and subsequently **35** (405 mg, 711 μmol, 6%).

N,*N*'-Di(2-ethylhexyl)-2-bromonaphthalene diimide (**35**):

Yield: 405 mg (711 μmol, 6%) of an orange solid

$C_{30}H_{37}BrN_2O_4$ [569.53]

^{1}H-NMR (400.1 MHz, $CDCl_3$):

δ [ppm] = 8.93 (s, 1 H), 8.81 (d, ^{3}J = 7.6 Hz, 1 H), 8.76 (d, 1 H, ^{3}J = 7.6 Hz), 4.25–4.05 (4 H, NCH_2), 2.05–1.80 (2 H, C*H*), 1.48–1.18 (16 H, CH_2), 0.96–0.91 (6 H, CH_3), 0.91–0.85 (6 H, CH_3).

^{13}C-NMR (100.6 MHz, $CDCl_3$):

δ [ppm] = 163.0 (quart), 162.4 (quart), 162.3 (quart), 161.5 (quart), 138.7 (tert), 131.9 (tert), 130.9 (tert), 128.85 (quart), 128.79 (quart), 126.9 (quart), 126.13

(quart), 126.06 (quart), 125.9 (quart), 124.1 (quart), 45.2 (sec), 44.9 (sec), 38.1 (tert), 37.9 (tert), 30.82 (sec), 30.79 (sec), 28.8 (sec), 28.7 (sec), 24.2 (sec), 24.1 (sec), 23.23 (sec), 23.16 (sec), 14.2 (2 × prim), 10.74 (prim), 10.71 (prim).

N,*N*'-Di(2-ethylhexyl)-2,6-dibromonaphthalene diimide (**36**):

Yield: 2.71 g (4.18 mmol, 37%) of a yellow solid

$C_{30}H_{36}Br_2N_2O_4$ [648.43]

^{1}H-NMR (400.1 MHz, $CDCl_3$):

δ [ppm] = 9.00 (s, 2 H), 4.21–4.10 (m, 4 H, NCH_2), 1.99–1.90 (m, 2 H, C*H*), 1.44–1.24 (16 H, CH_2), 0.94 (t, ^3J = 7.5 Hz, 6 H, CH_3), 0.89 (t, ^3J = 7.2 Hz, 6 H, CH_3).

5.2.2 Syntheses of Squaraine Monomers M1–M22

The squaraine monomer **M5**[157, 338] was synthesised according to literature procedures.

*Synthesis of **M1***

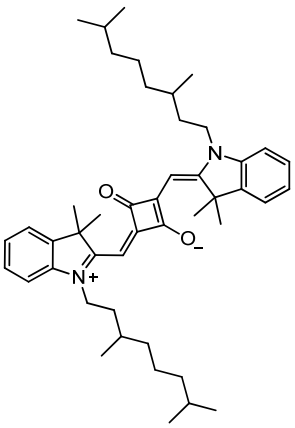

1-(3,7-Dimethyloctyl)-3,3-dimethyl-3*H*-indol-1-ium tosylate (**2**) (414 mg, 878 μmol) and 3,4-dihydroxycyclobut-3-ene-1,2-dione (50.1 mg, 439 μmol) were dissolved in pyridine (2 ml) and a mixture of toluene and 1-butanol (1:1, 40 ml) and refluxed for 4 h using a *Dean-Stark* trap. The solvent was evaporated under reduced pressure and the residue purified by flash chromatography (eluent: PE/EA 5:2 → 2:1). The crude product was dissolved in little DCM and an excess of hexane was added. The mixture was allowed to stand overnight. The precipitate was filtered and washed with hexane.

Yield: 178 mg (263 μmol, 60%) of a shiny green solid

$C_{46}H_{64}N_2O_2$ [677.01]

^{1}H-NMR (600.1 MHz, $CDCl_3$):

δ[ppm] = 7.36–7.34 (m, 2 H), 7.32–7.28 (m, 2 H), 7.16–7.12 (m, 2 H), 6.97–6.94 (m, 2 H), 5.96 (s, 2 H), 4.10–3.80 (m, 4 H, NCH_2), 1.84–1.74 (14 H, H-9, C*H*), 1.63–1.56 (m, 4 H, CH_2), 1.56–1.47 (m, 2 H, C*H*), 1.41–1.11 (12 H, CH_2), 1.04 (d, ^3J = 6.2 Hz, 6 H, CH_3), 0.86 (d, ^3J = 6.7 Hz, 12 H, CH_3).

^{13}C-NMR (150.9 MHz, $CDCl_3$):

δ [ppm] = 182.3 (quart), 179.6 (quart), 169.8 (quart), 142.4 (2 × quart), 127.7 (tert), 123.6 (tert), 122.3 (tert), 109.2 (tert), 86.4 (tert), 49.3 (quart), 42.1 (sec), 39.1 (sec), 37.1 (sec), 33.8 (sec), 31.2 (tert), 27.9 (tert), 27.0 (prim), 24.6 (sec), 22.7 (prim)[1], 22.6 (prim)[1], 19.6 (prim).

ESI-MS pos (high resolution): $[M^{\cdot+}]$

calc.: 676.49623 m/z

found: 676.49621 m/z Δ = 0.03 ppm.

*Synthesis of **M2***

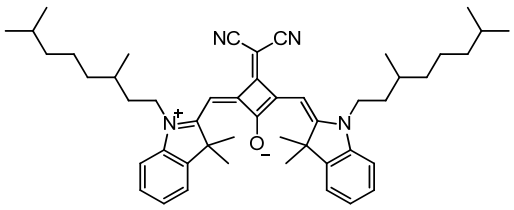

1-(3,7-Dimethyloctyl)-3,3-dimethyl-3*H*-indol-1-ium tosylate (**2**) (200 g, 424 μmol), **3** (64.5 mg, 202 μmol), and pyridine (7.5 ml) were refluxed in a mixture of toluene and 1-butanol (1:1, 16 ml) for 18 h. The solvent was evaporated and the residue purified by flash chromatography (eluent: DCM) and dried in vacuo. The product was recrystallised from hexane.

Yield: 100 mg (138 μmol, 68%) of green crystals

$C_{49}H_{64}N_4O$ [725.06]

^{1}H-NMR (600.1 MHz, $CDCl_3$):

δ [ppm] = 7.38–7.32 (4 H), 7.22–7.18 (m, 2 H), 7.03 (d, ^3J = 7.9 Hz, 2 H), 6.49 (s, 2 H, H-6), 4.10–3.98 (m, 4 H, NCH_2), 1.82–1.74 (14 H, H-9, C*H*), 1.70–1.58 (m,

[1] The signal of the primary C-atoms splits into two signals of equal intensity even though they are supposed just to give one single signal. Possibly this is due to the alkyl side chain, which has a stereocenter but is of racemic character.

4 H, CH_2), 1.55–1.48 (m, 2 H, C*H*), 1.42–1.29 (m, 4 H, CH_2), 1.30–1.18 (m, 4 H, CH_2), 1.18–1.11 (m, 4 H, CH_2), 1.03 (d, ^3J = 6.5 Hz, 6 H, CH_3), 0.86 (d, ^3J = 6.6 Hz, 12 H, CH_3).

^{13}C-NMR (150.9 MHz, $CDCl_3$):

δ[ppm] = 173.2 (quart), 171.7 (quart), 167.7 (quart), 166.6 (quart), 142.5 (quart), 141.9 (quart), 128.0 (tert), 124.5 (tert), 122.3 (tert), 118.9 (quart), 109.9 (tert), 89.0 (tert), 49.4 (quart), 42.9 (sec), 40.8 (quart), 39.1 (sec), 37.1 (sec), 34.1 (sec), 30.9 (tert), 28.0 (tert), 26.55 (prim)[1], 26.53 (prim)[1], 24.6 (sec), 22.7 (prim)[1], 22.6 (prim)[1], 19.7 (prim).

ESI-MS pos (high resolution): [M^{+}]

calc.: 724.50746 m/z

found: 724.50728 m/z Δ = 0.25 ppm.

*Synthesis of **M3***

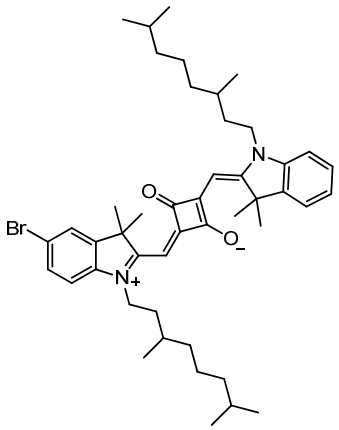

Semisquaraine **10** (154 mg, 324 μmol) and 1-(3,7-dimethyloctyl)-3,3-dimethyl-3*H*-indol-1-ium tosylate (**2**) (153 mg, 324 μmol) were dissolved in pyridine (4 ml) and a mixture of toluene and 1-butanol (1:1, 40 ml) and refluxed using a *Dean-Stark* trap for 17 h. The solvent was removed under reduced pressure and the residue was purified by

[1] The signal of the primary C-atoms splits into two signals of equal intensity even though they are supposed just to give one single signal. Possibly this is due to the alkyl side chain, which has a stereocenter but is of racemic character.

flash chromatography (eluent: DCM/Et_2O 40:1). The crude product was recrystallised from hexane.

Yield: 209 mg (276 μmol, 85%) of a green solid

$C_{46}H_{63}BrN_2O_2$ [755.91]

^{1}H-NMR (400.1 MHz, $CDCl_3$):

δ [ppm] = 7.43–7.41 (m, 1 H, C*H*), 7.39 (dd, ^3J = 8.4 Hz, ^4J = 2.0 Hz, 1 H, C*H*), 7.38–7.35 (m, 1 H, C*H*), 7.34–7.29 (m, 1 H, C*H*), 7.19–7.14 (m, 1 H, C*H*), 7.01–6.97 (m, 1 H, C*H*), 6.78 (d, ^3J = 8.4 Hz, 1 H, C*H*), 5.99 (s, 1 H, C*H*), 5.92 (s, 1 H, C*H*), 4.10–3.98 (m, 2 H, NCH_2), 3.98–3.84 (m, 2 H, NCH_2), 1.83–1.74 (14 H, H-9, C*H*), 1.57–1.47 (4 H, CH_2), 1.44–1.11 (14 H, C*H*, CH_2), 1.07–1.01 (m, 6 H, CH_3), 0.91–0.85 (12 H, CH_3).

^{13}C-NMR (150.9 MHz, $CDCl_3$):

δ [ppm] = 182.2 (quart), 181.2 (quart), 178.8 (quart), 170.8 (quart), 168.2 (quart), 144.2 (quart), 142.4 (quart), 142.2 (quart), 141.6 (quart), 130.6 (tert), 127.8 (tert), 125.7 (tert), 124.0 (tert), 122.4 (tert), 116.1 (quart), 110.1 (tert), 109.5 (tert), 86.8 (tert), 86.7 (tert), 49.5 (quart), 49.1 (quart), 42.3 (sec), 42.1 (sec), 39.133 (sec), 39.130 (sec), 37.093 (sec), 37.087 (sec), 33.9 (sec), 33.6 (sec), 31.2 (tert), 31.1 (tert), 27.94 (tert), 27.93 (tert), 27.1 (prim), 26.9 (prim), 24.7 (2 × sec), 22.7 (prim), 22.6 (prim), 19.6 (2 × prim).

*Synthesis of **M4***

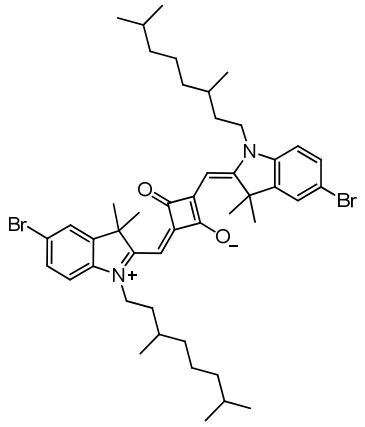

5-Bromo-1-(3,7-dimethyloctyl)-3,3-dimethyl-3*H*-indol-1-ium tosylate (**5**) (2.46 g, 4.48 mmol), and 3,4-dihydroxycyclobut-3-ene-1,2-dione (255 mg, 2.24 mmol) were dissolved in pyridine (5 ml) and a mixture of toluene and 1-butanol (1:1, 40 ml) and refluxed for 17 h using a *Dean-Stark* trap. The solvent was removed under reduced pressure and the residue purified by flash chromatography (eluent: DCM/EA 2:1 → 3:2). The crude product was dissolved in little DCM and an excess of hexane was added. The mixture was allowed to stand overnight. The precipitate was filtered and washed with hexane.

Yield: 1.51 g (1.81 mmol, 81%) of a shiny green solid

$C_{46}H_{62}Br_2N_2O_2$ [834.81]

^{1}H-NMR (600.1 MHz, $CDCl_3$):

δ [ppm] = 7.44 (d, ^4J = 1.8 Hz, 2 H, H-4), 7.41 (dd, ^3J = 8.4 Hz, ^4J = 1.9 Hz, 2 H, H-6), 6.81 (d, ^3J = 8.3 Hz, 2 H, H-7), 5.94 (s, 2 H, H-8), 4.10–3.80 (m, 4 H, NCH_2), 1.88–1.72 (14 H, H-9, C*H*), 1.63–1.55 (m, 4 H, CH_2), 1.55–1.47 (m, 2 H, C*H*), 1.40–1.30 (m, 4 H, CH_2), 1.29–1.10 (8 H, CH_2), 1.03 (d, ^3J = 6.1 Hz, 6 H, CH_3), 0.86 (d, ^3J = 6.7 Hz, 12 H, CH_3).

^{13}C-NMR (150.9 MHz, $CDCl_3$):

δ [ppm] = 182.1 (quart), 180.5 (quart), 169.3 (quart), 144.3 (quart), 141.4 (quart), 130.7 (tert), 125.7 (tert), 116.6 (quart), 110.5 (tert), 87.0 (tert), 49.3 (quart), 42.2

(sec), 39.1 (sec), 37.1 (sec), 33.7 (sec), 31.1 (tert), 27.9 (tert), 27.01 (prim)[1], 27.00 (prim)[1], 24.6 (sec), 22.67 (prim)[1], 22.56 (prim)[1], 19.6 (prim).

ESI-MS pos (high resolution): [$M^{\cdot+}$]

calc.: 832.31726 m/z

found: 832.31727 m/z Δ = 0.01 ppm.

*Synthesis of **M6***

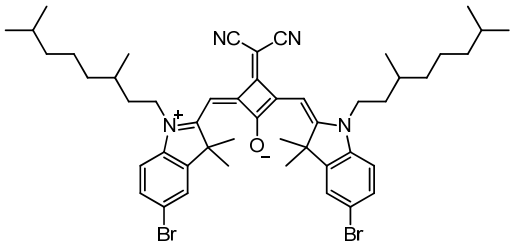

5-Bromo-1-(3,7-dimethyloctyl)-3,3-dimethyl-3*H*-indol-1-ium tosylate (**5**) (1.12 g, 2.03 mmol), **3** (325 mg, 1.02 mmol), pyridine (7.5 ml), and a mixture of toluene and 1-butanol (1:1, 40 ml) were refluxed for 17 h using a *Dean-Stark* trap. The solvent was removed under reduced pressure and the residue purified by flash chromatography (eluent: DCM).

Yield: 737 mg (835 μmol, 82%) of a shiny red violet solid

$C_{49}H_{62}Br_2N_4O$ [882.85]

^{1}H-NMR (600.1 MHz, CD_2Cl_2):

δ [ppm] = 7.50 (d, ^4J = 1.9 Hz, 2 H, H-4), 7.48 (dd, ^3J = 8.3 Hz, ^4J = 1.9 Hz, 2 H, H-6), 6.96 (d, ^3J = 8.4 Hz, 2 H, H-7), 6.46 (s, 2 H, H-8), 4.06–3.93 (m, 4 H, NCH_2), 1.80–1.71 (14 H, H-9, C*H*), 1.67–1.55 (m, 4 H, CH_2), 1.55–1.47 (m, 2 H, C*H*), 1.41–1.30 (m, 4 H, CH_2), 1.29–1.10 (8 H, CH_2), 1.01 (d, ^3J = 6.5 Hz, 6 H, CH_3), 0.86 (d, ^3J = 6.6 Hz, 12 H, CH_3).

[1] The signal of the primary C-atoms splits into two signals of equal intensity even though they are supposed just to give one single signal. Possibly this is due to the alkyl side chain, which has a stereocenter but is of racemic character.

^{13}C-NMR (150.9 MHz, CD_2Cl_2):

δ [ppm] = 173.2 (quart), 171.6 (quart), 167.9 (quart), 167.2 (quart), 144.8 (quart), 141.4 (quart), 131.2 (tert), 126.0 (tert), 118.9 (quart), 117.7 (quart), 111.8 (tert), 89.7 (tert), 49.8 (quart), 43.4 (sec), 40.9 (quart), 39.4 (sec), 37.4 (sec), 34.2 (sec), 31.20 (tert), 28.3 (tert), 26.61 (prim)[1], 26.57 (prim)[1], 25.0 (sec), 22.8 (prim)[1], 22.7 (prim)[1], 19.7 (prim).

ESI-MS pos (high resolution): [M^{+}]

calc.: 880.32849 m/z

found: 880.32851 m/z Δ = 0.02 ppm.

*Synthesis of **M7***

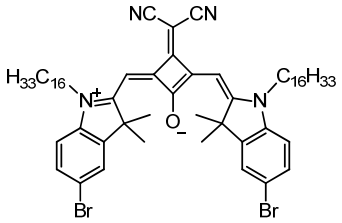

A mixture of 5-bromo-1-hexadecyl-2,3,3-trimethyl-3*H*-indolium iodide (**6**) (1.57 g, 2.66 mmol) and **3** (425 mg, 1.33 mmol) was refluxed in 1-butanol/pyridine 1:1 (30 ml) for 17 h. The solvent was removed under reduced pressure and the residue was purified by flash chromatography (eluent: DCM).

Yield: 599 mg (570 μmol, 43%) of a purple solid

$C_{61}H_{86}Br_2N_4O$ [1051.17]

^{1}H-NMR (400.1 MHz, CD_2Cl_2):

δ [ppm] = 7.50 (d, ^{4}J = 1.7 Hz, 2 H, H-4), 7.48 (dd, ^{3}J = 8.3 Hz, ^{4}J = 2.0 Hz, 2 H, H-6), 6.96 (d, ^{3}J = 8.4 Hz, 2 H, H-7), 6.50 (s, 2 H, H-8), 3.97 (t, ^{3}J = 7.6 Hz, 4 H,

[1] The signal of the primary C-atoms splits into two signals of equal intensity even though they are supposed just to give one single signal. Possibly this is due to the alkyl side chain, which has a stereocenter but is of racemic character.

N-CH_2), 1.79 (m, 4 H, NCH_2CH_2), 1.75 (s, 12 H, H-9), 1.47–1.20 (52 H, CH_2), 0.88 (t, ^3J = 6.8 Hz, 6 H, CH_3).

^{13}C-NMR (150.9 MHz, $CDCl_3$):

δ [ppm] = 172.9 (quart), 171.3 (quart), 167.9 (quart), 167.0 (quart), 144.4 (quart), 141.1 (quart), 131.0 (tert), 125.7 (tert), 118.1 (quart), 117.6 (quart), 111.4 (tert), 89.6 (tert), 49.4 (quart), 44.6 (sec), 41.2 (quart), 31.9 (sec), 29.69 (sec), 29.68 (sec), 29.67 (sec), 29.65 (sec), 29.65 (sec), 29.60 (sec), 29.54 (sec), 29.40 (sec), 29.36 (sec), 29.35 (sec), 27.3 (sec), 26.7 (sec), 26.6 (prim), 22.7 (sec), 14.1(prim).

ESI-MS pos (high resolution): [M^{+}]

calc.: 1048.51629 m/z

found: 1048.51633 m/z Δ = 0.04 ppm.

*Synthesis of **M8***

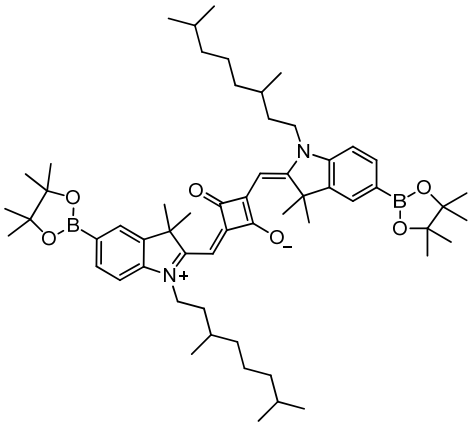

Squaraine **M4** (1.00 g, 1.20 mmol), bis(pinacolato)diboron (852 mg, 3.35 mmol) and KOAc (376 mg, 3.83 mmol) were suspended in dry 1,4-dioxane (33 ml) under nitrogen atmosphere and the mixture was degassed in a stream of nitrogen for 15 min. $Pd(PhCN)_2Cl_2$ (23.0 mg, 60.0 μmol) and dppf (33.0 mg, 60.0 μmol) were added and the mixture refluxed for 18 h. The solvent was evaporated under reduced pressure and the residue purified by flash chromatography (eluent: PE/EA 1:1 → DCM/EA 1:1).

Yield: 973 mg (1.05 mmol, 87%) of a shiny green solid

$C_{58}H_{86}B_2N_2O_6$ [928.94]

^{1}H-NMR (600.1 MHz, $CDCl_3$):

δ [ppm] = 7.78 (dd, ^3J = 7.9 Hz, ^4J = 1.0 Hz, 2 H, H-6), 7.76 (s, 2 H, H-4), 6.95 (d, ^3J = 7.9 Hz, 2 H, H-7), 5.99 (s, 2 H, H-8), 4.10–3.85 (m, 4 H, NCH_2), 1.88–1.70 (14 H, H-9, C*H*), 1.62–1.55 (m, 4 H, CH_2), 1.55–1.44 (m, 2 H, C*H*), 1.40–1.28 (28 H, CH_2, CH_3), 1.28–1.10 (8 H, CH_2), 1.03 (d, ^3J = 6.1 Hz, 6 H, CH_3), 0.86 (d, ^3J = 6.6 Hz, 12 H, CH_3).

^{13}C-NMR (150.9 MHz, $CDCl_3$):

δ [ppm] = 182.2 (quart), 180.2 (quart), 170.2 (quart), 144.9 (quart), 141.6 (quart), 135.1 (tert), 128.3 (tert), 123.9 (quart), 108.6 (tert), 87.1 (tert), 83.9 (quart), 49.1 (quart), 42.2 (sec), 39.1 (sec), 37.1 (sec), 33.8 (sec), 31.1 (tert), 27.9 (tert),

27.01 (prim)[1], 27.00 (prim)[1], 24.8 (prim), 24.6 (sec), 22.7 (prim)[1], 22.6 (prim)[1], 19.6 (prim).

*Synthesis of **M9***

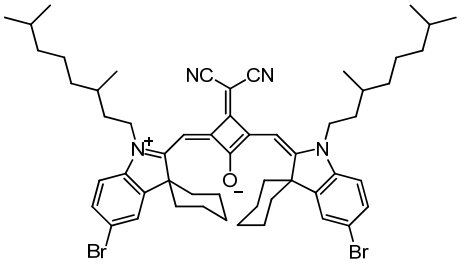

Compound **13** (300 mg, 508 μmol), **3** (81.0 mg, 254 μmol), and pyridine (3 ml) were refluxed in a mixture of toluene and 1-butanol (1:1, 20 ml) for 18 h. The solvent was evaporated and the residue purified by flash chromatography (eluent: DCM) and dried in vacuo. The product was recrystallised from hexane.

Yield: 173 mg (180 μmol, 71%) of a green-red solid

$C_{55}H_{70}Br_2N_4O$ [962.98]

^{1}H-NMR (600.1 MHz, $CDCl_3$):

δ[ppm] = 7.96 (d, ^4J = 1.8 Hz, 2 H, H-4), 7.50 (dd, ^3J = 8.5 Hz, ^4J = 1.9 Hz, 2 H, H-6), 6.92 (d, ^3J = 8.5 Hz, 2 H, H-7), 6.40 (s, 2 H, H-8), 4.15–3.98 (m, 4 H, NCH_2), 2.72–2.60 (4 H), 2.40–2.27 (2 H), 1.97–1.84 (10 H), 1.77–1.68 (2 H), 1.66–1.58 (2 H), 1.58–1.46 (4 H), 1.44–1.38 (4 H), 1.38–1.27 (4 H), 1.27–1.09 (8 H), 1.00 (d, ^3J = 6.5 Hz, 6 H, CH_3), 0.85 (d, ^3J = 6.6 Hz, 12 H, CH_3).

^{13}C-NMR (150.9 MHz, $CDCl_3$):

[1] The signal of the primary C-atoms splits into two signals of equal intensity even though they are supposed just to give one single signal. Possibly this is due to the alkyl side chain, which has a stereocenter but is of racemic character.

δ[ppm] = 173.3 (quart), 171.4 (quart), 167.5 (quart), 166.5 (quart), 142.1 (quart), 141.7 (quart), 130.9 (tert), 128.9 (tert), 118.8 (quart), 116.6 (quart), 111.5 (tert), 89.6 (tert), 53.9 (quart), 43.3 (sec), 40.8 (quart), 39.1 (sec), 37.0 (sec), 33.9 (sec), 33.4 (2 × sec), 30.8 (tert), 28.0 (tert), 24.6 (sec), 22.7 (prim)[1], 22.6 (prim)[1] , 21.8 (sec), 21.1 (2 × sec), 19.6 (prim).

ESI-MS pos (high resolution): [$M^{\cdot+}$]

calc.: 960.39109 m/z

found: 960.39082 m/z Δ = 0.28 ppm.

*Synthesis of **M10***

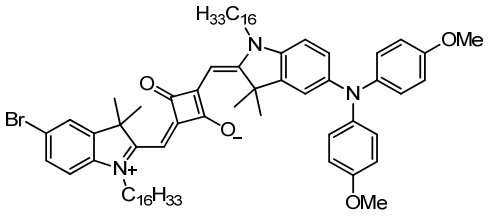

Semisquaraine acid **11** (135 mg, 242 μmol) and **15** (179 mg, 242 μmol) were dissolved in pyridine (5 ml) and a mixture of toluene and 1-butanol (1:1, 35 ml) and refluxed for 18 h using a *Dean-Stark* trap. The solvent was evaporated under reduced pressure and the residue purified by flash chromatography (eluent: PE/EA 2:1 → 1:1 → 1:2 → 1:4). The product was further purified by recycling GPC in $CHCl_3$.

Yield: 90.0 mg (78.0 μmol, 32%) of a red-blue solid

$C_{72}H_{100}BrN_3O_4$ [1151.49]

^{1}H-NMR (400.1 MHz, d^6-acetone):

δ[ppm] = 7.60 (d, ^4J = 2.0 Hz, 1 H), 7.45 (dd, ^3J = 8.5 Hz, ^4J = 2.0 Hz, 1 H), 7.20 (d, ^3J = 8.6 Hz, 1 H), 7.14 (d, ^3J = 8.5 Hz, 1 H), 7.11 (d, ^4J = 2.2 Hz, 1 H), 7.06–

[1] The signal of the primary C-atoms splits into two signals of equal intensity even though they are supposed just to give one single signal. Possibly this is due to the alkyl side chain, which has a stereocenter but is of racemic character.

7.00 (AA', 4 H), 6.93–6.88 (BB', 4 H), 6.87 (dd, ^3J = 8.6 Hz, ^4J = 2.2 Hz, 1 H), 5.96 (s, 1 H), 5.85 (s, 1 H), 4.18 (t, ^3J = 7.4 Hz, 2 H, CH_2), 4.11–3.96 (m, 2 H, CH_2), 3.80 (s, 6 H, CH_3), 1.91–1.79 (4 H, CH_2), 1.77 (s, 6 H, CH_3), 1.71 (s, 6 H, CH_3), 1.55–1.37 (8 H, CH_2), 1.35–1.20 (44 H, CH_2), 0.93–0.83 (6 H, CH_3).

^{13}C-NMR (150.9 MHz, $CDCl_3$):

δ[ppm] = 182.4 (2 × quart), 180.2 (quart), 176.0 (quart), 170.7 (quart), 167.0 (quart), 155.8 (quart), 146.4 (quart), 144.1 (quart), 143.8 (quart), 141.9 (quart), 141.0 (quart), 135.9 (quart), 130.4 (tert), 126.1 (tert), 125.5 (tert), 120.7 (tert), 115.8 (tert), 115.5 (quart), 114.8 (tert), 110.2 (tert), 110.0 (tert), 88.8 (tert), 88.5 (tert), 55.5 (prim), 49.8 (quart), 48.7 (quart), 44.1 (sec), 43.5 (sec), 31.9 (2 × sec), 29.693 (sec), 29.688 (sec), 29.684 (sec), 29.677 (sec), 29.672 (sec), 29.662 (sec), 29.65 (3 × sec), 29.63 (sec), 29.60 (sec), 29.59 (sec), 29.54 (sec), 29.52 (sec), 29.48 (2 × sec), 29.37 (sec), 29.35 (3 × sec), 27.3 (sec), 27.2 (prim), 27.1 (2 × sec), 26.8 (sec), 26.7 (prim), 22.7 (2 × sec), 14.1 (2 × prim).

ESI-MS pos (high resolution): [M^{+}]

calc.: 1149.68917 m/z

found: 1149.68966 m/z Δ = 0.43 ppm.

*Synthesis of **M11***

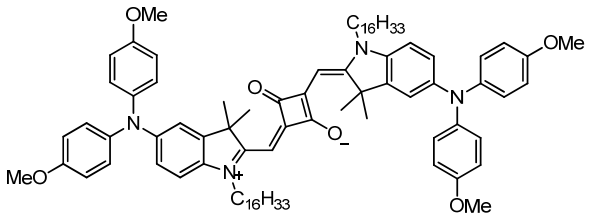

Compound **15** (600 mg, 812 μmol) was dissolved in pyridine (6 ml) and added to a solution of 3,4-dihydroxycyclobut-3-ene-1,2-dione (42.1 mg, 369 μmol) in a mixture of toluene and 1-butanol (1:1, 60 ml) under nitrogen atmosphere. The reaction mixture was

refluxed for 18 h using a *Dean-Stark* trap. The solvent was evaporated under reduced pressure and the residue was purified by flash chromatography (PE/EA 2:1 → 1:1 → 2:3). The product was recrystallised from acetone.

Yield: 191 mg (147 μmol, 40%) of a dark blue powder

$C_{86}H_{114}N_4O_6$ [1299.85]

^{1}H-NMR (600.1 MHz, CD_2Cl_2):

δ[ppm] = 7.04–6.97 (10 H), 6.87–6.77 (12 H), 5.80 (s, 2 H, H-8), 4.05–3.90 (m, 4 H, NCH_2), 3.78 (s, 12 H, OCH_3) 1.81–1.74 (m, 4 H, NCH$_2$CH_2), 1.65 (s, 12 H, H-9), 1.45–1.38 (m, 4 H, CH_2), 1.37–1.32 (m, 4 H, CH_2), 1.32–1.18 (44 H, CH_2), 0.87 (t, ^3J = 7.2 Hz, 6 H, CH_3).

^{13}C-NMR (150.9 MHz, CD_2Cl_2):

δ[ppm] = 182.2 (quart), 177.6 (quart), 168.8 (quart), 156.0 (quart), 145.8 (quart), 143.7 (quart), 141.6 (quart), 137.1 (quart), 126.1 (tert), 121.4 (tert), 116.6 (tert), 114.9 (tert), 110.0 (tert), 86.3 (tert), 55.8 (prim), 49.5 (quart), 44.0, 32.3, 30.04, 30.032, 30.028, 30.01, 30.00, 29.97, 29.91, 29.86, 29.73, 29.70, 27.39, 27.36, 23.0 (each sec), 27.0 (prim), 14.2 (prim).

ESI-MS pos (high resolution): [M^{+}]

calc.: 1298.87329 m/z

found: 1298.87329 m/z Δ = 0.00 ppm.

*Synthesis of **M12***

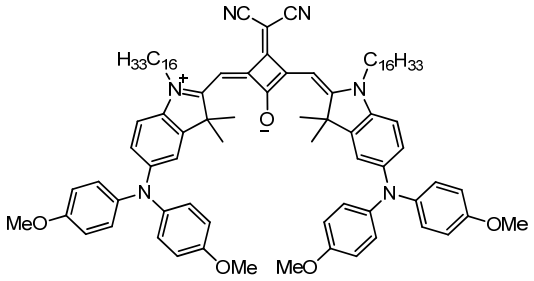

To a solution of **15** (450 mg, 609 μmol) in pyridine (7 ml) **3** (97.0 mg, 305 μmol) was added in a mixture of toluene and 1-butanol (1:1, 40 ml) and the mixture was refluxed

for 18 h. The solvent was removed under reduced pressure and the residue dried in vacuo. Flash chromatography was used for purification (eluent: pentane/acetone 5:1). The crude product was dissolved in little acetone and an excess of hexane was added. The mixture was allowed to stand overnight. The precipitate was filtered and washed with hexane.

Yield: 132 mg (98.0 μmol, 32%) of a dark blue powder

$C_{89}H_{114}N_6O_5$ [1347.90]

^{1}H-NMR (600.1 MHz, C_6D_6):

δ[ppm] = 7.19 (d, ^4J = 2.1 Hz, 2 H, H-4), 7.12–7.07 (AA', 8 H), 6.95 (dd, ^3J = 8.6 Hz, ^4J = 2.2 Hz, 2 H, H-6), 6.83 (s, 2 H), 6.77–6.73 (BB', 8 H), 6.41 (d, ^3J = 8.7 Hz, 2 H, H-7), 3.63 (t, ^3J = 7.5 Hz, 4 H, NCH_2), 3.31 (s, 12 H, OCH_3), 1.78 (s, 12 H, CH_3), 1.73–1.65 (m, 4 H, CH_2), 1.50–1.42 (m, 4 H, CH_2), 1.39–1.22 (48 H, CH_2), 0.92 (t, ^3J = 7.1 Hz, 6 H, CH_3).

^{13}C-NMR (150.9 MHz, C_6D_6):

δ[ppm] = 173.5 (quart), 170.1 (quart), 168.2 (quart), 165.9 (quart), 156.6 (quart), 146.7 (quart), 144.4 (quart), 141.6 (quart), 136.5 (quart), 126.4 (tert), 121.4 (tert), 119.4 (quart), 116.2 (tert), 115.3 (tert), 110.7 (tert), 89.8 (tert), 55.1 (prim), 49.6 (quart), 44.4 (sec), 41.7 (quart), 32.4 (sec), 30.24 (sec), 30.23 (3 × sec), 30.18 (sec), 30.16 (sec), 30.09 (sec), 29.92 (sec), 29.87 (sec), 29.81 (sec), 27.7 (sec), 27.0 (sec), 26.9 (prim), 23.2 (sec), 14.4 (prim).

ESI-MS pos (high resolution): [M^{+}]

calc.: 1346.88452 m/z

found: 1346.88486 m/z Δ = 0.25 ppm.

*Synthesis of **M13***

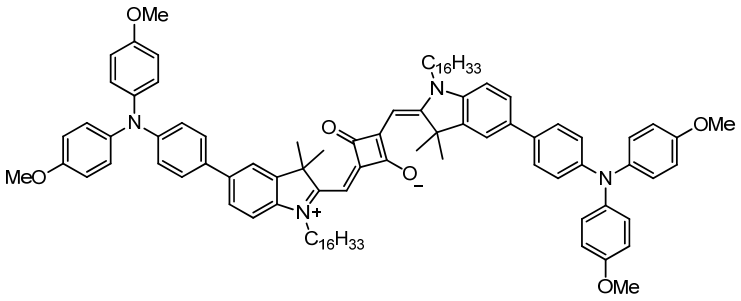

Squaraine **M5** (400 mg, 399 μmol), **17** (378 mg, 877 μmol), and aqueous Na_2CO_3 solution (1 M, 2.23 ml, 2.23 mmol) were dissolved in dry toluene (15 ml) under inert nitrogen atmosphere and degassed with a nitrogen stream for 10 min. $Pd(PPh_3)_4$ (18.4 mg, 16.0 μmol) was added and the solution refluxed for 2 d. After cooling to rt, DCM (30 ml) and H_2O (30 ml) were added and the layers separated. The organic layer was washed with H_2O (3 × 30 ml), dried over $MgSO_4$ and the solvent evaporated under reduced pressure. The residue was dissolved in DCM (20 ml) and washed again with H_2O (2 × 20 ml) and concentrated $Na_2S_2O_3$ solution (20 ml). The mixture was dried over $MgSO_4$ and the solvent evaporated under reduced pressure. The residue was purified by flash chromatography (eluent: PE/EA 5:2 → 2:1 → 1:1 → 3:4 → 1:2) but traces of monosubstituted squaraine were found in the product fraction. The product was then purified by recrystallisation from acetone where only disubstituted squaraine crystallised.

Yield: 274 mg (189 μmol, 47%) of a blue-green solid

$C_{98}H_{122}N_4O_6$ [1452.04]

^{1}H-NMR (600.1 MHz, CD_2Cl_2):

δ [ppm] = 7.53 (d, ^4J = 1.6 Hz, 2 H, H-4), 7.50 (dd, ^3J = 8.2 Hz, ^4J = 1.8 Hz, 2 H, H-6), 7.44–7.41 (AA', 4 H), 7.09–7.06 (AA', 8 H), 7.04 (d, ^3J = 8.2 Hz, 2 H, H-7), 6.98–6.95 (BB', 4 H), 6.87–6.84 (BB', 8 H), 5.93 (s, broad, 2 H, H-8), 4.19–3.92 (m, 4 H, NCH_2), 3.79 (s, 12 H, OCH_3), 1.82 (m, 4 H, NCH_2CH_2), 1.79 (s, 12 H, H-9), 1.45 (m, 4 H, CH_2), 1.37 (m, 4 H, CH_2), 1.32–1.20 (44 H, CH_2), 0.86 (t, ^3J = 7.1 Hz, 6 H, CH_3).

^{13}C-NMR (150.9 MHz, CD_2Cl_2):

δ[ppm] = 182.3 (quart), 179.4 (quart), 169.7 (quart), 156.4 (quart), 148.5 (quart), 143.2 (quart), 141.8 (quart), 141.1 (quart), 136.9 (quart), 132.7 (quart), 127.5 (tert), 127.0 (tert), 126.1 (tert), 120.9 (tert), 120.6 (tert), 115.0 (tert), 110.0 (tert), 87.0 (tert), 55.8 (prim), 49.6 (quart), 44.1, 32.3, 30.043, 30.039, 30.03, 30.01, 30.00, 29.97, 29.91, 29.85, 29.73, 29.70, 27.41, 27.38 (each sec), 27.2 (prim), 23.03 (sec), 14.2 (prim).

ESI-MS pos (high resolution): [M^{+}]

calc.: 1450.93589 m/z

found: 1450.93590 m/z Δ = 0.01 ppm.

*Synthesis of **M14** and **M15***

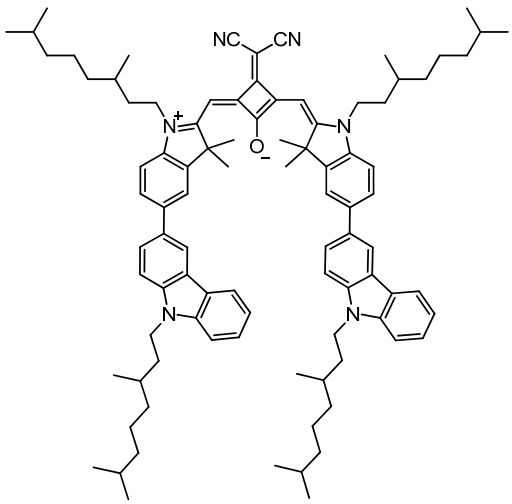

M14

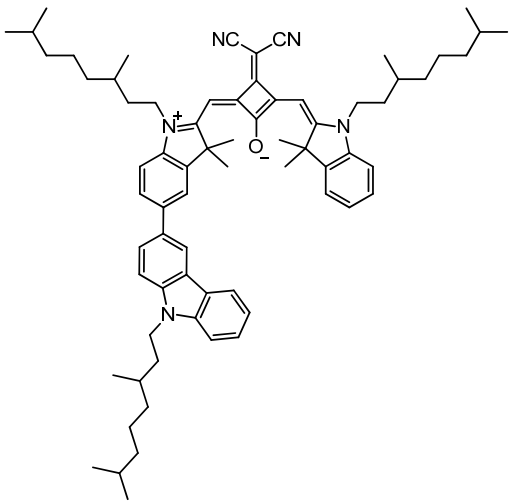

M15

Under nitrogen atmosphere, squaraine **M6** (250 mg, 283 μmol) and **20** (270 mg, 623 μmol) were dissolved in dry toluene (10 ml). An aqueous solution of Na_2CO_3 (1 M, 1.68 ml, 1.68 mmol) was added and the mixture was degassed in a stream of nitrogen for 15 min. $Pd(PPh_3)_4$ (25.4 mg, 22.0 μmol) was added and the reaction mixture was refluxed for 5 d. DCM (50 ml) was added and the mixture was washed with H_2O (3 × 30 ml). The organic layer was dried over Na_2SO_4 and the solvent was evaporated

under reduced pressure. The residue was purified by flash chromatography (eluent: PE/DCM 1:1) and subsequent preparative recycling GPC.

M14:

Yield: 256 mg (192 μmol, 68%) of a green solid

$C_{93}H_{118}N_6O$ [1335.98]

^{1}H-NMR (600.1 MHz, $CDCl_3$):

δ[ppm] = 8.30–8.28 (m, 2 H, C*H*), 8.19–8.16 (m, 2 H, C*H*), 7.73–7.68 (4 H, C*H*), 7.67–7.64 (m, 2 H, C*H*), 7.53–7.46 (4 H, C*H*), 7.45–7.41 (m, 2 H, C*H*), 7.29–7.24 (m, 2 H, C*H*), 7.16–7.11 (m, 2 H, C*H*), 6.54 (s, 2 H, C*H*), 4.42–4–31 (m, 4 H, NCH_2), 4.18–4.07 (m, 4 H, NCH_2), 1.96–1.81 (16 H, CH, CH_3), 1.78–1.48 (12 H, C*H*, CH_2), 1.47–1.11 (24 H, CH_2), 1.08–1.04 (12 H, CH_3), 0.91–0.82 (24 H, CH_3).

^{13}C-NMR (150.9 MHz, $CDCl_3$):

δ[ppm] = 173.4 (quart), 171.3 (quart), 167.8 (quart), 165.9 (quart), 143.2 (quart), 140.8 (quart), 140.7 (quart), 139.8 (quart), 138.2 (quart), 131.6 (quart), 127.1 (tert), 126.0 (tert), 125.0 (tert), 123.5 (quart), 122.9 (quart), 121.2 (tert), 120.5 (tert), 119.03 (quart), 119.00 (tert), 118.8 (tert), 110.2 (tert), 108.9 (tert), 108.8 (tert), 89.2 (tert), 49.6 (quart), 43.0 (sec), 41.4 (sec), 40.7 (quart), 39.20 (sec), 39.18 (sec), 37.2 (sec), 37.1 (sec), 35.6 (sec), 34.2 (sec), 30.93 (tert), 30.91 (tert), 27.9 (tert), 28.0 (tert), 26.8 (prim)[1], 26.7 (prim)[1], 24.63 (sec), 24.62 (sec), 22.70 (prim)[1], 22.66 (prim)[1], 22.62 (prim)[1], 22.58 (prim)[1], 19.8 (prim), 19.7 (prim).

[1] The signal of the primary C-atoms splits into two signals of equal intensity even though they are supposed just to give one single signal. Possibly this is due to the alkyl side chain, which has a stereocenter but is of racemic character.

ESI-MS pos (high resolution): [M^{+}]

calc.: 1334.93616 m/z

found: 1334.93551 m/z Δ= 0.49 ppm.

M15:

Yield: 16.0 mg (15.5 μmol, 5%) of a green solid.

$C_{71}H_{91}N_5O$ [1030.52]

^{1}H-NMR (600.1 MHz, $CDCl_3$):

δ[ppm] = 8.29–8.28 (m, 1 H, C*H*), 8.20–8.16 (m, 1 H, C*H*), 7.72–7.66 (2 H, C*H*), 7.66–7.63 (1 H, C*H*), 7.52–7.47 (2 H, C*H*), 7.45–7.41 (1 H, C*H*), 7.38–7.35 (m, 1 H, C*H*), 7.34–7.31 (m, 1 H, C*H*), 7.29–7.27 (m, 1 H, C*H*), 7.22–7.17 (m, 1 H, C*H*), 7.14–7.11 (m, 1 H, C*H*), 7.05–7.01 (m, 1 H, C*H*), 6.53 (s, 1 H, C*H*), 6.49 (s, 1 H, C*H*), 4.41–4–30 (m, 2 H, NCH_2), 4.19–3.98 (4 H, NCH_2), 1.95–1.83 (8 H, C*H*, CH_3), 1.82–1.75 (7 H, C*H*, CH_3), 1.74–1.47 (9 H, C*H*, CH_2), 1.46–1.10 (18 H, CH_2), 1.06 (d, ^3J = 6.5 Hz, 6 H, CH_3), 1.04 (d, ^3J = 6.5 Hz, 3 H, CH_3), 0.89–0.84 (18 H, CH_3).

^{13}C-NMR (150.9 MHz, $CDCl_3$):

δ[ppm] = 173.3 (quart), 171.6 (quart), 171.4 (quart), 167.7 (quart), 166.3 (quart), 166.2 (quart), 143.2 (quart), 142.4 (quart), 142.0 (quart), 140.8 (quart), 140.6 (quart), 139.8 (quart), 139.3 (quart), 131.6 (quart), 128.0 (tert), 127.1 (tert), 126.0 (tert), 125.0 (tert), 124.4 (tert), 123.5 (quart), 122.9 (quart), 122.3 (tert), 121.2 (tert), 120.5 (tert), 119.01 (tert), 118.8 (tert) 110.3 (tert), 109.9 (tert), 108.9 (tert), 108.8 (tert), 89.3 (tert), 89.0 (tert), 49.6 (quart), 49.4 (quart), 43.1 (sec), 42.8 (sec), 41.4 (sec), 40.8 (2 × quart), 39.20 (sec), 39.17 (sec), 39.16 (sec), 37.2 (sec), 37.13 (sec), 37.12 (sec), 35.6 (sec), 34.2 (sec), 34.1 (sec), 30.92 (tert), 30.91 (tert), 30.90 (tert), 27.98 (tert), 27.97

(tert) 27.94 (tert), 26.71 (prim)[1], 26.68 (prim)[1], 26.60 (prim)[1], 26.58 (prim)[1], 24.62 (2 × sec), 24.60 (sec), 22.70 (prim)[1], 22.69 (prim)[1], 22.66 (prim)[1], 22.61 (prim)[1], 22.60 (prim)[1], 22.58 (prim)[1], 19.8 (prim), 19.72 (prim), 19.69 (prim).

*Synthesis of **M16***

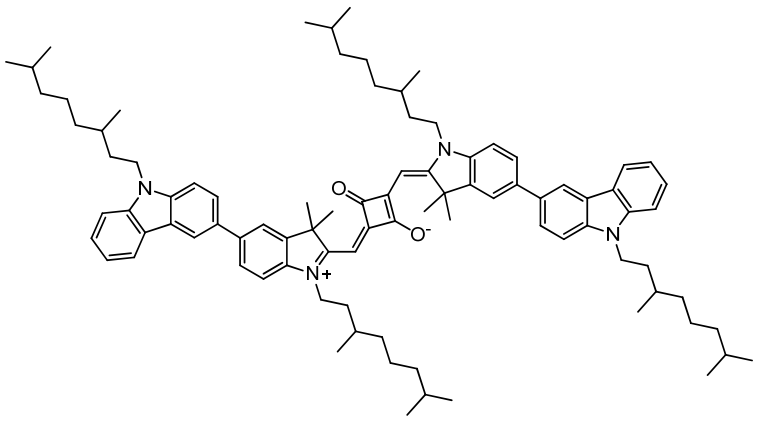

Under nitrogen atmosphere, squaraine **M4** (250 mg, 299 μmol) and **20** (286 mg, 659 μmol) were dissolved in dry toluene (20 ml). An aqueous solution of Na_2CO_3 (1 M, 1.68 ml, 1.68 mmol) was added and the mixture was degassed in a stream of nitrogen for 15 min. $Pd(PPh_3)_4$ (27.7 mg, 24.0 μmol) was added and the reaction mixture was refluxed for 5 d. DCM (50 ml) was added and the mixture was washed with H_2O (3 × 30 ml). The organic layer was dried over Na_2SO_4 and the solvent was evaporated under reduced pressure. The residue was purified by flash chromatography (eluent: DCM → DCM/Et_2O 40:1) and the product recrystallised from acetone.

Yield: 276 mg (214 μmol, 72%) of a shiny red solid

$C_{90}H_{118}N_4O_2$ [1287.93]

[1] The signal of the primary C-atoms splits into two signals of equal intensity even though they are supposed just to give one single signal. Possibly this is due to the alkyl side chain, which has a stereocenter but is of racemic character.

^{1}H-NMR (600.1 MHz, $CDCl_3$):

δ[ppm] = 8.31–8.29 (m, 2 H, C*H*), 8.20–8.17 (m, 2 H, C*H*), 7.71 (dd, ^{3}J = 8.4 Hz, ^{4}J = 1.8 Hz, 2 H, C*H*), 7.67 (d, ^{4}J = 1.8 Hz, 2 H, C*H*), 7.65 (dd, ^{3}J = 8.4 Hz, ^{4}J = 1.8 Hz, 2 H, C*H*), 7.57–7.41 (6 H, C*H*), 7.28–7.25 (m, 2 H, C*H*), 7.06 (d, ^{3}J = 8.4 Hz, 2 H, C*H*), 6.01 (s, 2 H, C*H*), 4.41–4.24 (m, 4 H, NCH_2), 4.06–3.88 (m, 4 H, NCH_2), 1.97–1.82 (16 H, C*H*, CH_3), 1.74–1.47 (12 H, C*H*, CH_2), 1.47–1.11 (24 H, CH_2), 1.09 (d, ^{3}J = 8 Hz, 6 H, CH_3), 1.06 (d, ^{3}J = 6.6 Hz, 6 H, CH_3), 0.89 (d, ^{3}J = 6.6 Hz, 12 H, CH_3), 0.87 (d, ^{3}J = 6.6 Hz, 12 H, CH_3).

^{13}C-NMR (150.9 MHz, $CDCl_3$):

δ[ppm] = 182.5 (quart), 179.0 (quart), 169.5 (quart), 143.0 (quart), 141.2 (quart), 140.8 (quart), 139.7 (quart), 138.3 (quart), 131.8 (quart), 126.8 (tert), 125.9 (tert), 125.0 (tert), 123.5 (quart), 122.9 (quart), 121.3 (tert), 120.5 (tert), 118.9 (tert), 118.7 (tert), 109.4 (tert), 108.9 (tert), 108.7 (tert), 86.7 (tert), 49.4 (quart), 42.2 (sec), 41.3 (sec), 39.2 (sec), 39.1 (sec), 37.2 (sec), 37.1 (sec), 35.6 (sec), 33.9 (sec), 31.2 (tert), 30.9 (tert), 29.7 (tert), 28.0 (tert), 27.2 (prim), 24.7 (sec), 24.6 (sec), 22.7 (prim), 22.6 (prim), 19.8 (prim), 19.6 (prim).

ESI-MS pos (high resolution): [$M^{\cdot+}$]

calc.: 1286.92493 m/z

found: 1286.92570 m/z Δ= 0.60 ppm.

*Synthesis of **M17***

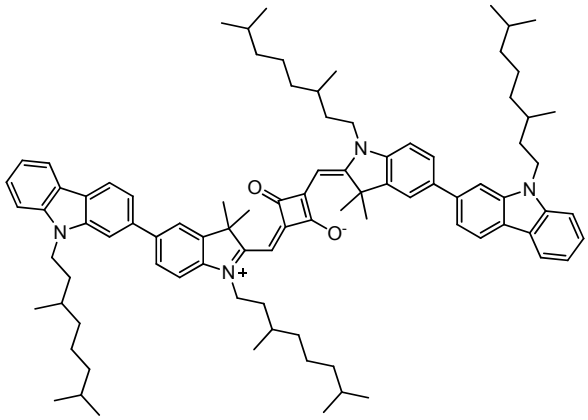

Under nitrogen atmosphere, squaraine **M4** (250 mg, 299 μmol) and **23** (286 mg, 659 μmol) were dissolved in dry toluene (20 ml). An aqueous solution of Na_2CO_3 (1 M, 1.68 ml, 1.68 mmol) was added and the mixture was degassed in a stream of nitrogen for 15 min. $Pd(PPh_3)_4$ (27.7 mg, 24.0 μmol) was added and the reaction mixture was refluxed for 5 d. DCM (50 ml) was added and the mixture was washed with H_2O (3 × 30 ml). The organic layer was dried over Na_2SO_4 and the solvent was evaporated under reduced pressure. The residue was purified by flash chromatography (eluent: PE/DCM 1:2) and the product recrystallised from acetone.

Yield: 215 mg (167 μmol, 56%) of a shiny green golden solid

$C_{90}H_{118}N_4O_2$ [1287.93]

^{1}H-NMR (600.1 MHz, $CDCl_3$):

δ [ppm] = 8.17–8.14 (m, 2 H, C*H*), 8.13–8.11 (m, 2 H, C*H*), 7.69–7.65 (4 H, C*H*), 7.56–7.53 (m, 2 H, C*H*), 7.50–7.44 (4 H, C*H*), 7.44–7.40 (m, 2 H, C*H*), 7.26–7.23 (m, 2 H, C*H*), 7.09–7.05 (m, 2 H, C*H*), 6.02 (s, 2 H, C*H*), 4.45–4–32 (m, 4 H, NCH_2), 4.16–4.01 (m, 4 H, NCH_2), 1.98–1.82 (16 H, C*H*, CH_3), 1.78–1.45 (12 H, C*H*, CH_2), 1.44–1.11 (24 H, CH_2), 1.10–1.02 (12 H, CH_3), 0.89 (d, ^3J = 6.4 Hz, 12 H, CH_3), 0.83 (d, ^3J = 6.8 Hz, 12 H, CH_3).

^{13}C-NMR (150.9 MHz, $CDCl_3$):

δ [ppm] = 182.4 (quart), 179.4 (quart), 169.6 (quart), 143.0 (quart), 141.7 (quart), 140.9 (quart), 140.8 (quart), 138.6 (quart), 138.3 (quart), 127.2 (tert), 125.7

(tert), 122.7 (quart), 122.1 (quart), 121.6 (tert), 120.7 (tert), 120.1 (tert), 119.0 (tert), 118.4 (tert), 109.4 (tert), 108.6 (tert), 106.8 (tert), 86.8 (tert), 49.4 (quart), 42.3 (sec), 41.2 (sec), 39.19 (sec), 39.17 (sec), 37.15 (sec), 39.13 (sec), 35.6 (sec), 33.9 (sec), 31.2 (tert), 30.9 (tert), 27.96 (tert), 27.94 (tert), 27.19 (prim)[1], 27.18 (prim)[1], 24.7 (sec), 24.6 (sec) 22.70 (prim)[1], 22.65 (prim)[1], 22.60 (prim)[1], 22.57 (prim)[1], 19.8 (prim), 19.6 (prim).

ESI-MS pos (high resolution): $[M^{\cdot+}]$

calc.: 1286.92493 m/z

found: 1286.92540 m/z Δ= 0.37 ppm.

*Synthesis of **M18***

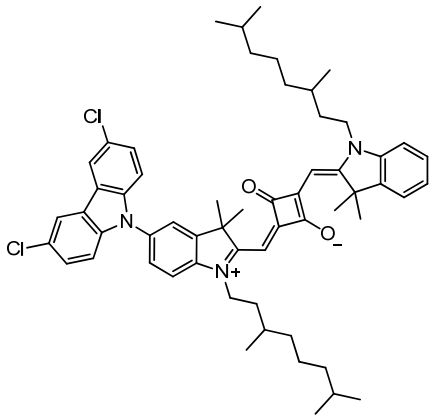

Under nitrogen atmosphere, **S24** (190 mg, 251 μmol), 3,6-dichloro-9*H*-carbazole (59.3 mg, 251 μmol), P*t*Bu$_3$ (1 M in toluene, 15.0 μl, 10.1 μmol) and NaO*t*Bu (36.2 mg, 377 μmol) were dissolved in dry toluene (10 ml). The mixture was degassed with a stream of nitrogen for 10 min. $Pd_2dba_3 \cdot CHCl_3$ (10.4 mg, 10.1 μmol) was added and the reaction mixture was stirred at 80°C for 18 h. The solvent was removed under reduced pressure and the residue was dissolved in DCM. The organic phase was washed with H_2O (3 × 50 ml), dried over Na_2SO_4 and the solvent removed under reduced pressure.

[1] The signal of the primary C-atoms splits into two signals of equal intensity even though they are supposed just to give one single signal. Possibly this is due to the alkyl side chain, which has a stereocenter but is of racemic character.

The crude product was purified by flash chromatography (eluent: DCM → DCM/Et_2O 40:1).

Yield: 98.0 mg (108 μmol, 43%) of a blue solid

$C_{58}H_{69}Cl_2N_3O_2$ [911.10]

^{1}H-NMR (400.1 MHz, $CDCl_3$):

δ [ppm] = 8.05 (dd, ^4J = 2.0 Hz, ^5J = 0.4 Hz, 2 H, C*H*), 7.44–7.36 (5 H, C*H*), 7.36–7.30 (m, 1 H, C*H*), 7.24–7.23 (1 H, C*H*)*, 7.21–7.16 (m, 1 H, C*H*), 7.11–7.08 (m, 1 H, C*H*), 7.02–6.69 (m, 1 H, C*H*), 6.02 (s, 1 H, C*H*), 6.01 (s, 1 H, C*H*), 4.10–3.95 (4 H, NCH_2), 1.86–1.78 (14 H, C*H*, CH_3), 1.72–1.60 (4 H, CH_2), 1.58–1.49 (2 H, CH), 1.48–1.12 (12 H, CH_2), 1.09 (d, ^3J = 6.1 Hz, 3 H, CH_3), 1.05 (d, ^3J = 6.2 Hz, 3 H, CH_3), 0.88 (d, ^3J = 6.6 Hz, 6 H, CH_3), 0.86 (d, ^3J = 6.6 Hz, 6 H, CH_3).* *That signal appears as a dublett but only dubletts of dubletts are expected in such a system. Therefore, one aromatic proton, which is missing, might be covered by the signal of the NMR-solvent between 7.27–7.25.*

^{13}C-NMR (100.6 MHz, $CDCl_3$):

δ [ppm] = 182.0 (quart), 178.7 (quart), 171.3 (quart), 168.2 (quart), 142.5 (quart), 142.3 (quart), 142.2 (quart), 142.1 (quart), 140.0 (2 × quart), 132.0 (quart), 127.9 (tert), 126.8 (2 × tert), 126.7 (tert), 125.8 (2 × quart), 124.2 (tert), 123.4 (2 × quart), 122.4 (tert), 121.3 (tert), 120.2 (2 × tert), 111.0 (2 × tert), 109.6 (2 × tert), 87.0 (2 × tert), 49.7 (quart), 49.1 (quart), 42.4 (sec), 42.2 (sec), 39.2 (sec), 39.1 (sec), 37.2 (sec), 37.1 (sec), 34.0 (sec), 33.8 (sec), 31.3 (tert), 31.2 (tert), 28.0 (tert), 27.9 (tert), 27.3 (prim), 26.9 (prim), 24.70 (sec), 24.65 (sec), 22.71 (prim)[1], 22.68 (prim)[1], 22.60 (prim)[1], 22.57 (prim)[1], 19.7 (prim), 19.6 (prim). *Two quarternary carbons missing.*

[1] The signal of the primary C-atoms splits into two signals of equal intensity even though they are supposed just to give one single signal. Possibly this is due to the alkyl side chain, which has a stereocenter but is of racemic character.

ESI-MS pos (high resolution): [M^{+}]

calc.: 909.47614 m/z

found: 909.47604 m/z Δ = 0.11 ppm.

*Synthesis of **M19***

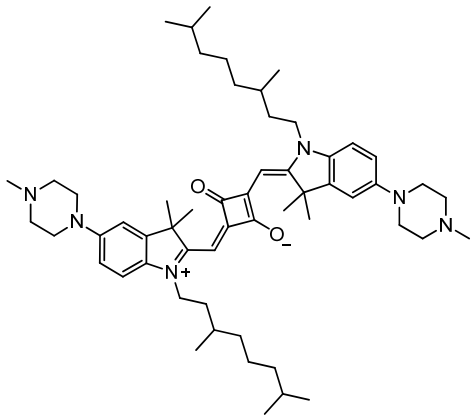

Compound **24** (133 mg, 334 μmol) and 3,4-dihydroxycyclobut-3-ene-1,2-dione (19.1 mg, 167 μmol) were refluxed in toluene/1-butanol 1:1 (40 ml) using a *Dean-Stark* trap for 18 h. The solvent was removed under reduced pressure and the residue was purified by flash chromatography (eluent: MeOH → MeOH/NEt_3 10:1). The crude product was dissolved in little DCM and an excess of hexane was added. The mixture was allowed to stand overnight. The precipitate was filtered and washed with hexane to give a purple solid.

Yield: 66.0 mg (75.6 μmol, 45%) of purple solid

$C_{56}H_{84}N_6O_2$ [873.31]

^{1}H-NMR (600.1 MHz, $CDCl_3$):

δ [ppm] = 6.98–6.96 (2 H, C*H*), 6.85–6.82 (4 H, C*H*), 5.85 (s, 2 H, C*H*), 4.05–3.85 (m, 4 H, CH_2), 3.20 (t, ^3J = 5.1 Hz, 8 H, NCH_2), 2.61 (t, ^3J = 4.7 Hz, 8 H, NCH_2), 2.37 (s, 6 H, NCH_3), 1.82–1.74 (14 H, CH_3, C*H*), 1.62–1.54 (m, 4 H, CH_2), 1.54–1.47 (m, 2 H, C*H*), 1.40–1.29 (m, 4 H, CH_2), 1.28–1.09 (8 H, CH_2), 1.02 (d, ^3J = 6.1 Hz, 6 H, CH_3), 0.86 (d, ^3J = 6.6 Hz, 12 H, CH_3).

^{13}C-NMR (150.9 MHz, $CDCl_3$):

δ [ppm] = 182.5 (quart), 177.2 (quart), 168.7 (quart), 148.7 (quart), 143.5 (quart), 135.8 (quart), 115.0 (tert), 111.7 (tert), 109.4 (tert), 85.8 (tert), 55.1 (sec), 50.1 (sec), 49.4 (quart), 46.1 (prim), 42.1 (sec), 39.1 (sec), 37.1 (sec), 33.8 (sec), 31.2 (tert), 27.9 (tert), 27.14 (prim)[1], 27.13 (prim)[1], 24.6 (sec), 22.7 (prim)[1], 22.6 (prim)[1], 19.6 (prim).

ESI-MS pos (high resolution): [M^{+}]

calc.: 872.66503 m/z

found: 872.66524 m/z Δ = 0.24 ppm.

*Synthesis of **M20***

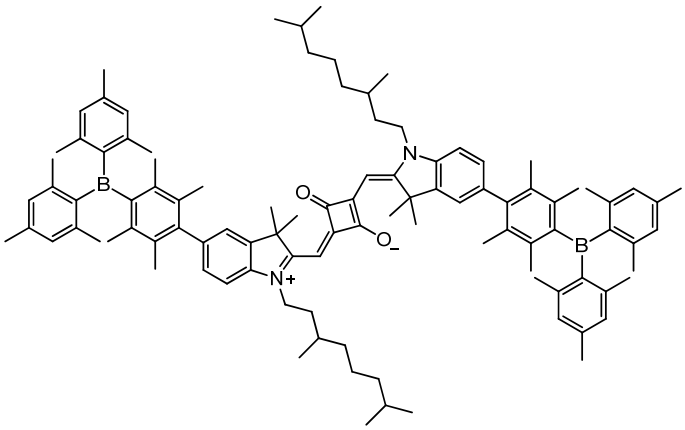

Squaraine **M8** (110 mg, 119 μmol), **34** (115 mg, 249 μmol), an aqueous solution of Na_2CO_3 (1 M, 665 μl, 665 μmol), and dry toluene (8 ml) were placed in a *Schlenk* tube under nitrogen atmosphere and degassed in a stream of nitrogen for 10 min. $Pd(PPh_3)_4$ (11.0 mg, 9.50 μmol) was added and the solution refluxed for 5 d. The solvent was removed under reduced pressure and the crude product was dissolved in little DCM. An excess of hexane was added and the mixture was allowed to stand overnight. The precipitate was filtered and washed with hexane.

[1] The signal of the primary C-atoms splits into two signals of equal intensity even though they are supposed just to give one single signal. Possibly this is due to the alkyl side chain, which has a stereocenter but is of racemic character.

Yield: 133 mg (93.0 μmol, 78%) of a blue solid

$C_{102}H_{130}B_2N_2O_2$ [1437.76]

^{1}H-NMR (600.1 MHz, $CDCl_3$):

δ[ppm] = 7.09 (d, ^4J = 1.2 Hz, 2 H, H-4), 7.03 (dd, ^3J = 8.0 Hz, ^4J = 1.4 Hz, 2 H, H-6), 6.98 (d, ^3J = 8.0 Hz, 2 H, H-7), 6.78–6.73 (8 H), 5.98 (s, 2 H, H-8), 4.14–3.88 (4 H, NCH_2), 2.280 (s, 6 H, CH_3), 2.275 (s, 6 H, CH_3), 2.05 (s, 6 H, CH_3), 2.04–2.01 (18 H, CH_3), 1.99 (s, 6 H, CH_3), 1.98 (s, 6 H, CH_3), 1.89–1.78 (26 H, CH_3, CH), 1.74–1.62 (m, 4 H, CH_2), 1.57–1.50 (m, 2 H, CH), 1.45–1.12 (12 H, CH_2), 1.07 (d, ^3J = 6.2 Hz, 6 H, CH_3), 0.87 (d, ^3J = 6.6 Hz, 12 H, CH_3).

^{13}C-NMR (150.9 MHz, $CDCl_3$):

δ[ppm] = 182.5 (quart), 178.9 (quart), 169.7 (quart), 147.7 (quart), 144.74 (quart), 144.67 (quart), 142.4 (quart), 140.82 (quart), 140.79 (quart), 140.75 (quart), 140.68 (quart), 139.2 (quart), 139.1 (quart), 139.0 (quart), 135.2 (quart), 131.3 (quart), 128.8 (2 × tert), 128.74 (tert), 128.68 (tert), 128.65 (tert), 123.7 (tert), 108.7 (tert), 86.3 (tert), 49.3 (quart), 42.3 (sec), 39.2 (sec), 37.1 (sec), 33.9 (sec), 31.3 (tert), 28.0 (tert), 27.1 (prim), 24.7 (sec), 23.2 (2 × prim), 22.9 (prim), 22.8 (prim), 22.7 (prim)[1], 22.6 (prim)[1], 21.23 (prim), 21.22 (prim), 20.3 (2 × prim), 19.6 (prim), 17.8 (2 × prim).

ESI-MS pos (high resolution): [$M^{\cdot+}$]

calc.: 1435.03856 m/z

found: 1435.03813 m/z Δ = 0.30 ppm.

[1] The signal of the primary C-atoms splits into two signals of equal intensity even though they are supposed just to give one single signal. Possibly this is due to the alkyl side chain, which has a stereocenter but is of racemic character.

*Synthesis of **M21** and **M22***

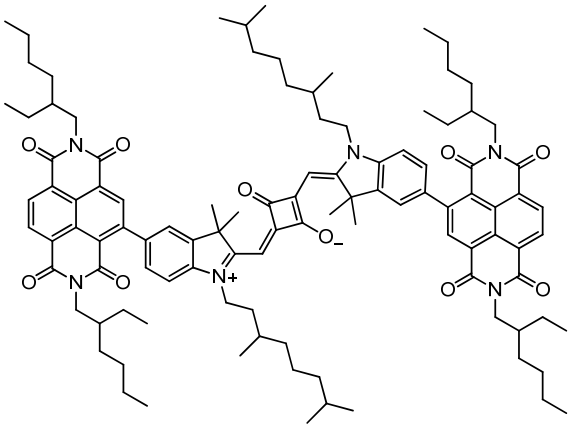

M21

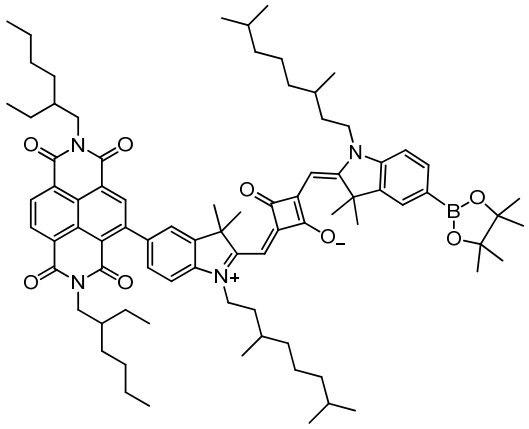

M22

Squaraine **M8** (150 mg, 162 μmol), **35** (111 mg, 324 μmol), and an aqueous solution of Na_2CO_3 (2 M, 2.00 ml, 4.00 mmol) were dissolved in 1,4-dioxane (6 ml) under nitrogen atmosphere and the mixture was degassed in a stream of nitrogen for 10 min. $Pd(PPh_3)_4$ (15.0 mg, 13.0 μmol) was added and the solution refluxed for 18 h. Aqueous HCl (1 M, 2 ml) was added and the solution diluted with H_2O (20 ml). The mixture was extracted with DCM (3 × 20 ml) and the solvent removed under reduced pressure. The residue was purified by flash chromatography (eluent: PE/EA 4:1) and preparative recycling GPC ($CHCl_3$).

M21:

Yield: 22.0 mg (13.0 μmol, 8%) of a blue solid

$C_{106}H_{136}N_6O_{10}$ [1654.25]

^{1}H-NMR (600.1 MHz, $CDCl_3$):

δ [ppm] = 8.82 (d, ^3J = 7.6 Hz, 2 H), 8.75 (d, ^3J = 7.7 Hz, 2 H), 8.63 (s, 2 H), 7.41 (dd, ^3J = 8.0 Hz, ^4J = 1.5 Hz, 2 H), 7.37 (d, ^4J = 1.3 Hz, 2 H), 7.09 (d, ^3J = 8.2 Hz, 2 H), 6.05 (s, 2 H), 4.20–3.98 (12 H, NCH_2), 1.98–1.91 (m, 2 H, C*H*), 1.91–1.82 (16 H, CH_3, C*H*), 1.72–1.63 (m, 4 H, CH_2), 1.57–1.51 (m, 2 H, C*H*), 1.46–1.14 (44 H, CH_2), 1.09 (d, ^3J = 6.1, 6 H, CH_3), 0.94 (t, ^3J = 7.3 Hz, 6 H, CH_3), 0.92–0.84 (30 H, CH_3).

^{13}C-NMR (150.1 MHz, $CDCl_3$):

δ[ppm] = 182.3 (quart), 180.3 (quart), 169.8 (quart), 163.3 (quart), 163.1 (quart), 163.0 (quart), 162.7 (quart), 147.7 (quart), 142.7 (quart), 142.5 (quart), 135.8 (tert), 131.4 (tert), 129.6 (tert), 128.3 (tert), 128.1 (quart), 126.8 (quart), 126.5 (quart), 126.0 (quart), 125.5 (quart), 123.1 (tert), 122.8 (quart), 115.4 (quart), 109.2 (tert), 87.3 (tert), 49.3 (quart), 44.6 (sec), 44.5 (sec), 42.4 (sec), 39.2 (sec), 37.93 (tert), 37.88 (tert), 37.1 (sec), 33.9 (sec), 31.3 (tert), 30.72 (sec), 30.69 (sec), 28.6 (2 × sec), 28.0 (tert), 27.1 (prim), 24.7 (sec), 24.1 (sec), 24.0 (sec), 23.05 (sec), 23.01 (sec), 22.7 (prim)[1], 22.6 (prim)[1], 19.6 (prim), 14.1 (2 × prim), 10.8 (prim), 10.6 (prim).

ESI-MS pos (high resolution): [M^{+}]

calc.: 1653.03125 m/z

found: 1653.03165 m/z Δ = 0.25 ppm.

M22:

Yield: 21.0 mg (16.3 μmol, 10%) of a blue solid

$C_{82}H_{111}BN_4O_8$ [1291.60]

^{1}H-NMR (600 MHz, $CDCl_3$):

δ[ppm] = 8.82 (d, ^{3}J = 7.7 Hz, 1 H), 8.75 (d, ^{3}J = 7.7 Hz, 1 H), 8.63 (s, 1 H), 7.79 (dd, ^{3}J = 7.9 Hz, ^{4}J = 0.9 Hz, 1 H), 7.77 (s, 1 H), 7.41 (dd, ^{3}J = 8.0 Hz, ^{4}J = 1.7 Hz, 1 H), 7.36 (d, ^{4}J = 1.6 h, 1 H), 7.09 (d, ^{3}J = 8.2 Hz, 1 H), 6.96 (d, ^{3}J = 7.9 Hz, 1 H), 6.03 (s, 1 H), 6.00 (s, 1 H), 4.20–3.94 (8 H, NCH_2), 1.98–1.91 (m, 1 H, C*H*), 1.91–1.74 (15 H, CH_3, C*H*), 1.73–1.63 (4 H, CH_2), 1.57–1.47 (2 H, C*H*), 1.46–1.11 (28 H, CH_2), 1.36 (s, 12 H, CH_3), 1.09 (d, ^{3}J = 6.1 Hz,

[1] The signal of the primary C-atoms splits into two signals of equal intensity even though they are supposed just to give one single signal. Possibly this is due to the alkyl side chain, which has a stereocenter but is of racemic character.

3 H, CH_3), 1.03 (d, ^3J = 6.1 Hz, 3 H, CH_3), 0.93 (t, ^3J = 7.5 Hz, 3 H, CH_3), 0.91–0.83 (21 H, CH_3).

^{13}C-NMR (150 MHz, $CDCl_3$):

δ [ppm] = 182.3 (2 × quart), 180.6 (quart), 180.0 (quart), 170.5 (quart), 169.5 (quart), 163.3 (quart), 163.1 (quart), 163.0 (quart), 162.7 (quart), 147.7 (quart), 144.9 (quart), 142.8 (quart), 142.4 (quart), 141.6 (quart), 135.8, (tert), 135.6 (quart), 135.1 (tert), 131.4 (tert), 130.4 (tert), 128.31 (tert), 128.25 (tert), 128.1 (quart), 126.8 (quart), 126.5 (quart), 126.0 (quart), 125.2 (quart), 124.0 (quart), 123.1 (tert), 122.7 (quart), 109.1 (tert), 108.7 (tert), 87.22 (tert), 87.18 (tert), 83.9 (2 × quart), 49.2 (2 × quart), 44.6 (sec), 44.5 (sec), 42.4 (sec), 42.2 (sec), 39.2 (sec), 39.1 (sec), 37.92 (tert), 37.87 (tert), 37.14 (sec), 37.07 (sec), 33.9 (sec), 33.8 (sec), 31.3 (tert), 31.2 (tert), 30.72 (sec), 30.68 (sec), 28.6 (2 × sec), 28.0 (tert), 27.9 (tert), 27.1 (prim), 27.00 (prim)[1], 26.99 (prim)[1], 24.8 (prim), 24.7 (sec), 24.6 (sec), 24.1 (sec), 24.0 (sec), 23.04 (sec), 23.01 (sec), 22.70 (prim)[1], 22.66 (prim)[1], 22.60 (prim)[1], 22.56 (prim)[1], 19.6 (2 × prim), 14.065 (prim), 14.060 (prim), 10.7 (prim), 10.6 (prim).

ESI-MS pos (high resolution): [M^{+}]

calc.: 1289.85258 m/z

found: 1289.85343 m/z Δ = 0.66 ppm.

[1] The signal of the primary C-atoms splits into two signals of equal intensity even though they are supposed just to give one single signal. Possibly this is due to the alkyl side chain, which has a stereocenter but is of racemic character.

5.2.3 Synthesis of Polymers P1–P13

The polymer **P2**[157] was synthesised according to literature procedure.

*Synthesis of **P1A***

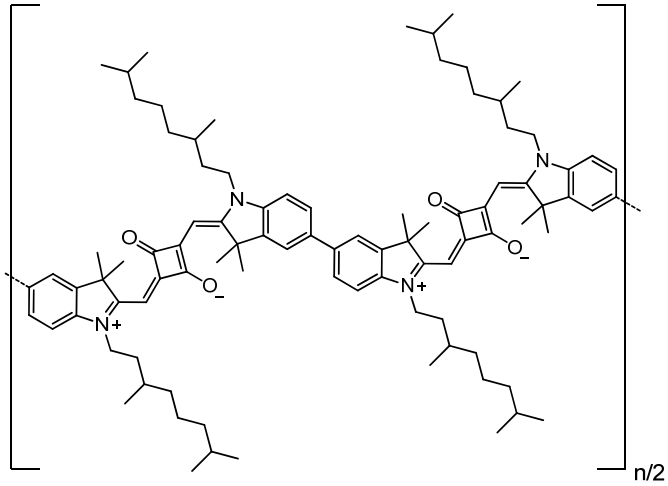

A mixture of $Ni(COD)_2$ (237 mg, 862 μmol), 2,2'-bipyridine (135 mg, 862 μmol), 1,5-cyclooctadiene (93.0 mg, 862 μmol), degassed dry toluene (2 ml), and degassed dry DMF (2 ml) was stirred at rt under nitrogen atmosphere for 30 min. A solution of squaraine **M4** (300 mg, 359 μmol) in degassed dry toluene (6 ml) and degassed dry DMF (6 ml) was added and the mixture was stirred at rt for 5 d. The reaction mixture was poured into MeOH/HCl (20%) (4:1; 500 ml) and stirred for 18 h. The precipitate was filtered through a blue ribbon filter and washed with MeOH. The solid was purified by subsequent *Soxhlet* extractions in hexane, acetone, and THF. Each extraction was carried out until no colouring of the solvent was detected anymore. The remaining solid was dissolved in $CHCl_3$ (30 ml) and dripped into MeOH/HCl (20%) (4:1; 500 ml). The precipitate was filtered through a blue ribbon filter and washed with MeOH.

Yield: 190 mg (~ 281 μmol, ~ 78%) of a purple solid

$(C_{46}H_{62}N_2O_2)_n$ $[675.00]_n$

^{1}H-NMR (400.1 MHz, $CDCl_3$):

δ [ppm] = 7.60–7.44 (4 H), 7.12–6.97 (2 H), 6.17–5.99 (2 H), 4.22–3.92 (4 H), 1.93–1.78 (14 H), 1.70–1.60 (4 H), 1.59–1.49 (2 H), 1.46–1.12 (12 H), 1.10–1.03 (6 H), 0.90–0.81 (12 H).

*Synthesis of **P1B***

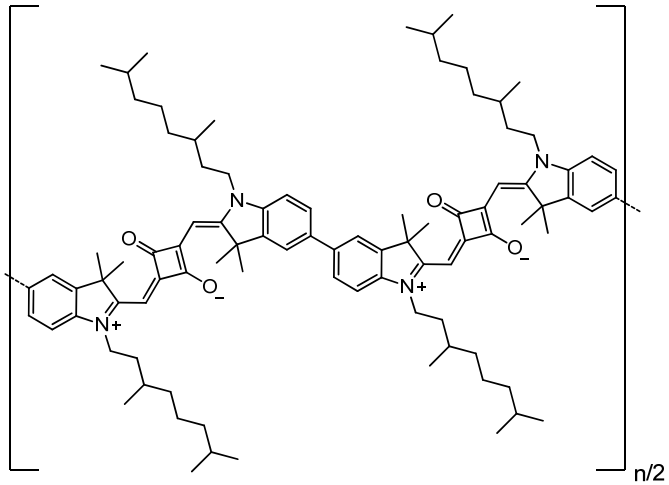

A mixture of $Ni(COD)_2$ (187 mg, 678 μmol), 2,2'-bipyridine (106 mg, 678 μmol), 1,5-cyclooctadiene (73.4 mg, 678 μmol), and degassed dry DMF (4 ml) was stirred at rt under nitrogen atmosphere for 30 min. A solution of **M3** (236 mg, 283 μmol) in degassed dry DMF (10 ml) was added and the resulting mixture was stirred at rt for 6 d. The reaction mixture was poured into MeOH/HCl (20%) (4:1; 500 ml) and stirred for 4 h. The purple precipitate was filtered through a blue ribbon filter and washed with MeOH. The solid was purified by subsequent *Soxhlet* extractions in hexane and acetone. Each extraction was carried out until no colouring of the solvent could be detected anymore. The remaining solid was dissolved in $CHCl_3$ (10 ml) and dripped into MeOH/HCl (20%) (4:1; 500 ml). The purple precipitate was filtered through a blue ribbon filter and washed with MeOH.

Yield: 84.0 mg (~ 124 μmol, ~ 44%) of a purple solid

$(C_{46}H_{62}N_2O_{2)n}$ $[675.00]_n$

^{1}H-NMR (400.1 MHz, $CDCl_3$):

δ [ppm] = 7.59–7.48 (4 H), 7.08–6.99 (2 H), 6.10–5.87 (2 H), 4.26–3.86 (4 H), 1.93–1.75 (14 H), 1.73–1.60 (4 H), 1.59–1.49 (2 H), 1.46–1.12 (12 H), 1.10–1.03 (6 H), 0.90–0.81 (12 H).

*Synthesis of **P3***

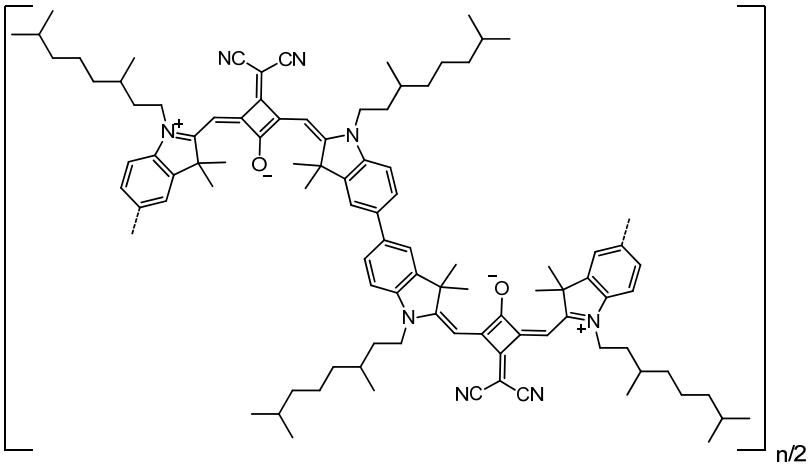

A mixture of $Ni(COD)_2$ (224 mg, 816 μmol), 2,2'-bipyridine (127 mg, 816 μmol), 1,5-cyclooctadiene (88.0 mg, 816 μmol), degassed toluene (2 ml), and degassed DMF (2 ml) was stirred at 65°C under nitrogen atmosphere for 30 min. A solution of squaraine **M6** (300 mg, 340 μmol) in degassed toluene (4 ml) and degassed DMF (4 ml) was added and the resulting mixture was stirred at 65°C for 6 d. The reaction mixture was poured into MeOH/HCl (20%) (4:1, 500 ml) and stirred for 5 h. The purple precipitate was filtered off and washed consecutively with hexane, MeOH and acetone using a *Soxhlet* extractor. Each washing ran overnight. The major part remained in the acetone fraction (192 mg, 265 μmol 78%) with very little solid that remained insoluble in acetone. Preparative GPC was used to separate the acetone fraction into two batches of different molecular weight and to isolate the cyclic trimer **Tri1** (see p. 323).

Yield: **P3–1**: 58 mg (~ 80.2 μmol, ~ 24%), **P3–2**: 53 mg (~ 73.3 μmol, ~ 22%).

$(C_{49}H_{62}N_4O)_n$ $[723.05]_n$

^{1}H-NMR (400.1 MHz, $CDCl_3$):

δ [ppm] = 7.64–7.44 (4 H), 7.18–7.04 (2 H), 6.62–6.44 (2 H), 4.23–3.87 (4 H), 1.92–1.58 (18 H), 1.58–1.46 (2 H), 1.46–1.10 (12 H), 1.10–0.98 (6 H), 0.92–0.76 (12 H).

*Synthesis of **P4***

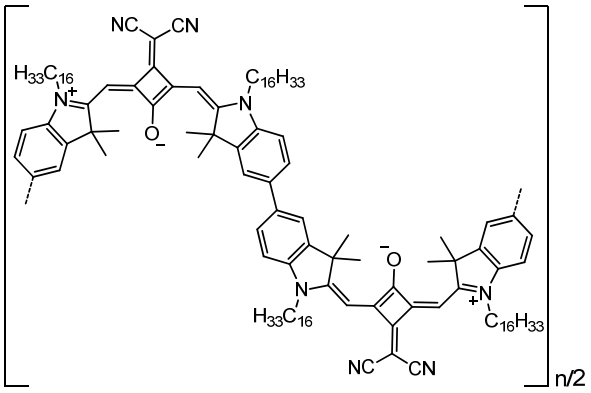

A mixture of $Ni(COD)_2$ (152 mg, 571 μmol), 2,2'-bipyridine (89.0 mg, 571 μmol), 1,5-cyclooctadiene (62.0 mg, 571 μmol), degassed toluene (1 ml), and degassed DMF (2 ml) was stirred at 65°C under nitrogen atmosphere for 30 min. A solution of squaraine **M7** (250 mg, 238 μmol) in degassed toluene (4.5 ml) and degassed DMF (3.5 ml) was added and the resulting mixture was stirred at rt for 6 d. The reaction mixture was poured into MeOH/HCl (20%) (4:1, 500 ml) and stirred for 90 min. The purple precipitate was filtered off and washed consecutively with hexane and MeOH using a *Soxhlet* extractor. Each washing ran overnight. The remaining solid was dissolved in $CHCl_3$ (30 ml) and poured into MeOH/HCl (20%) (4:1, 500 ml). The resulting precipitate was filtered off and dried under high vacuum. The product was obtained as purple solid (167 mg, 187 μmol 78%). Preparative GPC was used to separate the acetone fraction into two batches of different molecular weight and to isolate the cyclic trimer **Tri2** (see p. 324).

Yield: **P4–1**: 61 mg (~ 68.4 μmol, ~ 29%), **P4–2**: 40 mg (~ 44.9 μmol, ~ 19%).

$(C_{61}H_{86}N_4O)_n$ $[891.36]_n$

^{1}H-NMR (400.1 MHz, $CDCl_3$):

δ [ppm] = 7.66–7.44 (4 H), 7.20–7.06 (2 H), 6.66–6.46 (2 H), 4.20–3.80 (4 H), 1.92–1.74 (16 H), 1.54–1.42 (4 H), 1.42–1.33 (4 H), 1.33–1.12 (44 H), 0.90–0.81 (6 H).

*Synthesis of **P5***

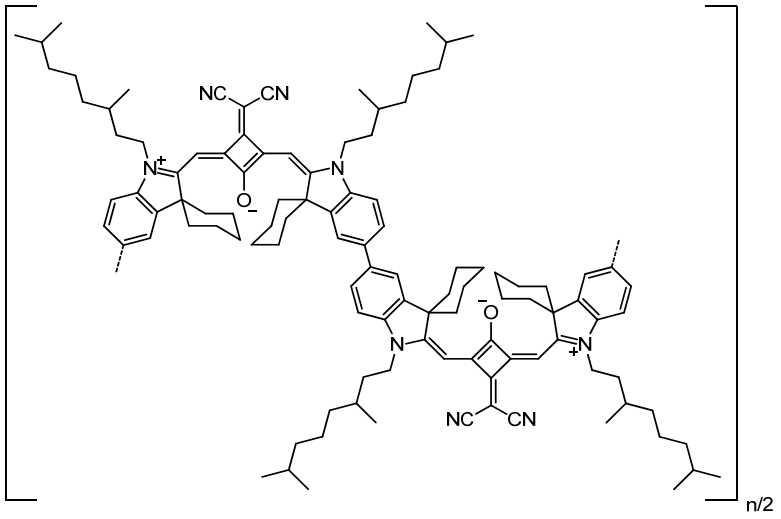

A mixture of $Ni(COD)_2$ (206 mg, 748 μmol), 2,2'-bipyridine (117 mg, 748 μmol), 1,5-cyclooctadiene (81.0 mg, 748 μmol), degassed toluene (3 ml), and degassed DMF (3 ml) was stirred at 65°C under nitrogen atmosphere for 30 min. A solution of squaraine **M9** (300 mg, 312 μmol) in degassed toluene (5 ml) and degassed DMF (5 ml) was added and the resulting mixture was stirred at 65°C for 6 d. The reaction mixture was poured into MeOH/HCl (20%) (4:1, 500 ml) and stirred for 5 h. The purple precipitate was filtered off and washed consecutively with hexane, MeOH, and acetone using a *Soxhlet* extractor. Each washing ran until no colouring of the solvent could be detected anymore. The remaining solid was dissolved in little DCM and poured into an excess of hexane. The resulting precipitate was filtered off and dried under high vacuum (148 mg, 184 μmol 59%). Preparative GPC was used to to isolate the cyclic trimer **Tri3** (see p. 326) and to remove further small oligomers from the polymer fraction.

Yield: 98 mg (122 μmol, 39%)

$(C_{55}H_{70}N_4O)_n$ $[803.17]_n$

^{1}H-NMR (400.1 MHz, $CDCl_3$):

δ [ppm] = 8.22–7.91 (2 H), 7.70–7.52 (2 H), 7.24–7.06 (2 H), 6.53–6.40 (2 H), 4.41–3.91 (4 H), 2.97–2.58 (4 H), 2.51–2.25 (2 H), 2.20–1.74 (12 H), 1.74–1.10 (22 H), 1.08–0.93 (6 H), 0.92–0.74 (12 H).

*Synthesis of **P6***

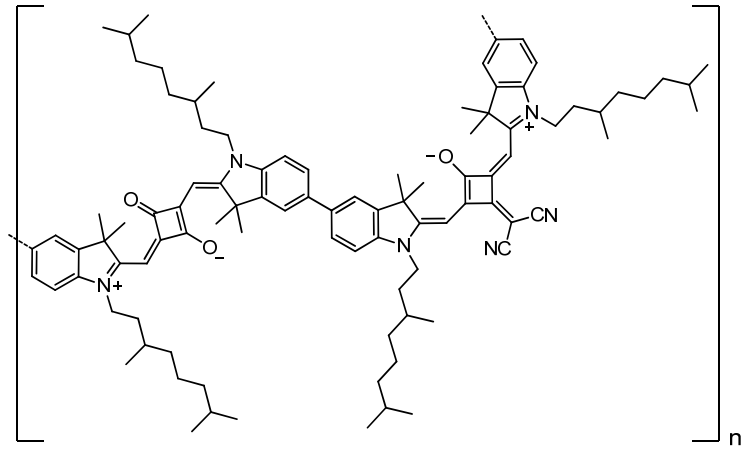

Squaraine **M8** (170 mg, 183 μmol), squaraine **M6** (162 mg, 183 μmol) and $NaHCO_3$ (615 mg, 7.32 mmol) were dissolved in dry THF (16 ml) and H_2O (4 ml) under nitrogen atmosphere. The mixture was degassed in a stream of nitrogen for 10 min and $Pd(PPh_3)_4$ (4.23 mg, 3.66 μmol) was added. The solution was stirred at 105°C for 6 d. Brine (20 ml) and $CHCl_3$ (20 ml) were added and the layers were separated. The organic layer was washed with brine (2 × 20 ml) and H_2O (20 ml) and the solvent was evaporated under reduced pressure. The residue was dissolved in $CHCl_3$ (10 ml) and the solution dripped into MeOH/H_2O (4:1, 500 ml). The precipitate was filtered and washed with MeOH and H_2O. The crude product was purified by subsequent *Soxhlet* extractions using MeOH, hexane, and acetone. The remaining solid was dissolved in little $CHCl_3$ and dripped into MeOH. The precipitate was filtered and washed with MeOH.

Yield: 88.0 mg (~ 62.9 μmol, ~ 34%) of a ruby coloured solid

$(C_{95}H_{124}N_6O_3)_n$ $[1398.04]_n$

^{1}H-NMR (400.1 MHz, $CDCl_3$):

δ[ppm] = 7.62–7.47 (8 H), 7.14–7.01 (4H), 6.55 (2 H), 6.01 (2 H), 4.26–3.88 (8 H), 1.97–1.76 (24 H), 1.76–1.46 (16 H), 1.46–1.11 (24 H), 1.11–0.98 (12 H), 0.93–0.77 (24 H).

*Synthesis of **P7***

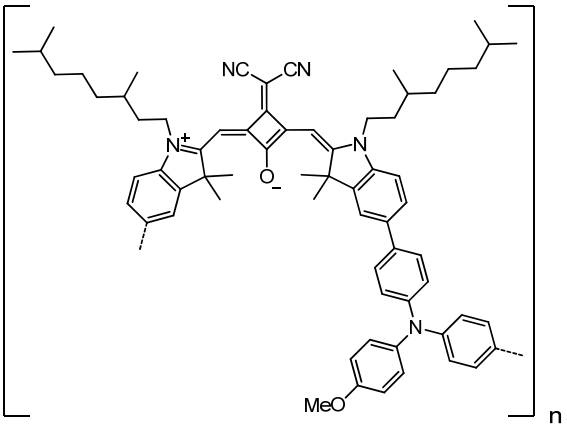

Squaraine **M6** (211 mg, 240 μmol), **26** (126 mg, 240 μmol), and $NaHCO_3$ (805 mg, 9.58 mmol) were dissolved in H_2O (4 ml) and THF (16 ml) under nitrogen atmosphere and degassed in a stream of nitrogen for 10 min. $Pd(PPh_3)_4$ (2.77 mg, 2.40 μmol) was added and the mixture was stirred at 100°C for 5 d. The mixture was extracted with $CHCl_3$ (40 ml) and washed with H_2O (3 × 40 ml). The solvent was evaporated, the residue dissolved in little $CHCl_3$ and dripped into hexane. The precipitate was filtered through a blue ribbon filter and washed with hexane. The residue was washed consecutively with hexane and acetone using a *Soxhlet* extractor. Preparative GPC was used to isolate a cyclic dimer **Dim1** (see p. 322) out of the hexane fractions (both filtrate and *Soxhlet*).

$(C_{68}H_{77}N_5O_2)_n$ $[996.37]_n$

Yield: 68.0 mg (~ 68.2 μmol, ~ 29%)

^{1}H-NMR (400.1 MHz, $CDCl_3$):

δ [ppm] = 7.60–7.40 (8 H), 7.19–7.13 (6 H), 7.10–7.03 (2 H), 6.94–6.86 (2 H), 6.52 (s, 2 H), 4.16–3.92 (4 H, NCH_2), 3.83 (s, 3 H, OCH_3), 1.90–1.73 (14 H, CH_3, CH), 1.73–1.59 (4 H, CH_2), 1.59–1.47 (m, 2 H, CH), 1.46–1.12 (12 H), 1.05 (d, ^3J = 6.3 Hz, 6 H, CH_3), 0.87 (d, ^3J = 6.6 Hz, 12 H, CH_3).

*Synthesis of **P8***

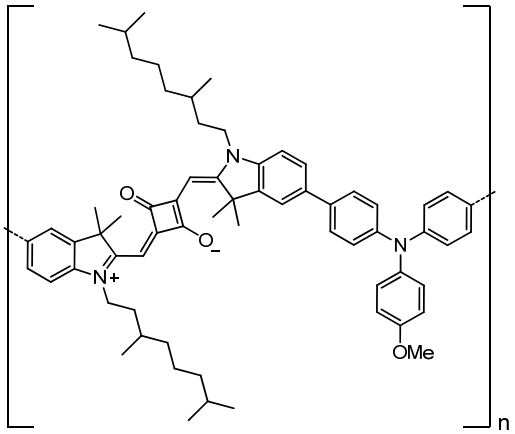

Squaraine **M4** (200 mg, 240 μmol), **26** (126 mg, 240 μmol) and $NaHCO_3$ (805 mg, 9.58 mmol) were dissolved in H_2O (4 ml) and THF (16 ml) under nitrogen atmosphere and degassed in a stream of nitrogen for 10 min. $Pd(PPh_3)_4$ (2.77 mg, 2.40 μmol) was added and the mixture was stirred at 100°C for 5 d. The mixture was extracted with $CHCl_3$ (40 ml) and washed with H_2O (3 × 40 ml). The solvent was evaporated, the residue dissolved in little $CHCl_3$ and dripped into hexane. The precipitate was filtered and washed consecutively with acetone, DCM, and $CHCl_3$ using a *Soxhlet* extractor. A major part remained insoluble in $CHCl_3$, so the fraction soluble in $CHCl_3$ but insoluble in DCM was used. The solid was dissolved in $CHCl_3$ and dripped into MeOH (400 ml). The precipitate was filtered through a blue ribbon filter and washed with MeOH.

Yield: 57.0 mg (~ 60.1 μmol, ~ 25%)

$(C_{65}H_{77}N_3O_3)_n$ $[948.33]_n$

^{1}H-NMR (400.1 MHz, $CDCl_3$):

δ [ppm] = 7.58–7.42 (8 H), 7.21–7.13 (6 H), 7.04–6.97 (2 H), 6.94–6.86 (2 H), 5.99 (s, 2 H), 4.20–3.90 (4 H), 3.84 (s, 3 H), 1.94–1.78 (14 H), 1.78–1.59 (4 H), 1.59–1.47 (2 H), 1.45–1.10 (12 H), 1.10–1.00 (6 H), 0.90–0.82 (12 H).

*Synthesis of **P9***

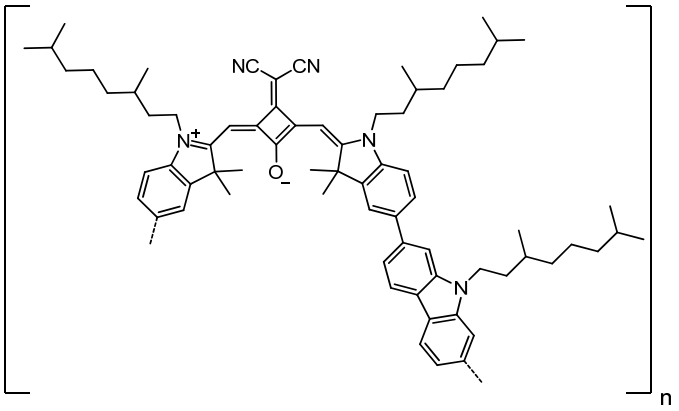

Under nitrogen atmosphere, a mixture of squaraine **M6** (200 mg, 227 μmol), **29** (127 mg, 227 μmol), an aqueous solution of Na_2CO_3 (1 M, 1.27 ml, 1.27 mmol) and dry toluene (10 ml) was degassed in a stream of nitrogen for 15 min. $Pd(PPh_3)_4$ (20.9 mg, 18.0 μmol) was added and the mixture refluxed for 4 d. The solvent was removed under reduced pressure and the residue was dissolved in $CHCl_3$ (50 ml) and washed with H_2O (3 × 30 ml). The solvent was evaporated under reduced pressure and the crude product was washed consecutively with hexane, MeOH, and acetone using a *Soxhlet* extractor. The residue was dissolved in little $CHCl_3$ and dripped into MeOH. The product was filtered through a blue ribbon filter and washed with MeOH.

Yield: 168 mg (~ 163 μmol, ~ 72%) of a shiny green solid

$(C_{71}H_{89}N_5O)_n$ $[1028.50]_n$

^{1}H-NMR (400.1 MHz, $CDCl_3$):

δ [ppm] = 8.24–8.08 (2 H), 7.79–7.62 (4 H), 7.62–7.43 (4 H), 7.20–7.08 (2 H), 6.57 (s, 2 H), 4.54–4.30 (2 H), 4.20–3.96 (4 H), 2.06–1.75 (15 H), 1.75–1.47 (9 H), 1.46–0.97 (27 H), 0.93–0.80 (18 H).

*Synthesis of **P10***

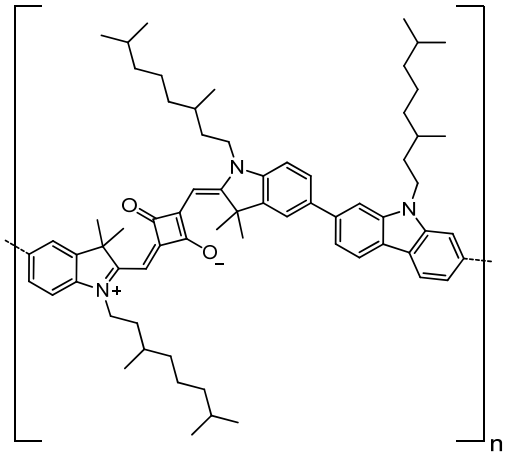

Under nitrogen atmosphere, a mixture of squaraine **M8** (200 mg, 215 μmol), **28** (100 mg, 215 μmol), $NaHCO_3$ (723 mg, 8.61 mmol), dry THF (16 ml), and H_2O (4 ml) was degassed in a stream of nitrogen for 15 min. $Pd(PPh_3)_4$ (4.98 mg, 4.31 μmol) was added and the mixture refluxed for 6 d. $CHCl_3$ (30 ml) and brine (30 ml) were added, the phases separated and the organic phase washed with brine (2 × 30 ml) and H_2O (30 ml). The solvent was evaporated and the residue dissolved in $CHCl_3$ and dripped into MeOH/H_2O (4:1; 500 ml). The precipitate was filtered through a blue ribbon filter and washed with MeOH. The crude product was washed consecutively with hexane, MeOH and acetone using a *Soxhlet* extractor. The remaining solid was dissolved in little $CHCl_3$ and dripped into MeOH. The violet precipitate was filtered through a blue ribbon filter and washed with MeOH.

Yield: 179 mg (~ 183 μmol, ~ 85%) of a violet solid

$(C_{68}H_{89}N_3O_2)_n$ $[980.45]_n$

^{1}H-NMR (400.1 MHz, $CDCl_3$):

δ [ppm] = 8.22–8.10 (2 H), 7.79–7.41 (8 H), 7.16–7.03 (2 H), 6.04 (s, 2 H), 4.60–4.26 (2 H), 4.26–3.88 (4 H), 2.0–1.78 (15 H), 1.74–1.52 (9 H), 1.52–1.02 (27 H), 0.92–0.85 (12 H), 0.84–0.78 (6 H).

*Synthesis of **P11***

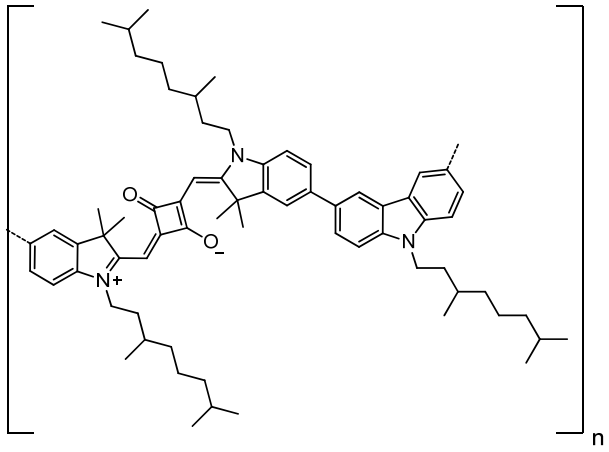

Squaraine **M4** (200 mg, 240 μmol) and **32** (134 mg, 240 μmol) were dissolved in dry toluene (10 ml) under nitrogen atmosphere. An aqueous solution of Na_2CO_3 (1 M, 1.68 ml, 1.68 mmol) was added and the mixture was degassed in a stream of nitrogen for 15 min. $Pd(PPh_3)_4$ (22.1 mg, 19.0 μmol) was added and the reaction mixture was refluxed for 90 h. The solvent was removed under reduced pressure, the residue was dissolved in $CHCl_3$ (50 ml) and the organic layer was washed with H_2O (3 × 30 ml). The solvent was removed under reduced pressure and the crude product was further washed consecutively with hexane, MeOH, acetone, and EA using a *Soxhlet* extractor. The remaining solid was dissolved in little $CHCl_3$ and dripped into MeOH. The violet precipitate was filtered through a blue ribbon filter and washed with MeOH.

Yield: 148 mg (~ 150.9 μmol, ~ 63%) of a blue-violet solid

$(C_{68}H_{89}N_3O_2)_n$ $[980.46]_n$

^{1}H-NMR (400.1 MHz, $CDCl_3$):

δ [ppm] = 8.42–8.27 (2 H), 7.77–7.63 (6 H), 7.52–7.45 (2 H), 7.17–7.03 (2 H), 6.10–5.95 (2 H), 4.50–4.23 (2 H), 4.22–3.88 (4 H), 2.0–1.78 (15 H), 1.74–1.48 (9 H), 1.48–0.99 (27 H), 0.93–0.76 (18 H).

*Synthesis of **P12***

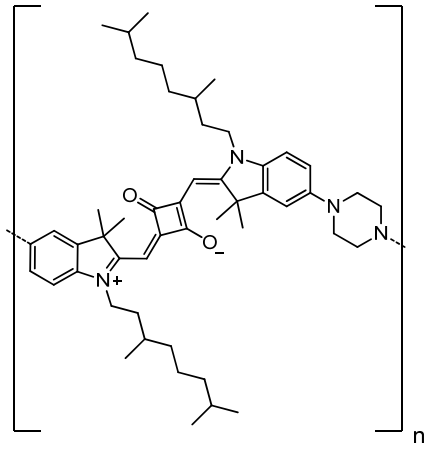

Under nitrogen atmosphere, a degassed solution of toluene and 1-butanol (1:1; 80 ml) was added to **33** (227 mg, 334 μmol) and 3,4-dihydroxycyclobut-3-ene-1,2-dione (38.0 mg, 334 μmol). The mixture was refluxed using a *Dean-Stark* trap under the absence of light for 6 d. The solvent was removed under reduced pressure and the residue was dissolved in $CHCl_3$ (14 ml) and dripped into MeOH/H_2O (4:1; 400 ml). The precipitate was filtered through a blue ribbon filter and washed with MeOH. The crude product was washed consecutively with hexane, MeOH, and acetone using a *Soxhlet* extractor. The remaining solid was dissolved in little $CHCl_3$ (9 ml) and dripped into MeOH/H_2O (6:1). The violet precipitate was filtered through a blue ribbon filter and washed with MeOH.

Yield: 127 mg (~ 167 μmol, ~ 50%) of a violet solid

$(C_{50}H_{70}N_4O_2)_n$ $[759.12]_n$

^{1}H-NMR (400.1 MHz, $CDCl_3$):

δ [ppm] = 7.14–6.64 (6 H), 5.89 (2 H), 4.18–3.78 (4 H), 3.52–3.09 (8 H), 1.93–1.68 (14 H), 1.68–1.47 (6 H), 1.46–1.10 (12 H), 1.10–0.99 (6 H), 0.92–0.77 (12 H).

*Synthesis of **P13***

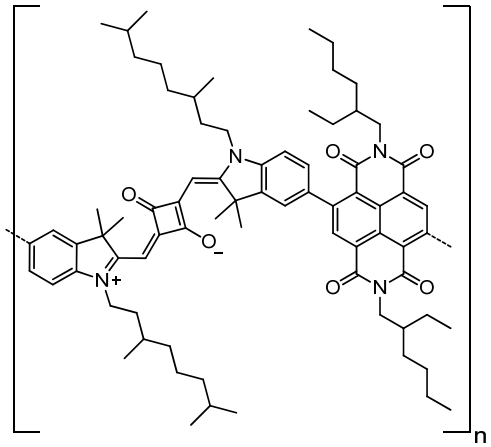

Compound **36** (140 mg, 215 μmol), squaraine **M8** (200 mg, 215 μmol), and $NaHCO_3$ (723 mg, 8.61 mmol) were dissolved in THF (16 ml) and H_2O (4 ml) under nitrogen atmosphere and the solution was degassed in a stream of nitrogen for 15 min. $Pd(PPh_3)_4$ (4.98 mg, 4.31 μmol) was added and the resulting mixture was refluxed for 6 d. $CHCl_3$ (30 ml) and brine (30 ml) were added and the layers were separated. The organic layer was washed with brine (2 × 30 ml) and H_2O (30 ml) and the solvent was removed under reduced pressure. The residue was dissolved in $CHCl_3$ (15 ml) and dripped into MeOH/H_2O (4:1, 350 ml). The precipitate was filtered off, placed in a *Soxhlet* extractor and was subsequently washed with hexane, MeOH, acetone, and DCM. The remaining solid was dissolved in little $CHCl_3$ and dripped into an excess of MeOH. The product was filtered and washed with MeOH.

Yield: 137 mg (118 μmol, 55%) of a voluminous purple solid

$(C_{76}H_{98}N_4O_6)_n$ [1163.62]

^{1}H-NMR (600.1 MHz, $CDCl_3$):

δ[ppm] = 8.70 (s, 2 H), 7.50–7.35 (4 H), 7.18–7.02 (2 H), 6.06 (s, 2 H), 4.32–3.74 (8 H, NCH_2), 2.10–1.75 (16 H, CH_3, C*H*), 1.75–1.63 (4 H, CH_2), 1.63–1.50 (2 H, C*H*), 1.50–1.24 (28 H, CH_2), 1.24–1.04 (6 H, CH_3), 0.96–0.80 (24 H, CH_3).

5.2.4 Synthesis of Cyclic Squaraines

Synthesis of ***Dim1***

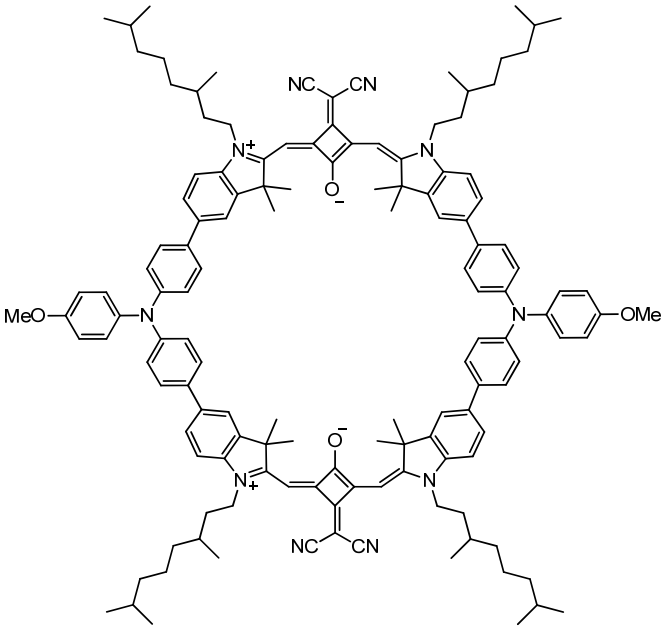

The dimer **Dim1** was obtained as a side product of the synthesis of polymer **P7** (p. 315). It was isolated out of the hexane fractions of the filtrate of the precipitation and the *Soxhlet* extraction by preparative recycling GPC in $CHCl_3$.

Yield: 3.00 mg (1.51 μmol, 1%)

$C_{136}H_{154}N_{10}O_4$ [1992.75]

^{1}H-NMR (400.1 MHz, $CDCl_3$):

δ [ppm] = 7.58–7.47 (16 H), 7.23–7.17 (12 H), 7.10–7.05 (4 H), 6.94–6.89 (4 H), 6.62–6.49 (4 H), 4.17–3.94 (8 H, NCH_2), 3.85 (s, 6 H, OCH_3), 1.95–1.78 (28 H, CH_3, CH), 1.77–1.59 (8 H, CH_2), 1.58–1.48 (4 H, CH), 1.47–1.13 (24 H, CH_2), 1.05 (d, ^3J = 6.4 Hz, 12 H, CH_3), 0.87 (d, ^3J = 6.6 Hz, 24 H, CH_3).

ESI-MS pos (high resolution): [M^{+}]

calc.: 1991.21490 m/z

found: 1991.21554 m/z Δ = 0.32 ppm.

Synthesis of ***Tri1***

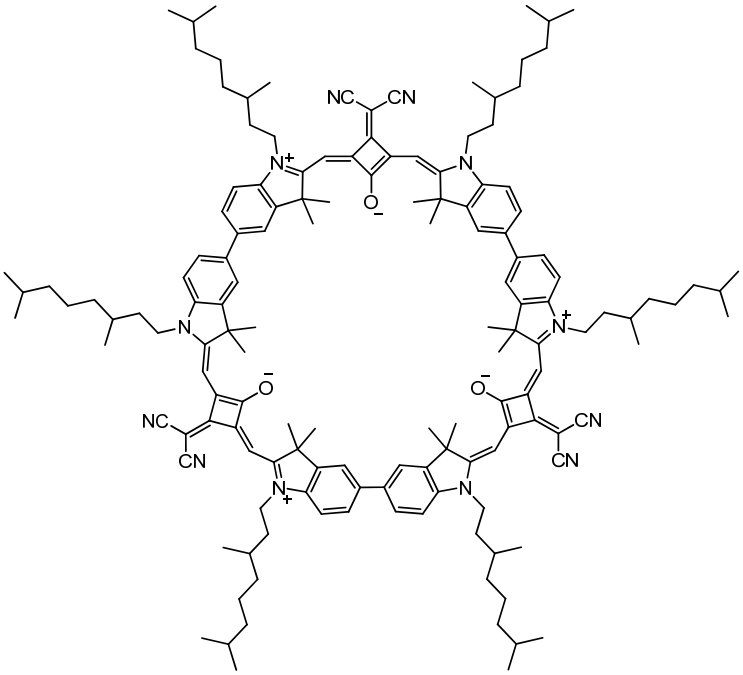

The trimer **Tri1** was obtained as a side product of the synthesis of polymer **P3** (p. 311). It was isolated by preparative recycling GPC in $CHCl_3$ in the process of the splitting of the main polymer batch. It was further purified by flash chromatography (eluent: DCM/MeOH 200:1) and HPLC (flow 10 ml/min: eluent: DCM/MeOH 600:1).

Yield: 14.0 mg (6.80 μmol, 6%) of a dark red solid

$C_{147}H_{186}N_{12}O_3$ [2169.13]

^{1}H-NMR (600.1 MHz, $CDCl_3$):

δ[ppm] = 7.74 (dd, ^3J = 8.3 Hz, ^4J = 1.6 Hz, 6 H, H-6), 7.56 (d, ^4J = 1.4 Hz, 6 H, H-4), 7.15 (d, ^3J = 8.3 Hz, 6 H, H-7), 6.64 (s, 6 H, H-8), 4.17–4.04 (m, 12 H, NCH_2), 1.90–1.81 (42 H, CH_3, CH), 1.74–1.63 (m, 12 H, CH_2), 1.56–1.50 (m, 6 H, CH), 1.45–1.33 (12 H, CH_2), 1.32–1.22 (12 H, CH_2), 1.20–1.15 (12 H, CH_2), 1.07 (d, ^3J = 6.3 Hz, 18 H, CH_3), 0.89–0.86 (36 H, CH_3).

^{13}C-NMR (150.9 MHz, $CDCl_3$):

δ[ppm] = 174.3 (quart), 171.2 (quart), 167.8 (quart), 166.3 (quart), 143.8 (quart), 141.4 (quart), 135.9 (quart), 125.8 (tert), 119.7 (tert), 118.8 (quart), 110.4 (tert), 89.6 (tert), 49.3 (quart), 43.1 (sec), 41.2 (quart), 39.2 (sec), 37.2 (sec),

34.3 (sec), 31.0 (tert), 28.0 (tert), 26.70 (prim)[1], 26.67 (prim)[1], 24.6 (sec), 22.7 (prim)[1], 22.6 (prim)[1], 19.7 (prim).

ESI-MS pos (high resolution): $[M^{\cdot\,++}]$

calc.: 1083.73800 m/z

found: 1083.73987 m/z Δ = 1.73 ppm.

*Synthesis of **Tri2***

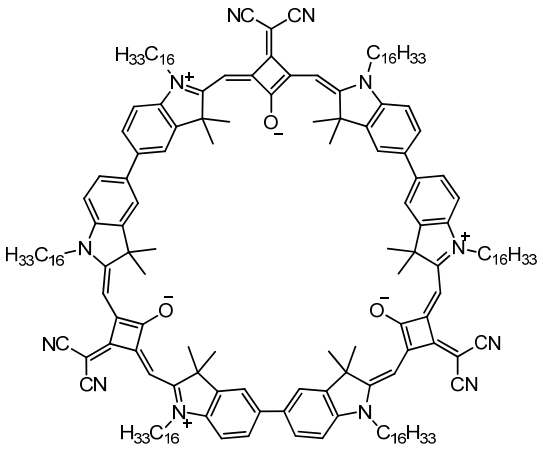

The trimer **Tri2** was obtained as a side product of the synthesis of polymer **P4** (p. 312). It was isolated by preparative recycling GPC in $CHCl_3$ in the process of the splitting of the main polymer batch. It was further purified by flash chromatography (eluent: DCM/MeOH 200:1) and HPLC (flow 10 ml/min: eluent: DCM/MeOH 600:1).

Yield: 13.0 mg (4.86 μmol, 6%) of a dark red solid

$C_{183}H_{258}N_{12}O_3$ [2674.09]

[1] The signal of the primary C-atoms splits into two signals of equal intensity even though they are supposed just to give one single signal. Possibly this is due to the alkyl side chain, which has a stereocenter but is of racemic character.

^{1}H-NMR (600.1 MHz, $CDCl_3$):

δ [ppm] = 7.75 (dd, ^{3}J = 8.3 Hz, ^{4}J = 1.4 Hz, 6 H, H-6), 7.57 (d, ^{4}J = 1.1 Hz, 6 H, H-4), 7.17 (d, ^{3}J = 8.3 Hz, 6 H, H-7), 6.66 (s, 6 H, H-8), 4.12–4.04 (m, 12 H, NCH_2), 1.93–1.85 (m, 12 H, CH_2), 1.83 (s, 36 H, CH_3), 1.54–1.45 (m, 12 H, CH_2), 1.42–1.34 (m, 12 H, CH_2), 1.34–1.19 (132 H, CH_2), 0.87 (t, ^{3}J = 6.9 Hz, 18 H, CH_3).

^{13}C-NMR (150.9 MHz, $CDCl_3$):

δ [ppm] = 173.0 (quart), 171.3 (quart), 167.9 (quart), 166.4 (quart), 143.8 (quart), 141.5 (quart), 135.8 (quart), 125.8 (tert), 119.7 (tert), 118.9 (quart), 110.6 (tert), 89.7 (tert), 49.2 (quart), 44.6 (sec), 41.2 (quart), 31.9 (sec), 29.69 (sec), 29.684 (sec), 29.681 (sec), 29.66 (sec), 29.65 (sec), 29.62 (sec), 29.57 (sec), 29.45 (sec), 29.42 (sec), 29.3 (sec), 27.5 (sec), 26.8 (sec), 26.7 (prim), 22.7 (sec), 14.1 (prim).

ESI-MS pos (high resolution): [$M^{\cdot\cdot+++}$]

calc.: 1336.01970 m/z

found: 1336.01980 m/z Δ = 0.08 ppm.

Synthesis of ***Tri3***

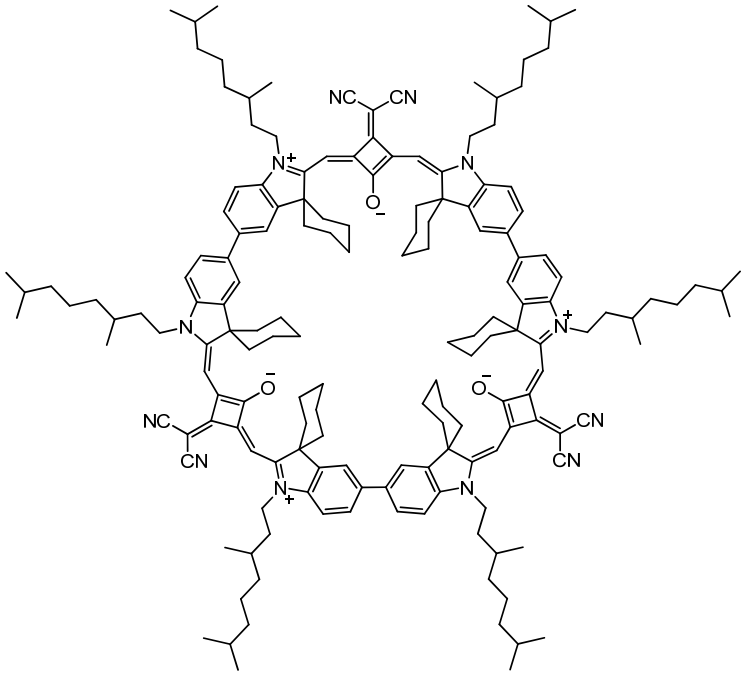

The trimer **Tri3** was obtained as a side product of the synthesis of polymer **P5** (p.313). It was isolated by preparative recycling GPC in $CHCl_3$ out of the main polymer batch and the *Soxhlet* filtrates. It was further purified by flash chromatography (eluent: DCM/MeOH 200:1) and HPLC (flow 10 ml/min: eluent: DCM/MeOH 600:1).

Yield: 16.0 mg (6.64 μmol, 6%) of a dark red solid

$C_{165}H_{210}N_{12}O_3$ [2409.52]

^{1}H-NMR (600.1 MHz, $CDCl_3$):

δ[ppm] = 8.19–8.09 (6 H, H-4), 7.74 (dd, ^3J = 8.4 Hz, ^4J = 1.1 Hz, 6 H, H-6), 7.18 (d, ^3J = 8.4 Hz, 6 H, H-7), 6.55 (s, 6 H, H-8), 4.25–4.02 (m, 12 H, NCH_2), 2.86–2.68 (12 H), 2.66–2.45 (6 H), 2.11–1.93 (12 H), 1.93–1.78 (24 H), 1.77–1.60 (12 H), 1.58–1.50 (6 H), 1.50–1.13 (48 H), 1.09 (d, ^3J = 6.4 Hz, 18 H), 0.88 (d, ^3J = 6.6 Hz, 36 H).

ESI-MS pos (high resolution): [$M^{+\cdot}$]

calc.: 2407.66434 m/z

found: 2407.66214 m/z Δ = 0.92 ppm.

Synthesis of ***Tet1***

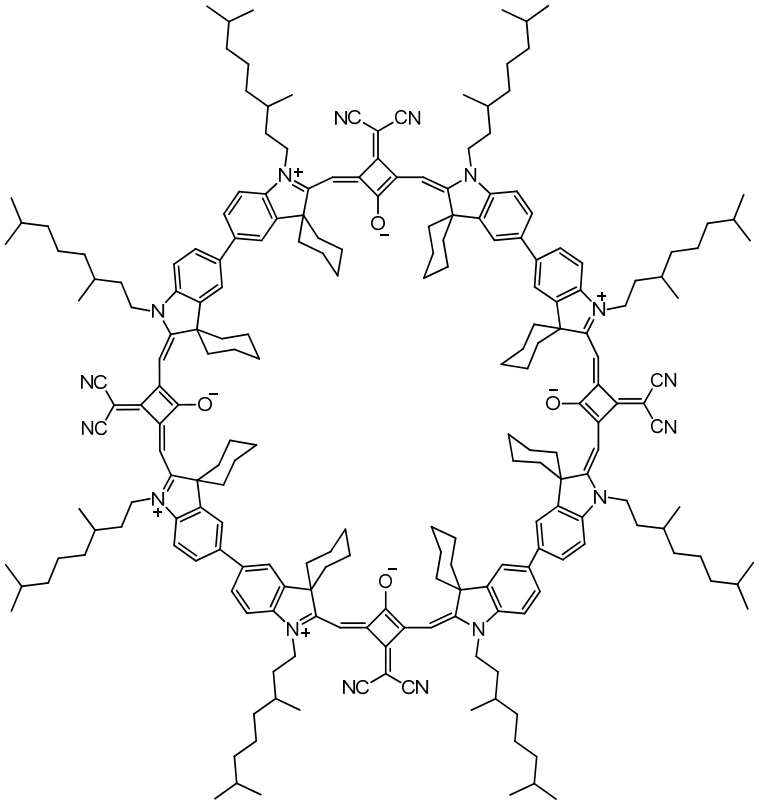

The tetramer **Tet1** was obtained as a side product of the synthesis of polymer **P5** (p. 313). It was isolated by preparative recycling GPC in $CHCl_3$ out of the main polymer batch and the *Soxhlet* filtrates and was further purified by flash chromatography (eluent: DCM/MeOH 200:1).

Yield: 2.00 mg (623 nmol, ~ 1%) of a green solid

$C_{220}H_{280}N_{16}O_4$ [3212.69]

^{1}H-NMR (600.1 MHz, $CDCl_3$):

δ[ppm] = 8.13–8.06 (8 H), 7.60 (d, ^3J = 8.4 Hz, 8 H), 7.16 (d, ^3J = 8.4 Hz, 8 H), 6.47 (s, 8 H), 4.31–4.03 (16 H), 2.86–2.66 (16 H), 2.51–2.30 (8 H), 2.16–1.46 (72 H), 1.45–1.09 (64 H), 1.09 (d, ^3J = 6.3 Hz, 24 H), 0.88 (d, ^3J = 6.6 Hz, 48 H).

ESI-MS pos (high resolution): $[M^{\cdot\cdot++}]$

calc. for x + 2: 1606.11262 m/z

found for x + 2: 1606.11305 m/z Δ = 0.27 ppm.

6 Literature

[1] S. Cohen, J. R. Lacher, J. D. Park, *J. Am. Chem. Soc.* **1959**, *81*, 3480-3480.

[2] D. G. Maahs, D. P. Hegenberg, *Angew. Chem.* **1966**, *78*, 927-931.

[3] A. H. Schmidt, *Synthesis* **1980**, 961-994.

[4] A. Treibs, K. Jacob, *Angew. Chem.-Int. Edit.* **1965**, *4*, 694-695.

[5] A. Treibs, K. Jacob, *Liebigs Ann. Chem.* **1966**, *699*, 153-167.

[6] H.-E. Sprenger, W. Ziegenbein, *Angew. Chem.* **1967**, *79*, 581-582.

[7] W. Ziegenbein, H. E. Sprenger, *Angew. Chem.-Int. Edit.* **1966**, *5*, 893-894.

[8] H. E. Sprenger, W. Ziegenbein, *Angew. Chem.-Int. Edit.* **1966**, *5*, 894.

[9] A. Treibs, K. Jacob, *Liebigs Ann. Chem.* **1968**, *712*, 123-137.

[10] S. Yagi, H. Nakazumi, *Topics Heterocyc. Chem.* **2008**, *14*, 133-181.

[11] S. Cohen, S. G. Cohen, *J. Am. Chem. Soc.* **1966**, *88*, 1533-1536.

[12] D. Keil, H. Hartmann, *Dyes Pigm.* **2001**, *49*, 161-179.

[13] L. A. Wendling, S. K. Koster, J. E. Murray, R. West, *J. Org. Chem.* **1977**, *42*, 1126-1130.

[14] S. Y. Wang, L. Hall, V. V. Diev, R. Haiges, G. D. Wei, X. Xiao, P. I. Djurovich, S. R. Forrest, M. E. Thompson, *Chem. Mater.* **2011**, *23*, 4789-4798.

[15] S. Bruck, C. Krause, R. Turrisi, L. Beverina, S. Wilken, W. Saak, A. Lutzen, H. Borchert, M. Schiek, J. Parisia, *Phys. Chem. Chem. Phys.* **2014**, *16*, 1067-1077.

[16] T. Lin, B. X. Peng, *Dyes Pigm.* **1999**, *43*, 73-76.

[17] D. E. Lynch, K. A. Byriel, *Cryst. Eng.* **1999**, *2*, 225-239.

[18] A. S. Tatikolov, S. M. B. Costa, *J. Photochem. Photobiol. A-Chem.* **2001**, *140*, 147-156.

[19] U. Mayerhöffer, F. Würthner, *Angew. Chem.-Int. Edit.* **2012**, *51*, 5615-5619.

[20] K. Jyothish, M. Hariharan, D. Ramaiah, *Chem. Eur. J.* **2007**, *13*, 5944-5951.

[21] Y. Xu, Z. Li, A. Malkovskiy, S. Sun, Y. Pang, *J. Phys. Chem. B* **2010**, *114*, 8574-8580.

[22] U. Mayerhöffer, F. Würthner, *Chem. Sci.* **2012**, *3*, 1215-1220.

[23] A. J. McKerrow, E. Buncel, P. M. Kazmaier, *Can. J. Chem.-Rev. Can. Chim.* **1995**, *73*, 1605-1615.

[24] J. Wojtyk, A. McKerrow, P. Kazmaier, E. Buncel, *Can. J. Chem.-Rev. Can. Chim.* **1999**, *77*, 903-912.

[25] G. de Miguel, M. Ziolek, M. Zitnan, J. A. Organero, S. S. Pandey, S. Hayase, A. Douhal, *J. Phys. Chem. C* **2012**, *116*, 9379-9389.

[26] J. Fu, L. A. Padilha, D. J. Hagan, E. W. Van Stryland, O. V. Przhonska, M. V. Bondar, Y. L. Slominsky, A. D. Kachkovski, *J. Opt. Soc. Am. B-Opt. Phys.* **2007**, *24*, 67-76.

[27] S. Ohira, I. Rudra, K. Schmidt, S. Barlow, S. J. Chung, Q. Zhang, J. Matichak, S. R. Marder, J. L. Brédas, *Chem. Eur. J.* **2008**, *14*, 11082-11091.

[28] U. Mayerhöffer, B. Fimmel, F. Würthner, *Angew. Chem.-Int. Edit.* **2012**, *51*, 164-167.

[29] S. Webster, S. A. Odom, L. A. Padilha, O. V. Przhonska, D. Peceli, H. H. Hu, G. Nootz, A. D. Kachkovski, J. Matichak, S. Barlow, H. L. Anderson, S. R. Marder, D. J. Hagan, E. W. Van Stryland, *J. Phys. Chem. B* **2009**, *113*, 14854-14867.

[30] S. Kuster, T. Geiger, *Dyes Pigm.* **2012**, *95*, 657-670.

[31] K. D. Volkova, V. B. Kovalska, A. L. Tatarets, L. D. Patsenker, D. V. Kryvorotenko, S. M. Yarmoluk, *Dyes Pigm.* **2007**, *72*, 285-292.

[32] A. L. Tatarets, I. A. Fedyunyayeva, T. S. Dyubko, Y. A. Povrozin, A. O. Doroshenko, E. A. Terpetschnig, L. D. Patsenker, *Anal. Chim. Acta* **2006**, *570*, 214-223.

[33] A. L. Tatarets, I. A. Fedyunyaeva, E. Terpetschnig, L. D. Patsenker, *Dyes Pigm.* **2005**, *64*, 125-134.

[34] U. Mayerhöffer, M. Gsänger, M. Stolte, B. Fimmel, F. Würthner, *Chem. Eur. J.* **2013**, *19*, 218-232.

[35] L. V. Reis, J. P. Serrano, P. Almeida, P. F. Santos, *Dyes Pigm.* **2009**, *81*, 197-202.

[36] S. H. Kim, S. K. Han, J. J. Kim, S. H. Hwang, C. M. Yoon, S. R. Keum, *Dyes Pigm.* **1998**, *39*, 77-87.

[37] S. Webster, D. Peceli, H. Hu, L. A. Padilha, O. V. Przhonska, A. E. Masunov, A. O. Gerasov, A. D. Kachkovski, Y. L. Slominsky, A. I. Tolmachev, V. V. Kurdyukov, O. O. Viniychuk, E. Barrasso, R. Lepkowicz, D. J. Hagan, E. W. Van Stryland, *J. Phys. Chem. Lett.* **2010**, *1*, 2354-2360.

[38] B. Radaram, T. Mako, M. Levine, *Dalton Trans.* **2013**, *42*, 16276-16278.

[39] A. Ajayaghosh, E. Arunkumar, J. Daub, *Angew. Chem.-Int. Edit.* **2002**, *41*, 1766-1769.

[40] B. A. Rao, H. Kim, Y. A. Son, *Sens. Actuator B-Chem.* **2013**, *188*, 847-856.

[41] J. V. Ros-Lis, R. Martínez-Máñez, F. Sancenón, J. Soto, M. Spieles, K. Rurack, *Chem. Eur. J.* **2008**, *14*, 10101-10114.

[42] J. V. Ros-Lis, R. Martínez-Máñez, J. Soto, *Chem. Commun.* **2002**, 2248-2249.

[43] J. V. Ros-Lis, B. Garcia, D. Jiménez, R. Martínez-Máñez, F. Sancenón, J. Soto, F. Gonzalvo, M. C. Valldecabres, *J. Am. Chem. Soc.* **2004**, *126*, 4064-4065.

[44] J. V. Ros-Lis, M. D. Marcos, R. Martínez-Máñez, J. Soto, *Angew. Chem.-Int. Edit.* **2005**, *44*, 4405-4407.

[45] J. V. Ros-Lis, R. Casasús, M. Comes, C. Coll, M. D. Marcos, R. Martínez-Máñez, F. Sancenón, J. Soto, P. Amorós, J. El Haskouri, N. Garró, K. Rurack, *Chem. Eur. J.* **2008**, *14*, 8267-8278.

[46] E. Climent, A. Agostini, M. E. Moragues, R. Martínez-Máñez, F. Sancenón, T. Pardo, M. D. Marcos, *Chem. Eur. J.* **2013**, *19*, 17301-17304.

[47] S. L. Luo, E. L. Zhang, Y. P. Su, T. M. Cheng, C. M. Shi, *Biomaterials* **2011**, *32*, 7127-7138.

[48] J. Fan, Z. Y. Wang, H. J. Zhu, N. Y. Fu, *Sens. Actuator B-Chem.* **2013**, *188*, 886-893.

[49] E. Terpetschnig, H. Szmacinski, J. R. Lakowicz, *Anal. Chim. Acta* **1993**, *282*, 633-641.

[50] M. Sameiro, T. Goncalves, *Chem. Rev.* **2009**, *109*, 190-212.

[51] E. Arunkumar, N. Fu, B. D. Smith, *Chem. Eur. J.* **2006**, *12*, 4684-4690.

[52] J. J. Gassensmith, E. Arunkumar, L. Barr, J. M. Baumes, K. M. DiVittorio, J. R. Johnson, B. C. Noll, B. D. Smith, *J. Am. Chem. Soc.* **2007**, *129*, 15054-15059.

[53] J. R. Johnson, N. Fu, E. Arunkumar, W. M. Leevy, S. T. Gammon, D. Piwnica-Worms, B. D. Smith, *Angew. Chem.-Int. Edit.* **2007**, *46*, 5528-5531.

[54] A. N. Bashkatov, E. A. Genina, V. I. Kochubey, V. V. Tuchin, *J. Phys. D-Appl. Phys.* **2005**, *38*, 2543-2555.

[55] V. Rapozzi, L. Beverina, P. Salice, G. A. Pagani, M. Camerin, L. E. Xodo, *J. Med. Chem.* **2010**, *53*, 2188-2196.

[56] R. R. Avirah, D. T. Jayaram, N. Adarsh, D. Ramaiah, *Org. Biomol. Chem.* **2012**, *10*, 911-920.

[57] F.-P. Gao, Y.-X. Lin, L.-L. Li, Y. Liu, U. Mayerhöffer, P. Spenst, J.-G. Su, J.-Y. Li, F. Würthner, H. Wang, *Biomaterials* **2014**, *35*, 1004-1014.

[58] L. Beverina, M. Crippa, M. Landenna, R. Ruffo, P. Salice, F. Silvestri, S. Versari, A. Villa, L. Ciaffoni, E. Collni, C. Ferrante, S. Bradamante, C. M. Mari, R. Bozio, G. A. Pagani, *J. Am. Chem. Soc.* **2008**, *130*, 1894-1902.

[59] M. Emmelius, G. Pawlowski, H. W. Vollmann, *Angew. Chem.-Int. Edit.* **1989**, *28*, 1445-1471.

[60] K.-Y. Law, *Chem. Rev.* **1993**, *93*, 449-486.

[61] S. A. Odom, S. Webster, L. A. Padilha, D. Peceli, H. Hu, G. Nootz, S. J. Chung, S. Ohira, J. D. Matichak, O. V. Przhonska, A. D. Kachkovski, S. Barlow, J. L. Brédas, H. L. Anderson, D. J. Hagan, E. W. Van Stryland, S. R. Marder, *J. Am. Chem. Soc.* **2009**, *131*, 7510-7511.

[62] S. Webster, J. Fu, L. A. Padilha, O. V. Przhonska, D. J. Hagan, E. W. Van Stryland, M. V. Bondar, Y. L. Slominsky, A. D. Kachkovski, *Chem. Phys.* **2008**, *348*, 143-151.

[63] L. Beverina, M. Crippa, P. Salice, R. Ruffo, C. Ferrante, I. Fortunati, R. Signorini, C. M. Mari, R. Bozio, A. Facchetti, G. A. Pagani, *Chem. Mater.* **2008**, *20*, 3242-3244.

[64] C. Toro, L. De Boni, S. Yao, J. P. Ritchie, A. E. Masunov, K. D. Belfield, F. E. Hernandez, *J. Chem. Phys.* **2009**, *130*, 214504.

[65] E. Collini, S. Carlotto, C. Ferrante, R. Bozio, A. Polimeno, J. Bloino, V. Barone, E. Ronchi, L. Beverina, G. A. Pagani, *Phys. Chem. Chem. Phys.* **2011**, *13*, 12087-12094.

[66] K. D. Belfield, M. V. Bondar, H. S. Haniff, I. A. Mikhailov, G. Luchita, O. V. Przhonska, *ChemPhysChem* **2013**, *14*, 3532-3542.

[67] D. Scherer, R. Dörfler, A. Feldner, T. Vogtmann, M. Schwoerer, U. Lawrentz, W. Grahn, C. Lambert, *Chem. Phys.* **2002**, *279*, 179-207.

[68] D. E. Lynch, U. Geissler, I. R. Peterson, M. Floersheimer, R. Terbrack, L. F. Chi, H. Fuchs, N. J. Calos, B. Wood, C. H. L. Kennard, G. J. Langley, *J. Chem. Soc., Perkin Trans* **1997**, *2*, 827-832.

[69] M. Gsänger, E. Kirchner, M. Stolte, C. Burschka, V. Stepanenko, J. Pflaum, F. Würthner, *J. Am. Chem. Soc.* **2014**, *136*, 2351-2362.

[70] D. Rocca, R. Gebauer, F. De Angelis, M. K. Nazeeruddin, S. Baroni, *Chem. Phys. Lett.* **2009**, *475*, 49-53.

[71] T. Geiger, S. Kuster, J. H. Yum, S. J. Moon, M. K. Nazeeruddin, M. Grätzel, F. Nüesch, *Adv. Funct. Mater.* **2009**, *19*, 2720-2727.

[72] J. Park, C. Barolo, F. Sauvage, N. Barbero, C. Benzi, P. Quagliotto, S. Coluccia, D. Di Censo, M. Grätzel, M. K. Nazeeruddin, G. Viscardi, *Chem. Commun.* **2012**, *48*, 2782-2784.

[73] T. Maeda, N. Shirna, T. Tsukamoto, S. Yagi, H. Nakazumi, *Synth. Met.* **2011**, *161*, 2481-2487.

[74] T. Maeda, Y. Hamamura, K. Miyanaga, N. Shima, S. Yagi, H. Nakazumi, *Org. Lett.* **2011**, *13*, 5994-5997.

[75] A. Dualeh, J. H. Delcamp, M. K. Nazeeruddin, M. Grätzel, *Appl. Phys. Lett.* **2012**, *100*, 173512.

[76] C. H. Chang, Y. C. Chen, C. Y. Hsu, H. H. Chou, J. T. Lin, *Org. Lett.* **2012**, *14*, 4726-4729.

[77] G. M. Shivashimpi, S. S. Pandey, R. Watanabe, N. Fujikawa, Y. Ogomi, Y. Yamaguchi, S. Hayase, *J. Photochem. Photobiol. A-Chem.* **2014**, *273*, 1-7.

[78] J.-H. Yum, P. Walter, S. Huber, D. Rentsch, T. Geiger, F. Nesch, F. D. Angelis, M. Grätzel, M. K. Nazeeruddin, *J. Am. Chem. Soc.* **2007**, *129*, 10320-10321.

[79] S. Alex, U. Santhosh, S. Das, *J. Photochem. Photobiol. A-Chem.* **2005**, *172*, 63-71.

[80] S. Kuster, F. Sauvage, M. K. Nazeeruddin, M. Graetzel, F. A. Nueesch, T. Geiger, *Dyes Pigm.* **2010**, *87*, 30-38.

[81] T. Maeda, S. Arikawa, H. Nakao, S. Yagi, H. Nakazumi, *New J. Chem.* **2013**, *37*, 701-708.

[82] D. Kuang, P. Walter, F. Nuesch, S. Kim, J. Ko, P. Comte, S. M. Zakeeruddin, M. K. Nazeeruddin, M. Grätzel, *Langmuir* **2007**, *23*, 10906-10909.

[83] Y. S. Chen, Z. H. Zeng, C. Li, W. B. Wang, X. S. Wang, B. W. Zhang, *New J. Chem.* **2005**, *29*, 773-776.

[84] G. Cicero, G. Musso, A. Lamberti, B. Camino, S. Bianco, D. Pugliese, F. Risplendi, A. Sacco, N. Shahzad, A. M. Ferrari, B. Ballarin, C. Barolo, E. Tresso, G. Caputo, *Phys. Chem. Chem. Phys.* **2013**, *15*, 7198-7203.

[85] U. Mayerhöffer, K. Deing, K. Gruß, H. Braunschweig, K. Meerholz, F. Würthner, *Angew. Chem.-Int. Edit.* **2009**, *48*, 8776-8779.

[86] K. C. Deing, U. Mayerhöffer, F. Würthner, K. Meerholz, *Phys. Chem. Chem. Phys.* **2012**, *14*, 8328-8334.

[87] W. Kylberg, Y. Zhang, A. Aebersold, F. A. de Castro, T. Geiger, J. Heier, S. Kuster, C. Q. Ma, P. Bäuerle, F. Nüesch, J. N. Tisserant, R. Hany, *Org. Electron.* **2012**, *13*, 1204-1212.

[88] T. Maeda, T. Tsukamoto, A. Seto, S. Yagi, H. Nakazumi, *Macromol. Chem. Phys.* **2012**, *213*, 2590-2597.

[89] D. B. Yang, Q. Q. Yang, L. Yang, Q. Luo, Y. Huang, Z. Y. Lu, S. L. Zhao, *Chem. Commun.* **2013**, *49*, 10465-10467.

[90] L. Beverina, M. Drees, A. Facchetti, M. Salamone, R. Ruffo, G. A. Pagani, *Eur. J. Org. Chem.* **2011**, 5555-5563.

[91] D. Bagnis, L. Beverina, H. Huang, F. Silvestri, Y. Yao, H. Yan, G. A. Pagani, T. J. Marks, A. Facchetti, *J. Am. Chem. Soc.* **2010**, *132*, 4074-4075.

[92] F. Silvestri, M. D. Irwin, L. Beverina, A. Facchetti, G. A. Pagani, T. J. Marks, *J. Am. Chem. Soc.* **2008**, *130*, 17640-17641.

[93] S. Wang, E. I. Mayo, M. D. Perez, L. Griffe, G. Wei, P. I. Djurovich, S. R. Forrest, M. E. Thompson, *Appl. Phys. Lett.* **2009**, *94*, 233304.

[94] G. Wei, S. Wang, K. Renshaw, M. E. Thompson, S. R. Forrest, *ACS Nano* **2010**, *4*, 1927-1934.

[95] G. D. Wei, R. R. Lunt, K. Sun, S. Y. Wang, M. E. Thompson, S. R. Forrest, *Nano Lett.* **2010**, *10*, 3555-3559.

[96] B. E. Lassiter, G. D. Wei, S. Y. Wang, J. D. Zimmerman, V. V. Diev, M. E. Thompson, S. R. Forrest, *Appl. Phys. Lett.* **2011**, *98*.

[97] G. Wei, X. Xiao, S. Wang, J. D. Zimmerman, K. Sun, V. V. Diev, M. E. Thompson, S. R. Forrest, *Nano Lett.* **2011**, *11*, 4261-4264.

[98] G. Wei, X. Xiao, S. Wang, K. Sun, K. J. Bergemann, M. E. Thompson, S. R. Forrest, *ACS Nano* **2012**, *6*, 972-978.

[99] X. Xiao, G. Wei, S. Wang, J. D. Zimmerman, C. K. Renshaw, M. E. Thompson, S. R. Forrest, *Adv. Mater.* **2012**, *24*, 1956-1960.

[100] J. D. Zimmerman, X. Xiao, C. K. Renshaw, S. Wang, V. V. Diev, M. E. Thompson, S. R. Forrest, *Nano Lett.* **2012**, *12*, 4366-4371.

[101] K. N. Liang, M. S. Farahat, J. Perlstein, K. Y. Law, D. G. Whitten, *J. Am. Chem. Soc.* **1997**, *119*, 830-831.

[102] H. J. Chen, W. G. Herkstroeter, J. Perlstein, K. Y. Law, D. G. Whitten, *J. Phys. Chem.* **1994**, *98*, 5138-5146.

[103] A. Ajayaghosh, P. Chithra, R. Varghese, K. P. Divya, *Chem. Commun.* **2008**, 969-971.

[104] A. Ajayaghosh, P. Chithra, R. Varghese, *Angew. Chem.-Int. Edit.* **2007**, *46*, 230-233.

[105] J. Gerold, U. Holzenkamp, H. Meier, *Eur. J. Org. Chem.* **2001**, 2757-2763.

[106] S. Yagi, T. Ohta, N. Akagi, H. Nakazumi, *Dyes Pigm.* **2008**, *77*, 525-536.

[107] S. Yagi, Y. Nakasaku, T. Maeda, H. Nakazumi, Y. Sakurai, *Dyes Pigm.* **2011**, *90*, 211-218.

[108] W. V. Moreshead, O. V. Przhonska, M. V. Bondar, A. D. Kachkovski, I. H. Nayyar, A. E. Masunov, A. W. Woodward, K. D. Belfield, *J. Phys. Chem. C* **2013**, *117*, 23133-23147.

[109] Y.-Y. Chen, J. H.K. Hall, *Polym. Bull.* **1986**, *16*, 419-425.

[110] E. E. Havinga, W. Tenhoeve, H. Wynberg, *Synth. Met.* **1993**, *55*, 299-306.

[111] G. Brocks, A. Tol, *J. Phys. Chem.* **1996**, *100*, 1838-1846.

[112] E. E. Havinga, W. t. Hoeve, H. Wynberg, *Polym. Bull.* **1992**, *29*, 119-126.

[113] E. E. Havinga, A. Pomp, W. Tenhoeve, H. Wynberg, *Synth. Met.* **1995**, *69*, 581-582.

[114] C. R. Chenthamarakshan, A. Ajayaghosh, *Chem. Mater.* **1998**, *10*, 1657-1663.

[115] H.-C. Lu, W.-T. Whang, B.-M. Cheng, *Synth. Met.* **2010**, *160*, 1002-1007.

[116] H. C. Lu, W. T. Whang, B. M. Cheng, *Chem. Phys. Lett.* **2010**, *500*, 267-271.

[117] H. C. Lu, W. T. Whang, B. M. Cheng, *J. Mater. Chem.* **2011**, *21*, 2568-2576.

[118] C. R. Chenthamarakshan, J. Eldo, A. Ajayaghosh, *Macromolecules* **1999**, *32*, 5846-5851.

[119] C. R. Chenthamarakshan, A. Ajayaghosh, *Tetrahedron Lett.* **1998**, *39*, 1795-1798.

[120] C. R. Chenthamarakshan, J. Eldo, A. Ajayaghosh, *Macromolecules* **1999**, *32*, 251-257.

[121] J. Eldo, A. Ajayaghosh, *Chem. Mater.* **2002**, *14*, 410-418.

[122] A. Ajayaghosh, J. Eldo, *Org. Lett.* **2001**, *3*, 2595-2598.

[123] J. Y. Wu, E. F. Huo, Z. B. Wu, Z. Y. Lu, M. G. Xie, Q. Jiang, *e-Polymers* **2007**, ISSN 1618-7229.

[124] E. F. Huo, J. Y. Wu, B. F. Song, Y. Li, Q. Jiang, M. G. Xie, *Chin. Chem. Lett.* **2007**, *18*, 1531-1534.

[125] Q. Q. Shi, W. Q. Chen, J. F. Xiang, X. M. Duan, X. W. Zhan, *Macromolecules* **2011**, *44*, 3759-3765.

[126] W. Zhang, F. Tao, K. G. Meng, L. Y. Xi, Z. Wang, Y. Li, Q. Jiang, *Polym. Bull.* **2012**, *68*, 349-360.

[127] W. Zhang, F. Tao, K. G. Meng, Z. Wang, L. Y. Xi, Y. Li, Q. Jiang, *J. Mater. Sci.* **2011**, *46*, 5363-5370.

[128] M. A. B. Block, S. Hecht, *Macromolecules* **2004**, *37*, 4761-4769.

[129] E. G. McRae, M. Kasha, in *Physical Processes in Radiation Biology* (Eds.: L. Augstein, R. Mason, B. Rosenberg), New York, **1964**, pp. 23-42.

[130] M. Kasha, H. R. Rawls, M. Ashraf El-Bayoumi, *Pure Appl. Chem.* **1965**, *11*, 371-392.

[131] M. Kasha, *Radiat. Res.* **1963**, *20*, 55-71.

[132] A. I. Kiprianov, *Russ. Chem. Rev.* **1971**, *40*, 594-607.

[133] J. A. Funkhouser, W. R. Brode, *J. Am. Chem. Soc.* **1934**, *56*, 2172-2173.

[134] K. Shibata, *Bull. Chem. Soc. Jpn.* **1953**, *26*, 105-108.

[135] L. G. S. Brooker, L. A. Smith, *J. Am. Chem. Soc.* **1937**, *59*, 67-74.

[136] E. E. Jelley, *Nature* **1936**, *138*, 1009-1010.

[137] G. Scheibe, *Angew. Chem.* **1937**, *50*, 212-219.

[138] J. Frenkel, *Phys. Rev.* **1931**, *37*, 17-44.

[139] W. T. Simpson, D. L. Peterson, *J. Chem. Phys.* **1957**, *26*, 588-593.

[140] T. Förster, *Discussions of the Faraday Society* **1959**, 7-17.

[141] E. W. Knapp, *Chem. Phys.* **1984**, *85*, 73-82.

[142] P. B. Walczak, A. Eisfeld, J. S. Briggs, *J. Chem. Phys.* **2008**, *128*, 044505.

[143] F. Bloch, *Z. Physik* **1929**, *52*, 555-600.

[144] G. H. Wannier, *Phys. Rev.* **1937**, *52*, 191-197.

[145] G. Scheibe, *Kolloid-Zeitschrift* **1938**, *82*, 1-14.

[146] E. E. Sheepwash, P. A. Rowntree, A. L. Schwan, *J. Labelled Compd. Radiopharm.* **2008**, *51*, 391-398.

[147] R. I. Zubatyuk, V. N. Baumer, A. L. Tatarets, L. D. Patsenker, O. V. Shishkin, *Acta Crystallogr. Sect. E.-Struct Rep. Online* **2004**, *60*, O2252-O2254.

[148] M. V. Reddington, *Bioconjugate Chem.* **2007**, *18*, 2178-2190.

[149] J. E. Lewis, M. Maroncelli, *Chem. Phys. Lett.* **1998**, *282*, 197-203.

[150] O. V. Przhonska, D. J. Hagan, E. Novikov, R. Lepkowicz, E. W. Van Stryland, M. V. Bondar, Y. L. Slominsky, A. D. Kachkovski, *Chem. Phys.* **2001**, *273*, 235-248.

[151] R. A. Negres, O. V. Przhonska, D. J. Hagan, E. W. Van Stryland, M. V. Bondar, Y. L. Slominsky, A. D. Kachkovski, *IEEE J. Sel. Top. Quantum Electron.* **2001**, *7*, 849-863.

[152] C. D. Entwistle, T. B. Marder, *Chem. Mater.* **2004**, *16*, 4574-4585.

[153] M. E. Glogowski, J. L. R. Williams, *J. Organomet. Chem.* **1981**, *218*, 137-146.

[154] S. I. Hauck, K. V. Lakshmi, J. F. Hartwig, *Org. Lett.* **1999**, *1*, 2057-2060.

[155] N. G. Connelly, W. E. Geiger, *Chem. Rev.* **1996**, *96*, 877-910.

[156] D. Tsiplakides, D. Archonta, C. G. Vayenas, *Top. Catal.* **2007**, *44*, 469-479.

[157] S. F. Völker, Diploma thesis, Julius-Maximilians Universität (Würzburg), **2009**.

[158] M. Kasha, E. G. McRae, *Physical processes in radiation biology* **1964**, 23-42.

[159] E. G. McRae, M. Kasha, *The molecular exciton model*, Academic Press, New York 3, **1964**.

[160] J. J. P. Stewart, Stewart Computational Chemistry, Colorado Springs, CO, USA, HTTP://openMOPAC.net, **2008**.

[161] Version 2.0 ed., Fujitsu Ltd, **1997-1998**.

[162] S. J. Strickler, R. A. Berg, *J. Chem. Phys.* **1962**, *37*, 814-822.

[163] J. Knoester, *Proc. Int. Sch. Phys. "Enrico Fermi"* **2002**, *149*, 149-186.

[164] J. A. Leegwater, *J. Phys. Chem.* **1996**, *100*, 14403-14409.

[165] G. D. Scholes, C. Smyth, *J. Chem. Phys.* **2014**, *140*, 110901.

[166] G. D. Scholes, *Annu. Rev. Phys. Chem.* **2003**, *54*, 57-87.

[167] W. J. D. Beenken, T. Pullerits, *J. Chem. Phys.* **2004**, *120*, 2490-2495.

[168] N. V. Tkachenko, *Optical Spectroscopy*, Elsevier, Amsterdam, **2006**.

[169] G. Paillotin, C. E. Swenberg, J. Breton, N. E. Geacintov, *Biophys. J.* **1979**, *25*, 513-533.

[170] M. M. L. Grage, Y. Zaushitsyn, A. Yartsev, M. Chachisvilis, V. Sundström, T. Pullerits, *Phys. Rev. B* **2003**, *67*, 205207.

[171] H. v. Amerongen, L. Vulkanas, R. v. Grondelle, *Photosynthetic Excitons*, Singapore, **2000**.

[172] M. A. Stevens, C. Silva, D. M. Russell, R. H. Friend, *Phys. Rev. B* **2001**, *63*, 165213.

[173] E. Engel, K. Leo, M. Hoffmann, *Chem. Phys.* **2006**, *325*, 170-177.

[174] J. Larsen, B. Brüggemann, T. Polívka, V. Sundström, E. Åkesson, J. Sly, M. J. Crossley, *J. Phys. Chem. A* **2005**, *109*, 10654-10662.

[175] M. N. Berberan-Santos, E. N. Bodunov, B. Valeur, *Chem. Phys.* **2005**, *315*, 171-182.

[176] N. Banerji, *J. Mater. Chem. C* **2013**, *1*, 3052-3066.

[177] J. M. Lim, P. Kim, M.-C. Yoon, J. Sung, V. Dehm, Z. Chen, F. Wurthner, D. Kim, *Chem. Sci.* **2013**, *4*, 388-397.

[178] T. Pullerits, S. Hess, J. L. Herek, V. Sundström, *J. Phys. Chem. B* **1997**, *101*, 10560-10567.

[179] D. Beljonne, G. Pourtois, C. Silva, E. Hennebicq, L. M. Herz, R. H. Friend, G. D. Scholes, S. Setayesh, K. Müllen, J. L. Brédas, *Proc. Natl. Acad. Sci. U.S.A.* **2002**, *99*, 10982-10987.

[180] I. Hwang, G. D. Scholes, *Chem. Mater.* **2011**, *23*, 610-620.

[181] T. Geiger, H. Benmansour, B. Fan, R. Hany, F. Nuesch, *Macromol. Rapid Commun.* **2008**, *29*, 651-658.

[182] P. E. Shaw, A. Ruseckas, I. D. W. Samuel, *Adv. Mater.* **2008**, *20*, 3516-3520.

[183] Y. Tamai, Y. Matsuura, H. Ohkita, H. Benten, S. Ito, *J. Phys. Chem. Lett.* **2014**, *5*, 399-403.

[184] H. Marciniak, X.-Q. Li, F. Würthner, S. Lochbrunner, *J. Phys. Chem. A* **2010**, *115*, 648-654.

[185] V. Sundström, T. Gillbro, R. A. Gadonas, A. Piskarskas, *J. Chem. Phys.* **1988**, *89*, 2754-2762.

[186] E. Rousseau, M. Van der Auweraer, F. C. De Schryver, *Langmuir* **2000**, *16*, 8865-8870.

[187] C. Lambert, J. Schelter, T. Fiebig, D. Mank, A. Trifonov, *J. Am. Chem. Soc.* **2005**, *127*, 10600-10610.

[188] G. R. Freeman, H. A. Levy, G. M. Brown, *Acta Crysallogr., Sect. A25* **1969**, S145-146.

[189] A. Midya, Z. Xie, J.-X. Yang, Z.-K. Chen, D. J. Blackwood, J. Wang, S. Adams, K. P. Loh, *Chem. Commun.* **2010**, *46*, 2091-2093.

[190] M. Tavasli, S. Bettington, M. R. Bryce, A. S. Batsanov, A. P. Monkman, *Synthesis* **2005**, 1619-1624.

[191] S. F. Völker, M. Renz, M. Kaupp, C. Lambert, *Chem. Eur. J.* **2011**, *17*, 14147-14163.

[192] S. F. Völker, T. Dellermann, H. Ceymann, M. Holzapfel, C. Lambert, *J. Polym. Sci., Part A: Polym. Chem.* **2014**, *52*, 890-911.

[193] F. Silvestri, I. López-Duarte, W. Seitz, L. Beverina, M. V. Martínez-Díaz, T. J. Marks, D. M. Guldi, G. A. Pagani, T. Torres, *Chem. Commun.* **2009**, 4500-4502.

[194] L. A. Padilha, S. Webster, H. H. Hu, O. V. Przhonska, D. J. Hagan, E. W. Van Stryland, M. V. Bondar, I. G. Davydenko, Y. L. Slominsky, A. D. Kachkovski, *Chem. Phys.* **2008**, *352*, 97-105.

[195] M. Rudolph, S. W. Feldberg, Bioanalytical Systems Inc, West Lafayette, USA, **1994-2002**.

[196] A. J. Bard, L. R. Faulkner, *Electrochemical Methods Fundamentals and Applications*, 2nd ed., Wiley, New York, **2001**.

[197] S. Amthor, B. Noller, C. Lambert, *Chem. Phys.* **2005**, *316*, 141-152.

[198] J. F. Morin, M. Leclerc, D. Ades, A. Siove, *Macromol. Rapid Commun.* **2005**, *26*, 761-778.

[199] C. J. Xia, R. C. Advincula, *Chem. Mater.* **2001**, *13*, 1682-1691.

[200] M. B. Robin, P. Day, *Adv. Inorg. Chem. Radiochem.* **1967**, *10*, 247-422.

[201] C. Lambert, S. Amthor, J. Schelter, *J. Phys. Chem. A* **2004**, *108*, 6474-6486.

[202] C. Lambert, G. Nöll, *J. Am. Chem. Soc.* **1999**, *121*, 8434-8442.

[203] P. J. Low, M. A. J. Paterson, H. Puschmann, A. E. Goeta, J. A. K. Howard, C. Lambert, J. C. Cherryman, D. R. Tackley, S. Leeming, B. Brown, *Chem. Eur. J.* **2004**, *10*, 83-91.

[204] S. Barlow, C. Risko, S. J. Chung, N. M. Tucker, V. Coropceanu, S. C. Jones, Z. Levi, J. L. Brédas, S. R. Marder, *J. Am. Chem. Soc.* **2005**, *127*, 16900-16911.

[205] K. Lancaster, S. A. Odom, S. C. Jones, S. Thayumanavan, S. R. Marder, J. L. Brédas, V. Coropceanu, S. Barlow, *J. Am. Chem. Soc.* **2009**, *131*, 1717-1723.

[206] M. Kaupp, M. Renz, M. Parthey, M. Stolte, F. Würthner, C. Lambert, *Phys. Chem. Chem. Phys.* **2011**, *13*, 16973-16986.

[207] G. Nöll, M. Avola, M. Lynch, J. Daub, *J. Phys. Chem. C* **2007**, *111*, 3197-3204.

[208] C. Lambert, G. Nöll, M. Zabel, F. Hampel, E. Schmälzlin, C. Bräuchle, K. Meerholz, *Chem. Eur. J.* **2003**, *9*, 4232-4239.

[209] S. A. Odom, K. Lancaster, L. Beverina, K. M. Lefler, N. J. Thompson, V. Coropceanu, J. L. Bredas, S. R. Marder, S. Barlow, *Chem. Eur. J.* **2007**, *13*, 9637-9646.

[210] J. C. Lacroix, K. I. Chane-Ching, F. Maquère, F. Maurel, *J. Am. Chem. Soc.* **2006**, *128*, 7264-7276.

[211] M. Büschel, A. Ajayaghosh, E. Arunkumar, J. Daub, *Org. Lett.* **2003**, *5*, 2975-2978.

[212] G. Sauve, P. V. Kamat, K. G. Thomas, K. J. Thomas, S. Das, M. V. George, *J. Phys. Chem.* **1996**, *100*, 2117-2124.

[213] R. A. Binstead, B. Jung, A. D. Zuberbühler, Spectrum Software Associates, Marlborough (USA), **1993**, p. Program for Multivariate Data Analysis.

[214] J. Salbeck, U. Schoberl, K. M. Rapp, J. Daub, *Z. Phys. Chemie-Int. J. Res. Phys. Chem. Chem. Phys.* **1991**, *171*, 191-212.

[215] D. Patra, D. Sahu, H. Padhy, D. Kekuda, C. W. Chu, H. C. Lin, *J. Polym. Sci. Pol. Chem.* **2010**, *48*, 5479-5489.

[216] N. Berton, I. Fabre-Francke, D. Bourrat, F. Chandezon, S. Sadki, *J. Phys. Chem. B* **2009**, *113*, 14087-14093.

[217] I. Noviandri, K. N. Brown, D. S. Fleming, P. T. Gulyas, P. A. Lay, A. F. Masters, L. Phillips, *J. Phys. Chem. B* **1999**, *103*, 6713-6722.

[218] T. Förster, *Ann. Phys. (Berlin)* **1948**, *2*, 55-75.

[219] C. J. Brabec, S. Gowrisanker, J. J. M. Halls, D. Laird, S. J. Jia, S. P. Williams, *Adv. Mater.* **2010**, *22*, 3839-3856.

[220] A. Facchetti, *Chem. Mater.* **2011**, *23*, 733-758.

[221] H. Usta, A. Facchetti, T. J. Marks, *Acc. Chem. Res.* **2011**, *44*, 501-510.

[222] T. Kobayashi, in *Luminescence efficiencies and time-dependence: Insights into the nature of the emitting species in conjugated polymers* (Ed.: N. S. Sariciftci), World Scientific, **1998**.

[223] I. D. W. Samuel, G. Rumbles, R. H. Friend, in *Primary Photoexcitations in Conjugated Polymers: Molecular Excitation versus Semiconductor Band Model* (Ed.: N. S. Sariciftci), World Scientific, **1998**.

[224] E. Collini, G. D. Scholes, *Science* **2009**, *323*, 369-373.

[225] C. Deibel, T. Strobel, V. Dyakonov, *Adv. Mater.* **2010**, *22*, 4097-4111.

[226] I. A. Howard, R. Mauer, M. Meister, F. Laquai, *J. Am. Chem. Soc.* **2010**, *132*, 14866-14876.

[227] F. B. Dias, S. King, A. P. Monkman, Perepichka, II, M. A. Kryuchkov, I. F. Perepichka, M. R. Bryce, *J. Phys. Chem. B* **2008**, *112*, 6557-6566.

[228] J. Huang, Y. S. Wu, H. B. Fu, X. W. Zhan, J. N. Yao, S. Barlow, S. R. Marder, *J. Phys. Chem. A* **2009**, *113*, 5039-5046.

[229] M. Scarongella, A. Laktionov, U. Rothlisberger, N. Banerji, *J. Mater. Chem. C* **2013**, *1*, 2308-2319.

[230] X. J. Yang, T. E. Dykstra, G. D. Scholes, *Phys. Rev. B* **2005**, *71*, 045203.

[231] E. Collini, G. D. Scholes, *J. Phys. Chem. A* **2009**, *113*, 4223-4241.

[232] A. Ruseckas, P. Wood, I. D. W. Samuel, G. R. Webster, W. J. Mitchell, P. L. Burn, V. Sundström, *Phys. Rev. B* **2005**, *72*, 115214.

[233] K. Johnson, Y.-S. Huang, S. Huettner, M. Sommer, M. Brinkmann, R. Mulherin, D. Niedzialek, D. Beljonne, J. Clark, W. T. S. Huck, R. H. Friend, *J. Am. Chem. Soc.* **2013**, *135*, 5074-5083.

[234] S. Gélinas, J. Kirkpatrick, I. A. Howard, K. Johnson, M. W. B. Wilson, G. Pace, R. H. Friend, C. Silva, *J. Phys. Chem. B* **2013**, *117*, 4649-4653.

[235] S. Yamaguchi, T. Shirasaka, K. Tamao, *Org. Lett.* **2000**, *2*, 4129-4132.

[236] R. Stahl, C. Lambert, C. Kaiser, R. Wortmann, R. Jakober, *Chem. Eur. J.* **2006**, *12*, 2358-2370.

[237] S. Chopin, F. Chaignon, E. Blart, F. Odobel, *J. Mater. Chem.* **2007**, *17*, 4139-4146.

[238] D. Gosztola, M. P. Niemczyk, W. Svec, A. S. Lukas, M. R. Wasielewski, *J. Phys. Chem. A* **2000**, *104*, 6545-6551.

[239] X. W. Zhan, A. Facchetti, S. Barlow, T. J. Marks, M. A. Ratner, M. R. Wasielewski, S. R. Marder, *Adv. Mater.* **2011**, *23*, 268-284.

[240] R. S. K. Kishore, O. Kel, N. Banerji, D. Emery, G. Bollot, J. Mareda, A. Gomez-Casado, P. Jonkheijm, J. Huskens, P. Maroni, M. Borkovec, E. Vauthey, N. Sakai, S. Matile, *J. Am. Chem. Soc.* **2009**, *131*, 11106-11116.

[241] F. Würthner, S. Ahmed, C. Thalacker, T. Debaerdemaeker, *Chem. Eur. J.* **2002**, *8*, 4742-4750.

[242] F. Chaignon, M. Falkenström, S. Karlsson, E. Blart, F. Odobel, L. Hammarström, *Chem. Commun.* **2007**, *1*, 64-66.

[243] P. Piyakulawat, A. Keawprajak, J. Wlosnewski, M. Forster, U. Asawapirom, *Synth. Met.* **2011**, *161*, 1238-1244.

[244] L. E. Polander, A. S. Romanov, S. Barlow, D. K. Hwang, B. Kippelen, T. V. Timofeeva, S. R. Marder, *Org. Lett.* **2012**, *14*, 918-921.

[245] S. V. Bhosale, M. B. Kalyankar, S. J. Langford, E. F. Reid, C. F. Hogan, *New J. Chem.* **2009**, *33*, 2409-2413.

[246] P. Gawrys, D. Djurado, J. R. Rimarcik, A. Kornet, D. Boudinet, J. M. Verilhac, V. Lukes, I. Wielgus, M. Zagorska, A. Pron, *J. Phys. Chem. B* **2010**, *114*, 1803-1809.

[247] J. H. Klein, T. L. Sunderland, C. Kaufmann, M. Holzapfel, A. Schmiedel, C. Lambert, *Phys. Chem. Chem. Phys.* **2013**, *15*, 16024-16030.

[248] C. Thalacker, C. Roger, F. Würthner, *J. Org. Chem.* **2006**, *71*, 8098-8105.

[249] M. Jaggi, B. Schmid, S. X. Liu, S. V. Bhosale, S. Rivadehi, S. J. Langford, S. Decurtins, *Tetrahedron* **2011**, *67*, 7231-7235.

[250] K. Cai, Q. F. Yan, D. H. Zhao, *Chem. Sci.* **2012**, *3*, 3175-3182.

[251] M. J. Frisch, G. W. Trucks, H. B. Schlegel, G. E. Scuseria, M. A. Robb, J. R. Cheeseman, G. Scalmani, V. Barone, B. Mennucci, G. A. Petersson, H. Nakatsuji, M. Caricato, X. Li, H. P. Hratchian, A. F. Izmaylov, J. Bloino, G. Zheng, J. L. Sonnenberg, M. Hada, M. Ehara, K. Toyota, R. Fukuda, J. Hasegawa, M. Ishida, T. Nakajima, Y. Honda, O. Kitao, H. Nakai, T. Vreven, J. J. A. Montgomery, J. E. Peralta, F. Ogliaro, M. Bearpark, J. J. Heyd, E. Brothers, K. N. Kudin, V. N. Staroverov, T. Keith, R. Kobayash, J. Normand, K. Raghavachari, A. Rendell, J. C. Burant, S. S. Iyengar, J. Tomasi, M. Cossi, N. Rega, J. M. Millam, M. Klene, J. E. Knox, J. B. Cross, V. Bakken, C. Adamo, J. Jaramillo, R. Gomperts, R. E. Stratmann, O. Yazyev, A. J. Austin, R. Cammi, C. Pomelli, J. W. Ochterski, R. L. Martin, K. Morokuma, V. G. Zakrzewski, G. A. Voth, P. Salvador, J. J. Dannenberg, S. Dapprich, A. D. Daniels, O. Farkas, J. B. Foresman, J. V. Ortiz, J. Cioslowski, D. J. Fox, Gaussian, Inc., Wallingford CT, **2010**.

[252] J. J. P. Stewart, 13.159W ed., Stewart Computational Chemsitry, **2012**.

[253] A. Weller, *Z. Phys. Chem.* **1982**, *133*, 93-98.

[254] CambridgeSoft, Revision 12.0.2.1076 ed., Cambridge, U.K., **2010**.

[255] I. H. M. van Stokkum, D. S. Larsen, R. van Grondelle, *Biochim. Biophys. Acta* **2004**, *1657*, 82-104.

[256] T. Elsaesser, W. Kaiser, *Annu. Rev. Phys. Chem.* **1991**, *42*, 83-107.

[257] A. Pigliucci, G. Duvanel, L. M. L. Daku, E. Vauthey, *J. Phys. Chem. A* **2007**, *111*, 6135-6145.

[258] A. Pigliucci, E. Vauthey, *Chimia* **2003**, *57*, 200-203.

[259] E. Busby, E. C. Carroll, E. M. Chinn, L. L. Chang, A. J. Moulé, D. S. Larsen, *J. Phys. Chem. Lett.* **2011**, *2*, 2764-2769.

[260] S. Tretiak, A. Saxena, R. L. Martin, A. R. Bishop, *Phys. Rev. Lett.* **2002**, *89*, 097402.

[261] S. Westenhoff, W. J. D. Beenken, R. H. Friend, N. C. Greenham, A. Yartsev, V. Sundström, *Phys. Rev. Lett.* **2006**, *97*, 166804.

[262] R. E. Di Paolo, J. Seixas de Melo, J. Pina, H. D. Burrows, J. Morgado, A. L. Macanita, *ChemPhysChem* **2007**, *8*, 2657-2664.

[263] M. M. L. Grage, P. W. Wood, A. Ruseckas, T. Pullerits, W. Mitchell, P. L. Burn, I. D. W. Samuel, V. Sundström, *J. Chem. Phys.* **2003**, *118*, 7644-7650.

[264] C. K. Min, T. Joo, M. C. Yoon, C. M. Kim, Y. N. Hwang, D. Kim, N. Aratani, N. Yoshida, A. Osuka, *J. Chem. Phys.* **2001**, *114*, 6750-6758.

[265] D. M. Jonas, M. J. Lang, Y. Nagasawa, T. Joo, G. R. Fleming, *J. Phys. Chem.* **1996**, *100*, 12660-12673.

[266] I. Pugliesi, U. Megerle, S. L. Suraru, F. Würthner, E. Riedle, S. Lochbrunner, *Chem. Phys. Lett.* **2011**, *504*, 24-28.

[267] A. Heckmann, C. Lambert, *Angew. Chem.-Int. Edit.* **2012**, *51*, 326-392.

[268] B. M. Aveline, S. Matsugo, R. W. Redmond, *J. Am. Chem. Soc.* **1997**, *119*, 11785-11795.

[269] S. F. Nelsen, H. Q. Tran, M. A. Nagy, *J. Am. Chem. Soc.* **1998**, *120*, 298-304.

[270] F. Zieschang, A. Schmiedel, M. Holzapfel, K. Ansorg, B. Engels, C. Lambert, *J. Phys. Chem. C* **2013**, *117*, 19816-19831.

[271] U. Rösch, S. Yao, R. Wortmann, F. Würthner, *Angew. Chem.-Int. Edit.* **2006**, *45*, 7026-7030.

[272] A. D. Becke, *J. Chem. Phys.* **1993**, *98*, 5648-5652.

[273] M. J. e. a. Frisch, Gaussian, Inc., Wallingford, CT, **2004**.

[274] P. C. Hariharan, J. A. Pople, *Theor. Chim. Acta* **1973**, *28*, 213-222.

[275] C. T. Lee, W. T. Yang, R. G. Parr, *Phys. Rev. B* **1988**, *37*, 785-789.

[276] E. Mena-Osteritz, F. Zhang, G. Götz, P. Reineker, P. Bäuerle, *Beilstein J. Nanotechnol.* **2011**, *2*, 720-726.

[277] C. Y. Mang, J. Zhou, C. P. Liu, K. C. Wu, *Chin. J. Chem.* **2009**, *27*, 2323-2328.

[278] K. Y. Law, *J. Phys. Chem.* **1987**, *91*, 5184-5193.

[279] K. Y. Law, *J. Phys. Chem.* **1989**, *93*, 5925-5930.

[280] K. Y. Law, *Chem. Phys. Lett.* **1992**, *200*, 121-124.

[281] B. Kippelen, J. L. Brédas, *Energy Environ. Sci.* **2009**, *2*, 251-261.

[282] A. Mishra, P. Bäuerle, *Angew. Chem.-Int. Edit.* **2012**, *51*, 2020-2067.

[283] W. J. Potscavage, A. Sharma, B. Kippelen, *Acc. Chem. Res.* **2009**, *42*, 1758-1767.

[284] M. C. Scharber, D. Mühlbacher, M. Koppe, P. Denk, C. Waldauf, A. J. Heeger, C. J. Brabec, *Adv. Mater.* **2006**, *18*, 789-794.

[285] C. Deibel, V. Dyakonov, *Rep. Prog. Phys.* **2010**, *73*.

[286] C. J. Brabec, G. Zerza, G. Cerullo, S. De Silvestri, S. Luzzati, J. C. Hummelen, S. Sariciftci, *Chem. Phys. Lett.* **2001**, *340*, 232-236.

[287] P. Schilinsky, C. Waldauf, C. J. Brabec, *Appl. Phys. Lett.* **2002**, *81*, 3885-3887.

[288] Y. Z. Lin, Y. F. Li, X. W. Zhan, *Chem. Soc. Rev.* **2012**, *41*, 4245-4272.

[289] Y. F. Li, *Acc. Chem. Res.* **2012**, *45*, 723-733.

[290] G. Li, R. Zhu, Y. Yang, *Nat. Photonics* **2012**, *6*, 153-161.

[291] Y. S. Liu, C. C. Chen, Z. R. Hong, J. Gao, Y. Yang, H. P. Zhou, L. T. Dou, G. Li, *Sci. Rep.* **2013**, *3*, DOI:10.1038/srep03356.

[292] M. A. Green, K. Emery, Y. Hishikawa, W. Warta, E. D. Dunlop, *Prog. Photovolt: Res. Appl* **2014**, *22*, 1-9.

[293] C. Cabanetos, A. El Labban, J. A. Bartelt, J. D. Douglas, W. R. Mateker, J. M. J. Fréchet, M. D. McGehee, P. M. Beaujuge, *J. Am. Chem. Soc.* **2013**, *135*, 4656-4659.

[294] M. T. Dang, L. Hirsch, G. Wantz, *Adv. Mater.* **2011**, *23*, 3597-3602.

[295] L. Luer, H. J. Egelhaaf, D. Oelkrug, G. Cerullo, G. Lanzani, B. H. Huisman, D. de Leeuw, *Org. Electron.* **2004**, *5*, 83-89.

[296] T. Stubinger, W. Brutting, *J. Appl. Phys.* **2001**, *90*, 3632-3641.

[297] J. L. Brédas, D. Beljonne, V. Coropceanu, J. Cornil, *Chem. Rev.* **2004**, *104*, 4971-5003.

[298] J. J. M. Halls, J. Cornil, D. A. dos Santos, R. Silbey, D. H. Hwang, A. B. Holmes, J. L. Brédas, R. H. Friend, *Phys. Rev. B* **1999**, *60*, 5721-5727.

[299] W. L. Ma, C. Y. Yang, X. Gong, K. Lee, A. J. Heeger, *Adv. Funct. Mater.* **2005**, *15*, 1617-1622.

[300] R. A. Marsh, J. M. Hodgkiss, S. Albert-Seifried, R. H. Friend, *Nano Lett.* **2010**, *10*, 923-930.

[301] A. A. Paraecattil, N. Banerji, *J. Am. Chem. Soc.* **2014**, *136*, 1472-1482.

[302] L. M. Chen, Z. R. Hong, G. Li, Y. Yang, *Adv. Mater.* **2009**, *21*, 1434-1449.

[303] Z. J. Chen, A. Lohr, C. R. Saha-Möller, F. Würthner, *Chem. Soc. Rev.* **2009**, *38*, 564-584.

[304] J. W. Ryan, T. Kirchartz, A. Viterisi, J. Nelson, E. Palomares, *J. Phys. Chem. C* **2013**, *117*, 19866-19874.

[305] V. Steinmann, N. M. Kronenberg, M. R. Lenze, S. M. Graf, D. Hertel, K. Meerholz, H. Bürckstümmer, E. V. Tulyakova, F. Würthner, *Adv. Energy Mater.* **2011**, *1*, 888-893.

[306] Y. Matsuo, Y. Sato, T. Niinomi, I. Soga, H. Tanaka, E. Nakamura, *J. Am. Chem. Soc.* **2009**, *131*, 16048-16050.

[307] J. G. Xue, B. P. Rand, S. Uchida, S. R. Forrest, *Adv. Mater.* **2005**, *17*, 66-71.

[308] S. W. Chiu, L. Y. Lin, H. W. Lin, Y. H. Chen, Z. Y. Huang, Y. T. Lin, F. Lin, Y. H. Liu, K. T. Wong, *Chem. Commun.* **2012**, *48*, 1857-1859.

[309] J. Y. Zhou, X. J. Wan, Y. S. Liu, Y. Zuo, Z. Li, G. R. He, G. K. Long, W. Ni, C. X. Li, X. C. Su, Y. S. Chen, *J. Am. Chem. Soc.* **2012**, *134*, 16345-16351.

[310] Y. M. Sun, G. C. Welch, W. L. Leong, C. J. Takacs, G. C. Bazan, A. J. Heeger, *Nat. Mater.* **2012**, *11*, 44-48.

[311] Y. Chen, X. Wan, G. Long, *Acc. Chem. Res.* **2013**, *46*, 2645-2655.

[312] D. Mühlbacher, M. Scharber, M. Morana, Z. G. Zhu, D. Waller, R. Gaudiana, C. Brabec, *Adv. Mater.* **2006**, *18*, 2884-2889.

[313] S. Albrecht, S. Janietz, W. Schindler, J. Frisch, J. Kurpiers, J. Kniepert, S. Inal, P. Pingel, K. Fostiropoulos, N. Koch, D. Neher, *J. Am. Chem. Soc.* **2012**, *134*, 14932-14944.

[314] R. C. Coffin, J. Peet, J. Rogers, G. C. Bazan, *Nat. Chem.* **2009**, *1*, 657-661.

[315] H. X. Zhou, L. Q. Yang, A. C. Stuart, S. C. Price, S. B. Liu, W. You, *Angew. Chem.-Int. Edit.* **2011**, *50*, 2995-2998.

[316] T. Y. Chu, J. P. Lu, S. Beaupre, Y. G. Zhang, J. R. Pouliot, S. Wakim, J. Y. Zhou, M. Leclerc, Z. Li, J. F. Ding, Y. Tao, *J. Am. Chem. Soc.* **2011**, *133*, 4250-4253.

[317] C. M. Amb, S. Chen, K. R. Graham, J. Subbiah, C. E. Small, F. So, J. R. Reynolds, *J. Am. Chem. Soc.* **2011**, *133*, 10062-10065.

[318] P. Khoram, Master thesis, Friedrich-Alexander Universität Erlangen-Nürnberg (Erlangen-Nürnberg), **2013**.

[319] J. M. Lobez, T. L. Andrew, V. Bulovic, T. M. Swager, *ACS Nano* **2012**, *6*, 3044-3056.

[320] L. Q. Yang, H. X. Zhou, S. C. Price, W. You, *J. Am. Chem. Soc.* **2012**, *134*, 5432-5435.

[321] T. Ameri, P. Khoram, J. Min, C. J. Brabec, *Adv. Mater.* **2013**, *25*, 4245-4266.

[322] J. S. Huang, T. Goh, X. K. Li, M. Y. Sfeir, E. A. Bielinski, S. Tomasulo, M. L. Lee, N. Hazari, A. D. Taylor, *Nat. Photonics* **2013**, *7*, 480-486.

[323] M. Campoy-Quiles, T. Ferenczi, T. Agostinelli, P. G. Etchegoin, Y. Kim, T. D. Anthopoulos, P. N. Stavrinou, D. D. C. Bradley, J. Nelson, *Nat. Mater.* **2008**, *7*, 158-164.

[324] Y. Zhao, Z. Y. Xie, Y. Qu, Y. H. Geng, L. X. Wang, *Appl. Phys. Lett.* **2007**, *90*, 043504.

[325] S. R. Tseng, Y. S. Chen, H. F. Meng, H. C. Lai, C. H. Yeh, S. F. Horng, H. H. Liao, C. S. Hsu, *Synth. Met.* **2009**, *159*, 137-141.

[326] P. Klán, J. Wirz, *Photochemistry of Organic Compounds*, Wiley-Blackwell, **2009**.

[327] B. Stender, S. F. Völker, C. Lambert, J. Pflaum, *Adv. Mater.* **2013**, *25*, 2943-2947.

[328] R. Sens, K. H. Drexhage, *J. Lumin.* **1981**, *24-5*, 709-712.

[329] *Innovative Instruments, Inc.*, *Tampa, USA*.

[330] V. V. Pavlishchuk, A. W. Addison, *Inorg. Chim. Acta* **2000**, *298*, 97-102.

[331] C. Kaiser, A. Schmiedel, M. Holzapfel, C. Lambert, *J. Phys. Chem. C* **2012**, *116*, 15265-15280.

[332] I. H. M. van Stokkum, D. S. Larsen, R. van Grondelle, *Biochim. Biophys. Acta-Bioenerg.* **2004**, *1657*, 82-104.

[333] R. Abbel, M. Woffs, R. A. A. Bovee, J. L. J. van Dongen, X. Lou, O. Henze, W. J. Feast, E. W. Meijer, A. Schenning, *Adv. Mater.* **2009**, *21*, 597-602.

[334] T. Zimmermann, *J. Heterocycl. Chem.* **2002**, *39*, 255-262.

[335] S. Amthor, C. Lambert, *J. Phys. Chem. A* **2006**, *110*, 1177-1189.

[336] Z. Jin, B. L. Lucht, *J. Am. Chem. Soc.* **2005**, *127*, 5586-5595.

[337] Z. B. Zhang, M. Fujiki, H. Z. Tang, M. Motonaga, K. Torimitsu, *Macromolecules* **2002**, *35*, 1988-1990.

[338] S. F. Völker, S. Uemura, M. Limpinsel, M. Mingebach, C. Deibel, V. Dyakonov, C. Lambert, *Macromol. Chem. Phys.* **2010**, *211*, 1098-1108.

7 Table of Formulas

Precursors

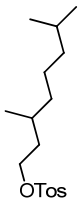

1

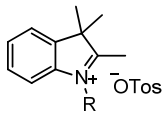

2

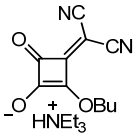

3

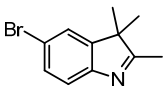

4

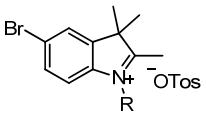

5

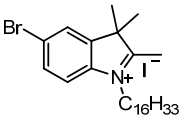

6

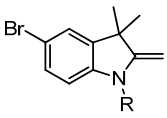

7

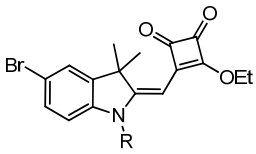

8

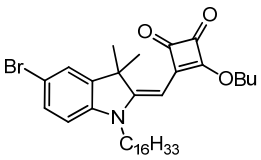

9

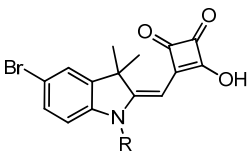

10

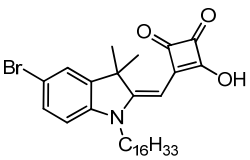

11

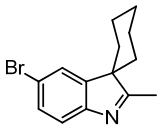

12

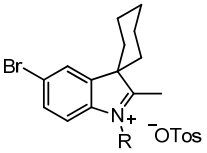

13

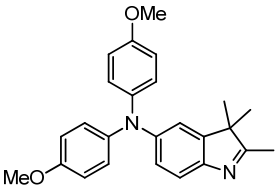

14

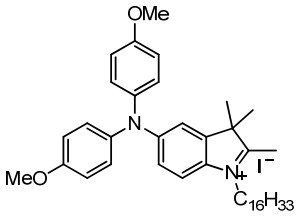

15

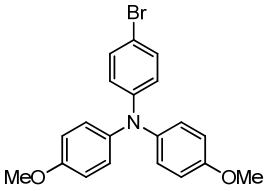

16

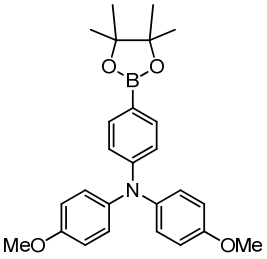

17

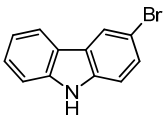

18

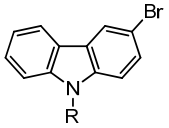

19

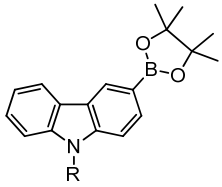

20

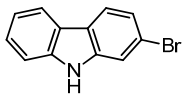

21

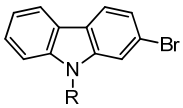

22

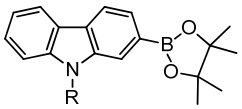

23

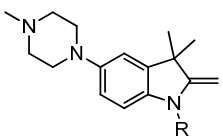

24

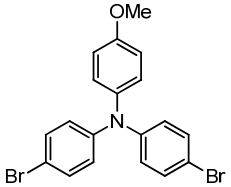

25

R =

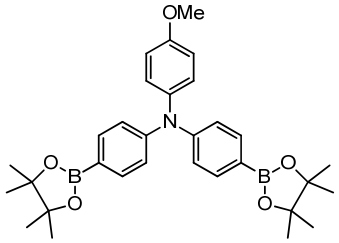

26

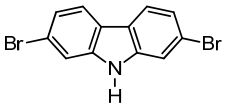

27

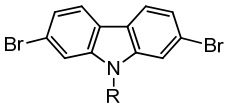

28

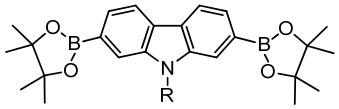

29

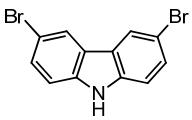

30

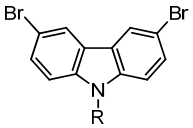

31

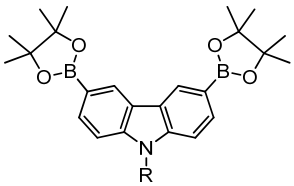

32

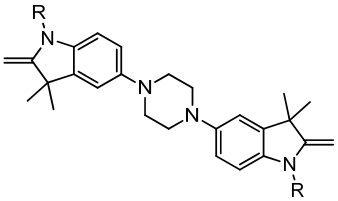

33

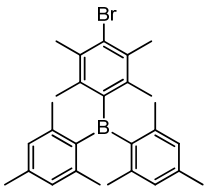

34

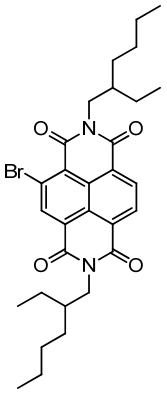

35

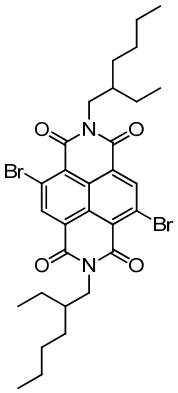

36

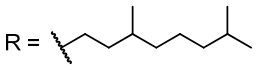

Squaraine Monomers

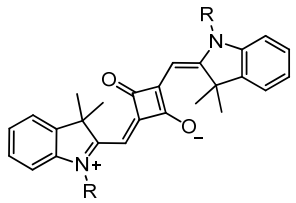

M1

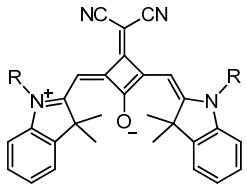

M2

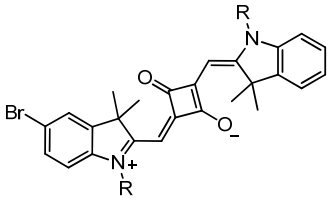

M3

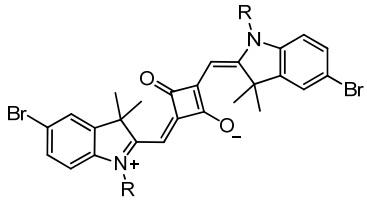

M4

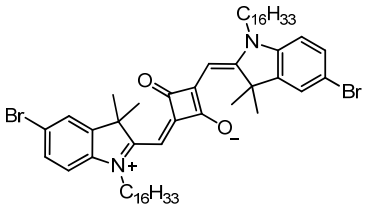

M5

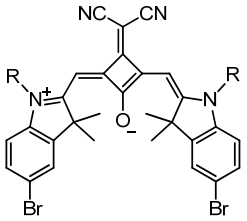

M6

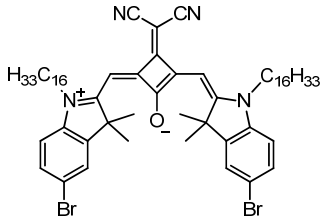

M7

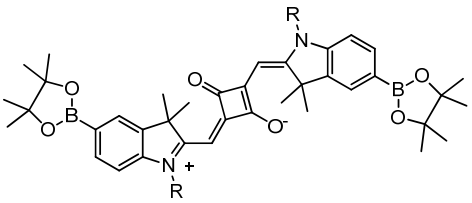

M8

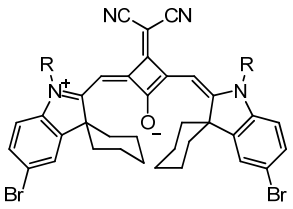

M9

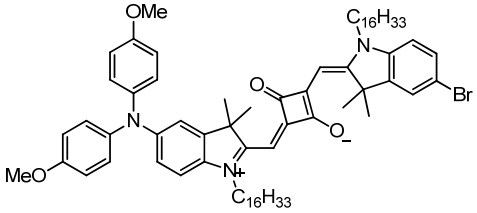

M10

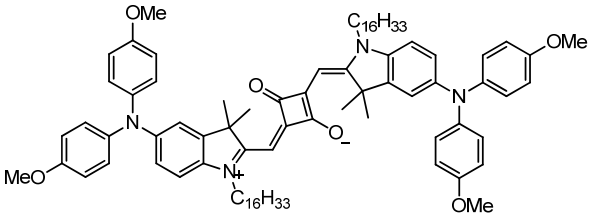

M11

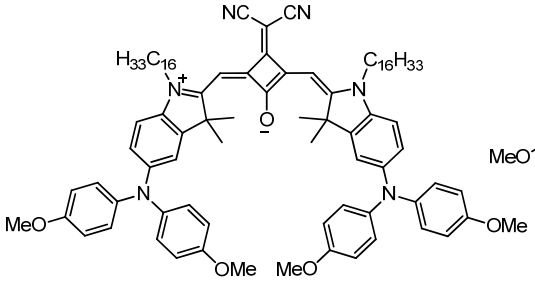

M12

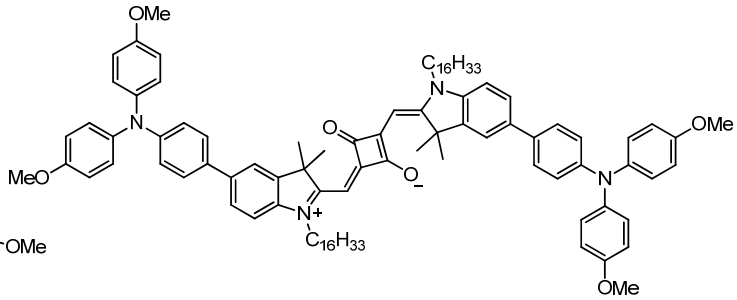

M13

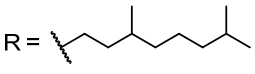

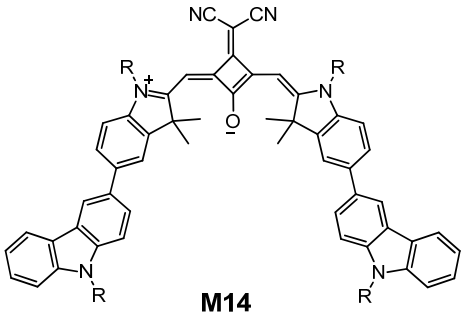

M14

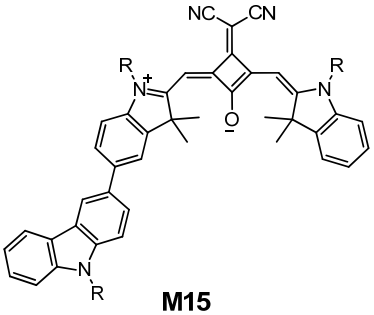

M15

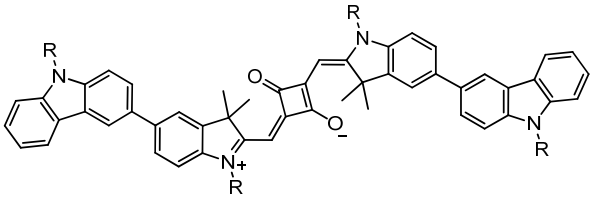

M16

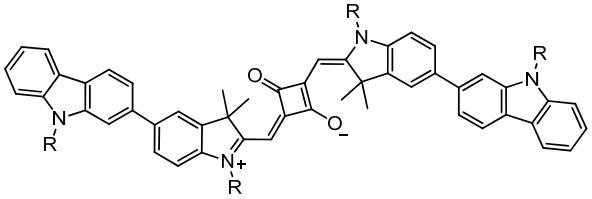

M17

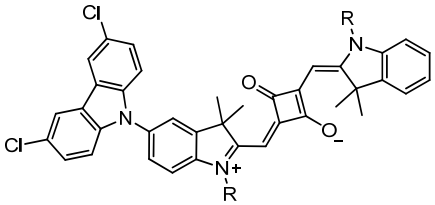

M18

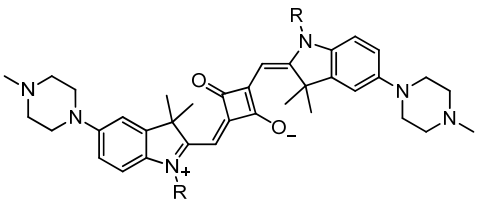

M19

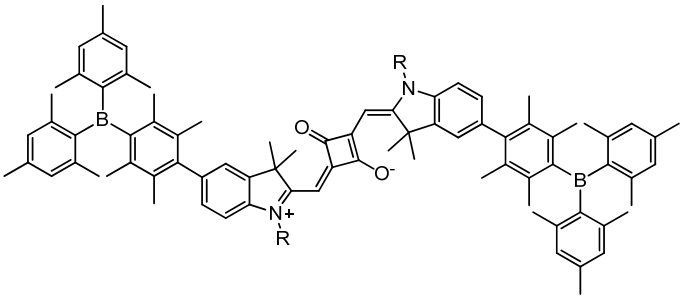

M20

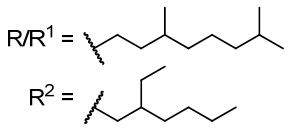

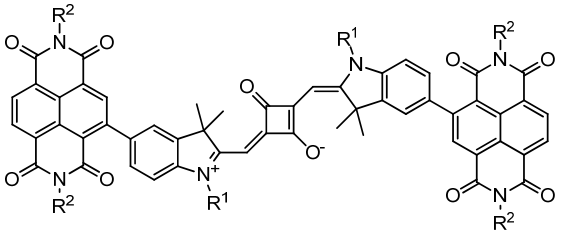

M21

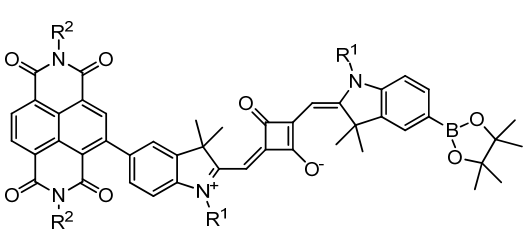

M22

Squaraine Polymers

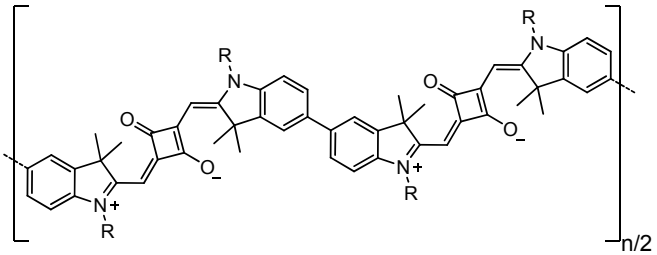

P1

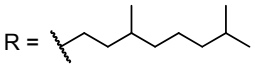

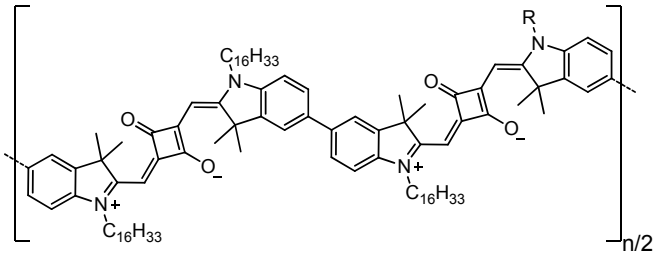

P2

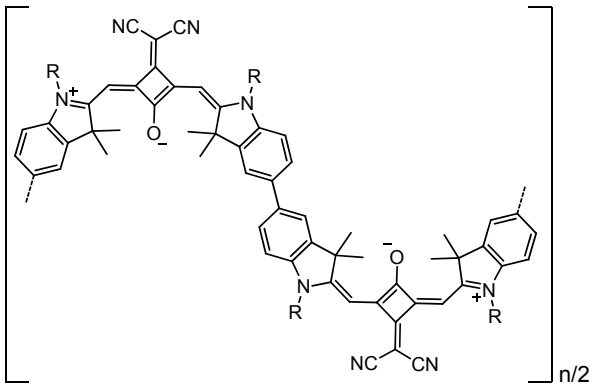

P3

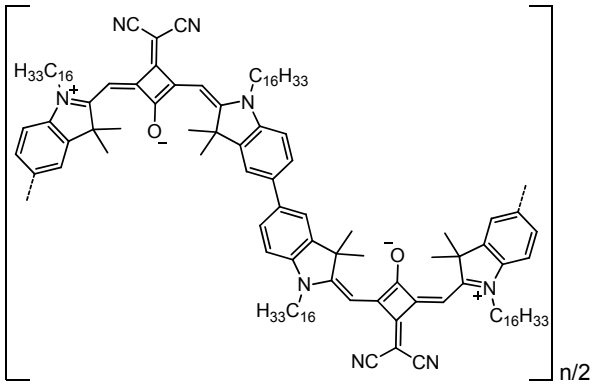

P4

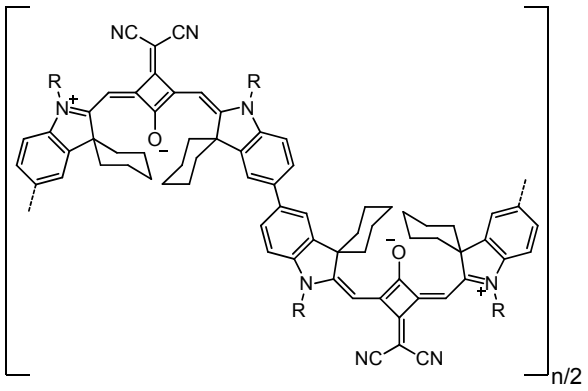

P5

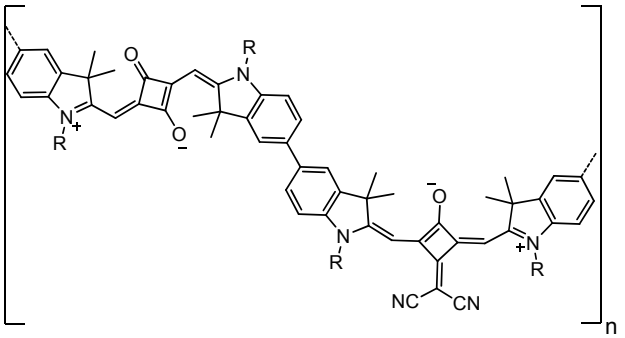

P6

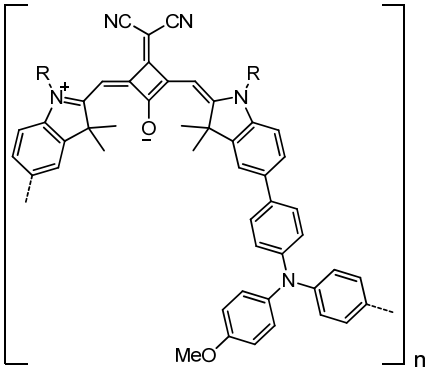

P7

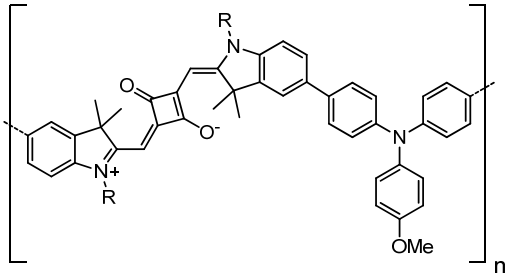

P8

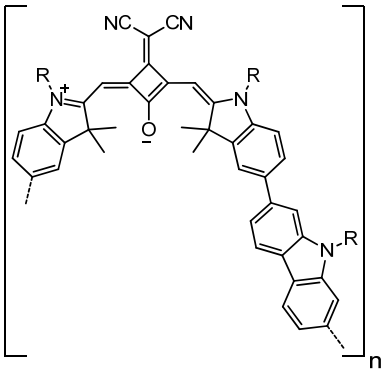

P9

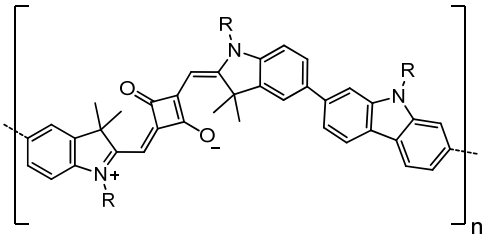

P10

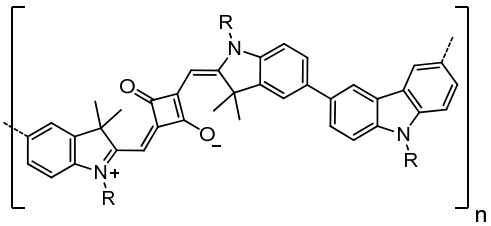

P11

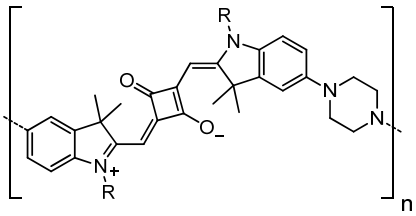

P12

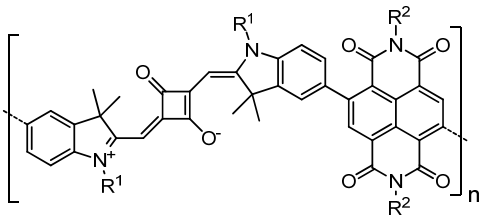

P13

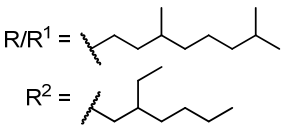

Squaraine Macrocycles

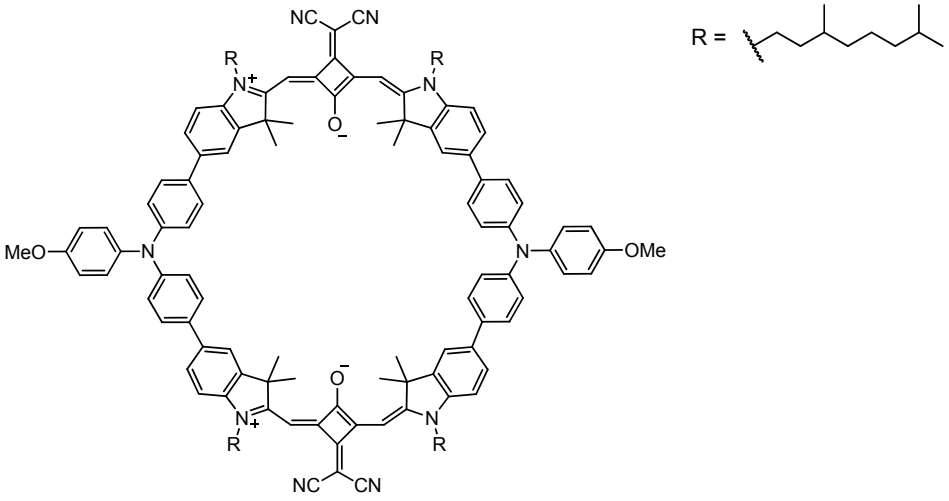

Dim1

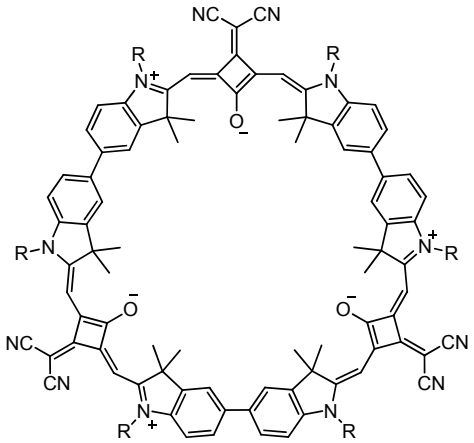

Tri1

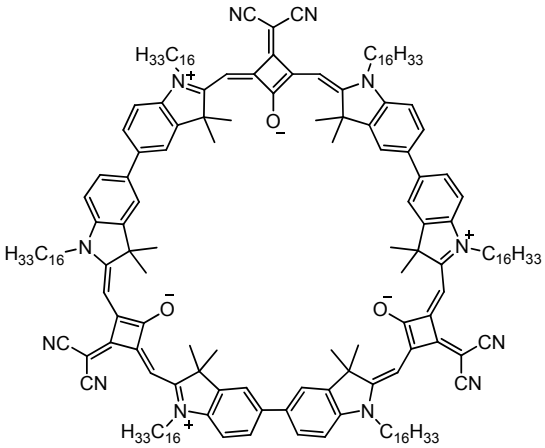

Tri2

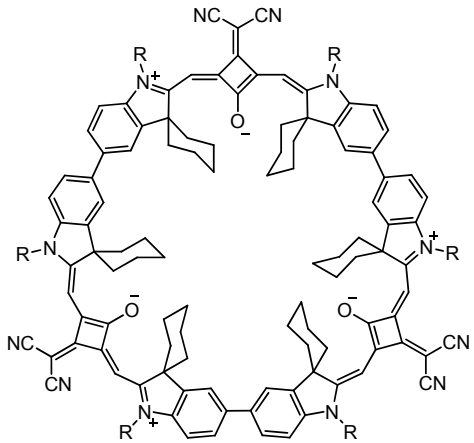

Tri3

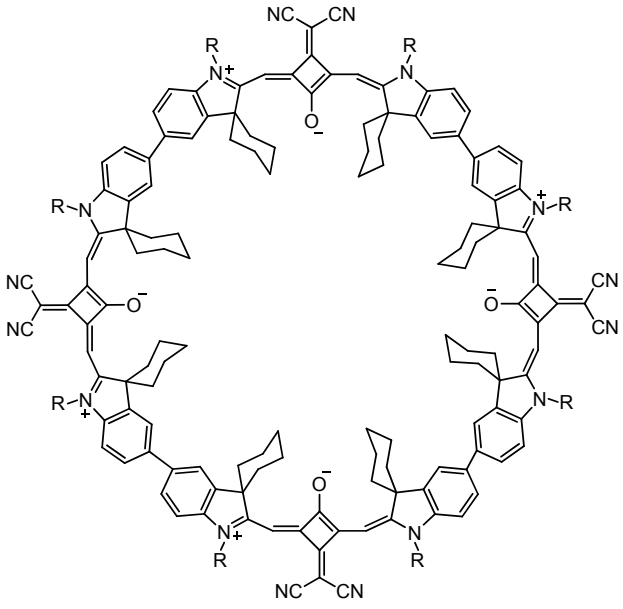

Tet1

8 Zusammenfassung

In dieser Arbeit wurde die Synthese sowie die spektroskopische und elektrochemische Untersuchung einer Reihe unterschiedlichster Squarainfarbstoffe präsentiert. Darüber hinaus wurde in diversen Kooperationen deren Verwendung in optoelektronischen Bauteilen wie z.B. organischen Solarzellen und OLEDs untersucht. Die große Vielfalt der Squaraine basierte auf zwei Indoleninsquarain Stammverbindungen. Das Squarain **M1** ist ein klassisches Squarain und zeigt eine *trans*-Konfiguration der Indoleningruppen zueinander. In **M2** wurde ein Sauerstoffatom durch eine Dicyanomethylengruppe ausgetauscht, was zu einer höheren Elektronenakzeptorstärke sowie einer *cis*-Konfiguration des Squarains führt.

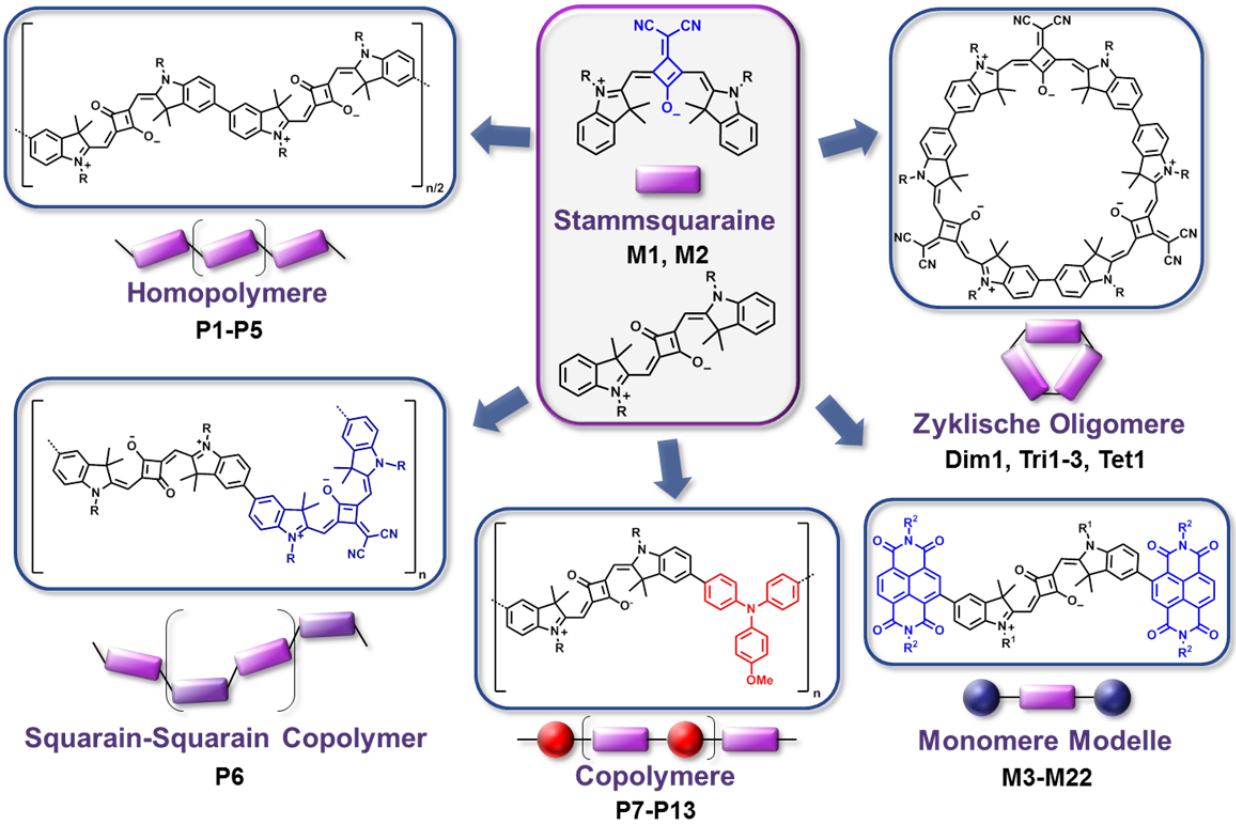

Die Vielfalt der darauf basierenden Squaraine beinhaltete neben den unsubstituierten Referenzverbindungen funktionalisierte Squaraine, donor- und akzeptorsubstitutierte monomere Modellverbindungen, Donor- und Akzeptor-Squarain Copolymere, reine

Squarain Homopolymere, ein Squarain-Squarain Copolymer sowie diverse konjugierte makrozyklische Squaraine.

Um überhaupt diese Vielfalt synthetisieren zu können, wurde zunächst eine Reihe monomerer Squaraine mit Brom- oder Borestergruppen synthetisiert, welche sich mittels Pd-katalysierter *Suzuki*-Kupplung in donor- und akzeptorsubstituierte monomere Modelle und Copolymere überführen ließen. Des Weiteren wurden die bromfunktionalisierten Squaraine mittels der Ni-unterstützten *Yamamoto*-Kupplung zu Homopolymeren und den entsprechenden Makrozyklen umgesetzt.

Das Absorptionsmaximum der Referenzverbindung **M1** lag bei ~ 15500 cm^{-1}. Das von **M2** lag aufgrund der erhöhten Akzeptorstärke des zentralen Bausteins bei ~ 14300 cm^{-1}. Die Extinktionskoeffizienten waren erwartungsgemäß squaraintypisch hoch mit Werten von ~ 300000 $M^{-1}\,cm^{-1}$, bzw. 200000 $M^{-1}\,cm^{-1}$. Es wurde gezeigt, dass die Einführung von funktionellen Gruppen (**M3–M9**), zusätzlichen Elektronendonoren (**M10–M19**) oder -akzeptoren (**M20–M22**) an der Peripherie zu einer Rotverschiebung des Absorptionsmaximums führte, wobei das Ausmaß der Verschiebung von der σ- und/oder π-Donorstärke der Substituenten abhing.

Im Falle der di- und triarylaminsubstituierten Squaraine **M10–M13** und der dibromierten Squaraine **M5** und **M7** wurde die elektronische Struktur der Mono- und Diradikal(di)kationen untersucht, wofür das Zusammenspiel von Cyclovoltammetrie, Spektroelektrochemie und DFT-Rechnungen notwendig war. Es wurde gezeigt, dass sämtliche Monoradikalkationen den Cyanincharakter beibehalten und vollständig delokalisierte Verbindungen der *Robin-Day* Klasse III sind, was auf das niedrige Redoxpotential der Squarainbrücke zurückzuführen war. Mit einem *N*-*N*-Abstand von 26 Bindungen zwischen den zusätzlichen Redoxzentren ist $\mathbf{M13}^{+\bullet}$ dadurch das nach bestem Wissen längste komplett delokalisierte Bis(triarylamin) Radikalkation. Die Situation der Diradikaldikationen war etwas komplexer. Die theoretischen Berechnungen ergaben für die diarylaminsubstituierten Squaraine einen energetisch günstigsten Zustand, welcher aus gleichen Anteilen eines offenschaligen Singulett- und Triplettzustandes bestand. Darüber hinaus beherrschten die HOMO–1→HOMO Übergänge die

Absorptionsspektren der Diradikaldikationen, in welchen auch direkt der Einfluss der *cis*-/*trans*-Konfiguration ersichtlich war.

Basierend auf den Donor–Squarain Modellverbindungen (**M10–M19**) wurde eine Reihe von Donor–Squarain Copolymere (**P7–P12**) synthetisiert, um eine weitere Rotverschiebung des Absorptionsmaximums sowie eine Verbreiterung der Absorptionsbande zu erreichen. Die Auswirkungen waren allerdings sehr gering und sowohl die optischen als auch die elektrochemischen Eigenschaften unterschieden sich kaum von denen der Modellverbindungen. Als Ursache wurde zum einen der durch die Brücke vergrößerte Abstand der Squaraine zueinander ausgemacht, welcher eine Verminderung der Exzitonkopplungsenergie bewirkte. Zum anderen zeigten semiempirische Berechnungen, dass die Brücken etwas aus der Ebene der Squaraine verdrillt waren, was zu einer Verminderung der konjugativen Effekte zwischen den Squarainen führte. Zusammenfassend lässt sich sagen, dass das Konzept eine breite niederenergetische Absorption der Farbstoffe zu schaffen, indem man die Squaraineinheiten mit zusätzlichen Elektronendonoren verbrückt, für die präsentierten Systeme nicht funktioniert hat.

Das Anbringen der starken NDI Elektronenakzeptoren an einem Squarain führte zu **M21** dem außergewöhnlichsten Modell in dieser Arbeit. Anstelle der allgemein bei Squarainen vorgefundenen scharfen niederenergetischen Absorptionsbande, zeigte **M21** eine stark verbreiterte und solvensabhängige Bande. Spektroelektochemische Experimente und semiempirische Rechnungen konnten zeigen, dass es sich dabei um eine Überlagerung des klassischen squarainlokalisierten HOMO→LUMO Übergangs sowie eines partiellen Squarain→NDI "charge transfer" Übergangs handelte. Letzterer verschwand bei der Oxidation von **M21** zum Monokation und dessen Absorptionsspektrum war nahezu ein Abbild dessen eines reinen Squarainmonokations. Sowohl das Modell **M21** als auch das Polymer **P13** zeigten niedrige Bandlücken von 1.05–1.20 eV, welche die niedrigsten aller Verbindungen in dieser Arbeit darstellten. Transiente Absorptionsmessungen zeigten außerdem für beide Farbstoffe die extrem schnelle Ausbildung eines ladungsgetrennten Zustandes binnen weniger ps. Auch die Rekombination in den Grundzustand erfolgte innerhalb weniger ps. Im Polymer wurde

kaum ein weiterer Ladungs- oder Energietransfer während der Lebenszeit des angeregten Zustandes beobachtet, was darauf schließen ließ, dass der ladungsgetrennte Zustand auf benachbarten Squarain/NDI Einheiten lokalisiert war und nicht den Polymerstrang entlang wanderte.

Mittels der Ni-unterstützten *Yamamoto*-Kupplung wurden die Homopolymere **P1–P5** synthetisiert. Diese zeigten eine stark rotverschobene und verbreiterte Absorption im roten bis nah-infraroten Bereich, im Gegensatz zu den Donor–Squarain Copolymeren, sowie eine scharfe Fluoreszenz. Diese Eigenschaften wurden hauptsächlich auf die Exzitonenkopplung von lokalisierten angeregten Zuständen und der Präsenz unterschiedlicher Strukturen der Polymere zurückgeführt. Eine lineare J-artige Struktur führte zu der intensivsten und zugleich niederenergetischsten Bande von **P1** und **P2**, während eine zick-zack Struktur auch zu Absorptionen höherer Energie führte. Bei den Polymeren **P3** und **P4** wurden gleich mehrere Fraktionen unterschiedlicher Molmassenverteilung untersucht. Auch hier war eine gestreckte J-artige Struktur verantwortlich für die niederenergetischste Absorption, während eine helikale H-artige Struktur für die Absorptionen bei höherer Energie verantwortlich war. Der Anteil zu welchem diese unterschiedlichen Strukturen gebildet wurden zeigte sich abhängig von der Kettenlänge der Polymere als auch des Lösungsmittels. Absorptionsmessungen von Dünnfilmen zeigten, dass die ursprünglich in Lösung vorliegenden Strukturen zum Teil auch im Dünnfilm erhalten blieben, jedoch durch Tempern verändert werden konnten. Durch eine Kontrolle dieser Strukturbildung könnten auch die optischen Eigenschaften gezielt beeinflusst werden. Trotz der starken elektronischen Kopplung der Squaraineinheiten im angeregten Zustand zeigte sich außerdem, dass die Redoxpotentiale sich zu denen der monomeren Stammverbindungen kaum unterschieden und somit nur eine vernachlässigbare Interaktion im Grundzustand vorlag.

Des Weiteren wurde ein Squarain-Squarain Copolymer (**P6**) synthetisiert, welches aus alternierenden Einheiten der Stammverbindungen **M1** und **M2** bestand. Ähnlich wie bei den Homopolymeren waren eine starke Verbreiterung sowie eine Rotverschiebung der niederenergetischen Absorption zu beobachten. Darüber hinaus zeigte das Polymer eine markante Bande bei höherer Energie, welche mittels einer Erweiterung des

Exzitonenmodells für Copolymere erklärt werden konnte. In Toluol zeigte sich die niederenergetischste Absorptionsbande außergewöhnlich intensiv und schmal, was auf sogenanntes „exchange narrowing“ zurückgeführt wurde. Dieses könnte aus einer sehr geordneten J-artigen Struktur, welche wohl nur in Toluol vorlag, resultiert haben. Transiente Absorptionsmessungen zeigten eine starke Abhängigkeit der Abklingkurven von der Pumpenergie, insbesondere zu frühen Zeiten. Dies wurde auf das Auftreten von Mehrfachanregung (begünstigt durch den hohen Extinktionskoeffizienten) eines Polymerstranges und darauf folgender Exziton-Exziton Auslöschung zurückgeführt. Die statische Exziton-Exziton Auslöschung war der ratenbestimmende Schritt des Abklingprozesses, da sehr große Exzitondiffusionskonstanten bestimmt wurden. Dies war im Gegensatz zu anderen konjugierten Polymeren, in deren Dünnfilm die Exzitondiffusion als ratenbestimmender Schritt bestimmt wurde.

Zusammengefasst lässt sich sagen, dass für Polymere welche ausschließlich aus Squaraineinheiten bestanden, die Exzitonenkopplung von Chromophoren mit starken Übergangsdipolmomenten eine vielversprechende Weise war, die optischen Eigenschaften zu verändern.

Als Nebenprodukt der Polykondensationsreaktionen wurden in niedrigen Ausbeuten mittels Recycling-GPC beispiellose zyklische konjugierte Oligosquaraine erhalten, wie zum Beispiel ein mit Triarylaminen verbrücktes Dimer (**Dim1**) sowie einige Homotrimere (**Tri1–3**) und ein Homotetramer (**Tet1**). Insbesondere die Absorptions- und Fluoreszenzeigenschaften der Trimere waren außergewöhnlich. Sie zeigten mehrere Fluoreszenzbanden im NIR Spektralbereich die einen Bereich von ~ 8000–12500 cm^{-1} (800–1250 nm) abdeckten. Ersten theoretischen Berechnungen zu Folge, waren die zyklischen Trimere nicht vollständig planar, sondern lagen als eine Mischung aus planaren und abgewinkelten Squaraineinheiten vor, welche für diese besonderen Eigenschaften verantwortlich waren. Nichtsdestotrotz fehlten noch endgültige Ergebnisse der Berechnungen um dies mit endgültiger Sicherheit zu sagen.

Im letzten Abschnitt wurde die Verwendung einiger Substanzen in optoelektronischen Bauteilen beschrieben. Die Homopolymere **P1–P4** wurden in binären BHJ Solarzellen untersucht, welche allerdings nur eine geringe Effizienz zeigten, insbesondere aufgrund

geringer Kurzschlussströme. Die Verwendung von **P3** und **P4** führte zwar zu höheren Leerlaufspannungen, bedingt durch die Dicyanomethylengruppe und das resultierende niedrigere HOMO Energielevel, allerdings blieben sowohl die Effizienz als auch die Kurzschlussströme niedrig. Weder für die unterschiedlichen Molmassenverteilungen der Polymerfraktionen, noch für die unterschiedlichen Alkylketten konnte ein Trend bezüglich der Leistung der Solarzellen bestimmt werden. In den ternären BHJ Solarzellen wurden kleine Mengen von entweder Monomer **M14** oder den Polymeren **P1A**, **P4–1** oder **P13** zu einem P3HT/PCBM System beigemischt. Dadurch sollte ein zusätzlicher Weg für den Elektronen- oder Energietransport geschaffen und höhere Effizienzen erzielt werden. Jedoch führte keine der Verbindungen zu einer Verbesserung des Systems, sondern es wurden verringerte Kurzschlussströme beobachtet, welche auch zu geringerer Effizienz führten. Die niedrigen Kurzschlussströme deuteten an, dass die Morphologie der Squaraine der limitierende Faktor war. Es ist vorstellbar, dass die Dimethylgruppe am Heterozyklus der Squaraineinheit eine vorteilhafte Anordnung der Chromophore sterisch verhinderte, welche zu effizienterem Ladungs- oder Energietransport hätte führen können.

Das Monomer **M6** wurde als Dotiersubstanz zu einem Polymer (**SY-PPV**) in einer OLED beigemischt und fungierte erfolgreich als NIR-Emitter. Schon bei geringen Mengen des Squarains wurde die Fluoreszenz des Polymers gelöscht und stattdessen Fluoreszenz aus dem Squarain beobachtet. Bei Elektrolumineszenzmessungen reichten geringere Mengen (0.5 Gew.-%) als bei Photolumineszenzmessungen, um die Fluoreszenz des Polymers vollständig zu löschen. Dies deutete darauf hin, dass abgesehen von FRET zusätzliche Quenchmechanismen, wie Ladungsträgerdynamiken, in den elektrisch betriebenen Bauteilen eine Rolle spielten.

9 Appendix

9.1 List of Publications

1. *Polymeric Squaraine Dyes as Electron Donors in Bulk Heterojunction Solar Cells*, S. F. Völker, S. Uemura, M. Limpinsel, M. Mingebach, C. Deibel, V. Dyakonov, C. Lambert, *Macromol. Chem. Phys.* **2010**, *211*, 1098-1108.

2. *Squaraine Dyes as Efficient Coupling Bridges between Triarylamine Redox Centres*, S. F. Völker, M. Renz, M. Kaupp, C. Lambert, *Chem. Eur. J.* **2011**, *17*, 14147-14163.

3. *Exciton Coupling Effects in Polymeric cis-Indolenine Squaraine Dyes*, S. F. Völker, C. Lambert, *Chem. Mater.* **2012**, *24*, 2541-2553.

4. *Charge Transfer Dynamics in Squaraine-Naphthalene Diimide Copolymers*, S. F. Völker, A. Schmiedel, M. Holzapfel, C. Böhm, C. Lambert, *Phys. Chem. Chem. Phys.* **2013**, *15*, 19831-19844.

5. *Optoelectronic Processes in Squaraine Dye-Doped OLEDs for Emission in the Near-Infrared*, B. Stender, S. F. Völker, C. Lambert, J. Pflaum, *Adv. Mater.* **2013**, *25*, 2943-2947.

6. *Synthesis, Electrochemical, and Optical Properties of Low Band Gap Homo- and Copolymers Based on Squaraine Dyes*, S. F. Völker, T. Dellermann, H. Ceymann, M. Holzapfel, C. Lambert, *J. Polym. Sci., Part A: Polym. Chem.* **2014**, *52*, 890-911.

7. *Singlet-Singlet Exciton Annihilation in an Exciton-Coupled Squaraine-Squaraine Copolymer: A Model towards Hetero-J-Aggregates,* S. F. Völker, A. Schmiedel,

M. Holzapfel, K. Renziehausen, V. Engel, C. Lambert, *J. Chem. Phys. C.* **2014**, *accepted*.

9.2 Conference Contributions

1. Talk: *Dynamics in Excited Squaraine Polymers*, S. F. Völker, A. Schmiedel, M. Holzapfel, K. Renziehausen, V. Engel, C. Lambert "FOR 1809 Workshop", 04/2014, Schmerlenbach, Germany.

2. Talk: *Photoinduced Processes in Squaraine Polymers*, S. F. Völker, A. Schmiedel, M. Holzapfel, C. Böhm, C. Lambert, "KOPO 2013 Conference", 09/2013, Retzbach, Germany.

3. Poster: *POLYMERIC SQUARAINE DYES - Spectroscopic and Electrochemical Properties of Homopolymers and Donor/Acceptor Bridged Copolymers*, S. F. Völker, C. Lambert, "The 11th International Symposium on Functional π–Electron Systems (Fπ11)", 06/2013, Arcachon, France.

4. Poster: *POLYSQUARAINE DYES – From Homopolymers to Donor- and Acceptor-Squaraine Copolymers*, S. F. Völker, C. Lambert, "FOR 1809 Workshop", 10/2012, Niederstetten, Germany.

5. Poster: *Polymeric cis-Indolenine Squaraine Dyes and Cyclic Trimers*, S. F. Völker, C. Lambert, "Inauguration Party & Workshop Solar Technologies go Hybrid", 10/2012, Munich, Germany.

6. Poster: *Squaraine Dyes: Diversity and Properties*, S. F. Völker, H. Ceymann, C. Lambert, "GRK 1221 Workshop", 10/2012, Schöntal, Germany.

7. Poster: *Polymeric cis-Indolenine Squaraine Dyes and Conjugated Cyclic Trimer*, S. F. Völker, C. Lambert, "XXIV IUPAC Symposium of Photochemistry", 07/2012, Coimbra, Portugal.

8. Poster: *Redox Properties of Triarylamine/Bisphenylamine Substituted Indolenine Squaraines*, S. F. Völker, M. Renz, M. Kaupp, C. Lambert, "The 10th International Symposium on Functional π-Electron Systems (Fπ10)", 10/2011, Bejing, China.

9. Poster: *Triarylamine/Bisphenylamine-functionalized Indolenine Squaraines: Synthesis and Redox Properties*, S. F. Völker, M. Renz, M. Kaupp, C. Lambert, "Electronic Properties of π-Conjugated Materials II", 09/2011, Würzburg, Germany.

10. Poster: *Squaraine Polymer for use in Organic Solar Cells and Properties of Molecular Triarylamine-Squaraine-Conjugates*, S. F. Völker, C. Lambert, "GRK 1221 Workshop", 10/2010, Zeilitzheim, Germany.

11. Poster: *Squaraine Polymer for use in Organic Solar Cells and Properties of Molecular Triarylamine-Squaraine-Conjugates*, S. F. Völker, C. Lambert, "22nd Lecture Conference of the GDCh-Division of Photochemistry", 09/2010, Erlangen, Germany.

12. Talk: *Organic Solar Cells with Squaraine Polymers*, S. F. Völker, M. Limpinsel, C. Deibel, C. Lambert, "GRK 1221 Workshop", 10/2009, Niederstetten, Germany.

13. Poster: *Organic Solar Cells with Squaraine Polymers*, S. F. Völker, M. Limpinsel, C. Deibel, C. Lambert, "ICP2009 – XXIV International Conference on Photochemistry, 07/2009, Toledo, Spain.

9.3 Danksagung

Abschließend möchte ich mich bei allen Personen bedanken, die, in welcher Form auch immer, zum Gelingen dieser Arbeit beigetragen haben.

Benedikt Stender und *Prof. Dr. Jens Pflaum* für die sehr angenehme und erfolgreiche Zusammenarbeit und den überaus sympathischen Gesprächen rund um den Kickertisch.

Dr. Manuel Renz und *Prof. Dr. Martin Kaupp* für theoretische Berechnungen und insbesondere *Martin* für diverse schöne Abende auf dem Fussballplatz.

Dr. Markus Mingebach, *Dr. Shinobu Uemura*, *Moritz Limpinsel*, *Prof. Dr. Carsten Deibel* und *Prof. Dr. Vladimir Dyakonov* für die Herstellung und Untersuchung der binären Solarzellen.

Klaus Renziehausen, *Christoph Brüning* und *Prof. Dr. Volker Engel* für die Berechnung von Absorptions- und Fluoreszenzspektren.

Parisa Khoram, *Dr. Tayebeh Ameri* und *Prof. Dr. Christoph Brabec* für die unkomplizierte Zusammenarbeit und die Anfertigung und Untersuchung der ternären Solarzellen.

Federico Koch und *Prof. Dr. Tobias Brixner* für die Aufnahme von 2D transienten Absorptionsspektren und die zugehörigen Diskussionen zu unserem leider noch nicht abgeschlossenen Projekt, und vor allem *Fede* für höchst angenehme Zeiten auf unzähligen Workshops und auch abseits der Uni.

Markus Braun für seine allseits gutgelaunte Hilfestellung bei sämtlichen Anliegen und diversen kurzweiligen Gesprächen über Reisen, Politik, etc.

Michael Ramold für sämtliche Sonderanfertigungen im Labor und seine unkomplizierte Art.

Den Angestellten des Instituts für Organische Chemie: *Anette Krug*, *Petra Leckert*, *Dr. Christian Stadler*, *Dr. Alfons Ledermann*, *Dipl. Ing. Bernd Brunner*, *Matthias Fromm* und *Jonathan Landeck*.

Dr. Matthias Grüne und *Elfriede Ruckdeschel* für ihre überaus zuvorkommende Art, die Einweisung in die NMR Geräte und die Messungen unzähliger NMR-Spektren.

Antje Hautzinger, *Fritz Dadrich* und *Dr. Michael Büchner* für die Anfertigung zahlloser Massenspektren.

Insbesondere gilt der Dank den aktuellen und ehemaligen AK Mitgliedern (HEY, auf S.1 anfangen zu lesen!), die immer wussten eine angenehme Atmosphäre innerhalb und außerhalb des Labors zu schaffen.

Markus Steeger („Gargamel“): Danke für die megagute jahrelange Zusammenarbeit in der Box, für Dein Gefühl wann man mal ruhig sein muss („Markus, halt jetzt die Klappe!“) und Dein großes Wissen und den vielen Ideen zu sämtlichen Laborproblemen. Deinem horizontalen Laternendropkick sollte übrigens ein Denkmal gebaut werden. Und auch wenn Dich Deine unwiderstehliche Lache etwas verrückt(er) erscheinen lässt, so macht sie doch alles gleich etwas sonniger.

Fabian Zieschang: Danke für die jahrelange kompromisslose Freundschaft und den damit verbunden Bierchen, Urlauben und sonstigen Aktivitäten nach einem langen Tag im Labor. Wahrscheinlich haben wir mitunter mehr Zeit miteinander verbracht als *Nadja* und Du (Danke *Nadja* ;-)). Danke auch dafür, dass Du mehr als nur einmal ein gutes Gespür hattest, wann am besten ein Bier kalt zu stellen ist. Ach ja, auf ausdrücklichen und persönlichen Wunsch: U+2665 U+2665 U+2665!

Johannes Klein: Danke für unzählige Weineinkäufe inkl. Verkostung zum Wohle der AK-Feiern. Ist nicht einfach den gemeinen Franken zu knacken aber wir waren ein eingespieltes Team. 13 Weine sprechen eine deutliche Sprache. Auch nett, dass Du nicht militant versucht hast den Hobby- und Teilzeitvegetarismus zu verbreiten und dafür, dass Du den Laden gerade am Laufen hältst. Ist dir hoch anzurechnen…beides. Unvergessen auch die unterhaltsamen Tagungsaufenthalte in Peking und Portugal sowie Deine Zurückhaltung und Dein Charme („Verlierer! Verlierer!….!!!“)

Harald Ceymann: Danke für die Hauptrolle in lustigen Anekdoten rund um Treppenhäuser, natürlich für die Leitung der Logistikabteilung bei den ChemCups sowie für die entspannt kollegialen gemeinsamen Synthesen. Auch Deiner aufopferungsvollen Arbeit rund um den Grillrost sei gebührend gedankt, auch wenn Deine übliche Schoki-Fleisch-Diät Normalsterbliche schnell dahinraffen würde.

Julian Schäfer: Danke für Deine herrlich entspannte und lustige Art die ich immer zu schätzen wusste und Deiner Begeisterungsfähigkeit für Quatsch, Kaffee, Wein und Whisk(e)y (in der Reihenfolge). Die Frage guter oder böser Zwilling war schon fast geklärt, aber der Chilitopf hat die Entscheidung dann doch noch erst mal vertagt.

Stefan Riese: Danke für Deine ausgeglichene Art am späten Abend, Deinen Aktivitäten als Crash Test Dummy zwischen Bahnhof und Laby und vor allem Deinen höchst angenehmen Humor.

Maximillian Schreck: Danke für Deinen Wissensdurst und den anderen Durst, dessen Entgegenwirken in diversen Lokalitäten und auf grandiosen Konzerten immer ein pures Vergnügen war. Außerdem schön dass hinter Deiner primären höflichen Ader noch ne komplett durchgeknallte Sekundäre steckt.

Nina Schopf: Danke für leckere Muffins und Kuchen und die ruhige und besonnene Art, welche Dich vermutlich den Herrenhaushalt hier ertragen lässt.

Dr. Guillaume Grellaud: Merci, pour expliquer le (la?) difference d'une „Mousse *au* pamplemousse" et une „Mousse *de* pamplemousse".

Theresa Dellermann („Schlumpfine"): Ein riesiges DANKESCHÖN für die irrsinnig viele und gute Arbeit (Wahnsinn!) bei mir im Labor und für drei Monate gute-Laune-Sonnenschein (auch wenn es einmal ein Nogger brauchte) während Deiner Bachelorarbeit. Es hätte niemand besseren zu keinem besseren Zeitpunkt geben können! Danke vor allem auch für immer kurzweilige und schöne Zeiten außerhalb der Uni.

Julia Ehbets: Danke für die schöne Zeit während Deines F-Praktikums und auch der Zeit außerhalb des Labors inkl. der Gespräche im strömenden Regen. Schön dass Du am Ball geblieben bist.

Meinem Praktikanten *Christian Saalfrank*: Danke für ein paar lustige Wochen im Labor und der zahllosen Desserts.

Meiner Laborantin *Nadja Behr*: Danke für die aufopferungsvolle Arbeit bis zum Umfallen und dafür, dass Du immer weiter aufgeblüht bist.

Christoph Böhm: Danke dass nach Deiner Bachelorarbeit zumindest manche Stellen im Labor nicht blau eingefärbt waren.

Dr. Conrad Kaiser: Danke für Dein buntes Naturell und dafür, dass man im Labor immer mal wieder lachen und/oder mit dem Kopf schütteln musste. Außerdem danke, dass man immer aktuell wusste, wo man einen Touchscreen einbauen kann.

Dr. Nina Dürrbeck: Danke natürlich erstmal für Deine grandiosen und unermüdlichen Korrekturlesearbeiten sowie der, zumindest den Umständen entsprechenden, äußerst angenehmen Zeit im 3. Stock und der gemeinsamen sportlichen Aktivitäten außerhalb unseres Büros.

Dr. Christian Müller, einstiger Laborchef 116: Danke für Deine Führung der „Goldene Generation", die gute Stimmung (nicht Musik) im Labor und Deine Begeisterungsfähigkeit für alles was mit Essen und Trinken zu tun hat. Dein zweiter Platz in der Residenz und der „Frieden von Toledo" waren Meilensteine im Buffetbusiness. Ich hab Dir in Toledo gesagt die Kroketten sind eine Falle. Vor allem

aber die Zeiten nach Ladenschluss werden in bester Erinnerung bleiben. Ach ja, *Fabi* hat Dich am Dienstag im Reu vermisst.

Dr. Dörte Reitzenstein: Danke für die Einführung in die GPC. Ich glaub der neue Apparat hätte Dir auch gefallen.

Dr. Barbara Geiß: Danke für Deine Energie und der Gewissheit, Dich immer mal wieder im Nachti oder einem Weinetablissement unverhofft anzutreffen. PARTYYYY.

Alexander Heckmann: Denke für Deine immer etwas spezielleren, aber kurzweiligen Weltansichten.

Martin Bauer: Danke für meine ersten blauen Zipfel, das tägliche Kickerheft und die Inspiration zu einer ausgewogenen Ernährung.

Han Lu: Danke für Dein leckere Essen und vor allem den chinesisch Crash-Kurs, der es mir erlaubt in China ein oder vier Bier zu bestellen. Ebay π Joe!

Michael Moos: Danke für schöne Zeiten während des Studiums und Deinen jetzigen Tätigkeiten als unser „Mädchen für alles“. Und obacht beim Fahrradfahren!

Dr. Marco Holzapfel: Danke für die Auswertung der transienten Absorptions-messungen und für die theoretischen Berechnungen.

Alexander Schmiedel: Danke für die Aufnahmen der transienten Absorptionsspektren.

Christel Wendinger: Danke für diverse lustige Anekdoten, Laborarbeiten und den leckeren Apfelkuchen.

ERNIES&LamBERT, die ChemCup Sieger 2010: Danke für einen der grossartigsten Tage überhaupt.

Dr. Herbert Bezdek: Danke für zwei schöne Jahre im Chemie-Leistungskurs, welche wohl letztendlich mitunter ausschlaggebend für das Chemiestudium waren.

Mein besonderer Dank gilt auch meinen Freunden *Mark*, *Christin*, *Nadja*, *Jo*, *Chrissi*, *Nina*, *Jürgen*, *Georg*, *Moe*, *Andre*, *Bettina*, *Eva*, *Sabbel*, *Sebi*, *Yasmin*, *Lui*, *Thomas*, *Sofie*, *Stephan,…*, die mich über die Jahre in Würzburg begleitet haben und immer für den nötigen Ausgleich gesorgt haben. Ohne geht’s nicht! DANKE!

Abschließend möchte ich mich bei meiner Familie bedanken. Vor allem bei meinem Bruder, meiner Mutter und ihrem Mann (und meinem guten Kumpel) Bernd, meinem Vater und seiner Lebensgefährtin sowie meinen Großeltern für die immerwährende Unterstützung und das uneingeschränkte Vertrauen darin, mich einfach mal machen zu lassen. VIELEN VIELEN DANK!